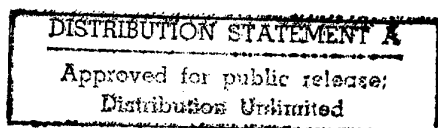


# **IUTAM**

## **Symposium on Statistical Energy Analysis**

**8-11 July 1997**

### **PROGRAMME**



**19980514 065**

**Chilworth Conference Centre  
University of Southampton  
Southampton, UK**

# REPORT DOCUMENTATION PAGE

Form Approved  
OMB No. 0704-0188

Public reporting burden for this collection of information is estimated to average 1 hour per response, including the time for reviewing instructions, searching existing data sources, gathering and maintaining the data needed, and completing and reviewing the collection of information. Send comments regarding this burden estimate or any other aspect of this collection of information, including suggestions for reducing this burden, to Washington Headquarters Services, Directorate for Information Operations and Reports, 1215 Jefferson Davis Highway, Suite 1204, Arlington, VA 22202-4302, and to the Office of Management and Budget, Paperwork Reduction Project (0704-0188), Washington, DC 20503.

1. <b>AGENCY USE ONLY</b> (Leave blank)		2. <b>REPORT DATE</b> 1997	3. <b>REPORT TYPE AND DATES COVERED</b> Preconference Literature 8 - 11 July 1997	
4. <b>TITLE AND SUBTITLE</b> IUTAM Symposium on Statistical Energy Analysis			5. <b>FUNDING NUMBERS</b> N00014-97-1-0571	
6. <b>AUTHOR(S)</b> Professor G M L Gladwell, Editor				
7. <b>PERFORMING ORGANIZATION NAME(S) AND ADDRESS(ES)</b> Professor Frank Fahy University of Southampton\Institute of Sound and Vibration Research Highfield Southampton SO17 1BJ United Kingdom			8. <b>PERFORMING ORGANIZATION REPORT NUMBER</b>	
9. <b>SPONSORING/MONITORING AGENCY NAME(S) AND ADDRESS(ES)</b> Technical Director Office of Naval Research International Field Office Europe PSC 802 Box 39 FPO, AE 09499-0700			10. <b>SPONSORING/MONITORING AGENCY REPORT NUMBER</b>	
11. <b>SUPPLEMENTARY NOTES</b>				
12a. <b>DISTRIBUTION AVAILABILITY STATEMENT</b> Approved for public release, distribution is unlimited			12b. <b>DISTRIBUTION CODE</b>	
13. <b>ABSTRACT</b> (Maximum 200 words) This was the first international scientific gathering devoted specifically to Statistical Energy Analysis which was first introduced nearly forty years ago. Abstracts were invited from 33 persons suggested by the Scientific and Organising Committee of which 30 were agreed by the committees to be converted to full papers. All the discussion sessions were tape recorded for subsequent transcription: it is hoped to include a synopsis in the edited proceedings.  The papers fell into three categories: theoretical developments; developments of experimental technique; practical applications. The first category included papers on the newly introduced smoothed energy flow and asymptotic wave propagation approaches to high frequency structural vibration analysis. The second category included papers on two new experimental techniques, namely input power modulation and energy impulse response measurement. The third category included a number of illustrations of the growing sophistication and utilisation of commercial SEA software, of which four versions were on display throughout the Symposium. The very lively discussion periods provided an excellent opportunity for individual scientists and engineers to air fundamental questions, to exchange views and experiences and to indicate their personal priorities for future research.				
14. <b>SUBJECT TERMS</b> Energy propagation, energy models, energy analysis, energy flow, continuum dynamics, vibrational energy, statistical energy analysis (SEA)			15. <b>NUMBER OF PAGES</b>	
			16. <b>PRICE CODE</b>	
17. <b>SECURITY CLASSIFICATION OF REPORT</b>	18. <b>SECURITY CLASSIFICATION OF THIS PAGE</b>	19. <b>SECURITY CLASSIFICATION OF ABSTRACT</b>	20. <b>LIMITATION OF ABSTRACT</b>	



# **Symposium on Statistical Energy Analysis**

**Sponsored by:**

**Office of Naval Research Europe**

**International Union of Theoretical and Applied Mechanics**

**Kluwer academic publishers**

**8-11 July 1997**

**Chilworth Conference Centre  
University of Southampton  
Southampton, UK**

# **IUTAM Symposium on Statistical Energy Analysis**

## **8-11 July 1997, Southampton, UK**

### *Scientific Committee*

Dr E Baba, Japan  
Professor V V Bolotin, Russia  
Professor H Davies, Canada  
Professor F J Fahy, UK  
Professor J L Guyader, France  
Professor M Heckl\*, Germany  
Professor T Kihlman, Sweden  
Professor D Y Maa, Peoples Republic of China  
Dr G Maidanik, USA  
Professor W G Price, UK  
Professor W Schiehlen (Ex-Officio Member)

### *Organising Committee*

Professor R J Craik, UK  
Professor F J Fahy, UK  
Dr K H Heron, UK  
Professor A J Keane, UK  
Professor R S Langley, UK  
Professor W G Price, UK  
Dr I Roebuck, UK  
Dr J Woodhouse, UK

### **Short Summary of Scientific Progress Achieved**

This was the first international scientific gathering devoted specifically to Statistical Energy Analysis which was first introduced nearly forty years ago. Abstracts were invited from 33 persons suggested by the Scientific and Organising Committee of which 30 were agreed by the committees to be converted to full papers. Complete sets of working papers, produced according to the format ultimately required by the publishers, were made available to the participants. All paper presentations were allocated 30 minutes and the ratio of discussion time to delivery time was 37%. All the discussion sessions were tape recorded for subsequent transcription: it is hoped to include a synopsis in the edited proceedings.

The Symposium opened with a Presidential address from Professor F Ziegler and a personal perspective on SEA from Professor B L Clarkson, past member of Council of IUTAM. The papers fell into three categories: theoretical developments; developments of experimental technique; practical applications. The first category included papers on the newly introduced smoothed energy flow and asymptotic wave propagation approaches to high frequency structural vibration analysis. The second category included papers on two new experimental techniques, namely input power modulation and energy impulse response measurement. The third category included a number of illustrations of the growing sophistication and utilisation of commercial SEA software, of which four versions were on display throughout the Symposium. The very lively discussion periods provided an excellent opportunity for individual scientists and engineers to air fundamental questions, to exchange views and experiences and to indicate their personal priorities for future research.

It was concluded that, although SEA now forms the basis of high frequency vibrational analysis by engineers in many industries, further research is required on the question of the influence of system topology on vibrational energy flow behaviour, and that criteria for subsystem selection are still largely lacking. It was also agreed that more work needs to be

---

\* Deceased



done on error and confidence analysis. The question of the influence of junction damping on the validity of the SEA equations was raised but not resolved.

### Countries represented and number of participants

Australia (1), Austria (3), Belgium (5), Canada (1), China (1), United Kingdom (20), France (12), Germany (3), Italy (1), Japan (1), New Zealand (1), Poland (1), Russia (2), Sweden (6), The Netherlands (3), USA (7). Number of participants: 68.

### Proceedings of the Symposium

The papers will be submitted to Professor G M L Gladwell for editing, before being printed by Kluwer Academic Publications early in 1998.

### Financial support

The Symposium was sponsored by the International Union of Theoretical and Applied Mechanics, the US Office of Naval Research (Europe) and Kluwer Academic Publications. 8 participants were assisted in varying degrees with travel, registration and subsistence costs (1 Austria, 1 China, 1 France, 1 New Zealand, 1 Poland, 2 Russia, 1 Sweden).

### Scientific Programme

<b>Chairman: W G Price</b>	
R S Langley	Some perspectives on wave-mode duality in SEA
A Carcaterra	Wavelength scale effects on energy propagation in structures
A Bocquillet, M N Ichchou, P Moron and L Jezequel	On the validity domain of some high frequency energy models
Y I Bobrovnikskii	Some energy relations for mechanical systems
<b>Chairman: R S Langley</b>	
G Orefice, J L Guyader and C Cacciolati	The energetic mean mobility approach (EMMA)
B R Mace and P J Shorter	Irregularity, damping and coupling strength in SEA
R G DeJong	An approach to the statistical energy analysis of strongly coupled systems
<b>Chairman: R J M Craik</b>	
J T Xing and W G Price	The energy flow equation of continuum dynamics
C Fredö	A note on conservative and non-conservative coupling
K H Heron	Predictive SEA using line wave impedances
P G Bremner and T E Burton	Statistical energy analysis of beams which are line-connected to plates
M Beshara and A J Keane	Vibrational energy flows between two plates forming an 'L'-shape and joined by compliant and dissipative couplings

J E Manning	SEA coupling factors for regular and irregular structures
<b>Chairman: I Roebuck</b>	
I Honda and K Ohta	Prediction of structure borne sound of low modal density structure by using SEA
M Blakemore and J Woodhouse	Power-flow analysis of quasi-one-dimensional systems with distributed coupling
D G Karczub and M P Norton	The estimation of dynamic stress and strain in beams, plates and shells using strain-velocity relationships
A K Belyaev	Statistical energy analysis of the parametric resonance in structural members
<b>Chairman: K H Heron</b>	
G Maidanik and J Dickey	On the external input power into coupled structures
G I Schuëller and H J Pradlwarter	Statistical energy analysis in view of stochastic modal analysis
K-O Lundberg	Input power modulation method
F J Fahy and P P James	An indicator of coupling strength between SEA subsystems
L Hermans, K De Langhe and L Demeestere	On the calculation of confidence levels of the experimentally derived internal and coupling loss factors
<b>Chairman: A J Keane</b>	
N Lalor	The practical implementation of SEA
X Huang, M J Moeller, J J Lee and R E Powell	Application of statistical energy analysis (SEA) to the development of a light truck sound package
G Borello	Predicting noise transmission in a truck cabin using the statistical energy analysis approach
S Finnveden	Prediction of vibration of fluid-filled pipes
A Adobes, L Ricol and Y Roussel	SEA for predicting the efficiency of noise reduction solutions applied to an air conditioner unit
Yao De-Yuan	Statistical energy analysis of nonconservatively coupled systems and its applications to engineering
<b>Chairman: F J Fahy</b>	
P Geissler	Calculation of structure-borne sound radiation from automotive mufflers using SEA
R J M Craik	Sound transmission through buildings using SEA

## IUTAM SYMPOSIUM ON STATISTICAL ENERGY ANALYSIS

CHILWORTH CONFERENCE CENTRE, UNIVERSITY OF SOUTHAMPTON

8-11 JULY 1997

Dear Symposiast

We bid you welcome to Southampton and to the IUTAM Symposium on Statistical Energy Analysis. It has been our long held ambition to arrange an international gathering of persons active in the development and application of SEA. We wish to offer our sincere gratitude to the Council of the International Union of Theoretical and Applied Mechanics for accepting our proposal to organise a symposium on this approach to modelling the vibrational and acoustical behaviour of complex mechanical systems which has undergone a long period of gestation before maturing into a widely used engineering tool, increasingly supported by a rapidly growing supply of commercial software.

Under the guidance of the members of our distinguished International Scientific Committee, we have invited participants from the broad spectrum of SEAFarers - academics, consultants, industrial engineers, software developers and research students - and aimed to reflect the balance of worldwide activity in SEA, although some eminent members of the SEA community have sadly been unable to attend. We are particularly disappointed that Professor Richard Lyon and Dr Gideon Maidanik, two of the principal originators of SEA, cannot be with us. We shall also greatly miss our late, dear colleague, Professor Manfred Heckl.

We wish to acknowledge with gratitude the generous sponsorship by IUTAM and the US Office of Naval Research, Europe, which, in addition to helping us to restrict the registration fee to a modest amount, has assisted a number of young researchers, and colleagues working in less favourable economic circumstances than ourselves, to participate. We also wish to thank Kluwer Academic Publishers for financial support.

It is not conventional to provide written communications to IUTAM symposia, but we felt that their availability would enhance the effectiveness of the proceedings. This file contains copies of all papers available at the time of copying. We apologise for any deficiencies in legibility, but wish to point out that the official proceedings, included in the registration fee, will be printed by Kluwer during the next six months, after editing by the appointed editor, and will be despatched to each participant in due course. We hope to be able to include summaries of the discussions in the proceedings, so that the pearls of wisdom will not be lost to posterity.

As you will appreciate, the organisation of an international symposium requires dedicated effort over a lengthy period from the home team. We wish to place on record our appreciation of the contributions of our colleagues on the National organising committee and, in particular, to Miss Sue Hellon who has somehow managed to handle the many administrative and secretarial demands of organisation in addition to her already onerous duties as secretary to the ISVR Fluid Dynamics and Acoustics Group.

SEA is by no means set in stone: many fundamental technical and practical problems still need to be resolved. We are confident that your participation in this symposium will result in significant advances in this direction. We wish you a pleasant and profitable sojourn with us here in Southampton.

Geraint Price

Co-Chairmen

Frank Fahy

**IUTAM SYMPOSIUM ON STATISTICAL ENERGY ANALYSIS**  
**CHILWORTH CONFERENCE CENTRE, UNIVERSITY OF SOUTHAMPTON**  
**8-11 JULY 1997**

**SCIENTIFIC COMMITTEE**

Dr E Baba, Japan  
Professor V V Bolotin, Russia  
Professor H Davies, Canada  
Professor F J Fahy, UK  
Professor J L Guyader, France  
Professor M Heckl\*, Germany  
Professor T Kihlman, Sweden  
Professor D Y Maa, Peoples Republic of China  
Dr G Maidanik, USA  
Professor W G Price, UK  
Professor W Schiehlen (Ex-Officio Member)

**NATIONAL ORGANISING/SCIENTIFIC COMMITTEE**

Professor R J Craik, UK  
Professor F J Fahy, UK  
Dr K H Heron, UK  
Professor A J Keane, UK  
Professor R S Langley, UK  
Professor W G Price, UK  
Dr I Roebuck, UK  
Dr J Woodhouse, UK

---

\* Deceased

# IUTAM SYMPOSIUM ON STATISTICAL ENERGY ANALYSIS

## Visit to the Institute of Sound and Vibration Research

**Thursday 10 July 1997**

Coach leaves: Chilworth Conference Centre at 1400  
University of Southampton at 1700

1430	Introduction to ISVR, Professor Frank Fahy (Tizard 3017)			
	<b>Group A</b>	<b>Group B</b>	<b>Group C</b>	<b>Group D</b>
1500	FDA (Tizard 2031)	RL (Building 15)	SPC (Tizard 3051)	VD (Building 19)
1520	HS (Tizard 2704)	FDA (Tizard 2031)	RL (Building 15)	SPC (Tizard 3051)
1540	SD (Building 19)	HS (Tizard 2704)	FDA (Tizard 2031)	RL (Building 15)
1600	SPC (Tizard 3051)	SD (Building 19)	HS (Tizard 2704)	FDA (Tizard 2031)
1620	VD (Building 19)	VD (Building 19)	SD (Building 19)	HS (Tizard 2704)
1640	RL (Building 15)	SPC (Tizard 3051)	VD (Building 19)	SD (Building 19)

Groups of 7 to 8 persons

FDA	Fluid Dynamics and Acoustics Group	MCMW, KRH, PPG, RHGT, ADP, SJH
HS	Human Sciences Group	NJM, HES
SPC	Signal Processing and Control Group	MJ, JS
VD	Vehicle Dynamics Group	LB, DJT, SJG
SD	Structural Dynamics Group	ARB, RMG, SLA
RL	Rayleigh Laboratories	RAD, DRP, OK, PAD

**Tuesday 8 July 1997**

**Chairmen**

Morning session:           WG Price

Afternoon session:       R S Langley

<b>0900</b>	C G Rice	Welcome to University of Southampton
<b>0910</b>	W Schiehlen	Welcome to the Symposium
<b>0925</b>	B L Clarkson	SEA: A personal perspective
<b>0945</b>	R S Langley	Some perspectives on wave-mode duality in SEA
<b>1015</b>	A Carcaterra	Wavelength scale effects on energy propagation in structures
<b>1045</b>	<b>Discussion</b>	
<b>1110</b>	<b>Coffee</b>	
<b>1130</b>	A Bocquillet, M N Ichchou, P Moron and L Jezequel	On the validity domain of some high frequency energy models
<b>1200</b>	Y I Bobrovnikskii	Some energy relations for mechanical systems
<b>1230</b>	<b>Discussion</b>	
<b>1300</b>	<b>Lunch</b>	
<b>1430</b>	G Orefice, J L Guyader and C Cacciolati	The energetic mean mobility approach (EMMA)
<b>1500</b>	B R Mace and P J Shorter	Irregularity, damping and coupling strength in SEA
<b>1530</b>	<b>Tea</b>	
<b>1600</b>	R G DeJong	An approach to the statistical energy analysis of strongly coupled systems
<b>1630</b>	<b>Discussion</b>	
<b>1700</b>	<b>Close</b>	

**Wednesday 9 July 1997**

**Chairmen**

Morning session: R J M Craik

Afternoon session: I Roebuck

<b>0900</b>	J T Xing and W G Price	The energy flow equation of continuum dynamics
<b>0930</b>	C Fredö	A note on conservative and non-conservative coupling
<b>1000</b>	<b>Discussion</b>	
<b>1025</b>	<b>Coffee</b>	
<b>1045</b>	K H Heron	Predictive SEA using line wave impedances
<b>1115</b>	P G Bremner and T E Burton	Statistical energy analysis of beams which are line-connected to plates
<b>1145</b>	M Beshara and A J Keane	Vibrational energy flows between two plates forming an 'L'-shape and joined by compliant and dissipative couplings
<b>1215</b>	J E Manning	SEA coupling factors for regular and irregular structures
<b>1245</b>	<b>Discussion</b>	
<b>1315</b>	<b>Lunch</b>	
<b>1430</b>	I Honda and K Ohta	Prediction of structure borne sound of low modal density structure by using SEA
<b>1500</b>	M Blakemore and J Woodhouse	Power-flow analysis of quasi-one-dimensional systems with distributed coupling
<b>1530</b>	<b>Tea</b>	
<b>1600</b>	D G Karczub and M P Norton	The estimation of dynamic stress and strain in beams, plates and shells using strain-velocity relationships
<b>1630</b>	A K Belyaev	Statistical energy analysis of the parametric resonance in structural members
<b>1700</b>	<b>Discussion</b>	
<b>1730</b>	<b>Close</b>	

**Thursday 10 July 1997**

**Chairman**

Morning session: K H Heron

<b>0900</b>	G Maidanik and J Dickey	On the external input power into coupled structures
<b>0930</b>	G I Schuëller and H J Pradlwarter	Statistical energy analysis in view of stochastic modal analysis
<b>1000</b>	<b>Discussion</b>	
<b>1025</b>	<b>Coffee</b>	
<b>1045</b>	K-O Lundberg	Input power modulation method
<b>1115</b>	F J Fahy and P P James	An indicator of coupling strength between SEA subsystems
<b>1145</b>	L Hermans, K De Langhe and L Demeestere	On the calculation of confidence levels of the experimentally derived internal and coupling loss factors
<b>1215</b>	<b>Discussion</b>	
<b>1300</b>	<b>Lunch</b>	
<b>1400</b>	Depart by coach for visit to Winchester and ISVR	
<b>1700</b>	Coach leaves ISVR to return to Chilworth	
<b>1730</b>	Coach leaves Winchester to return to Chilworth	
<b>1900</b>	Depart by coach for Dinner at Towles Restaurant in Lymington	



**Friday 11 July 1997**

**Chairmen**

Morning session: A J Keane

Afternoon session: F J Fahy

<b>0900</b>	N Lalor	The practical implementation of SEA
<b>0930</b>	X Huang, M J Moeller, J J Lee and R E Powell	Application of statistical energy analysis (SEA) to the development of a light truck sound package
<b>1000</b>	G Borello	Predicting noise transmission in a truck cabin using the statistical energy analysis approach
<b>1030</b>	<b>Discussion</b>	
<b>1045</b>	<b>Coffee</b>	
<b>1100</b>	S Finnveden	Prediction of vibration of fluid-filled pipes
<b>1130</b>	A Adobes, L Ricol and Y Roussel	SEA for predicting the efficiency of noise reduction solutions applied to an air conditioner unit
<b>1200</b>	Yao De-Yuan	Statistical energy analysis of nonconservatively coupled systems and its applications to engineering
<b>1230</b>	<b>Discussion</b>	
<b>1300</b>	<b>Lunch</b>	
<b>1400</b>	P Geissler	Calculation of structure-borne sound radiation from automotive mufflers using SEA
<b>1430</b>	R J M Craik	Sound transmission through buildings using SEA
<b>1500</b>	<b>General discussion</b>	
<b>1600</b>	<b>Close of Symposium</b>	

**IUTAM SYMPOSIUM ON STATISTICAL ENERGY ANALYSIS**  
**CHILWORTH CONFERENCE CENTRE, UNIVERSITY OF SOUTHAMPTON**

**8-11 JULY 1997**

**Attendance List**

Mr A Adobes	Electricité de France, France
Dr A K Belyaev	Johannes Kepler University of Linz, Austria
Miss M Beshara	University of Oxford, UK
Dr M Blakemore	Litton Data Systems, UK
Dr Y Bobrovnikski	Russian Academy of Sciences, Russia
Mr A Bocquillet	Ecole Centrale de Lyon, France
Professor V V Bolotin	Russian Academy of Sciences, Russia
Dr M Bonilha	United Technologies Research Center, USA
Mr I Bosmans	Katholieke Universiteit Leuven, Belgium
Mr P Bremner	Vibro-Acoustic Sciences Inc, USA
Dr C B Burroughs	The Pennsylvania State University, USA
Dr C Cabos	Germanischer Lloyd, Germany
Dr A Carcaterra	INSEAN, Italy
Miss C Chabrier	INRS, France
Professor B L Clarkson	Former Director of ISVR and former Principal of University College Swansea, UK
Professor R J M Craik	Heriot Watt University, UK
Professor H G Davies	University of New Brunswick, Canada
Dr R G De Jong	Calvin College, USA
Dr C A F De Jong	TNO, The Netherlands
Dr K De Langhe	LMS Numerical Technologies, Belgium
Professor Yao De-Yuan	Beijing Institute of Technology, China
Dr J Dickey	The John Hopkins University, USA
Mr D Eaton	European Space Agency, The Netherlands
Professor F J Fahy	University of Southampton, UK
Dr S Finnveden	KTH, Sweden
Dr C Fredö	Ingemansson Technology, Sweden

Mr P Geissler	Müller-BBM, Germany
Dr B M Gibbs	University of Liverpool, UK
Professor J-L Guyader	INSA de Lyon, France
Mr L Hermans	LMS International, Belgium
Professor K H Heron	DERA Farnborough, UK
Dr I Honda	Mitsubishi Heavy Industries Ltd, Japan
Mr M Iadevaia	LMS International, Belgium
Mr P P James	SEP, France
Dr D G Karczub	University of Western Australia, Australia
Professor A J Keane	University of Southampton, UK
Professor T Kihlman	Chalmers University of Technology, Sweden
Dr N Lalor	University of Southampton, UK
Professor R S Langley	University of Southampton, UK
Mr W Lie	Luleå University of Technology, Sweden
Mr K-O Lundberg	Lund Institute of Technology, Sweden
Dr J E Manning	Cambridge Collaborative Inc, USA
Mr L Maxit	INSA de Lyon, France
Mr M Moeller	Ford Motor Company, USA
Miss I Moens	Katholieke Universiteit Leuven, Belgium
Mr T Monger	DERA Farnborough, UK
Mr G Orefice	INSA de Lyon, France
Dr R Panuszka	University of Cracow, Poland
Dr H J Pradiwarter	University of Innsbruck, Austria
Professor W G Price	University of Southampton, UK
Mr M Rehfeld	Saint Gobain Vitrage, France
Mr L Ricol	Electricité de France, France
Prof Dr-Ing W O Schiehlen	University of Stuttgart, Germany
Prof Dr G I Schüeller	University of Innsbruck, Austria
Mr P Shorter	University of Auckland, New Zealand
Mr M G Smith	University of Southampton, UK
Dr J A Steel	Heriot Watt University, UK

Mr M Stubbs	DERA Haslar, UK
Dr R M Thompson	DERA Haslar, UK
Mr D Trentin	SEGIME, France
Miss S Vanpeperstraete	Aerospatiale, France
Dr Ir G Verbeek	Eindhoven University of Technology, The Netherlands
Dr M Villot	CSTB, France
Mr A Wilson	Chalmers University of Technology, Sweden
Dr J Woodhouse	University of Cambridge, UK
Professor J T Xing	University of Southampton, UK

## SOME PERSPECTIVES ON WAVE-MODE DUALITY IN SEA

R.S. LANGLEY

*Department of Aeronautics and Astronautics,  
University of Southampton,  
Southampton, SO17 1BJ, U.K.*

### 1. Introduction

It is well known that the response of a vibrating system can be viewed either in terms of modes or in terms of elastic wave motion. Both types of description are used extensively in Statistical Energy Analysis (SEA): the fundamental principles which underlie the method are normally expressed in modal terms, whereas wave based arguments are often used to yield practical estimates of key SEA parameters such as coupling loss factors. There has been much previous discussion regarding the relationship between the wave and modal descriptions, and the current view is perhaps best summarised by quoting the following extracts from Lyon and DeJong [1]: "we must emphasise that it is always possible, *at least in principle*, to arrive at the same conclusions by either [the wave or mode] approach"; "modal bandwidth is a very difficult concept to explain by a wave analysis and spatial decay of vibration is an equally difficult concept to explain by using a modal description"; "the wave-mode duality is useful for mean value estimates, but a wave analysis of variance by its nature disregards spatial coherence effects that are essential to the correct calculation of variance". To this can be added the following quote from Fahy [2]: "just how pure standing wave fields can be created in any elastic system, by reflection of waves from boundaries of arbitrary geometry, is something of a mystery". The relationships between the wave and modal descriptions of vibration are explored in the present paper, with the aim of clarifying the extent to which each allows a "physical" insight into the nature of the system response.

Initially, wave and modal descriptions of both the free and forced vibrations of a one-dimensional system are considered in Section 2. It is well known that the modes of such a system can be expressed very simply in terms of standing waves, although the relationship between the wave and modal descriptions of the forced response is less clear: a mode which is excited off-resonance no longer represents a simple combination of freely propagating elastic waves. It is shown here that a wave description of the forced response can be converted into a modal description by means of the Mittag-Leffler expansion [3], and the physical implications of this result are explored. Two-dimensional systems are then considered in Sections 3 and 4: a simply supported plate which is subjected to a point load is studied in Section 3, and this

example is used to show that any "physical" description of the response in terms of elastic wave motion is non-unique. The special case of a plane wave description of the motion of a two-dimensional system is considered in Section 4, and it is found that such a description, although valid in principle, leads to severe ill-conditioning which prevents precise resolution of the plane wave amplitudes. In this sense, the "mystery" alluded to by Fahy [2] cannot be resolved.

## 2. One-Dimensional Systems

### 2.1 FREE VIBRATION

This section is concerned with the vibration of a one-dimensional waveguide of length  $L$ . For the present purposes it is convenient to assume that the waveguide can carry only one type of propagating wave, and the wavenumber at frequency  $\omega$  is written as  $k$ . The system might represent a rod, a string, or a beam, provided that in the latter case any evanescent wave components decay rapidly across the system and hence need not be considered as a second wavetype. It can be noted that the present restriction on the nature of the system is imposed only to simplify the mathematical development and hence clarify the physical aspects of the system behaviour - it can readily be shown that the main results derived in what follows are also applicable to a complex system which displays multiple wavetypes.

The free vibration of the system can in general be expressed as a sum of right- and left-going wave components so that

$$u(x) = A_R e^{-ikx} + A_L e^{ikx}, \quad (1)$$

where  $u(x)$  is the system displacement at position  $x$  and the time dependency  $\exp(i\omega t)$  has been implicitly assumed. If the reflection coefficients at the ends of the system ( $x=0$  and  $x=L$ ) are written as  $R_1 = \exp(i\phi_1)$  and  $R_2 = \exp(i\phi_2)$  then equation (1) will only represent a valid description of the response if the following conditions are met

$$A_R = R_1 A_L, \quad A_L e^{ikL} = R_2 A_R e^{-ikL}. \quad (2,3)$$

If the frequency  $\omega$  is such that equations (2) and (3) are satisfied, then the response described by equation (1) is self sustaining and it can be deduced that the system is vibrating in a natural mode. The natural frequencies which satisfy equations (2) and (3) are given by the roots of the following equation

$$1 - R_1 R_2 e^{-2ikL} = 0 \quad \Rightarrow \quad 2kL = (\pm 2\pi n) + \phi_1 + \phi_2. \quad (4)$$

If equation (4) is satisfied then equation (1) can be re-expressed in the form of a real mode shape so that

$$u(x) = (\rho\gamma)^{-1/2} \cos(kx - \phi_1/2), \quad \gamma = L/2 + (1/4k)[\sin\phi_1 + \sin\phi_2], \quad (5,6)$$

where  $\rho$  is the mass per unit length of the system, and the factor  $\gamma$  has been introduced to scale the mode shape to unit generalised mass.

It is clear from the foregoing analysis that the modes of a one-dimensional system can be expressed very simply in terms of travelling wave components, and hence wave-mode duality in this sense is obvious. It should be emphasised however that this duality applies *only* when the mode is vibrating freely at its natural frequency. If the mode is *forced* at an off-resonant frequency then the mode shape, equation (5), is unchanged, but the wavenumber  $k$  is no longer compatible with the vibration frequency: the modal response cannot therefore be expressed simply in terms of two wave components, and wave-mode duality (in the simple single mode sense) breaks down. The precise relationship between the wave and modal descriptions of forced vibration is considered in the following section.

## 2.2 FORCED VIBRATION

In this section the one-dimensional system is taken to be subjected to a harmonic point load of complex amplitude  $P$  which is applied at the position  $x = x_0$ . To develop a wave description of the system response, it can firstly be noted that were the point load to act on an infinite system then a right and a left going wave of amplitude  $A_0 = -iP/2\rho c_g \omega$  would be generated, where  $c_g$  is the group velocity of the system [4]. The response of the finite system is produced by multiple reflection of these two components from the system boundaries: by adopting a ray tracing approach, it can readily be shown that the response at the position  $x = x_1$  is given by

$$u(x_1) = A_0 e^{-ik(x_1-x_0)} (1 + R_1 e^{-2ikx_0}) [1 + R_2 e^{-2ik(L-x_1)}] \sum_{n=0}^{\infty} R_1^n R_2^n e^{-2ikLn}. \quad (7)$$

The summation term in this expression represents an infinite series of "round trips" undertaken by the wave components. By evaluating the summation, equation (7) can be re-expressed in the form

$$u(x_1) = A_0 e^{-ik(x_1-x_0)} (1 + R_1 e^{-2ikx_0}) [1 + R_2 e^{-2ik(L-x_1)}] / (1 - R_1 R_2 e^{-2ikL}). \quad (8)$$

The wavenumber  $k$  which appears in equations (7) and (8) will be complex in the presence of damping, so that  $k = k_0 - i\omega\eta/2c_g$ , where  $k_0$  is the wavenumber of the undamped system and  $\eta$  is the system loss factor. Clearly the response yielded by equation (8) will display a peak in the vicinity of a system natural frequency, since

equation (4) is satisfied by the resonant wavenumber of the undamped system. In more detail, the denominator of equation (8) gives an indication of the "dynamic range" of the system response as a function of frequency, since it is readily shown that

$$1 - e^{-\pi m} \leq 1 - R_1 R_2 e^{-2ikL} \leq 1 + e^{-\pi m}, \quad m = \omega \eta L / \pi c_g, \quad (9,10)$$

where  $m$  is by definition the *modal overlap* of the system. It then follows that

$$(1 - R_1 R_2 e^{-2ikL})_{\max} / (1 - R_1 R_2 e^{-2ikL})_{\min} = \coth(\pi m / 2). \quad (11)$$

This expression agrees with results derived by Skudrzyk [5] and Langley [6] regarding the envelope of the frequency response function of a dynamic system: the ratio of the peaks to the troughs is found to be approximately  $\coth(\pi m / 2)$ . The analysis contained in references [5] and [6] is based on a modal, rather than a wave, analysis, and thus the recovery of equation (11) in the present work is an indication of wave-mode duality. In more general terms, it is not immediately obvious how equation (8) can be related to a modal expansion representation of the response. Progress in this regard can be made by considering the Mittag-Leffler expansion of a function  $f(\omega)$ , which states that [3]

$$f(\omega) = f(0) + \sum_r b_r [1 / (\omega - \omega_r) + 1 / \omega_r], \quad (12)$$

where  $\omega_r$  are the poles of the function and  $b_r$  are the residues. If equation (12) is applied to the system velocity,  $v(\omega) = i\omega u(\omega)$ , then the relevant poles are given by those frequencies for which equation (4) is satisfied. Now it can be noted that the wavenumber solutions ( $k$ ) to equation (4) are *real*, which means that, in the presence of damping, the associated frequencies must be *complex*. Furthermore, the reflection coefficients satisfy the condition  $\phi_i(-k) = -\phi_i(k)$ , which means that any solution  $k$  to equation (4) is accompanied by a second solution  $-k$ . It follows from these arguments that the relevant poles are

$$\omega_r = \pm \omega_{nr} (1 + i\eta / 2), \quad (13)$$

where  $\omega_{nr}$  is the  $r$ th undamped natural frequency of the system. In order to calculate the residue associated with the  $r$ th pole, the following quantity is required

$$\left. \frac{\partial}{\partial \omega} (1 - R_1 R_2 e^{-2ikL}) \right|_{\omega = \omega_r} = (i / c_g) [2L - (\partial \phi_1 / \partial k) - (\partial \phi_2 / \partial k)]_{\omega = \omega_r}. \quad (14)$$

In order to evaluate the derivatives which appear on the right hand side of this expression, it can be noted that for massless end fixtures each of the reflection



coefficients  $R_i$  must have the form  $(k-i\mu)/(k+i\mu)$ , where  $\mu$  is a real constant. It then follows that  $\partial\phi_i/\partial k = -(\sin\phi_i/k)$ , so that equation (14) becomes

$$\frac{\partial}{\partial\omega} \left( 1 - R_1 R_2 e^{-2ikL} \right) \Big|_{\omega=\omega_r} = 4i\gamma/c_g, \quad (15)$$

where  $\gamma$  is given by equation (6). Given this result, it can readily be shown that the application of the Mittag-Leffler expansion to equation (8) yields

$$v(\omega) = i\omega u(\omega) = (i\omega/\rho\gamma) \sum_r \frac{P \cos(k_r x_0 - \phi_r/2) \cos(k_r x_1 - \phi_r/2)}{\omega_{nr}^2 (1+i\eta) - \omega^2}. \quad (16)$$

This result is precisely the expression for the system velocity which is yielded by a modal approach.

Although equations (8) and (16) demonstrate wave-mode duality in a mathematical sense (in that the modal result can be derived directly from the wave result), there is no clear physical connection between the two approaches: away from a resonance the modes combine in a complex way to reproduce the travelling wave result, with no single mode being associated with a clearly definable form of wave motion. For broad band excitation the situation is somewhat different, in that the response will be dominated by "resonant modes", and as shown in Section 2.1, each resonant mode can be represented by two travelling waves. The extent to which these results are also applicable to two-dimensional systems is considered in the following sections.

### 3. Two-Dimensional Systems: Initial Example

#### 3.1 THE SYSTEM CONSIDERED

As a preliminary introduction to the behaviour of two-dimensional systems, attention is focused here on the example of a simply supported rectangular plate which is subjected to a point load. This example highlights certain features of the response which are further explored in Section 4 with regard to both free and forced vibrations. The plate is taken to have the planform dimensions  $L_1 \times L_2$  and a co-ordinate system  $(x_1, x_2)$  is centred at the lower left-hand corner of the plate so that  $0 \leq x_1 \leq L_1$  and  $0 \leq x_2 \leq L_2$ . A harmonic point load of frequency  $\omega$  and complex amplitude  $P$  is applied at the point  $(x_{10}, x_{20})$ ; it is convenient for the present purposes to derive an expression for the response of the plate by employing the method of images. With this approach, the finite plate is replaced by an infinite plate which is subjected to an infinite array of point loads: the point loads which lie outside the boundary of the finite plate represent the effect of reflections from the plate boundaries. Each

boundary reflection changes the sign of the point load, and the net effect is that the infinite plate is subjected to the following loading distribution

$$F(x_1, x_2) = P \sum_{n_1=-\infty}^{\infty} [\delta(x_1 - x_{10} - 2n_1 L_1) - \delta(x_1 + x_{10} - 2n_1 L_1)] \times \sum_{n_2=-\infty}^{\infty} [\delta(x_2 - x_{20} - 2n_2 L_2) - \delta(x_2 + x_{20} - 2n_2 L_2)], \quad (17)$$

where  $\delta$  is the Dirac delta function. An expression for the response of the plate is most easily obtained by applying the method of Fourier transforms; the spatial Fourier transform of the force represented by equation (17) is given by

$$F(k_1, k_2) = \frac{P}{4\pi^2} \int_{-\infty}^{\infty} \int_{-\infty}^{\infty} F(x_1, x_2) e^{ik_1 x_1 + ik_2 x_2} dx_1 dx_2 = g(k_1, k_2) \sum_{n_1=-\infty}^{\infty} e^{2ik_1 n_1 L_1} \sum_{n_2=-\infty}^{\infty} e^{2ik_2 n_2 L_2}, \quad (18)$$

where

$$g(k_1, k_2) = (P / 4\pi^2) (e^{ik_1 x_{10} + ik_2 x_{20}} - e^{-ik_1 x_{10} + ik_2 x_{20}} - e^{ik_1 x_{10} - ik_2 x_{20}} + e^{-ik_1 x_{10} - ik_2 x_{20}}). \quad (19)$$

The response of the plate then has the form [4]

$$u(x_1, x_2) = \sum_{n_1=-\infty}^{\infty} \sum_{n_2=-\infty}^{\infty} \int_{-\infty}^{\infty} \int_{-\infty}^{\infty} \frac{g(k_1, k_2) e^{-ik_1 x_1 - ik_2 x_2 + 2ik_1 n_1 L_1 + 2ik_2 n_2 L_2}}{D(k_1^2 + k_2^2)^2 (1 + i\eta) - \rho h \omega^2} dk_1 dk_2, \quad (20)$$

where  $D$  is the flexural rigidity of the plate,  $\rho h$  is the mass per unit area, and  $\eta$  is the loss factor. As detailed in the following sub-sections, equation (20) provides a useful starting point from which both modal and wave descriptions of the system response can be derived.

### 3.2 MODAL REPRESENTATION

Equation (20) can be used to derive a modal representation of the system response by performing the two summations *before* the integration is carried out. In this regard it can be noted that

$$\sum_{n_1=-\infty}^{\infty} e^{2ik_1 n_1 L_1} = \frac{\pi}{L_1} \sum_{r=-\infty}^{\infty} \delta(k_1 - r\pi / L_1), \quad \sum_{n_2=-\infty}^{\infty} e^{2ik_2 n_2 L_2} = \frac{\pi}{L_2} \sum_{s=-\infty}^{\infty} \delta(k_2 - s\pi / L_2), \quad (21,22)$$

so that equation (20) then yields

$$u(x_1, x_2) = (4P / \rho h L_1 L_2) \sum_{r=1}^{\infty} \sum_{s=1}^{\infty} \frac{\sin(k_{1r} x_{10}) \sin(k_{2s} x_{20}) \sin(k_{1r} x_1) \sin(k_{2s} x_2)}{\omega_{rs}^2 (1 + i\eta) - \omega^2}, \quad (23)$$

where  $\omega_{rs}$  is the  $rs$  natural frequency of the plate and

$$k_{1r} = r\pi / L_1, \quad k_{2s} = s\pi / L_2, \quad \omega_{rs}^2 = (D / \rho h)(k_{1r}^2 + k_{2s}^2)^2. \quad (24-26)$$

Equation (23) is the standard modal representation of the system response.

### 3.3 WAVEGUIDE REPRESENTATION

A wave based description of the system response can be derived from equation (20) by summing only over  $n_2$  before performing the integration. In this case the equation becomes

$$u(x_1, x_2) = (\pi / L_2) \sum_{n_1=-\infty}^{\infty} \sum_{s=-\infty}^{\infty} \int_{-\infty}^{\infty} \frac{g(k_1, k_{2s}) e^{-ik_1 x_1 - ik_{2s} x_2 + 2ik_1 n_1 L_1}}{D(k_1^2 + k_{2s}^2)^2 (1 + i\eta) - \rho h \omega^2} dk_1, \quad (27)$$

where  $k_{2s}$  is given by equation (25). Now from the definition of  $g(k_1, k_2)$ , equation (19), this result can be rewritten in the form

$$u(x_1, x_2) = (P / \pi L_2) \sum_{s=1}^{\infty} \sin k_{2s} x_{20} \sin k_{2s} x_2 \sum_{n_1=-\infty}^{\infty} \int_{-\infty}^{\infty} \frac{(e^{ik_1 x_{10}} - e^{-ik_1 x_{10}}) e^{-ik_1 x_1 + 2ik_1 n_1 L_1}}{D(k_1^2 + k_{2s}^2)^2 (1 + i\eta) - \rho h \omega^2} dk_1. \quad (28)$$

The integral over  $k_1$  can be performed by noting that the integrand has four poles: if  $Dk_{2s}^4 < \rho h \omega^2$  then two of the poles are predominantly real, corresponding to propagating wave motion - the pole with a positive real part has a negative imaginary part and vice-versa. The other two poles are predominantly imaginary, corresponding to evanescent wave motion. For  $Dk_{2s}^4 > \rho h \omega^2$  all four poles are predominantly imaginary: the excitation frequency can be said to be below the cut-on frequency for propagating wave motion. In evaluating equation (28), the integration contour should be taken around the upper half-plane for  $x_1 \pm x_{10} - 2n_1 L_1 < 0$  and around the lower half-plane for  $x_1 \pm x_{10} - 2n_1 L_1 > 0$  (the notation  $\pm x_{10}$  is used here to represent either of the two terms which appear in the numerator of the integrand). In either case, only two of the poles contribute to the integral; a typical contribution to the total response arising from this procedure will have the form

$$u_r(x_1, x_2) = (iP / 2L_2) \sum_{s=1}^{\infty} \sin k_{2s} x_{20} \sin k_{2s} x_2 \sum_{n_1=0}^{\infty} \frac{e^{ik_1 (\pm x_{10} - x_1)} e^{2ik_1 n_1 L_1}}{Dk_1 k^2 (1 + i\eta)}, \quad (29)$$

where  $k_{1r}$  is the relevant pole. The summation over  $n_1$  can now be performed to yield

$$u_r(x_1, x_2) = (iP / 2L_2) \sum_{s=1}^{\infty} \sin k_{2s} x_{20} \sin k_{2s} x_2 \frac{e^{ik_{1s}(\pm x_{10} - x_1)}}{Dk_{1s} k^2 (1 + i\eta)} \left( \frac{1}{1 - e^{2ik_{1s} L_1}} \right). \quad (30)$$

This contribution has a very similar appearance to equation (8), the response of a one-dimensional waveguide. In fact, the present approach is entirely equivalent to representing the response of the plate as a Lévy series of the type

$$u(x_1, x_2) = \sum_{s=1}^{\infty} u_s(x_1) \sin(s\pi x_2 / L_2). \quad (31)$$

With this approach, each of the functions  $u_s(x_1)$  satisfies a one-dimensional differential equation, and the system can be considered to be comprised of a series of waveguides which run in the  $x_1$ -direction. Each waveguide can be analysed by using the method outlined in section 2.2, and equations (29) and (30) represent a statement of this fact - the total response is produced by multiple reflections of (damped) waves which propagate in the  $x_1$ -direction. Clearly this approach provides a "physical" wave-based view of the system response, but it should be noted that this view is not unique. The system response could just as readily be expanded as a Lévy series in the transverse direction, so that the wave motion is taken to propagate in the  $x_2$ -direction; within the present analytical framework, this would amount to evaluating equation (20) by summing only over  $n_1$  before performing the integration.

### 3.4 CYLINDRICAL WAVE REPRESENTATION

A further wave-based description of the system response can be obtained by performing the integral which appears in equation (20) *before* evaluating either of the summations. The integral yields the Hankel function representation of the response of an infinite plate to a point load, and when this result is summed over all  $n_1$  and  $n_2$  (i.e. over the whole array of sources acting on the infinite plate) the following expression for the total response is obtained.

$$u(x_1, x_2) = (-iP / 8Dk^2) \sum_n (\pm 1) [H_0^{(2)}(kr_n) - H_0^{(2)}(ikr_n)]. \quad (32)$$

Here the index  $n$  covers the whole set of sources, and  $r_n$  represents the distance of the  $n$ th source from the point  $(x_1, x_2)$ . The  $\pm 1$  which appears inside the summation arises from the fact that successive reflections reverse the sign of the sources, as discussed in Section 3.1. Equation (32) provides a "physical" description of the system response in terms of a source cylindrical wave which undergoes multiple reflections at the systems boundaries.

### 3.5 PLANE WAVE REPRESENTATION

It has been shown that equation (20) can be used to derive both wave and modal descriptions of the response of a simply supported plate to an applied point load. The wave approach is often considered to provide the more "physical" description of the nature of the response (in terms of the propagation of damped waves), but an important issue which arises from the present work is that the wave description is not unique for a two-dimensional system. In SEA, a "wave description" is normally taken to mean a description in terms of damped *plane* waves, and such a description has not arisen naturally from equation (20). A description of this type could however be obtained by putting  $k_1 = k \cos \theta$  and  $k_2 = k \sin \theta$ , and converting the double integral which appears in equation (20) to an integral over  $k$  and  $\theta$ . The poles of the integral over  $k$  occur at the plane wavenumbers of the plate, and in principle the resulting expression for the response could be interpreted as a complex superposition of plane wave components. Rather than pursue this line of approach for the special case of the simply supported plate, the more general issue of the validity or otherwise of a plane wave description for arbitrarily shaped components is considered in the following section.

### 4. Two-Dimensional Systems: Plane Wave Description

It is well known that the modes of a simply supported plate can be represented by four mutually reflecting plane wave components. Furthermore, the modes of more complex systems of rectangular planform can be represented by a combination of four plane waves and a system of edge waves - this forms the basis of Bolotin's asymptotic method [6], which has been interpreted in terms of waves by Langley [7]. Bolotin's method is not applicable to arbitrary shaped components however, and thus it is not clear how plane waves might interact to produce modes in this type of system. Furthermore a plane wave representation of the *forced* harmonic response is not straight forward for any type of component. These issues can be investigated by writing the forced response of an arbitrary plate in the form

$$u(x_1, x_2) = \int_0^{2\pi} A(\theta) e^{-ix_1 k \cos \theta - ix_2 k \sin \theta} d\theta + \int_0^{2\pi} B(\theta) e^{-x_1 k \cos \theta - x_2 k \sin \theta} d\theta + u_p(x_1, x_2), \quad (33)$$

where  $k$  is the (damped) plane wavenumber associated with the excitation frequency  $\omega$ , and  $u_p(x_1, x_2)$  is a particular integral representing the response of an infinite plate to the applied loading. The description afforded by equation (33) can be shown to be complete - for example, if  $A(\theta)$  and  $B(\theta)$  are expanded as Fourier series then the equation represents an expansion in terms of a complete set of Bessel functions. A numerical scheme for computing the response of the plate can be devised by re-writing equation (33) in the form

$$u(x_1, x_2) = \sum_{n=1}^N A_n e^{-ix_1 k \cos \theta_n - ix_2 k \sin \theta_n} + \sum_{n=1}^N B_n e^{-x_1 k \cos \theta_n - x_2 k \sin \theta_n} + u_p(x_1, x_2), \quad (34)$$

where the coefficients  $A_n$  and  $B_n$  can be found by applying  $2N$  boundary conditions. This technique can be viewed as a version of the Trefftz method [9], and recent work in the Japanese literature has considered precisely this approach [10]. If the method can be applied successfully, then it will lead to a very clear description of the response of the system in terms of plane wave (propagating and evanescent) components. However, an investigation of the approach has shown that the method is subject to severe ill-conditioning; this is illustrated in what follows by the derivation of the condition number for an example problem.

To demonstrate the main features of the response description afforded by equation (34), it is convenient to consider the special case of a clamped circular membrane. In this case  $B_n = 0$ , since no evanescent waves arise in a membrane, and the boundary condition is  $u = 0$  on the circular boundary. By writing  $x_1 = r \cos \phi$  and  $x_2 = r \sin \phi$ , where  $r$  and  $\phi$  are polar co-ordinates, the boundary condition can be applied at  $N$  discrete points to yield

$$\sum_{n=1}^N A_n e^{-iRk \cos(\theta_n - \phi_m)} = -u_{pm}, \quad m = 1, 2, \dots, N, \quad (35)$$

where  $R$  is the radius of the membrane and  $\phi_m$  is the polar angle of the  $m$ th boundary point. Clearly equation (35) can be written in the matrix form

$$\mathbf{CA} = -\mathbf{u}_p, \quad (36)$$

where the vector  $\mathbf{A}$  contains the unknown wave amplitudes. The numerical stability of equation (36) is governed by the condition number  $\kappa$  of the matrix  $\mathbf{C}$ . Regardless of the nature of  $\mathbf{C}$ , the condition number is related to the eigenvalues of the matrix  $\mathbf{C}^T \mathbf{C}$ ; in the special case where  $\mathbf{C}$  is Hermitian, the condition number is related directly to the eigenvalues of  $\mathbf{C}$  - in fact  $\kappa$  is given by the ratio of the largest eigenvalue of  $\mathbf{C}$  to the smallest eigenvalue. For the present problem,  $\mathbf{C}$  can be made Hermitian by considering an undamped system ( $k$  real) and selecting  $\phi_n = \theta_n + \pi/2$  (which requires  $N$  to be divisible by four), in which case the entries of  $\mathbf{C}$  have the form  $C_{mn} = \exp\{ikR \sin[(m-n)2\pi/N]\}$ . Now it can readily be verified that the vector  $(1 -1 \ 1 -1 \dots 1 -1)$  is an eigenvector of  $\mathbf{C}$ , and furthermore this eigenvector can be expected to be associated with the smallest eigenvalue of the matrix,  $\lambda_{\min}$  say. It then follows that

$$\lambda_{\min} = \sum_{n=0}^{N-1} (-1)^n e^{-ikR \sin(n2\pi/N)} \approx 2(-i)^{N/2} N J_{N/2}(kR). \quad (37)$$

This result has been derived by expanding each exponential term in the summation as a Fourier series in the variable  $\theta = n2\pi/N$  - to leading order, all terms cancel except those involving the Bessel function  $J_{N/2}$ . Now the largest eigenvalue of  $C$  is bounded by the column norm, and hence a reasonable approximation is  $\lambda_{\max} = N$ . It then follows that the condition number is given by

$$\kappa = |\lambda_{\max} / \lambda_{\min}| \approx [2 J_{N/2}(kR)]^{-1} \approx \sqrt{\pi N / 4} (N / ekR)^{N/2}, \quad (38)$$

where the final expression is valid for large  $N$ . Equation (38) has been validated numerically by directly computing the condition number of  $C$  for a range of cases. Clearly the condition number grows very rapidly with  $N$ : for example, if the vibrational wavelength is equal to the membrane diameter, so that  $kR = \pi$ , then  $\kappa = 540$  for  $N = 16$ ,  $\kappa = 7.6e+09$  for  $N = 32$ , and  $\kappa = 6.97e+28$  for  $N = 64$ . Thus any attempt to finely resolve the detail of the wave amplitude distribution  $A(\theta)$  will be thwarted by ill conditioning - the physical reason for this can be traced to the fact that any two neighbouring waves  $A_n$  and  $A_{n+1}$  become very closely aligned, and they interact spatially with a very long "beat" wavelength; the plate (or membrane) appears relatively small on the scale of this beat wavelength, and hence the two waves produce near identical motion over the plate, which gives rise to ill conditioning. There is a kind of uncertainty principle at work here: increased angular resolution on  $A(\theta)$  leads inevitably to decreased spatial resolution between the wave components and hence ill conditioning.

Equation (34) has been applied by the author to a clamped skew plate. It has been found that the solution yielded by the method passes through three phases with increasing  $N$ : (i) for small  $N$  the problem is well conditioned but the solution is inaccurate; (ii) for moderate  $N$  the problem is reasonably well conditioned and a very accurate result is obtained for the physical plate response - even so, the wave amplitude distribution  $A(\theta)$  yielded by the method is not meaningful, since the results are erratic and show no convergence with  $N$ ; (iii) for higher values of  $N$  the problem is ill conditioned and the results are very poor. This confirms that a plane wave description of the response is possible in principle, although precise determination of the wave amplitude distribution is not possible due to ill-conditioning.

## 5. Conclusions

This paper has considered various aspects of wave-mode duality in one- and two-dimensional systems. For one-dimensional systems it has been shown that the modes of vibration can readily be expressed in terms of standing waves, although it should be noted that this representation is only valid at resonance - away from resonance, the modal wavelength is not commensurate with the wavelength of a propagating wave, and simple wave-mode duality breaks down. More generally it has been shown that the forced response of a one-dimensional system can be derived by employing a ray

tracing procedure, and this wave based description can be converted into a modal description via the Mittag-Leffler expansion.

Two-dimensional systems have been explored by considering initially the response of a simply supported plate to a harmonic point load. Equation (20) represents a general result for the response of the plate which can be manipulated to yield both the modal description and a number of (non-unique) wave descriptions. The issue of a plane wave description of the response of an arbitrary component has also been explored, and it has been shown that a form of uncertainty principle applies: the precise distribution of plane wave amplitudes cannot be determined due to ill-conditioning.

The non-uniqueness of the various wave based descriptions raises an interesting question as to whether the wave viewpoint can actually be considered to offer a more "physical" insight into the nature of the system response. In classical mechanics one tends to expect a "physical" description of the behaviour of a system to explain what the system is "really" doing, and such a description might be expected to be unique. The modal description is unique, in that the mode shapes are well defined, or alternatively in that the Mittag-Leffler expansion of the system response is well defined. However, the concern in SEA is with coupled systems rather than with single structural elements, and the modes employed are those of the uncoupled subsystems: this re-introduces the issue of non-uniqueness, since the subsystem modes can be defined under a variety of boundary conditions - for example free, or blocked (with the addition of "static" modes to make the modal basis complete). Clearly the wave and modal descriptions of the system behaviour are mutually compatible, and neither can claim to offer a definitive (or unique) physical insight into the system dynamics.

## 6. References

1. Lyon, R.H., and DeJong, R.G.: *Theory and Application of Statistical Energy Analysis, Second Edition*, Butterworth-Heinemann, Boston, 1995.
2. Fahy, F.J.: *Sound and Structural Vibration: Radiation, Transmission and Response*, Academic Press, London, 1985.
3. Spiegel, M.R.: *Theory and Problems of Complex Variables*, McGraw-Hill, New York, 1964.
4. Cremer, L., Heckl, M., and Ungar, E.E.: *Structure-borne sound*, Springer, Berlin, 1988.
5. Skudrzyk, E.J.: The mean-value method of predicting the dynamic response of complex vibrators, *Journal of the Acoustical Society of America* 67 (1980), 1105-1135.
6. Langley, R.S.: Spatially averaged frequency response envelopes for one- and two-dimensional structural components, *Journal of Sound and Vibration* 178 (1994), 483-500.
7. Bolotin, V.V.: *Random Vibrations of Elastic Systems*, Martinus Nijhoff, The Hague, 1984.
8. Langley, R.S.: An elastic wave technique for the free vibration analysis of plate assemblies, *Journal of Sound and Vibration* 145 (1991), 261-277.
9. Kita, E., and Kamiya, N.: Trefftz method: an overview, *Advances in Engineering Software* 24 (1995), 3-12.
10. Urata, Y., and Horide, A.: Analysis of lateral vibration of plates by the use of analytic solutions discretized on boundaries, 1st report: arbitrarily convex shaped plates with clamped and free edges (in Japanese), *Transactions of the Japanese Society of Mechanical Engineers* 61 (1995), 4153-4159.



## WAVELENGTH SCALE EFFECTS ON ENERGY

### PROPAGATION IN STRUCTURES

A. CARCATERRA

*Insean, Italian Ship Model Basin  
Via di Vallerano, 139, Roma, Italy*

#### 1. Introduction

In the field of energy transmission in dynamical systems the Statistical Energy Analysis (S.E.A.) is, at present, the most acknowledged contribution. Based on the thermal exchange of mechanical energy, S.E.A. provides information on the stored and dissipated energy and on the transmitted power between coupled dynamic systems. In spite of the particular simplicity of this energetical formulation, the research of a solid theoretical basis of S.E.A. instances has required, and still imposes, a remarkable effort to the scientific community [1-6].

In these last ten years several methods have been developed to meet new arising requirements. In these methods [7-9] the extension of the original S.E.A. statements is performed. While in S.E.A. complex structures of finite size are considered, in the new approaches the same thermal relationships are directly translated into differential form.

Aim of this work is to reconsider the thorny but fascinating problem of the vibrational conductivity under the light of the wavelength scale effect. The basic idea is that the wave energy transmission is dominated by the ratio between the characteristic length  $d$  of the system and the characteristic wavelength  $\lambda$  generated by the excitation. More precisely the non-dimensional value of the ratio  $\mu = d / \lambda$  seems to separate two different energy rate conditions: the small and the large  $\mu$  scale range.

#### 2. Energy Balance Equation and Constitutive Relationships

The Poynting vector is defined as  $\underline{I} = \underline{\sigma} \underline{v}$ , where  $\underline{\sigma}$  and  $\underline{v}$  are the stress tensor and the velocity vector, respectively. It gives, by its modulus and direction, the power flow through a continuous medium. The power balance is:  $\text{div } \underline{I} + \Pi_{\text{diss}} = \frac{\partial e}{\partial t}$ ,

being  $\Pi_{\text{diss}}, \frac{\partial e}{\partial t}$  the dissipated power and the time derivative of the total energy (kinetic and potential) respectively.

## A. CARCATERRA

The transmission potential function has been introduced in [10]. A general definition of  $\psi$  is given by:  $\underline{L} = \text{grad } \psi$ . The power balance equation therefore becomes:  $\nabla^2 \psi + \Pi_{\text{av}} = \frac{\partial e}{\partial t}$ .

The problem of providing the energy constitutive relationships consists of the following steps:

- determination of the correlation  $\psi = \psi(e)$ ;
- determination of the correlation  $\Pi_{\text{av}} = \Pi_{\text{av}}(e)$ .

When harmonic motion and time-average are considered, the following constitutive equation is accepted:  $\Pi_{\text{av}} = 2\eta \omega \langle e \rangle$ ,  $\langle e \rangle = \frac{1}{2T} \int_{-T}^T \frac{1}{2} \rho \omega^2 \dot{w}^2 dt$ , where  $\eta$ ,

$\omega$  and  $T$  are the loss factor, the circular frequency and the period of oscillation, respectively. As a consequence of this assumption the time derivatives into the energy balance disappear. In this case the potential of transmission depends on two different terms, and only one (thermal contribution,  $t$ ) is proportional to the local stored energy:  $\psi = \psi_t + \psi_d = \alpha \langle e \rangle + \psi_d$ , while the second term  $\psi_d$  (deviation,  $d$ ) has a more complex form [10].

In the present paper a study of the power transfer through regions of characteristic finite size  $d$  of a dynamical system is proposed. More precisely the importance of the ratio between the characteristic size  $d$  and the characteristic wavelength  $\lambda$  is analysed.

Therefore the following time and spatial moving-average energy is considered:

$$\langle \bar{e}(x, y, z) \rangle = \frac{1}{d^3} \int_D \langle e(\xi, \eta, \zeta) \rangle d\xi d\eta d\zeta; \quad D \equiv \{x < \xi < x + d, y < \eta < y + d, z < \zeta < z + d\}$$

### 3. Asymptotic Thermal Effects on a Discrete Linear Array

The equation of motion for a linear spring-mass system is:

$$m \frac{d^2}{dt^2} u_i + k(u_i - u_{i-1}) - k(u_{i+1} - u_i) = 0$$

Let us find a solution of the form:  $u_i(t) = U_i e^{j\omega t}$ ,  $U_i = z^i$ , where  $z$  is an unknown complex constant. Two cases are discussed:

- Below the cut-off frequency:  $\omega \leq 2 \omega_n$

In this condition the two  $z$  values, roots of the characteristic polynomial, are complex and conjugate. When  $\omega \ll \omega_n$  a first order Taylor expansion in terms of the ratio  $\omega / \omega_n$  leads to the expression:

$$z_{\pm}(\omega) \approx e^{\pm j \left( \frac{\omega}{\omega_n} \right)} \Rightarrow u(i, t) = z_{+}^{-1}(\omega) e^{j\omega t} \approx e^{j\omega t - j \left( i \frac{\omega}{\omega_n} \right)}$$

that is a propagative-nature solution.

- Above the cut-off frequency:  $\omega > 2 \omega_n$

## WAVELENGTH SCALE EFFECTS

When the frequency is above the cut-off limit, no wave propagates through the linear chain. The solutions  $z_+$ ,  $z_-$  are both real, with modulus less than one. This circumstance leads to an extinction of the motion  $\left( \lim_{i \rightarrow \infty} z_i = 0 \right)$  along the chain from the reference station. When  $\omega \gg \omega_*$ , the following approximation holds for the two roots:

$$z_+(\omega) = \gamma^{-1}(\omega), \quad z_-(\omega) = \gamma(\omega), \quad \gamma(\omega) = -\left(\frac{\omega}{\omega_*}\right)^2.$$

Below the cut-off frequency and in the absence of damping, the phenomenon presents exactly the same propagation characteristic as in a continuous waveguide. In [10] the energy distribution equation is determined and it does not exhibit a thermal behaviour.

Above the cut-off frequency a sort of thermal effect can be observed. The chain motion, when  $\omega \gg \omega_*$ , is well approximated by the form:  $U_i \approx U_0 \gamma^i$ ,  $\langle e \rangle_i \approx U_0^2 \gamma^{2i}$ . Therefore the chain asymptotic energy  $\langle e \rangle_i^*$  obeys the law:

$$\langle e \rangle_{i+1}^* - 2\langle e \rangle_i^* + \langle e \rangle_{i-1}^* - \left(\frac{\omega}{\omega_*}\right)^2 \langle e \rangle_i^* = 0. \text{ This result is suggestive for several reasons. In}$$

fact a smooth thermal-like asymptotic trend of energy is exhibited by the discrete system even in absence of damping, when using the time-average kinetic energy. This is a peculiar characteristic of these systems, that they don't share with the continuous ones.

Let be  $d$  the distance between two consecutive masses along the chain; the thermal energy behaviour is possible only when the wavelength is much bigger than  $2d$  (equivalent to the condition  $\omega \gg \omega_*$ ). The asymptotic limit expressed by eq (5) is therefore reached when  $\mu = 2d/\lambda \rightarrow \infty$ . Here  $\mu$  draws the bound between two complete different energy propagation domains. This sudden change, when the frequency crosses the cut-off limit, is not present in continuous systems, mainly because of the absence of the cut-off phenomenon. The crossing is, in that case, smooth and involves the space average energy, but  $\mu$  plays its role in a similar manner, at least for one-dimensional systems.

### 4. Asymptotic Thermal Effects in One-Dimensional Waveguides

The solution for a harmonically vibrating beam is:  $w = (a_- e^{i k_- x} + a_+ e^{-i k_+ x}) e^{i \omega t}$ ,

being  $k$  the complex wavenumber and  $a_-$ ,  $a_+$  the wave phasors, depending on the boundary conditions. The time and space-average energy, defined by  $\langle \bar{e}(x) \rangle = \frac{1}{d} \int_{x-d/2}^{x+d/2} \langle e(\xi) \rangle d\xi$ , after some mathematics, can be written as:

$$\langle \bar{e} \rangle = \kappa_* \left[ \left( \frac{e^{i \mu} - 1}{i \mu e^{i \mu/2}} \right) \cdot \left( a e^{-i k_+ \frac{d}{2}} + b e^{-i k_- \frac{d}{2}} \right) + c \left( \frac{\sin(2 \pi \mu)}{2 \pi \mu} \right) \cos(2 k_* x + \varphi) \right] = \langle \bar{e} \rangle_+ + \langle \bar{e} \rangle_- \quad (6)$$

## A. CARCATERRA

$$a = |a_+|^2, \quad b = |a_-|^2, \quad c = 2|a_+ a_-|, \quad \varphi = \angle(a_+, a_-)$$

where  $t$  and  $d$  indicate thermal and deviation component respectively. The first,  $\langle \bar{e} \rangle_t$ , smooth, is governed by exponential terms and is thermal; on the contrary the second one,  $\langle \bar{e} \rangle_d$ , is harmonically oscillating. Under this point of view the situation does not differ so much from that obtained by using only the time-average energy [10]. The relevant difference is here related to the presence of the  $\mu$  dependent factors in the energy expression. Those terms control, through  $\mu$ , the relative amplitude of the two energy contributions and their asymptotic properties (as  $\mu \rightarrow \infty$  or  $\mu \rightarrow 0$ ) reveal two different energy rate regions: the small and the large  $\mu$  scale range.

When the local energy value is accounted for, corresponding to  $d \rightarrow 0$ , no space-average is performed. In this case  $\mu \rightarrow 0$  and from the last written equation it is apparent that the factors involving  $\mu$  in the energy expression tend both to 1. Therefore the thermal and non-thermal components are of the same order of magnitude. On the contrary the opposite asymptotic limit,  $\mu \rightarrow \infty$ , definitely increases the amplitude of the thermal components, while the non-thermal one tends to vanish. Moreover if  $\mu = n/2$  (for an integer  $n$ ) the amplitude of the non-thermal component is zero.

It can be concluded that the thermal conductivity has an asymptotic validity in the sense previously defined i.e.:  $\lim_{\mu \rightarrow \infty} \langle \bar{e} \rangle = \langle \bar{e} \rangle^* = \langle \bar{e} \rangle_t$ .

To point out better this wavelength scale effect, it is interesting to estimate the thermal and non-thermal transmission potentials. It is:  $\psi = -\frac{8c^2}{\eta \omega} \langle \bar{e} \rangle_d + \psi_t$ . Moreover

$$\text{the property holds: } \psi_t(x, \mu) = 0 \quad \begin{cases} \mu \rightarrow \infty, & (\text{asymptotic property}) \\ \mu = \frac{n}{2}, & n = 1, 2, 3, \dots \end{cases}$$

Therefore it can be concluded that, for the beam, the time and space-average asymptotic energy  $\langle \bar{e} \rangle^*$  satisfies the conductivity vibrational principle.

### 5. Asymptotic Bounds in Two Dimensional Waveguides: Non-Thermal Energy Components

In plates we can represent the solution as obtained by superposition of an infinite number of plane waves travelling in any possible direction. The displacement  $w$  can be expressed as an integral of the form:

$$w(x) = \int_0^\pi \bar{a}_+(\theta) e^{-i/2(\theta)} z + \bar{a}_-(\theta) e^{i/2(\theta)} z \, d\theta$$

## WAVELENGTH SCALE EFFECTS

where  $\underline{k}(\theta) = k_s (1 - j\eta/4) \underline{n}(\theta)$  is the complex wave vector,  $\underline{n}(\theta)$  the unit vector associated to the  $\theta$  direction of propagation and  $\underline{r} \equiv \{x, y\}$  the position vector. The time and space-average energy associated to the displacement field is (omitting the heavy mathematics):

$$\langle \bar{\epsilon} \rangle = \sum_{i=1}^4 \int_0^\pi \int_0^\pi \frac{A_i(\theta_1, \theta_2) \bar{E}_i(\underline{r}, \theta_1, \theta_2)}{d^2} d\theta_1 d\theta_2$$

where:

$$A_1 = a_+(\theta_1) a_+(\theta_2), A_2 = a_+(\theta_1) a_-(\theta_2), A_3 = a_-(\theta_1) a_+(\theta_2), A_4 = a_-(\theta_1) a_-(\theta_2),$$

$$\bar{E}_i(\underline{r}, \theta_1, \theta_2) = \int_{x-d/2}^{x+d/2} \int_{y-d/2}^{y+d/2} e^{z_1 \xi} d\xi d\eta = \frac{e^{z_1 \xi} \cdot e^{v_{1x} \xi} - 1}{v_{1x} v_{1y}} \cdot \frac{e^{v_{1x} \xi} - 1}{e^{v_{1x} d/2}} \cdot \frac{e^{v_{1y} \xi} - 1}{e^{v_{1y} d/2}}$$

and

$$v_1 = j[k^*(\theta_2) - k(\theta_1)], v_2 = -j[k^*(\theta_2) + k(\theta_1)], v_3 = j[k^*(\theta_2) + k(\theta_1)], v_4 = -j[k^*(\theta_2) - k(\theta_1)]$$

In the previous expression of the energy field two main contribution can be separated.

In fact it is easy to show that the following decomposition holds:

$$\begin{aligned} \langle \bar{\epsilon} \rangle &= \sum_{i=1}^4 \int_0^\pi \int_0^\pi \frac{A_i(\theta_1, \theta_2) \bar{E}_i(\underline{r}, \theta_1, \theta_2)}{d^2} [1 - \delta(\theta_1 - \theta_2)] d\theta_1 d\theta_2 \\ &+ \sum_{i=1}^4 \int_0^\pi \frac{A_i(\theta, \theta) \bar{E}_i(\underline{r}, \theta, \theta)}{d^2} d\theta = \langle \bar{\epsilon} \rangle_{int} + \langle \bar{\epsilon} \rangle_{cwe} \end{aligned}$$

where  $\delta$  is the Dirac's generalized function and the two energy components are named *interference wave energy* (iwe) and *coincident wave energy* (cwe) respectively. The first is related to incident waves propagating along different directions, while the second is due to the waves propagating in a given direction.

The explicit form of the cwe is instead recovered by using the expression of  $\underline{v}_i(\theta_1, \theta_2)$ , given before, when  $\theta_1 = \theta_2 = \theta$ . It holds:

$$v_1 = -k_s \frac{\eta}{2} \underline{n}, v_2 = -2jk_s \underline{n}, v_3 = k_s \frac{\eta}{2} \underline{n}, v_4 = 2jk_s \underline{n}, \text{ where } \underline{n} \equiv \{\cos \theta, \sin \theta\}.$$

Substituting into the cwe expression one obtains, after some mathematics:

$$\langle \bar{\epsilon} \rangle_{cwe,1} = \kappa_r \int_0^\pi \left( \frac{(e^{i\pi\mu\cos\theta} - 1)(e^{i\pi\mu\cos\theta} - 1)}{(\pi\mu\eta)^2 \sin 2\theta e^{i\pi\mu\frac{\eta}{2}(\cos\theta + \cos\theta)}} \right) \cdot \left( A_1 e^{-i\pi\mu\frac{\eta}{2}\sin\theta} + A_2 e^{i\pi\mu\frac{\eta}{2}\sin\theta} \right) d\theta$$

$$\langle \bar{\epsilon} \rangle_{cwe,d} = \kappa_r \int_0^\pi \left( \frac{\sin(2\pi\mu\cos\theta)\sin(2\pi\mu\sin\theta)}{(\pi\mu)^2 \sin 2\theta} \right) \cdot |A_2| \cos(2k_s \underline{n} \underline{r} - \varphi)$$

# A. CARCATERRA

$$\langle \bar{e} \rangle_{cwe} = \langle \bar{e} \rangle_{cwe,1} + \langle \bar{e} \rangle_{cwe,2}$$

where  $\varphi = \angle A_1$ . The analogy between this part of the plate and the beam energy is complete. In fact the first term is thermal and satisfies the conductivity law. On the contrary the second one is non-thermal but has the same asymptotic properties discussed in section 4 about the beam energy. Therefore the  $\langle \bar{e} \rangle_{cwe}$  provides substantially a thermal energy contribution. Proceeding in the same manner shown in section 4, when high  $\mu$  values are considered (i.e.  $\langle \bar{e} \rangle_{cwe,2}$  vanishes), the asymptotic

cwe energy obeys the thermal law i.e.:  $\nabla^2 \langle \bar{e} \rangle_{cwe}^* - \left( \frac{\eta \omega}{c_t} \right)^2 \langle \bar{e} \rangle_{cwe}^* = 0$ . The asymptotic

transmission potential is:  $\psi_{cwe}^* = \left( \frac{2\omega}{c_t k_s} \right)^2 \langle \bar{e} \rangle_{cwe}^*$ .

It is important to notice that the possibility to split the cwe energy into two independent components, is related to the form of the  $\underline{v}_i$  vectors. They are in fact two reals ( $i=1,4$ ) and two purely imaginary ( $i=2,3$ ).

Let us examine the part of energy related to the waves interference. It is convenient to introduce the notations:

$$A_i(\theta_1; \theta_2) \bar{E}_i(\underline{r}, \theta_1; \theta_2) = F_i(\theta_1; \theta_2) e^{z_i \cdot \underline{r}}, \quad \underline{v}_i(\theta_1; \theta_2) = k_i \underline{z}_i(\theta_1; \theta_2).$$

The  $\underline{v}_i, \underline{z}_i$  vectors are now generally complex and, thus, the integrand contains both evanescent and harmonic factors coupled. After some mathematical manipulations it holds:

$$\langle \bar{e} \rangle_{cwe} = \sum_{i=1}^4 \int_0^\pi \int_0^\pi \left( F_i^R \cos(\underline{v}_i' \cdot \underline{r}) - F_i^I \sin(\underline{v}_i' \cdot \underline{r}) \right) e^{z_i' \cdot \underline{r}} [1 - \delta(\theta_1 - \theta_2)] d\theta_1 d\theta_2$$

$$\text{where: } F_i(\mu, \theta_1, \theta_2) = A_i(\theta_1, \theta_2) \frac{(e^{2\pi\mu z_{i1}^R} e^{2\pi j\mu z_{i1}^I} - 1)(e^{2\pi\mu z_{i2}^R} e^{2\pi j\mu z_{i2}^I} - 1)}{(2\pi\mu)^2 z_{i1} z_{i2} e^{-\pi\mu z_{i1}^R} e^{-\pi\mu z_{i1}^I} e^{-\pi\mu z_{i2}^R} e^{-\pi\mu z_{i2}^I}}$$

and the symbols  $R$  and  $I$  indicate real and imaginary part respectively, and the dependence on  $\mu$  is explicitly indicated. This energy does not satisfy the thermal equation, as it can be proved by direct substitution. Therefore it is worthwhile to analyse the trend of the functions  $F_i$  versus  $\mu$ .

The exponents affecting the asymptotic trend of these functions are only the real ones. Therefore, the asymptotic analysis of  $F_i$  involves the general function  $\frac{e^{2\pi\mu}}{\mu e^{2\pi\mu}}$ . It

follows:  $\lim_{\mu \rightarrow \infty} \frac{e^{2\pi\mu}}{\mu e^{2\pi\mu}} = \begin{cases} 0 & \text{if } \alpha < 0 \\ \infty & \text{if } \alpha > 0 \end{cases}$ .

## WAVELENGTH SCALE EFFECT

Since  $\alpha$  is the real or imaginary part of the generic  $\underline{z}_i$  vector, when  $\theta_i, \theta$ , vary in the integration region  $\Theta = [0; \pi] \times [0; \pi]$   $\alpha$  belongs to the interval  $-\eta/2 < \alpha < \eta/2$ . Therefore in the part of  $\Theta$  in which  $\alpha > 0$ ,  $F_i$  tends to zero when  $\mu$  increases; but in the remaining part of  $\Theta$  it tends to infinite. Looking at the  $\underline{z}_i$  vector expressions, one is easily convinced that for each region  $\mathcal{R} \subseteq \Theta$  over which  $\alpha < 0$  exists a corresponding  $\mathcal{R} \subseteq \Theta$ , of equal area, over which  $\alpha > 0$ . Consequently the integrand of the *interference wave energy* has globally the same exponential increasing trend as the contributions in the integral of the *coincident wave energy*. Thus a non-thermal component definitely exists, even when asymptotics is considered. It should also be noticed that the combined effect of an increasing and a decreasing component of *iwe* can determine a relative minimum in its contribution to the total energy.

### 6. Experimental Validation of Theory

The rest of this paper describes some experiments designed with the aim of validating the theoretical predictions.

The experimental tests have been performed on one beam and one plate excited in the high frequency range. In fact the wished variations of the  $\mu$  parameter imply the use of short wavelengths to avoid the construction of very large structures. Moreover the thermal analogy is essentially formulated to perform a convenient analysis in the high frequency range. Consequently a very fine measurement grid is necessary and a laser measurement technique is used both for the beam and the plate.

Goal of the experimental analysis is to check how the wavelength scale effect, *i.e.*  $\mu$ , acts on the energy transfer law.

To this aim a single meaningful parameter is proposed as an indicator of the tendency of the energy to elude the thermal law, or as a measure of the deviation energy component.

In the following the relative energy error criterion is presented for the plate case, being it totally analogous in the simpler beam case.

The vibrational conductivity equation is:

$$\nabla^2 \langle \bar{e} \rangle - \beta^2 \langle \bar{e} \rangle = 0, \quad (7)$$

where  $\beta$  is a constant depending on the loss factor, the frequency and the wave phase speed traveling along the structure. Its actual value for the real structure under study is only roughly evaluable due to the uncertainties affecting the mentioned quantities. It is thus preferable to determine it during the experiment, following the identification procedure explained later on.

By laser, the velocity phasor  $w_{i,j}$  in each point of the measurement grid  $P_{i,j}$  is available. Therefore the energy density distribution over the grid is determined as:  $\langle e \rangle_{i,j} = \kappa_r w_{i,j}^* w_{i,j}$ .

Let us divide the structure into rectangular regions, or cells  $C_{i,j}$ , of characteristic sizes  $d_x, d_y$ . Time and space-average energy can be computed, for each cell, as:

## A. CARCATERRA

$$\langle \bar{\varepsilon} \rangle_{i,j} = \frac{1}{d_x d_y} \sum_{i,j} \langle \varepsilon \rangle_{i,j} = \frac{1}{d_x d_y} \sum_{i,j} \langle \varepsilon(P_{i,j}) \rangle \quad \text{where } P_{i,j} \in C_{i,j}$$

At a fixed frequency  $\omega$ , a corresponding wavelength  $\lambda$  is generated. Therefore for each decomposition into cells of characteristic sizes  $d_x, d_y$ , a related value of the

$\mu$  parameter is determined, for example, as follows:  $\mu = \frac{d}{\lambda} = \frac{\sqrt{d_x d_y}}{\lambda}$ . By varying the characteristic dimension of the cells, at a fixed frequency, the wished  $\mu$  parameter variations are obtained and, in correspondence, several distributions of the related average energy  $\langle \bar{\varepsilon}(\mu) \rangle_{i,j}$  are computed.

Since the aim of the experiments is to check the limit of validity of the thermal formulation for the energy transmission expressed by (7), the simplest way to solve the problem is to compute the error equation substituting the measured energy distribution into the thermal balance equation (7). Expressing the energy balance between the cells one has:

$$\frac{\langle \bar{\varepsilon}(\mu) \rangle_{i,j} - 2\langle \bar{\varepsilon}(\mu) \rangle_{i,j} + \langle \bar{\varepsilon}(\mu) \rangle_{i-1,j}}{d_x^2} + \frac{\langle \bar{\varepsilon}(\mu) \rangle_{i,j} - 2\langle \bar{\varepsilon}(\mu) \rangle_{i,j} + \langle \bar{\varepsilon}(\mu) \rangle_{i,j-1}}{d_y^2} - \beta^2 \langle \bar{\varepsilon}(\mu) \rangle_{i,j} = \varepsilon(\mu)_{i,j}$$

$\varepsilon(\mu)$  is the non-thermal power component, i.e. the error affecting the thermal hypothesis.

The value of the  $\beta$  coefficient is determined, by a least square procedure, imposing that the global thermal error over the whole structure, i.e.  $\varepsilon(\mu) = \sum_{i,j} \varepsilon^2(\mu)_{i,j}$ , be minimum. This value ( $\beta_{opt}$ ) provides the best fit of the

energetic experimental data by the vibrational conductivity hypothesis. The global thermal error  $\varepsilon(\mu)$  accounts for the square of the total non-thermal power flow.

In the following it is preferable to refer it to the total dissipated power in the structure in order to obtain a more significant non-dimensional relative

$$\text{error: } \varepsilon_{rel}(\mu) = \frac{\sqrt{\varepsilon(\mu)}}{\beta_{opt}^2 E(\mu)}, \quad E(\mu) = \sum_{i,j} \langle \bar{\varepsilon}(\mu) \rangle_{i,j}.$$

Aim of the experimental analysis is to evaluate the behaviour of  $\varepsilon_{rel}(\mu)$  versus  $\mu$ , to check if the energetic transmission effects predicted by theory are met in practice.

## 7. Experimental Set Up and Results

The first set of experiments were performed on a hanged aluminum beam, whose length is 1.4 m. It was attached to a frame structure, by two elastic wires.

A damping layer was applied on the beam surface. It introduces an important increment in damping and in mass per unit length but not in the beam stiffness.



## WAVELENGTH SCALE EFFECTS

A laser head was used to perform the velocity measurements (over 140 points) in order to recover the kinetic energy distribution. The maximum range of  $\mu$ , allowed by the available measurement chain, is  $0 < \mu < 3$ .

The trend error, as defined in section 6, is plotted in figg. 1, 2, 3 versus  $\mu$ , at frequencies 8 kHz, 12 kHz and for random vibrations with flat excitation spectrum in the range 8-10 kHz respectively.

The asymptotic limit of the error as  $\mu$  increases is apparent. Moreover the sudden decrement in correspondence of the critical values  $\mu = 0.5, 1, 1.5, 2, 3$  are also clear (see sec. 4). The agreement with theory seems to be very good.

The experimental set up for the plate (0.6 m x 0.8 m) test is analogous to that described for the beam.

The maximum tested frequency is fixed at 4 kHz and a point force is applied to the plate in  $x=0.5, y=0.5$ . The minimum wavelength is estimated to be about 4 cm. The corresponding maximum number of points in the measurement rectangular grid is  $128 \times 64 = 8192$ . The plate is hanged by two elastic wires and the coupling between the exciter and the plate is obtained by a sting connector.

The procedure described in section 6 is applied to produce the error parameter for the previous test case and its trend is shown in fig. 4. In fig. 5 the error parameter is plotted for a random force test (frequency 3.5-4.5 kHz). The trend of the  $\varepsilon(\mu)$  curves show the different behaviour of the plate energy with respect to that of the beam. A direct comparison is shown in fig. 6. In fact in the plate test relevant errors are present even when the  $\mu$  parameter is considerably high (about 4). Moreover it is important to point out that in this last region the cell size (20 cm) approaches dimensions comparable with those of the plate.

Another difference with respect to the beam is the absence of the zero values in correspondence of some multiples of wavelength fractions as predicted by theory (see sec. 5).

## 8. Conclusions

The developed analysis highlights different scale laws in the mechanical energy transmission. The  $\mu$  parameter controls this characteristic scale. In the small scale transmission range ( $\mu < 1$ ) the vibrational conductivity principle fails for every type of considered structure: beams and plates. In the large scale range ( $\mu \gg 1$ ) the beam substantially obeys the thermal law, but the plate does not. A physical explanation, based on the *coincident* and the *interference wave energy* is proposed to justify these different behaviours.

In two-dimensional systems, although in the large  $\mu$  scale range the non-thermal components (related to the *interference wave energy*) can be reduced, they significantly contribute to the total energy field.

About two or three-dimensional structures it seems that the asymptotic thermal limit is reached very slowly as  $\mu$  increases, *i.e.* only when performing spatial-average over the entire structure, or over so large portions of it, that the real advantage with respect the classical Statistical Energy Analysis is doubtful.

## A. CARCATERRA

### Aknowledgments

The author wish to express his acknowledgement to Aldo Sestieri, professor at the Department of Mechanics and Aeronautics of the University of Rome, for his continuos suggestions and the useful discussions on the subject exposed in the paper.

This work was partly supported by the Italian Ministry of Merchant Marine in the frame of the INSEAN (Italian Ship Model Basin) research program 1991-93, and partly by MURST (Ministero Università e Ricerca Scientifica) through grant 60%.

### References

1. Fahy, F.J., Yao De Yuan, 'Power flow between non-conservatively coupled oscillators' *J. Sound and Vibration* (1987) **114**, 1-11.
2. Woodhouse, J., 'An Approach to the Theoretical Background of the Statistical Energy Analysis Applied to Structural Vibration', *J. Acoust. Soc. of Amer.*, vol.69, n.6 (1981).
3. Maidanik, G., Dickey, J., 'Wave Derivation of the Energetics of Driven Coupled One-Dimensional Dynamic Systems', *J. Sound and Vibration* (1990) **139**(1).
4. Keane, A.J., Price W.G., 'Energy flows between arbitrary configurations of conservatively-coupled multi-modal elastic subsystems', *Proc. of the Royal Society of London, A* **436**, 537-568.
5. Langley, R.S., 'A General Derivation of the Statistical Energy Analysis Equations for Coupled Dynamic Systems', *J. Sound and Vibration* (1989) **135**(3).
6. B. R. Mace, 'On the statistical energy analysis hypothesis of coupling power proportionality and some implications of its failure', *J. Sound and Vibration* (1994) **178**(1), 95-112.
7. D.J. Nefske, S.H. Sung, 'Power Flow Finite Element Analysis of Dynamic Systems: Theory and Apllication to Beams', Statistical Energy Analysis, *American Society of Mechanical Engineers*, NCA vol.3, (1987).
8. Le Bot, A., Jezequel, L., 'Energy formulation for one dimensional problems', *Proc. of the Institute of Acoustics* **15**(3), 561-568, 1993.
9. Bouthier, O.M., Bernhard, R.J., 'Simple models of energetics of transversely vibrating plates', *J. Sound and Vibration*, vol **182**, 129-164, 1995.
10. Carcaterra, A., Sestieri, A., 'Energy Density Equations and Power Flow in Structures', *J. Sound and Vibration* (1995) **188**(2), 269-282.

## WAVELENGTH SCALE EFFECTS

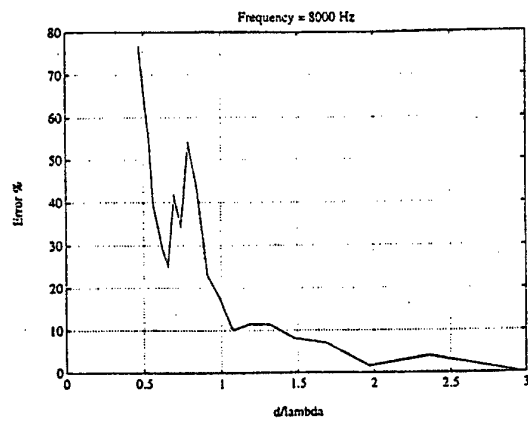


Figure 1

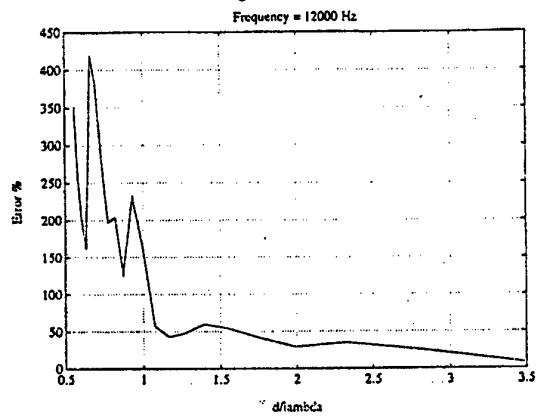


Figure 2

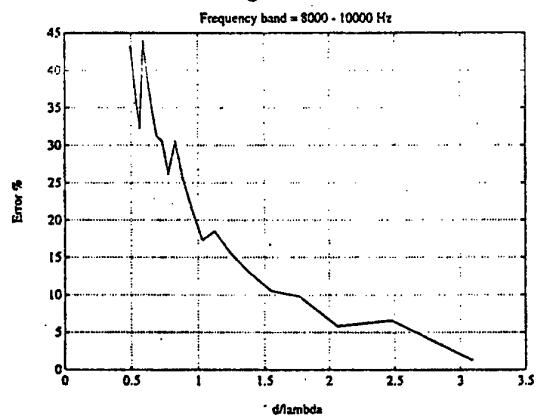


Figure 3

A. CARCATERRA

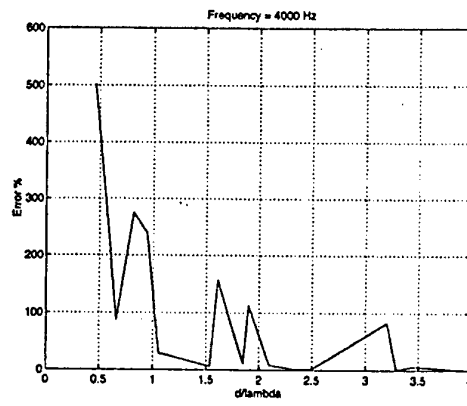


Figure 4

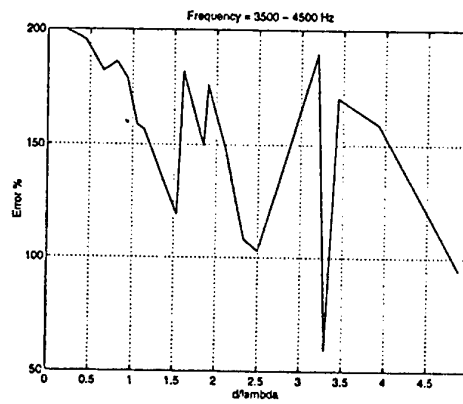


Figure 5

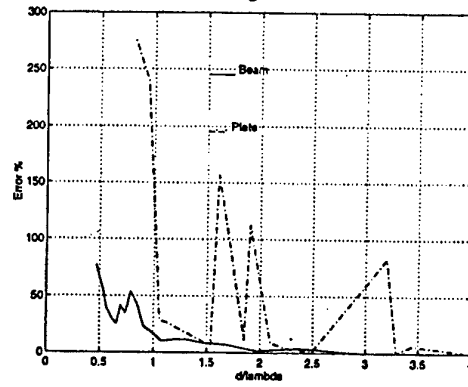


Figure 6

A. BOCQUILLET

## ON THE VALIDITY DOMAIN OF SOME HIGH FREQUENCY ENERGY MODELS.

A. BOCQUILLET, M. N. ICHCHOU, P. MORON & L. JEZEQUEL

*EQUIPE DYNAMIQUE DES SYSTEMES ET DES STRUCTURES  
ECOLE CENTRALE DE LYON - 69131 ECULLY CEDEX  
FRANCE.*

### ABSTRACT

The high frequency structural/acoustic dynamics has become a subject of increasing interest over the last few years. Special methods like the (SEA) have been developed to describe structural/acoustic response in this field. Recently, new original strategies like the Wave intensity Analysis (WIA) or a class of models called simplified energy methods (SEM) appeared to avoid (SEA) deficiencies. Two forms of the energy flow methods has been developed for (SEM). The first one is a pure differential energetic equation and is established using a plane wave hypothesis. The second form of the energy flow methods takes a pure integral form and is established from a cylindrical wave hypothesis and using Huygens principle.

This paper proposes some comparative results in attempt to clarify the validity domain and the main restrictions of each high frequency model. For this purpose, the system into consideration is a complex plate configuration. A numerical study is proposed in order to compare the energy models results to a semi-analytic "exact" prediction of the energy level of the system. Several structural parameters are considered (damping ratio....) to realise a parametric survey.

### 1- INTRODUCTION

The (SEA) is until nowadays, the main predicting method of the high and mid-frequency vibration through complex structures. It seeks to calculate the spatial average of energy for each sub-system by considering the power balance. Researches into the (SEA) validity have shown that it only applies to structures which are reverberant and have a high modal overlap. Besides, Guyader *et al.* has shown that (SEA) over-estimates the vibration energy levels between two steel plates in L-shape. Therefore, it seems to be important to investigate some alternative techniques.

## ON THE VALIDITY DOMAIN OF SOME H.F. ENERGY MODELS

The first one has been developed by R.S. Langley. It is a natural extension of the (SEA) and is called Wave Intensity Analysis (WIA). It relaxes the implicit wave field assumption of the SEA as well as the modal equi-repartition of energy. The two other possible (SEA) improvement methods are the so-called differential simplified energy method and the integral simplified energy method. They represent two different formulations derived from the same high frequency hypotheses. The (SEM) is a power flow model based on the original work by Belov, Rybak and Tartakovski, who first derived a differential equation of the heat conduction type to characterise the "spread" of energy throughout an absorbing structure. Since, power flow methods have been implemented in the case of Euler-Bernoulli beams, membranes, Kirchchov-Love plates and many coupling problems.

In what follows, we first present the (SEA) and (WIA) fundamental hypotheses and equations. Secondly, we present the two (SEM) formulations. Next, we focus on the coupling relationships used in the (SEM) formulations. Lastly, a numerical study is proposed in order to compare the four energy models with exact results.

### 2- BRIEF DESCRIPTION OF THE CONSIDERED ENERGY METHODS

#### 2.1. STATISTICAL ENERGY ANALYSIS (SEA) AND WAVE INTENSITY TECHNIQUE (WIA)

The main goal of the (SEA) is the prediction of the distribution of energy associated to the modal densities for each sub-system. Statements such as weak coupling, (subject of important debate), equi-repartition of energy between the modes present in high density for any sub-system, random stationary excitation forces and no correlation between the forces conservative coupling, are the (SEA) Hypotheses.

They involve that each sub-system should be reverberant enough to consider diffuse fields. They involve too a high modal overlap factor for each sub-system. The dissipated power and the power exchanged by two sub-systems may be expressed in the following forms:

$$\begin{aligned} [\eta] \{ \langle E \rangle \} &= \{ \langle P_{inj} \rangle \} / \omega_c \\ \text{où : } [\eta] &= \left[ \delta_{rs} \sum_i \eta_{ist} - (1 - \delta_{rs}) \eta_{rs} \right]_{s,r} \text{ et } \eta_{rr} = \eta_r \end{aligned} \quad (2.1)$$

The coupling loss factors are given by the following expression ([6]):

$$\eta_{ij} = \frac{c_{gi} L}{\pi \omega S} \int_0^{\frac{\pi}{2}} \tau_{ij}(\theta) \cos(\theta) d\theta \quad (2.2)$$

where  $\tau_{ij}$  are then transmission efficiencies of the coupled sub-systems.

The (WIA) appears to be a natural extension of the (SEA) approach. As a matter of fact, this method takes up the main (SEA) assumptions, relaxing nevertheless the diffuse

wave field assumptions and considering the wave field homogeneous random. Thereby, the directional dependencies of the wave intensity and energy density in each sub-system are represented by Fourier Series. Furthermore, if a single term of the series is used, the (WIA) recovers the (SEA) form in the coupling loss coefficients expressions. Moreover, it is interesting to notice from a modal point of view, that the standard assumption of energy equirepartition between the modes of a particular sub-system, is relaxed ([2]). Under the assumption that the dynamic response of each component is represented in terms of a random wave field, the total energy density may be expressed as:

$$\langle E \rangle = 2 \langle T \rangle = \sum_j \int_{-\infty}^{+\infty} \int_{-\infty}^{+\infty} \langle W \rangle_j(\theta, \omega) d\theta d\omega \quad (2.3)$$

with  $\langle W \rangle_j(\theta, \omega) = 2 \rho \omega^2 S_j(\theta, \omega)$ ,  $S_j$  spectral density,  $W_j$  being the density of a particular wave type which is attributable to a plane wave of pulsation  $\omega$ , and propagating into the  $\theta$  direction (cf. Figure 1).

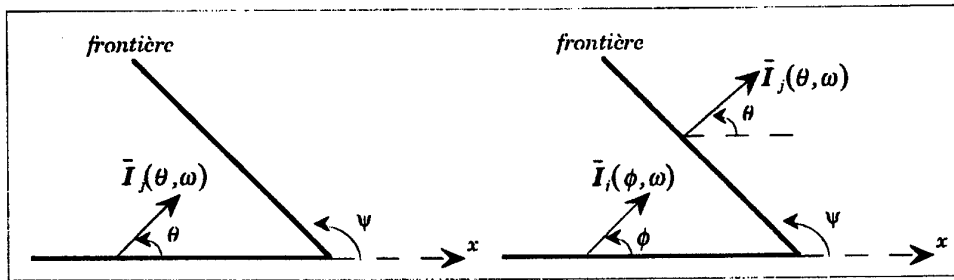


Figure 1. Boundary description according to Wave Intensity Analysis.

The power flow vector (or intensity) associated to a particular wave type has the general expression:

$$\langle \bar{I} \rangle_j(\theta, \omega) = c_{e,j} \langle W \rangle_j(\theta, \omega) \bar{u}(\theta) \quad (2.4)$$

where  $\bar{u}(\theta)$  is the unit directional vector of the power flow. In order to find the quantities, we have to consider the energy flow equilibrium equation for the heading  $\theta$  of the wave of type  $j$ :

$$\langle P_{inj} \rangle_j(\theta, \omega) = \langle P_{dis} \rangle_j(\theta, \omega) + \langle P_{en} \rangle_j(\theta, \omega) - \langle P_{ei} \rangle_j(\theta, \omega) \quad (2.5)$$

where  $\langle P_{inj} \rangle_j$  is the injected power due to external forces,  $\langle P_{dis} \rangle_j$  the dissipated power,  $\langle P_{ei} \rangle_j$  the power entering the sub-structure through boundary, and  $\langle P_{en} \rangle_j$  the outgoing power. After having expressed the two last powers in terms of the intensity vector and

## ON THE VALIDITY DOMAIN OF SOME H.F. ENERGY MODELS

next in terms of energy density as well as the dissipated power, the power equilibrium ([2]) may be written in the form:

$$[C]\{\langle W \rangle_{jp} / v_j\} = P \quad (2.6)$$

with

$$\langle W \rangle_j(\theta, \omega) = \sum_p \langle W \rangle_{jp}(\omega) N_p^j(\theta),$$

$$C_{jp, is} = \delta_{ij} \left\{ \omega \eta_i v_j \int_0^{2\pi} N_p^j(\theta) N_s^i(\theta) d\theta + (\omega/2\pi c_j) \sum_k L_k \int N_p^j(\theta) N_s^i(\theta) \cos(\theta + \pi/2 - \psi_k) d\theta \right. \\ \left. - (\omega/2\pi c_j) \sum_m L_m \int N_p^j(\theta) N_s^i(\phi_{mi}) \cos(\theta + \pi/2 - \psi_m) \tau_{ij}^m(\phi_{mi} + \pi/2 - \psi_m) d\theta \right\}$$

and

$$P_{jp} = \int_0^{2\pi} P_{inj}^j(\theta, \omega) N_p^j(\theta) d\theta.$$

In practice, two further hypotheses are made as far as the N functions are concerned. If the considered panel has only horizontal reflecting boundaries, the appropriate Fourier components are  $\cos(n\theta)$ . If it has horizontal and vertical reflecting boundaries, the Fourier components must have the form  $\cos(2n\theta)$  with n even integer.

### 2.2. SEM ENERGY MODELS

The first step in the energy method development is the well known energy flow balance written in harmonic form. In this case, the time is removed and the following expression is obtained; if  $\langle \cdot \rangle$  is the temporal average and  $\underline{\cdot}$  indicates (MES) hypotheses:

$$\nabla \cdot \langle \underline{\bar{I}} \rangle + \eta \omega \langle \underline{e} \rangle = \langle \underline{p}_{inj} \rangle. \quad (2.7)$$

In the following, a hysteretic damping model is considered. The assumption set required to derive the (SEM) is:

- (i) ♦ *Linear, Elastic, dissipative and isotropic systems.*
- (ii) ♦ *Slight hysteretic damping loss factor.*
- (iii) ♦ *Steady state conditions with harmonic excitation  $\omega$ .*
- (iv) ♦ *Far from singularities, evanescent waves are neglected.*
- (v) ♦ *The interferences between propagative waves are not considered.*

The assumptions (1), (2), (3) define the general context of the study, the assumption (2) involves that the wave numbers are approximately equal to the undamped axes. The



assumption (5) has been introduced by Ichchou and Jezequel in order to generalize the space average concept developed by Bouthier and Bernhard ([9]). It means that in the mid and high frequency range, we assume the decorrelation between the propagative waves. At this stage, the relevant relation between a partial active energy flow and energy density may be expressed in the following form:

$$\langle \bar{I} \rangle = c_g \langle e \rangle \bar{u} \quad (2.8)$$

### 2.2.1 Differential (SEM):

The parameter  $c_g$  is the group velocity concerning the wave type  $j$ . Since we assume that the dynamical behaviour of our system may be approximated by a **plane wave field** solution, it can be stated:

$$\langle \bar{I} \rangle = -\frac{c_g^2}{\eta \omega} \vec{\text{grad}}(\langle e \rangle) \quad (2.9)$$

Thereby, the power flow balance (cf. Eq. (2.7)) may be expressed in the form by using Eq. (2.9):

$$-\frac{c_g^2}{\eta \omega} \Delta \langle e \rangle + \eta \omega \langle e \rangle = \langle p_{inj} \rangle \quad (2.10)$$

In this study, we only consider the bending waves propagating in the plate

### 2.2.2 Integral Simplified Energy Method

A. Le Bot [8] has adopted an integral formulation of the (SEM). The energy fields are written by applying the Huygens Principle.

The scheme of this method is based upon the definition of a energy travelling wave in a infinite isotropic medium of dimension 2, excited by a driving point  $S_0$ . Accounting for the relationship linking the energy density to the energy flow Eq. (2.8), the power balance leads to the distribution equation:

$$\frac{\partial \langle e \rangle}{\partial r} + \frac{\langle e \rangle}{r} + \frac{\eta \omega}{c_g} \langle e \rangle = \delta_{S_0}, \quad (2.11)$$

whose kernel  $G$  constitute the fondamentale propagative wave:

$$G(S_0, M) = \frac{e^{-\frac{\eta \omega}{c} r}}{2\pi r}.$$

$G$  describes in this case a **cylindrical wave propagation**.

The associated energy flow vector is expressed as follows:

## ON THE VALIDITY DOMAIN OF SOME H.F. ENERGY MODELS

$$\bar{H}(S_o, M) = c_r \frac{e^{-\frac{\eta \omega}{c_r}}}{2\pi r} \bar{u}_{S_o, M}$$

The expressions of the fields  $\langle \bar{I} \rangle$  and  $\langle \bar{e} \rangle$  involve a boundary repartition of secondary sources  $\sigma$ , in addition to the primary sources  $\rho$ . The principle of superposition on energy variables is valid since interferences coming from different sources are neglected. So we write for  $M \in \Omega$ :

$$\begin{aligned} \langle \bar{e} \rangle (M) &= \int_{\Omega} \rho(S) G(S, M) dS + \int_{\partial\Omega} \sigma(P) f(P, \bar{u}_{MP} \cdot \bar{n}_P) G(P, M) dP \\ \langle \bar{I} \rangle (M) &= \int_{\Omega} \rho(S) \bar{H}(S, M) dS + \int_{\partial\Omega} \sigma(P) f(P, \bar{u}_{MP} \cdot \bar{n}_P) \bar{H}(P, M) dP, \end{aligned}$$

where  $f(P, \cdot)$  is the directivity of the boundary source  $P$ .

The power balance at any boundary point  $P$  exhibits a Fredholm equation of the second kind on  $\sigma$  [8]:

$$\begin{aligned} \sigma(P) &= \frac{1 - \alpha(P)}{\gamma(P)} \left\{ \int_{\Omega} \rho(S) G(S, P) dS + \int_{\partial\Omega} \sigma(P') f(P', \bar{u}_{PP'} \cdot \bar{n}_{P'}) G(P', P) \bar{u}_{PP'} \cdot \bar{n}_P dP' \right\} \quad (2.12) \\ \text{with } \begin{cases} \gamma(P) = \int_{-\pi/2}^{\pi/2} f(P, \theta) d\theta, \\ \alpha(P) \text{ absorption coefficient.} \end{cases} \end{aligned}$$

This formulation, quite similar to the description given by R.N.Miles [11] for acoustic fields, proposes further applications in high frequency dynamic. It has been generalized to the case of structures with several types of waves and coupled sub-systems.

### 3- NOTES CONCERNING THE COUPLING RELATIONSHIPS

This section summarizes some of the results concerning the description of the energy exchange according to each energy based method. As mentioned in several references dealing with high frequency dynamics, this particular point is one of the major sources of errors and discrepancies in the energy methods predictions. Indeed, the use of energy variables (scalar) rather than the displacement field (vector) introduces difficulties concerning the characterization of discontinuities.

The technique which has been employed in this paper for the coupling loss factors determination is purely "propagative". It is based upon the calculation for the interested system of the reflection and transmission efficiencies. The knowledge of those parameters allows the determination of energy levels from (SEA), (WIA) thanks to expression (2.6) and finally (SEMI) using relationships given below in section 3.2. However, the use of reflection and transmission efficiencies in the context of (SEMD) formalism is not immediate. Nefske and Sung [12] who proposed one of the earlier work

concerning the use of the thermal analogy to predict the high frequency dynamics, report in their paper a relationship able to couple two Euler Bernoulli beams.

Assuming pure conservative coupling, Nefske [12] express the power exchange between subsystem 1 to subsystem 2, by

$$-(c_{g1}^2/\eta\omega)de_1/dx = -(c_{g2}^2/\eta\omega)de_2/dx = \tau_{12}c_1 e_1 - \tau_{21}c_2 e_2 \quad (2.13)$$

Recently R. S. Langley [13] generalises this relationship in the case of two pure bending plate junction. The relationship proposed is then:

$$-(c_{g1}^2/\eta\omega)\nabla e_1 \cdot \bar{n}_1 = -(c_{g2}^2/\eta\omega)\nabla e_2 \cdot \bar{n}_1 = (\omega/L)[S_1\eta_{12} e_1 - S_2\eta_{21} e_2],$$

where

$$\eta_{12} = (c_{g1}L/\omega\pi S_1) \int_0^\pi \tau_{12}(\theta) \begin{pmatrix} \cos(\theta) \\ \sin(\theta) \end{pmatrix} \cdot \bar{n}_1 d\theta$$

Some authors have considered the differential energy equation (2.10), boundary condition and coupling conditions in depth. For instance, the general form of the boundary conditions for one propagative mode is given in reference [12], in one dimension by the following relationship:

$$(c_g^2/\eta\omega)de/dx = \frac{1-\zeta}{1+\zeta} e \quad (2.14)$$

$\zeta$  designate the reflection efficiency of the boundary.

For non dissipative boundary, the reflection efficiency is equal to 1, and the expression (2.14) leads to the expected results showing that no energy flow through the boundary. In the case of monodimensional coupled systems, Cho and Bernhard [14], Ichchou and Jezequel [4] and Djimadoun and Guyader [15] proposed similar relationships put into the practical form:

$$\begin{aligned} -(c_{g1}^2/\eta\omega)de_1/dx &= \frac{\tau_{12}}{\zeta_{12} + \zeta_{21}} c_{g1} e_1 - \frac{\tau_{21}}{\zeta_{12} + \zeta_{21}} c_{g2} e_2 \\ -(c_{g2}^2/\eta\omega)de_2/dx &= \frac{\tau_{12}}{\zeta_{12} + \zeta_{21}} c_{g1} e_1 - \frac{\tau_{21}}{\zeta_{12} + \zeta_{21}} c_{g2} e_2 \end{aligned} \quad (2.15)$$

where  $\zeta_{12}$ ,  $\zeta_{21}$ ,  $\tau_{12}$  and  $\tau_{21}$  are respectively the reflection and the transmission efficiencies.

A generalisation of this relationship to plate interfaces has been proposed by Cho [14] and Ichchou [4]. It may be noticed that the expression (2.15) and (2.13) are different.

## ON THE VALIDITY DOMAIN OF SOME H.F. ENERGY MODELS

The fact that both (SEA) and the differential (SEM) use averaged values of the transmission efficiencies has to be noticed, whereas (WIA) and the integral form of (SEM) use non diffuse transmission and reflection efficiencies.

### 3.2 BOUNDARY CONDITIONS FOR THE INTEGRAL SIMPLIFIED ENERGY METHOD

The analysis of coupled structures needs the knowledge of the transmission and reflexion efficiencies of plane waves on boundaries. Considering two coupled subsystems  $\Omega_1$  and  $\Omega_2$ , the field  $\langle I_{em}^1 \rangle$  emitted in system  $\Omega_1$  in direction  $\theta$  by a point of boundary separating the two domains, is chosen as the contribution of:

$$\langle I_{em}^1 \rangle (\theta) = R_1(\theta) \langle I_{inc}^1 \rangle (\theta_{inc}^1(\theta)) + T_{21}(\theta) \langle I_{inc}^2 \rangle (\theta_{inc}^2(\theta)).$$

$\theta_{inc}^1(\theta)$  is the incident angle of the wave reflecting on the border in the direction  $\theta$  and  $\theta_{inc}^2$  defines the direction of the incident wave being transmitted in direction  $\theta$  through the boundary.

The subsequent linear relations define the coupling conditions linking the unknowns  $\sigma_1$  and  $\sigma_2$  associated respectively to  $\Omega_1$  and  $\Omega_2$ . For  $P \in \partial\Omega_1 \cap \partial\Omega_2$ :

$$\begin{cases} \sigma_1(P) = \frac{1}{\gamma_1(P)} \left\{ \int_{\Omega_1} R_1 \rho(S) G_1(S, P) \bar{u}_{SP} \cdot \bar{n}_P^1 dS + \int_{\partial\Omega_1} R_1 \sigma_1(P') f_1(P', \bar{u}_{PP'} \cdot \bar{n}_{P'}) G_1(P', P) \bar{u}_{PP'} \cdot \bar{n}_P^1 dP + \right. \\ \quad \left. \int_{\Omega_2} T_{21} \rho(S) G_2(S, P) \bar{u}_{SP} \cdot \bar{n}_P^2 dS + \int_{\partial\Omega_2} T_{21} \sigma_2(P') f_2(P', \bar{u}_{PP'} \cdot \bar{n}_{P'}) G_1(P', P) \bar{u}_{PP'} \cdot \bar{n}_P^2 dP \right\} \\ \sigma_2(P) = \frac{1}{\gamma_2(P)} \left\{ \int_{\Omega_2} R_2 \rho(S) G_2(S, P) \bar{u}_{SP} \cdot \bar{n}_P^2 dS + \int_{\partial\Omega_2} R_2 \sigma_2(P') f_2(P', \bar{u}_{PP'} \cdot \bar{n}_{P'}) G_2(P', P) \bar{u}_{PP'} \cdot \bar{n}_P^2 dP + \right. \\ \quad \left. \int_{\Omega_1} T_{12} \rho(S) G_1(S, P) \bar{u}_{SP} \cdot \bar{n}_P^1 dS + \int_{\partial\Omega_1} T_{12} \sigma_1(P') f_1(P', \bar{u}_{PP'} \cdot \bar{n}_{P'}) G_1(P', P) \bar{u}_{PP'} \cdot \bar{n}_P^1 dP \right\} \end{cases}$$

The numerical implementation of such a system is easily obtained by a collocation method and a rough discretisation of the boundary unknowns  $\sigma_i$ .

## 4- COMPARATIVE RESULTS AND PARAMETRIC SURVEY

### 4.1. CASE STUDIED

The system which has been considered is a planar coupling between two bending rectangular plates. Geometrical and physical characteristics of such plates are close to those used by Langley [13].

## A. BOCQUILLET

The following parameters will not vary during the numerical tests: Young modulus  $E=2e11 \text{ N/m}^2$ , mass density  $\rho=7800 \text{ kg/m}^3$  et  $\nu=0.3$ . The width of the plates is taken equal to 1 m. The summary of the numerical tests is given below. Let us note that five computation have been made for each case. The numerical computation of the "exact" solution which is given using the classical direct stiffness method, but also the energetic predictions of the four considered energy methods.

### 4.2. DAMPING INFLUENCE

The damping influence is an important way to qualify the reverberation of tested plates. In the following simulation, three damping cases are tested. Note that the considered plates are assumed to have similar damping ratio. The overall characteristics of the plates tested are summerised in Table 1.

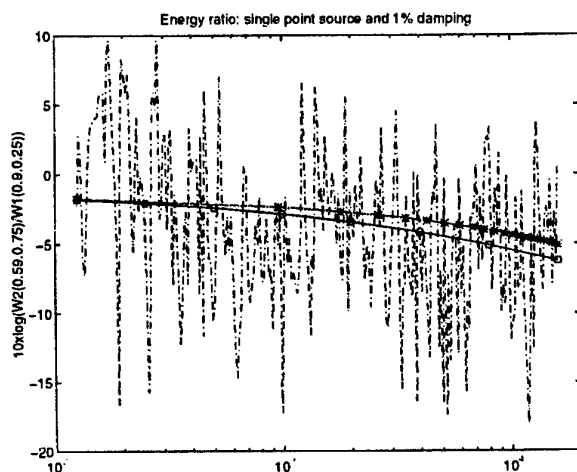
Two kinds of computations are achivied regarding to the nature of the excitation source. In the first case, single point source is considered whilst the second case deals with multi-point source.

TABLE 1. Plates characteristics : study of the damping influence

	Plate 1			Plate 2		
	Length	Thickness	$\eta$	Length	Thickness	$\eta$
Case 1	1.2 m	4 mm	1 %	0.7 m	3 mm	1 %
Case 2	1.2 m	4 mm	5 %	0.7 m	3 mm	5 %
Case 3	1.2 m	4 mm	10 %	0.7 m	3 mm	10 %

The frequency range is fixed in the band [125 Hz - 16000 Hz]. The exact result required 200 interpolating functions. The WIA results is computed following the indications given in [2], and seems to converge using three angular interpolating functions. Finally, the DSEM is computed using a semi-analytic result from a dynamical stiffness energy based calculation.

#### 4.2.1. Single point source case



## ON THE VALIDITY DOMAIN OF SOME H.F. ENERGY MODELS

Figure 1. Energy ratio comparison in 1% damping case: "--" exact energy ratio values.  
"-o-" DMES energy ratio values & "-\*-"- IMES energy ratio values.

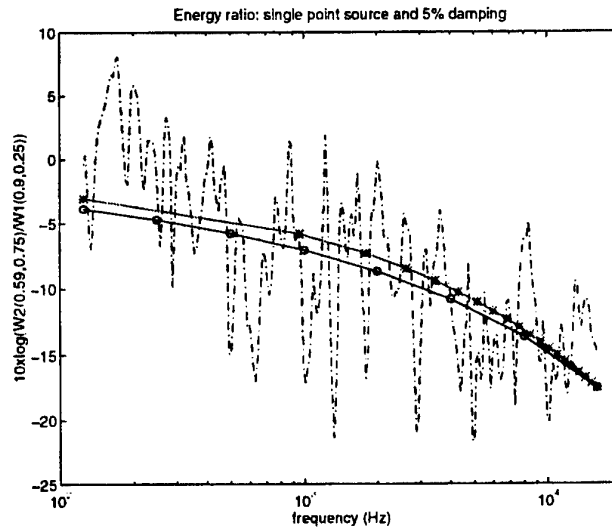


Figure 2. Energy ratio comparison in 5% damping case: "--" exact energy ratio values.  
"-o-" DMES energy ratio values & "-\*-"- IMES energy ratio values.

The first presented case considers single point source. In this case, the plate 1 is excited in point (0.595 m; 0.54 m), the energy is calculated in point (0.9 m; 0.25 m) of plate 1 and in point (0.59 m; 0.75 m) of plate 2. Figures 1 to 3 show the comparison between exact energy ratio and those calculated from (DSEM) and (ISEM). The (SEA) and (WIA) results are not computed as the energy equi-repartition is not guaranteed in this case.

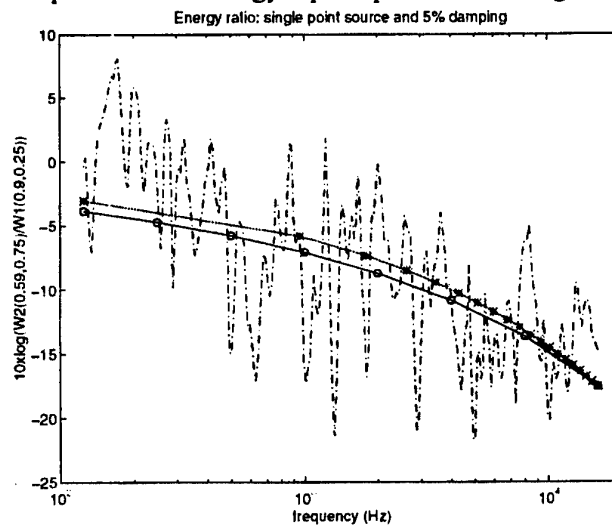


Figure 3. Energy ratio comparison in 10% damping case: "--" exact energy ratio values. "-o-" DMES energy ratio values & "-\*-"- IMES energy ratio values.

Figures 2 to 4 show the general adequation of the simplified energy predictions with the exact results. Hence, (DSEM) and (ISEM) give from a radically different formalism very close results. It can be also seen that the obtained results are in good agreement with the expected averaged exact results for reverberant and non reverberant case.

#### 4.2.2. Multi-point source case.

In this case, eight point sources are considered, in order to approach the delta-correlated random loading required specially by (SEA) and (WIA). Indeed, it is known that the exact calculation to delta-correlated source is equal to the result which is obtained when the response is averaged over the ponctual load. Here, the following point sources are (dimensions in m):

$$\begin{aligned} & (0.595; 0.540) \quad (0.595; 0.300) \quad (0.400; 0.600) \quad (0.400; 0.500) \\ & (0.850; 0.750) \quad (0.850; 0.700) \quad (0.230; 0.450) \quad (0.230; 0.900) \end{aligned}$$

The results presented in the following figures shows a comparison between the energy methods presented in the beginning of this paper and an averaged exact result. The exact result is obtained as an average value over eight ponctual loads and over the energy at eight points in each considered plate. A third octave band and an octave band frequency average of the obtained results is then computed.

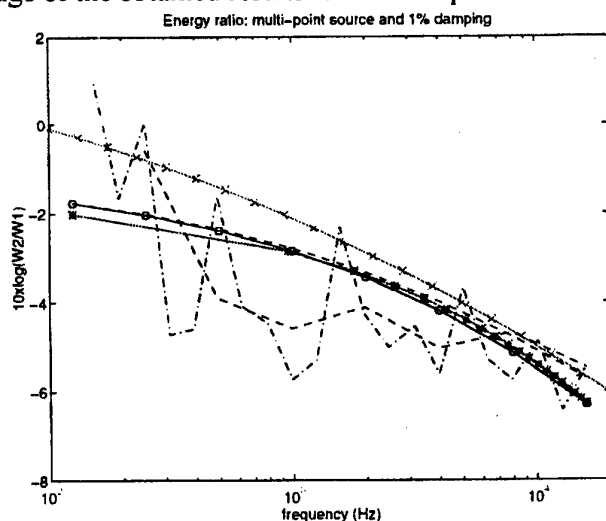


Figure 5. Energy ratio comparison in 1% damping case: "--" exact energy ratio values. '-.-' third octave band exact results. '--' octave band exact result. '--' SEA result. '-x-' WIA results. "-o-" DMES energy ratio values & "-\*- " IMES energy ratio values.

The comparison between the energy predictions and the frequency averaged results for 1 % damping ratio show that (DSEM), (ISEM) and (SEA) give very close results. This remarks, according to the authors experience, seems to be valid for a great number of tested reverberant cases. The (WIA) result seems to follow better the third octave band result in this case.

## ON THE VALIDITY DOMAIN OF SOME H.F. ENERGY MODELS

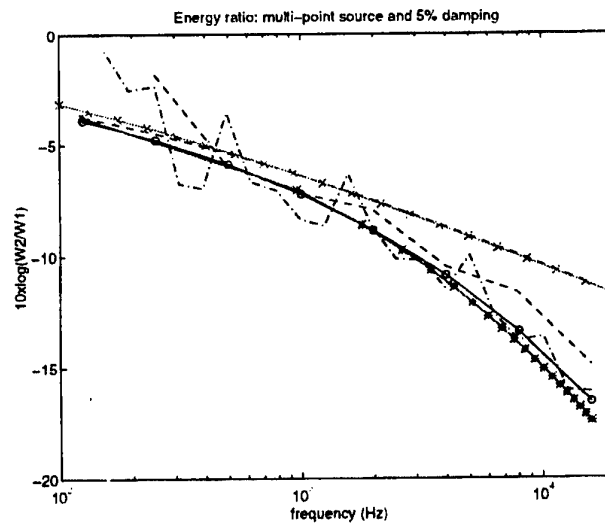


Figure 6. Energy ratio comparison in 5% damping case: "--" exact energy ratio values. '-.-' third octave band exact results. '-' octave band exact result. '--' SEA result. '-x-' WIA results. "-o-" DMES energy ratio values & "-\*-" IMES energy ratio values.

For 5 % and 10 % damping ratio, the tested systems are less reverberant. In this case, an energy accurate prediction is obtained using (DSEM) and (ISEM). The predictions of those methods are once again very close (around 2 dB of discrepancy). Those energy methods seem to give better predictions than (SEA) and (WIA). We verify the deficiencies of (SEA) and (WIA) in the case of non reverberant structures.

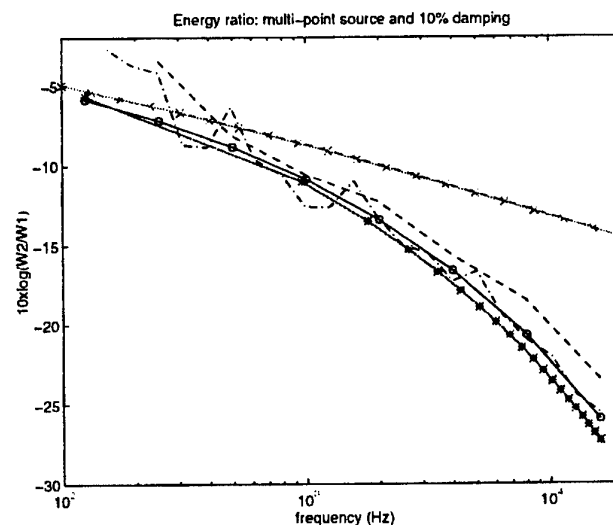


Figure 7. Energy ratio comparison in 10% damping case: "--" exact energy ratio values. '-.-' third octave band exact results. '-' octave band exact result. '--' SEA result. '-x-' WIA results. "-o-" DMES energy ratio values & "-\*-" IMES energy ratio values.



## 5- CONCLUDING REMARKS

Four energy methods have been presented, performed and compared in the cases of two coupled plates and three coupled plates. The conclusions are, *regarding to numerical simulation presented in this paper*:

- \* (SEA) and (WIA) provide good results when the structures are sufficiently reverberant, but overestimate the energy levels without giving the correct trend, when the structures are not reverberant. (WIA) improve (SEA) results for reverberant coupled plates.

- \* (SEA), (ISEM) and (DSEM) give very close results for reverberant coupled plates.

- \* (DSEM) and (ISEM) give accurate energy levels and provides good asymptotic trends. It provides suitable results in both reverberants and no reverberant configurations. Moreover, (DSEM) and (ISEM) allow a spatial determination of high energy field.

An important addition to the present work would be the comparison of the predicted energy levels with experimental results. This investigation is in progress and will provide a check of the energy assumptions.

## 6- REFERENCES

- [1] Keane A.J. and Price W. G. (1997) *A statistical energy analysis: An overview with applications in structural dynamics*, Cambridge University Press.
- [2] Langley R.S. (1992) A wave intensity technique for the analysis of high frequency vibrations, *Journal of Sound and Vibrations*, vol.159, page 483-502.
- [3] Langley R.S. (1991) Analysis of beam and plate vibrations, *Journal of Sound and Vibrations*, vol.150 (1), page 47-65.
- [4] Ichchou M.N. (1996) *Formulation énergétiques pour l'étude des moyennes et hautes fréquences des systèmes : Théorie et applications*, PHD thesis, Ecole Centrale de Lyon.
- [5] Boisson C., Guyader J.L., Millot P. and Lesueur C. (1982) Energy transmission in finite coupled plates. Part II: Application to an L shaped structure, *Journal of Sound and Vibration*, Vol. 81 (1), Page. 93-105.
- [6] Wohler W., Beckman T. and Schreckenbach H. (1981) Coupling loss factors for Statistical Energy Analysis of sound transmission at rectangular slab joints. part 1, *Journal of Sound and Vibration*, Vol. 77, Page. 323-334.
- [7] Rybak S.A., Belov V.D. and Tartakovskii B.D. (1977) Propagation of vibrational energy in absorbing structures, *Soviet Physic Acoustic*, vol. 23, Page 115-119.
- [8] Le Bot A., Ichchou M.N. and Jezequel L. (1995) Smooth energy formulation for multi-dimensional problem. Proceedings of Euro-Noise 95, Lyon, page 423-428.

## ON THE VALIDITY DOMAIN OF SOME H.F. ENERGY MODELS

- [9] Bouthier O.M. and Bernhard R.T. (1995) Simple models of energy of transversely vibrating plates. *Journal of Sound and Vibration*, vol. 153, page 1-19.
- [10] Boisson C., Guyader J.L., Millot P. and Lesueur C. (1982) Energie transmission in finite coupled plates. *Journal of Sound and Vibration*, vol. 81, page 93-105.
- [11] Miles R.N. (1983) Sound field in a rectangular enclosure with diffusely reflecting boundaries. *Journal of Sound and Vibration*, vol 92, page 203-226.
- [12] Nefske D. J. and Sung S. H. (1987) Power flow element analysis of dynamic systems: Basic theory and application to beams. *NCA application*, vol. 3, page 47-54.
- [13] Langley R.S. (1995) On the vibrational conductivity approach to high frequency dynamics for two dimensional structural components, *Journal of sound and vibration*, vol. 182(4), page 637-657.
- [14] Cho P. E. (1993) *Energy Flow Analysis of Coupled Structures*, Master. Science. Thesis. Purdue University.
- [15] Djimadoun M. (1995) *Prévision des Vibrations Stationnaires et Instationnaires aux Moyennes Fréquences: Approche en Energie Moyenne et Approche par Admittance Impulsionnelle*. Thèse d'université N° 93 ISAL 0111, Insa de Lyon.
- [16] Guyader J. L., Boisson C. and Lesueur C. (1982) Energy transmission in finite coupled plates. part I: Theory. *Journal of sound and vibration*, vol. 81(1), page 81-92.

## SOME ENERGY RELATIONS FOR MECHANICAL SYSTEMS

YU.I.BOBROVNITSKII

*Mechanical Engineering Research Institute of Russian Academy of Sciences, M.Kharitonievski, 4, Moscow 101830, Russia*

### 1. Introduction

A damped linear NDOF mechanical system vibrating harmonically under the action of external forces is considered. The goal is to derive some relations between various quadratic vibration characteristics—energy, power flow and others. These relations turn out to be useful for estimating SEA parameters of the system via data measured on a part of the system DOF's.

The approach used is based on the representation of a linear quantity (displacement, force, etc.) by a sum of two independent alternating in time components (sine- and cosine-components) and a quadratic quantity by three independent components: direct one and two similar alternating components of double frequency. The relations obtained connect the components of various linear and quadratic quantities.

Two applications are presented. In the first one, a physical meaning of the famous Maxwell-Betty reciprocity theorem is given. It is shown that, for harmonic motion, the theorem means the equality of the alternating components of the cross power flow of two sets of external forces. In the second application it is shown how to calculate the total energy, loss factor and other characteristics of the whole system driven on a part of DOF's using only the responses measured at the driven points.

### 2. Representation of the vibration field characteristics

We consider a linear system with  $n$  DOF's whose vibrations are described by a matrix equation

$$M\ddot{\mathbf{u}}(t) + C\dot{\mathbf{u}}(t) + K\mathbf{u}(t) = \mathbf{f}(t) \quad (1)$$

where  $M$ ,  $C$  and  $K$  are mass, damping and stiffness  $n \times n$ -matrices with real-valued elements,  $\mathbf{u}(t) = [u_1(t), \dots, u_n(t)]^T$  is a  $n$ -vector of displacements,

$\mathbf{f}(t) = [f_1(t), \dots, f_n(t)]^T$  is a vector of the external forces,  $T$  means transposition. It is assumed that all three matrices in Eq.(1) are symmetric, i. e. there are no gyroscopic elements in the system. The damping matrix  $C$  is not proportional to  $M$  or  $K$ . The equation (1) thus models rather general mechanical system.

We confine the consideration to time harmonic motion of frequency  $\omega$ . Beside the complex representation commonly used in mechanics and acoustics

$$\mathbf{f}(t) = \text{Re}(\mathbf{f}e^{-i\omega t}), \quad \mathbf{u}(t) = \text{Re}(\mathbf{u}e^{-i\omega t}) \quad (2)$$

with the complex amplitudes

$$\mathbf{f} = [f_1, \dots, f_n]^T, \quad \mathbf{u} = [u_1, \dots, u_n]^T, \quad (3)$$

the real-valued representation, taken from electricity, is also used:

$$\begin{aligned} \mathbf{f}(t) &= \mathbf{f}_c \cos \omega t + \mathbf{f}_s \sin \omega t, \\ \mathbf{u}(t) &= \mathbf{u}_c \cos \omega t + \mathbf{u}_s \sin \omega t, \end{aligned} \quad (4)$$

where  $\mathbf{f}_{c,s}$  and  $\mathbf{u}_{c,s}$  are  $n$ -vectors with real-valued elements. Complex amplitudes (3) relate to cosine- and sine-amplitudes in representation (4) as

$$\mathbf{f} = \mathbf{f}_c + i\mathbf{f}_s, \quad \mathbf{u} = \mathbf{u}_c + i\mathbf{u}_s. \quad (5)$$

We also use the velocity vector  $\mathbf{v}(t)$  represented in the same manner

$$\mathbf{v}(t) = \text{Re}(\mathbf{v}e^{-i\omega t}) = \mathbf{v}_c \cos \omega t + \mathbf{v}_s \sin \omega t,$$

where

$$\mathbf{v} = -i\omega\mathbf{u} = \mathbf{v}_c + i\mathbf{v}_s, \quad \mathbf{v}_c = \omega\mathbf{u}_s, \quad \mathbf{v}_s = -\omega\mathbf{u}_c. \quad (6)$$

Substitution of the representations (2)-(6) into Eq.(1) gives the relation between the external forces and responses, in the complex form:

$$\mathbf{f} = Z\mathbf{v}, \quad Z = C + iX, \quad X = \frac{1}{\omega}K - \omega M, \quad (7)$$

where  $Z$  is the impedance matrix with complex entries, and in the real form:

$$\mathbf{f}_c = C\mathbf{v}_c - X\mathbf{v}_s, \quad \mathbf{f}_s = X\mathbf{v}_c - C\mathbf{v}_s, \quad (8)$$

where the resistance(damping) matrix  $C$  and the reactance matrix  $X$  have real-valued entries.

The following vibration energy characteristics will be considered further:

We confine the consideration to time harmonic motion of frequency  $\omega$ . Beside the complex representation commonly used in mechanics and acoustics

$$\mathbf{f}(t) = \text{Re}(\mathbf{f}e^{-i\omega t}), \quad \mathbf{u}(t) = \text{Re}(\mathbf{u}e^{-i\omega t}) \quad (2)$$

with the complex amplitudes

$$\mathbf{f} = [f_1, \dots, f_n]^T, \quad \mathbf{u} = [u_1, \dots, u_n]^T, \quad (3)$$

the real-valued representation, taken from electricity, is also used:

$$\begin{aligned} \mathbf{f}(t) &= \mathbf{f}_c \cos \omega t + \mathbf{f}_s \sin \omega t, \\ \mathbf{u}(t) &= \mathbf{u}_c \cos \omega t + \mathbf{u}_s \sin \omega t, \end{aligned} \quad (4)$$

where  $\mathbf{f}_{c,s}$  and  $\mathbf{u}_{c,s}$  are  $n$ -vectors with real-valued elements. Complex amplitudes (3) relate to cosine- and sine-amplitudes in representation (4) as

$$\mathbf{f} = \mathbf{f}_c + i\mathbf{f}_s, \quad \mathbf{u} = \mathbf{u}_c + i\mathbf{u}_s. \quad (5)$$

We also use the velocity vector  $\mathbf{v}(t)$  represented in the same manner

$$\mathbf{v}(t) = \text{Re}(\mathbf{v}e^{-i\omega t}) = \mathbf{v}_c \cos \omega t + \mathbf{v}_s \sin \omega t,$$

where

$$\mathbf{v} = -i\omega \mathbf{u} = \mathbf{v}_c + i\mathbf{v}_s, \quad \mathbf{v}_c = \omega \mathbf{u}_s, \quad \mathbf{v}_s = -\omega \mathbf{u}_c. \quad (6)$$

Substitution of the representations (2)-(6) into Eq.(1) gives the relation between the external forces and responses, in the complex form:

$$\mathbf{f} = Z\mathbf{v}, \quad Z = C + iX, \quad X = \frac{1}{\omega}K - \omega M, \quad (7)$$

where  $Z$  is the impedance matrix with complex entries, and in the real form:

$$\mathbf{f}_c = C\mathbf{v}_c - X\mathbf{v}_s, \quad \mathbf{f}_s = X\mathbf{v}_c - C\mathbf{v}_s, \quad (8)$$

where the resistance(damping) matrix  $C$  and the reactance matrix  $X$  have real-valued entries.

The following vibration energy characteristics will be considered further:

where  $\mathbf{v}^*$  is the Hermitian conjugate for  $\mathbf{v}$ , i. e. complex conjugate plus transposition. The real part of the complex power flow is the direct component (11), and

$$F_q = (\mathbf{v}_c^T \mathbf{f}_s - \mathbf{v}_s^T \mathbf{f}_c) / 2 \quad (16)$$

is the so called reactive power flow. The latter does not relate to any physically meaningful part of the instantaneous power flow (10) and cannot be obtained from the direct and alternating components (11) and (12). It characterises the part of the velocity vector  $\mathbf{v}(t)$  which is in quadrature with the external forces. Thus the power flow is represented by four independent real-valued characteristics  $F_0$ ,  $F_c$ ,  $F_s$  and  $F_q$ . The first three are the components (one direct and two alternating) of the instantaneous power flow, the fourth one reflects phase property of response with respect to the external force (see next section).

Other quadratic quantities (9) can be represented in the similar manner. However, unlike the power flow, they all have zero reactive component and thus are described by three real-valued components—one direct and two alternating components. For example, for the kinetic energy these components are

$$\begin{aligned} T_0 &= (\mathbf{v}_c^T M \mathbf{v}_c + \mathbf{v}_s^T M \mathbf{v}_s) / 4, \\ T_c &= (\mathbf{v}_c^T M \mathbf{v}_c - \mathbf{v}_s^T M \mathbf{v}_s) / 4, \\ T_s &= \mathbf{v}_c^T M \mathbf{v}_s / 2, \\ T_q &= 0. \end{aligned} \quad (17)$$

They can also be expressed through the complex amplitudes of velocity (6):

$$T = T_c + iT_s = \mathbf{v}^T M \mathbf{v} / 4, \quad T_0 = \mathbf{v}^* M \mathbf{v} / 4, \quad (18)$$

etc.

### 3. Relations between the energy characteristics

If the equations (7), (8) are substituted into the equations for various components of the energy characteristics (9), i. e. into equations (11)–(16) and others, one can express these components through the velocity amplitudes  $\mathbf{v}_c$ ,  $\mathbf{v}_s$  and  $\mathbf{v}$  and the system matrices  $M$ ,  $C$ ,  $K$  and obtain equations similar to Eqs (17) and (18) (they are omitted here to save space). When all these equations are compared, the following relations can be derived:

$$\begin{aligned} F_0 &= \Phi_0, \\ F_c &= \Phi_c + 2\omega E_s, \\ F_s &= \Phi_s - 2\omega E_c, \\ F_q &= -2\omega L_0. \end{aligned} \quad (19)$$

$$\begin{aligned}
F(t) &= \mathbf{v}^T(t) \mathbf{f}(t) \text{ — power flow into the system,} \\
T(t) &= \frac{1}{2} \mathbf{v}^T(t) M \mathbf{v}(t) \text{ — kinetic energy,} \\
W(t) &= \frac{1}{2} \mathbf{u}^T(t) K \mathbf{u}(t) \text{ — potential energy,} \\
E(t) &= T(t) + W(t) \text{ — total energy,} \\
L(t) &= T(t) - W(t) \text{ — Lagrange function,} \\
\Phi(t) &= \mathbf{v}^T(t) C \mathbf{v}(t) \text{ — loss power.}
\end{aligned} \tag{9}$$

Each of these quadratic quantities as a function of time can be represented as a sum of three components. Let's consider the power flow into the system. Substitution of Eq. (4) into the first equation (9), after the obvious trigonometric manipulations, yields

$$F(t) = \mathbf{v}^T(t) \mathbf{f}(t) = F_0 + F_c \cos 2\omega t + F_s \sin 2\omega t, \tag{10}$$

where

$$F_0 = (\mathbf{v}_c^T \mathbf{f}_c + \mathbf{v}_s^T \mathbf{f}_s) / 2 \tag{11}$$

is the direct (time-averaged) component, and

$$\begin{aligned}
F_c &= (\mathbf{v}_c^T \mathbf{f}_c - \mathbf{v}_s^T \mathbf{f}_s) / 2, \\
F_s &= (\mathbf{v}_c^T \mathbf{f}_s + \mathbf{v}_s^T \mathbf{f}_c) / 2
\end{aligned} \tag{12}$$

are the amplitudes of the cosine and sine alternating components of double frequency. The three components in Eq. (10) are independent in the sense that they are orthogonal in the time interval  $2\pi/\omega$ . For the alternating components a complex amplitude can be introduced by analogy with Eq. (5):

$$F = F_c + iF_s; \quad F_c \cos 2\omega t + F_s \sin 2\omega t = \operatorname{Re}(F e^{-2i\omega t}). \tag{13}$$

It is easy to verify that this complex amplitude is simply a product of the complex amplitudes of the velocity and the force (5).

$$F = \frac{1}{2} \mathbf{v}^T \mathbf{f} = F_c + iF_s. \tag{14}$$

In literature the complex power flow is often used

$$F^* = \frac{1}{2} \mathbf{v}^* \mathbf{f} = F_0 + iF_q, \tag{15}$$





The first relation (19) is evident from the physical point of view: the time-averaged power flow  $F_0$  into the system is equal to the time-averaged power dissipated in the system,  $\Phi_0$ . The next two relations (19) say that the alternating power flow components,  $F_c$  and  $F_s$ , not only supply the dampers in the system by the energy but also cause the variations of the total energy  $E_c$  and  $E_s$ . The last relation (19) gives a physical meaning to the reactive power flow  $F_q$ : it is proportional to the time-averaged function of Lagrange  $L_0$ , i. e. to the difference between the averaged kinetic energy and potential energy,  $L_0 = T_0 - W_0$ . It is known that the averaged kinetic energy  $T_0$  is equal to the averaged potential energy  $W_0$  only at the natural frequencies. When  $T_0 > W_0$ , the system behaves with respect to external forces as mass-controlled, when  $L_0 < 0$ , its behaviour is spring-controlled. Hence, the reactive power flow  $F_q$ , according to Eq. (19), can be considered as a measure of closeness to a resonance. It is worth noting that the first three relations (19) are equivalent to the energy conservation law

$$F(t) = \frac{dE(t)}{dt} + \Phi(t) \quad (20)$$

Equations (19) can also be represented in the complex form as

$$F = \Phi - i2\omega E, \quad F' = \Phi_0 - i2\omega L_0, \quad (21)$$

where  $F$  and  $F'$  are given in Eqs (14) and (15), and  $\Phi = \Phi_c + i\Phi_s$ ,  $E = E_c + iE_s$  are the complex amplitudes of the alternating components of the loss power and total energy of the system.

A number of useful energy relations can be derived by considering vibrations caused by two groups of the external harmonic forces,  $\mathbf{f}^{(1)}(t)$  and  $\mathbf{f}^{(2)}(t)$ , of frequency  $\omega$ .

When these forces act separately, the response velocities are  $\mathbf{v}^{(1)}(t)$  and  $\mathbf{v}^{(2)}(t)$ , and when they act simultaneously,  $\mathbf{f}(t) = \mathbf{f}^{(1)}(t) + \mathbf{f}^{(2)}(t)$ , the response, due to linearity of the system, is a sum:  $\mathbf{v}(t) = \mathbf{v}^{(1)}(t) + \mathbf{v}^{(2)}(t)$ . The power flow in the latter case is composed by four terms

$$F(t) = \mathbf{v}^T(t) \cdot \mathbf{f}(t) = F^{11}(t) + F^{22}(t) + F^{12}(t) + F^{21}(t), \quad (22)$$

where terms  $F^{11}(t)$  and  $F^{22}(t)$  correspond to separate action, and terms

$$F^{12}(t) = [\mathbf{v}^{(1)}(t)]^T \mathbf{f}^{(2)}(t), \quad F^{21}(t) = [\mathbf{v}^{(2)}(t)]^T \mathbf{f}^{(1)}(t) \quad (23)$$

are the instantaneous cross power flows.

Each term in the right hand side of Eq. (22), including the cross terms (23), can be represented as a sum of the direct and the alternating components like in Eq. (10). With the help of equations (7), (8) one can express all the components of the energy characteristics (9) through the system matrices  $M$ ,  $C$ ,  $K$  and the velocities  $\mathbf{v}_{c,s}^{(1,2)}$ .

Omitting the cumbersome manipulations, one can derive the following relations between the cross-energy characteristics:

$$A_j^{12} - A_j^{21} = 0, \quad A_q^{12} + A_q^{21} = 0 \quad (24)$$

for  $j = 0, c, s$  and  $A = T, W, E, L, \Phi$ —see Eq. (9);

$$F_c^{12} - F_c^{21} = 0, \quad F_s^{12} - F_s^{21} = 0; \quad (25)$$

$$F_0^{12} + F_0^{21} = 2\Phi_0^{12}, \quad F_q^{12} - F_q^{21} = 2\Phi_q^{12}. \quad (26)$$

The relations (24)–(26) establish all possible reciprocity properties of the system under study. One of these properties is considered in the next section.

#### 4. Physical meaning of the Maxwell-Betty's reciprocity theorem

In its very general form the reciprocity principle in mechanics and acoustics can be formulated as follows[1]: the response of a linear system to a harmonic concentrated force will not change if the driven and observation points are interchanged.

Mathematically, this principle is usually written in the form of reciprocity theorems which relate responses of the system to two arbitrary groups of external forces. One of such theorems, the famous Maxwell-Betty's theorem, can be written, for the NDOF-system under study, as the equality[2]

$$[\mathbf{u}^{(1)}]^T \mathbf{f}^{(2)} = [\mathbf{u}^{(2)}]^T \mathbf{f}^{(1)} \quad \text{or} \quad [\mathbf{v}^{(1)}]^T \mathbf{f}^{(2)} = [\mathbf{v}^{(2)}]^T \mathbf{f}^{(1)}, \quad (27)$$

where  $\mathbf{f}^{(j)}$  are the complex amplitudes of two groups of external forces, and  $\mathbf{u}^{(j)}$ ,  $\mathbf{v}^{(j)}$  are the complex amplitudes of displacement and velocity of corresponding responses,  $j = 1, 2$ . The physical meaning of the theorem is obvious for static ( $\omega = 0$ ): The first Eq. (27) is equality of the cross-works of the two groups of forces [2], but in dynamics the meaning is not so obvious and, to the author's knowledge, has not been discussed earlier [3].

Here we demonstrate that the Maxwell-Betty's theorem (27) physically means *the equality of the alternating components of the instantaneous cross-power flows* for two groups of external forces.

To prove this statement it is sufficient to show that the second equation (27) is equivalent to the relations (25). As it is seen from the Eq. (14), left-hand side of the Eq. (27) is the complex amplitude  $F^{12}$  of the alternating component of the cross power flow (23):  $F^{12} = F_c^{12} + iF_s^{12}$ . The right-hand side of Eq. (27) is the complex amplitude

of an alternating component of  $F^{21} = F_c^{21} + iF_s^{21}$ . Thus, the Maxwell-Betty's theorem (27) is the equality of the complex amplitudes of the alternating components of the cross-power flows.

As it can be seen from Eq. (26), the relations between the direct and the reactive components of the cross-power flows are more complicated. In the simplest case, when the system is lossless, the reactive components of the cross-power flow are equal, and the direct components have opposite signs.

### 5. A structure driven at one or several points

In this section, a finite linear structure driven at one or several points by harmonic forces is considered. It is supposed that a NDOF model of this structure (i. e. the matrices  $M$ ,  $C$ ,  $K$  in Eq. (1)) is not known. Available (measured) are only the external forces and the response (velocity) at the driven points. The question which is discussed here is the following: what can be said about the vibration field of the *whole* structure and, specifically, is it possible to estimate the total vibration energy of the structure and its loss factor using only the data measured at the driven points?

As it is shown below, the answer is: some energy characteristics can be exactly calculated from these data, some cannot. For the latter characteristics approximate estimates are proposed.

To use the relations obtained above we assume that the structure can, in principle, be modelled by a NDOF-system of the type as in Eq. (1). For simplicity we consider the case when only one external harmonic force acts upon the structure (let it be  $f_1(t)$  acting as the first DOF of the model) and the only known response is the velocity  $v_1(t)$  of the first DOF. Thus the problem is to compute the time averaged energy characteristics (9) using only the functions  $f_1(t)$  and  $v_1(t)$  as input data.

Using these input data, i.e. the complex amplitudes of the force and the response,  $f_1$  and  $v_1$ , and their sine- and cosine-amplitudes, one can immediately compute:

$$\text{-- complex input impedance: } z_{in} = f_1 / v_1 \quad (28)$$

as a function of frequency,

$$\text{-- the instantaneous power flow into the system: } F(t) = f_1(t)v_1(t)$$

and all the quantities related to it, i. e. the real-valued components  $F_0$ ,  $F_c$ ,  $F_s$ ,  $F_q$  or their complex equivalents  $F = f_1 v_1 = F_c + iF_s$  and  $F' = f_1 v_1^* = F_0 + iF_q$ .

From these data, using the relations (19) one can obtain exact values of the loss power  $\Phi_0$ , i. e. the energy dissipated in the structure during one second, and the time averaged Lagrange function, i. e. the difference between the averaged kinetic energy and the averaged potential energy:  $L_0 = T_0 - W_0$ . Unfortunately, that is all that can be

calculated exactly. The most needed in practice characteristics—the time averaged total energy  $E_0$  and the loss factor of the structure

$$\eta = \Phi_0 / \omega E_0 \quad (29)$$

do not relate to the input data directly. So, in what follows, two methods for estimating these, based on the obtained above relations, are presented.

As it is seen from the second and the third relations (19), one can exactly compute the quantities  $(E_c - \Phi_s / 2\omega)$  and  $(E_s + \Phi_c / 2\omega)$ , i. e. the alternating components of the total energy contaminated by the damping terms. If the losses in the system are small, these additional terms can be neglected and the estimates for the alternating energy amplitudes are

$$\begin{aligned} E_c &\cong -F_s / 2\omega, \quad E_s \cong -F_c / 2\omega, \\ E_{alt} &= (E_c^2 + E_s^2)^{1/2} \cong (F_c^2 + F_s^2)^{1/2} / 2\omega. \end{aligned} \quad (30)$$

Since the instantaneous total energy is always positive,  $E(t) > 0$ , the alternating energy amplitude cannot exceed the direct component  $E_0$ . Hence, the inequality

$$E_0 > E_{alt} \quad (31)$$

gives a lower estimate for the time-averaged total energy of the system, while the inequality

$$\eta < 2F_0 / (F_c^2 + F_s^2)^{1/2} \quad (32)$$

is an upper estimate for the loss factor of the system.

Another estimates for the time-averaged total energy can be derived from the input impedance (28). As it is shown in [4], the total energy of the system equals

$$E_0 = -\frac{1}{4} |v_1|^2 \operatorname{Im} \frac{\partial z_{in}}{\partial \omega} \quad (33)$$

Strictly speaking, this equation is valid only for lossless mechanical systems, for which the input impedance is purely imaginary. We propose here to use the Eq. (33) for estimating the time-averaged total energy  $E_0$  of systems with losses. Since the steady power flow  $F_0$  can also be represented via the input impedance

$$F_0 = \frac{1}{2} \operatorname{Re}(f_1 v_1^*) = \frac{1}{2} |v_1|^2 \operatorname{Re} z_{in},$$

the loss factor (29) of the system can also be estimated through the input impedance as

$$\eta \cong -2 \operatorname{Re} z_{in} / \operatorname{Im} \left( \omega \frac{\partial z_{in}}{\partial \omega} \right). \quad (34)$$

Combining the expression for the time-averaged Lagrange function  $L_0$  (see the last relation (19)) with the estimate (31) or (33), one can also obtain estimates for the kinetic energy and the potential energy separately:

$$\begin{aligned} T_0 &\cong (E_0 - F_0 / 2\omega) / 2, \\ W_0 &\cong (E_0 + F_0 / 2\omega) / 2, \end{aligned} \quad (35)$$

which characterise the velocity and strain amplitudes averaged over time and structure. The author verified the estimates (30)-(35) in computer simulation on two mechanical systems: a single DOF-system and a finite free rod. The SDOF consists of a mass, spring and dashpot, the motion is described by one-dimensional equation (1). The rod executes longitudinal vibrations due to a harmonic force at one end and is described by the classical Bernoulli's equation of motion with the complex Young module[5]. The main results are the following.

The best estimates give the equations (33)-(35). For the SDOF, they give the exact values of the energies and loss factor. For the rod, the estimates (33)-(35) are close to the actual values in all the frequency region excluding narrow bands around the natural frequencies of the rod which cause antiresonances with respect to the given force. Figure 1 shows the rod response at the driven point and Figure 2 presents the loss factor (29) as a function of frequency. It is seen that the estimate (34) is good everywhere but the bands near three antiresonant frequencies. The explanation is rather simple. Eq.(34) is exact for a lossless system and gives a good approximation for a damped system at frequencies where damping does not effect considerably on the input impedance. But at the antiresonant frequencies, the system behaviour is damping-controlled and Eq.(34) gives erroneous results.

As for equations (31),(32), they give only one-side bounds and can hardly be used as estimates - see curve 3 in Figure 2.

## 6. References

1. Rayleigh, J.W.S.: *Theory of Sound*, Vols. I and II, Dover Publication, New York, 1945.
2. Love, A.E.H.: *A treatise on the Mathematical Theory of Elasticity*, Dover Publication, New York, 1944.
3. Bobrovnikskii, Yu.I.: Physical meaning of the Maxwell-Betty's reciprocity theorem, *Acoustical Physics*, 42(1996), 234-235.
4. Bobrovnikskii, Yu.I.: Energy relations for acousto-structural waveguides, in *Proceedings of 13th International Congress on Acoustics*, Vol.III, Belgrade, Yugoslavia, 1989, pp.389-392.
5. Graff, K.F.: *Wave Motion in Elastic Solids*, Clarendon Press, Oxford, 1975.

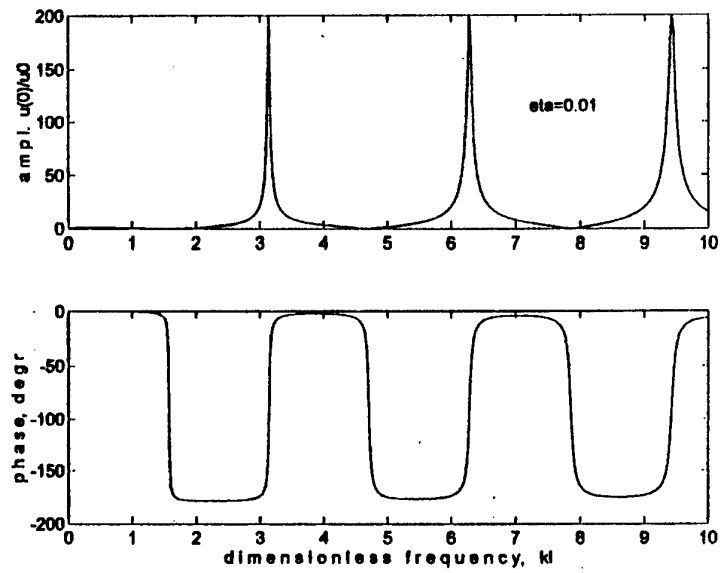


Figure 1. Amplitude and phase of the rod response at the driven point vs frequency; the material loss factor is 0.01.

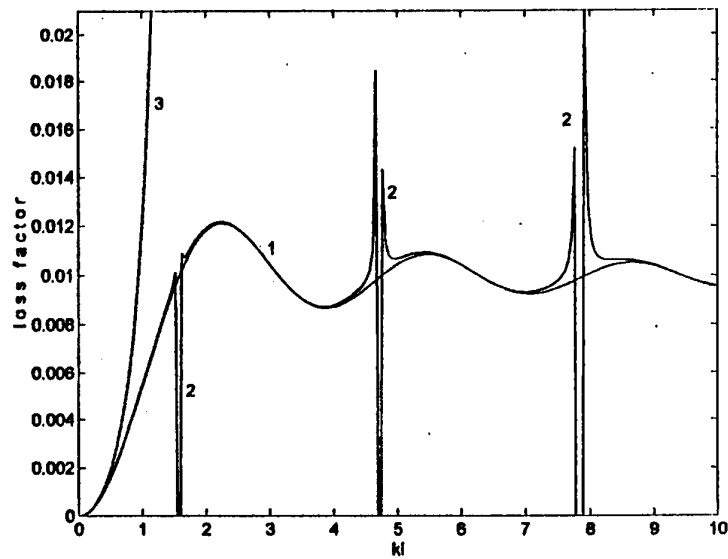


Figure 2. The rod vibration loss factor vs frequency: 1 - exact, 2 - estimate (34), 3 - upper bound (32).

# THE ENERGETIC MEAN MOBILITY APPROACH (EMMA)

G. OREFICE, J.L. GUYADER AND C. CACCIOLATI  
*Laboratoire Vibrations Acoustique*  
*bat 302 INSA de LYON, 69629 Villeurbanne, FRANCE*

The concept of energetic mobility is presented; its use on a single structure and its use for an approximate prediction of the exchanged powers and of the local energies after rigid coupling, on an assembly is exposed. The concept of frequency averaged active power source is also proposed. Numerical simulations illustrate this method for two different homogeneous and heterogeneous substructures rigidly linked at several points.

## 1. Prelude

The energetic mobility finds its natural place at the cross point of three different trends:

- the proposals to achieve a *local* energetic prediction on assemblies, that is not allowed by usual SEA (see [7], [6], [8])
- the wish of avoiding the description of the energy equations like those developed by [1], [9], often limited to simple homogeneous structures ...
- the attempts to use exclusively frequency band averaged quantities, [14], [5], [4] which can better represent the properties of similar industrial structures (see [13], [3], ...).

## 2. Main scope and kernel of the method

Let us assume an **energetic additivity** of the contributions of several local frequency averaged active powers  $P_e$ , injected at points  $e$ , on a separate structure, with linear behavior, to obtain the frequency averaged squared velocity ("FASV") at any point  $m$ , as follows:

$$\langle |V_m|^2 \rangle \approx \sum_{e=1}^{N_e} H_{me} P_e \quad (1)$$

where the brackets  $\langle \rangle$  indicate a frequency average on the band  $\Delta f$  and  $H_{me}$  are the energetic mobilities.

On an assembly of two substructures  $S^I$  and  $S^{II}$ , rigidly coupled at  $N_c$  points, let us then develop the FASV at coupling points  $c$  (or  $k$ ), as sum of the contributions of the external active injected powers  $P_e$  and of the exchanged ones  $P_k$  (the quantities *after coupling* are crown by a tilde ):

$$\langle |\widetilde{V}_c^I|^2 \rangle \approx \sum_{e=1}^{N_e^I} H_{ce}^I \widetilde{P}_e^I + \sum_{k=1}^{N_c} H_{ck}^I \widetilde{P}_k^I \quad (2)$$

and

$$\langle |\widetilde{V}_c^{II}|^2 \rangle \approx \sum_{e=1}^{N_e^{II}} H_{ce}^{II} \widetilde{P}_e^{II} + \sum_{k=1}^{N_c} H_{ck}^{II} \widetilde{P}_k^{II} \quad (3)$$

Our **energetic connectivity**, consists in writing, the following *coupling relations* at each rigidly coupled point  $c$  (or  $k$ ), on  $S^I$  and on  $S^{II}$ :

- the frequency averaged squared velocities are equal

$$\langle |\widetilde{V}_c^I|^2 \rangle = \langle |\widetilde{V}_c^{II}|^2 \rangle \quad (4)$$

- the frequency averaged active exchanged powers are opposite

$$\widetilde{P}_c^I = -\widetilde{P}_c^{II} \quad (5)$$

Solving the above equations, one gets then the frequency averaged active exchanged powers, from the external injected ones, as:

$$\{\widetilde{P}_c^I\} \approx [H_{ck}^I + H_{ck}^{II}]^{-1} \{[H_{ke}^{II}]\{\widetilde{P}_e^{II}\} - [H_{ke}^I]\{\widetilde{P}_e^I\}\} \quad (6)$$

and the FASV at any point  $m$ , after coupling, for instance on  $S^I$ , is:

$$\langle |\widetilde{V}_m^I|^2 \rangle \approx \sum_{e=1}^{N_e^I} H_{me}^I \widetilde{P}_e^I + \sum_{c=1}^{N_c} H_{mc}^I \widetilde{P}_c^I \quad (7)$$

Notice that relations (4) and (5) are exact, while relation (1) is not. Thanks equations (6) and (7) we are able to predict the frequency averaged kinetic energy density at any point of an assembly, using exclusively frequency averaged quantities of the uncoupled substructures, i.e. *without any phase information between the loads* (in fact we will see that the frequency averaged active powers injected at an uncoupled point are almost unchanged after coupling).

### 3. Energetic mobility for a separate structure

The classical mobility  $Y_{me} = \frac{V_m}{F_e}$  (see [11]), on a structure with linear behavior, links the velocity  $V_m$  at point  $m$  to the load  $F_e$  at point  $e$ .



We use the classical mobilities to define our **energetic mobility**  $H_{me}$ , between these points m and e, as follows:

$$H_{me} = \frac{\langle |Y_{me}|^2 \rangle}{\langle \text{Re}\{Y_{ee}\} \rangle} \quad (8)$$

We will show now that this quantity represents a good estimation for the ratio between the FASV at point m and the frequency averaged active power injected at point e,  $P_e = \langle \text{Re}\{F_e V_e^*\} \rangle$ .

### 3.1. SHORT DEMONSTRATION FOR $H_{ME} \approx \frac{\langle |V_M|^2 \rangle}{P_E}$

In fact our energetic mobility (8) can be written:  $H_{me} = \frac{\langle |Y_{me}|^2 \rangle \langle |F_e|^2 \rangle}{\langle \text{Re}\{Y_{ee}\} \rangle \langle |F_e|^2 \rangle}$  and, if we assume (or notice) that:

**H. 1**  $|F_e|^2$  and  $|Y_{me}|^2$  are frequency uncorrelated

**H. 2**  $|F_e|^2$  and  $\text{Re}\{Y_{ee}\}$  are frequency uncorrelated

("frequency uncorrelated" means that the respective distributions of these functions in respect to the frequency are statistically independent) the products of the means can be replaced by the means of the products:

$$H_{me} \approx \frac{\langle |Y_{me}|^2 |F_e|^2 \rangle}{\langle \text{Re}\{Y_{ee}\} |F_e|^2 \rangle} \quad (9)$$

The last equation is evidently another form of the researched one:

$$H_{me} \approx \frac{\langle |V_m|^2 \rangle}{P_e} \quad (10)$$

### 3.2. SHORT DEMONSTRATION FOR $\langle |V_M|^2 \rangle \approx \sum_{E=1}^{N_E} H_{ME} P_E$

The energetic additivity also lets itself be demonstrated quite easily.

We consider a separate structure loaded by  $N_e$  forces at points e (or f).

The exact velocity obtained at point m is then given by  $V_m = \sum_{e=1}^{N_e} Y_{me} F_e$  and one writes the following *exact expressions*:

- the frequency averaged squared velocity at point m is

$$\langle |V_m|^2 \rangle = \sum_{e=1}^{N_e} (\langle |Y_{me}|^2 |F_e|^2 \rangle + \sum_{f \neq e=1}^{N_e} \langle \text{Re}\{Y_{me} F_e Y_{mf}^* F_f^*\} \rangle) \quad (11)$$

- the frequency averaged active powers injected at points e are

$$P_e = \langle \text{Re}\{Y_{ee}\} |F_e|^2 \rangle + \sum_{f \neq e=1}^{N_e} \langle \text{Re}\{F_e F_f^* Y_{ef}^*\} \rangle \quad (12)$$

Then, using the simply assumption that

**H. 3**  $F_e$  and  $Y_{me}$  are frequency uncorrelated

one can neglect the second terms of (11) and (12), (because one takes an average on values which oscillate about zero), compared to the first ones (which are averages of strictly positive values), and one obtains the two following relations:

$$P_e = \langle \text{Re}\{F_e V_e^*\} \rangle \approx \langle |F_e|^2 \rangle \langle \text{Re}\{Y_{ee}\} \rangle \quad (13)$$

(using also H2) and

$$\langle |V_m|^2 \rangle \approx \sum_{e=1}^{N_e} \langle |Y_{me}|^2 \rangle \langle |F_e|^2 \rangle \quad (14)$$

the last one can be further approximated by:

$$\langle |V_m|^2 \rangle \approx \sum_{e=1}^{N_e} \frac{\langle |Y_{me}|^2 \rangle}{\langle \text{Re}\{Y_{ee}\} \rangle} \frac{\langle |F_e|^2 \rangle}{\langle \text{Re}\{Y_{ee}\} \rangle} \quad (15)$$

where the energetic mobilities  $H_{me}$  appear, multiplied by  $P_e$ .  
The energetic additivity is nothing else as:

$$\langle |V_m|^2 \rangle \approx \sum_{e=1}^{N_e} H_{me} P_e \quad (16)$$

This additivity means that *it is possible to find a frequency averaged kinetic energy density, only in terms of frequency averaged active injected powers, i.e. without any phase information between the loads.*

Let us also notice that (13) means that *the frequency averaged active powers are almost the same, when injected "separately" or "together".*

#### 4. Energetic mobility for coupled structures

We consider now two structures, rigidly linked together at  $N_c$  points  $c$  (or  $k$ ). Assumption H3 cannot hold, as the coupling forces  $F_c$  depend on  $Y_{ce}$ :

$$\{\widetilde{F}_c^I\} = [Y_{ck}^I + Y_{ck}^{II}]^{-1} \{[Y_{ke}^{II}]\{\widetilde{F}_e^{II}\} - [Y_{ke}^I]\{\widetilde{F}_e^I\}\} \quad (17)$$

More physically, we cannot assume that the exchanged powers act together as they were separate (as with the previous relation (13)) because they obviously don't exist without the external injected ones !

The previous expression for some transfer energetic mobilities must be corrected to verify the energetic additivity, for each coupling point  $c$  :

- on substructure  $S^I$ , if the excited point  $e$  is different to  $c$

$$H_{ce}^I = \frac{\langle |Y_{ce}^I|^2 \rangle}{\langle \text{Re}\{Y_{ee}^I\} \rangle} \alpha_c^I \quad (18)$$

- on substructure  $S^{II}$ , if the excited point  $e$  is different to  $c$ :

$$H_{ce}^{II} = \frac{\langle |Y_{ce}^{II}|^2 \rangle}{\langle \text{Re}\{Y_{ee}^{II}\} \rangle} \alpha_c^{II} \quad (19)$$

in all other cases (for any points  $m$  and  $e$ ), as previous,

$$H_{me}^I = \frac{\langle |Y_{me}^I|^2 \rangle}{\langle \text{Re}\{Y_{ee}^I\} \rangle} \quad \text{and} \quad H_{me}^{II} = \frac{\langle |Y_{me}^{II}|^2 \rangle}{\langle \text{Re}\{Y_{ee}^{II}\} \rangle} \quad (20)$$

We use (for each coupling point) the following **correcting factors**:

$$\alpha_c^I = \frac{H_c^I + H_c^{II}}{H_c^I \frac{\langle \text{Re}\{Y_c^I\} \rangle}{\langle \text{Re}\{Y_c^{II}\} \rangle} + H_c^{II} + 2 \langle \text{Re}\{Y_c^I\} \rangle} \quad (21)$$

and (also only in terms of frequency averaged quantities)

$$\alpha_c^{II} = \frac{H_c^I + H_c^{II}}{H_c^I + H_c^{II} \frac{\langle \text{Re}\{Y_c^{II}\} \rangle}{\langle \text{Re}\{Y_c^I\} \rangle} + 2 \langle \text{Re}\{Y_c^{II}\} \rangle} \quad (22)$$

#### 4.1. HOW TO FIND THE CORRECTING FACTORS

For one rigid coupled point  $c$ , if only subsystem  $S^I$  is externally excited by  $F_e$ , the exact frequency averaged exchanged power becomes:

$$\widetilde{P}_c^I = - \langle |\widetilde{F}_e^I|^2 \text{Re}\{Y_c^I\} \frac{|Y_{ce}^I|^2}{\text{Re}\{Y_e^I\} |Y_c^I|^2 + |Y_c^{II}|^2 + 2\text{Re}\{Y_c^I Y_c^{II*}\}} \text{Re}\{Y_c^{II}\} \rangle \quad (23)$$

Then, assuming that

**H. 4**  $Y_c^I$  and  $Y_c^{II}$  are frequency uncorrelated

one can neglect the second term in the following mean product

$$\langle \text{Re}\{Y_c^I Y_c^{II*}\} \rangle = \langle \text{Re}\{Y_c^I\} \text{Re}\{Y_c^{II}\} \rangle - \langle \text{Im}\{Y_c^I\} \text{Im}\{Y_c^{II*}\} \rangle$$

(because the product of the imaginary parts oscillates about zero, while the real parts are always positive) and one replaces the mean product of the real parts by the product of the mean real parts:

$$\langle \text{Re}\{Y_c^I\} \text{Re}\{Y_c^{II}\} \rangle \approx \langle \text{Re}\{Y_c^I\} \rangle \langle \text{Re}\{Y_c^{II}\} \rangle$$

Applying also H1, H2, H3, one gets the following approximate power :

$$\widetilde{P}_c^I \approx -\widetilde{P}_e \frac{\langle |Y_{ce}^I|^2 \rangle}{\langle \text{Re}\{Y_e^I\} \rangle} \frac{1}{\frac{\langle |Y_c^I|^2 \rangle \langle \text{Re}\{Y_c^I\} \rangle}{\langle \text{Re}\{Y_c^I\} \rangle \langle \text{Re}\{Y_c^{II}\} \rangle} + \frac{\langle |Y_c^{II}|^2 \rangle}{\langle \text{Re}\{Y_c^{II}\} \rangle} + 2 \langle \text{Re}\{Y_c^I\} \rangle} \quad (24)$$

where some energetic mobilities appear again :

$$\widetilde{P}_c^I \approx -\widetilde{P}_e \frac{\langle |Y_{ce}^I|^2 \rangle}{\langle \text{Re}\{Y_e^I\} \rangle} \frac{1}{H_c^I \frac{\langle \text{Re}\{Y_c^I\} \rangle}{\langle \text{Re}\{Y_c^{II}\} \rangle} + H_c^{II} + 2 \langle \text{Re}\{Y_c^I\} \rangle} \quad (25)$$

one recognizes then the previous correcting factor  $\alpha_c^I$  and gets

$$\widetilde{P}_c^I \approx -\widetilde{P}_e \frac{\langle |Y_{ce}^I|^2 \rangle}{\langle \text{Re}\{Y_e^I\} \rangle} \frac{\alpha_c^I}{H_c^I + H_c^{II}} \approx -\widetilde{P}_e \frac{H_{ce}^I}{H_c^I + H_c^{II}} \quad (26)$$

The last expression is conform to (6). The same factors  $\alpha_c$  were found analytically to work also for two coupling points.

**N.B.** In the symmetric coupling of two identical substructures, assumption H4 does not hold, the correcting factors  $\alpha_c$  are not valid, but fortunately they are also not necessary in this case (see [12]).

#### 4.2. THE CONCEPT OF MEAN ACTIVE POWER SOURCES

We also must underline that *the external mean active powers injected at uncoupled points, often can be considered as unchanged after coupling:*

$$\widetilde{P}_e \approx P_e \quad (27)$$

In fact  $P_e = \langle \text{Re}\{F_e V_e^*\} \rangle$  can also be written as:

$$P_e \approx \langle \text{Re}\{Y_{ee}\} \rangle \langle |F_e|^2 \rangle$$

and the mean input mobility at e is quite unchanged by coupling at c:

$$\langle \text{Re}\{Y_{ee}\} \rangle \approx \langle \text{Re}\{\widetilde{Y}_{ee}\} \rangle$$

Then, **force sources are also "mean active power sources"**, because

$$\langle |F_e|^2 \rangle = \langle |\widetilde{F}_e|^2 \rangle \text{ implies } \widetilde{P}_e \approx P_e$$

In the same manner,  $P_e = \langle \text{Re}\{F_e V_e^*\} \rangle$  can also be written as:

$$P_e \approx \langle \text{Re}\{Z_{ee}\} \rangle \langle |V_e|^2 \rangle$$

Then we can affirm that **velocity sources are also "mean active power sources"**, because

$$\langle |V_e|^2 \rangle = \langle |\widetilde{V}_e|^2 \rangle \text{ also implies } \widetilde{P}_e \approx P_e$$

Let us conclude by a slogan: **"we are all mean active power sources!"**.

## 5. Numerical Simulations

We will not submerge the reader with a detailed analysis of all the numerical cases treated to better understand the concept of energetic mobility; our wish is now to simply illustrate the different possibilities announced in the previous analytical part, through some numerical samples.

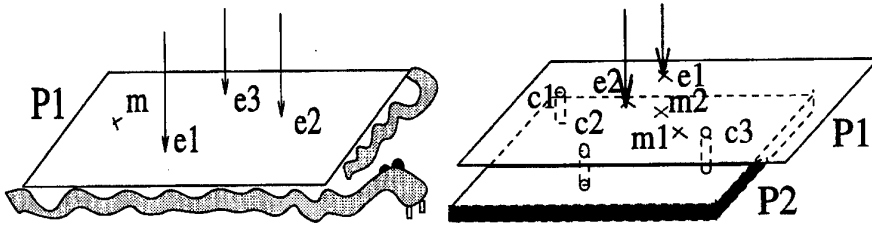


Figure 1. Simply Supported plates, alone or rigidly coupled

### 5.1. ON A SINGLE STRUCTURE

We compare (in Figure 2), on an homogeneous thin supported plate, the energetic mobility  $H_{me1}$  and the ratio between the FASV at point m and the frequency averaged active power injected at point e1, when the plate is loaded at three points. We do this for two types of loads: force sources and velocity sources. We can also report that increasing the structural

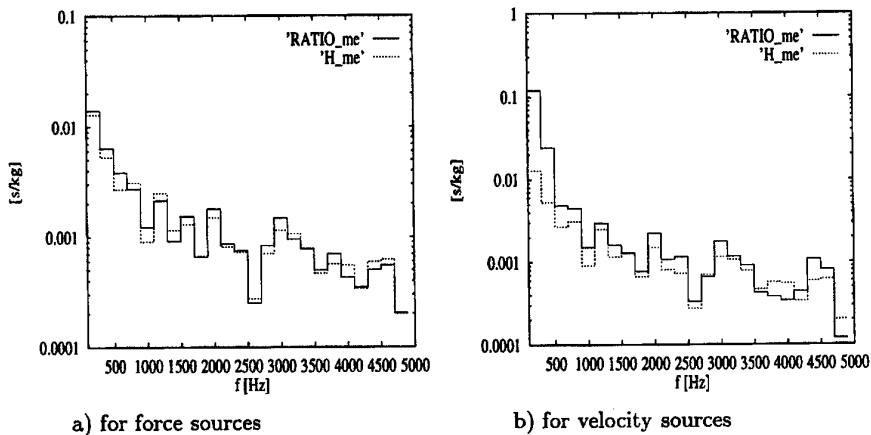


Figure 2. Comparison between  $H_{me1}$  and the ratio  $\frac{\langle |V_m|^2 \rangle}{\langle \text{Re}\{F_{e1} V_{e1}^* \} \rangle}$

damping, reduces the differences ("error on the definition").

We further can compare (in Figure 3) the result of the energetic additivity with the exact calculation of the FASV at a point  $m$ .

Data of plate P1 are in appendix; results are similar at any other point.

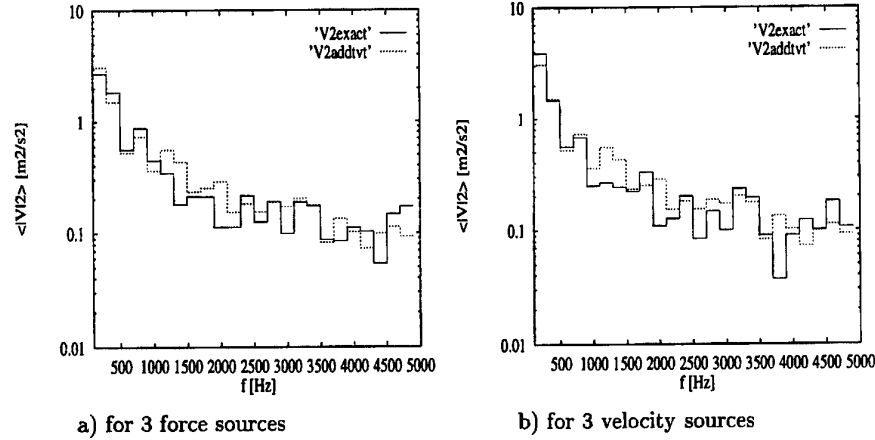


Figure 3. Comparison between the exact  $\langle |V_m|^2 \rangle$  and the one given by (1)

We can report again that increasing the structural damping, also increases this "error of the energetic additivity" in the high frequency domain, where the classical mobilities become smoothed; on the other hand, increasing the bandwidth reduces this error.

This indicates that the error depends on the number of fluctuations in the averaging frequency band, rather then on the modal overlap, or on the modal density: *another logic as the usual one applied to energetic problems is here required to handle to the energetic mobilities.*

## 5.2. ON AN ASSEMBLY OF TWO DIFFERENT SUBSTRUCTURES

We take now two simply supported plates, P1, identical to the previous and P2, for times thicker and something smaller. Three rigid links are taken at points  $c1$ ,  $c2$ ,  $c3$ . Two forces load at points  $e1$  and  $e2$ , on P1 (see appendix). We compare (on Figure 4) the exact FASV after coupling at  $c2$  (the worst result), with those obtained by (6), at coupling point  $c2$ .

Better results are obtained at the others coupling points (for instance  $c1$ ) and at others uncoupled points (for instance  $m$  on P2).

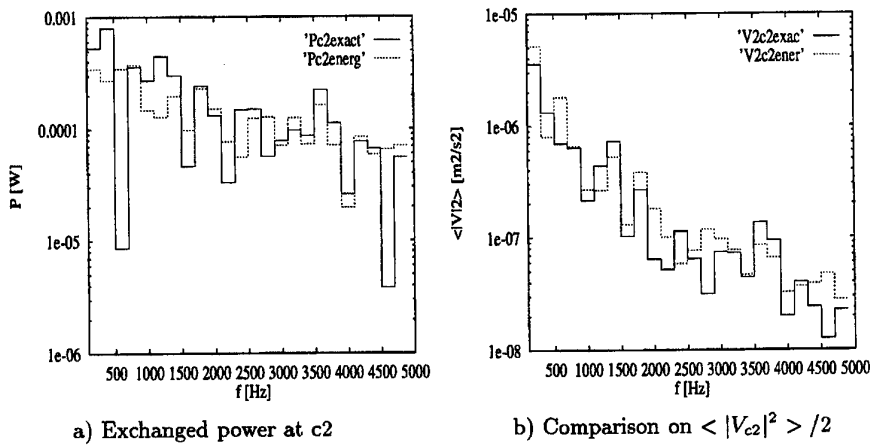


Figure 4. Comparison between exact and energetic calculations: the worst case

### 5.3. ON AN ASSEMBLY OF TWO DIFFERENT, HETEROGENEOUS STRUCTURES

We add on P1 some point attached masses, link P1 to P2 and perform the same calculations, as in the previous case (see Figure 5). This case is quite

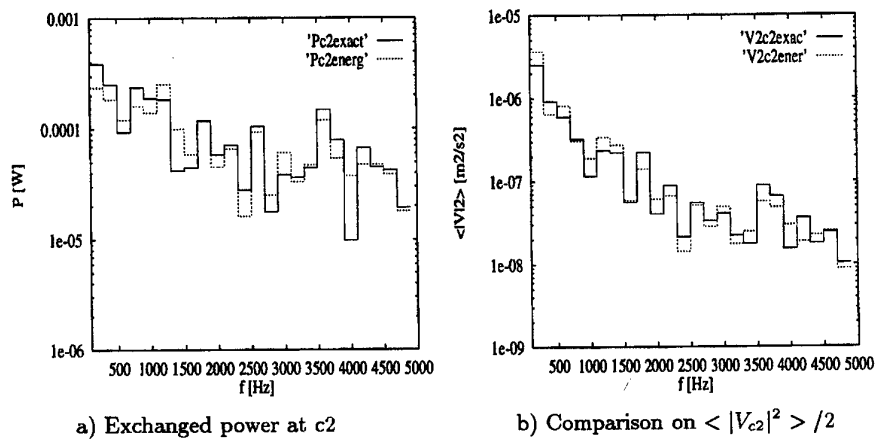


Figure 5. Comparison between exact and energetic calculations: P1 heterogeneous

complete: we can analyse the coupling at one heterogeneity, the load on one heterogeneity and all the possible transfers involving an heterogeneity.





## 6. Conclusions

The **energetic mobility** links the frequency averaged (f.a.) active injected power at a point to the f. a. squared velocity obtained at another point.

An **energetic additivity** allows one to calculate the f. a. squared velocity obtained at a point  $m$  loading a structure at several points  $e$ , using exclusively the f.a. active injected powers, that is to say, **without any phase information between the loads**.

A general **energetic connectivity** allows one to predict f.a. quantities, like the local squared velocities and the local active exchanged powers, on an assembly, only as function of the f.a. quantities on each substructure, before coupling (point injected powers or squared velocities).

The f.a. active power injected at an uncoupled point, is found to be almost unchanged by coupling, whatever are the forces. We can then consider any loading system as a **"mean power source"**.

The Energetical Mean Mobility Approach (EMMA) is approximate but applies quite well even to **heterogeneous structures**, because its ingredients are the classical mobilities, which can furthermore be directly measured on industrial systems. EMMA is also quite robust because it uses only frequency averaged quantities, which vary less on similar industrial systems. An experimental application of the method will be soon presented and the sensitivity to some parameters will be also described.

## Acknowledgements

This work was supported by EDF (Électricité de France) - DER Clamart, and INRS (Institut National de Recherche sur la Sécurité) - MAV, Vandoeuvre, France. In particular we wish to thank E. Luzzato and T. Loyau for their kind suggestions.

## References

1. Bouthier, O.M. and Bernhard, R.J. *American Institute of Aeronautics and Astronautics Journal*, Vol. 30no. 3, pp. 616-623
2. Cacciolati, C. and Guyader, J.L. (1994) Measurement of SEA coupling loss factors using point mobilities, *Phil. Trans. R. Soc. Lond.*, Vol. no. A346, pp. 465-475
3. DeJong, R.G. (1992) Statistical measures of the response fuctions of simple and complex structures, *Proceedings of internoise '96*, Vol. 6, pp. 2885-2890
4. Delattre, F., Gotteland M. and Lesueur, C. (1993) Frequency smoothing through cepstral and flow graph analysis, *Acoustic's93 I.S.V.R.*, pp. 259-272
5. Girard, A. and Defosse, H. (1990) Frequency response smoothing, matrix assembly and structural paths: a new approach for structural dynamics up to high frequencies, *Journal of Sound and Vibration*, Vol. 137no. 1, pp. 53-68
6. Shankar, K. and Keane, A.J. (1995) A study of the vibrational energies of two coupled beams by finite element and green function (receptance) methods, *Journal*

- of *Sound and Vibration*, Vol. 181no. 5, pp. 801-838
7. Koss, L.L. (1995) Frequency response functions for power and connectivity, *Journal of Sound and Vibration*, Vol. 181no. 4, pp. 709-725
  8. Lasé, Y., Ichchou, M.N., Jezequel, L. and Aquilina, R. (1993) Calculating transfer functions using a new energetic method, *Cetim 93, 3th International Congress on Intensimetry*
  9. LeBot, A. and Ricol, L. (1995) Integral equation instead of heat conduction equation for medium and high frequencies, *Proceedings of internoise 95*, Vol. 43 no. 2, pp. 579-582
  10. Manning, J.E. (1994) Formulation of SEA parameters using mobility functions, *Phil. Trans. R. Soc. Lond.*, Vol. no. A346, pp. 477-488
  11. O'Hara, J. (1967) Mechanical impedance and mobility concepts, *Journal of the Acoustical Society of America*, Vol. 41no. 5, pp. 1180-1184
  12. Orefice, G., Cacciolati, C. and Guyader, J.L. (1996) An energetic Mobility for Structures assembling, *Proceedings of internoise '96*, Vol. 6, pp. 3042-3046
  13. Plunt, J. (1996) Generic limitations of vibro-acoustic prediction methods for product noise, *Proceedings of internoise '96*, Vol. 6, pp. 3047-3051
  14. Skudrzyk, E. (1980) The mean-value method of predicting the dynamic response of complex vibrators, *Journal of the Acoustical Society of America*, Vol. 67 no. 4, pp. 1105-1135

## Appendix

### DATA USED IN THE NUMERICAL SIMULATIONS

Plate P1. Dimensions:  $L_x = 1.0[m]$ ,  $L_y = 0.7[m]$ ,  $h = 0.001[m]$ ;  
 Material:  $\rho = 7800[kg/m^3]$ ,  $E = 2.110^{11}[Pa]$ ,  $\nu = 0.33$ ,  $\eta = 0.01$ .  
 Modal density: 0.2; modal overlap: 0.4 to 10.8; number of modes: 40 to 47;  
 mean wavelength  $\lambda = 0.22$  to  $0.046[m]$  for 200 Hz wide frequency bands.  
 Loaded points: e1(0.4;0.2), e2(0.7;0.3), e3(0.5;0.6). Measured point m(0.2;0.5).  
 Force sources:  $F_e = 1/Y_{ee}$  and velocity sources:  $V_e = 1[m/s]$ .  
 Plate P2. Dimensions:  $L_x = 0.9[m]$ ,  $L_y = 0.7[m]$ ,  $h = 0.004[m]$ ;  
 Material:  $\rho = 7800[kg/m^3]$ ,  $E = 2.110^{11}[Pa]$ ,  $\nu = 0.33$ ,  $\eta = 0.01$ .  
 Modal density: 0.05; modal overlap: 0.08 to 1.3; number of modes: 8 to 11;  
 mean wavelength  $\lambda = 0.44$  to  $0.09[m]$ , for 200 Hz wide frequency bands.  
 Assembly of P1 and P2.  
 Coupling points (the same on both plates): c1(0.2;0.5), c2(0.4;0.2), c3(0.7;0.3).  
 Measured points: m2(0.5;0.6) on P2 and m1(0.6;0.3) on P1; loaded points  
 e1(0.5;0.6), e2(0.4;0.4) on P1. Constant unit loading forces  $F_e = 1[N]$ .  
 Mean active injected powers given by  $P_e = \langle Re\{Y_{ee}\} \rangle$  (i.e. considered as  
 separate sources).  
 Plate P1 with point attached masses: 0.1kg at point c1(0.2;0.5), 0.2kg at  
 point e1(0.5;0.6) and 0.5kg at point m1(0.6;0.3).  
 The excited and linked points are unchanged, so are the external loads.

## IRREGULARITY, DAMPING AND COUPLING STRENGTH IN S.E.A.

B. R. MACE and P. J. SHORTER  
*Department of Mechanical Engineering*  
*The University of Auckland*  
*New Zealand*

Common experience indicates that SEA predictions tend to become more accurate as damping levels increase and are more accurate for subsystems which are irregular. This paper discusses some reasons for this behaviour and suggests measures by which these effects can be quantified in terms of wave or modal parameters. These reasons involve wave coherence, global mode localisation and orthogonality of global modes within each subsystem. Particular reference is made to the SEA of a system comprising two, coupled subsystems and numerical examples are given for the case of two coupled plates.

### 1. Introduction

Inaccuracy of SEA predictions can be attributed to two main causes. First, the fundamental underlying assumptions in SEA may fail, so that the SEA equations may not predict the frequency and ensemble average behaviour of the system under consideration, even over wide bandwidths. When this is the case, the system is said to be strongly coupled, while the SEA equations hold for a weakly coupled system. Secondly, there may be large variability between the frequency average response for a particular realisation of the system and the ensemble and frequency average of SEA. This may be due to averages being taken over relatively narrow bands (finite frequency band averaging effects) or perhaps to there being only modest levels of uncertainty in the system (so-called mid-frequency range effects). In this paper only weak/strong coupling issues are of concern, with frequency averages assumed to be taken over a frequency band  $\Omega$  which is wide, containing many modes of vibration.

It is as well to emphasise the difference between strongly (weakly) coupled and well (poorly) coupled subsystems. In this paper two subsystems are said to be well coupled if energy can pass freely through the coupling between them - typically the transmission coefficient of their coupling is large and so, too, is the appropriate coupling loss factor. Strong or weak coupling, on the other hand, gives an indication of the qualitative nature of energy flow through a system and depends not only on coupling transmission but also on energy dissipation within the subsystems - typically this depends on the relative magnitudes of coupling and damping loss factors.

Damping can be quantified in terms of loss factor  $\eta$ , modal overlap  $M$  (here,  $M = n\Delta$  is the product of the asymptotic modal density  $n$  of the structure and the half-power bandwidth  $\Delta$ ) or the decay in amplitude experienced by a wave as it propagates through the system. As damping increases so the system becomes more weakly coupled and SEA predictions tend to become more accurate. When weakly coupled the system response depends only on the gross subsystem properties (area, modal density etc.) and energy flow though a coupling depends only on local system properties. When the coupling is strong (i.e., when the damping is light enough) the response becomes dependent on the detailed properties of the subsystems under consideration (specific shape etc.) and energy transmission depends on global properties. Hence system detail, and subsystem irregularity, become important. Irregularity, be it in geometric or physical properties, is a somewhat nebulous quantity: systems may appear more or less irregular, but quantifying the degree of irregularity is less straightforward.

In the next section a wave interpretation is reviewed. Here the strength of coupling depends on the coherence of waves incident on the coupling between two subsystems. Damping and irregularity both decrease these coherence effects. This is followed by a discussion in terms of the global modes of the structure. In this case damping effects are described in terms of modal overlap, while irregularity is quantified in terms of global mode localisation and the orthogonality of global modes within each subsystem. Finally this global mode view is rephrased in terms of subsystem or local modes.

Particular reference is made here to the SEA of a system comprising just two subsystems,  $a$  and  $b$ , which have the same (small) loss factor. Subsystem  $a$  is excited by "rain-on-the-roof" excitation. The SEA equations relating ensemble (and broadband frequency) averages are

$$P_{in,a} = \omega\eta E_a + P_{ab}; \quad 0 = \omega\eta E_b + P_{ba}; \quad P_{ab} = \omega\eta_{ab} E_a - \omega\eta_{ba} E_b \quad (1)$$

where  $P_{in}$  and  $P_{ab}$  are the input and coupling powers,  $E$  the subsystem energy,  $\omega$  is the centre frequency and  $\eta_{ab}$  is the coupling loss factor. Furthermore  $n_a\eta_{ab} = n_b\eta_{ba}$ . Numerical examples are presented for a system comprising two plates, coupled along a straight edge and with all edges simply supported. Irregularity is introduced by allowing the plates to have varying shapes while their gross properties (e.g., their areas, which are fixed in the ratio 1:1.4) and the length of the coupled edge (0.9) remain constant. An analytical solution exists for rectangular plates [1], other results being predicted from traditional SEA [2] and from finite element calculations [3].

## 2. Irregularity, Damping and SEA: a Wave Perspective

The failure of SEA can be described in terms of wave coherence [4]. Consider the line of coupling between two, 2-dimensional subsystems  $a$  and  $b$  as shown in Figure 1. Time harmonic waves  $a^+$  and  $b^-$  are incident on the coupling at an angle  $\theta$  and at frequency  $\omega$ . (For simplicity it is assumed that the subsystems have the same

wavenumber.) They give rise to transmitted and reflected waves where, for example,  $a^- = r_{aa}(\theta)a^+ + t(\theta)b^-$ . If the coupling is conservative then [4]

$$\begin{aligned} P_{ab} &= P_{sea} - P_{coh}; \\ P_{sea} &= T^2 P_{inc,a} - T^2 P_{inc,b} \end{aligned} \quad (2)$$

where  $P_{sea}$  is the coupling power assumed in the normal wave approach to SEA [2],  $P_{inc,a}$  and  $P_{inc,b}$  are the incident powers and  $T(\theta) = |t(\theta)|$ . The coherent power

$$P_{coh} = \frac{1}{2} (tr_a^* a^+ b^- + t^* r_a a^+ b^-) \quad (3)$$

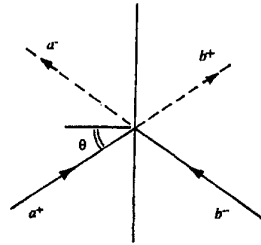


Figure 1. Wave transmission and reflection at a boundary between two subsystems.

depends on both the amplitudes of and the relative phase between the incident waves,  $*$  denoting the complex conjugate. Generally waves are incident at all angles  $\theta$ , the powers then being integrals over  $\theta$ .

For discrete frequency excitation of a specific system by a single source, the wave amplitudes are of course coherent. In the traditional wave approach to SEA [2] it is assumed, however, that the frequency average coherent power  $\langle P_{coh} \rangle_\Omega$  is negligibly small ( $\langle \rangle$  denotes an average quantity). The argument for making this assumption arises from the observation that the relative phase between  $a^+$  and  $b^-$  typically varies very rapidly with frequency. Similarly the ensemble can be defined by assuming this relative phase (and perhaps other dynamic properties) is random. One might then assume the average coherent power is negligible.

The frequency or ensemble average coherent power can, however, be very substantial, so that  $P_{sea}$  becomes an inaccurate estimate of  $P_{ab}$ . The coupling is then strong, in a wave sense. This is because the incident waves are caused in part by reflections of the outgoing waves from distant parts of the structure. Certain frequencies, and hence certain values of the relative phase, correspond to system resonance, and hence large wave amplitudes, and give a disproportionate contribution to the frequency or ensemble average coherent power. If both outgoing waves produce significant reflections then  $\langle P_{coh} \rangle$  can be very substantial.

The average coherent power is always positive and is found to depend on a coupling strength parameter  $\gamma$  where

$$\gamma^2 = \frac{T^2}{\mu_a \mu_b} \quad (4)$$

and where, for a given  $\theta$ ,  $\mu_{a,b}$  relates the amplitude of an outgoing wave to that of its reflection from distant parts of the structure, which later returns to the coupling (e.g.,  $|b^-(\theta)| = \exp(-\mu_b(\theta)) |b^+(\theta)|$ ). If  $\gamma \gg 1$  the coupling is strong: waves are transmitted well, attenuated poorly and transmission through a coupling depends on the global

properties of the structure (i.e., reflections from parts distant from the coupling). The coupling power is predicted poorly by  $P_{sea}$ . Weak coupling, on the other hand, occurs if  $\gamma \ll 1$ . Attenuation is relatively strong, transmission relatively weak and local (i.e., coupling) properties determine local transmission. Now the traditional wave approach to SEA gives accurate predictions. In general waves are incident at all angles  $\theta$ , and  $\max(\chi(\theta))$  gives a somewhat conservative estimate of the overall strength of coupling.

Increasing damping increases  $\mu$  (since waves attenuate more rapidly as they propagate) and hence decreases  $\gamma$ , the strength of coupling and  $\langle P_{coh} \rangle$ . Increasing irregularity scatters some of the energy carried by a wave leaving the coupling at angle  $\theta$  into wave components which propagate in different directions. Hence the coherent reflection which arrives back at the coupling at the same angle  $\theta$  is decreased and so, too, is the consequent contribution to  $\langle P_{coh} \rangle$ . The relative phase of waves incident at different angles varies along the line of coupling, so that they give very small contributions to the total coherent power, this being the integral along the line of coupling. Thus  $\gamma$  includes the effects of both dissipation and subsystem irregularity.

In principle, reflection coefficients can be calculated numerically for couplings and subsystems. For the case of rectangular plates this is straightforward. The response is then found by a Fourier series decomposition into components with specific trace wavenumbers [1], each trace wavenumber component being transmitted, reflected and propagating without being scattered into other trace wavenumber components. In this sense, two rectangular plates can be regarded as the most regular of systems. Figure 2 shows an example, where the coupling power is compared to the traditional SEA expression [2] as a function of  $\mu_{a0} = \mu_a(\theta=0)$ . The value of  $\mu_{a0}$  at which  $\max(\chi(\theta)) = \chi(0) = 1$  is shown, this marking the transition from strong to weak coupling as  $\mu_{a0}$  increases. For very low levels of damping the SEA estimate of coupling power from equation (1) tends to a value corresponding to equipartition of energy, namely

$$\left( \frac{P_{ab}}{P_{in}} \right)_{equip} = \frac{n_b}{n_a + n_b} \quad (5)$$

For high  $\mu_{a0}$ ,  $P_{ab}$  tends to a value independent of geometry and determined by the coupling loss factor. Clearly, coherence effects in the regular, rectangular system are very significant when the coupling is strong. Introducing non-uniformity into the end supports [5] or the coupling [6] causes a trace wavenumber component to be scattered into components of different directionality, the irregularity thus introduced

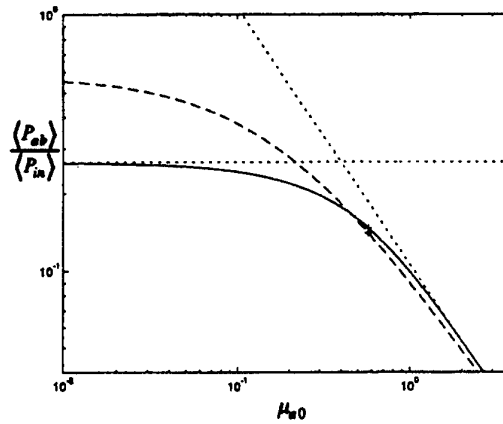


Figure 2. Coupling power: — theory, rectangular plates [1]; --- traditional SEA [2]; ..... low and high  $\mu_{a0}$  limits,  $\gamma_0 = 1$ . Plate properties:  $E=2.1 \times 10^{11}$ ,  $\rho=8 \times 10^3$ ,  $\nu=0.3$ , thickness=0.01.

causing the average coherent power to be reduced.

### 3. Global Modes of Vibration

In this section the response of a system comprising two subsystems is described in terms of the global modes of vibration. Expressions are developed for the time and frequency average input power and subsystem energies in terms of the mode shapes. The dependence of these quantities on system irregularity and modal overlap is then explored. It is assumed here for simplicity that the density is constant throughout the system, damping is proportional so that the response can be decomposed in terms of the undamped global modes of vibration, all modes have equal (small) loss factor  $\eta$  and that time and frequency average kinetic and potential energies are equal.

#### 3.1 GLOBAL MODAL DECOMPOSITION

The response at point  $x_2$  per unit time harmonic force at point  $x_1$  can be written as a sum of global mode components as

$$u(\omega, x_1, x_2) = \sum_j \alpha_j(\omega) \phi_j(x_1) \phi_j(x_2) \quad (6)$$

where  $\phi_j(x)$  is the  $j$ 'th mode shape and where

$$\alpha_j(\omega) = \frac{1}{\omega_j^2(1 + i\eta) - \omega^2} \quad (7)$$

is the modal receptance,  $\omega_j$  being the  $j$ 'th natural frequency. The mode shapes are assumed to be mass normalised so that

$$\int \rho \phi_j(x) \phi_k(x) dx = \delta_{jk} \quad (8)$$

where  $\rho$  is the density. The time average input power and kinetic energy density at  $x_2$  are given by

$$\begin{aligned} P_{in}(\omega, x_1) &= \frac{2\eta}{\omega} \sum_j \omega_j^2 \beta_{jj}(\omega) \rho \phi_j^2(x_1) \\ D_T(\omega, x_2) &= \frac{1}{4} \rho \omega^2 |u(\omega, x_1, x_2)|^2 = \sum_{j,k} \beta_{jk}(\omega) [\rho \phi_j(x_1) \phi_k(x_1)] [\rho \phi_j(x_2) \phi_k(x_2)] \\ \beta_{jk}(\omega) &= \omega^2 \text{Re} \{ \alpha_j(\omega) \alpha_k^*(\omega) \} / 4\rho \end{aligned} \quad (9)$$

Note that the input power is a sum of modal contributions while the kinetic energy density depends on cross-modal terms. Typically  $\beta_{jk}(\omega)$  is very small if neither mode  $j$  nor mode  $k$  is resonant at frequency  $\omega$ , is moderate if one mode is resonant and very large if both modes are resonant.

### 3.1.1 Frequency average response

Suppose now that broadband excitation of constant unit power spectral density acts over a bandwidth  $\Omega$ . Frequency averages of equations (9) can be taken, the frequency average kinetic energy density, for example, being

$$\langle D_T(x_2) \rangle_\Omega = \sum_{j,k} \Gamma_{jk} [\rho \phi_j(x_1) \phi_k(x_1)] [\rho \phi_j(x_2) \phi_k(x_2)]; \quad \Gamma_{jk} = \frac{1}{\Omega} \int_\Omega \beta_{jk}(\omega) d\omega \quad (10)$$

Note that if the damping is light then  $\alpha_j$  shows a distinct resonance peak around its natural frequency  $\omega_j$ . Then  $\Gamma_{jk}$  tends to be small except for those mode pairs  $j$  and  $k$  which are resonant in  $\Omega$  and which "overlap", i.e., whose natural frequencies lie within each others bandwidths. The terms  $\Gamma_{jj}$  are necessarily large if  $\omega_j$  lies in  $\Omega$ . For such resonant modes  $\Gamma_{jk}$  closely approximates the integral over  $(0, \infty)$  and

$$\Gamma_{jj} \approx \frac{1}{\Omega} \frac{\pi}{8\rho\omega\eta}; \quad \Gamma_{jk} \approx \xi_{jk} \Gamma_{jj}; \quad \xi_{jk} = \left(1 + (\omega_j - \omega_k)^2 / \Delta^2\right)^{-1} \quad (11)$$

where  $\Delta = \omega\eta$  and where  $\omega$  is now the centre frequency of  $\Omega$ .

### 3.1.2 Subsystem responses

Let statistically independent excitations (i.e., "rain-on-the-roof") be applied at all points  $x_1$  in subsystem  $a$ . The total kinetic energies in subsystems  $a$  and  $b$  are then found by integrating equation (10) over  $x_1$  and  $x_2$  and are given by

$$\begin{aligned} \langle T_a \rangle &= \sum_{j,k} \Gamma_{jk} \psi_{jk}^{(a)2}; \quad \langle T_b \rangle = \sum_{j,k} \Gamma_{jk} \psi_{jk}^{(a)} \psi_{jk}^{(b)}; \\ \psi_{jk}^{(a)} &= \int_a \rho \phi_j(x_1) \phi_k(x_1) dx_1; \quad \psi_{jk}^{(b)} = \int_b \rho \phi_j(x_2) \phi_k(x_2) dx_2 \end{aligned} \quad (12)$$

where the integrations in  $\psi_{jk}^{(a,b)}$  are carried out over subsystems  $a$  and  $b$  respectively. The input power is given to a good approximation by

$$\langle P_{in} \rangle = 2\omega\eta \sum_j \Gamma_{jj} \psi_{jj}^{(a)} = 2\omega\eta (\langle T_a \rangle + \langle T_b \rangle) \quad (13)$$



### 3.2 DEPENDENCE ON IRREGULARITY AND MODAL OVERLAP

Equations (12) and (13) indicate how the frequency average input power and coupling power  $\langle P_{ab} \rangle = 2\omega\eta\langle T_b \rangle$  depend on the global mode shapes through the terms  $\psi_{jk}^{(a,b)}$ . These are here termed the kinetic energy distribution factors for the  $(j,k)$ 'th mode pair. Since the mode shapes are mass normalised then

$$\psi_{jj}^{(a)} + \psi_{jj}^{(b)} = 1; \quad \psi_{jk}^{(a)} + \psi_{jk}^{(b)} = 0, \quad j \neq k \quad (14)$$

For  $j = k$ ,  $\psi_{jj}^{(a)}$  indicates the proportion of kinetic energy stored in subsystem  $a$  when the system vibrates in the  $j$ 'th mode. For  $j \neq k$ ,  $\psi_{jk}^{(a)}$  gives a measure of the orthogonality of the mode pair over subsystem  $a$ .

Equation (12) can be re-written as

$$\langle T_b \rangle = \sum_j \Gamma_{jj} \psi_{jj}^{(a)} \psi_{jj}^{(b)} - \sum_{j,k \neq j} \Gamma_{jk} (\psi_{jk}^{(a)})^2 \quad (15)$$

When the modal overlap  $M$  is small, the terms  $\Gamma_{jk}$  are small and the first sum on the right of this equation dominates. The cross-modal terms become increasingly important as  $M$  increases. Some aspects of this behaviour will now be amplified and approximations developed assuming that  $\Gamma_{jk}$  are given by equations (11).

#### 3.2.1 Low modal overlap - global mode localisation

If the modal overlap is small ( $M \ll 1$ ), the response (i.e., the kinetic energy, equation (15)) in the undriven subsystem is dominated by the terms  $\Gamma_{jj}$ . Thus

$$\langle T_b \rangle \approx \sum_j \Gamma_{jj} \psi_{jj}^{(a)} \psi_{jj}^{(b)}; \quad \frac{P_{ab}}{P_{in}} = \frac{\sum_j \Gamma_{jj} \psi_{jj}^{(a)} \psi_{jj}^{(b)}}{\sum_j \Gamma_{jj} \psi_{jj}^{(a)}} \quad (16)$$

This is in contrast to the SEA prediction in the strong coupling, equipartition limit (5). Large contributions to the response, and hence large contributions to the coupling power, arise from those modes for which the product  $\psi_{jj}^{(a)} \psi_{jj}^{(b)} = \psi_{jj}^{(a)} (1 - \psi_{jj}^{(a)})$  is large. Such modes are not only relatively well excited (i.e.,  $\psi_{jj}^{(a)}$  large), but also respond relatively strongly in the undriven subsystem (i.e.,  $\psi_{jj}^{(b)}$  large). Modes whose mode shapes are large only within one subsystem are localised within that subsystem: they are either weakly excited or respond weakly in subsystem  $b$ , and hence give only a small contribution to the response there. Thus  $\psi_{jj}^{(a)} \psi_{jj}^{(b)}$  indicates the degree to which the  $j$ 'th mode is localised within one subsystem or the other.

If  $\Gamma_{jj}$  is the same for all modes in  $\Omega$ , then the response for low  $M$  can be written as

$$\frac{P_{ab}}{P_{in}} = \lambda \left( \frac{P_{ab}}{P_{in}} \right)_{equip} ; \lambda = \frac{\langle \psi_{ji}^{(a)} \psi_{ji}^{(b)} \rangle_j}{\langle \psi_{ji}^{(a)} \rangle_j \langle \psi_{ji}^{(b)} \rangle_j} \quad (17)$$

The localisation parameter  $\lambda$  is related to system irregularity. It determines the response in the low modal overlap limit, is equal to 1 for highly irregular systems (for which the SEA equipartition estimate is accurate) and decreases as the amount of irregularity decreases. In terms of global modes, then, irregularity can be quantified partly by the degree to which global mode localisation occurs.

**Numerical examples.** Figure 3 shows frequency average power ratios for two-plate systems of different geometry found by finite element analysis [3] as functions of  $\mu_{w0}$  for a rectangular plate. Each plate is either rectangular (R), quadrilateral (Q) or pentagonal (P) in shape. Also shown are the rectangular plate and SEA theoretical predictions. For strong coupling (low enough  $\mu_{w0}$ ) plate shape is important.

Figure 4 shows  $\psi_{ji}^{(a)}$  for the first 120 modes of the 2-plate system. Results for both RR (i.e., coupled rectangular-rectangular plates) and PP plates are given. There is a marked tendency for the RR global modes (i.e., the modes of the more regular system) to be more localised, in that the energy is stored primarily within one or the other plate (i.e.,  $\psi_{ji}^{(a)}$  is either small or large). The kinetic energy for each of the global modes of the PP plate system, on the other hand, tends to be more evenly distributed between the two plates. Figure 5 shows the

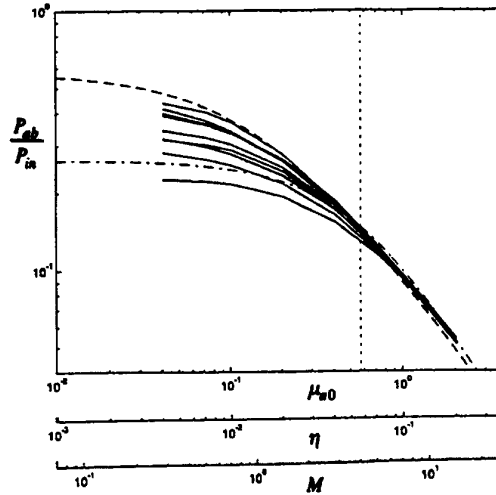


Figure 3. Coupling power per unit input power: ensemble averages: --- rectangular plates; - - - traditional SEA; — 400 Hz frequency averages, centre frequency 1 kHz, various plate systems.

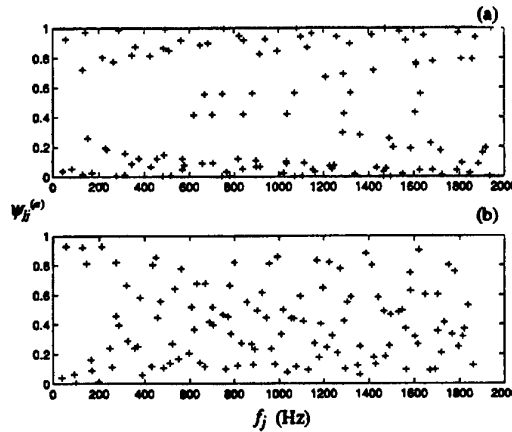


Figure 4. Global mode localisation:  $\psi_{ji}^{(a)}$  as a function of natural frequency  $f_j$ , first 120 modes of (a) RR and (b) PP plate systems.

cumulative probability distribution for  $\psi_{jj}^{(a)}$  for the first 120 modes of each system. This illustrates again the tendency for global mode localisation to occur to a greater degree in the regular RR plates than in the irregular PP plates. The result of this is that the response in the undriven plate and the coupling power are substantially less for the RR plates in the low  $\mu_0$ , low  $M$  region. Table 1 shows the localisation parameters  $\lambda$  calculated for RR and PP systems. The values of  $\lambda$  depend on the specific modes in  $\Omega$ , with  $\lambda$  being consistently smaller for the regular, RR plates, for which  $P_{ab}$  is then also smaller (Figure 3).

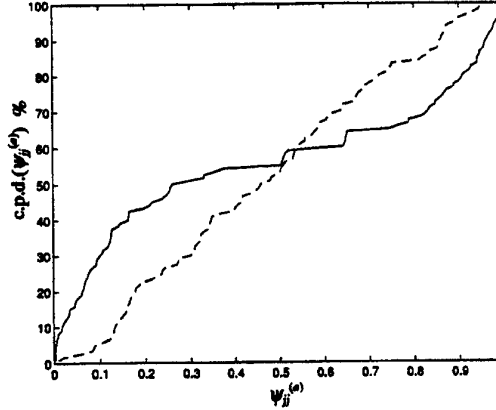


Figure 5. Cumulative probability distribution of  $\psi_{jj}^{(a)}$ , first 120 modes of —RR and --- PP plates.

	RR plates		PP plates	
	(a)	(b)	(a)	(b)
$\langle \psi_{jj}^{(a)} \rangle$	0.410	0.423	0.408	0.405
$\lambda$	0.405	0.376	0.725	0.763

TABLE 1. Mode shape statistics, RR and PP plates.  
(a) first 120 modes and (b) 400Hz band,  
centre frequency 1kHz

### 3.2.2 Higher $M$ - global mode shape orthogonality

As the modal overlap  $M$  increases so cross-modal interaction terms become important,  $\Gamma_{jk}$  being substantial for modes that overlap. Since  $\xi_{jk}$  monotonically increases, these cross-modal terms give negative contributions to both  $\langle P_{ab} \rangle$  and  $\langle T_b \rangle$  (equation (15)), which consequently decrease as  $M$  increases.

As  $M \rightarrow \infty$  then  $\langle P_{ab} \rangle$  and  $\langle T_b \rangle \rightarrow 0$  as one would expect. This can be shown by reordering the summations and integrations in equation (12) and noting that global mode shape incoherence implies

$$\sum_{n=1}^{\infty} \phi_n(x_i) \phi_n(x_j) = \delta_{ij} \quad (18)$$

Rewriting  $\langle T_b \rangle$  in terms of the interactions between neighbouring modes gives

$$\langle T_b \rangle = \sum_j \Gamma_{jj} \psi_{jj}^{(a)} \psi_{jj}^{(b)} - \sum_j \Gamma_{jj} \left[ \sum_{m=-(j-1), m \neq 0}^{\infty} \xi_{j,j+m} \psi_{j,j+m}^{(a)} \right]^2 \quad (19)$$

If only those modes lying in  $\Omega$  are included in the sums and if  $\Gamma_{jj}$  is constant for all such modes then

$$\frac{P_{ab}}{P_{in}} = \left\{ \lambda - \sum_m v_m(M) \right\} \left( \frac{P_{ab}}{P_{in}} \right)_{equip} ; \quad v_m(M) = \frac{\langle \xi_{j,j+m} \psi_{j,j+m}^{(a)2} \rangle_j}{\langle \psi_{jj}^{(a)} \rangle_j \langle \psi_{jj}^{(b)} \rangle_j} \quad (20)$$

where  $v_m$  represents the average interaction of a mode with its  $m$ 'th neighbour. For finite  $M$ , and especially if  $M \sim 1$ , these expressions depend on the detailed statistics of  $\psi_{j,j+m}^{(a)}$  and the specific natural frequency separations that determine  $\xi_{j,j+m}$ . Neglecting non-resonant modes (i.e., modes outside  $\Omega$ ) can lead to noticeable errors if  $M$  is large.

Because of the clear band-pass nature of  $\xi_{j,j+m}$ , the sum over  $m$  can be truncated to exclude modes which do not overlap. Indeed, as an approximation one can regard  $\xi_{j,j+m}$  as a band pass filter of width  $\pi\Delta$ , and truncate the sums at  $\pm\pi M/2$  so that only those modes whose natural frequencies lie within each others noise bandwidths  $\pi\Delta/2$  remain. The coupling power is approximately then

$$\frac{P_{ab}}{P_{in}} \sim \left\{ \lambda - \pi M \langle v'_m \rangle_{|m| \leq \pi M/2} \right\} \left( \frac{P_{ab}}{P_{in}} \right)_{equip} ; \quad v'_m = \frac{\langle \psi_{j,j+m}^{(a)2} \rangle_j}{\langle \psi_{jj}^{(a)} \rangle_j \langle \psi_{jj}^{(b)} \rangle_j} \quad (21)$$

These equations indicate how the response varies with modal overlap and irregularity: for very low  $M$ , the response is determined by global mode localisation (i.e.,  $\lambda$ ); for moderate  $M$  localisation and cross-modal orthogonality within a subsystem (i.e.,  $v_m$ ) determine the response; for high  $M$  cross-modal terms dominate, the response tending to zero. There is a clear tendency for regular systems to have small  $v_m$  for small  $m$ . In this case the low modal overlap response which is determined by  $\lambda$  persists to relatively higher levels of damping than in irregular systems.

**Numerical examples.** Figure 6 shows  $\psi_{j,j+m}^{(a)}$  for two-plate RR and PP systems. For RR plates few mode pairs interact strongly, with many  $\psi_{j,j+m}^{(a)}$  being negligible. This is particularly

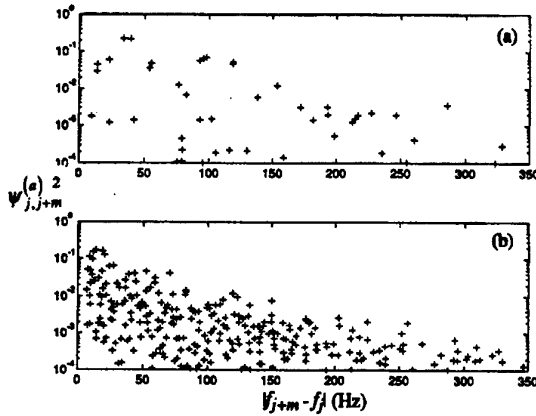


Figure 6. Cross-modal interaction:  $\psi_{j,j+m}^{(a)}$  as a function of natural frequency separation, frequency band 800-1200 Hz: (a) RR and (b) PP plate systems.

true for low  $m$ . This is because in this regular case the global modes form clear groups, each with an integral number of half-wavelengths across the plate width. Modes within each group are generally relatively well spaced (i.e., neighbouring modes have different numbers of half wavelengths across the plate) and modes from different groups are orthogonal. Irregular plates do not have this distinct modal structure. Thus significant cross-modal interaction occurs at a higher level of damping for the rectangular, regular system.

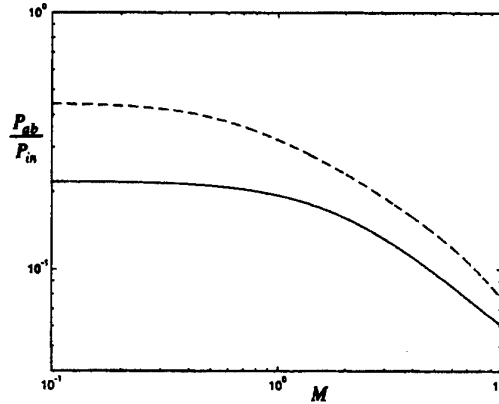


Figure 7. Frequency average coupling power, equation (20), frequency band 800-1200 Hz: — RR and --- PP plate systems.

Figure 7 shows the frequency average coupling powers for the two systems, calculated from equation (20). There is close agreement with the finite element calculations (Figure 3) except when  $M$  is large. This is due to the contributions of non-resonant modes outside  $\Omega$ , which have been ignored in equation (20).

#### 4. Irregularity and Coupling Power: Local Modes

The previous section requires that a global modal analysis be performed. In order to reduce computational effort it becomes useful to describe the global modes in terms of local modal properties. In this section expressions for the response are given using component mode synthesis [7], from which the previous parameters can be derived.

For time harmonic excitation of component mode  $s$  in subsystem  $a$ , the response of the  $r$ 'th component mode and the consequent kinetic energy in subsystem  $b$  are

$$\mathbf{q}_r = \sum_{j=1}^{n_{\text{global}}} \mathbf{P}_{(r,j)} \mathbf{P}_{(s,j)} \alpha_j f_{(s)}; \quad \langle T_b \rangle = \frac{\omega^2}{4} \text{Re} \{ \mathbf{q}_{(b)}^T \mathbf{M}_{(b)} \mathbf{q}_{(b)} \} \quad (22)$$

where  $\mathbf{M}_{(b)}$  is the subsystem mass matrix,  $f_s$  is the magnitude of the force applied to component mode  $s$  and  $\mathbf{P}$  is a matrix of global mode shapes, whose elements are component mode responses. For uncorrelated broad band component mode excitation,  $\langle T_b \rangle$  can be found by summing over all modes ( $s \in a$ ) and integrating over  $\Omega$  to give

$$\langle T_b \rangle = \sum_{m,p}^{n_{\text{global}}} \left( \sum_{j,k \in b} \mathbf{M}_{(j,k)b} \mathbf{P}_{(k,m)} \mathbf{P}_{(j,p)} \right) \left( \sum_{s \in a} |f_{(s)}|^2 \mathbf{P}_{(s,m)} \mathbf{P}_{(s,p)} \right) \left\langle \frac{\omega^2}{4} \text{Re} \{ \alpha_m \alpha_p^* \} \right\rangle_{\Omega} \quad (23)$$

In practice, uncorrelated component modal excitation approximates "rain-on-the-roof" excitation. In the notation of the previous section equation (23) can be written as

$$\langle T_b \rangle = \sum_{m,p}^{n_{\text{total}}} \psi_{mp,M}^{(b)} \psi_{mp,F}^{(a)} \Gamma_{mp} \quad (24)$$

where the distribution factors are weighted by the mass matrix and excitation distribution respectively. Similar expressions can be found for the potential energy.

## 5. Concluding Remarks

This paper discussed some aspects of irregularity, damping and coupling strength with particular reference to the SEA of a system comprising two subsystems. In summary, the coupling is weak (in a wave sense) if wave coherence effects are negligible, this being the case if  $\max(\gamma) \leq 1$ . In this case  $P_{\text{sea}}$  is an accurate estimate of the frequency and ensemble average coupling power  $P_{ab}$ . When the coupling is strong, the response depends on the detailed, rather than the gross, subsystem properties.

In the strong coupling regime, a wave analysis can be used to find the response by including the effects of reflections from distant parts of the system. Alternatively, global mode properties can be used to relate the system response to the normal SEA estimate. When the damping (i.e., the modal overlap) is very small, global mode localisation determines the response in a frequency band through the parameter  $\lambda$ . As the modal overlap increases, cross-modal interaction effects become more important. These manifest themselves through terms  $\psi_{jk}^{(a,b)}$  which quantify the orthogonality of the  $(j,k)$ 'th modal pair within subsystem  $a$  or  $b$ . To calculate the response a global modal analysis is required. While an individual mode is sensitive to uncertainties in system properties, averages over a number of modes are relatively insensitive.

## 6. References

- 1 Wester, E.C.N. and Mace, B.R. (1996) Statistical Energy Analysis of two edge-coupled rectangular plates: ensemble averages, *J Sound Vibration* 193(4), 793-822
- 2 Lyon, R. and DeJong R.G. (1995) *Theory and application of Statistical Energy Analysis*, 2<sup>nd</sup> Edition, Butterworth-Heinemann
- 3 Mace, B.R. and Rosenberg, J. The SEA of two coupled plates : An investigation into the effects of subsystem irregularity, submitted to the *J Sound Vibration*
- 4 Mace, B.R. (1995) Wave coherence, coupling power and Statistical Energy Analysis, *J Sound Vibration* 199(3), 369-380
- 5 Wester, E.C.N. (1996) A wave approach to the SEA of a coupled rectangular plate system involving a non-uniform boundary condition, *Proceedings of Internoise 96* 2909-2914
- 6 Wester, E.C.N. and Mace, B.R. A wave analysis of energy flow between two, non-uniformly coupled rectangular plates, *Proceedings of Internoise 97* (to appear).
- 7 Craig, R.R. (1995) Substructure methods in vibration, 50<sup>th</sup> Anniversary design issue: *Trans ASME* 117, 207-213

# AN APPROACH TO THE STATISTICAL ENERGY ANALYSIS OF STRONGLY COUPLED SYSTEMS

R.G. DeJONG  
*Calvin College, Engineering Department*  
*3201 Burton Street, S.E.*  
*Grand Rapids, MI 49546 USA*

## 1. Introduction

One of the issues in the development of the SEA theory has been the validity of the method for the case of strongly coupled subsystems. In the earliest paper presenting the SEA formulation, Lyon and Maidanik [1] used a light coupling assumption to derive the fundamental power flow equations for two coupled resonators. In a later paper Scharton and Lyon [2] removed the light coupling assumption by redefining the subsystem "blocked" energies. The validity of applying SEA to strongly coupled subsystems has been questioned by a number of people [3, 4].

In this paper the SEA coupling formulation is developed to include arbitrarily strong coupling and validations are included using numerical and experimental results. It is shown that the limiting case for the SEA validity is not strong coupling but low modal overlap. In some cases strong coupling increases the system modal overlap and actually improves the predictive accuracy of the SEA model. However, strong coupling does make the inverse problem of back-calculating coupling factors from measured results more unstable.

## 2. Coupled Subsystems

The SEA method is based on a statistical analysis of the power flow between coupled modes in a system. A simple case is depicted in Fig. 1, where a vibrating system is considered to be the connection of two distinct subsystems, attached at a junction. The modes of the complete system can be considered to be the sum of the coupled modes of the two

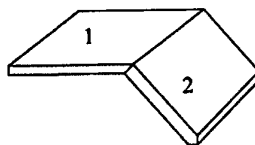


Figure 1. Vibrating System Consisting of Two Coupled Subsystems

subsystems. Mathematically this is described by a pair of differential equations for the response  $u$  with excitation  $p$  of the form

$$\begin{aligned} m_1 \frac{\partial^2 u_1}{\partial t^2} + r_1 \frac{\partial u_1}{\partial t} + \Lambda_1 u_1 &= p_1 + \mu_{12} \frac{\partial^2 u_2}{\partial t^2} + \gamma_{12} \frac{\partial u_2}{\partial t} + \kappa_{12} u_2 \\ m_2 \frac{\partial^2 u_2}{\partial t^2} + r_2 \frac{\partial u_2}{\partial t} + \Lambda_2 u_2 &= p_2 + \mu_{21} \frac{\partial^2 u_1}{\partial t^2} + \gamma_{21} \frac{\partial u_1}{\partial t} + \kappa_{21} u_1 \end{aligned} \quad (1)$$

where  $m$  is the mass,  $r$  is the dissipation, and  $\Lambda$  is the spatial derivative operator. The vibration response of either subsystem is driven in part by the motion of the other subsystem at the junction through inertial ( $\mu$ ), gyroscopic ( $\gamma$ ), and elastic ( $\kappa$ ) operators.

For linear and passive subsystems the uncoupled natural modes are found by solving two individual eigenvalue problems with the junction motion restrained (blocked)

$$\begin{aligned} m_1 \frac{\partial^2 u_1^{(b)}}{\partial t^2} + r_1 \frac{\partial u_1^{(b)}}{\partial t} + \Lambda_1 u_1^{(b)} &= p_1 \\ m_2 \frac{\partial^2 u_2^{(b)}}{\partial t^2} + r_2 \frac{\partial u_2^{(b)}}{\partial t} + \Lambda_2 u_2^{(b)} &= p_2 \end{aligned} \quad (2)$$

For subsystems with proportionate damping (or an approximation for light damping), two sets of undamped and orthogonal natural modes,  $\phi_{1\alpha}$  and  $\phi_{2\sigma}$ , are found with associated natural frequencies,  $\omega_\alpha$  and  $\omega_\sigma$ .

The responses of the "unblocked" system are then expanded in terms of the blocked mode shapes having modal amplitudes  $U$  and modal excitations  $P$ , yielding a set of coupled equations

$$\begin{aligned} M_1 \left[ \frac{d^2 U_\alpha}{dt^2} + \omega_\alpha \eta_\alpha \frac{dU_\alpha}{dt} + \omega_\alpha^2 U_\alpha \right] &= P_\alpha + \sum_\sigma \left[ \mu_{\alpha\sigma} \frac{d^2 U_\sigma}{dt^2} + \gamma_{\alpha\sigma} \frac{dU_\sigma}{dt} + \kappa_{\alpha\sigma} U_\sigma \right] \\ M_2 \left[ \frac{d^2 U_\sigma}{dt^2} + \omega_\sigma \eta_\sigma \frac{dU_\sigma}{dt} + \omega_\sigma^2 U_\sigma \right] &= P_\sigma + \sum_\alpha \left[ \mu_{\sigma\alpha} \frac{d^2 U_\alpha}{dt^2} + \gamma_{\sigma\alpha} \frac{dU_\alpha}{dt} + \kappa_{\sigma\alpha} U_\alpha \right] \end{aligned} \quad (3)$$

For each  $\alpha$  and  $\sigma$  these equations are identical to those of the general pair of coupled resonators shown in Fig. 2. Scharton and Lyon [2] have shown that the frequency averaged power flow  $\Pi_{12}$  between the coupled resonators is given by

$$\Pi_{12} = B_{12}(E_1 - E_2) \quad (4)$$



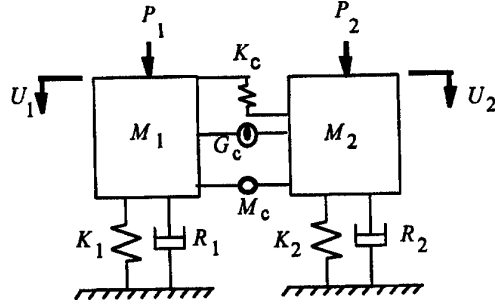


Figure 2. Coupled Resonators

where the energies are  $E_1 = (M_1 + M_c/4)(dU_1/dt)^2$ ,  $E_2 = (M_2 + M_c/4)(dU_2/dt)^2$ .  $B_{12}$  is a complicated function of the system parameters, but not of the energy levels. This result is valid for *arbitrarily large* coupling parameters  $K_c$ ,  $G_c$ , and  $M_c$ . The subsystem energies are defined in a way which includes some of the energy of the coupling elements.

Fahy and Yao [5] have shown that this result does not hold for dissipative coupling elements. However, for the most common cases where the dissipative coupling forces are small compared to the other coupling forces, Eq. (4) is a good approximation.

Applying Eq. (4) to the system in Fig. 1, the average net power flow is found by averaging the value of  $B_{12}$  over a frequency band  $\Delta\omega$  containing  $N_1$  and  $N_2$  modes in subsystems 1 and 2, respectively. This gives

$$\langle \Pi_{12} \rangle = \langle B_{12} \rangle N_1 N_2 \left( \frac{E_1}{N_1} - \frac{E_2}{N_2} \right) \quad (5)$$

where

$$\langle B_{12} \rangle = \frac{\pi}{2 \Delta\omega} \left( \mu^2 \omega^2 + (\gamma^2 + 2\mu\kappa) + \kappa^2 / \omega^2 \right)$$

and

$$\begin{aligned} \mu &= (M_c/4) / \sqrt{(M_1 + M_c/4)(M_2 + M_c/4)} \\ \gamma &= G_c / \sqrt{(M_1 + M_c/4)(M_2 + M_c/4)} \\ \kappa &= K_c / \sqrt{(M_1 + M_c/4)(M_2 + M_c/4)} \end{aligned}$$

It is interesting to note that in this form the frequency averaged coupling parameter is independent of the damping in the system.

An alternate form for Eq. (5) is obtained by defining the coupling loss factors  $\eta_{12} = \langle B_{12} \rangle N_2 / \omega$  and  $\eta_{21} = N_1 \eta_{12} / N_2$ . Then

$$\langle \Pi_{12} \rangle = \omega (\eta_{12} E_1 - \eta_{21} E_2) \quad (6)$$

### 3. Power Flow through Edge Coupling

The SEA coupling parameters in Eq. (6) for connected subsystems can be derived from both a wave formulation and a modal formulation. A convenient model to validate the power flow derivations for a subsystem connected at an edge point is shown in Fig. 3. In this case the power flow from the longitudinal motion of a bar into an ideal viscous dashpot  $R$  is evaluated. This simulates the net power flow out of a subsystem at a junction but does not include the energy returned by the reverberation of the receiving subsystem.

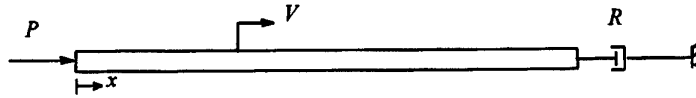


Figure 3. 1-D Bar with Edge Power Flow

In the wave formulation a wave traveling in the  $+x$  direction with velocity amplitude  $V_{\text{inc}} = V_+ \exp(ikx - i\omega t)$  is considered to be incident on the dashpot termination of the bar ( $x = L$ ). A wave  $V_{\text{ref}} = V_- \exp(-ikx - i\omega t)$  will be reflected from the end, and some power,  $\Pi_{\text{abs}}$ , will be absorbed by the dashpot. With the boundary condition,  $i\omega R V = ES \partial V / \partial x$  at  $x = L$ , it is convenient to define a termination absorption coefficient as

$$\alpha = \frac{\Pi_{\text{abs}}}{\Pi_{\text{inc}}} = 1 - \frac{|V_-|^2}{|V_+|^2} = \frac{4(R/\rho S c_L)}{(1 + R/\rho S c_L)^2} \quad (7)$$

$E$  is the elastic modulus,  $\rho$  is the density and  $S$  is the cross-sectional area of the bar with  $c_L = \sqrt{E/\rho}$  and  $k = \omega/c_L$ .

The wave solution assumes that the incident and reflected waves are incoherent, so the total mean-square velocity is,  $\langle V^2 \rangle = \langle V_{\text{inc}}^2 \rangle + \langle V_{\text{ref}}^2 \rangle = (2 - \alpha) \langle V_{\text{inc}}^2 \rangle$ . The absorbed power can be related to the SEA expression for dissipated power to find an expression for the effective loss factor  $\eta$

$$\eta = \frac{\alpha \Pi_{\text{inc}}}{\omega M \langle V^2 \rangle} = \frac{c_L}{\omega L} \frac{\alpha}{2 - \alpha} \quad (8)$$

In the modal formulation the wave equation,  $\rho \partial V^2 / \partial t^2 = E \partial V^2 / \partial x^2$ , for the longitudinal velocity  $V$  is solved with the boundary condition  $i\omega P = ES \partial V / \partial x$  at the excitation point ( $x = 0$ ), and  $i\omega RV = ES \partial V / \partial x$  at the dashpot ( $x = L$ ). This gives the bar response function

$$\frac{V}{P} = \frac{1}{\rho S c_L} \frac{\cos k(L-x) - i(R/\rho S c_L) \sin k(L-x)}{(R/\rho S c_L) \cos kL - i \sin kL} \quad (9)$$

The bar energy is proportional to the mean square velocity. Averaging  $V^2$  over the length of the bar and over frequency (above the first resonance) for a constant amplitude excitation gives

$$\frac{\langle V^2 \rangle}{\langle P^2 \rangle} = \frac{1}{\rho S c_L} \frac{1 + (R/\rho S c_L)^2}{2(R/\rho S c_L)} \quad (10)$$

This result can be related to the SEA power flow relation

$$\begin{aligned} \Pi_{\text{in}} &= \Pi_{\text{out}} \\ \frac{\langle P^2 \rangle}{\rho S c_L} &= \omega \eta M \langle V^2 \rangle \end{aligned} \quad (11)$$

where  $\eta$  is the loss factor and  $M = \rho S L$ . Solving for the loss factor gives

$$\eta = \frac{c_L}{\omega L} \frac{2(R/\rho S c_L)}{1 + (R/\rho S c_L)^2} \quad (12)$$

This expression for the loss factor can be related to the boundary absorption coefficient  $\alpha$  using Eq. (7)

$$\eta = \frac{c_L}{\omega L} \frac{\alpha}{2 - \alpha} \quad (13)$$

which is identical to the result in Eq. (8) obtained from the wave formulation.

For the case of edge connected subsystems, such as shown in Fig. 4, the absorption coefficient used above is replaced with a transmission coefficient, defined in the wave formulation as

$$\tau_{12} = \frac{\Pi_{\text{tra}}}{\Pi_{\text{inc}}} = \frac{4 R_1 R_2}{|Z_1 + Z_2|^2} \quad (14)$$

where  $R$  is the real part of the subsystem connection impedance  $Z$ . With no significant power dissipation at the connection,  $\Pi_{\text{ref}} = (1 - \tau_{12}) \Pi_{\text{inc}}$ .

In the wave formulation the power transmitted into subsystem 2 is assumed to be incoherent with the power transmitted back into subsystem 1. Then,

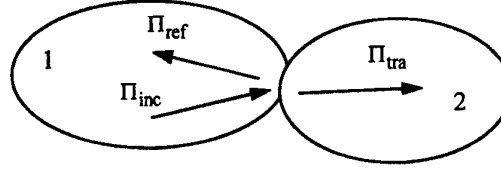


Figure 4. Edge Connected Subsystems

$$\Pi_{\text{tra}} = \Pi_{1 \rightarrow 2} = \omega \eta_{12} E_1 \quad (15)$$

Also, the incident and reflected waves are assumed to be incoherent, so

$$E_1 = M_1 \left( \langle V_{\text{inc}}^2 \rangle + \langle V_{\text{ref}}^2 \rangle \right) = 2 M_1 G_1 (\Pi_{\text{inc}} + \Pi_{\text{ref}}) \quad (16)$$

where  $G_1$  is the subsystem conductance (real part of mobility).

Combining Eqs. (14-16) gives an expression relating  $\eta$  to  $\tau$

$$\eta_{12} = \frac{1}{2 \omega M_1 G_1} \frac{\tau_{12}}{2 - \tau_{12}} \quad (17)$$

In the modal formulation subsystem 1 is considered to be driven with excitation  $P_1$  at point  $a$ . The SEA power balance relation for subsystem 1 is

$$\begin{aligned} \Pi_{1,\text{in}} &= \Pi_{1,\text{diss}} + \Pi_{12} \\ \langle P_1^2 \rangle G_{1a} &= \omega \eta_1 E_1 + \langle V_j^2 \rangle R_{2j} \end{aligned} \quad (18)$$

where  $G_{1a}$  is the input conductance of the excitation,  $\eta_1$  is the damping loss factor of subsystem 1,  $V_j$  is the junction velocity, and  $R_{2j}$  is the input resistance of subsystem 2 at the junction. The SEA power balance relation for subsystem 2 is

$$\begin{aligned} \Pi_{12} &= \Pi_{2,\text{diss}} \\ \langle V_j^2 \rangle R_{2j} &= \omega \eta_2 E_2 \end{aligned} \quad (19)$$

Combining these two power balance equations gives

$$\frac{\langle V_j^2 \rangle}{\langle P_1^2 \rangle} = \frac{G_{1a}}{R_{2j}} \frac{\eta_2 E_2}{\eta_1 E_1 + \eta_2 E_2} \quad (20)$$

Next, a reciprocal condition is considered in which the connection junction is driven with  $P_{j'}$  resulting in a junction velocity  $V_j = P_{j'} / (Z_{1j} + Z_{2j})$ . The SEA power balance relation for subsystem 1 in this case is

$$\begin{aligned} \Pi_{1, \text{in}'} &= \Pi_{1, \text{diss}'} \\ \langle V_j^2 \rangle R_{1j} &= \omega \eta_1 M_1 \langle V_1^2 \rangle \end{aligned} \quad (21)$$

These two conditions are related by the reciprocity relation which, when averaged over point  $a$ , is

$$\frac{\langle V_j^2 \rangle}{\langle P_1^2 \rangle} = \frac{\langle V_1^2 \rangle}{\langle P_{j'}^2 \rangle} \quad (22)$$

Combining Eqs. (20-22) gives

$$4 \omega \eta_1 M_1 \left\langle \frac{G_1}{1 + (\eta_1 E_1) / (\eta_2 E_2)} \right\rangle = \frac{4 R_{1j} R_{2j}}{|Z_{1j} + Z_{2j}|^2} = \tau_{12} \quad (23)$$

In principle Eq. (23) could be averaged over frequency for a particular modal solution for the two subsystems in a manner similar to that done for the response of the 1-D bar in Eq. (9). However, an approximate general formulation can be found by noting that  $G_1$  peaks at the resonances of the system (for light damping), at which frequencies the reverberant energy ratio is

$$\frac{E_1}{E_2} = \frac{\eta_2 + \eta_{21}}{\eta_{12}} \quad (24)$$

The frequency averaged transmission coefficient is then given by

$$\langle \tau_{12} \rangle = \frac{4 \omega \eta_1 M_1 \langle G_1 \rangle}{1 + \frac{\eta_1}{\eta_2} \frac{\eta_2 + \eta_{21}}{\eta_{12}}} \quad (25)$$

Solving for  $\eta_{12}$ , using  $\langle G_1 \rangle = (\pi/2)(n(\omega)_1/M_1)$  and  $\eta_{21} = \eta_{12}(n(\omega)_1/n(\omega)_2)$ , where  $n(\omega)$  is the subsystem modal density, and defining the modal overlap factors,  $(\pi/2)\beta = (\pi/2)\omega \eta n(\omega)$ , gives

$$\eta_{12} = \frac{1}{\pi \omega n(\omega)_1} \frac{\langle \tau_{12} \rangle}{2 - \langle \tau_{12} \rangle \left( \frac{1}{\pi \beta_1} + \frac{1}{\pi \beta_2} \right)} \quad (26)$$

When the modal overlap increases to unity (which is the upper limit of this approximation), Eq. (26) is identical to Eq. (17). This indicates that the wave solution assumption of incoherence is valid in finite systems only for high modal overlap. The form of Eq. (26) is not convenient to use at low modal overlap because of the subtraction in the denominator. The average transmission coefficient is also a function of the modal overlap.

A better correction for low modal overlap can be obtained using the example shown in Fig. 5 of two beams connected at a right angle. The frequency dependent transmission coefficient for flexural motion is plotted in Fig. 5a using an exact impedance formulation. Also plotted are the calculated frequency averaged values and the infinite system value  $\tau_{12,\infty}$  (used in the wave solution). The normalized coupling loss factor values are plotted in Fig. 5b.

Also plotted in Fig. 5b is an curve-fit approximation for the coupling loss factor based on two limiting values. First, for high modal overlap the coupling loss factor converges to the infinite system value. Second, for low modal overlap the coupling loss factor is reduced by the factor  $(2\pi(\beta_1 + \beta_2))^2$ . A convenient curve-fit is

$$\eta_{12} = \frac{1}{\pi \omega n(\omega)_1} \frac{\tau_{12,\infty}}{2 - \tau_{12,\infty}} \left( 1 + \left( \frac{1}{2\pi(\beta_1 + \beta_2)} \right)^8 \right)^{-1/4} \quad (27)$$

This result is valid for point-coupled subsystems. For line and area connections an additional term is needed to take into account the effects of wavelength matching along the connection [6].

For systems with more than two subsystems the modal overlap includes the coupling as well as the damping loss factor. This is seen in the example shown in Fig. 6 where the two beams used previously have an additional beam attached. The modal response is more dense, and modal overlap is achieved at lower frequencies.

While edge connected subsystems are considered to be strongly coupled when the value of the transmission coefficient approaches unity, the next two sections consider even more strongly coupled subsystems.

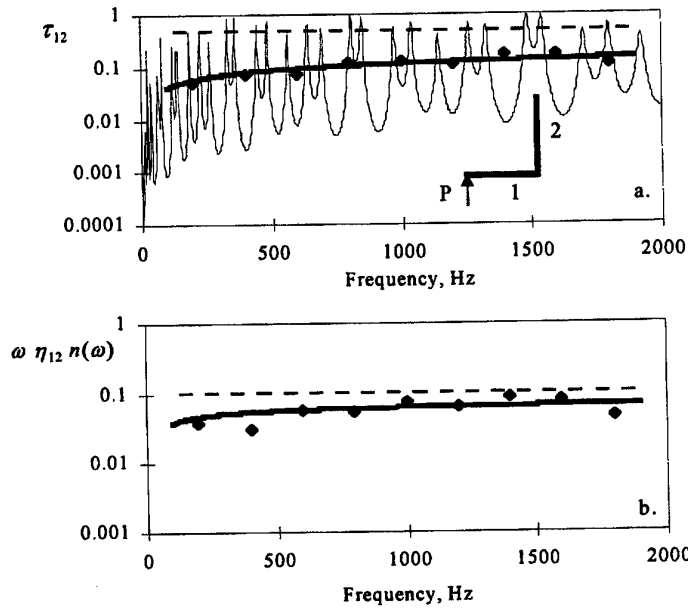


Figure 5. Transmission Coefficient and Coupling Loss Factor for Edge Connected Beams;  
 — Analytical Solution, ♦ 400 Hz Average, — Using Eq. (27), - - - Infinite System Values

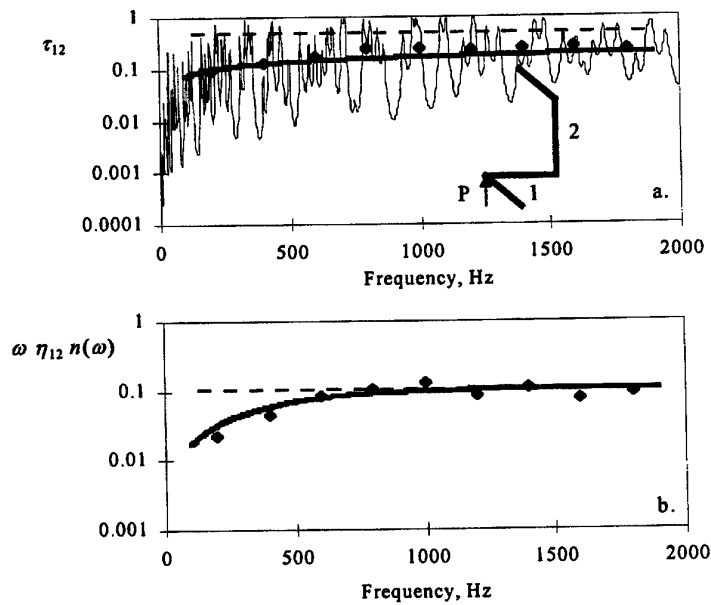


Figure 6. Transmission Coefficient and Coupling Loss Factor for Edge Connected Beams;  
 — Analytical Solution, ♦ 400 Hz Average, — Using Eq. (27), - - - Infinite System Values

#### 4. Beam-Plate System

One example of strongly coupled subsystems is the case of a beam attached to a plate along its length as illustrated in Fig. 7. In some cases it is desirable to define separate subsystems for the plate and the beam modes. The question is how to define the subsystems in keeping with the "blocked" subsystem definitions used above. This can be answered by evaluating the impedance of the beam-plate junction.

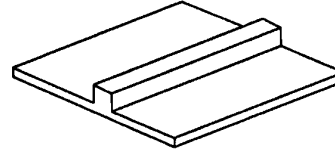


Figure 7. Beam on a Plate

The drive-point impedance of the beam-plate junction can be evaluated using the wavenumber integral formulation

$$\frac{1}{Z_{bp}} = \frac{1}{2\pi} \int_{-\infty}^{\infty} \frac{e^{-ik_x x} dk_x}{Z'_b(k_x) + Z'_p(k_x)} \quad (28)$$

where the line impedances as a function of the wavenumber  $k_x$  along the length of the beam are given by

$$\begin{aligned} Z'_b &= \frac{i}{\omega} B_b (k_x^4 - k_b^4) \\ Z'_p &= \frac{i}{\omega} 4B'_p k_p^2 \left( \frac{1}{\sqrt{k_p^2 - k_x^2}} - \frac{1}{\sqrt{k_p^2 + k_x^2}} \right)^{-1} \end{aligned} \quad (29)$$

$B_b$  is the bending rigidity and  $k_b$  is the free bending wavenumber of the beam.  $B'_p$  is the bending rigidity per unit length and  $k_p$  is the free bending wavenumber of the plate.

A numerical evaluation of this integral (with care in dealing with the branch cut in the complex square root function) for a particular case is shown in Fig. 8. This impedance should be the sum of the two SEA subsystem impedances. At low frequencies the junction impedance converges to the free plate impedance. However, at high frequencies the junction impedance does not converge to the free beam impedance. Rather, it converges to the impedance of an equivalent beam constrained by the elasticity of the plate. This equivalent beam can be approximated by including a plate width equal to  $1/k_b$ , as illustrated in Fig. 8. A similar result is obtained for the torsion of the beam.

As an illustration of the use of these subsystems in an SEA model, a ribbed plate tested by Heckl [7] (see Fig. 9) is analyzed. Three sections of the plate are used, each with bending and inplane modes modeled separately. An equivalent beam is used with bending and torsional modes modeled separately. Fig. 9 shows a good comparison between the SEA model and the measurements.



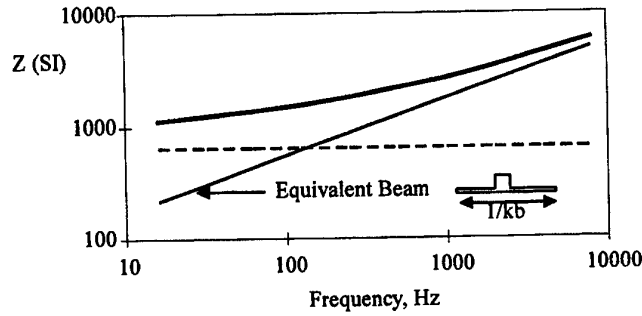


Figure 8. Impedances of Beam-Plate System;  
 — Junction Numerical Solution,  
 --- Flat Plate, — Equivalent Beam

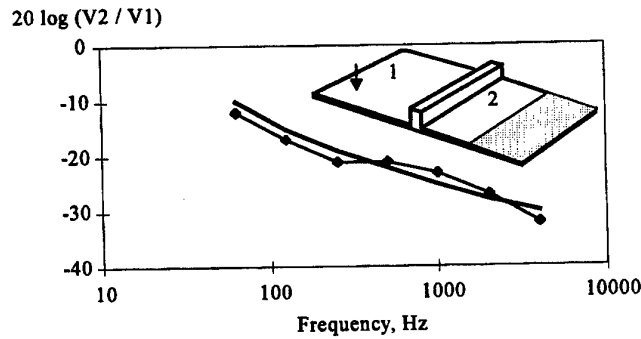


Figure 9. Vibration Ratio across a Beam on a Plate;  
 ♦ Measurements, — SEA Model

### 5. Fluid-loaded Plate

Another example of strongly coupled subsystems is the case of a plate in contact with a fluid of significant impedance. The impedance of a line force driving on the plate is given by

$$\frac{1}{Z'_{fp}} = \frac{1}{2\pi} \int_{-\infty}^{\infty} \frac{e^{-ik_y y} dk_y}{Z''_p(k_y) + Z''_f(k_y)}$$

where  $Z''_p$  and  $Z''_f$  are the area impedances of the plate and fluid, respectively [8].

Fig. 10 shows a numerical evaluation of the impedance for steel in water compared to the two asymptotes of a free plate and one with the fluid inertia loading. Using this result in

an SEA model for the transmission across a simple support on a fluid-loaded plate, the results shown in Fig. 11 are obtained.

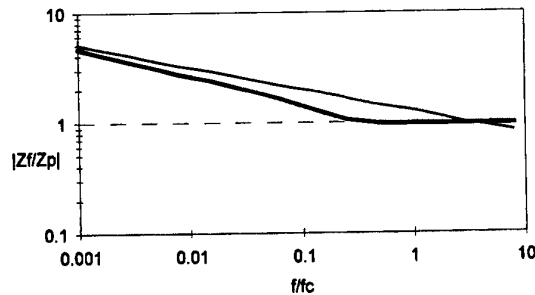


Figure 10. Impedances of Fluid-loaded Plate;  
— Numerical Solution, - - - Free Plate, — Fluid-loading

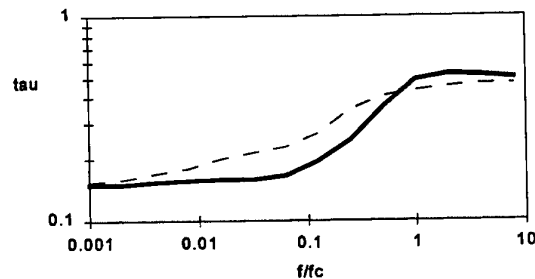


Figure 11. Transmission Coefficient of Fluid-loaded Plate across  
a Simple Support; — Numerical Solution, - - - SEA Model

## 6. References

1. Lyon, R.H. and Maidanik, G., "Power Flow Between Linearly Coupled Oscillators," *J.A.S.A.* **34**, 623-639 (1962)
2. Scharton, T.D. and Lyon, R.H., "Power Flow and Energy Sharing in Random Vibration," *J.A.S.A.* **43**, 1332-1343 (1968)
3. Woodhouse, J., "An Approach to the Theoretical Background of Statistical Energy Analysis Applied to Structural Vibration," *J.A.S.A.* **69**, 1695-1709 (1981)
4. Norton, M.P., *Fundamentals of Noise and Vibration Analysis for Engineers*, Cambridge University Press, Cambridge, 1989
5. Fahy, F.J. and Yao, D., "Power Flow Between Non-conservatively Coupled Oscillators," *J.S.V.* **114**(1), 1-11 (1987)
6. Lyon, R.H. and DeJong, R.G., *Theory and Application of Statistical Energy Analysis*, Butterworth-Heinemann, Boston, 1995
7. Heckl, M., "Wave Propagation on Beam-Plate Systems," *J.A.S.A.* **33**, 640-651 (1961)
8. Crighton, D.G., "The Free and Forced Waves on a Fluid-loaded Elastic Plate," *J.S.V.* **63**(2), 225-235 (1979)

# THE ENERGY FLOW EQUATION OF CONTINUUM DYNAMICS

J. T. XING<sup>1,2</sup> \*

*Solid Mechanics Centre, Beijing University of Aeronautics and Astronautics, Beijing 100083, People's Republic of China<sup>1</sup>*

W. G. PRICE

*Department of Ship Science, University of Southampton, Highfield, Southampton SO17 1BJ, U.K<sup>2</sup>*

**Abstract.** A mathematical model is developed to describe the energy flow equation associated with the dynamics of a viscoelastic continuum excited externally and subject to boundary conditions. The model is applied to a selection of simple examples to illustrate the concepts of an energy flow density vector, energy flow line, energy potential and an energy equipotential surface. On this basis, a brief comparison between mechanical and thermal energy flows is conducted.

**Key words:** Energy Flow Equation, Energy Flow Density Vector, Viscoelastic Continuum

## 1. Introduction

Based on the fundamental equations and principles of continuum mechanics, a general theoretical approach is developed to assess directly the energy flow or power flow in a general continuum subject to external excitation and prescribed boundary conditions. To achieve this aim, the proposed mathematical model examines the energy transmitted from point to point within the continuum through an energy flow density vector being functionally dependent on a stress tensor and a velocity vector. This allows determination of the rate of energy flow at each point in a defined direction, the construction of energy flow equations and their time averaged forms as well as defining the energy flow line, the energy flow potential and equipotential surface within the continuum.

The proposed mathematical model generalises the more traditional approaches adopted in statistical energy analyses or power flow analyses as described by Lyon and Maidanik (1962), Scharton and Lyon (1968), Lyon (1975), Goyder and White (1980a,b,c), Fahy (1994), Keane and Price (1997) and many others in their investigations of high frequency excited dynamical

---

\* JTX expresses his thanks to NSFC for supporting the related research in China.

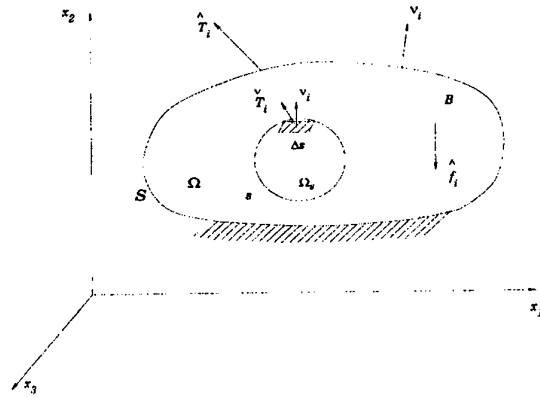


Figure 1. Energy transmission from one part to another in the continuum

systems. Normally, for a specific dynamical system, e.g. two oscillators or rods connected through a spring-dashpot coupling, the relevant equations of motion are derived and through their analysis and solution the energy flow or power flow passing through the system caused by an external excitation is evaluated. In this paper, following the original discussion on the flux of energy in vibratory motion described by Love (1927), we investigate and develop energy flow concepts from a more generic viewpoint, presenting energy flow equations derived from the equations of continuum mechanics.

This is illustrated by a brief description of the proposed mathematical model developed from the linear field equations associated with the dynamics of a viscoelastic continuum. By this means, the energy flow equations are derived for dynamically excited systems, such as a rod in tension or compression, a rod in torsion, a Timoshenko beam, a shear plate and a circular plate under a concentrated load. Furthermore, on this basis, the hypothesis, proposed by Nefske and Sung (1987) and investigated by Wohlever and Bernhard (1992) and Carcaterra and Sestieri (1995), that the flow of mechanical energy through a structure may be modelled in a manner similar to the flow of thermal energy in a heat conduction problem is investigated.

## 2. Viscoelastic Continuum and Energy Flow Mathematical Model

It is assumed that the continuum and structures under investigation in this paper are constructed of materials described by a linear Voigt viscoelastic model (see, for example, Fung 1977). Let us examine the motion of a continuum system  $B$  from time  $t_0$  to  $t_1$ , ( $t_1 > t_0$ ) as schematically illustrated in

# ENERGY FLOW EQUATION

figure 1. In the frame of the Lagrangian coordinate  $x_i$ , ( $i=1,2,3$ ), the continuum occupies the domain  $\Omega$  with surface  $S$  which has the unit vector  $\nu_i$  defined along the outer normal. In this study it is assumed that the variables  $u_i$  and  $v_i$  represent displacement and velocity, respectively;  $\sigma_{ij}$  a stress tensor;  $e_{ij}$  a strain tensor;  $C_{ijkl}$  an elastic constant tensor;  $d_{ijkl}$  a viscous constant tensor;  $S_u$  displacement boundary with a prescribed displacement  $\hat{u}_i$ ;  $S_T$  traction boundary with a prescribed traction  $\hat{T}_i$ ;  $\hat{f}_i$  a body force per unit volume acting in the continuum and  $\rho$  the density of the continuum. Under these circumstance the linear field equations describing the dynamics of the continuum system are expressed as:

$$\text{Dynamic equation: } \sigma_{ij,j} + \hat{f} = \rho v_{i,t}, \quad (1)$$

$$\text{Constitutive equation: } \sigma_{ij} = C_{ijkl}e_{kl} + d_{ijkl}e_{kl,t}, \quad (2)$$

$$\text{Displacement-strain relation: } e_{ij} = (u_{i,j} + u_{j,i})/2, \quad (3)$$

$$\text{Displacement-velocity relation: } v_i = u_{i,t}, \quad (4)$$

$$\text{Boundary conditions: } u_i = \hat{u}_i \quad \text{on } S_u, \quad (5)$$

$$\sigma_{ij}\nu_j = \hat{T}_i \quad \text{on } S_T, \quad (6)$$

where, for example,  $v_{i,t} = \partial v_i / \partial t$ ,  $\sigma_{ij,j} = \sigma_{ij} / \partial x_j$ , etc.

## Energy Flow Density Vector

The energy transmission from one part to another in a continuum excited by external forces can be investigated by analysing the energy flow across the closed surface  $s$  within the continuum  $B$  illustrated in figure 1. Let  $\Delta s$  denote an elemental surface on  $s$  and  $\nu_i$  an unit normal to  $\Delta s$  with its positive direction pointing outward from the (negative) interior to the (positive) exterior. The interactions between material lying on either side of this surface cause internal actions defined by the traction or stress vector  $\hat{T}_i$  representing the force per unit area acting on the surface  $s$ . Through the rate of work done by this traction  $\hat{T}_i$ , the rate of energy flow along the direction  $\nu_i$  is given by

$$q^\nu = -v_i \hat{T}_i. \quad (7)$$

A positive value of  $q^\nu$  represents the transmission of energy per unit time through the unit area  $\Delta s$  from the material within  $s$  to the outside.

It follows from Cauchy's formula (see, for example, Green and Zerna 1954), the traction

$$\hat{T}_i = \sigma_{ij}\nu_j, \quad (8)$$

and hence the rate of energy flow

$$q^\nu = -v_i \sigma_{ij}\nu_j = q_j \nu_j. \quad (9)$$

Here, the energy flow density vector

$$q_j = -v_i \sigma_{ij} = -\sigma_{ji} v_i \quad (10)$$

is defined by the dot product of the velocity  $v_i$  and stress tensor  $\sigma_{ij}$  and is a vector field function dependent on the coordinate  $x_i$  and the time  $t$ . In a continuum mechanics approach this energy flow density vector  $q_j$  specifies the energy transmission from one part to another in the dynamical system and allows the determination of the rate of energy flow at each point in or on the continuum in any direction with unit normal  $\nu_i$  through application of equation (9).

#### *Energy Flow Line*

An energy flow line is defined as a line in the direction of the energy flow in the continuum, and satisfies the differential equations

$$dx_1/q_1 = dx_2/q_2 = dx_3/q_3. \quad (11)$$

These energy flow lines are the vector lines of the vector field of the energy flow density  $q_i$  and give a geometrical description of the vector field.

#### *Energy Flow Potential*

If the vector field of energy flow density  $q_i$  is assumed irrotational, there exists a single-valued function  $\varphi$ , called an *energy flow potential* satisfying the relation

$$q_i = -\partial\varphi/\partial x_i = -\varphi_{,i}. \quad (12)$$

The necessary and sufficient conditions for the existence of the energy flow potential is the irrotational condition of the vector field  $q_i$ , i.e.

$$\epsilon_{ijk} q_{k,j} = \epsilon_{ijk} (v_r \sigma_{rk})_{,j} = 0, \quad (13)$$

where  $\epsilon_{ijk}$  is the permutation symbol. Based on Stokes theorem (see, for example, Fung 1977), the energy flow line in a single connected domain of continuum will not be a closed line, if there exists an energy flow potential.

Equation (12) shows that when an energy flow potential exists the energy flow lines are everywhere perpendicular to a system of surfaces, viz. the equipotential surfaces  $\varphi = \text{constant}$ . Again, if from the point  $(x_1, x_2, x_3)$  a linear element  $dl$  extends in the direction  $(\frac{dx_1}{dl}, \frac{dx_2}{dl}, \frac{dx_3}{dl})$ , the rate of energy flow resolved in this direction is

$$q^l = -\varphi_{,i} dx_i/dl = -\partial\varphi/\partial l. \quad (14)$$

The rate of energy flow in any direction is therefore equal to the rate of decrease of  $\varphi$  in that direction.

## ENERGY FLOW EQUATION

Taking  $dl$  in the direction of the normal to the surface  $\varphi = \text{constant}$ , we see that if a series of such surfaces are drawn corresponding to equidistant values of  $\varphi$ , the rate of energy flow at any point will be inversely proportional to the distance between two consecutive surfaces in the neighbourhood of the point. Hence, if any equipotential surface intersects itself, the rate of energy flow is zero at the intersection. The intersection of two distinct equipotential surfaces would imply an infinite rate of energy flow.

### *Input, Absorption and Transmission of Energy*

At every point in the continuum there occurs a dynamical physical process involving an input, absorption and transmission of energy. Their rates are defined as follows.

*Rate of energy input* represents the rate at which energy enters the continuum and this is defined by the power of the applied external body force  $\hat{f}_i$  at the input point in the continuum, i.e.

$$\pi^I = v_i \hat{f}_i = \hat{q}_f. \quad (15)$$

*Rate of energy absorption* describes the ability of the continuum to absorb energy and equals the sum of the rate of change of mechanical energy  $\dot{E}$  and the rate of energy dissipation  $\dot{D}$ , i.e.

$$\pi^A = \dot{E} + \dot{D}. \quad (16)$$

Here the densities of mechanical energy  $E$ , kinematic energy  $K$ , strain energy  $U$  and energy dissipation  $D$  are defined as

$$E = K + U, \quad U = C_{ijkl} e_{ij} e_{kl} / 2, \quad K = \rho v^2 / 2, \quad D = \int_{t_0}^t d_{ijkl} e_{kl,t} e_{ij,t} dt. \quad (17)$$

*Rate of energy transmission* is the difference between the rates of energy input and absorption, i.e.

$$\pi = \pi^I - \pi^A. \quad (18)$$

This describes the ability of the continuum to transmit energy from a point.

### *Energy Flow Equation*

From the governing equations of the continuum expressed in equations (1)-(6), Xing and Price (1997) show that the equation of energy flow balance of the continuum takes the form

$$q_{j,j} = \hat{q}^I - \dot{E} - \dot{D} = \pi^I - \pi^A = \pi, \quad q^\nu = \hat{q}_u \quad \text{on } S_u, \quad q^\nu = \hat{q}_T \quad \text{on } S_T, \quad (19)$$

where the boundary energy flows  $\hat{q}_u$  on the displacement boundary  $S_u$  and  $\hat{q}_T$  on the traction boundary  $S_T$  are respectively given by

$$\hat{q}_u = -\nu_i \sigma_{ij} \hat{u}_{j,t}, \quad \hat{q}_T = -v_i \hat{T}_i. \quad (20)$$

This equation defined at any point in the continuum states that the divergence of the energy flow density vector ( $q_{j,j}$ ) equals the rate of energy transmission  $\pi$ , being the difference between the rates of energy input ( $\pi^I$ ) and absorption ( $\pi^A$ ).

The application of the time average operation to the local equation of energy flow balance expressed in equation (19) gives the following time averaged equation of energy flow balance

$$\langle q_j \rangle_{,j} = \langle \dot{q}_f \rangle - \langle \dot{E} \rangle - \langle \dot{D} \rangle = \langle \pi \rangle, \quad \langle q^\nu \rangle = \langle \dot{q}_u \rangle \text{ on } S_u, \quad \langle q^\nu \rangle = \langle \dot{q}_T \rangle \text{ on } S_T. \quad (21)$$

For the case of a harmonic motion or a stationary random process (see, for example, Newland 1975; Price and Bishop 1974) in the absence of any body forces it follows that the results of the time averaged equation of energy flow balance in equation (21) reduces to the simpler form

$$\langle q_j \rangle_{,j} = -\langle \dot{D} \rangle, \quad \langle q^\nu \rangle = \langle \dot{q}_u \rangle \text{ on } S_u, \quad \langle q^\nu \rangle = \langle \dot{q}_T \rangle \text{ on } S_T. \quad (22)$$

If the energy flow potential expressed in equation (12) exists, this equation can be further expressed as

$$\langle \varphi \rangle_{,jj} = \langle \dot{D} \rangle, \quad \langle \varphi \rangle_{,j} \nu_j = -\langle \dot{q}_u \rangle \text{ on } S_u, \quad \langle \varphi \rangle_{,j} \nu_j = -\langle \dot{q}_T \rangle \text{ on } S_T. \quad (23)$$

These two equations state that for the case of a harmonic motion or a stationary random process in the absence of any body forces, the time average of the energy flow distribution in the continuum is only dependent on the distribution of the material damping. Furthermore, if there exists no damping, the time average of the possible energy flow potential must satisfy the Laplace equation.

To illustrate these concepts, this mathematical model is applied to a selection of simple examples as demonstrated in the following sections.

### 3. Rod in Tension or Compression

In this example, it is assumed that the longitudinal axis of the rod ( $0 \leq x \leq x_1$ ) coincides with the x-axis of a rectangular Cartesian axis system. The governing equations describing the linear dynamics of a Voigt viscoelastic rod with unit sectional area are as follows.

$$\text{Dynamic equation: } T_{,x} + \hat{f} = \rho v_{,t}, \quad (24)$$

$$\text{Constitutive equation: } T = Ce + de_{,t}, \quad (25)$$

$$\text{Displacement-strain relation: } e = u_{,x}, \quad (26)$$

$$\text{Displacement-velocity relation: } v = u_{,t}, \quad (27)$$

$$\text{Boundary conditions: } T = \hat{T}, \quad x = 0, \quad (28)$$

$$u = \hat{u}, \quad x = x_1. \quad (29)$$



## ENERGY FLOW EQUATION

The energy flow density vector  $q$ , the energy flow potential  $\varphi$  and the energy flow equation are respectively written as

$$q = -vT, \quad q = -\varphi_{,x}, \quad (30)$$

$$q_{,x} = \hat{q}_f - \dot{E} - \dot{D}, \quad q = \hat{q}_0 \text{ on } x = 0, \quad q = \hat{q}_1 \text{ on } x = x_1, \quad (31)$$

where

$$\begin{aligned} \hat{q}_f &= v\hat{f}, & \hat{q}_0 &= -v_0\hat{T}, & \hat{q}_1 &= -T_1\hat{u}_{,t}, \\ K &= \rho v^2/2, & U &= Ce^2/2, & D &= \int_{t_0}^t de_{,t}e_{,t}dt. \end{aligned}$$

For stationary random processes, it follows from equation (31) that the time averaged equations take the form

$$\langle q \rangle_{,x} = \langle \hat{q}_f \rangle - \langle \dot{D} \rangle, \quad \langle q \rangle = \langle \hat{q}_0 \rangle \text{ on } x = 0, \quad \langle q \rangle = \langle \hat{q}_1 \rangle \text{ on } x = x_1. \quad (32)$$

### 4. Rod in Torsion

Let us assume that the longitudinal axis of the rod coincides with the  $z$ -axis of a cylindrical coordinate system;  $M$ ,  $\hat{m}$  and  $\theta$  represent the internal torque, the distributed torque and the twist of the rod, respectively. The governing equations of the rod in torsion are represented as

$$\text{Dynamic equation: } M_{,z} + \hat{m} = \rho J \omega_{,t}, \quad (33)$$

$$\text{Constitutive equation: } M = GJe + de_{,t}, \quad (34)$$

$$\text{Displacement-strain relation: } e = \theta_{,z}, \quad (35)$$

$$\text{Displacement-velocity relation: } \omega = \theta_{,t}, \quad (36)$$

$$\text{Boundary conditions: } M = \hat{M}, \quad z = 0, \quad (37)$$

$$\theta = \hat{\theta}, \quad z = z_1. \quad (38)$$

The energy flow density vector  $q$ , the energy flow potential  $\varphi$  and the energy flow equation are respectively expressed in the following way:

$$q = -\omega M, \quad q = -\varphi_{,z}, \quad (39)$$

$$q_{,z} = \hat{q}_f - \dot{E} - \dot{D}, \quad q = \hat{q}_0, \quad z = 0, \quad q = \hat{q}_1, \quad z = z_1, \quad (40)$$

where

$$\begin{aligned} \hat{q}_f &= \omega \hat{m}, & \hat{q}_0 &= -\omega_0 \hat{M}, & \hat{q}_1 &= -M_1 \hat{\theta}_{,t}, \\ K &= \rho J \omega^2/2, & U &= GJe^2/2, & D &= \int_{t_0}^t de_{,t}e_{,t}dt. \end{aligned}$$

## 5. Timoshenko Beam

The governing equations describing the linear dynamics of a Timoshenko beam in bending are as follows (Timoshenko et al 1974):

$$\text{Dynamic equations: } Q_{,x} + \hat{f} = \rho A v_{,t}, \quad M_{,x} - Q = \rho I \omega_{,t}, \quad (41)$$

$$\text{Constitutive equations: } M = C J \kappa + d_M \kappa_{,t}, \quad (42)$$

$$Q = G A \gamma + d_Q \gamma_{,t}, \quad (43)$$

$$\text{Geometrical relations: } \kappa = \psi_{,x}, \quad \gamma = \psi + w_{,x}, \quad (44)$$

$$\text{Deflection-velocity relations: } v = w_{,t}, \quad \omega = \psi_{,t}, \quad (45)$$

$$\text{Boundary conditions: } M = \hat{M}, \quad Q = \hat{Q}, \quad x = 0, \quad (46)$$

$$w = \hat{w}, \quad \psi = \hat{\psi}, \quad x = x_1. \quad (47)$$

The energy flow density vector  $q$  and the energy flow potential  $\varphi$  are respectively defined as

$$q = -(vQ + \omega M), \quad \varphi = -\varphi_{,x}. \quad (48)$$

The energy flow equations and their time averaged forms for stationary random processes are the same as those derived in equations (31) and (32), respectively. However, in this case, the relevant quantities are defined as follows:

$$\begin{aligned} \hat{q}_0 &= -(v_0 \hat{Q} + \omega_0 \hat{M}), \quad \hat{q}_1 = -(Q_1 \hat{w}_{,t} + M_1 \hat{\psi}_{,t}), \quad K = \rho(Av^2 + I\omega^2)/2, \\ \hat{q}_f &= v\hat{f}, \quad U = (CJ\kappa^2 + GA\gamma^2)/2, \quad D = \int_{t_0}^t (d_M \kappa_{,t} \kappa_{,t} + d_Q \gamma_{,t} \gamma_{,t}) dt. \end{aligned}$$

## 6. Shear Plate

In the following analysis, the subscripts  $\alpha$  and  $\beta$  take values 1 or 2 and the repeated subscript summation convention applies. For example, the plate stress-resultants described by the transverse shear force  $Q_\alpha$  and the moment  $M_{\alpha\beta}$  per unit length, the unit outward normal vector  $\nu_\alpha$  and the unit tangent vector  $\tau_\alpha$  of the midplane of the plate have components  $Q_1, Q_2, M_{11}, M_{12}$ , etc. This notation allows the governing equations describing the linear dynamics of a shear plate to be expressed in the forms (Reismann and Pawlik 1980):

$$\text{Dynamic equations: } Q_{\alpha,\alpha} + \hat{f} = \rho h v_{,t}, \quad (49)$$

$$M_{\alpha\beta,\beta} - Q_\alpha = \rho I \omega_{\alpha,t}, \quad (50)$$

## ENERGY FLOW EQUATION

$$\text{Constitutive equations: } M_{\alpha\beta} = D[(1-\mu)\kappa_{\alpha\beta} + \mu\kappa\delta_{\alpha\beta}] + d_M[(1-\mu)\kappa_{\alpha\beta,t} + \mu\kappa_{,t}\delta_{\alpha\beta}], \quad (51)$$

$$Q_\alpha = Gh\gamma_\alpha + d_Q\gamma_{\alpha,t}, \quad (52)$$

$$\text{Geometrical relations: } \kappa_{\alpha\beta} = (\psi_{\alpha,\beta} + \psi_{\beta,\alpha})/2, \quad (53)$$

$$\gamma_\alpha = \psi_\alpha + w_{,\alpha}, \quad \kappa = \psi_{\alpha,\alpha}, \quad (54)$$

$$\text{Deflection-velocity relations: } v = w_{,t}, \quad \omega_\alpha = \psi_{\alpha,t}, \quad (55)$$

$$\text{Boundary conditions: } w = \hat{w}, \quad \psi^\nu = \hat{\psi}^\nu \quad \text{on } S_d, \quad (56)$$

$$M^\nu = M_{\alpha\beta}\nu_\alpha\nu_\beta = \hat{M}^\nu \quad \text{on } S_f, \quad (57)$$

$$Q^\nu + M_{,\tau}^{\nu\tau} = \hat{Q}^\nu + \hat{M}_{,\tau}^{\nu\tau} \quad \text{on } S_f, \quad (58)$$

where

$$M^{\nu\tau} = \epsilon_{3\alpha\beta}\nu_\alpha M_\beta^\nu = \epsilon_{3\alpha\beta}\nu_\alpha M_{\beta\gamma}\nu_\gamma. \quad (59)$$

The energy flow density vector  $q_\alpha$  is defined as

$$q_\alpha = -(vQ_\alpha + \omega_\beta M_{\beta\alpha}). \quad (60)$$

If  $q_{2,1} = q_{1,2}$ , there exists an energy potential  $\varphi$  satisfying

$$q_\alpha = -\varphi_{,\alpha}. \quad (61)$$

The energy flow equation is

$$q_{\alpha,\alpha} = \hat{q}_f - \dot{E} - \dot{D}, \quad q^\nu = \hat{q}_d^\nu \quad \text{on } S_d, \quad q^\nu = \hat{q}_f^\nu \quad \text{on } S_f, \quad (62)$$

where

$$\begin{aligned} \hat{q}_f &= v\hat{f}, \quad \hat{q}_d^\nu = -(\hat{w}_{,t}Q^\nu + \hat{\psi}_{,t}^\nu M^\nu), \quad \hat{q}_f^\nu = -(\hat{Q}^\nu w_{,t} + \hat{\psi}_{,t}^\nu \hat{M}^\nu), \\ K &= \rho(hv^2 + I\omega_\alpha\omega_\alpha)/2, \quad U = [D(1-\mu)\kappa_{\alpha\beta}\kappa_{\alpha\beta} + \mu\kappa\kappa + Gh\gamma_\alpha\gamma_\alpha]/2, \\ D &= \int_{t_0}^t (d_M\kappa_{\alpha\beta,t}\kappa_{\alpha\beta,t} + d_Q\gamma_{\alpha,t}\gamma_{\alpha,t})dt. \end{aligned}$$

## 7. Circular Plate under Concentrated Load

Let us examine a clamped, circular plate of radius  $a$ , acted upon by a transverse concentrated load  $\hat{f} = F(t)$  at the centre of the plate. In this example, it is convenient to use a plane polar coordinate system  $(r, \theta)$ . Because of axial symmetry, the rotation  $\psi_\theta = 0$  and the rotation  $\psi_r$  and the deflection  $w$  of the plate are functions dependent only on  $r$  and  $t$ . According to the equations given in section 6, the energy flow equations described in equations (62) reduce to

$$(rq_r)_{,r}/r = w_{,t}F(t)\delta(r) - \dot{E} - \dot{D} \quad \text{for } 0 < r < a, \quad q_r(a, t) = 0, \quad (63)$$

assuming  $q_r(0, t)$  is bounded. The energy flow density vector  $q_r$  lies along the radial direction and the energy flow lines are a set of lines radiating from the centre of the plate. Furthermore, from equation (61), the energy flow potential  $\phi$  can be obtained and the resultant equipotential surfaces are a set of increasing radial circles around the centre of the plate.

An integration of equation (63) over the circular area of radius  $r$ , ( $r \leq a$ ), gives

$$2\pi r q_r = w_{,t}(0, t)F(t) - \int_0^r 2\pi r \dot{E} dr - \int_0^r 2\pi r \dot{D} dr. \quad (64)$$

For a stationary random process or a sinusoidal excitation, the time average of this equation takes the form

$$2\pi r \langle q_r \rangle = \langle w_{,t}(0, t)F(t) \rangle - \int_0^r 2\pi r \langle \dot{D} \rangle dr. \quad (65)$$

Letting the integration radius  $r = a$  and using the boundary condition given in equation (63) produces the result

$$\langle w_{,t}(0, t)F(t) \rangle = \int_0^a 2\pi r \langle \dot{D} \rangle dr. \quad (66)$$

This demonstrates that the average energy input of the load is totally absorbed by the damping of the material of the plate. If the latter is neglected then the average energy input of the load must be zero to keep the motion of the plate bounded.

## 8. Discussion: Energy Flow Potential and Thermal Analogy

In some analyses of power flow, it has been hypothesized that the energy flux density may be represented by a gradient of total energy density (for example, Nefske and Sung, 1987). As previously discussed, the necessary and sufficient conditions for the existence of an energy flow potential expressed in equation (12) is that the energy flow density vector field is irrotational, i.e. equation (13) is valid. For the structural members described in sections 3-5, this condition is valid and an energy potential exists. As an example, let us further investigate the rod in tension or compression as described in section 3. From equations (30)-(31) it follows that

$$q = \int_0^x (\hat{q}_f - \dot{E} - \dot{D}) dx + \hat{q}_0, \quad \hat{q}_1 = \int_0^{x_1} (\hat{q}_f - \dot{E} - \dot{D}) dx + \hat{q}_0, \quad (67)$$

$$\phi = - \int_0^x \left[ \int_0^\xi (\hat{q}_f - \dot{E} - \dot{D}) d\xi + \hat{q}_0 \right] dx + \phi(0, t), \quad (68)$$

## ENERGY FLOW EQUATION

where  $\phi(0, t)$  denotes the value of the energy flow potential  $\phi$  at the end  $x = 0$  which is assumed zero if this end is chosen as the base point of the energy flow potential. Equation (68) shows that the energy flow potential depends on the rate of energy input  $\dot{q}_f$ , the rate of change of mechanical energy  $\dot{E}$  and the rate of energy dissipation  $\dot{D}$ . Therefore, in a general case, it may be difficult to represent it only by the total mechanical energy density  $E$ .

To examine the thermal energy analogy hypothesis, let us assume that the rod discussed in section 3 is now replaced by a semi-infinite nonviscous rod (i.e.  $\dot{D} = 0$ ) such that  $x_1 = \infty$  with no waves reflected. It is thus of interest to examine how the energy of the wave produced by the force applied at  $x = 0$  transmits along the rod. The general solution of this problem is represented by

$$u(x, t) = f(x - ct). \quad (69)$$

This corresponds to the following densities of strain and kinetic energy and energy flow density vector

$$U = \frac{C}{2} f'^2, \quad K = \frac{\rho c^2}{2} f'^2, \quad q = Cc f'^2, \quad (70)$$

respectively, where  $f'(\xi) = df/d\xi$ . Using the relation  $c^2 = C/\rho$  and equation (17), we obtain

$$U = K = \frac{E}{2}, \quad q = cE. \quad (71)$$

From the energy flow equation (31), the energy transmission along the rod is given by the first order partial differential equation

$$cE_{,x} + E_{,t} = 0, \quad (72)$$

subject to the boundary condition  $E(0, t) = \dot{q}/c$  at  $x = 0$ . The behaviour of this equation is not similar to the one representing the flow of thermal energy in a heat conduction problem, (see, for example, Courant & Hilbert 1962). If the rod is of finite length, reflected waves occur at  $x_1$  and this simple equation becomes invalid. Therefore, from this analysis, we conclude that, in general, there lacks a direct similarity between the flow of mechanical energy through a structural system and the flow of thermal energy in a heat conduction problem confirming the findings of Carcaterra & Sestieri (1995) and the development of any hypothesis or modelling based on such analogy is of limited value.

## References

- Carcaterra, A. and Sestieri, A. (1995) Energy density equations and power flow in structures, *Journal of Sound and Vibration* **188**(2), 269-282.

- Courant, R. & Hilbert, D. (1962) *Methods of mathematical physics*, Interscience, New York.
- Fahy, F. J. (1994) Statistical energy analysis: a critical overview, *Phil. Trans. R. S. Lond. A* **346**, 431-447.
- Fung, Y. C. (1977) *A first course in continuum mechanics*, Prentice-Hall, New Jersey.
- Goyder, H. G. D. and White, R. G. (1980a) Vibrational power flow from machines into buildup structures, part I: introduction and approximate analysis of beam and plate-like foundations, *Journal of Sound and Vibration* **68**(1), 59-75.
- Goyder, H. G. D. and White, R. G. (1980b) Vibrational power flow from machines into buildup structures, part II: wave propagation and power flow in beam-stiffened plates, *Journal of Sound and Vibration* **68**(1), 77-96.
- Goyder, H. G. D. and White, R. G. (1980c), Vibrational power flow from machines into buildup structures, part III: power flow through isolation systems, *Journal of Sound and Vibration* **68**(1), 97-117.
- Green, A. E. and Zerna, W. (1954) *Theoretical elasticity*, Oxford University Press.
- Keane, A. J. and Price, W. G., eds. (1997) *Statistical energy analysis: an overview, with applications in structural dynamics*, Cambridge University Press.
- Love, A. E. H. (1927) *A treatise on the mathematical theory of elasticity*, 4th ed., Cambridge University Press.
- Lyon, R. H. and Maidanik, G. (1962) Power flow between linearly coupled oscillators, *J. Acoust. Soc. Amer.* **34**(5), 623-639.
- Lyon, R. H. (1975) *Statistical energy analysis of dynamic systems*, MIT Press, Cambridge Massachusetts.
- Nefske, D. J. and Sung, S. H. (1987) Power flow finite element analysis of dynamic systems: basic theory and application to beams, in K. H. Hsu, D. J. Nefske and A. Akay (eds.), *Statistical energy analysis*, (ASME special publication NCA-3), ASME, New York.
- Newland, D. E. (1975) *An introduction to random vibrations and spectral analysis*, 2nd ed., Longman, London.
- Price, W. G. and Bishop, R. E. D. (1974) *Probabilistic theory of ship dynamics*, Chapman and Hall, London.
- Reismann, H. and Pawlik, P. S. (1980) *Elasticity theory and applications*, Wiley, New York.
- Scharton, T. D. and Lyon, R. H. (1968) Power flow and energy sharing in random vibration, *J. Acoust. Soc. Amer.* **43**(6), 1332-1343.
- Timoshenko, S. P., Young, D. H. and Weaver, W. (1974) *Vibration problems in engineering*, 4th ed., Wiley, New York.
- Wohlever, J. C. and Bernhard, R. J. (1992) Mechanical energy flow models of rods and beams, *Journal of Sound and Vibration* **153**(1), 1-19.
- Xing, J. T. and Price, W. G. (1997) An energy or power flow analysis based on continuum dynamics, (To appear).

## A NOTE ON CONSERVATIVE AND NON-CONSERVATIVE COUPLING

C. R. FREDÖ  
*Ingemansson Technology AB*  
*Box 276, S-401 24 Gothenburg, Sweden*

### 1. Introduction

**Statistical Energy Analysis (SEA)** [1] is a useful tool for investigating transmission paths for sound and vibration. A well-known disadvantage of SEA is that it is difficult to treat systems in which high losses occurs between the subsystems. A solution to this dilemma would be to include the non-conservative coupling element as a subsystem and, by this way turn the system into a conservatively coupled case. However, it is well known that the conventional three-subsystem model [2] cannot be collapsed into a meaningful non-conservatively coupled two-subsystem model. The problem can therefore not always be avoided by introduction of an additional subsystem. Practical problems may as well arise for cases where it is problematic to excite the intermediate element.

This fact highlights that the conventional three-subsystem model is a reduced model. It has been previously shown by several authors [3-6] that a conservatively coupled three-subsystem model requires introduction of so called indirect couplings to become complete.

The indirect couplings account for the transfer of power across subsystem 2. This type of coupling is believed to account for the non-resonant transfer path between subsystems 1 and 3 and, in fact, has been included in SEA for some special cases. Most notable is the so called 'mass-law' another example is coupling via the stiffness of the intermediate element.

The subsystem response in SEA is normally considered to be resonant. A non-resonant path across an intermediate subsystem does therefore not effect the resonant energy of the intermediate subsystem. One motivation to why indirect transmission is considered to be non-resonant is that the non-resonant part of the energy in a subsystem cannot store energy and, thus is inefficient at destroying power in this element.

However, the non-resonant behaviour of the subsystem can yield a mechanism that is effective at transferring power across the element.

As mentioned above, the so-called 'mass-law' of a limp wall between two rooms is a well known example of non-resonant transmission. The vibrational level of the wall does not matter as long as it is not related to the indirect transmission, e.g. vibration introduced from structural coupling does not effect the sound transmission since a limp wall is unable to radiate this vibration into any of the connecting rooms. Another motivation is that the transmission across a limp wall is invariant to dissipation in the wall. The transmission mechanism must therefore be non-resonant

It may at first seem strange to connect indirect couplings that are insensitive to the dissipation in the intermediate element with non-conservative coupling that consumes power in the element. However, an energy flow model that incorporates indirect and direct coupling can be shown to yield a complete solution for the conservatively coupled three-subsystem case. It should therefore be possible to obtain information about the non-conservatively coupled case simply by reducing the information that is used to yield the complete solution. The order of presentation is therefore to first examine the conservatively case and thereafter to continue with the non-conservatively coupled case.

## 2. Theory

The investigated case consists of three rectangular plates coupled along simply supported joints, as depicted in Figure 1(a). The interaction between the plates is carried out by moments. Excitation is provided by forces of rain-on-the-roof character. The analysis is based on thin plate theory with homogeneous, isotropic plates of uniform thickness and applies for modal and viscous damping. Only viscous damping will be discussed as modal damping complicates the presentation. The model can be applied to plate edge boundary conditions that allow the eigenmodes to be divided in separate shape functions. Note that the plates incorporate bending (out-of-plane) motion only.

The approach which is used in this study was originally developed for beams by Davies *et al* [7] and later extended to plates by Dimitriadis *et al* [8,6]. The derivation is lengthy and the idea is therefore to sketch only the basic steps of the analysis and their outcome. A more detailed examination is given in references [6,9]

The power that is injected into the subsystems, the power that is transmitted across the junctions, the kinetic energy for the plates and the power that is dissipated in each subsystem can be written as

$$\begin{Bmatrix} S_{P_{in,1}} \\ S_{P_{in,2}} \\ S_{P_{in,3}} \end{Bmatrix} = \begin{bmatrix} V_1 & 0 & 0 \\ 0 & V_2 & 0 \\ 0 & 0 & V_3 \end{bmatrix} \begin{Bmatrix} S_1 \\ S_2 \\ S_3 \end{Bmatrix} = [V] \begin{Bmatrix} S_1 \\ S_2 \\ S_3 \end{Bmatrix}, \quad (1)$$



$$\begin{Bmatrix} S_{P_{1 \rightarrow 2}} \\ S_{P_{3 \rightarrow 2}} \end{Bmatrix} = \begin{bmatrix} PP_{21} & PP_{12} & PP_{13} \\ PP_{31} & PP_{32} & PP_{23} \end{bmatrix} \begin{Bmatrix} S_1 \\ S_2 \\ S_3 \end{Bmatrix} = [PP] \begin{Bmatrix} S_1 \\ S_2 \\ S_3 \end{Bmatrix}, \quad (2)$$

$$\begin{Bmatrix} S_{E_1} \\ S_{E_2} \\ S_{E_3} \end{Bmatrix} = \begin{bmatrix} R_{11} & R_{12} & R_{13} \\ R_{21} & R_{22} & R_{23} \\ R_{31} & R_{32} & R_{33} \end{bmatrix} \begin{Bmatrix} S_1 \\ S_2 \\ S_3 \end{Bmatrix} = [R] \begin{Bmatrix} S_1 \\ S_2 \\ S_3 \end{Bmatrix}, \quad (3)$$

and

$$\begin{Bmatrix} S_{P_{dis,1}} \\ S_{P_{dis,2}} \\ S_{P_{dis,3}} \end{Bmatrix} = \begin{bmatrix} U_{11} & U_{12} & U_{13} \\ U_{21} & U_{22} & U_{23} \\ U_{31} & U_{32} & U_{33} \end{bmatrix} \begin{Bmatrix} S_1 \\ S_2 \\ S_3 \end{Bmatrix} = [U] \begin{Bmatrix} S_1 \\ S_2 \\ S_3 \end{Bmatrix} \quad (4)$$

for subsystems 1, 2 and 3, respectively. The direction of the arrow in the subscript of the energy flow  $S_{P_{i \rightarrow j}}$  indicates the direction of the energy flow that is considered to have positive sign. The rain-on-the-roof excitations are denoted as  $S_j$ .

The content of equation (3) is similar to what has been obtained previously by other authors. Equation (3) is identical to the so called "energy influence coefficients" that were introduced by Guyader *et al* in reference [10]. Equation (3) is similar (and in some situations identical) to the "Greens function" that Langley used in reference [4].

The power balance can also be expressed as a function of the energy flow and the power that is dissipated in each subsystem, i.e. as

$$\begin{Bmatrix} S_{P_{in,1}} \\ S_{P_{in,2}} \\ S_{P_{in,3}} \end{Bmatrix} = [V] \begin{Bmatrix} S_1 \\ S_2 \\ S_3 \end{Bmatrix} = ([U] + [PP]) \begin{Bmatrix} S_1 \\ S_2 \\ S_3 \end{Bmatrix}. \quad (5)$$

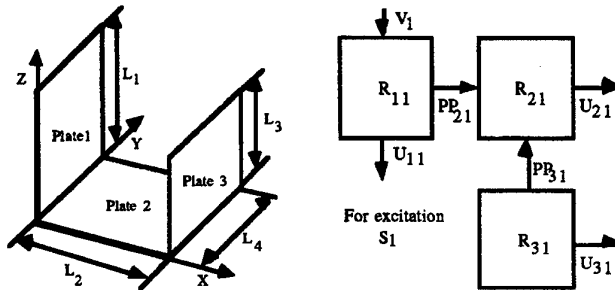


Figure 1 a) The U-shaped plate assembly. The plates are considered to be rectangular, thin and simply supported in the analytical model. b) The conceptual energy flow balance for the case where rain-on-the-roof excitation acts in plate 1.

### 2.1. CONSERVATIVE COUPLING: UNCOUPLED SUBSYSTEM ENERGY

The average energy of an uncoupled plate that is subjected to rain-on-the-roof excitation can be shown to be [6,7]

$$\langle E_{av,j} \rangle = \frac{\pi S_j}{2\epsilon_j A_j} n_j(\omega) \quad , \text{ and } \theta_j = \frac{\pi S_j}{2\epsilon_j A_j} \quad , \quad (6a,b)$$

where the energy per mode is signified by  $\theta_j$  and the average density of uncoupled modes is denoted as  $n_j(\omega)$ . Specific viscous damping is denoted as  $\epsilon_j$  and plate area is denoted  $A_j$ . A feature which is oftentimes forgotten is that the excitation ( $S_j$ ) is a part of the energy per uncoupled mode (it would otherwise be normalised with respect to the spectral density of the excitation). This fact implies that the average energy per uncoupled mode, by definition, must be zero for a receiving subsystem when excitation occurs only in the sending subsystem.

This fact is, perhaps better understood if one states that a receiving subsystem cannot be uncoupled if it receives power from another subsystem that is connected to it. The receiving subsystem must in this situation, by definition, be of the coupled type.

The dissipative powers fulfil

$$\frac{U_{13}}{U_{31}} = \frac{\epsilon_1 A_1}{\epsilon_3 A_3} \quad , \quad \frac{U_{12}}{U_{21}} = \frac{\epsilon_1 A_1}{\epsilon_2 A_2} \quad \text{and} \quad \frac{U_{32}}{U_{23}} = \frac{\epsilon_3 A_3}{\epsilon_2 A_2} \quad , \quad (6c-e)$$

which happens to be the same as the ratio between the uncoupled average energies per mode. This fact can be used together with the knowledge that the energy flow out from subsystem 1 equals the power that is dissipated in subsystems 2 and 3

$$PP_{21} = U_{21} + U_{31} \quad , \text{ and that } PP_{31} = U_{31} \quad . \quad (6f,g)$$

Similar findings apply for the other energy flow components.

The energy flow can thus be re-expressed as a function of the average uncoupled, i.e. as

$$S_{P_{1 \rightarrow 2}} = U_{21} \left( S_1 - \frac{\epsilon_1 A_1}{\epsilon_2 A_2} S_2 \right) + U_{31} \left( S_1 - \frac{\epsilon_1 A_1}{\epsilon_3 A_3} S_3 \right) = \omega \eta_{12} n_1 (\theta_1 - \theta_2) + \omega \eta'_{13} n_1 (\theta_1 - \theta_3). \quad (7a)$$

and

$$S_{P_{3 \rightarrow 2}} = U_{23} \left( S_3 - \frac{\epsilon_3 A_3}{\epsilon_2 A_2} S_2 \right) + U_{13} \left( S_3 - \frac{\epsilon_3 A_3}{\epsilon_1 A_1} S_1 \right) = \omega \eta_{32} n_3 (\theta_3 - \theta_2) + \omega \eta'_{31} n_3 (\theta_3 - \theta_1). \quad (7b)$$

Equation (7a,b) shows that the conservatively coupled three-subsystem case can be put in a form where the energy flows become functions of the average energy per mode. Two additional, so called, indirect couplings must be introduced to yield this solution.

## 2.2. CONSERVATIVE COUPLING: COUPLED SUBSYSTEM ENERGY

Equation (1) can be rewritten as a function of subsystem energy

$$\begin{Bmatrix} S_{P_{in,1}} \\ S_{P_{in,2}} \\ S_{P_{in,3}} \end{Bmatrix} = [V][R]^{-1} \begin{Bmatrix} S_{E_1} \\ S_{E_2} \\ S_{E_3} \end{Bmatrix} = \omega \begin{bmatrix} \eta_{11} + \eta_{12} + \eta'_{13} & -\eta_{21} & -\eta'_{31} \\ -\eta_{12} & \eta_{22} + \eta_{21} + \eta_{23} & -\eta_{32} \\ -\eta'_{13} & -\eta_{23} & \eta_{33} + \eta'_{31} + \eta_{32} \end{bmatrix} \begin{Bmatrix} S_{E_1} \\ S_{E_2} \\ S_{E_3} \end{Bmatrix}. \quad (8)$$

The form of equation (8) is found if the parts of equation (5) is solved separately and thereafter assembled. No terms in the matrix  $[V][R]^{-1}$  become zero as is normally assumed in SEA. Therefore, coupling coefficients should also be introduced for the two plates that are not directly coupled to each other, i.e. indirect couplings should be included to yield a complete solution for the power input balance.

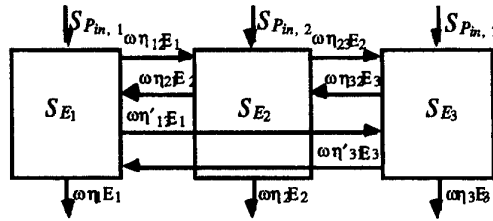


Figure 2. The extended energy flow model with its subsystems, kinetic energies ( $S_{Ej}$ ), power inputs ( $S_{Pj}$ ), energy flow components ( $\omega \eta_{ij} E_j$ ) and power losses ( $\omega \eta_j E_j$ ). Note that the spectral density of the subsystem energy is abbreviated to  $E_j$  for the energy flow components and the power losses.

## 2.3. TERMINOLOGY

The energy flows of equation (2) can be rewritten to become a function of coupled subsystem energy

$$\begin{Bmatrix} S_{P_{1 \rightarrow 2}} \\ S_{P_{3 \rightarrow 2}} \end{Bmatrix} = [PP][R]^{-1} \begin{Bmatrix} S_{E_1} \\ S_{E_2} \\ S_{E_3} \end{Bmatrix} = \begin{bmatrix} (\eta_{12} + \eta'_{13}) & -\eta_{21} & -\eta'_{31} \\ -\eta'_{13} & -\eta_{23} & (\eta_{32} + \eta'_{31}) \end{bmatrix} \begin{Bmatrix} S_{E_1} \\ S_{E_2} \\ S_{E_3} \end{Bmatrix}. \quad (9)$$

Comparison of equation (7) and equation (9) shows that the energy flows can be expressed as a function of uncoupled and as a function of coupled subsystem energy. Scrutiny of the equations shows that the couplings change when they are changed to from a function of uncoupled to become a function of coupled energy. The change in the couplings is the same as

$$\begin{pmatrix} \langle E_{av, 1} \rangle \\ \langle E_{av, 2} \rangle \\ \langle E_{av, 3} \rangle \end{pmatrix} = \begin{bmatrix} \pi n_1 / 2 \epsilon_1 A_1 & 0 & 0 \\ 0 & \pi n_2 / 2 \epsilon_2 A_2 & 0 \\ 0 & 0 & \pi n_3 / 2 \epsilon_3 A_3 \end{bmatrix} [R]^{-1} \begin{pmatrix} S_{E_1} \\ S_{E_2} \\ S_{E_3} \end{pmatrix}, \quad (10)$$

which can differ markedly from unity.

Equation (10) shows that it is advisable to ideologically separate couplings that refer to the uncoupled case from those that belong to the coupled case. The couplings, again, change if the energy flows ( $P_{ij}$ ) are instead extracted from ensembles or other 'statistical' situations rather than from the single case in equation (7a,b).

Discussion can therefore easily be confused when these factors cannot be clearly distinguished from each other. The following terminology is therefore adopted: factors that refer to average energy per mode (and a weak coupling approx. of coupled energy) and energy flows that refer to 'statistical' (archetypal) situations are termed Coupling Loss Factors (CLFs) (as is commonplace today); factors that refer to average uncoupled energy and energy flows for a particular case is termed Uncoupled Energy Flow Coefficients (UEFCs); and factors that refer to coupled subsystem energy and energy flows for a particular case are termed Coupled Energy Flow Coefficients (CEFCs).

The CLF, the UEFC and the CEFC are expected to become identical in situations where the archetypal trend starts to show in the single case. Note that the notation in the algebra does not cater for the above mentioned differences and that the same coefficients merrily are used for various coupling types without further censure.

#### 2.4. NON-CONSERVATIVE COUPLING: UNCOUPLED SUBSYSTEM ENERGY

The flow of energy in equation (7a,b) becomes

$$S_{P_{1 \rightarrow 2}} = \omega \eta_{12} n_1 \theta_1 + \omega \eta'_{13} n_1 (\theta_1 - \theta_3), \text{ and } S_{P_{3 \rightarrow 2}} = \omega \eta_{32} n_3 \theta_3 + \omega \eta'_{31} n_3 (\theta_3 - \theta_1) \quad (11a,b)$$

respectively, when no excitation occurs in subsystem 2, i.e. when, by definition  $\theta_2 = 0$ . Unfortunately, equation (11a,b) does not support 'energy flow reciprocity' which makes it less attractive for introduction into a non-conservative two-subsystem model.

However, it can be seen from equation (11a,b) that the energy flow that is communicated between subsystems 1 and 3 yields a transmission path that fulfils the requirement of 'energy flow reciprocity' and is

$$S_{P_{1 \rightarrow 3}} = \omega \eta'_{13} n_1 (\theta_1 - \theta_3). \quad (12)$$

The case that is considered to produce positive values for  $S_{P_{1 \rightarrow 3}}$  is when energy flows in the direction from subsystem 1 to subsystem 3 equation (12) applies for energy-flow across the *fictitious* subsystem interface of Figure 3(b).

The power balance can, after some steps of algebra, be stated as

$$S_{P_{in},1} = \omega (\eta_1 + \eta_{12} + \eta'_{13}) n_1 \theta_1, \text{ and } S_{P_{in},3} = \omega (\eta_3 + \eta_{32} + \eta'_{31}) n_3 \theta_3, \quad (13a,b)$$

for subsystems 1 and 3, respectively (Figure 3(c)).

Introducing the weak coupling approximation  $E_j = n_j \theta_j$  for the coupled subsystem energy yields, after some extra steps and further motivation, the approximate power balance

$$\begin{Bmatrix} S_{P_{in},1} \\ S_{P_{in},3} \end{Bmatrix} = \omega \begin{bmatrix} (\eta_1 + \eta_{12} + \eta'_{13}) & -\eta'_{31} \\ -\eta'_{13} & (\eta_3 + \eta_{32} + \eta'_{31}) \end{bmatrix} \begin{Bmatrix} S_{E_1} \\ S_{E_3} \end{Bmatrix}. \quad (14a,b)$$

The difference between equation (13a,b) and equation (14a,b) may at first seem surprising but is invoked by that fact that a response (that is larger than zero) cannot exist in the receiving subsystem in equation (13a,b) without violating the total power balance of the system.

Equation (14a,b) shows that the non-conservative case can be introduced into SEA if indirect Coupling Loss Factors (CLFs) and suitable radiation factors are derived. However, few indirect CLFs are available today. Development of such factors is desirable as it shows promise at expanding the applicability of SEA to a wider range of cases.

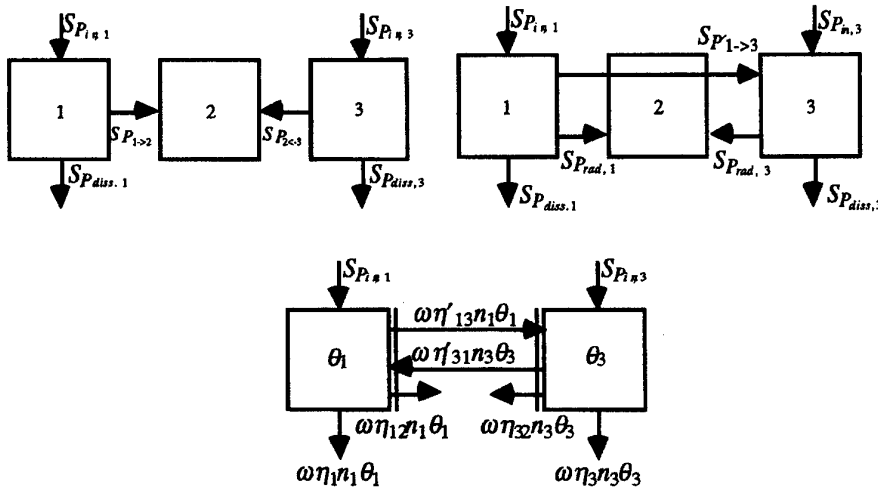


Figure 3 a) The energy flow model in which the physical subsystem interfaces are used. b) The conceptual energy flow balance in which the energy flows of Figure 3(a) are re-expressed into one indirect and two radiating paths. c) The non-conservatively coupled energy flow model the way it can be expressed in SEA. The dashed lines symbolise the fictitious subsystem interface that must be introduced into the model.

## 2.5. NON-CONSERVATIVE COUPLING: COUPLED SUBSYSTEM ENERGY

Most measurements or calculations refer to systems in which a response occurs in the receiving subsystem. It is obvious that such cases, by definition, must refer to coupled rather than uncoupled subsystem energy. The weak coupling approximation of the coupled subsystem energy may not be sufficient for all of these cases.

The experience from the discussion above is that one should be cautious not to take the benefits of the uncoupled subsystem energy for granted also for coupled subsystem energy. A separate evaluation is therefore motivated for this kind of subsystem response coordinate.

The power that is injected into the subsystems, the kinetic energy for the plates and the energy flow out of plates 1 and 3 and the power that is dissipated in the plates can be written as

$$\begin{Bmatrix} S_{P_{in,1}} \\ S_{P_{in,3}} \end{Bmatrix} = \begin{bmatrix} V_1 & 0 \\ 0 & V_3 \end{bmatrix} \begin{Bmatrix} S_1 \\ S_3 \end{Bmatrix} = [V'] \begin{Bmatrix} S_1 \\ S_3 \end{Bmatrix}, \quad (15)$$

$$\begin{Bmatrix} S_{E_1} \\ S_{E_3} \end{Bmatrix} = \begin{bmatrix} R_{11} & R_{13} \\ R_{31} & R_{33} \end{bmatrix} \begin{Bmatrix} S_1 \\ S_3 \end{Bmatrix} = [R'] \begin{Bmatrix} S_1 \\ S_3 \end{Bmatrix}, \quad (16)$$

and

$$\begin{Bmatrix} S_{P_{1 \rightarrow}} \\ S_{P_{3 \rightarrow}} \end{Bmatrix} = \begin{bmatrix} PP_{21} & PP_{13} \\ PP_{31} & PP_{23} \end{bmatrix} \begin{Bmatrix} S_1 \\ S_3 \end{Bmatrix}, \quad (17)$$

respectively. Note that equation (17) does not contain the symmetry that is required.

The energy flow out from the subsystems can be rewritten as

$$\begin{aligned} \begin{Bmatrix} S_{P_{1 \rightarrow}} \\ S_{P_{3 \rightarrow}} \end{Bmatrix} &= \begin{bmatrix} U_{21} - PP_{31} & PP_{13} \\ PP_{31} & U_{23} - PP_{13} \end{bmatrix} \begin{Bmatrix} S_1 \\ S_3 \end{Bmatrix} = ([U'] + [PP']) [R']^{-1} \begin{Bmatrix} S_1 \\ S_3 \end{Bmatrix} = \\ &= \omega \left( \begin{bmatrix} \eta_{12(1)} & \eta_{32(1)} \\ \eta_{12(3)} & \eta_{32(3)} \end{bmatrix} + \begin{bmatrix} \eta'_{13} & -\eta'_{31} \\ -\eta'_{13} & \eta'_{31} \end{bmatrix} \right) \begin{Bmatrix} S_{E_1} \\ S_{E_3} \end{Bmatrix}, \quad (18) \end{aligned}$$

where the power that is dissipated in the intermediate element (the  $U_{ij}$  terms on the diagonal) has been separated from the energy flow between subsystems 1 and 3.

Equation (15) thus becomes

$$\begin{Bmatrix} S_{P_{in,1}} \\ S_{P_{in,3}} \end{Bmatrix} = [V'] [R']^{-1} \begin{Bmatrix} S_{E_1} \\ S_{E_3} \end{Bmatrix} = \omega \begin{bmatrix} (\eta_{11} + \eta_{12(1)} + \eta'_{13}) & -(\eta'_{31} + \eta_{32(1)}) \\ -(\eta_{12(3)} + \eta'_{13}) & (\eta_{33} + \eta'_{31} + \eta_{32(3)}) \end{bmatrix} \begin{Bmatrix} S_{E_1} \\ S_{E_3} \end{Bmatrix}, \quad (19)$$

when it is rewritten to become a function of coupled subsystem energy.

Two additional, (off-diagonal) radiation factors can be seen to appear in equation (18). Therefore, no terms in the matrix  $[V][R]^{-1}$  can be separated purely from a knowledge of the power inputs and subsystem responses. To access the complete information content in the right hand side of equation (19) requires explicit knowledge of the energy flows and the dissipative powers. Therefore, the input power balance must be given the simplified interpretation

$$\begin{aligned} \begin{Bmatrix} S_{Pin,1} \\ S_{Pin,3} \end{Bmatrix} &= \omega \begin{bmatrix} (\alpha_1 + \alpha_{12} + \alpha'_{13}) & -\alpha'_{31} \\ -\alpha'_{13} & (\alpha_3 + \alpha_{32} + \alpha'_{31}) \end{bmatrix} \begin{Bmatrix} S_{E1} \\ S_{E3} \end{Bmatrix} \\ &= \omega \begin{bmatrix} (\alpha_{1tor} + \alpha'_{13}) & -\alpha'_{31} \\ -\alpha'_{13} & (\alpha_{3tor} + \alpha'_{31}) \end{bmatrix} \begin{Bmatrix} S_{E1} \\ S_{E3} \end{Bmatrix} \end{aligned} \quad (20)$$

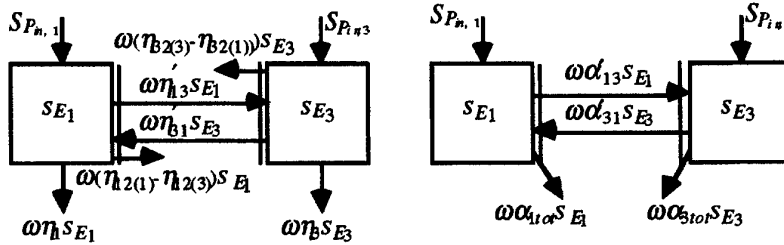


Figure 4. The energy flow model for the non-conservatively coupled two-subsystem case in which coupled subsystem energy is utilised. a) The complete model for the case of viscous damping. b) A simplified interpretation of the input power balance. The inclination of the two lowest arrows signifies that the radiation, re-radiation and dissipation is combined and treated as a single factor.

Note that the power input is explicitly balanced by equation (20). It is only the function of the *pseudo* coupling and loss factor data that is inaccurately interpreted with respect to the derivation of the energy-flow. The form of equation (20) is identical with the results of other authors, e.g. [11-13], even though types of subsystem response coordinates other than coupled subsystem energy have been used in these examinations.

Furthermore, comparison of the simplified interpretation (equation (20)) and the weak coupling approximation (equation (14a,b)) shows close similarity. Therefore, it may be anticipated that the simplified interpretation of the power balance improves when the coupled subsystem energy resembles the uncoupled subsystem energy.

However, one should be cautious not to draw too much on this similarity and the experience from the conservatively coupled two-subsystem case. The author's experience from numerical simulations is that the success of equation (20) does not depend on the strength of the indirect coupling. What matters is how large the on-diagonal radiation factor is in comparison with a subsystem's Dissipation Loss Factor (DLF). Cases in which one subsystem's DLF is smaller than its radiation factors can be shown to yield satisfactory estimates of the energy flow when this subsystem is the excited subsystem,

while poor results are obtained when the situation is the reverse and it instead becomes the receiving subsystem.

In short, such cases can be expected when a receiving subsystem is unable to destroy the power transfer from an indirectly connected subsystem (which is where the source is located). This type of cases is invoked when the receiving subsystem is either lightly damped or is unable to accumulate energy. Examples of the latter are when the subsystem is rigid, limp or at anti-resonant frequencies. An explanation for this 'asymmetric' behaviour is given below.

The power balance of the total system is obtained by summing the rows of equation (19), which yields

$$S_{P_{in,1}} + S_{P_{in,3}} = \omega \{ (\eta_1 + \eta_{12(1)} - \eta_{12(3)}) S_{E_1} + (\eta_3 - \eta_{32(1)} + \eta_{32(3)}) S_{E_3} \} \quad (21)$$

Comparison of the subsystem and total system power balances of equation (20) and equation (21), respectively, shows that

$$\begin{aligned} S_{P_{in,1}} - \omega (\eta_1 + \eta_{12(1)} - \eta_{12(3)}) S_{E_1} &= \omega (\eta'_{13} + \eta_{12(3)}) S_{E_1} - \omega (\eta'_{31} + \eta_{32(1)}) S_{E_3} = \\ &= \omega (\eta_3 - \eta_{32(1)} + \eta_{32(3)}) S_{E_3} \end{aligned} \quad (22a)$$

when  $S_{P_{in,3}} = 0$  and

$$\begin{aligned} S_{P_{in,3}} - \omega (\eta_3 - \eta_{32(1)} + \eta_{32(3)}) S_{E_3} &= \omega (\eta'_{31} + \eta_{32(1)}) S_{E_3} - \omega (\eta'_{13} + \eta_{12(3)}) S_{E_1} = \\ &= \omega (\eta_1 + \eta_{12(1)} - \eta_{12(3)}) S_{E_1} \end{aligned} \quad (22b)$$

when  $S_{P_{in,1}} = 0$ .

The actual energy flow is yielded by use of the indirect couplings. Examination of equations (22a,b) shows that the energy flow is likely to be overestimated since the off-diagonal radiation factors tend to be smaller than the on-diagonal radiation factors. The matrices that are involved shows that the off-diagonal radiation factors tend to be smaller than the on-diagonal radiation factors. Exceptions can be found, e.g. at frequencies where the kinetic energy is much larger in the receiving than in the excited subsystem. The determinant of matrix  $[R]$  is negative at such frequencies and, thus a sign change can be expected for the couplings. Furthermore, the on- and off-diagonal radiation factors cancel which reduces the error in the energy flow estimate. The effect of the off-diagonal radiation factors in equation (20) is that the energy flow is over-estimated.

Equations (22a,b) show that one excitation case can be poorly described while excitation of the other subsystem can yield good results, i.e. equation (22a,b) may independently yield a poor or reasonable approximation. It can be seen that the relative size of the radiation factor sum (e.g.  $\eta_{32(3)} - \eta_{32(1)}$ ) with respect to the dissipation loss factor (e.g.  $\eta_3$ ) of the receiving subsystem (e.g. 3) is what matters.

The author's experience from numerical examinations of the three-plate case suggests that successful application of equation (20) does not depend on whether the indirect energy flow is weak or strong. As mentioned above, it is the re-radiation strength of the receiving subsystem that matters. The energy flow that is communicated between subsystems 1 and 3 can be quite weak and equation (20) still yield valid results



as long as the re-radiation is small in comparison with the dissipation. This indicates that it should not matter whether large distances or several subparts exists between subsystem 1 and 3 or if the intermediate element is lightly or heavily damped.

The derivation of the above mentioned equations does only rely on the form of the power balances. It may therefore be speculated that they hold also for the case in which the intermediate element (subsystem 2) encircles subsystems 1 and 3. A possible future use of equation (20) may therefore be as an approximate tool in the experimental survey of dominant transmission paths in structures that are not (too) lightly damped. An examination of this kind was applied for joint with air-pumping and mechanical point connections in parallel by Sun *et al* [12]. The numerical survey implies that it should be possible to take the use of equation (20) even further (although with caution).

In sum, the DLFs and radiation factors must be separated for the non-conservatively coupled two subsystem model to yield the *actual* energy flow. The energy flows are otherwise incorrectly derived. Measuring the power inputs and subsystem energies of two non-conservatively coupled subsystems does not yield enough information to separate the DLFs from the radiation factors with the current approach. A simplified interpretation of the power balance (equation (20)) is therefore found necessary. The approximation of equation (20) is such that it tends to overestimate the energy flow.

The DLFs may be assessed from a separate measurement if they remain unchanged when the subsystems are decoupled. However, it should be recognised that the 'inverse' non-conservative power balance need not be used when the DLFs are already known. Instead, the energy flow can simply be derived from the dissipative and input powers of subsystems 1 and 3. The advantage of the non-conservatively coupled two-subsystem model is that it yields the radiation factors which may serve as a measure of the efficiency of the dissipative joint. However, most cases cannot be decoupled and practical application of this approach may thus be restricted.

### 3. Conclusions

Two non-conservatively coupled subsystems was demonstrated as a special case of the three-subsystem configuration. The physical subsystem interfaces cannot be directly applied in the non-conservatively coupled two-subsystem model for the simple reason that only a single interface can be used in the non-conservatively coupled two-subsystem model. A *fictional* interface was therefore introduced to account for the transfer of energy between the non-conservatively coupled subsystems.

Two kinds of non-conservatively coupled energy flow models were derived for cases in which uncoupled and coupled subsystem energies are used. The first type, that refers to uncoupled subsystem energy, can be used in a 'forward' fashion when setting up a SEA model, while the second type, that uses coupled subsystem energy, is appropriate for 'inverse' computational or experimental analysis procedures.

Two versions of the power balance were deduced for the coupled case. The first version contains a complete information set that cannot be revealed from the power

inputs to and responses of two subsystems. The crux of the matter for the non-conservatively coupled two-subsystem model is that four radiation factors must be used when the power input is expressed as a function of coupled subsystem energy. A second, simplified, version was therefore introduced for approximate analysis of the energy flows. This simplification can yield perfectly valid results when exciting in one of the subsystems and truly fail when the other subsystem is excited. The degree of approximation depends on how large the receiving subsystem's dissipation-loss and radiation factors are in comparison with each other.

A few speculations about extending the use of the non-conservative power balance were made to suggest directions for further research. The non-conservative two-subsystem case may be applied in the search of dominant transmission paths in structures that are not too lightly damped. However, un-cautious use of the simplified power balance is not recommended as it yields the energy flow by approximation only.

In conclusion, a dual interpretation of the conservatively coupled three-subsystem case and the non-conservatively coupled two-subsystem case can be made if indirect couplings are introduced. Further development of such factors for introduction to SEA is therefore desirable and may help expand the applicability of SEA.

## REFERENCES

1. R.H. Lyon 1975, *MIT Press, MA USA*. Statistical Energy Analysis of Dynamical Systems, Theory and Applications.
2. E. Eichler 1965, *Journal of Acoustical Society of America* **37**, 995 - 1007. Thermal circuit approach to vibrations in coupled systems and noise reduction of a rectangular box.
3. C.H. Hodges and J. Woodhouse 1986, *Reports in Progress in Physics* **49**, 107 - 170. Theories of noise and vibration transmission in complex structures.
4. R.S. Langley 1990, *Journal of Sound and Vibration* **141**(2), 207 - 219. A derivation of the Coupling Loss Factor used in Statistical Energy Analysis.
5. S. Finnveden 1990, *Proc. Inter-Noise 90* Gothenburg, 945 - 948. Energy flows within a three element structure with a statistical description of the design parameters.
6. C.R. Fredö 1995, *F95-02, PhD Thesis, Chalmers Univ. Tech.* Statistical energy analysis and the individual case.
7. H.G. Davies and M.A. Wahab 1981 *Journal of Sound and Vibration* **77**, 311 - 321. Ensemble averages of power flow in randomly excited coupled beams.
8. E.K. Dimitriadis and A.D. Pierce 1988, *Journal of Sound and Vibration* **123**(3), 397-412. Analytical solution for the power exchange between strongly coupled plates under random excitation: A test of Statistical Energy Analysis concepts.
9. C.R. Fredö. 1994-1996, Energy flow in three subsystem configurations, Parts 1-3. (*Journal of Sound and Vibration*, submitted for publication)
10. J.L. Guyader, C. Boisson and C. Lesueur 1982, *Journal of Sound and Vibration* **81**(1), 81-92. Energy transmission in finite coupled plates, part I: Theory.
11. J.C. Sun, N. Lalor and E.J. Richards 1987, *Journal of Sound and Vibration* **112**(2), 321-330. Power flow and energy balance of non-conservatively coupled structures, I: Theory.
12. J.C. Sun, L.C. Chow, N. Lalor and E.J. Richards 1987, *Journal of Sound and Vibration* **112**(2), 331-343. Power flow and energy balance of non-conservatively coupled structures, II: Experimental verification of theory.
13. Kishimoto and Bernstein 1995, *Journal of Sound and Vibration* **182**(1), 59-76. Thermodynamic modelling of interconnected systems, Part II: Dissipative coupling.

# **ERRATA: A NOTE ON CONSERVATIVE AND NON-CONSERVATIVE COUPLING**

Claes Fredö  
Ingemansson Technology AB

*Equation (2) should be renamed as equation (2a).* Manipulating the upper and lower rows of equation (2a) to include the energy flow to subsystem 2 yields that

$$\begin{pmatrix} S_{P_{1 \rightarrow}} \\ S_{P_{2 \rightarrow}} \\ S_{P_{3 \rightarrow}} \end{pmatrix} = \begin{bmatrix} PP_{21} & PP_{12} & PP_{13} \\ (-PP_{31}-PP_{21}) & (-PP_{32}-PP_{12}) & (-PP_{33}-PP_{23}) \\ PP_{31} & PP_{32} & PP_{23} \end{bmatrix} \begin{pmatrix} S_1 \\ S_2 \\ S_3 \end{pmatrix} = [PP^+] \begin{pmatrix} S_1 \\ S_2 \\ S_3 \end{pmatrix} \quad (2b)$$

The superscript + in the matrix  $[PP^+]$  signifies that a row has been added.

*The 3rd sentence in the paragraph before equation (5) should read*

Equation (3) is similar (and in some situations identical) to the energy part of the "Greens function" formulation that Langley used in reference [4].

*Equation (5) should read*

$$\begin{pmatrix} S_{P_{in,1}} \\ S_{P_{in,2}} \\ S_{P_{in,3}} \end{pmatrix} = [V] \begin{pmatrix} S_1 \\ S_2 \\ S_3 \end{pmatrix} = ([U] + [PP^+]) \begin{pmatrix} S_1 \\ S_2 \\ S_3 \end{pmatrix} \quad (5)$$

Summing the  $[U]$  and  $[PP^+]$  matrices for the dissipated power and the energy flow out of the subsystems, respectively yields the diagonal  $[V]$  matrix for the power input.

*The 1st sentence in the paragraph before equation (15) should read*

The experience from the discussion above is that one should be cautious to take the benefits of the uncoupled subsystem energy for granted also for coupled subsystem energy.

*Equation (17) should read*

$$\begin{pmatrix} S_{P'_{1 \rightarrow}} \\ S_{P'_{3 \rightarrow}} \end{pmatrix} = \begin{bmatrix} PP_{21} & PP_{13} \\ PP_{31} & PP_{23} \end{bmatrix} \begin{pmatrix} S_1 \\ S_3 \end{pmatrix} = [PP'] \begin{pmatrix} S_1 \\ S_3 \end{pmatrix} \quad (17)$$

## **Addendum**

The power input for the non-conservatively coupled case can be divided into the following subparts

$$\begin{pmatrix} S_{P_{in,1}} \\ S_{P_{in,3}} \end{pmatrix} = [V'] \begin{pmatrix} S_1 \\ S_3 \end{pmatrix} = ([U''] + ([U'] + [PP'])) \begin{pmatrix} S_1 \\ S_3 \end{pmatrix} \quad (19b)$$

where the power which is lost in the non-conservative junction is

$$\begin{pmatrix} S_{P'_{1 \rightarrow}} \\ S_{P'_{3 \rightarrow}} \end{pmatrix} = \begin{bmatrix} U_{21} & 0 \\ 0 & U_{23} \end{bmatrix} \begin{pmatrix} S_1 \\ S_3 \end{pmatrix} = [U'] \begin{pmatrix} S_1 \\ S_3 \end{pmatrix} \quad (19c)$$

and the power which is lost in the subsystem is

$$\begin{pmatrix} S_{P'_{diss,1}} \\ S_{P'_{diss,3}} \end{pmatrix} = \begin{bmatrix} U_{11} & U_{13} \\ U_{31} & U_{33} \end{bmatrix} \begin{pmatrix} S_1 \\ S_3 \end{pmatrix} = [U''] \begin{pmatrix} S_1 \\ S_3 \end{pmatrix} \quad (19d)$$

Re-expressing equation (19c) as a function of coupled subsystem energy yields four radiation factors. Re-expressing equation (19d) as a function of coupled subsystem energy yields two dissipation loss factors on the matrix diagonal.

## PREDICTIVE SEA USING LINE WAVE IMPEDANCES

K. H. HERON  
DERA  
*Aero-Structures Department*  
*Farnborough, Hants, GU14 0LX*  
*England*

### Abstract

Predictive SEA is mainly based on the wave approach. For plate networks the main computational procedure is associated with the calculation of the infinite plate to plate random incidence transmission coefficients. This paper outlines a method for such a procedure based upon generalising the 1D concept of a point impedance to 2D concept of a line wave impedance. Formulae are presented for the line wave impedance of an infinite Timoshenko beam and a thin semi-infinite plate, and for the cross line wave impedance of a strip plate of finite width.

These formulae are used to calculate plate to plate SEA coupling loss factors. Experimental results are compared with this theory for the particular case of an assembly consisting of two plates connected to the diagonally opposite flanges of an I-beam. Very good agreement is shown. The theory using strip plates is shown to be superior and asymptotic to two other approximate theories one of which can be assumed accurate at low frequencies and one at high frequencies.

The theory has been extensively validated against the measured response results from many test assemblies.

### 1. Introduction

Predictive theory based on the modal approach to SEA is very difficult to apply to complex structural assemblies, firstly because of the computational load and secondly because of the many assumptions that seem to be necessary. On the other hand the wave approach to the calculation of SEA coupling loss factors is computationally efficient and seems to be governed by a single assumption. This assumption, that the infinite canonical form of each junction need only be studied and that the resulting infinite transmission matrix can be used to calculate finite coupling loss factors, is clearly valid 'on the average' once wavelengths have become much smaller than typical subsystem lengths. In fact experience has shown this assumption to be valid

down to frequencies associated with modal overlap factors of about one, and for many vibro-acoustic problems such frequencies lie below the frequency range of interest.

Another advantage to the use of the wave approach is in the choice of SEA subsystems. At least for plate and beam assemblies this choice becomes somewhat automatic, as against involving engineering judgement, by the need to match a transmission matrix element to a coupling loss factor. Thus each wavetype within a plate or a beam has to be modelled as at least one subsystem.

The critical theory for predictive SEA is thus associated with the calculation of these infinite transmission matrices. This paper describes such a calculation procedure for a general line connection of plates. It is based on the use of line wave impedance matrices, analogous to the use of point impedance matrices for beam networks. Formulae are presented for the line wave impedance of semi-infinite plates, infinite beams and infinite strip plates. The method by which these can be used to calculate the required transmission matrices is described.

Predictions using this theory are then compared with the measured results from a two plate assembly. It is shown that typical connecting I-beams cannot be modelled using beam theory because of the dynamic behaviour of their webs, however by modelling the beam as a series of connected strip plates very good agreement is shown between theory and experiment.

## 2. Basic SEA theory

When plates are joined along a line the SEA coupling loss factor  $\eta_{ab}$  between plate *a* and plate *b* is normally calculated using the formula

$$\eta_{ab} = \frac{L k_a \tilde{\tau}_{ba}}{2\pi^2 \omega n_a}, \quad (1)$$

where  $\omega$  is the circular frequency,  $k_a$  and  $n_a$  are the wavenumber and modal density of plate *a* respectively,  $L$  is the length of the line connection, and  $\tilde{\tau}_{ba}$  is the infinite random incidence transmission coefficient between plate *a* and plate *b*. This infinite transmission coefficient is simply the transmission coefficient associated with the canonical junction of infinite extent.

Normally each plate will have three travelling wave types associated with it, one for the bending waves, one for the inplane compression waves and one for the inplane shear waves, and these will give rise to a transmission matrix of order three times the number of plates at the line junction. Through equation 1, this will result in a similar order matrix for the coupling loss factors between all the plate wave types.

Knowing the angle dependent plate to plate transmission coefficient  $\tau_{ba}(\theta_a)$  where  $\theta_a$  is the normal angle of incidence, the random incidence transmission coefficient  $\tilde{\tau}_{ba}$  is calculated using

$$\tilde{\tau}_{ba} = \int_0^{\pi/2} \tau_{ba}(\theta_a) \cos(\theta_a) d\theta_a. \quad (2)$$

Thus the calculation of the SEA coupling loss factor  $\eta_{ab}$  between plates at a line junctions is dependent on the calculation of  $\tau_{ab}(\theta_a)$ . The general calculation of  $\tau_{ab}(\theta_a)$  usually proceeds as follows.

A plane incident wave is assumed with a given incident angle  $\theta_a$ , for a given plate and given wavetype. The power incident on the line junction is then calculated together with the input velocity and the induced force on the junction at the plate edge. These calculations are simple functions of the plate supporting the incident wave and are independent of the other plates and the connection complexity of the junction.

This 'external' force is then imposed on the junction and the junction velocity calculated. It is then a relatively simple matter to use this junction velocity to deduce the various output wave type powers, and by dividing by the input power to calculate  $\tau_{ab}(\theta_a)$ . The major part of the procedure is thus associated with the calculation of the junction velocity from a knowledge of a given external force.

### 3. Line wave impedances

At a point connection there are six degrees of freedom but at a line connection there are only four. This is fundamental and simply associated with the geometrical relationships that must exist along a line once we assume all variables have a simple dependency in the direction of the line. Let the connection line be parallel to the  $x$  axis, then for a given trace wavenumber  $k$  (a simple function of the incident wave) all variables must have an  $x$  dependency of  $e^{-ikx}$ .

Now the usual line velocity and line force variables are taken to be

$$\begin{aligned} \mathbf{v}^T &= (v_x \quad v_y \quad v_z \quad w_x), \\ \mathbf{f}^T &= (f_x \quad f_y + ikm_z \quad f_z - ikm_y \quad m_x), \end{aligned} \quad (3)$$

where superscript T denotes a transpose,  $v$  represents linear velocity,  $w$  represents rotational velocity,  $f$  represents force, and  $m$  represents moment.

The aim herein is to generalise the well understood point impedance approach and define a suitable line wave impedance. Unfortunately some of the useful properties of a point impedance are lost if a line wave impedance is defined in terms of the above variables. However it is possible to overcome this problem by defining a new set of variables such that

$$\begin{aligned} \mathbf{v}^T &= (-ik^{-1}v_x \quad v_y \quad v_z \quad w_x), \\ \mathbf{f}^T &= (-ikf_x \quad f_y + ikm_z \quad f_z - ikm_y \quad m_x). \end{aligned} \quad (4)$$

This is a mathematical trick that is not essential but is very desirable, for if we now define a line wave impedance  $Z$  using the formula

$$\mathbf{f} = Z\mathbf{v}, \quad (5)$$

we find that all line wave impedance matrices are symmetric and furthermore that the line wave impedance matrix of a reactive element, such as a beam, is purely imaginary. Such properties are clearly analogous with the properties of point impedance matrices.

The change of variables is allowed, without loss, because any set of variables is acceptable provided we ensure conservation of power, that is

$$\text{power} \propto \mathbf{f}^H \mathbf{v} = \mathbf{f}'^H \mathbf{v}', \quad (6)$$

where superscript H denotes a complex conjugate transposition.

All the subsequent formulae in this paper use line variables defined by equation 4. Line wave impedances can be added together just like point impedances and cross line wave impedances can be used to model for example a strip plate just like a cross point impedance can be used to model a finite beam. Furthermore these impedances can be transformed to cope with small rigid offsets and rotations using the following transformation matrix

$$\Phi = \begin{bmatrix} 1 & 0 & 0 & 0 \\ 0 & \cos \phi & -\sin \phi & 0 \\ 0 & \sin \phi & \cos \phi & 0 \\ 0 & p \sin \phi - q \cos \phi & p \cos \phi + q \sin \phi & 1 \end{bmatrix}, \quad (7)$$

where the local axis is at position  $(0 \ p \ q)$  with respect to the global axis origin and the local y and z axes are at an angle  $\phi$  with respect to the global y and z axes. To transform a line wave impedance from local co-ordinates to global co-ordinates we simply use  $\Phi Z \Phi^T$ .

#### 4. The line wave impedance for a beam

The twelve cyclic equations for a Timoshenko beam can be used to generate its line wave impedance. This is done by imposing each of the four line forces in turn and calculating the line velocity responses to give the 4x4 line wave mobility matrix which can then be inverted to give the line wave impedance matrix. The assumption is that the beam is acting along a single connection line.

The problem associated with plates attached along different lines of the beam section, such as the opposite flanges of an I-beam, is better solved by modelling the beam as a series of strip plate elements rather than by introducing a special six degree of freedom element as cited in Langley and Heron (1990). Practically all engineering beams are thin sectioned beams and should be modelled as a series of strip plates in order to accurately predict the beam dynamics at the mid and high frequencies. Thus the beam formulae of this section should be used sparingly.

After some algebra, the line wave impedance for an infinite beam about its centroid can be shown to be given by the following formulae

$$i\omega Z_{\text{beam-centroid}} = \begin{bmatrix} L & 0 & 0 & 0 \\ 0 & F_x & 0 & -\epsilon_x k' \hat{B}_x \\ 0 & 0 & F_y & +\epsilon_y k' \hat{B}_y \\ 0 & -\epsilon_x k' \hat{B}_x & +\epsilon_y k' \hat{B}_y & T_{\text{centroid}} \end{bmatrix}, \quad (8)$$

$$L = k^2 (k^2 EA - \omega^2 m'), \quad (9)$$

$$F_y = k^4 \hat{B}_y - \omega^2 m' , \quad (10)$$

$$F_z = k^4 \hat{B}_z - \omega^2 m' , \quad (11)$$

$$k^2 \hat{B}_y = \frac{(k^2 B_y - \omega^2 H_y)}{1 + \frac{\epsilon_y}{\omega A} (k^2 B_y - \omega^2 H_y)} , \quad (12)$$

$$k^2 \hat{B}_z = \frac{(k^2 B_z - \omega^2 H_z)}{1 + \frac{\epsilon_z}{\omega A} (k^2 B_z - \omega^2 H_z)} , \quad (13)$$

$$T_{\text{centroid}} = k^2 GJ - \omega^2 H_x + \epsilon_y^2 k^4 \hat{B}_y + \epsilon_z^2 k^4 \hat{B}_z , \quad (14)$$

where  $E$  is Young's modulus,  $A$  is the cross sectional area,  $m'$  is the mass per unit length,  $B_y$  and  $B_z$  are the two bending stiffnesses,  $G$  is the shear modulus,  $\epsilon_y$  and  $\epsilon_z$  are the two thick bending shear coefficients,  $GJ$  is the torsional stiffness,  $H_x$ ,  $H_y$  and  $H_z$  are the three moments of inertia of the beam cross section and  $(\epsilon_y, \epsilon_z)$  is the position of the beam shear centre with respect to the centroid.

Using the transformation matrix of equation 7 the line wave impedance for an infinite beam about its shear axis can also be derived

$$i\omega Z_{\text{beam-shear}} = \begin{bmatrix} L & 0 & 0 & 0 \\ 0 & F_z & 0 & -\epsilon_z \omega^2 m' \\ 0 & 0 & F_y & +\epsilon_y \omega^2 m' \\ 0 & -\epsilon_z \omega^2 m' & +\epsilon_y \omega^2 m' & T_{\text{shear}} \end{bmatrix} , \quad (15)$$

$$T_{\text{shear}} = k^2 GJ - \omega^2 (H_x + m' \epsilon_y^2 + m' \epsilon_z^2) . \quad (16)$$

## 5. The line wave impedance for a semi-infinite plate

The line wave impedance for a thin isotropic semi-infinite plate is given in Langley and Heron (1990) and is reproduced here with a few slight changes associated with the new definition of a line wave impedance as described above.

$$Z_{\text{plate}} = \begin{bmatrix} 0 & 0 \\ Z_{\text{inplane}} & 0 \\ 0 & 0 \\ 0 & 0 \end{bmatrix} \begin{bmatrix} 0 \\ 0 \\ Z_{\text{bending}} \end{bmatrix} , \quad (17)$$

$$i\omega Z_{\text{inplane}} = \frac{\omega^2 m'' k_s^{-2}}{(k^2 - \gamma_s \gamma_s)} \begin{bmatrix} k^2 k_s^2 \gamma_s & k^2 (2k^2 - k_s^2 - 2\gamma_s \gamma_s) \\ k^2 (2k^2 - k_s^2 - 2\gamma_s \gamma_s) & k_s^2 \gamma_s \end{bmatrix} , \quad (18)$$

$$i\omega Z_{\text{bending}} = \omega^2 m'' k_b^{-4} \begin{bmatrix} \gamma_b \gamma_s (\gamma_b + \gamma_s) & \gamma_b \gamma_s + \sigma k^2 \\ \gamma_b \gamma_s + \sigma k^2 & (\gamma_b + \gamma_s) \end{bmatrix} , \quad (19)$$

$$\gamma_b^2 = k^2 - k_b^2 , \quad (20)$$

$$\gamma_s^2 = k^2 + k_b^2 , \quad (21)$$



$$\gamma_c^2 = k^2 - k_c^2, \quad (22)$$

$$\gamma_s^2 = k^2 - k_s^2, \quad (23)$$

$$Bk_c^4 = \omega^2 m'', \quad (24)$$

$$Ck_c^2 = \omega^2 m'', \quad (25)$$

$$Sk_s^2 = \omega^2 m'', \quad (26)$$

where  $B$ ,  $C$  and  $S$  are the bending, compression and shear stiffnesses of the plate,  $\sigma$  is Poisson's ratio and  $m''$  is the mass per unit area of the plate. Unlike in reference 1  $\mathbf{Z}_{\text{bending}}$  is now a symmetric matrix.

## 6. The cross line wave impedance for a strip plate

The cross line wave impedance for a thin isotropic strip plate is given below. The strip is assumed to occupy the  $0 < y < W$  part of the  $xy$  plane, where  $W$  is the strip plate width. As with the calculation of the impedance of a thin isotropic semi-infinite plate, the process is split into one involving the out-of-plane bending motion and one involving the inplane motion. Eight line variables needed here and they are chosen such that the first four refer to the edge at  $y=0$  and the last four refer to the edge at  $y=W$ . The  $8 \times 8$   $\mathbf{Z}_{\text{strip}}$  matrix is then made up as follows

$$\mathbf{Z}_{\text{strip}} = \begin{bmatrix} \mathbf{Z}_{\text{is-11}} & \mathbf{0} & \mathbf{Z}_{\text{is-12}} & \mathbf{0} \\ \mathbf{0} & \mathbf{Z}_{\text{out-11}} & \mathbf{0} & \mathbf{Z}_{\text{out-12}} \\ \mathbf{Z}_{\text{is-21}} & \mathbf{0} & \mathbf{Z}_{\text{is-22}} & \mathbf{0} \\ \mathbf{0} & \mathbf{Z}_{\text{out-21}} & \mathbf{0} & \mathbf{Z}_{\text{out-22}} \end{bmatrix}. \quad (27)$$

This impedance matrix can be transformed from local to global co-ordinates using the  $8 \times 8$  transformation matrix given by

$$\Phi_{\text{strip}} = \begin{bmatrix} \Phi_1 & \mathbf{0} \\ \mathbf{0} & \Phi_2 \end{bmatrix}, \quad (28)$$

where  $\Phi_1$  is the  $4 \times 4$  transformation matrix for the first edge of the strip with respect to the global co-ordinates chosen for this first edge connection point, and  $\Phi_2$  is the  $4 \times 4$  transformation matrix for the 'strip extension' with respect to the global co-ordinates chosen for this second edge connection point. The 'strip extension' refers to an imaginary plate occupying the  $W < y < \infty$  part of the  $xy$  plane.

After much algebra the out-of-plane cross line wave impedance  $\mathbf{Z}_{\text{out}}$  can be shown to be given by the following formula

$$i\omega \mathbf{Z}_{\text{out}} \Psi_r = \Psi_f, \quad (29)$$

where

$$\Psi_s = \begin{bmatrix} \zeta_0 & \zeta_0 & \zeta_1 & -\zeta_1 \\ \zeta_2 & -\zeta_2 & \zeta_3 & \zeta_3 \\ \zeta_0 P & \zeta_0 P^{-1} & \zeta_1 Q & -\zeta_1 Q^{-1} \\ \zeta_2 P & -\zeta_2 P^{-1} & \zeta_3 Q & \zeta_3 Q^{-1} \end{bmatrix}, \quad (30)$$

$$\Psi_f = \begin{bmatrix} \zeta_4 & -\zeta_4 & \zeta_5 & \zeta_5 \\ \zeta_6 & \zeta_6 & \zeta_7 & -\zeta_7 \\ -\zeta_4 P & \zeta_4 P^{-1} & -\zeta_5 Q & -\zeta_5 Q^{-1} \\ -\zeta_6 P & -\zeta_6 P^{-1} & -\zeta_7 Q & \zeta_7 Q^{-1} \end{bmatrix}, \quad (31)$$

and where

$$\begin{aligned} \zeta_0 &= 1 \\ \zeta_1 &= 1 \\ \zeta_2 &= -\gamma_b \\ \zeta_3 &= -\gamma_c \\ \zeta_4 &= \gamma_b(\gamma_b^2 - \sigma k^2) B \\ \zeta_5 &= \gamma_c(\gamma_c^2 - \sigma k^2) B \\ \zeta_6 &= \zeta_0 \zeta_5 \zeta_3^{-1} \\ \zeta_7 &= \zeta_1 \zeta_4 \zeta_2^{-1} \\ P &= e^{-\gamma_b W} \\ Q &= e^{-\gamma_c W} \end{aligned} \quad (32)$$

The inplane cross line wave impedance  $Z_{in}$  can similarly be shown to be given by the following formula

$$i\omega Z_{in} \Psi_s = \Psi_f, \quad (33)$$

where  $\Psi_s$  and  $\Psi_f$  are still given by equation 30 and equation 31 but where equation 32 is replaced by

$$\begin{aligned} \zeta_0 &= 1 \\ \zeta_1 &= \gamma_b \\ \zeta_2 &= \gamma_c \\ \zeta_3 &= k^2 \\ \zeta_4 &= 2k^2 \gamma_c S \\ \zeta_5 &= k^2(\gamma_b^2 + k^2) S \\ \zeta_6 &= \zeta_0 \zeta_5 \zeta_3^{-1} \\ \zeta_7 &= \zeta_1 \zeta_4 \zeta_2^{-1} \\ P &= e^{-\gamma_b W} \\ Q &= e^{-\gamma_c W} \end{aligned} \quad (34)$$

It can also be shown that in all cases  $D = \Psi_f \Psi_s^{-1}$  is a real symmetric matrix. Thus  $Z_{strip}$  is an imaginary 8x8 symmetric matrix; imaginary as expected because the strip

plate has no damping. It is possible to evaluate  $\mathbf{D}$  by numerically inverting  $\Psi$ , however this can cause numerical problems especially near  $W=0$ . The following algebraic formula for  $\mathbf{D}$  can be used instead.

$$\Delta \mathbf{D} = \begin{bmatrix} d_{11} & d_{12} & d_{13} & d_{14} \\ d_{12} & d_{22} & -d_{14} & d_{24} \\ d_{13} & -d_{14} & d_{11} & -d_{12} \\ d_{14} & d_{24} & -d_{12} & d_{22} \end{bmatrix}, \quad (35)$$

$$d_{11} = (\zeta_3 \zeta_4 - \zeta_2 \zeta_5) [\zeta_0 \zeta_3 (1+P^2)(1-Q^2) - \zeta_1 \zeta_2 (1-P^2)(1+Q^2)], \quad (36)$$

$$d_{12} = \zeta_0 \zeta_1 (\zeta_3 \zeta_4 + \zeta_2 \zeta_5) [4PQ - (1+P^2)(1+Q^2)] + (\zeta_0^2 \zeta_3 \zeta_5 + \zeta_1^2 \zeta_2 \zeta_4) (1-P^2)(1-Q^2), \quad (37)$$

$$d_{13} = 2(\zeta_2 \zeta_5 - \zeta_3 \zeta_4) [\zeta_0 \zeta_3 P(1-Q^2) - \zeta_1 \zeta_2 Q(1-P^2)], \quad (38)$$

$$d_{14} = 2\zeta_0 \zeta_1 (\zeta_2 \zeta_5 - \zeta_3 \zeta_4) [P(1+Q^2) - Q(1+P^2)], \quad (39)$$

$$d_{22} = \frac{\zeta_0 \zeta_1}{\zeta_2 \zeta_3} (\zeta_3 \zeta_4 - \zeta_2 \zeta_5) [\zeta_0 \zeta_3 (1-P^2)(1+Q^2) - \zeta_1 \zeta_2 (1+P^2)(1-Q^2)], \quad (40)$$

$$d_{24} = 2 \frac{\zeta_0 \zeta_1}{\zeta_2 \zeta_3} (\zeta_2 \zeta_5 - \zeta_3 \zeta_4) [\zeta_0 \zeta_3 Q(1-P^2) - \zeta_1 \zeta_2 P(1-Q^2)], \quad (41)$$

$$\Delta = 2\zeta_0 \zeta_1 \zeta_2 \zeta_3 [4PQ - (1+P^2)(1+Q^2)] + (\zeta_0^2 \zeta_3^2 + \zeta_1^2 \zeta_2^2) (1-P^2)(1-Q^2). \quad (42)$$

## 7. Experimental validation

An assembly consisting of two aluminium plates (thickness 2mm and 4mm) connected by an I beam was manufactured and is shown diagrammatically in figure 1. Damping material was attached to each plate in order to keep clear of SEA equipartition.

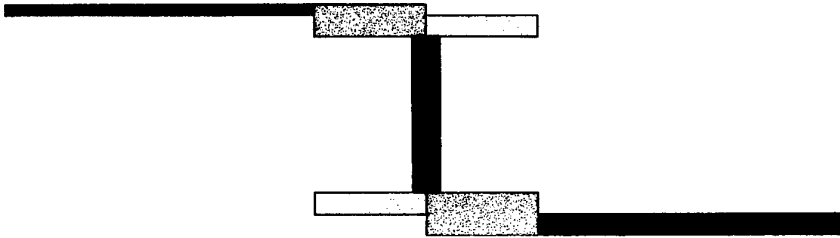


Figure 1 : The Z assembly

The structure was excited at five random positions on each plate and the response of each plate measured using five randomly positioned miniature accelerometers. This allowed full SEA inversion to be used to obtain the coupling loss factor matrix, and from this the in-situ damping levels for each plate. Taking account of both the direct vibration field associated with point excitation and the acoustic radiation damping, a simple mechanical loss factor was fitted to these data. The resultant assessed energy loss factor was 1.8% for both plates, constant across all frequencies. This value was inserted into all the SEA theoretical models; the in-plane loss factors were taken arbitrarily to be one third of this value.

This process of inverting the measured energy matrix to obtain the in-situ damping, then using these measured damping values in a theoretical prediction of response, and then comparing these predicted responses with the original measured responses needs a little explanation. The alternative and simpler approach would be to compare predicted and measured coupling loss factors. However there are two disadvantages to this alternative approach. Firstly the measured variance of the coupling loss factors is often large and secondly the measurements and inversion process has to assume a two subsystem model (i.e. no inplane motion) and thus the measured coupling loss factors are not necessarily what they seem. These effects can give a biased result and /or an inconclusive comparison with theory.

The approach adopted here is an attempt to bypass these problems by arguing that comparison with theory should occur in the response plane so that the theory can take full account of the inplane motion and then all that is needed is a good estimate of the damping. The best estimate of this is obtained from the inverted energy matrix on the assumption that any inplane motion energy losses are very small when compared to the out-of-plane losses.

Using this approach the results for the Z-assembly are shown in figure 2. The result are expressed in terms of the response velocity normalised to the input drive point velocity. The 90% confidence limits as well as the mean are plotted for the measurement results.

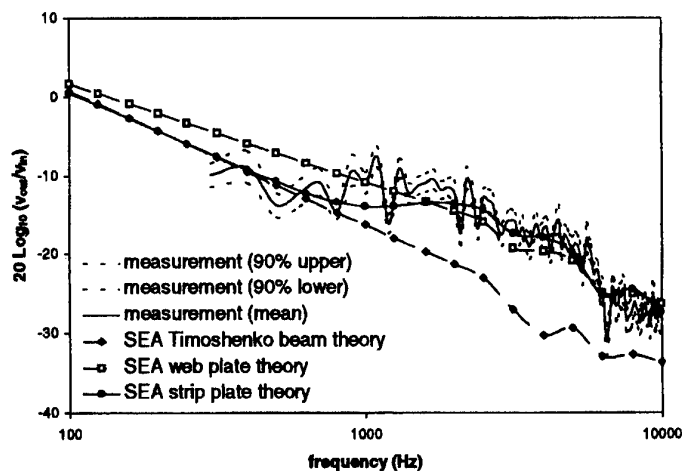


Figure 2 : Response of 2mm plate due to forcing on 4mm plate

Three theories are plotted on figure 2. The Timoshenko beam model was calculated by treating the I-beam (the centre section of figure 1) as a beam. The web plate theory was calculated by treating the web of the I-beam as an undamped SEA plate with the two flanges as coupling beams in a three plate SEA model. The strip plate theory was calculated using five strip plates, two semi-infinite plates and *no* beams as outlined in figure 1.

Treating the full I-beam as a beam is a good model at the lower frequencies but introduces errors in excess of 10dB at frequencies above 1kHz. Treating the web as an undamped SEA plate gives remarkably good agreement for frequencies above about 1kHz. It is to be expected that this model will be accurate at the highest frequencies but it is somewhat surprising that it is accurate down to 1kHz.

The strip plate model is remarkably accurate over the whole frequency range. It is asymptotic to the other two model and at about 1kHz predicts a smooth transition between these two approximate theories in good agreement with the measurements.

## 8. Discussion

The wave approach, as against the mode approach, is the usual method of calculating SEA coupling loss factors. This is mainly because the mode approach is inherently computationally expensive because it involves the evaluation of complicated integrals to deal with the necessary averages over space and frequency (Lyon and DeJong, 1995). Occasionally a particular junction is so complicated that the wave approach cannot be used because the junction is neither a point, a line or an area. In such situations a theoretical evaluation of the coupling may have to use the mode approach. However it is now clear that whenever possible the wave approach is to be preferred, if for no other reason than that of computational efficiency.

Furthermore the wave approach assumptions, as against the mode approach assumptions, can be more easily understood. Indeed the wave approach only assumes that a given infinite transmission coefficient is a good approximation to the transmission coefficient for the finite assembly. This will be valid at high frequencies where we can assume far boundary conditions to be unimportant as compared to the junction boundary under consideration. The lower limit of applicability is associated with the frequency at which the modal overlap factor (average modal bandwidth divided by average modal separation) is unity. This is not surprising because below this frequency individual modes can become important and this is equivalent to far boundary conditions becoming important.

The wave approach to the calculation of SEA coupling loss factors has been used from the earliest days in the development of predictive SEA, but perhaps it is only in recent times that it has been realised that further assumptions with regard to the connecting structure are unwise. For a general line connection between plates, the conclusion has to be drawn from the results of this paper that an accurate model of the dynamics associated with the connecting beam is necessary in order to accurately predict the SEA coupling loss factor.

Fortunately practically all engineering structures use thin sectioned beams and the strip plate theory presented herein is well suited to accurately model such connecting beams. It should be noted that *any* thin sectioned connecting beam (open, closed, multiply connected) can be modelled with this theory by using appropriate transformation matrices and applying the theorem of impedances addition.

The theory can be simply extended to include 'thick' isotropic plates and indeed any transversely isotropic plate although care is needed in dealing with the sixth rather than fourth order bending equations. The possible extension to anisotropic and curved plates introduces a further complication associated with the variation of group and phase velocity with heading direction and it is unclear as yet how this will be overcome.

Finally, the theory presented herein has been successfully used to predict the vibro-acoustic response of many test assemblies. These have included a box assembly of 50 plates (Heron, 1995) and a real helicopter fuselage modelled using 369 plates (Rossall and Wood, 1995); both of these structures were studied within the CEC Brite EuRam project RHINO (Reduction of helicopter interior noise) which concluded in 1996. More recently under the Anglo-French project DOVAC (DERA:ONERA vibro acoustic collaboration) the response of a 26 plate box assembly with 5 internal volumes was accurately predicted (Monger *et al.*, 1997).

## 9. Conclusions

A theory has been presented which can be used to predict plate to plate SEA coupling loss factors for a general junction consisting of thin isotropic plates connected by a thin sectioned isotropic beam of any cross-section.

Experimental results are compared with this theory for the particular case of an assembly consisting of two plates connected to the diagonally opposite flanges of an I-beam. Very good agreement is shown.

The theory is asymptotic to two other approximate theories one of which can be assumed accurate at low frequencies and one at high frequencies.

The theory has been extensively validated against the measured response results from many test assemblies.

## 10. References

- Heron, K.H. (1995), Predictive statistical energy analysis : A fifty plate case study, *CEAS/AIAA Aeroacoustics conference*, Munich, Germany.
- Langley, R.S. and Heron, K.H. (1990) Elastic wave transmission through plate/beam junctions, *J. Sound and Vibration* **143**(2), 241-253.
- Lyon, R.H. and DeJong, R.G. (1995) *Theory and application of statistical energy analysis*, second edition, Butterworth-Heinemann Publishers.
- Monger, T.J., Payne, A.P. and Heron, K.H. (1997) Statistical energy analysis : DOVAC box results, *Defence Evaluation and Research Agency DERA/ASD/TR97026/1*.
- Rossall, A.W. and Wood, P.C. (1995) The Westland 30 fuselage : SEA response survey : Measurements and predictions, CEC project RHINO, RH7D33.

## STATISTICAL ENERGY ANALYSIS OF BEAMS WHICH ARE LINE-CONNECTED TO PLATES

P. G. BREMNER AND T. E. BURTON

*Vibro-Acoustic Sciences Inc.*

*5355 Mira Sorrento Place, San Diego, California 92121*

### 1.0 Introduction

A beam which is line-connected to a plate is a commonly encountered arrangement in structure-borne noise studies (Figure 1). The modeling of the transmission of vibrational energy through this assembly using Statistical Energy Analysis (SEA) raises several issues. [1]

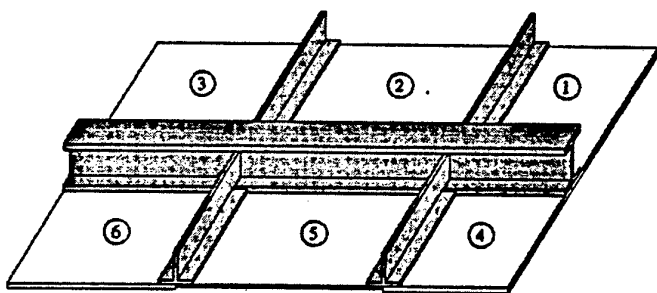


*Figure 1. A panel stiffened by spars and stringers can be modeled as plates (1-6) interconnected at beam-stiffened junctions.*

First, the motion of a beam is by definition completely defined by the motion of the junction. A panel facing an acoustic cavity is similar. Second, a plate can significantly load a line-connected beam, altering its in-situ free wavenumber and effective mass. Again, this is analogous to the familiar reactive (mass) loading of a panel facing a dense acoustic medium such as water [2]. Third, if a line-force source acts on the beam with a wavenumber different to the beam wavenumber, then power supplied to beam modes may be negligible but power supplied to the line-connected plate modes—through the non-resonant response of the beam—may be significant. This phenomenon could be likened to “mass law” transmission loss for the structure-acoustic coupling case.

In this paper, we pursue these issues for a single beam-stiffened junction of two plates.



## 2.0 EARLIER WORK

Goyder and White [3] provide an approximate analytical solution for the power flow of a beam connected to a panel along its length and excited by a point force. They observe that the poles of the mobility of the in-situ beam differ from those of the uncoupled beam. However, they find that power supplied to the in-situ beam can be estimated adequately using the mobility of the uncoupled beam. Their analysis is presented only for the case of a beam symmetrically coupled to two identical plates at its centroid, finite offsets being ignored. Torsion waves in the beam are treated in a similar manner, but there is no analysis of how the plate effects the other two beam wavefields: flexure in the plane of the plates and extensional waves.

Langley and Heron [4] show that a complete wave mechanics treatment of line-connected plates will yield power transmission coefficients and the corresponding coupling loss factors of SEA. They stiffen the junction with a general beam, considering shear flexibility, rotatory inertia, and offsets. The beam is not an SEA subsystem; the beam's response is considered only in the calculation of the matrices of plate-to-plate power transmission. Furthermore, the beam is undamped, so only reactive forces—stiffness and mass—operate at the junction.

In Langley and Heron, a diffuse vibration energy is assumed in the source plate, and power transmission characteristics are integrated over all incident angles. Each wave heading presents a different trace wavenumber to the beam at the junction. They show that total transmission ( $\tau = 1$ ) occurs between two identical, aligned plates at trace wavenumbers near the unconnected beam's free bending and torsion wavenumbers. They suggest that the maximum transmission occurs at the in-situ beam wavenumbers—that is, at the wavenumbers as modified by the plate(s) reactive loading of the beam. At this "in-situ" wavenumber, the beam impedance drops to zero, allowing un-attenuated transmission of vibration between identical plates.

The only deficiency of the model is that it does not directly accommodate the case of a power source applied to the beam or the case where the beam transmits energy to other structures (Figure 2).

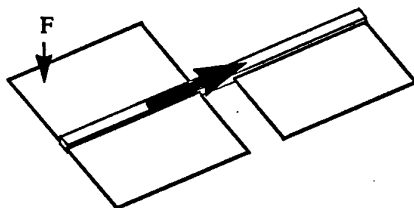


Figure 2. The heavy arrow shows a possibly important path of power flow that is missing from Langley and Heron's analysis.

One solution to this problem is to include the beam as a resonant subsystem in the SEA model. Then end-to-end transmission coefficients can accommodate axial flow of power along the beam.

## STATISTICAL ENERGY ANALYSIS OF IN-SITU BEAMS

### 3.0 In-Situ Wavenumbers

Following the work of Langley and Heron [4], the line impedance  $Z_B$  of the in-situ beam can be assembled from

- the free beam 4x4 line impedance matrix  $Z_b(k_x)$
- the plate 4x4 line (edge) impedance matrix  $Z_p(k_x)$
- a geometric offset transformation matrix  $R$

as follows:

$$Z_B(k_x) = \left( Z_b + \sum_{p=1}^{n_p} R Z_p R^T \right) \quad (1)$$

The plate's impedances loads the beam wavefields and couple them together. The eigenvector  $v$  of coupled wavefield velocities satisfies

$$Z_B(k_x) \cdot v = 0 \quad (2)$$

Setting the determinant of the beam junction impedance matrix to zero yields a characteristic equation whose roots represent the in-situ beam wavenumbers

$$\det[Z_B(k_x)] = 0 \quad (3)$$

### 3.1 ILLUSTRATIVE EXAMPLE

The interaction of the line impedances of the joined plates and beam controls the in-situ beam's free wavenumber. Here we consider the case of two 3mm-thick aluminium plates line-connected to a 25mm-by-10mm solid aluminium bar (Figure 3).

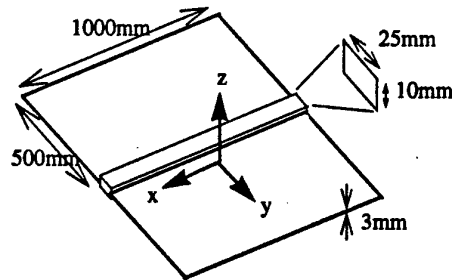


Figure 3. Two plates symmetrically welded to a solid beam

Without loss of generality, the location of the nominal line junction is taken to coincide with the centroid of the beam. The symmetric arrangement of the two plates leaves the two flexural wavefields uncoupled from each other and from the torsional and exten-

sional fields. The offsets of the edges of the plates from the junction ( $\pm 12.5$  mm) strongly influence the effective impedance of these plates and therefore must be considered.

Anticipating future experimental work, we shall present results over the frequency range 500–2000 Hz.

### 3.2 BEAM WEAK-AXIS BENDING LOADED BY PLATE BENDING

A comparison of line impedances of undamped beam and plates can shed light on the interaction of these subsystems. Figure 4 compares the absolute values of one component of these two impedances: that of flexural displacement in  $z$  (out of the plane of the plates).

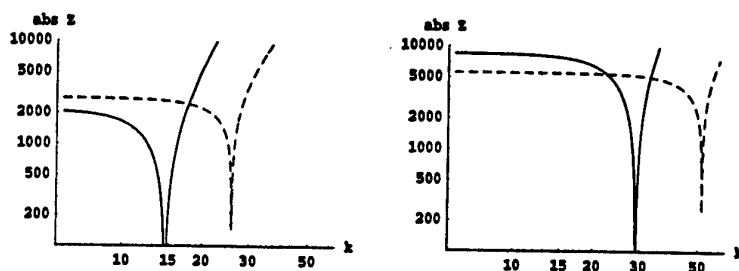


Figure 4. Absolute values of uncoupled transverse line impedances presented to the junction: at 500hz (left); at 2,000hz (right); — beam; - - - plate

The impedances of the two plates are combined and transformed to the centroid of the beam. The zero of the beam's impedance mark the free wavenumbers of the unconnected beam. The zero of the impedance of the two plates locate the free wavenumber of flexure in the plate—the trace wavenumber consistent with grazing waves in the plate and no out-ware radiation.

At low wavenumbers (at both frequencies shown), the plate's flexural impedance is of the same order as the beam flexural impedance. Thus, the loading of the plate can be expected to exert an significant but not overwhelming influence on the beam's in-site free wavenumber.

Figure 5 confirms this forecast. It follows the complex wavenumber of the beam at a fixed frequency of 500 Hz as the thickness of the two attached plates is increased from zero to the nominal 3mm in small steps. The transverse bending wavenumber of the in-situ beam increases slightly and becomes complex under the action of plate loading. An increase in the real part of wavenumber indicates that the plate's edge loading is mass-like. The finite imaginary part of the in-situ beam wavenumber indicates that some of the beam's energy radiates into the plate.

The offsets plate edges from the nominal junction play do not affect this result.

# STATISTICAL ENERGY ANALYSIS OF IN-SITU BEAMS

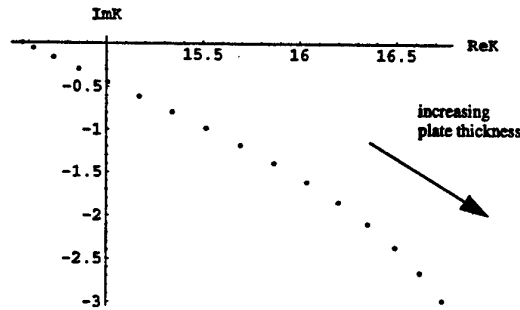


Figure 5. Locus of transverse flexural wavenumber of the in-situ beam at 500Hz as the thickness of the attached plates is increased from zero to 3mm

## 3.3 BEAM STRONG-AXIS BENDING LOADED BY PLATE EXTENSION

Line impedances of the beam and combined plates for in-plane flexure (considering the  $x$ -component of displacement and normal traction) are compared in Figure 6, again in terms of their absolute values.

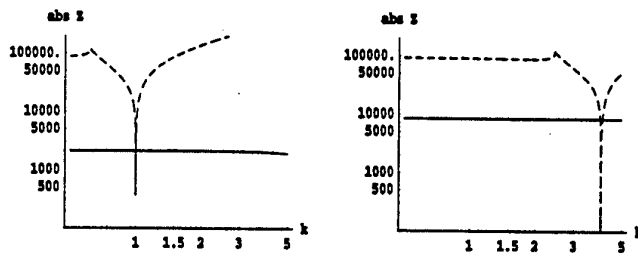


Figure 6. Absolute values of uncoupled in-plane line impedances presented to the junction; At 500hz (left); At 2,000hz (right); — beam; ----- plate

The plate's impedance is much greater than the beam's uncoupled in-plane bending impedance. In contrast to the out-of-plane component of impedance (see Figure 4), these impedances are of comparable magnitudes only very near the zero of the impedance of the plate. Owing to the coupling of extensional and shearing waves in the plates, the location of this zero is strongly affected by the offset of the edges from the junction.

Figure 7 plots this  $x$ -component of the plates' impedance versus frequency and (purely real) wavenumber.

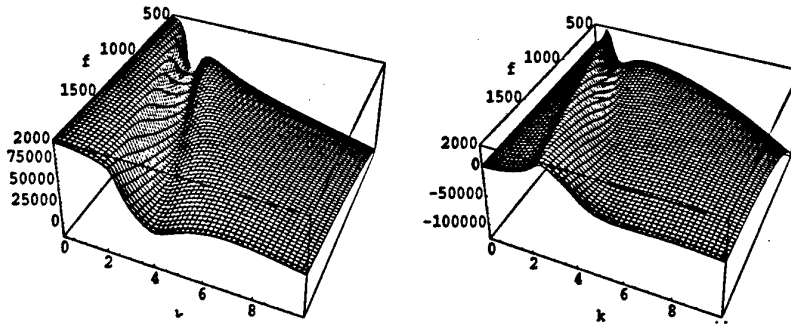


Figure 7. Uncoupled in-plane impedance of plate plotted versus both frequency and wavenumber; Real part (left); Imaginary part (right)

The sharp troughs shown in Figure 6 occur just to the right—at slightly higher wavenumbers—than the crest of the ridge in the imaginary part (right plot) of Figure 7.

Anticipating that the plates' stiffness will dominate the free wavenumber of in-plane flexure of the in-situ beam, we trace this complex wavenumber in Figure 8 as the stiffness of these plates is stiffened from zero to that of aluminium in small steps.

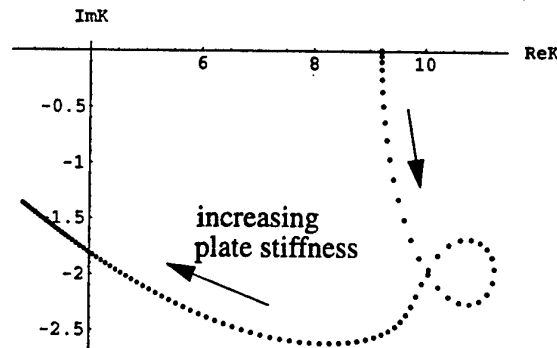


Figure 8. Locus of in-plane flexural wavenumbers of the in-situ beam at 500Hz as the plates' elastic modulus is increased.

The very first point in the plot incorporates some added mass. As stiffness is increased from zero, radiation resistance forms and increases (increasingly negative imaginary part of wavenumber). The loop in the figure marks comparable wavespeeds of in-plane flexure of the uncoupled beam and in-plane waves of the plate. The primary affect of further increases in plate stiffness is added stiffness (lower real part). Finally, the in-plane bending wavenumber for the in-situ beam is greatly reduced by the extensional stiffness in the plate.

## STATISTICAL ENERGY ANALYSIS OF IN-SITU BEAMS

### 4.0 SEA Modeling

We propose that the line-connected beam in a SEA model should be incorporated in two complementary ways, illustrated in Figure 9:

1. as a finite beam subsystem with four resonant wavefield energies (the two flexural waves discussed above plus extension and torsion) defined by in-situ wavenumber and mass density, and
2. as an infinite beam contributing line impedance to the junction between connected plate vibration wavefields.

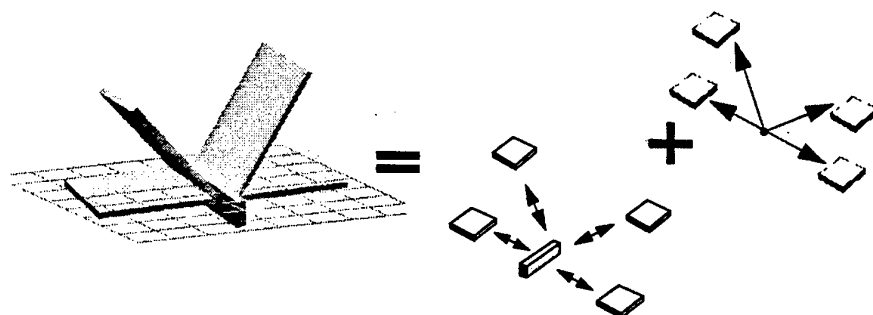


Figure 9. Both resonant and non-resonant behavior of beams in an SEA model

This approach implies that a combination of two uncorrelated energies describe the motion of the beam:

1. the SEA subsystem's modal energy concentrated at the in-situ beam wavenumber, whose amplitude is controlled by the balance between any power applied directly to the beam and the combination of damping loss in the beam and power radiation (loss) through coupling loss factors to connected plate(s)
2. a forced-response energy in the beam, driven by the incident plate waves over a whole spectrum of wavenumbers from zero to the cut-off wavenumbers  $\pm k_p$  of the plate.

#### 4.1 IN-SITU BEAM SUBSYSTEM PROPERTIES

The real part  $k_{Br}$  of the junction wavenumber can be used to define the in-situ beam free wavenumber. The modal density can be calculated from effective group velocity

$$\text{using } n_B = L / \left( \pi \left( \frac{\partial k_{Br}}{\partial \omega} \right) \right) .$$

## 4.2 COUPLING LOSS FACTORS

The imaginary part  $k_{Bi}$  of each of the in-situ beam's wavenumbers indicates that there is a radiation loss to the attached plate. In the proposed SEA model this is represented by a coupling loss factor between the beam subsystem and the plate.

### 4.2.1 Beam to Plate

Langley [6] has suggested that the coupling loss factor from the beam into the plates can be found by equating the in-situ beam's spatial rate of energy decay with the loss factor in a one-dimensional damped subsystem:

$$e^{-k_{Bi}x} \equiv e^{-(\omega\eta/2c_s)x} \quad (4)$$

It then follows that the total loss to the plates can be estimated for each in-situ wavefield as

$$\eta = 2(\partial\omega/\partial k_{Br})k_{Bi}/\omega \quad (5)$$

For the case where there are multiple plate wavefields participating at the junction, the coupling loss factor into each plate  $p$  can be apportioned according to the relative eigenvector-normalized power flows into each plate wavefield

$$\Pi_p = \text{Re} \left\{ \bar{\mathbf{v}}^T \mathbf{Z}_p \mathbf{v} \right\} \quad (6)$$

as follows

$$\eta_{Bp} = \eta \Pi_p / \left( \sum_p \Pi_p \right) \quad (7)$$

### 4.2.2 Plate-to-Beam

The corresponding plate-to-beam coupling loss factor is most conveniently estimated from the reciprocity relation

$$\eta_{pB} = (n_B/n_p)\eta_{Bp} \quad (8)$$

### 4.2.3 Plate-to-Plate Through an in-situ Beam

Langley and Heron [4] provide a complete formulation for general plate-to-plate energy transmission, incorporating the in-line beam in the calculation of the junction's power transmission coefficient. The coefficient  $\tau_{ij}$  for each incident wavefield is calculated versus the junction's trace wavenumber while assuming that the energy in the source plate is diffuse. Each coupling loss factor is calculated from the integral over all wavenumbers according to:

# STATISTICAL ENERGY ANALYSIS OF IN-SITU BEAMS

$$\eta_{ij} = \frac{c_i L}{2\pi\omega A} \int_0^\pi \tau_{ij}(\omega, \phi) \sin\phi d\phi \quad (9)$$

Langley and Heron's formulation does not automatically include the damping in the beam. The beam presents a purely imaginary (reactive) impedance to the incident plate wavefields. Power is either transmitted to another plate or reflected; no power is diverted to the beam. If damping were included in the beam, then the power transmission co-efficient  $\tau_{ij}(\omega, \phi)$  would never reach unity for any incident angle  $\phi$ .

## 4.3 NUMERICAL EXAMPLE

For the beam-plate assembly introduced in section 2, the energy transfer is evaluated and compared here the three different models illustrated in Figure 10:

1. Langley & Heron's method [4] without beam damping
2. Langley & Heron's method with beam damping of  $\eta=0.10$
3. Three subsystem model with beam damping of 0.10

In all cases the plate damping loss factor is 0.05.

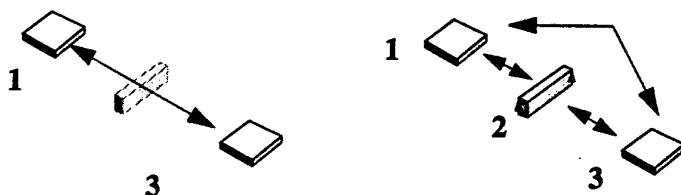


Figure 10. Models 1 and 2 (left); Model 3 (right)

In models 1 and 2, the two plate subsystems are directly connected. The beam is part of the junction. In model 2, a substantial loss factor of 0.1 is applied to the beam, simulating longitudinal transport of energy down the beam as shown in Figure 2. In model 3, the beam is a conventional subsystem, again with a loss factor 0.1.

Figure 11 compares predictions of the transfer function  $E_3/E_1$ —the ratio of energy in receiving plate 3 to driven plate 1—in dB for the three models. We may observe that

1. The inclusion of damping in the beam in model 2 does not significantly change the results compared to model 1.
2. The transfer function is smaller for the two-subsystem models (1 and 2) compared to the three-subsystem model—that is, more energy is predicted to reach the other plate when the beam is a separate SEA subsystem



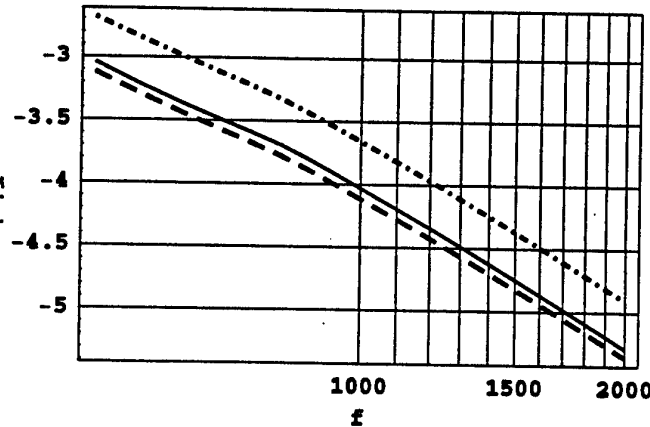


Figure 11. Normalized energy transfer functions  $E_3/E_1$  (dB); — Langley and Heron's method [4] with an undamped beam; - - - [4] with beam damping  $\eta=0.10$ ; - . - . resonant-beam subsystem with  $\eta=0.10$

Figure 12 suggests an explanation of the modestly higher transfer function predicted using model 3.

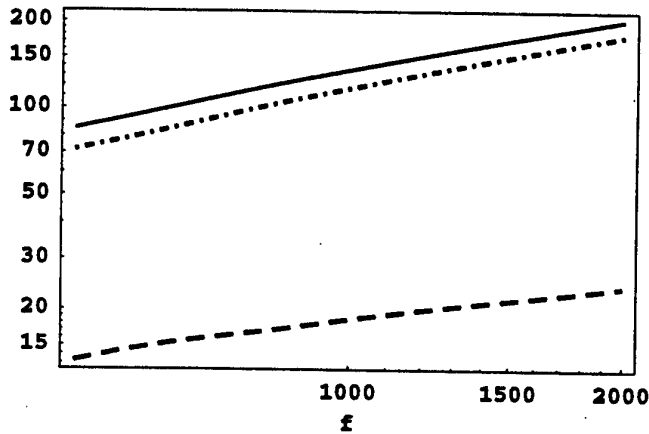


Figure 12. Components of power transmitted to plate subsystem 3; — total power; - - - power from beam subsystem 2; - . - . power from plate subsystem 1.

About 15% of total power transmitted to subsystem 3 comes from the beam (subsystem 2). This additional path is strong enough to explain the 0.5 dB increase in transfer function shown in Figure 11.

## STATISTICAL ENERGY ANALYSIS OF IN-SITU BEAMS

### 5.0 Conclusions

For the example studied, the inclusion of a resonant-beam subsystem contributes to the transfer of energy; model 3 predicts more transfer than models 1 and 2. Future experimental results may show which model is best.

The modest (though significant) difference between the three models is heartening, because the approach of Langley and Heron (model 1) has been validated, and because model 3 is more general, being able in principal to handle the energy flows in Figure 2.

### 6.0 Acknowledgments

The authors gratefully acknowledge the valuable contributions to this topic by Dr. Robin Langley of University of Southampton and Dr. Ken Heron of DERA Farnborough.

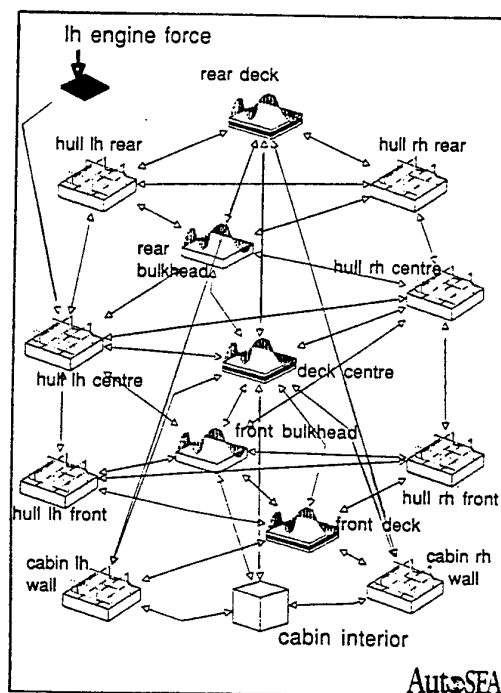
- [1] Lyon, R.H and DeJong, R. (1995) *Theory and Application of Statistical Energy Analysis*, 2nd ed., Butterworth-Heinemann, Newton Massachusetts.
- [2] Fahy, F.J. (1980) *Sound, Structures and their Interaction*, J. Wiley and Sons.
- [3] Goyder, H.G.D. and White, R.G. (1980) "Vibrational Power Flow from Machines into Built-Up Structures, Part II: Wave Propagation and Power Flow in Beam-Stiffened Plates" *J. Sound & Vibration* 68(1) 77-96.
- [4] Langley, R.S. and Heron, K.H. (1990) "Elastic Wave Transmission through Plate/Beam Junctions" *J. Sound & Vibration* 143(2) 241-253.
- [5] Burton, T.E. "AutoSEA v2.0 Theory and Quality Assurance Manual" Vibro-Acoustic Sciences Inc., to be published.
- [6] Langley, R.S. (1996) "An Approach to Modeling the In-Situ Dynamics of Beams", private communication.

# Executive Summary

## Ambient Noise Reduction in Ships & Offshore Structures

Industrial Design Study in Conjunction with MTD

- ✓ Offer Improved Specifications
- ✓ Assess Compliance with Specs
- ✓ Evaluate New Designs
- ✓ Identify Noise Paths
- ✓ Reduce Remedial Work Risk



## A better design technique for controlling noise.....

- Noise is an important design issue for marine structure designers and builders. Meeting regulations and clients' specifications for on-board noise is of growing concern.
- A survey has revealed that most designers and builders see the need for more sophisticated and reliable prediction and optimisation methods, to enable noise to be controlled to specific limits at the design stage and hence to comply with customers' specifications. Better design techniques can also assist competitiveness by aiding low noise design.
- A Managed Programme of the Marine Technology Directorate, which is being coordinated by Marinetechnics South Ltd, is combining the resources of a £0.5M research programme (now in mid-term) with multi-sponsor industrial design projects in order to develop the application of Statistical Energy Analysis (SEA) techniques for design relating to marine craft and offshore installations.
- Statistical Energy Analysis (SEA) is a noise and vibration modelling technique introduced 30 years ago, in particular to design spacecraft to resist damage from acoustically-induced vibration during the launch phase. SEA has since been developed for broader application, particularly for the prediction of sound levels in road vehicles, aircraft and buildings. Its advantage lies in rapid assessment of multiple noise paths.
- Commercial SEA applications packages are available and it is the aim of this study to develop and verify the particular aspects required to meet the needs of the marine industry. The technique will assist the evaluation of new designs and reduce risk in remedial work situations.
- The technique is complementary to Finite Element Analysis (FEA), already in widespread use for the dynamic analysis of structures and components. In fact, the latest developments include combined approaches, with FEA assisting SEA modelling.
- The application study is targeted at ships and offshore structures. A typical structure will be selected for testing the research developments.
- The intended project is costed at £65k over a period of 15 months.
- Sponsors will have the opportunity of influencing the direction and emphasis of the study, at the project definition stage and throughout, and will receive early information on technical progress in this important area of design.
- Proposed deliverables include design guidelines for aspects of SEA modelling particular to marine structure applications.

If you are interested in knowing more about this programme, please contact:

Neil Pinder, Programme Coordinator  
Marinetechnics South Ltd  
Tizard Building (ISVR)  
University of Southampton  
Highfield  
Southampton SO17 1BJ, UK

Tel: +44 (0)1703 593756  
Fax: +44 (0)1703 592728

# **ERRATA: A NOTE ON CONSERVATIVE AND NON-CONSERVATIVE COUPLING**

Claes Fredö  
Ingemansson Technology AB

Equation (2) should be renamed as equation (2a). Manipulating the upper and lower rows of equation (2a) to include the energy flow to subsystem 2 yields that

$$\begin{pmatrix} S_{P1 \rightarrow} \\ S_{P2 \rightarrow} \\ S_{P3 \rightarrow} \end{pmatrix} = \begin{bmatrix} PP_{21} & PP_{12} & PP_{13} \\ (-PP_{31}-PP_{21}) & (-PP_{32}-PP_{12}) & (-PP_{33}-PP_{23}) \\ PP_{31} & PP_{32} & PP_{23} \end{bmatrix} \begin{pmatrix} S_1 \\ S_2 \\ S_3 \end{pmatrix} = [PP^+] \begin{pmatrix} S_1 \\ S_2 \\ S_3 \end{pmatrix} \quad (2b)$$

The superscript + in the matrix  $[PP^+]$  signifies that a row has been added.

The 3rd sentence in the paragraph before equation (5) should read

Equation (3) is similar (and in some situations identical) to the energy part of the "Greens function" formulation that Langley used in reference [4].

Equation (5) should read

$$\begin{pmatrix} S_{P_{in,1}} \\ S_{P_{in,2}} \\ S_{P_{in,3}} \end{pmatrix} = [V] \begin{pmatrix} S_1 \\ S_2 \\ S_3 \end{pmatrix} = ([U] + [PP^+]) \begin{pmatrix} S_1 \\ S_2 \\ S_3 \end{pmatrix} \quad (5)$$

Summing the  $[U]$  and  $[PP^+]$  matrices for the dissipated power and the energy flow out of the subsystems, respectively yields the diagonal  $[V]$  matrix for the power input.

The 1st sentence in the paragraph before equation (15) should read

The experience from the discussion above is that one should be cautious to take the benefits of the uncoupled subsystem energy for granted also for coupled subsystem energy.

Equation (17) should read

$$\begin{pmatrix} S_{P'1 \rightarrow} \\ S_{P'3 \rightarrow} \end{pmatrix} = \begin{bmatrix} PP_{21} & PP_{13} \\ PP_{31} & PP_{23} \end{bmatrix} \begin{pmatrix} S_1 \\ S_3 \end{pmatrix} = [PP'] \begin{pmatrix} S_1 \\ S_3 \end{pmatrix} \quad (17)$$

## **Addendum**

The power input for the non-conservatively coupled case can be divided into the following subparts

$$\begin{pmatrix} S_{P_{in,1}} \\ S_{P_{in,3}} \end{pmatrix} = [V'] \begin{pmatrix} S_1 \\ S_3 \end{pmatrix} = ([U''] + ([U'] + [PP'])) \begin{pmatrix} S_1 \\ S_3 \end{pmatrix} \quad (19b)$$

where the power which is lost in the non-conservative junction is

$$\begin{pmatrix} S_{P'1 \rightarrow} \\ S_{P'3 \rightarrow} \end{pmatrix} = \begin{bmatrix} U_{21} & 0 \\ 0 & U_{23} \end{bmatrix} \begin{pmatrix} S_1 \\ S_3 \end{pmatrix} = [U'] \begin{pmatrix} S_1 \\ S_3 \end{pmatrix} \quad (19c)$$

and the power which is lost in the subsystem is

$$\begin{pmatrix} S_{P'_{diss,1}} \\ S_{P'_{diss,3}} \end{pmatrix} = \begin{bmatrix} U_{11} & U_{13} \\ U_{31} & U_{33} \end{bmatrix} \begin{pmatrix} S_1 \\ S_3 \end{pmatrix} = [U''] \begin{pmatrix} S_1 \\ S_3 \end{pmatrix} \quad (19d)$$

Re-expressing equation (19c) as a function of coupled subsystem energy yields four radiation factors. Re-expressing equation (19d) as a function of coupled subsystem energy yields two dissipation loss factors on the matrix diagonal.

# VIBRATIONAL ENERGY FLOWS BETWEEN TWO PLATES FORMING AN 'L'-SHAPE AND JOINED BY COMPLIANT AND DISSIPATIVE COUPLINGS

M. BESHARA

*Department of Engineering Science,  
University of Oxford,  
Parks Road, Oxford, OX1 3PJ, U.K.*

and

A.J. KEANE

*Department of Mechanical Engineering,  
University of Southampton,  
Highfield, Southampton, SO17 1BJ, U.K.*

## Abstract

The transmission of energy between two coupled plates has been extensively discussed in the literature of structural dynamics. In most of these studies it is assumed that the plates are rigidly joined and that no energy dissipation occurs at the joint, i.e., conservative coupling. In most practical cases, however, the plate elements forming a complex, built-up structure are joined together by welding or fasteners which give rise to energy dissipation in the joints via various forms of friction and damping.

Previous SEA based studies of the transmission of energy through dissipative joints, modelled by springs and viscous dampers, have shown that the effects of dissipation in such joints can give rise to significant changes in the various quantities used in SEA, and in particular to the coupling loss factors used by the method. In this work, the transmission of energy through a compliant and dissipative joint between two plates forming an 'L'-shape is investigated, using a receptance approach. The two plates are assumed to be thin, homogeneous and isotropic. Their common edge is taken to be simply supported so that the joint has relative motions only in its rotational degree of freedom, i.e., translation normal to the plate at the common edge is not permitted. The joint is then assumed to have a constant complex stiffness per unit length, denoted by  $K + i\omega\gamma$  (Nm per m radian). Exact formulae for the spectral densities of the energy flow through the joint, the energy dissipated at the joint and the power input into the plates are established for the case of excitation by random ergodic forcing.

The aim of this study is to examine the effects of the joint damping and compliance on the magnitudes of the energy flows through the joint and the energy levels in the two plates. Interest is focused on the power dissipated at the joint and the conditions under which this quantity is maximised. The coupling and coupling damping loss factors that would be used in an SEA model of this problem are also derived, using the power injection method. These are compared to the results obtained from using a wave

based approach with semi-infinite subsystem models.

### 1. Introduction

In this work, energy flow between two thin rectangular plates which are coupled together by compliant and dissipative joints is considered. This topic is one on which little attention seems to have been focused in the literature. The method adopted for the analysis is based on a receptance approach as used in previous works by Dimitriadis and Pierce[1] to gain an exact solution for the energy flow between two coupled plates, by Fredo[2] for the analysis of energy flows in three thin rectangular plates connected along two simply supported joints and by Kim *et al.*[3] for a general situation such that there are no limitations on the number of connected plates or the junction type. However, these studies have been mainly concerned with rigid or conservative joints. The work presented here addresses the less familiar case of compliant and non-conservative coupling[4]. Exact solutions for the spectral densities of the energy flows and energy levels are found. These results are utilised to derive the coupling and coupling damping loss factors used in SEA studies, by ensemble averaging of the various energy receptances. They are compared to those given by the wave approach for a model of two semi-infinite plates.

### 2. Theory

Consider two simply supported plates coupled together along a compliant and dissipative joint as shown in Figure 1. The plates are assumed to be thin, isotropic and homogeneous so that the classical thin plates theory holds. Each plate  $n$  has thickness  $h_n$ , mass per unit area  $\rho_n$ , viscous damping coefficient  $c_n$  and bending rigidity  $D_n$ . The dimensions of plate  $n$  are  $L_{x_n}$  and  $L_{y_n}$  and the mode shapes are denoted by  $\Psi_{n,i}(x)$  and  $\Phi_{n,j}(y)$ . The joint is assumed to have a constant complex rotational stiffness  $\Omega = K + i\gamma\omega$ , per unit of length. In this case, the coupling moment which acts on the first plate can be written in terms of the mode shapes of both plates as

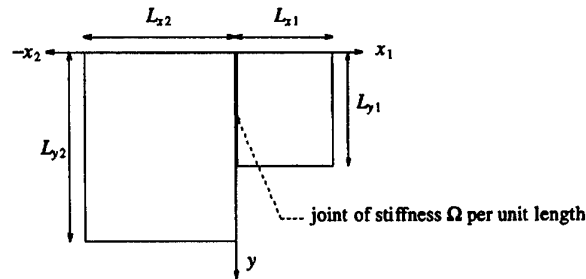


Figure 1. Two simply supported plates coupled together along a boundary to form an 'L'-shape.

$$M_{c1}(y, \omega) = \Omega \sum_j [\Theta_{2,j}(0, \omega) \Phi_{2,j}(y) - \Theta_{1,j}(0, \omega) \Phi_{1,j}(y)] \delta'(x_1 - 0) \quad (1)$$

The coupling moment on the second plate acts only on a length  $L_{y1}$  of its edge and is given by

$$M_{c2}(y, \omega) = \Omega \sum_j [\Theta_{1,j}(0, \omega) \Phi_{1,j}(y) - \Theta_{2,j}(0, \omega) \Phi_{2,j}(y)] U(y - L_{y1}) \delta'(x_2 - 0) \quad (2)$$

where  $U(y - y_1)$  is the unit step function acting at  $y = y_1$ . Using modal analysis, the rotation at the coupled edge of plate one due to the coupling moment distributed along its edge is given by

$$\theta_{c1}(0, y, \omega) = \sum_j G_{1,j\infty}(0, 0, \omega) \Phi_{1,j}(y) \Omega \left[ -\frac{2}{L_{y1}} \sum_k \Theta_{2,k}(0, \omega) q_{1,jk} - \Theta_{1,j}(0, \omega) \right] \quad (3)$$

and the rotation at the edge of plate two due to the coupling moment can be written similarly as follows

$$\theta_{c2}(0, y, \omega) = \sum_j G_{2,j\infty}(0, 0, \omega) \Phi_{2,j}(y) \Omega \frac{2}{L_{y2}} \left[ \sum_k \Theta_{1,k}(0, \omega) q_{1,kj} - \Theta_{2,k}(0, \omega) q_{2,jk} \right] \quad (4)$$

where

$$q_{1,jk} = \int_0^{L_{y1}} \Phi_{1,j}(y) \Phi_{2,k}(y) dy, \quad q_{2,jk} = \int_0^{L_{y1}} \Phi_{2,j}(y) \Phi_{2,k}(y) dy \quad (5,6)$$

Here  $G_{n,j\infty}(x, x^0, \omega)$  is the Green function which gives the  $j$ th component of rotation at point  $x$  of plate  $n$ , denoted by  $\Theta_{n,j}(x, \omega)$ , due to unit  $j$ th component of a modal expansion along the  $y$  axis of moment  $M_{n,j}(x, \omega)$  applied at point  $x^0$ , and is given by

$$G_{n,j\infty}(x, x^0, \omega) = \sum_i \frac{\Psi'_{n,i}(x) \Psi'_{n,i}(x^0)}{\rho_{sn} L_{xn} / 2 H_{n,ij}(\omega)} \quad (7)$$

where  $H_{n,ij}(\omega) = \omega_{n,ij}^2 - \omega^2 + ic_n \omega$  and  $\omega_{n,ij}$  is the natural frequency of mode  $ij$  of plate  $n$ . The compatibility conditions are next satisfied at the coupled edge, which require that the total rotation be equal to the rotation due to the external forcing plus the rotation due to the coupling moments, i.e.,

$$\begin{aligned} \sum_j \Theta_{1,j}(0, \omega) \Phi_{1,j}(y) &= \sum_j \Theta_{1,j}^0(0, \omega) \Phi_{1,j}(y) \\ &+ \sum_j G_{1,j\infty}(0, 0, \omega) \Omega \left[ -\frac{2}{L_{y1}} \sum_k q_{1,jk} \Theta_{2,k}(0, \omega) - \Theta_{1,j}(0, \omega) \right] \Phi_{1,j}(y) \quad (8) \end{aligned}$$

$$\begin{aligned} \sum_j \Theta_{2,j}(0, \omega) \Phi_{2,j}(y) &= \sum_j \Theta_{2,j}^0(0, \omega) \Phi_{2,j}(y) \\ &+ \sum_j G_{2,j\infty}(0, 0, \omega) \Omega \frac{2}{L_{y2}} \left[ \sum_k q_{1,kj} \Theta_{1,k}(0, \omega) - q_{2,jk} \Theta_{2,k}(0, \omega) \right] \Phi_{2,j}(y) \quad (9) \end{aligned}$$

These last two equations may be reduced to



$$\Theta_{1,j}(0,\omega) = \Theta_{1,j}^0(0,\omega) + G_{1,j\infty}(0,0,\omega)\Omega \left[ -\frac{2}{L_{y1}} \sum_k q_{1,jk} \Theta_{2,k}(0,\omega) - \Theta_{1,j}(0,\omega) \right], \quad (10-a)$$

$$\Theta_{2,j}(0,\omega) = \Theta_{2,j}^0(0,\omega) + G_{2,j\infty}(0,0,\omega)\Omega \left[ \sum_k q_{1,kj} \Theta_{1,k}(0,\omega) - q_{2,jk} \Theta_{2,k}(0,\omega) \right]. \quad (10-b)$$

As may be seen from the above equations, the coupling moment couples the modes in the  $y$  direction of both plates, so that each mode  $j$  of plate one interacts with all the modes in the  $y$  direction of plate two. Equations (10) represent an infinite set of coupled algebraic equations and therefore approximate solutions must be explored for a finite number of resonant modes  $n$  in the  $y$  direction for both plates, and so, the infinite set of equations (10) is transformed to two finite  $n \times n$  sets of algebraic equations which can be written as follows

$$\{\Theta_1(0,\omega)\} = \{\Theta_1^0(0,\omega)\} - \Omega [G_1] \left\{ \{\Theta_1(0,\omega)\} - \frac{2}{L_{y1}} [q_1] \{\Theta_2(0,\omega)\} \right\}, \quad (11-a)$$

$$\{\Theta_2(0,\omega)\} = \{\Theta_2^0(0,\omega)\} - \frac{2}{L_{y2}} \Omega [G_2] \left\{ [q_2] \{\Theta_2(0,\omega)\} - [q_1]^T \{\Theta_1(0,\omega)\} \right\}, \quad (11-b)$$

where

$$\{\Theta_1(0,\omega)\} = \begin{Bmatrix} \Theta_{1,1}(0,\omega) \\ \Theta_{1,2}(0,\omega) \\ \vdots \\ \Theta_{1,n}(0,\omega) \end{Bmatrix} \quad \text{and} \quad \{\Theta_2(0,\omega)\} = \begin{Bmatrix} \Theta_{2,1}(0,\omega) \\ \Theta_{2,2}(0,\omega) \\ \vdots \\ \Theta_{2,n}(0,\omega) \end{Bmatrix}. \quad (12,13)$$

$[G_1]$  is a diagonal matrix  $n \times n$  which has the elements  $G_{1,j\infty}(0,0,\omega)$  on its diagonal,  $[G_2]$  is defined similarly.  $[q_1]$  is matrix of dimensions  $n \times n$  which has  $q_{1,ij}$  on the  $i$ th line and  $j$ th column.  $[q_2]$  is defined similarly. Solving the two sets of algebraic equations together gives expressions for the modal rotations at the coupled edge in terms of the modal rotations at the edge due to external forcing alone. If the following notation is introduced

$$[Q_{11}] = [I] + \Omega [G_1] \quad , \quad [Q_{22}] = [I] + \frac{2}{L_{y2}} \Omega [G_2] [q_2] \quad (14,15)$$

$$[Q_{12}] = -\frac{2}{L_{y1}} \Omega [G_1] [q_1] \quad , \quad [Q_{21}] = -\frac{2}{L_{y2}} \Omega [G_2] [q_1]^T \quad (16,17)$$

then the solution of the previous equations can be written as follows

$$\begin{aligned} \{\Theta_1(0,\omega)\} &= [[Q_{11}] - [Q_{12}][Q_{22}]^{-1}[Q_{21}]]^{-1} \{\Theta_1^0(0,\omega)\} \\ &\quad + [[Q_{21}] - [Q_{22}][Q_{12}]^{-1}[Q_{11}]]^{-1} \{\Theta_2^0(0,\omega)\}, \quad (18-a) \\ \{\Theta_2(0,\omega)\} &= [[Q_{12}] - [Q_{11}][Q_{21}]^{-1}[Q_{22}]]^{-1} \{\Theta_1^0(0,\omega)\} \end{aligned}$$

$$+[[Q_{22}]-[Q_{21}][Q_{11}]^{-1}[Q_{12}]]^{-1}\{\Theta_2^0(0,\omega)\} \quad (18-b)$$

For convenience, these last two equations are written as follows

$$\begin{Bmatrix} \{\Theta_1(0,\omega)\} \\ \{\Theta_2(0,\omega)\} \end{Bmatrix} = \begin{bmatrix} [X_{11}] & [X_{12}] \\ [X_{21}] & [X_{22}] \end{bmatrix} \begin{Bmatrix} \{\Theta_1^0(0,\omega)\} \\ \{\Theta_2^0(0,\omega)\} \end{Bmatrix} \quad (19)$$

It is obvious that the modal rotation  $\{\Theta_{1,j}(0,\omega)\}$  is dependent on all the modal rotations  $\{\Theta_{n,j}^0(0,\omega)\}$  through the elements of the matrices  $[q_1]$  and  $[q_2]$ . When the mode shapes in the  $y$  direction are identical then the matrices  $[q_1]$  and  $[q_2]$  become diagonal and the previous equations are then decoupled. In this case the modal rotation  $\{\Theta_{n,j}(0,\omega)\}$  depends only on the characteristics of mode  $j$  of both plates while the other modes have no effect. Hence,

$$\Theta_{1,j}(0,\omega) = \frac{(1+\Omega G_{2,j\infty}(0,0,\omega))}{\Delta_j(\omega)} \Theta_{1,j}^0(0,\omega) + \frac{\Omega G_{1,j\infty}(0,0,\omega)}{\Delta_j(\omega)} \Theta_{2,j}^0(0,\omega), \quad (20-a)$$

$$\Theta_{2,j}(0,\omega) = \frac{\Omega G_{2,j\infty}(0,0,\omega)}{\Delta_j(\omega)} \Theta_{1,j}^0(0,\omega) + \frac{(1+\Omega G_{1,j\infty}(0,0,\omega))}{\Delta_j(\omega)} \Theta_{2,j}^0(0,\omega), \quad (20-b)$$

where  $\Delta_j(\omega) = 1 + \Omega (G_{1,j\infty}(0,0,\omega) + G_{2,j\infty}(0,0,\omega))$ .

### 3. Energy Flow, Energy Dissipation at the Joint and Input Power

The spectral density of the energy flow is given by

$$\Pi_{12}^I(\omega) = \int_0^{L_{y1}} i\Omega \omega S_{\theta_1, \theta_2}(y, \omega) dy + \int_0^{L_{y1}} \gamma \omega^2 S_{\theta_1, \theta_1}(y, \omega) dy \quad (21)$$

where the rotations at the edge  $\theta_1(y, \omega)$  and  $\theta_2(y, \omega)$  are given by  $\{\Theta_1(0, \omega)\}^T \{\Phi_{1,j}(y)\}$  and  $\{\Theta_2(0, \omega)\}^T \{\Phi_{2,j}(y)\}$ , respectively. Substituting in the expression for the energy flow gives

$$\begin{aligned} \Pi_{12}^I(\omega) = & i\Omega \omega \lim_{T \rightarrow \infty} \frac{2\pi}{T} [\{\Theta_1^*(0, \omega)\}^T [q_1] \{\Theta_2(0, \omega)\}] \\ & + \gamma \omega^2 L_{y1} / 2 \lim_{T \rightarrow \infty} \frac{2\pi}{T} [\{\Theta_1^*(0, \omega)\}^T \{\Theta_1(0, \omega)\}] \quad (22) \end{aligned}$$

Assuming that the forces acting on both plates are incoherent so that  $S_{\theta_{1j}^0, \theta_{2k}^0} = 0$ , the expression for the energy flow becomes

$$\begin{aligned} \Pi_{12}^I(\omega) = & \text{Re} \{ i\Omega \omega \{ \sum_j \sum_k [[X_{11}^*]^T [q_1] [X_{21}]]_{jk} S_{\theta_{1j}^0, \theta_{1k}^0} + \sum_j \sum_k [[X_{12}^*]^T [q_1] [X_{22}]]_{jk} S_{\theta_{1j}^0, \theta_{2k}^0} \} \\ & + \gamma \omega^2 L_{y1} / 2 \{ \sum_j \sum_k [[X_{11}^*]^T [X_{11}]]_{jk} S_{\theta_{1j}^0, \theta_{1k}^0} + \sum_j \sum_k [[X_{12}^*]^T [X_{12}]]_{jk} S_{\theta_{1j}^0, \theta_{2k}^0} \} \} \quad (23) \end{aligned}$$

As noted above, the effect of each mode in the  $y$  direction on each plate is not separable from the effects of the other modes. The energy flow from plate two to plate one is similarly given by the expression

$$\begin{aligned} \Pi_{21}^I(\omega) = & \text{Re}\{i\Omega\omega\left\{\sum_{j,k}[[X_{21}^*]^T[q_1]^T[X_{11}]]_{jk} S_{\Theta_{1,j}\Theta_{1,k}} + \sum_{j,k}[[X_{22}^*]^T[q_1]^T[X_{12}]]_{jk} S_{\Theta_{1,j}\Theta_{2,k}}\right\} \\ & + \gamma\omega^2\left\{\sum_{j,k}[[X_{21}^*]^T[q_2]^T[X_{21}]]_{jk} S_{\Theta_{1,j}\Theta_{1,k}} + \sum_{j,k}[[X_{22}^*]^T[q_2]^T[X_{22}]]_{jk} S_{\Theta_{1,j}\Theta_{2,k}}\right\}\} \quad (24) \end{aligned}$$

For the case of two plates which have the same width, the previous equations are simplified considerably. The energy flow from plate one to plate two can then be written as an infinite sum over the modes in the  $y$  direction as

$$\Pi_{12}^I(\omega) = \sum_j (i\Omega\omega L_y/2 S_{\Theta_{1,j}\Theta_{2,j}}(\omega) + \gamma\omega^2 L_y/2 S_{\Theta_{1,j}\Theta_{1,j}}(\omega)) = \sum_j \Pi_{12,j}^I(\omega) \quad (25)$$

where the  $j$ th component of the energy flow is

$$\begin{aligned} \Pi_{12,j}^I(\omega) = & i\Omega\omega L_y/2 \left[ \frac{\Omega G_{2,j\infty}(0,0,\omega) + |\Omega G_{2,j\infty}(0,0,\omega)|^2}{|\Delta_j(\omega)|^2} S_{\Theta_{1,j}\Theta_{1,j}}(\omega) \right. \\ & \left. + \frac{\Omega^* G_{1,j\infty}(0,0,\omega) + |\Omega G_{1,j\infty}(0,0,\omega)|^2}{|\Delta_j(\omega)|^2} S_{\Theta_{2,j}\Theta_{2,j}}(\omega) \right] \\ & + \gamma\omega^2 L_y/2 \left[ \frac{|1 + \Omega G_{2,j\infty}(0,0,\omega)|^2}{|\Delta_j(\omega)|^2} S_{\Theta_{1,j}\Theta_{1,j}}(\omega) + \frac{|\Omega G_{1,j\infty}(0,0,\omega)|^2}{|\Delta_j(\omega)|^2} S_{\Theta_{2,j}\Theta_{2,j}}(\omega) \right] \quad (26) \end{aligned}$$

The spectral density of the modal rotation of plate  $n$  along the common edge is written in terms of the spectral density of the modal forces as follows

$$S_{\Theta_{n,j}\Theta_{n,j}} = \sum_{i,k} \frac{\Psi'_{n,i}(0)\Psi'_{n,k}(0)}{(M_n/4)^2 H_{n,ij}^*(\omega)H_{n,kj}(\omega)} S_{F_{n,ij}F_{n,kj}}(\omega) \quad n=1,2 \quad (27)$$

so that the expression for the energy flow becomes

$$\begin{aligned} \Pi_{12,j}^I(\omega) = & \left[ \frac{-\omega|\Omega|^2 L_y/2}{|\Delta_j(\omega)|^2} \text{Im} \left[ \sum_r \frac{\Psi_{2,r}'(0)}{\rho_{s2} L_{x2}/2 H_{2,rj}(\omega)} \right] + \frac{\gamma\omega^2 L_y/2}{|\Delta_j(\omega)|^2} \right] \\ & \times \sum_{i,k} \frac{\Psi'_{1,i}(0)\Psi'_{1,k}(0)}{(M_1/4)^2 H_{1,ij}^*(\omega)H_{1,kj}(\omega)} S_{F_{1,ij}F_{1,kj}}(\omega) \\ & + \frac{\omega|\Omega|^2 L_y/2}{|\Delta_j(\omega)|^2} \text{Im} \left[ \sum_i \frac{\Psi_{1,i}'(0)}{\rho_{s1} L_{x1}/2 H_{1,ij}(\omega)} \right] \sum_m \frac{\Psi'_{2,r}(0)\Psi'_{2,m}(0)}{(M_2/4)^2 H_{2,rj}^*(\omega)H_{2,mj}(\omega)} S_{F_{2,rj}F_{2,mj}}(\omega) \quad (28) \end{aligned}$$

The expression for the energy flow from plate two to plate one is derived similarly. Lastly, the energy dissipated at the joint can be recovered from the energy balance at the joint. It is given by  $\Pi_{DC}(\omega) = \sum_j \Pi_{DC,j}(\omega)$  where  $\Pi_{DC,j}(\omega)$  is the sum of  $\Pi_{12,j}^I(\omega)$  and  $\Pi_{21,j}^I(\omega)$  and is given by

$$\begin{aligned} \Pi_{DC,j}(\omega) = & \frac{\gamma \omega^2 L_y / 2}{|\Delta_j(\omega)|^2} \sum_i \sum_k \frac{\Psi'_{1,i}(0) \Psi'_{1,k}(0)}{(M_1/4)^2 H_{1,ij}^*(\omega) H_{1,kj}(\omega)} S_{F_{1,ij} F_{1,kj}}(\omega) \\ & + \frac{\gamma \omega^2 L_y / 2}{|\Delta_j(\omega)|^2} \sum_r \sum_m \frac{\Psi'_{2,r}(0) \Psi'_{2,m}(0)}{(M_2/4)^2 H_{2,rj}^*(\omega) H_{2,mj}(\omega)} S_{F_{2,rj} F_{2,mj}}(\omega) \end{aligned} \quad (29)$$

The spectral density of the input power due to a vertical force applied to plate one is calculated from the product of force and velocity at the point of its application and is given by

$$\begin{aligned} \Pi_{N_1}(\omega) = & -i\omega \lim_{T \rightarrow \infty} \frac{2\pi}{T} \int_0^{L_x} \int_0^{L_y} v_1^*(x_1, y, \omega) f_1(x_1, y, \omega) dx_1 dy \\ = & -i\omega \lim_{T \rightarrow \infty} \frac{2\pi}{T} \sum_i \sum_j V_{1,ij}^*(\omega) F_{1,ij}(\omega) \end{aligned} \quad (30)$$

Substituting  $V_{1,ij}(\omega)$  by its value in terms of the modal forcing components and assuming that the forces acting on the two plates are incoherent, i.e.,  $S_{F_{2,kj} F_{1,ij}}(\omega) = 0$ , the input power to plate 1 is given by

$$\begin{aligned} \Pi_{N_1}(\omega) = & \frac{\omega}{M_1/4} \sum_i \sum_j \text{Im} \left\{ \frac{1}{H_{1,ij}^*(\omega)} \right\} S_{F_{1,ij} F_{1,ij}}(\omega) \\ & - \frac{\omega}{(M_1/4)^2} \sum_i \sum_j \left[ \sum_k \sum_r \sum_m \text{Im} \left\{ X_{21,kr} \frac{\Psi'_{1,i}(0) \Psi'_{1,m}(0) \Omega}{H_{1,ij}(\omega) H_{1,mr}(\omega)} \right\} \right. \\ & \times q_{1,jk} S_{F_{1,mr} F_{1,ij}}(\omega) - \sum_r \sum_m L_{y1} / 2 \text{Im} \left\{ X_{11,jr} \frac{\Psi'_{1,i}(0) \Psi'_{1,m}(0) \Omega}{H_{1,ij}(\omega) H_{1,mr}(\omega)} \right\} S_{F_{1,mr} F_{1,ij}}(\omega) \left. \right] \end{aligned} \quad (31)$$

For the special case when the plates have the same width, the expression for the spectral density of the input power to the first plate is written as

$$\begin{aligned} \Pi_{N_1}(\omega) = & \frac{\omega}{M_1/4} \sum_i \sum_j \text{Im} \left\{ \frac{1}{H_{1,ij}^*(\omega)} \right\} S_{F_{1,ij} F_{1,ij}}(\omega) \\ & + \frac{\omega L_y / 2}{(M_1/4)^2} \sum_i \sum_j \sum_m \text{Im} \left\{ \frac{\Psi'_{1,i}(0) \Psi'_{1,m}(0) \Omega}{H_{1,ij}(\omega) H_{1,mj}(\omega) \Delta_j(\omega)} \right\} S_{F_{1,mj} F_{1,ij}}(\omega) \end{aligned} \quad (32)$$

The expression for the input power to plate two can be derived similarly.

For the case of modally incoherent forcing, the spectral density of the driving forces is given by  $S_{f_n f_n}(\omega, x_n, \hat{x}_n, y, \hat{y}) = 4 S_{F_n F_n}(\omega) \delta(x_n - \hat{x}_n) \delta(y - \hat{y}) / A_n$  and the spectral density of the modal forces is then  $S_{F_n,ij} F_{n,kj}(\omega) = S_{F_n F_n}(\omega) \delta_{ik}$ . The spectral densities of the energy flows, energy dissipation at the joint and input power due to external forcing can then be recovered when these expressions for the modal forcing spectral densities are substituted in the equations above.

#### 4. Determination of Coupling and Coupling Damping Loss Factors for two Coupled Plates

In the previous sections, exact expressions for the various energy receptances for the case of two nonconservatively coupled plates have been derived. Assuming that deterministic knowledge of the plates is not available, their characteristics can only be described probabilistically. All energy receptances are then expressed as ensemble averages, which are taken across a supposedly infinite set of grossly similar systems, in which the individual members differ in some unpredictable detail. Thus, the ensemble averages of the input power, energy leaving one plate and energy dissipated internally and in the coupling damping are written as follows (assuming linear systems and independent ergodic random forcing and where ensemble averages are denoted by  $E[\cdot]$ ),

$$E[\Pi_{IN_1}(\omega)] = E[H_{IN_1}(\omega)] S_{F_1 F_1}(\omega), \quad E[\Pi_{DISS_1}(\omega)] = c_1 E[E_1(\omega)], \quad (33,34)$$

$$E[\Pi'_{12}(\omega)] = E[H_{12}(\omega)] S_{F_1 F_1}(\omega) + E[H_{DC_1}(\omega)] S_{F_1 F_1}(\omega) - E[H_{21}(\omega)] S_{F_2 F_2}(\omega), \quad (35)$$

$$E[\Pi_{DC}(\omega)] = E[H_{DC_1}(\omega)] S_{F_1 F_1}(\omega) + E[H_{DC_2}(\omega)] S_{F_2 F_2}(\omega). \quad (36)$$

The energy balance equation for subsystem one may be written as

$$E[\Pi_{IN_1}(\omega)] - E[\Pi_{DISS_1}(\omega)] - E[\Pi'_{12}(\omega)] = 0, \quad (37)$$

and similarly for subsystem two with that for the damper as

$$E[\Pi'_{12}(\omega)] + E[\Pi'_{21}(\omega)] = E[\Pi_{DC}(\omega)]. \quad (38)$$

Rearranging these equations (for white noise forcing) leads to the following equations, which are similar in structure to the traditional SEA equations,

$$E[\Pi'_{12}(\omega)] = \omega \eta_{12} E[E_1(\omega)] - \omega \eta_{21} E[E_2(\omega)] + \omega \zeta_{12} E[E_1(\omega)] \quad (39)$$

and

$$E[\Pi_{DC}(\omega)] = \omega \zeta_{12} E[E_1(\omega)] + \omega \zeta_{21} E[E_2(\omega)] \quad (40)$$

where

$$\omega \eta_{12} = c_1 E[H_{12}(\omega)] E[H_{IN_2}(\omega)] / D, \quad (41)$$

$$\omega \zeta_{12} = \frac{c_1}{D} \left\{ (E[H_{IN_2}(\omega)] - E[H_{21}(\omega)] - E[H_{DC_2}(\omega)]) E[H_{DC_1}(\omega)] - E[H_{12}(\omega)] E[H_{DC_2}(\omega)] \right\}, \quad (42)$$

and

$$D = (E[H_{IN_1}(\omega)] - E[H_{DC_1}(\omega)]) (E[H_{IN_2}(\omega)] - E[H_{DC_2}(\omega)])$$

$$\begin{aligned}
& -E[H_{12}(\omega)](E[H_{IN_2}(\omega)] - E[H_{DC_2}(\omega)]) \\
& -E[H_{21}(\omega)](E[H_{IN_1}(\omega)] - E[H_{DC_1}(\omega)])
\end{aligned} \quad (43)$$

and again the expressions for subsystem two,  $\eta_{21}$  and  $\zeta_{21}$  are similar.  $\eta_{12}$  is the coupling loss factor which relates the energy *transferred* to plate 2 to the energy level of plate 1.  $\eta_{21}$  is defined similarly.  $\zeta_{12}$  and  $\zeta_{21}$  are called the coupling damping loss factors and relate the energy dissipated in the coupling element to the energy levels of both plates. Hence, the CLF and CDLF are given in terms of the ensemble averages of the energy receptances which should be taken for the case of rain-on-the-roof driving to be consistent with the conventional assumptions of SEA. Note that the CLF and CDLF are both dependent on coupling damping.

TABLE 1. Parameters used in the examples

Parameter	Plate 1	Plate 2	Units
Mass density ( $\rho_s$ )	78.00	78.00	kg/m <sup>2</sup>
Length ( $L_x$ )	1.200	0.80	m
width ( $L_y$ )	1.0	1.0	m
Rigidity(D)	$1.923 \times 10^4$	$1.923 \times 10^4$	Nm
Damping strength (c)	10	10	s <sup>-1</sup>

### 5. Numerical Examples

Consider two simply supported plates coupled together where the first plate is driven by a rain-on-the-roof forcing. The properties of the two plates are given in Table (1). Interest is focused on the ratios of the energy dissipated in the joint and in plates one and two to the power input by the external forcing, denoted by  $R_d$ ,  $R_1$  and  $R_2$ , respectively. To begin with, the spring stiffness is given one of the values  $10^4$  N (= Nm/rad/m),  $10^6$  N and  $10^8$  N, respectively, while the damper strength is increased. The ratios  $R_d$ ,  $R_1$  and  $R_2$  are plotted in Figure 2. For the case of the weak spring, it is seen that when the damper strength is weak, most of the input power is dissipated in the first plate, while the energy transferred through, and dissipated in, the coupling damper are at minimum levels. As the damper strength increases, the energy dissipated in plate 1 drops until it reaches a minimum level for moderate coupling strength. The energy dissipated in plate 2 on the other hand increases as the coupling strength increases, as does the energy dissipated in the damper. It is seen that in this case the bulk of the input power is dissipated in the coupling damper with only a small percentage of the input power dissipated in plates 1 and 2. When the damper strength increases further, the ratio  $R_d$  decreases as the damper becomes blocked while, on the other hand,  $R_1$  and  $R_2$  increase again to reach constant levels for the limit of a rigid joint. When the three ratios  $R_d$ ,  $R_1$  and  $R_2$  are plotted for the case of the stiff spring of stiffness  $10^8$  N, it is noticed that the ratio  $R_d$  has the same pattern of behaviour as before and reaches a maximum at  $\gamma_0 = K_0/\omega$  but it is seen that this ratio is very small for all values of the damper strength, as might be expected since the damper is essentially always blocked by the very stiff spring. It follows that the power input is dissipated

mostly in the plates. In this case, the ratios  $R_1$  and  $R_2$  remain at nearly constant levels for all values of the damper strength, which represent the limit for a rigid joint.

## 6. Comparison with the Wave Approach

The coupling loss factors (CLF) used in SEA analyses can also be obtained based on a wave approach where the wave transmission and reflection coefficients across junctions of semi-infinite systems are used to indirectly evaluate the CLF. Following the traditional wave approach, see Lyon[5], the coupling loss factor (when the joint is dissipative) may be given by

$$\eta_{12}(\omega) = 2/\pi \int_0^{\pi/2} \frac{\tau_{12}(\theta, \omega) c_g L \sin \theta}{\omega A_1 (2 - \tau_{12}(\theta, \omega) - \nu_{12}(\theta, \omega))} d\theta \quad (44)$$

where  $c_g$  is the bending wave speed,  $A$  is the plate area and  $L$  is the length of the junction.  $\tau_{12}(\theta, \omega)$  and  $\nu_{12}(\theta, \omega)$  are the infinite wave transmission and dissipation coefficients which are functions of the wave heading angle at the junction, denoted by  $\theta$ . In order to obtain the values of the CLF,  $\tau_{12}(\theta, \omega)$  and  $\nu_{12}(\theta, \omega)$  are first determined for a model of two semi-infinite plates with compliant joint following a similar approach to Langely and Heron[6] and the coupling loss factors are then obtained using the equation above.

For the case of nonconservative coupling, formulae for the coupling damping loss factors can be developed using the same method adopted for the CLF. These may be shown to be related to the infinite system dissipation and transmission coefficients by the expression

$$\zeta_{12}(\omega) = 2/\pi \int_0^{\pi/2} \frac{\nu_{12}(\theta, \omega) c_g L \sin \theta}{\omega A_1 (2 - \tau_{12}(\theta, \omega) - \nu_{12}(\theta, \omega))} d\theta \quad (45)$$

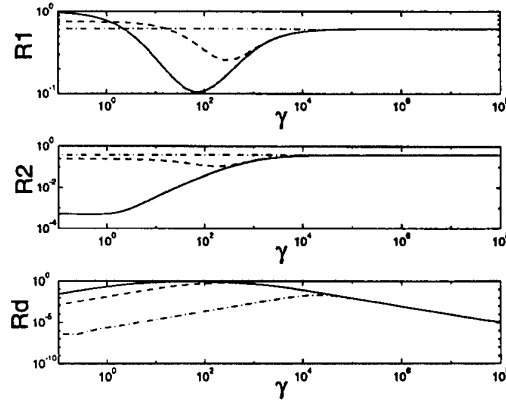


Figure 2. Variation in  $R_1$ ,  $R_2$  and  $R_d$  with  $\gamma_0$  for  $\omega=10000$  rad/sec for the case of two simply supported plates coupled through rotation; (—),  $K_0=1 \times 10^4$  N; (---),  $K_0=1 \times 10^6$  N and (-.-),  $K_0=1 \times 10^8$  N.

Figures 3 and 4 show the values of  $\eta_{12}$  and  $\zeta_{12}$  obtained by the wave approach compared with the results based on the deterministic analysis where arithmetic frequency averages are taken over a bandwidth of 300 Hertz. Plots are given for the case of low modal overlap factor (MOF) (which is associated with the example discussed above) and for MOF larger than unity (which is achieved by increasing the dimensions of both plates). Here the spring strength is taken to be weak while the damper strength is chosen so that the energy dissipation at the coupling is significant. It is noted that the results given by both methods are in agreement for large MOF, as expected, and that  $\zeta_{12}$  has significant values compared to  $\eta_{12}$ . The results are also in broad agreement for low MOF although the wave analysis fails to reveal much of the detail present in the modal approach.

## 7. Conclusions

A receptance approach has been presented for the analysis of energy flows and energy levels in thin rectangular plates coupled together by compliant and dissipative joints to form an 'L'-shape. It is shown that joint damping is most effective when the coupling is in the transitional region between weak and strong and that for strong coupling regimes, the nonconservative nature of the joint may be ignored with little error. The coupling and coupling damping loss factors used in SEA studies are also derived in terms of ensemble averages of the energy receptances and compared to those derived using a traditional wave approach. Reasonable agreement is obtained but some detail is lost when using the wave approach.

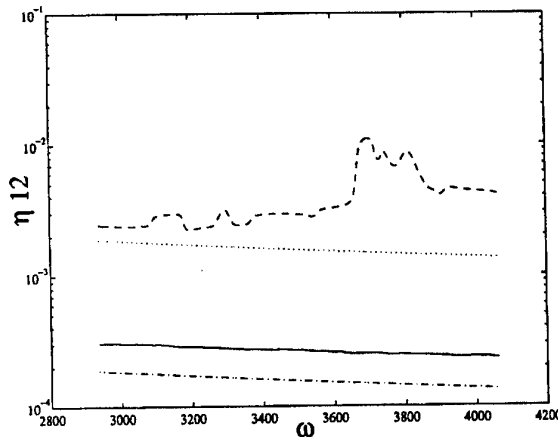


Figure 3.  $\eta_{12}$  calculated using the deterministic analysis and compared with the results of the wave approach for the case of two nonconservatively coupled plates; (—),  $\eta_{12}$  from equation (41) for modal overlap greater than one; (---),  $\eta_{12}$  from equation (41) for modal overlap much less than one; (-.-.),  $\eta_{12}$  from equation (44) for modal overlap greater than one; (...)  $\eta_{12}$  from equation (44) for modal overlap much less than one.



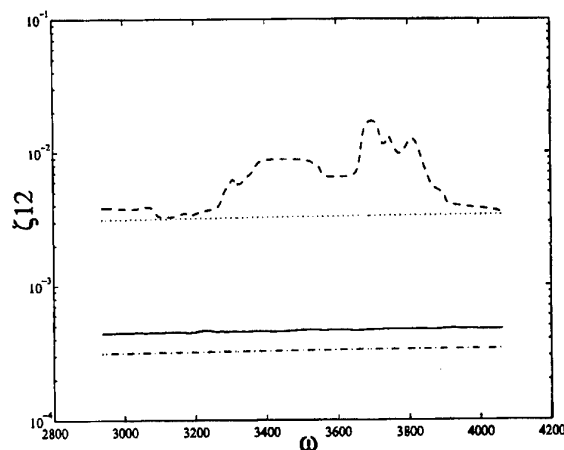
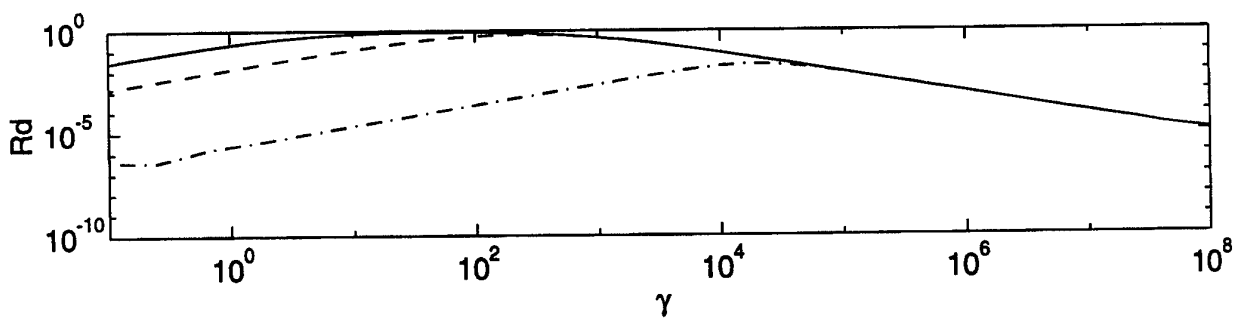
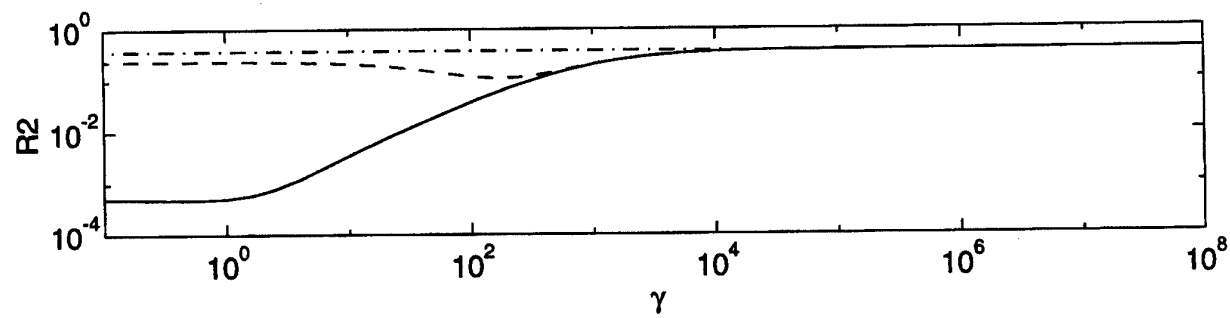
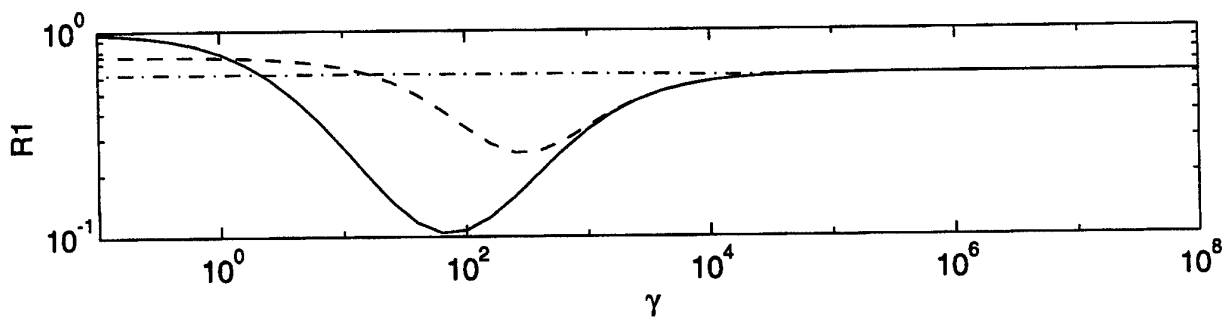
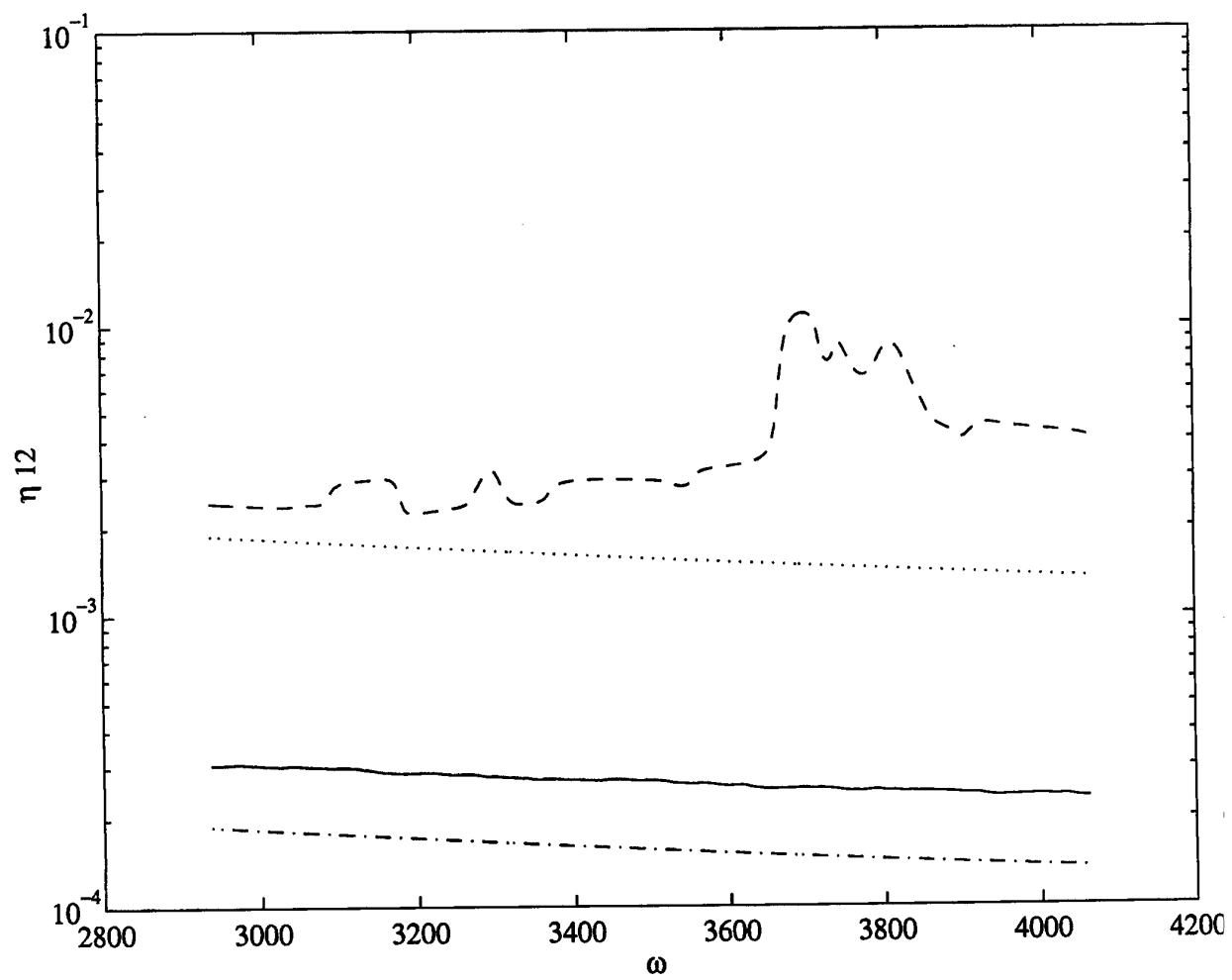


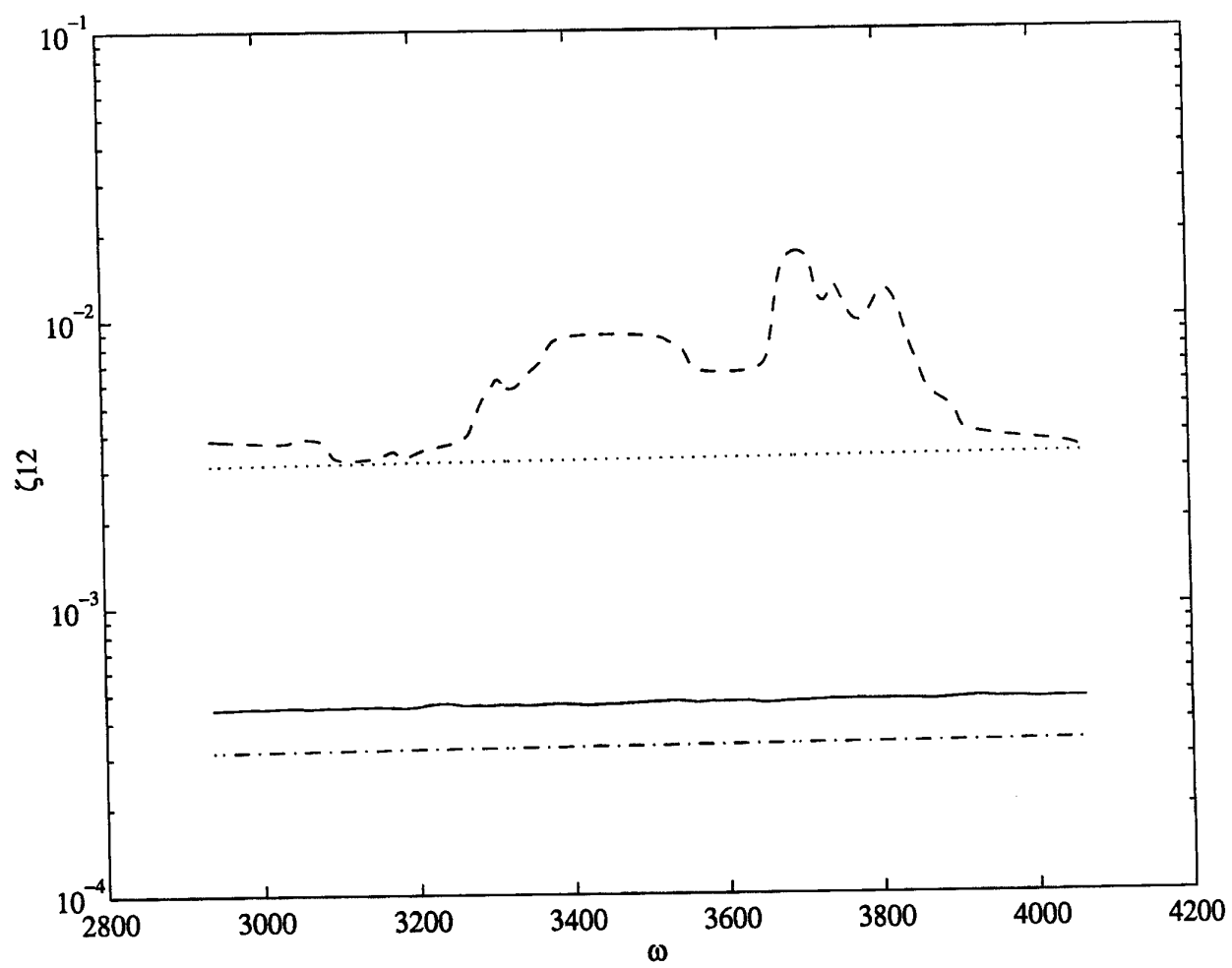
Figure 4.  $\zeta_{12}$  calculated using the deterministic analysis and compared with the results of the wave approach for the case of two nonconservatively coupled plates; (—),  $\zeta_{12}$  from equation (42) for modal overlap greater than one; (---),  $\zeta_{12}$  from equation (42) for modal overlap much less than one; (-.-),  $\zeta_{12}$  from equation (45) for modal overlap greater than one (....)  $\zeta_{12}$  from equation (45) for modal overlap much less than one.

## 8. References

1. E. K. Dimitriadis and A. D. Pierce, "Analytical Solution for the Power Exchange between Strongly Coupled Plates under Random Excitation: A Test of Statistical Energy Analysis Concepts," *J. Sound Vib.* **123**(3) pp. 497-412 (1988).
2. C. R. Fredo, "Statistical energy analysis and the individual case.," Ph.D. Thesis, Chalmers Institute of Technology, Sweden. (1995).
3. Hyun-Sil Kim, Hyun-Joo Kang, and Jae-Seung Kim, "Transmission of bending waves in inter-connected rectangular plates," *J. Acoust. Soc. Am* **96**(3) pp. 1557-1562 (1994).
4. M. Beshara and A. J. Keane, "Statistical energy analysis of multiple, non-conservatively coupled systems," *J. Sound Vib.* **198**(1) pp. 95-122 (1996).
5. R. H. Lyon, *Statistical Energy Analysis of Dynamical Systems : Theory and Applications*, MIT Press (1975).
6. R. S. Langley and K. H. Heron, "Elastic wave transmission through plate/beam junctions," *J. Sound Vib.* **143**(2) pp. 241-253 (1990).







## SEA COUPLING FACTORS FOR REGULAR AND IRREGULAR STRUCTURES

JEROME E. MANNING  
*Cambridge Collaborative, Inc.*  
*Cambridge, Massachusetts 02138-1002*

### Abstract

The research reported in this paper studies the coupling between regular, rectangular plates and irregular, five-sided plates separated by a beam. Both experimental and analytical results are reported. The coupling between irregular plates is found to follow the conventional SEA modeling procedure with a single subsystem representing the bending modes of each plate. The coupling between regular plates, however, requires a different modeling procedure, with the bending modes of each plate divided into subgroups according to wavenumber matching along the boundaries of the connection. The significance of this result for SEA modeling of realistic structures is studied by including the effect of irregular boundary impedances on the SEA modeling. Finite element results are used to show that irregular boundary impedances can have the same effect as irregular shapes, so that use of the conventional SEA modeling procedure may be acceptable for regular, rectangular plates in realistic systems such as vehicles, aircraft, and other products.

### 1. Introduction

There is a tendency in vibration and acoustic analysis to look for "exact" solutions. It is assumed that the response of a system can be predicted exactly as long as the parameters defining the system are specified exactly. Finite element and boundary element analyses are well known examples of deterministic prediction procedures in which greater accuracy is achieved by improving the accuracy of the model description.

Uncertainties in response prediction due to random excitation forces and manufacturing tolerances are accepted, but without enthusiasm. Randomness is associated with a lack of precision, since we can no longer predict the exact response at a single point in time and space. As scientists and engineers we hesitate to regard uncertainty and lack of precision as beneficial effects. However, randomness can bring about simplifications in the analysis, which we must regard favorably since a simplified analysis helps to reduce analysis time and cost.

Statistical analysis procedures allow predictions of the average response to be made in terms of average properties of the system being studied. Using these procedures we no longer look for "exact" solutions and therefore we no longer need to describe the system properties exactly. Of course, when we use a statistical analysis, we must accept a prediction that agrees with measured data only in an average sense.

Statistical energy analysis has become an accepted statistical analysis procedure for structural-acoustic problems [Manning 1997]. SEA takes advantage of the inherent randomness in these systems and allows predictions of the average response to be made using only average system properties. The simplicity of SEA is its strongest feature.

In nearly all SEA predictions the mean response is predicted. The variance of the response and other higher order statistics of the response are not considered. Therefore, it is difficult, if not impossible, to assess the accuracy of a SEA model based on a comparison between a prediction of the mean and measured data from one member of the ensemble of systems being considered. Thus, questions continue to arise about the reliability of the SEA predictions. When combined with measured data to validate the model predictions, SEA provides a useful technique to identify noise and vibration transmission paths and to study the sensitivity of system response on parameter variations. When no data are available to validate the prediction model, the reliability of the SEA prediction depends on the skill and experience of the analyst and the extent to which the response of the individual member of the ensemble of systems equals the ensemble average.

Due to the growing popularity of SEA there is significant work underway to quantify the assumptions made in SEA. Questions regarding the minimum number of subsystem modes, light coupling approximations, and the effect of low modal overlap are common. However, the statistical nature of SEA is often forgotten and the validity of the procedure is assessed by comparison with predictions or measurements on idealized, deterministic systems that are not statistical. When using SEA, more attention needs to be given to identify (at least qualitatively) the ensemble of random systems being considered.

## 2. SEA Assumptions

Statistical Energy Analysis requires that the system being modeled be divided into subsystems as described in Lyon and DeJong (1995). Each subsystem represents a group of modes, and it is assumed that each mode in the group has the same energy - at least within the statistical concept of the average energy over an ensemble of systems. For this equipartition of energy to occur, the modes in a subsystem should have similar excitation, damping, and coupling to other subsystems.

Subsystem divisions are generally made at the boundaries of physical substructures, so that the SEA model can be represented by a set of coupled plates, shells, beams, and acoustic spaces. Often only the bending modes of each substructure are considered. In more advanced models, both bending and inplane compression and shear modes are considered. The bending and inplane modes are placed in separate subsystems to satisfy the assumption of equipartition of energy within a subsystem.

SEA coupling factors are then calculated using asymptotic modal densities and impedances of infinite and semi-infinite systems. The shape of the substructures used in the model does not enter into these calculations, so that the distinction between regularly-shaped and irregularly-shaped structures is lost. The ensemble of systems consists of plates with equal area but different shapes.

Many of the early studies of SEA used irregular plates with no two boundaries parallel, e.g. Lyon and Eichler (1964). The irregular plate represented one member of an ensemble of plates with random shapes and boundary conditions, although the ensemble was not explicitly defined. In these early studies it was assumed that the irregular plate was a better representative of actual structures used in vehicles, aircraft, and other products. This assumption is often valid, but when it is not, predictions obtained using SEA may become unreliable.

Measurements on rectangular plates with idealized free, clamped, or simply-supported boundary conditions show significant deviations from the ensemble mean predicted by SEA. This deviation is due to the regular nature and symmetry of the rectangular plate. Measurements on irregular plates are found to be in better agreement with the SEA mean. Since the irregular plate does not always provide a good representation of a system, improvements in SEA modeling procedures for rectangular plates with idealized boundary conditions are needed.

## 2.1. SEA FIELD APPROXIMATIONS

In SEA reverberant and diffuse field approximations are often made to simplify the analysis of complex systems [Lyon and Maidanik 1962]. It is important, before developing a modeling procedure for regular and irregular structures and acoustic spaces, to discuss the meaning of these terms and the influence of structural irregularity on the validity of these approximations.

### 2.1.1. Direct and Reverberant Fields

In room acoustics, the sound field is commonly divided into a direct and reverberant field. The direct field is represented by sound waves emanating directly from a source before they have reflected from the walls of the room, as shown in Figure 1. The reverberant field is represented by waves that have reflected one or more times from the walls and other reflecting surfaces.

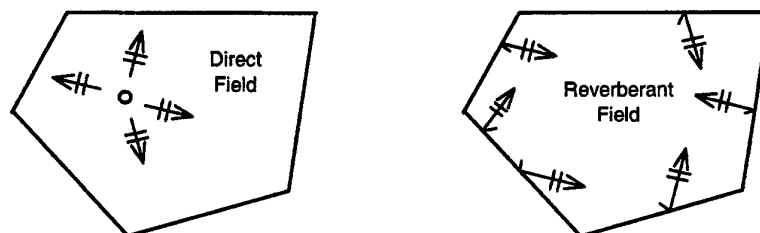


Figure 1. Direct and reverberant field representations

The relative importance of the direct and reverberant fields depends on the absorption within the room. In a room with low wall absorption, sound waves emanating from a source will propagate throughout the room reflecting many times from walls and other surfaces with little or no reduction in amplitude. In this case the reverberant field will dominate the overall acoustic field. For high absorption, the amplitude of the reflected waves will be significantly reduced at each reflection so that the direct field dominates.

The concept of direct and reverberant fields can be extended to structural vibrations. For example, in a lightly damped plate, the bending waves emanating from a point force excitation will propagate across the plate reflecting many times from the plate boundaries. The amplitude of these waves will decay slowly as the wave travels along the plate due to distributed damping mechanisms and on reflection due to damping or energy transmission at the edge of the plate. As in room acoustics, direct and reverberant fields can be defined. However, the fields may be more complex, since both bending and in-plane compression and shear waves exist.

Although studies of room acoustics are often based on wave descriptions of the direct and reverberant fields, a modal description can also be used to describe the field. The sound pressure in the room is described as a sum of modal responses as shown by Morse (1948). The reverberant field in a given band of frequencies is represented by the resonant response of modes with resonance frequencies within the band.

Description of the direct acoustic field is also possible using a summation of modal responses. However, such a description is much more complicated since a large number of modes must be included in the summation and the phase of the different modal responses must be correctly determined. Even with low damping, the direct field response in a given band of frequencies must take into account the response of modes with resonance frequencies both within and outside of the band.

In SEA, the subsystem damping is assumed to be sufficiently low that the response is dominated by the reverberant field. The direct field response is typically ignored. Thus, in cases where the direct field does play a significant role in the response calculation, the SEA formulation should be modified to include the direct field. Fortunately, this is a fairly simple procedure within the context of a statistical model of the subsystem as shown by Maidanik (1981).

#### 2.1.2. *Directive and Diffuse Fields*

In a diffuse acoustic field, sound waves are incident from all directions with equal and uncorrelated amplitudes. The reverberant field in a large room with low wall absorption and irregular boundaries will become asymptotically diffuse at higher frequencies as more and more modes contribute to the response.

In a rectangular room with rigid boundaries, the acoustic modes can be easily determined. Each mode can then be represented by a sum of eight traveling waves (one-dimensional and two-dimensional modes required fewer waves). The direction of travel is given by the wavenumber vector for the mode. Different modes will have different wavenumbers and different travel directions. At low frequencies, only a few modes contribute to the response so that only a few travel directions are involved in describing the response. At these low frequencies the field is not diffuse. However, at high frequencies, hundreds of modes will contribute to the response so that hundreds of travel



directions are involved. The use of a diffuse field at these high frequencies is a good approximation to the actual field.

The introduction of the statistical theory of room acoustics more than 50 years ago, e.g. Morse (1948), allows analysts to quantify the accuracy associated with the use of the diffuse field approximation for high frequency acoustic analysis. At low frequencies, where only a few modes contribute to the response, a deterministic analysis can be performed to identify the modes of a room and the response of each mode to a prescribed excitation. Acoustic finite element analysis and boundary element analysis allows this deterministic analysis to be carried out with great precision. At high frequencies, on the other hand, many hundreds of modes contribute to the room response. At these frequencies, the deterministic analysis of a room becomes too cumbersome and the implied accuracy of the predictions misleading since the analysis can't take into account the many small details of the room that influence the response. A statistical analysis becomes more useful. "The situation is analogous to the difference between the methods of statistical mechanics, which deal with the average behavior of a large number of bodies, and those of ordinary mechanics, which deal with the detailed motions of one or two bodies." [Morse, p. 383]

If a statistical description of a room is used, diffuse fields can be used to obtain predictions of the average behavior of members of an ensemble of rooms. Within the confines of a statistical solution, these predictions can be considered to be exact rather than approximate solutions useful only at high frequencies.

The concept of a diffuse field can be extended to structural vibrations. For example, we can consider a diffuse field of bending waves with energy incident on a point in the plate from all directions. In a rectangular plate with simply supported boundaries, each bending mode can be represented by a sum of four traveling waves as shown in Figure 2. As in the case of room acoustics the direction of travel is given by a

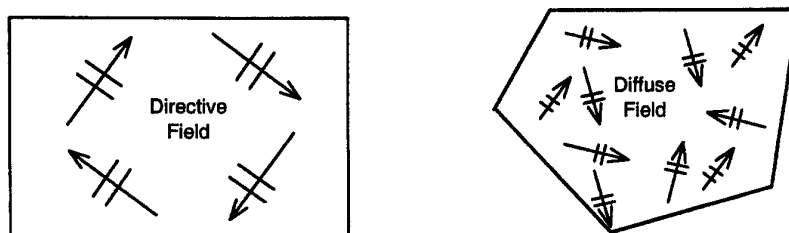


Figure 2. Directive and diffuse field representations for plate bending waves

wavenumber vector for the mode. For a single mode of the rectangular plate there are only four waves and four directions of travel. For this case the field will be quite directive. At sufficiently high frequencies where many modes contribute to the vibration field, each with a different directions of wave propagation, the field in the rectangular plate can become diffuse if all modes have the same energy and uncorrelated response amplitudes. On the other hand, even a single mode of the irregular plate requires a large

number of waves to represent the field. Thus, the diffuse field approximation may be valid for the irregular plate even when only a small number of modes contribute to the response.

In many applications SEA relies on the use of diffuse field models to represent both acoustic and vibration fields. Thus, from a deterministic point of view, SEA may be considered to be an approximate technique useful only at high frequencies. On the contrary, if we accept a statistical approach, SEA can be considered to be an exact technique, giving statistical estimates of the response of an ensemble of systems. However, in using a statistical approach it is dangerous to put too much confidence in a prediction of the ensemble average response, since the variance of the prediction over the different members of the ensemble may be large. If a prediction of the ensemble average response is used for product design, half of the products will fail!

The proper use of SEA requires that the statistical nature of the prediction be recognized. Predictions of the ensemble average response are useful only when the variance of the prediction is acceptably small.

**2.1.3. Coupling Factor Calculations Using Reverberant Diffuse Field Approximations**  
In SEA coupling loss factors are generally calculated using a wave approach. The acoustic or vibration fields in the two coupled subsystems are represented by reverberant diffuse fields and angle-averaged power transmission coefficients are used. The following steps are carried out.

*Step 1: Represent the field in each subsystem by a reverberant diffuse field.* The diffuse field consists of waves incident from all directions with equal and uncorrelated amplitudes. The energy density in a traveling wave is given by

$$e(\phi) = \omega^2 m \frac{1}{2} |A(\phi)|^2 \quad (1)$$

The energy density in the diffuse field is found by integrating over all angles of incidence. For example, in a two dimension field of bending waves on a plate, the energy density is given in terms of the incident wave amplitudes as

$$e = \omega^2 m \int_{-\pi}^{\pi} d\phi \frac{1}{2} |A(\phi)|^2 \quad (2)$$

If the field is also reverberant, the energy density will be uniformly distributed throughout the plate. The energy density can then be simply related to the total energy in the plate and its area,

$$e = \frac{E}{A_{plt}} \quad (3)$$

The wave amplitude in the diffuse field can be obtained from the plate energy as

$$|A(\phi)|^2 = \frac{1}{\pi \omega^2 m A_{plt}} E \quad (4)$$

*Step 2: Calculate the transmitted power.* The transmitted power is determined as the product of the incident power from the diffuse field and a power transmission coefficient. The intensity in a traveling wave is found by multiplying the energy density by the group speed,

$$\bar{i}(\varphi) = c_g e(\varphi) \bar{u} \quad (5)$$

where  $\bar{u}$  is a unit vector in the direction of wave propagation. Assuming the connection between subsystems to be at the edge of each subsystem, the intensity incident from a given angle is given by

$$i^{\text{incident}}(\varphi) = \frac{1}{\pi} \frac{E c_g}{2 A_{\text{plt}}} \quad (6)$$

The transmitted power is given in terms of a power transmission coefficient by

$$i^{\text{transmitted}}(\varphi) = i^{\text{incident}}(\varphi) \tau(\varphi) \quad (7)$$

The total power transmitted is found by integrating over the angles of incidence,

$$W^{\text{transmitted}} = \frac{E c_g}{2 A_{\text{plt}}} \frac{1}{\pi} \int_{-\pi/2}^{+\pi/2} d\varphi \tau(\varphi) \cos(\varphi) \quad (8)$$

$\bar{\tau}$

where  $\bar{\tau}$  is the angle-average transmission coefficient.

The net power transmitted between subsystems is the difference between power transmitted from  $i$  to  $j$  and the power from  $j$  to  $i$ . Since the diffuse fields in the two plates are assumed to be uncorrelated, the net power is given by

$$W_{i,j}^{\text{transmitted}} = \frac{L_{\text{jnc}}}{2} \left( \frac{c_{g,i} \bar{\tau}_{i,j}}{A_i} E_i - \frac{c_{g,j} \bar{\tau}_{j,i}}{A_j} E_j \right) \quad (9)$$

where  $L$  is the junction length. Note that the angle-averaged power transmission coefficients are not reciprocal due to the averaging.

*Step 3: Calculate the coupling loss factors.* In SEA the net power transmitted is given in terms of coupling loss factors as

$$W_{i,j}^{\text{transmitted}} = \omega \eta_{i,j} E_i - \omega \eta_{j,i} E_j \quad (10)$$

The coupling loss factors are now determined to be

$$\eta_{i,j} = \frac{c_{g,i} \bar{\tau}_{i,j}}{2 \omega A_i} L_{\text{jnc}} \quad \text{and} \quad \eta_{j,i} = \frac{c_{g,j} \bar{\tau}_{j,i}}{2 \omega A_j} L_{\text{jnc}} \quad (11)$$

The calculation of angle-average power transmission coefficients for plates is straight forward, though tedious for all but the simplest junctions. The integration over angle usually cannot be performed analytically so that some computational assistance is needed. Fortunately, numerical aids such as MATLAB make these calculations much simpler than they were when SEA was first developed, Heckl (1961).

### 3. Coupled Plate Results

Measurements were performed on coupled plates separated by a beam to demonstrate the effect of structural irregularity. First, measurements were taken on a regular structure consisting of two rectangular plates, as shown in Figure 3. Beams were placed on both

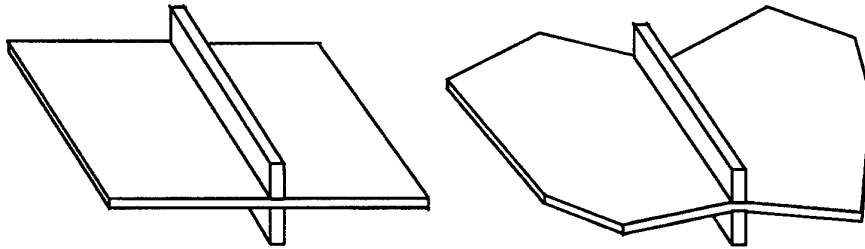


Figure 3. Coupled rectangular and irregular plates

sides of the plate to avoid the complexity due to the coupling of bending and inplane modes at an asymmetric connection. Similar measurements were then taken on a irregular structure consisting of two five-sided plates.

The baseline SEA model consists of four subsystems: two plate bending subsystems - one for each plate, a beam bending subsystem, and a beam torsion subsystem. The coupling factors between the two plates and the coupling factors from beam bending and beam torsion to plate bending were calculated following the approach used by Heckl (1961). Since diffuse fields are assumed for each plate, angle-averaged transmission coefficients were used in calculating the coupling factors. Damping loss factors were determined from decay-rate measurements and the energy flow equations were solved to determine the average vibration level for each plate. Results are shown in Figure 4.

Predictions from the baseline SEA model are seen to be in good agreement with measured data for the irregular plates. In this case the reverberant diffuse field assumption made in calculating the coupling factors is valid, at least at the higher frequencies above 1,250 Hz. Predictions for the coupled rectangular plates are in poor agreement with measured data even at high frequencies.

#### 3.1 WHEN SEA DOESN'T WORK

When SEA doesn't work it is usually a result of the reverberant diffuse field approximation. For one or more subsystems, the field is either not reverberant or not diffuse. A variety of new techniques have been identified to solve these problems. However, rather than replacing SEA with another technique, we should realize that SEA does not require the reverberant diffuse field approximation to be made.

SEA is often restricted to high modal overlap. However, when there is high modal overlap and the source is localized, the vibration field may also be localized due to the dominance of the direct field. In such a case we find that the approximation that the field is reverberant is not very accurate. The plate damping for the measurements

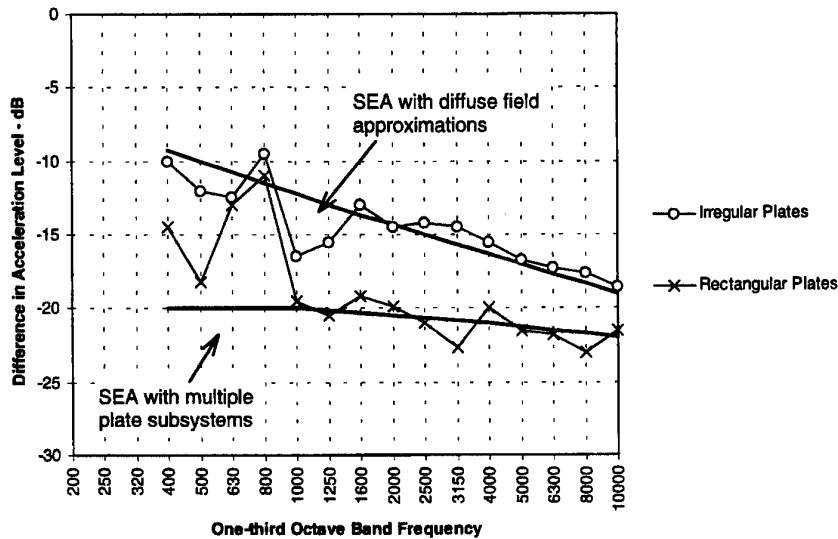


Figure 4. Mode shape and wave distribution for rectangular plate with simply-support boundary conditions

discussed above was sufficiently low that the modal overlap factor was not high, even though the modal densities were quite high. Thus, the assumption of a reverberant field is valid for both cases being considered. This may not be the case if the damping of one or both plates were increased.

As would be expected from the discussion earlier in this paper, the diffuse field approximation is not valid for the rectangular plates. Although the modal densities are high so that many waves could be excited in each plate, only those waves (or modes) that match the wavenumber of the bending and torsional waves of the beam are strongly excited in the receiving plate. Thus, equipartition of energy does not occur in the bending wave subsystem of the receiving plate. The field in the receiving plate cannot be modeled as diffuse, although it is reverberant.

To resolve this problem, the bending modes of each rectangular plate were divided into subsystems according to their coupling to the beam. Four bending subsystems were used for each plate: one for plate modes strongly coupled to the bending modes of the beam, one for plate modes strongly coupled to the torsional modes of the beam, one for plate modes coupled by mass-law beam response, and one for plate modes coupled by stiffness-controlled beam response. Coupling factors were calculated for these different subsystems using the same transmission coefficients used in the baseline SEA model, but without angle-averaging. The expanded SEA energy flow equations were solved and the energy of the four subsystems for each plate were added to predict the overall energy and average response level for the two plates. Results show a marked improvement over the baseline model at the higher frequencies above 1,000 Hz. At low frequencies, however, the expanded model underpredicts the response of the receiving plate. It is possible that at these lower frequencies, end conditions at the two ends of the

beam result in a more uniform distribution of coupling so that the transmission coefficients based on infinite beam and plate impedances are no longer valid. Further work is needed to extend the SEA predictions to these lower frequencies.

#### 4. Criteria For Structural Irregularity

The measurements conducted on coupled rectangular and irregular plates show that a conventional SEA analysis is valid only for the irregular plates. Although the SEA model can be expanded to obtain accurate predictions for the rectangular plate, some measure of irregularity must be identified so that the proper modeling technique can be employed. In many cases, the analyst's judgment must be used. Decisions are made based on the shape of the plate and its boundary conditions. In many problems of practical interest, structural irregularity can be assumed. For example, most plate structures in a modern automobile can be modeled as irregular plates. Many plate structures in satellites and other space vehicles can also be modeled as irregular plates due to the presence of components loading the plate.

Most cases where an irregular plate structure cannot be assumed occur in the laboratory. Idealized test setups with rectangular plates having simply-supported or free boundaries are often studied to gain a better understanding of vibration response and transmission mechanisms.

Finite element models can be used to gain a more quantitative understanding of irregularity. Finite element models were developed for three plate configurations. The first consists of a rectangular plate with simply supported boundaries. The modes for this plate can be easily calculated. Figure 5 shows a contour plot of the mode shape for a single plate mode. A regular pattern of nodes and anti-nodes is observed. A two-dimensional transform of the mode shape can be used to displace the waves required to represent the mode shape. Figure 5 also shows the wave distribution for the mode. Four peaks occur representing the four traveling waves required to represent the mode.

Figure 6 shows the same type of results for a plate with an irregular shape. In this case nodes and anti-nodes are observed, but there is no regular pattern. The wave distribution plot shows that many waves are needed to represent the vibration field of this mode.

Figure 7 shows results for the third case in which the modes of a rectangular plate with irregular boundary conditions were identified. The contour plot of a single mode shape shows nodes and anti-nodes, as for the other two cases. However, as in the case of the irregularly shaped plates, no pattern is observed. The wave distribution plot is similar to the plot for the irregularly shaped plate.

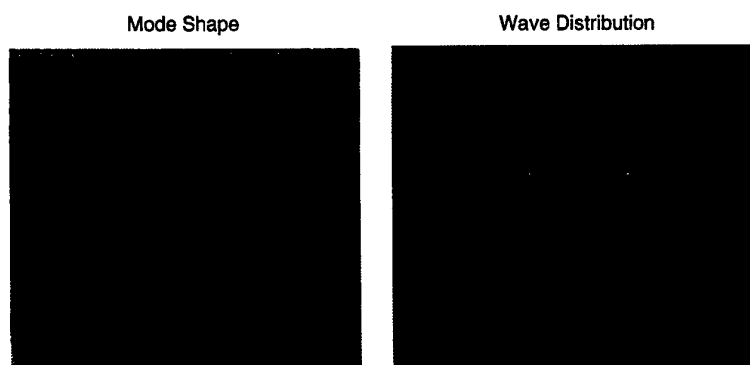


Figure 5. Mode shape and wave distribution for rectangular plate with simply-support boundary conditions

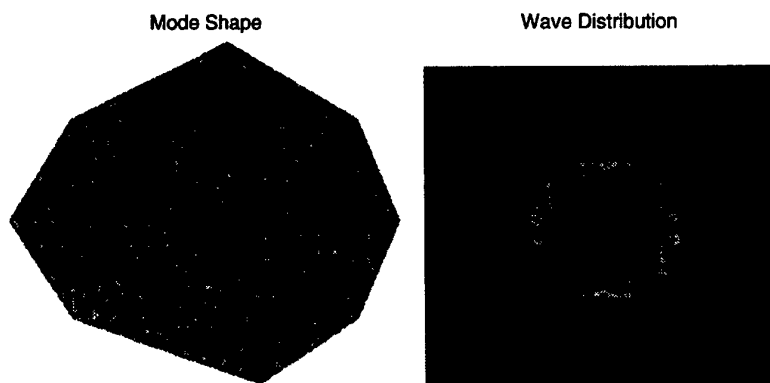


Figure 6. Mode shape and wave distribution for irregular plate with simply-support boundary conditions

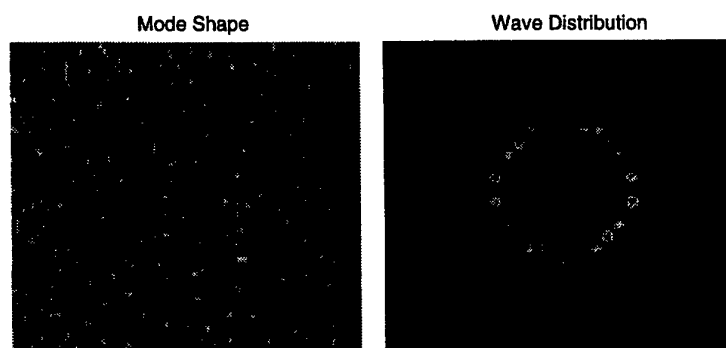


Figure 7. Mode shape and wave distribution for rectangular plate with irregular boundary conditions

## 5. Conclusions

Based on the work presented in this paper we conclude that SEA models can be used for both regular and irregular structures and acoustic spaces. However, models using coupling factors based on diffuse field representations of the vibration and acoustic fields in each subsystem should be limited to studies of irregular structures and acoustic spaces. System irregularity is seen to occur either because of irregular shapes or irregular boundary conditions. Both are fairly common in automotive, aerospace, and ship structures, so that the diffuse field representation continues to provide valid coupling factors for many cases of practical interest.

## Acknowledgments

This work was initiated at Bolt Beranek and Newman Inc. in 1969. It has recently been completed at Cambridge Collaborative, Inc. The author wishes to thank Jim Moore, who carried out the measurements on coupled plates almost 30 years ago. Appreciation is also given to Ms. Olga Chernets, who completed the finite element modal analysis using Ansys<sup>®</sup> and the wavenumber analysis using MATLAB<sup>®</sup>. SEA predictions were obtained using SEAM<sup>®</sup>.

## References

- Heckl, M. (1961) Wave Propagation on Beam-Plate Systems, *J. Acoust. Soc. Am.* **33** (5), 640-651.
- Lyon, R. H. and DeJong, R. G. (1995) *Theory and Application of Statistical Energy Analysis*, 2<sup>nd</sup> ed., Butterworth-Heinemann, Newton, MA.
- Lyon, R. H. and Maidanik, G. (1962) Power Flow between Linearly Coupled Oscillators, *J. Acoust. Soc. Am.* **34** (5), 623-639.
- Lyon, R. H. and Eichler, E. (1964) Random Vibration of Connected Structures, *J. Acoust. Soc. Am.* **36** (7), 1344-1354.
- Lyon, R. H. (1970) Application of a Disorder Measure to Acoustical and Structural Models, *ASME Journal of Engineering for Industry*, Paper No. 70-WA/DE-1.
- Maidanik, G. (1981) Extension and Reformulation of Statistical Energy Analysis with Use of Room Acoustics Concepts, *J. Sound and Vib.*, **78** (3), 417-423.
- Manning, J. E. (1997) Statistical Modeling of Vibrating Systems, Chapter 78 of *Encyclopedia of Acoustics*, edited by M. J. Crocker, John Wiley & Sons, Inc. New York, NY.
- Morse, P. M. (1948) Standing Waves of Sound, Ch. VIII in *Vibration and Sound*, 2<sup>nd</sup> ed., McGraw-Hill Book Company, Inc., New York, NY.
- Ansys is a registered trademark of Ansys, Inc., MATLAB is a registered trademark of The MathWorks, Inc., and SEAM is a registered trademark of Cambridge Collaborative, Inc.



## **Prediction of Structure Borne Sound of Low Modal Density Structure by Using SEA**

Iwao Honda, Kazuhide Ohta  
Mitsubishi Heavy Industries Ltd.  
5-717-1, Fukahori-machi, Nagasaki, Japan

### **1. Introduction**

The basic concept of the SEA method has been primarily developed for analyzing problems in the aerospace engineering field such as the acoustic fatigue of outer-skin and the reliability of electronic equipments due to high frequency vibration in space vehicles during flight. Nowadays, SEA, for the sake of its simplicity in power balance equation, has been recognized as useful and powerful tool for analyzing structure borne sound and practically utilized to assess the noise of products in the audible frequency range. In addition, with increasing needs for comfort in our living and working environment, requires the assessment of structure borne noise on a structure constructed with low and high modal density elements.

The SEA method regards each element in the system as a combination of equivalent oscillators and evaluates macroscopically the energy transmitting among them in the sense of statistical average in the considered frequency band. Though these assumptions are valid for the structure borne sound analysis of a structure which consists of weakly coupled elements in high frequencies, so called high modal density elements, the properties of structure borne energy propagation of low modal density elements are affected by eigen modes of each elements of a structure, and it is difficult to consider these elements as an aggregate of equivalent oscillators which have nearly equal excitation. In the case of low modal density and weakly coupled elements, these oscillators show the different dynamic characteristics and have different energy storage levels, energy transfer to modes of other subsystems, and energy dissipation. It is difficult to predict the transmission power based on the mean value of energy transfer parameters.

This paper presents a new prediction method of the structure borne sound of

structure which is constructed with low modal density and weakly coupled elements. This method is based on the SEA concepts, but the subsystem in this method consists of multi-oscillators which have different excitation by sources, coupling to other subsystems, and damping. The oscillators are excited by random moment and coupled with infinite elements. And the power flow among them are calculated using the natural frequencies and eigen modes.

In this paper, a system equation describing the energy flow is formulated with modal parameters of each elements and numerical simulation of plate structure are shown.

## 2. Numerical Formulation

### 2.1 Vibratory Energy

#### 2.1.1 Mean square velocity

Using modal parameters, such as modal mass  $m_n$ , mode shape  $\phi_n$ , modal damping  $\eta_n$  and eigenfrequency  $\omega_n$ , the vibration velocity  $v(x_r)$  caused by the distributed load  $p(x_r)$  is written as follows,

$$\begin{aligned} v(x_r, x_r; \omega) &= \sum_n \frac{j\omega \phi_n(x_r) \phi_n(x_r)}{m_n(\omega_n^2 - \omega^2 + j\eta_n \omega_n^2)} p(x_r) ds, \\ &= \sum_n j\omega G_n \phi_n(x_r) \phi_n(x_r) p(x_r) ds, \end{aligned} \quad (1)$$

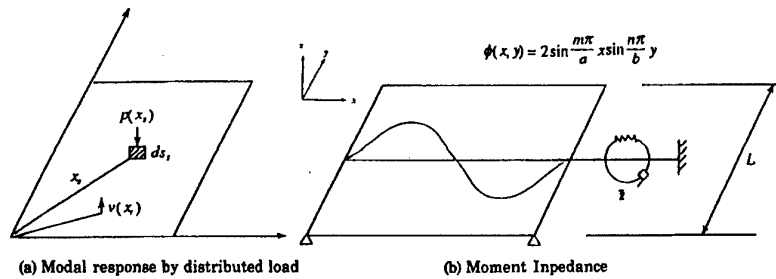


Figure 1 Calculation model for vibration energy and transmitting power

Now let us assume the spatially random load, the spatial average of the square velocity is given by

$$\begin{aligned} \overline{v^2}(x_r; \Omega) &= \int \omega^2 \sum_n |G_n|^2 \phi_n^2(x_r) \left| \int \phi(x_r) p(x_r) ds_r \right|^2 d\omega \\ &= \int \omega^2 \sum_n |G_n|^2 \phi_n^2(x_r) d\omega \overline{|P|^2} \\ \overline{|P|^2} &= \left| \int \phi(x_r) p(x_r) ds_r \right|^2 = \frac{1}{\bar{m}''} \int m''(x_r) \phi(x_r)^2 ds_r \int |p(x_r')|^2 ds_r, \end{aligned} \quad (2)$$

where  $m''$  and  $\bar{m}''$  denote the mass per unit area and the mean value of  $m''$ .

Integrating eq.(2) by the frequency range  $[\omega_1, \omega_2]$  yields the mean square velocity  $v_\Delta^2$  in the frequency band  $(\Omega, \Delta\omega)$

$$\begin{aligned}\overline{v_\Delta^2}(\Omega) &= \frac{1}{Sm^n} \sum \int \frac{\omega^2 \phi_n^2(x_r)}{m_n^2 \{(\omega_n^2 - \omega^2)^2 + \eta_n^2 \omega_n^4\}} d\omega |\overline{P}|^2 ds_r \\ &= \frac{1}{Sm^n} \sum \frac{1}{2m_n \eta_n \omega_n} g_n |\overline{P}|^2 \\ g_n &= \tan^{-1} \frac{2(\omega_2 - \omega_n)}{\eta_n \omega_n} - \tan^{-1} \frac{2(\omega_1 - \omega_n)}{\eta_n \omega_n}\end{aligned}\quad (3)$$

where  $\omega_1, \omega_2$  are the lowest and highest frequency respectively, and  $\Sigma$  shows the amount of eigen modes in frequency band  $(\Omega, \Delta\omega)$ , and  $|\overline{P}|^2/Sm^n$  denotes the equivalent input power and the parameter  $g_n$  means the contribution of the  $n$ -th oscillator, such as the  $n$ -th mode of element, for the mean square velocity  $v_\Delta^2(\Omega)$ .

#### 2.1.2 Kinetic energy

Let us suppose that the equivalent random load  $p_e(\omega, x_a)$  is uncorrelated in the time domain and in the spatial domain. The equivalent distributed load  $p_e(\omega, x_a)$  causes the vibration velocity  $v(\omega, x)$ , and the power spectrum of kinetic energy  $T_\Delta(\Omega)$  in the frequency band  $(\Omega, \Delta\omega)$  is written by

$$\begin{aligned}T_\Delta(\Omega) &= \frac{1}{2} \int \omega^2 \int m(x_r) \left| \int \sum_{n=1}^N v_n(\omega, x, x_r) p(\omega, x_r) ds_r \right|^2 ds d\omega \\ &\cong \frac{1}{2} \sum \frac{1}{2m_n \eta_n \omega_n} g_n |\overline{P}|^2 \\ |\overline{P}|^2 &= \int \phi_n^2(x_r) dx_r |\overline{P}|^2\end{aligned}\quad (4)$$

Using the kinetic energy  $T_\Delta$  in eq.(4), the modal energy of the element  $E_\Delta$  is expressed as follows,

$$E_\Delta(\Omega) = 2T_\Delta(\Omega) = \sum \frac{1}{2m_n \eta_n \omega_n} g_n |\overline{P}|^2 = \overline{Sm^n} \overline{v_\Delta^2}(\Omega) \quad (5)$$

#### 2.1.3 External input power

The power spectrum of input power by distributed load  $p(x_r)$  in the frequency band  $(\Omega, \Delta\omega)$  is given by

$$\begin{aligned}W(\Omega) &= \frac{1}{2} \int \text{Re} \left\{ \iint \sum_n j\omega G_n \phi_n(x_r) \phi_n(x_s) p(x_s) ds_s p^*(x_r) ds_r \right\} d\omega \\ &= \frac{1}{2} \frac{1}{Sm^n} \sum \frac{1}{m_n} g_n |\overline{P}|^2 \\ |\overline{P}|^2 &= \int |\phi(x_r) p(x_r) ds_r|^2\end{aligned}\quad (6)$$

#### 2.1.4 Transmitting power from $i$ -th element to $j$ -th one

Fig.1 illustrates a coupling model of a plate and an impedance element. Taking

the moment impedance of semi infinite plate into consideration, the transmitting power from the plate to the impedance element  $W_{\Delta}(\Omega)$  is written as follows,

$$\begin{aligned} W_{\Delta}(\Omega) &= \int \frac{1}{2} \int \operatorname{Re} \left\{ \int v(x_c; \omega) (Z(x_c; \omega) v(x_c; \omega))^* \right\} dx_c d\omega \\ &= \frac{1}{2} L \sum \frac{k_m^2}{m_n \eta_n \omega_n} g_n \operatorname{Re} \left\{ \bar{Z}(\Omega) \right\} |\bar{P}|^2 \end{aligned} \quad (7)$$

where  $k_m$ ,  $Z$ ,  $h$  are wave number, moment impedance and plate thickness respectively.

## 2.2 System equation of 2-element model

In this paper, let us approximate that the transmitting power from i-th element to j-th element is expressed as transmitting power from finite element i to semi infinite element j as shown in Fig.2. Using eqs.(5)–(7), the external input power of i-th element, the vibration energy, the dissipated energy and the transmitting power to j-th element are rewritten as follows,

$$\text{External input power} \quad W_i^o(\Omega) = \frac{1}{2} \frac{1}{S m_i} \sum \frac{1}{m_n} g_n |\bar{P}_0|^2 \quad (6')$$

$$\text{Vibration energy} \quad E_i(\Omega) = \sum \frac{1}{2 m_n \eta_n \omega_n} g_n |\bar{P}|^2 \quad (5')$$

$$\text{Dissipated power} \quad W_i^d(\Omega) = \omega \sum \eta_n \frac{1}{2 m_n \eta_n \omega_n} g_n |\bar{P}|^2 \quad (8)$$

$$\text{Transmitting power} \quad W_{ij}(\Omega) = \frac{1}{2} L \sum \frac{k_m^2 R_i(Z)}{m_n \eta_n \omega_n} g_n |\bar{P}|^2 \quad (7')$$

Taking the energy balance of i-th element into consideration yields the following equations,

$$\begin{aligned} W_i^o + W_{ij} &= W_i^d + W_j \\ \frac{1}{2} \frac{1}{S_i m_i} \sum \frac{1}{m_n} g_n |\bar{P}|^2 + \frac{1}{2} L_j \sum \frac{k_m^2 R_i(Z_i)}{m_n \eta_n \omega_n} g_i |\bar{P}_j|^2 \\ &= \omega \sum \eta_n \frac{1}{2 m_n \eta_n \omega_n} g_n |\bar{P}_i|^2 + \frac{1}{2} L_j \sum \frac{k_m^2 R_i(Z_j)}{m_n \eta_n \omega_n} g_n |\bar{P}_i|^2 \\ \frac{1}{S_i m_i} \sum \frac{1}{m_n} g_n |\bar{P}_0|^2 &= \omega \left\{ \sum \eta_n \frac{2}{2 m_n \eta_n \omega_n} g_n + L_j \sum \frac{k_m^2 R_i(Z_j)}{m_n \eta_n \omega_n} g_n \right\} |\bar{P}_i|^2 \\ &\quad - \omega L_j \sum \frac{k_m^2 R_i(Z_i)}{m_n \eta_n \omega_n} g_i |\bar{P}_j|^2 \end{aligned} \quad (9)$$

In the above eq.(9), the first term denotes internal dissipated power and transmitted power from i-th to j-th element, and the second term shows the transmitted power from j-th to i-th element. In each term, the denominator includes the internal loss factor  $\eta_n$ .

this shows the decreasing the loss factor increases the vibration energy. And in the term of transmitting power,  $L_{ij} \sum_m \text{Re}(Z_j) / m_n \eta_n \omega_n \omega$  denotes the coupling loss.

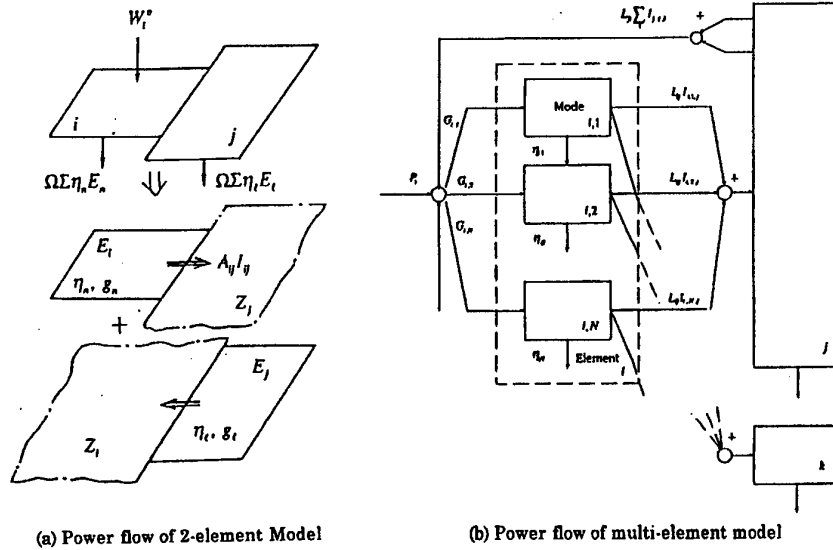


Figure 2 Power flow model taking the energy balance of i-th element into consideration

### 2.3 System equation of Multi-element

Taking consideration the energy balance in the multi-element system shown in Fig.2, the system equation is given by

$$\mathbf{G}\mathbf{P}_e = \mathbf{\Omega Y P}$$

$$\mathbf{G} = \left[ \text{diag.} \frac{1}{2} \frac{1}{S_i m_i} [\sum g_n] \right], \mathbf{P}_e = \{ \overline{p_1^e}, \overline{p_2^e}, \dots, \overline{p_N^e} \}, \mathbf{P} = \{ \overline{p_1}, \overline{p_2}, \dots, \overline{p_N} \}^T \quad (10)$$

$$\mathbf{Y}[\mathbf{Y}_i]: \begin{cases} Y_i = \sum \frac{1}{2m_n \omega_n} g_n + \frac{1}{\Omega} L_{ij} R_s(\bar{Z}_j) \sum \frac{1}{2\eta_n \omega_n} \frac{k_m^2}{m_n} g_n & i = j \\ Y_i = -\frac{1}{\Omega} L_{ji} R_s(\bar{Z}_j) \sum \frac{1}{2\eta_n \omega_n} \frac{k_m^2}{m_n} g_n & i \neq j \end{cases}$$

### 3. Numerical Simulation

#### 3.1 The effect of coupling stiffness

Fig. 3 shows the coupling stiffness based on the moment impedance of semi-infinite plate and the modal stiffness of plate. Fig.4 shows the effect of coupling stiffness on eigen frequencies. The coupling stiffness in Fig.3 and Fig.4 is formulated as follows

$$k_c = \text{Re}\{j\omega Z\} = \text{Re}\left\{\frac{j}{1 - j1.46 \ln 0.9ka} \frac{5.3Eh^3}{12(1-\nu^2)}\right\} \quad (11)$$

From the Fig.3 and Fig.4, it is found that the increase of frequency decreases the moment impedance, decreases the coupling stiffness based on the moment impedance. In the low coupling stiffness range, which means that the ratio of the coupling and the modal stiffness  $k_c/k_m$  is small enough, the influence of coupling stiffness is negligible, and the ratio of the coupling and the modal stiffness  $k_c/k_m$  of 10mm thick steel plate is small ( $k_c/k_m \ll 0.1$ ) in the frequency range over 10Hz. This shows that the two subsystems are weakly coupled.

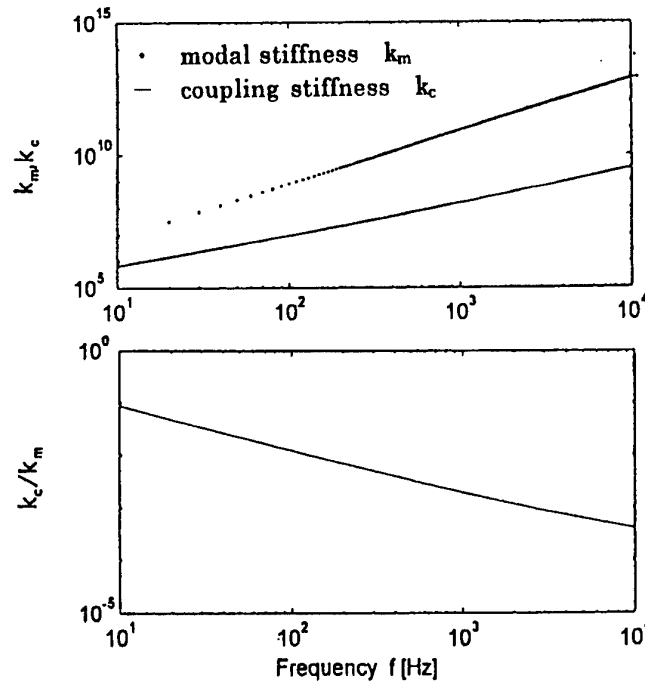


Figure 3 Relationship between modal stiffness and coupling stiffness

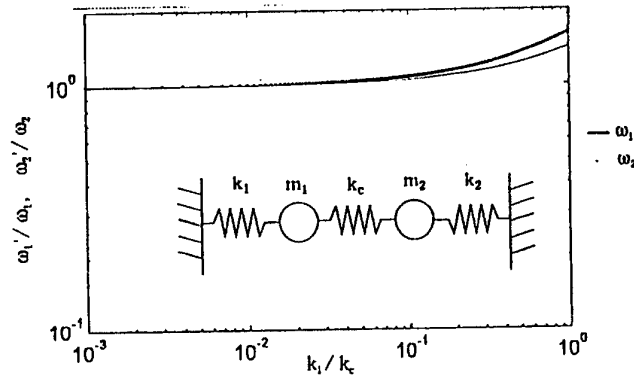


Figure 4 Effects of coupling stiffness on eigen frequencies

### 3.2 The relationship of parameter $g_n$ and mode count $\Delta N$

In order to consider the effect of each mode on the vibration energy in the frequency band  $(\Omega, \Delta\omega)$ , the system equation is formulated as the function of parameter  $g_n$  in this method. In the SEA method,  $\Sigma g_n$  is approximated to mode count  $\Delta N$  as follows,

$$\sum g_n = \sum \tan^{-1} \frac{2(\omega_2 - \omega_n)}{\eta_n \omega_n} - \tan^{-1} \frac{2(\omega_1 - \omega_n)}{\eta_n \omega_n} = \pi \Delta N \quad (12)$$

Fig.5 shows the relation ship between  $\Sigma g_n$  and  $\Delta N$ . In the frequency range which the mode count  $\Delta N$  is greater than 50, the amount of  $g_n$  is approximated as  $\Sigma g_n = \pi \Delta N$ , and the influence of internal loss factor is very small. And in the low modal density range, the effect of the internal loss factor is large and the error of the approximation by eq.(12) becomes large.

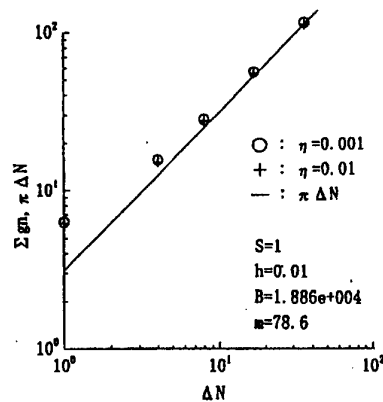


Figure 5 Relationship between mode counts and parameter  $g_n$

### 3.3 The vibration levels of 2-element system

In order to discuss the characteristics of the power transmission, the present method was applied to the 2-element plate model as shown in Tab.1.

Table 1 2-element model

	element 1	element 2
External Force [ $\text{N/m}^2\sqrt{\text{Hz}}$ ]	1.0	--
width and length [m]	5*5	5*a <sub>2</sub>
thickness [m]	0.01	h <sub>2</sub>
internal loss factor	0.005	$\eta_2$
Young's Modulus [Pa]	206*10 <sup>9</sup>	206*10 <sup>9</sup>
density [ $\text{kg/m}^3$ ]	7.86*10 <sup>3</sup>	7.86*10 <sup>3</sup>
Poisson's ratio	0.3	0.3

Fig.6 shows the relationship of the vibration levels and the thickness ratio  $h_2/h_1$  in the case  $a_2=5\text{m}$ , frequency  $\Omega=2\pi*31.5\text{rad/s}$ . The decrease of the thickness of the element 2 decreases the vibration level of element 2, and the vibration level of element 1 converges to the constant value, which is equal to the vibration level of 1-element model. And this means that the power transmitted to element 2 is decreased and all most of the vibration energy is dissipated in element 1 in the case of very small thickness ratio  $h_2/h_1$ . At the thickness ratio  $h_2/h_1=1.0$ , the vibration levels of each element becomes to neary equal value and the level is 3dB less than the vibration level of element 1 at  $h_2/h_1=0.1$ .

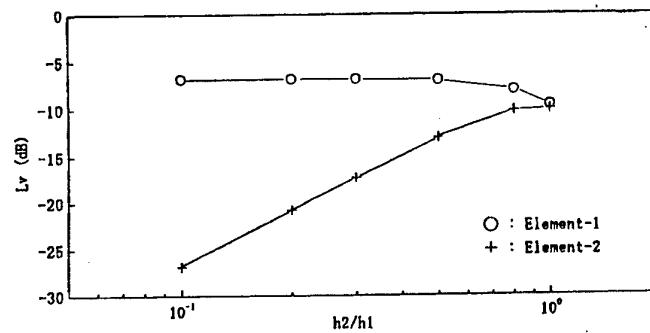


Figure 6 Effects of thickness ratio on vibration levels



Fig.7 shows the relationship of the length of elements  $a_2$  and the vibration levels at  $h_2/h_1=1.0$ , frequency  $\Omega=2\pi*31.5\text{rad/s}$ . The increase of the length of element 2 decreases the vibration energy of element 2. In this case, the coupling loss and the total input power are not changed and the total vibration energy of element 1 and 2 are constant. And the increase of the mass of element 2 bring forth the reduction of vibration level of element 2. The decrease of vibration level of element 1 means that the increase of the power transmission to element 2 caused by the decrease of vibration level of element 2.

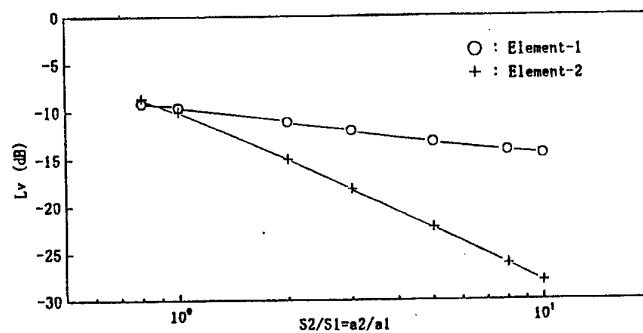


Figure 7 Effects of length of elements on vibration levels

Fig.8 shows the comparison of the calculated results of SEA and the presented method. The model is 2-element model and the dimension of both elements are  $5\text{m}*5\text{m}$  and  $0.01\text{m}$  thickness.

The vibration levels of this method is similar to the results of SEA. But the vibration level of element 2 is a few dB higher than SEA results at each frequency bands. And the total of the vibration level of presented method results are same with SEA results, this shows the distribution of energy is different from SEA results.

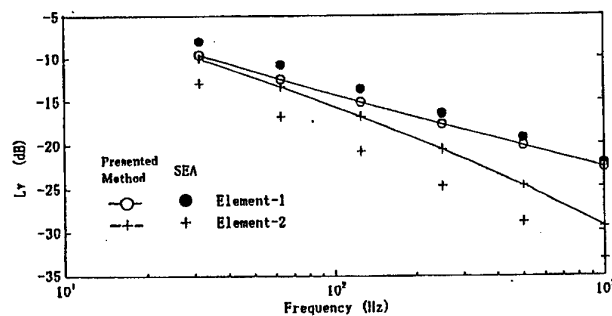


Figure 8 Comparison of vibration levels calculated by presented method and SEA

#### **4. Conclusions**

In order to estimate the vibratory characteristics of structure which is constructed with low modal density and weakly coupled elements, a new prediction method of the structure borne sound is presented. This method regards each element in the subsystem as a combination of modal oscillators and evaluates macroscopically the energy transmission among them in the considered frequency band, but the subsystem in this method is consists of multi oscillators which have different excitation by sources, coupling to other subsystems, and damping. And the power flow among them are calculated using the natural frequencies and eigen modes.

In this paper, a system equation describing the energy flow in the structures is formulated with modal parameters of each elements and numerical simulation of plate structure are shown.

#### **References**

- 1) Y.Irie et al. Prediction of Structure Borne Sound Transmission Using Statistical Energy Analysis, Bulletin of the M.E.S.J., Vol. 13, No. 2, pp.60-72, 1985
- 2) B.M.Gibbs : The Analysis of Bending Vibration of Plate Combinations at Low and High Frequencies, Proc. of INTER-NOISE 94
- 3) L.Cremer et al. : Structure-Borne Sound, Springer-Verlag
- 4) R.H.Lyon et al. : Theory and Application of Statistical Energy Analysis, Butterworth-Heinemann, 1995

# POWER-FLOW ANALYSIS OF QUASI-ONE-DIMENSIONAL SYSTEMS WITH DISTRIBUTED COUPLING

M. BLAKEMORE (1) AND J. WOODHOUSE (2)

- (1) Litton Data Systems Ltd  
Poseidon House, Castle Park, Cambridge CB3 0RD
- (2) Cambridge University Engineering Department  
Trumpington Street, Cambridge CB2 1PZ

## 1. Introduction

Prediction of the noise transmitted from machinery and flow sources on a submarine to the sonar arrays poses a complex problem. Vibrations in the pressure hull provide the main transmission mechanism. The pressure hull is characterised by the very large number of modes over the frequency range of interest (at least 100,000) and the high modal overlap, both of which place its analysis beyond the scope of finite element or boundary element methods. We present a method for calculating the transmission, which is broadly based on Statistical Energy Analysis, but extended in two important ways: (1) a novel subsystem breakdown which exploits the particular geometry of a submarine pressure hull; (2) the explicit modelling of response level variations within a subsystem. The method takes account of fluid-structure interaction, the underlying pass/stop band characteristics resulting from the near-periodicity of the pressure hull construction, the effect of vibration isolators such as bulkheads, and the cumulative effect of irregularities (e.g. attachments and penetrations).

## 2. Background

The sonar arrays we are concerned with are positioned on the forward flanks and the bow of the submarine. The sources of structure-borne sound include the propulsor, other machinery internal to the submarine, and the external flow. The principal machinery sources are mostly sited well aft of the arrays. The estimation of the noise transmitted from these sources to the arrays, over a range of frequencies up to a few kHz, poses a complex prediction problem. It is worth making three initial observations.

- (1) With regard both to flow sources and remote machinery the pressure hull itself provides the most important structural transmission path to the arrays, as opposed to the contribution from internal structure such as decks. This is mainly due to the large impedance mismatch at all junctions with the pressure hull, combined with the complex nature of these internal structures. Within the pressure hull, both flexural-like waves and in-surface waves (compression and shear) provide potentially important transmission mechanisms.
- (2) The pressure hull is made up of a cylindrical shell internally braced against external pressure by circumferential T-section frames. The frames are fairly

regularly spaced axially, and they are substantial enough to present a significant impedance to the pressure hull. They thus produce a characteristic pass- and stop-band frequency variation of the structure-borne transmission.

- (3) The submarine is divided into a small number of separate compartments by bulkheads. These are significant reflectors of structure-borne energy incident in the pressure hull, and need to be taken into account in any predictive procedure.

In the discussion that follows, therefore, we shall consider the combination only of the pressure hull (including the frames) and the bulkheads, in the presence of an external fluid. The external fluid has three distinct effects [1]: mass loading of the structure; adding effective damping through radiation; and fluid short-circuiting of vibration attenuators, including the frames and bulkheads.

The flat plate coincidence frequency (i.e. the frequency where flexural wavelengths match acoustic wavelengths (see [1]) is typically at the top end of the frequency range of interest here. Nevertheless, radiation loss from flexural waves on the structure still occurs below that frequency due to the effects of curvature and wave scattering by the frames. Indeed radiation damping tends to dominate intrinsic structural damping, producing loss factors typically in the region of  $10^{-2}$  to  $10^{-1}$ . Modal overlap is consequently high, and the global structure non-reverberant with regard to flexural-like waves (though local build-up of reverberant energy remains a possibility).

It is possible to design different frame spacings for different sections of the submarine such that pass bands in one section coincide with stop bands in another. In an "ideal" structure, it would then be theoretically possible to achieve extremely low transmission. The necessary variations in frame spacing are of the same order as those typically present (for other reasons) on a submarine. We shall see that the "ideal" low transmission is in practice short-circuited by the cumulative effect of small-scale irregularities in the structure, which produce a small but significant degree of coupling between the different wavetypes. For long range transmission, it is essential to include such effects in the prediction methodology. In this paper we propose a statistical approach to this problem based on an analysis of power flow on a ribbed cylinder. We shall begin by reviewing the underlying dispersion characteristics of the corresponding perfectly regular structure.

### 3. Dispersion characteristics of a fluid-loaded ribbed cylinder

Consider the vibration transmission characteristics of an infinite regularly-framed rotationally-symmetric fluid-loaded thin cylindrical shell. For such a structure, it is possible to decompose the global problem into a set of independent one-dimensional problems, indexed by "angular order"  $n = 0, 1, 2, \dots$ . Each component of the solution then has circumferential behaviour like  $\cos n\theta$  or  $\sin n\theta$ , where  $\theta$  is the circumferential angle. The detailed theory was described for the *in vacuo* case by Hodges *et al.* [2].

Fluid loading is formally incorporated into the scheme by adding to the kinetic energy extra terms representing the response of the fluid to radial motion of the shell, as determined by the kinematic boundary condition. This incorporates both mass loading and radiation damping. The determination of the fluid-loaded transmission modes then involves the solution of a matrix eigenvalue problem. This cannot however be solved by standard matrix procedures due to the non-algebraic frequency dependency in the fluid-loading terms. A non-linear equation solver is adopted. For each transmission mode,

## STATISTICAL POWER FLOW

several relevant quantities can be readily calculated from the eigen-solution, including the frequency, group velocity, radiation loss factor, mode shape and admittance.

These propagation modes are plotted in Fig. 1 on a frequency/angular order diagram. The waves are dispersive and the wavenumber spectrum exhibits very characteristic features, notably the pattern of pass and stop bands whose positions vary with angular order. This predicted pattern has been well validated by comparison with detailed model scale measurements both in air and in water.

The relative width of stop and pass bands depends on their position with respect to the "rib coincidence" line, along which the frames become essentially transparent to flexural waves in the cylinder shell. Its position is delineated by the bottom edge of the "Type C" band shown shaded on the figure. We can divide the propagation modes into four classes. For wavenumber-frequency values to the left of this line, the "Type L" flexural modes tend to have high axial group velocities and wide pass-bands, and usually have high radiation damping. Conversely the "Type R" modes to the right have high circumferential group velocities and narrow pass-bands, and low radiation damping. The transition region around the rib coincidence line is associated with "Type C" modes (the shaded region on the Figure). These have the broadest pass bands of all, giving them low spatial attenuation rates due to structural damping, and they also have rather low radiation damping. Finally it is useful to group all in-surface modes, including compression and shear types, into a single class, designated "IS". These are confined to the region to the left of the relevant line on the figure.

### 4. Statistical modelling

#### 4.1. REALISTIC STRUCTURES

This deterministic model of a perfectly regular structure is adequate to represent the characteristics of transmission over a few frame bays. However for long-range transmission on a realistic structure, a number of complicating factors need to be taken into account:

- (1) the finite length of the structure;
- (2) the effects of isolated attenuators (e.g. bulkheads);
- (3) the effects of distributed axial irregularities (e.g. variable frame spacings);
- (4) the effects of other irregularities (e.g. attachments, penetrations, constructional imperfections, partial frames etc.).

As discussed earlier, in the absence of other irregularities variable frame spacings can produce a theoretical flexural wave transmission which is extremely low. In this case, (4) above becomes crucially important — although the scattering from an individual irregularity is typically small, the cumulative effect is significant, producing a weak "diffusive" scatter between angular orders which can short-circuit the theoretical low transmission. Of course all the above effects can in principle be modelled deterministically, by augmenting the idealised theory. However this deterministic approach either loses accuracy (because the assumptions made in order to make the problem tractable become invalid) or the degree of complexity in the problem becomes unmanageable. It is inevitable then that we consider methodologies where the irregularities and their effects are represented statistically in some way.

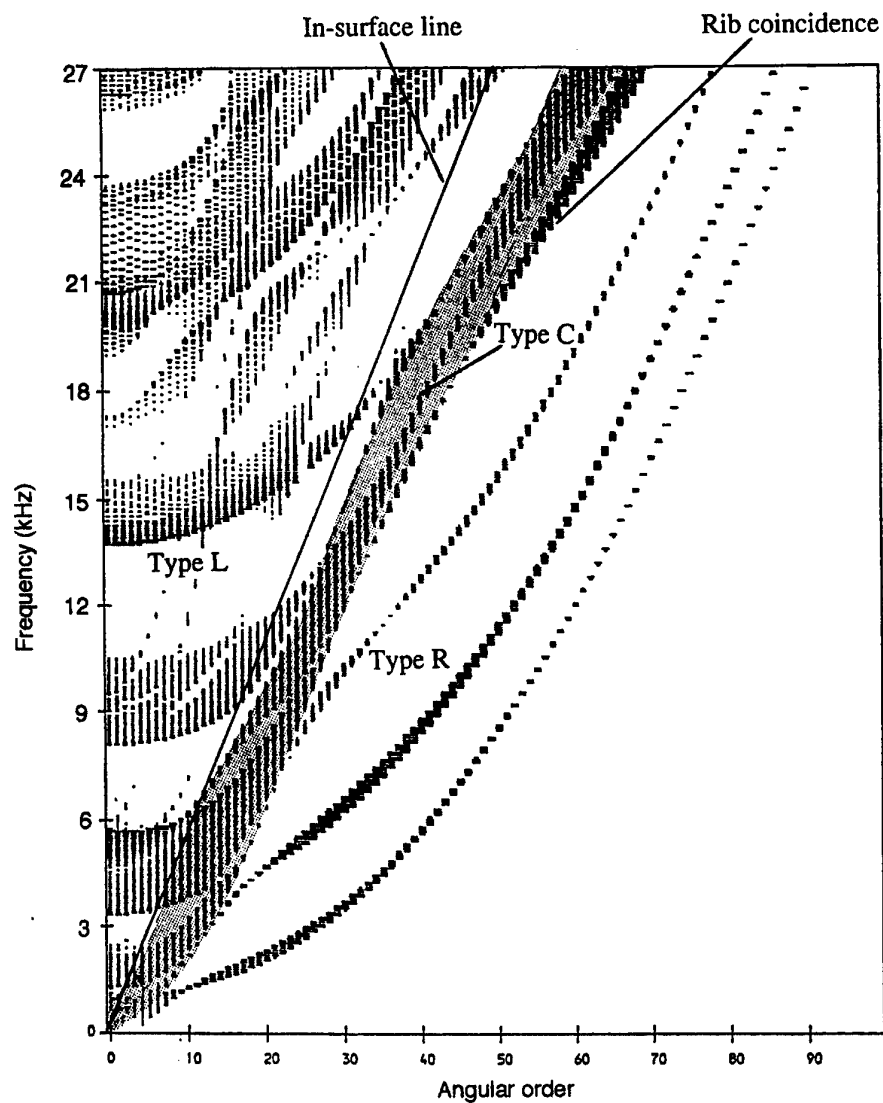


Figure 1: Pass- and stop-band structure for a typical ribbed-cylinder geometry, which corresponds to the small-scale model studied in [2].

## STATISTICAL POWER FLOW

### 4.2. SUBSYSTEM BREAKDOWN

We start by considering the standard statistical approach for structural vibration problems — Statistical Energy Analysis or SEA (see [3,4]). Within SEA, a structure is first divided into discrete subsystems within which response levels are assumed to be homogeneous. Linear equations are then set up to represent energy exchange and balance between these subsystems. By solving these, it is possible to deduce the response level within each subsystem in terms of the energy input from excitation sources.

Perhaps the most obvious subsystem breakdown of the pressure hull would be into individual frame bays, frames etc. However it is well known that a breakdown of a periodic or near-periodic structure into periodic elements in this way produces an SEA model with qualitatively the wrong behaviour (see [4]), essentially because SEA neglects coherence effects which are crucial in determining the transmission characteristics of the periodic structure.

Our approach is to take a macro-scale view of the pressure hull structure, regarding the ribbed cylinder as a kind of composite material with rather complicated dispersion characteristics for vibration transmission. We can then choose physical subsystems which are many frame bays in length. There are now the usual conflicting considerations with regard to SEA — breakdown into small subsystems produces high resolution, but larger subsystems may be necessary in order to satisfy the SEA requirement for high modal density and overlap per subsystem. Here we shall discuss a derivative of SEA — the statistical power flow method — which attempts to satisfy both objectives, using physical subsystems which are as large as is sensible, but allowing for variation of levels within each subsystem consistent with the known transmission and radiation characteristics of the various wavefields.

The first breakdown is into physical sections or “chunks”. There may be half a dozen or so chunks to a submarine, and they are what might most easily be inferred from a drawing, without any reference to vibration — the Main Machinery Compartment or Reactor Compartment, for example. They relate to sections of pressure hull in which we would expect no sudden changes in vibration levels or transmission characteristics. A chunk boundary would be placed at a significant reflector (e.g. a bulkhead) or a change in transmission characteristics (due to a change in mean frame spacing or shell thickness, say). Ideally a chunk should be many bays long, so that the infinite-cylinder dispersion characteristics can become established within a chunk. Such evidence as we have suggests that “many bays long” in this context means “at least three bays long”. A further breakdown into different wave types is now necessary, to represent in some way the wide range of transmission characteristics. Again, an extremely fine subdivision into individual propagation branches and individual angular orders is entirely feasible. However we have opted for a coarser breakdown into four wavetypes. These are the in-surface (IS) modes, and the flexural L-, C- and R-modes discussed earlier.

### 4.3. POWER-FLOW ANALYSIS WITHOUT COUPLING

This slightly unusual subsystem breakdown could, of course, be used with standard SEA. SEA parameters like modal densities and coupling loss factors are easily computed from the deterministic model discussed above. The difficulty for SEA is that many of the flexural subsystems are non-reverberant, largely due to the high rates of

radiation damping provided by the external fluid. Thus the assumption of homogeneous response within a subsystem — intrinsic to SEA — is invalid.

Instead, for these quasi-one-dimensional subsystems, it turns out to be quite easy to implement an analysis of power flow which ignores phase information but is otherwise in a certain sense "exact". This theory corresponds to "ASEA $\infty$ " as defined by Heron [5]. Consider two "chunks" of the pressure hull, coupled end-to-end, each carrying four subsystems. Since each chunk is a spatially-uniform section of ribbed cylinder, then a theory which ignores phase only requires two parameters to specify the complete energy field in any one subsystem: the amplitudes of the left-travelling and right-travelling "energy waves". For definiteness, define the amplitudes in the  $j$ th chunk such that the amplitudes of left-travelling energy density in the various internal subsystems are given at the right-hand end by the vector  $L_j$ , and the corresponding amplitudes of right-travelling energy at the left-hand end by the vector  $R_j$ . Each of these "energy waves" will decay exponentially as it travels, at a spatial rate determined by the subsystem damping factor and group velocity (suitably averaged over the frequency band under consideration). Apart from "near fields" around any localised energy source, the energy field in a given subsystem can be described exactly (within the context of a theory ignoring phase) as a linear combination of these two exponential basis functions.

It is now straightforward to obtain a closed set of equations for these energy amplitudes, by considering the reflection and transmission behaviour at the junction, together with perfectly-reflecting boundaries at the ends of the system. Some energy input is needed, of course. The simplest way to include this for a first examination of the results of this theory is to inject power at one end of the system at a known rate, and solve for the resulting distribution of energy density over the whole system. The system is illustrated schematically in Fig 2.

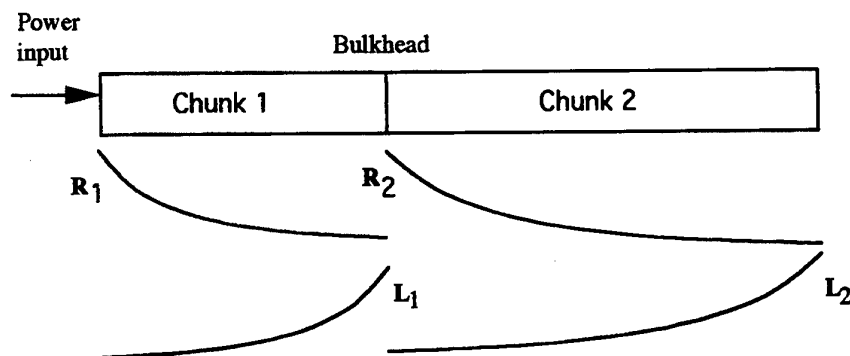


Figure 2: Schematic diagram of system and basis functions for "energy waves"

Energy associated with the different subsystems has different rates of exponential decay with distance. The amplitudes of the "energy waves" by the time they reach the far end of the chunks can thus be represented by two diagonal matrices  $\Lambda_1, \Lambda_2$  such that, for example, the right-travelling energy in chunk 1 has a vector of amplitudes at the right-hand end (i.e. the bulkhead) of  $\Lambda_1 R_1$ . The elements of these matrices are simply given by the exponential rates and the lengths of the chunks.



## STATISTICAL POWER FLOW

If we now define the power input to be a vector  $\mathbf{P}$ , and the matrices of reflection and transmission coefficients at the bulkhead are now called  $\rho, \tau$  respectively, then we can write down equations of energy-flux balance as follows:

$$\begin{aligned} \mathbf{R}_1 &= \Lambda_1 \mathbf{L}_1 + \mathbf{P} \\ \mathbf{L}_1 &= \rho \Lambda_1 \mathbf{R}_1 + \tau \Lambda_2 \mathbf{L}_2 \\ \mathbf{R}_2 &= \tau \Lambda_1 \mathbf{R}_1 + \rho \Lambda_2 \mathbf{L}_2 \\ \mathbf{L}_2 &= \Lambda_2 \mathbf{R}_2 \end{aligned} \quad (1)$$

It is straightforward to solve this set of linear equations, and hence find the energy distribution across the whole system. Examples will be shown shortly.

### 4.4. POWER-FLOW ANALYSIS WITH COUPLING

First, we discuss a development of the theory to allow for the scattering effects of irregularities. Motivated by SEA, the approach we propose here is a heat-diffusion analogy of the parallel energy paths within each chunk. We allow some "leakage" between the paths at a rate proportional to the local difference of "temperatures". For clarity of exposition, consider just two such coupled paths. The governing equations are assumed to take the form:

$$\begin{aligned} C_1 \frac{\partial^2 T_1}{\partial x^2} &= \Delta_1 T_1 + \alpha_{12} (T_1 - T_2) \\ C_2 \frac{\partial^2 T_2}{\partial x^2} &= \Delta_2 T_2 + \alpha_{12} (T_2 - T_1) \end{aligned} \quad (2)$$

where  $T_1, T_2$  are the SEA "temperature" variables for the two paths, i.e. the densities of energy-per-mode, and  $C_1, C_2$  are effective diffusivities. These diffusivities are determined by the requirement that, in the absence of the coupling term, each path should have the correct rate of spatial decay, as provided by the deterministic model. This requires

$$C_1 = \frac{c_g^2}{\Delta_1}, C_2 = \frac{c_g^2}{\Delta_2} \quad (3)$$

where  $c_g$  is the (appropriately averaged) group velocity. The loss coefficients  $\Delta_1, \Delta_2$  are the same as in standard SEA, and the coupling term involves the constant  $\alpha_{12}$  whose value, in practice, is determined empirically by matching the length-scales of breakthrough energy transport to those found from relevant measurements.

Generalised in the obvious way to allow for the four subsystems per chunk, these equations can be written

$$\begin{bmatrix} C_1 & 0 & 0 & 0 \\ 0 & C_2 & 0 & 0 \\ 0 & 0 & C_3 & 0 \\ 0 & 0 & 0 & C_4 \end{bmatrix} \begin{bmatrix} T_1'' \\ T_2'' \\ T_3'' \\ T_4'' \end{bmatrix} = \begin{bmatrix} \Delta_1 + \alpha_{12} + \alpha_{13} + \alpha_{14} & -\alpha_{12} & -\alpha_{13} & -\alpha_{14} \\ -\alpha_{12} & \ddots & \dots & \dots \\ -\alpha_{13} & \vdots & \ddots & \dots \\ -\alpha_{14} & \vdots & \vdots & \ddots \end{bmatrix} \begin{bmatrix} T_1 \\ T_2 \\ T_3 \\ T_4 \end{bmatrix} \quad (4)$$

But these are just the familiar equations for a four-degree-of-freedom vibrating system, with spatial derivatives in place of time derivatives, and with the two matrices on the left- and right-hand sides playing the roles of "mass" and "stiffness" matrices. We can

solve them by a "modal" transformation. The (generalised) eigenvalues of this pair of real, symmetric matrices give the spatial decay rates (squared) of the "modal" combinations of energy levels in the various subsystems. If we construct the matrix  $Q$  whose columns are the eigenvectors (normalised with the "mass matrix", i.e. the diagonal matrix of diffusivities), then it can be used to map energy vectors into and out of these "modal" combinations.

The result is that the analysis of the previous subsection carries over directly to this new case, provided only that we replace the matrices  $\Lambda_1, \Lambda_2$  by the combinations  $Q\Lambda_1Q^{-1}, Q\Lambda_2Q^{-1}$ , where the diagonal matrices  $\Lambda_1, \Lambda_2$  here are calculated like the earlier ones, but using the eigenvalues for the decay rates. This formalises the translation into and out of modal coordinates in order to calculate the energy decay factors from end to end of the chunks.

## 5. Example calculations

For the purposes of illustration, a submarine structure consisting of two "chunks" of pressure hull separated by a bulkhead (modelled as a thin flat plate) will be considered. The length of chunk A will be  $L_A = 10$  frame bays, and that of B will be  $L_B = 15$  bays. A normalised input of 1 Watt/Hz will be assumed into each of the four subsystems of chunk A at the end remote from the bulkhead. The ribbed cylinder geometry corresponds to the small-scale model studied in [2].

The spatial average of the SEA temperature (energy per mode) within each of the four subsystems of chunks A and B is plotted in Figs. 3(a)–(d), for the different subsystem types. Each graph displays results calculated using both "standard" SEA and the statistical power flow method without "leakage" coupling. On each graph the two predictions for chunk A (the driven section) are virtually indistinguishable. However within chunk B very large differences are observed, particularly for types R and C, corresponding to transmission modes having the most rapid spatial decay. In effect standard SEA is assuming that the energy incident on the chunk boundary is the same as the spatially averaged result. This is much greater than is actually the case (because of the rapid rate of spatial decay in some subsystems). Therefore a greater transfer of energy into chunk B is predicted, with consequently higher estimated levels.

These results may be compared directly with those in Figs. 4(a)–(d), which show the same comparison calculated with non-zero values for the coupling parameters  $\alpha_{ij}$ . These parameters are given the same value between every pair of subsystems in each chunk, purely for illustrative purposes. This models "a little coupling of everything to everything". To provide some idea of the magnitude of these coupling terms in the cases to be shown, they are expressed as a fraction of the damping rate  $\Delta_{struct}$  due to structural damping alone, since this is set at a constant value  $0.005\omega$  for all subsystems. The diagonal terms of the matrix appearing on the right-hand side of eq. (4) also contains the contribution from radiation damping, which varies with mode type and with frequency, and is in general much bigger than the structural contribution.

The coupling value used to compute Fig. 4 is only  $\Delta_{struct} / 1000$ . Even with this tiny amount of coupling, the very low levels predicted in chunk B for types R and C are substantially increased. The main mechanism for this is that the bulkhead forms only a very weak reflector for IS waves, and to a lesser extent for type L waves. Energy transmits into chunk B by these mechanisms, then can scatter back into types R and C. By the far end of chunk B, the SEA temperatures of types R and C had been raised, due

## STATISTICAL POWER FLOW

to the coupling, to the extent where they were comparable with that of type L.

To gain some physical insight into the effect of coupling, we present some plots of spatial energy distribution. The energy density is plotted at each mid-bay position. The bulkhead is at the end of bay 10, and an obvious drop of levels occurs there. Figures 5(a) and (b) show two representative results without coupling, for two different frequency bands. Figures 5(c) and (d) show the results for the same frequency band as Fig. 5(b), with coupling equal to  $\Delta_{struct}/1000$  (as in Fig. 4) and  $\Delta_{struct}/10$ , respectively.

The non-reverberant nature of some of the subsystems is immediately apparent in the cases without coupling. For the higher frequency shown here, in Fig. 5(b), the Type L modes particularly are showing a very rapid spatial decay. This can be attributed mainly to their high damping (predominantly by radiation). It is no wonder, with such extreme non-reverberant behaviour, that SEA does not predict the response at all accurately. Notice in Fig. 5(b) that because the Type L modes show rapid spatial decay and are also coupled to the Type IS modes, the resulting pattern has a local maximum near the bulkhead. What is happening is that energy initially fed into the Type L modes decays rapidly, so that little of it reaches the bulkhead. However, energy reaches the bulkhead quite efficiently via the Type IS modes, and some of it is then scattered into Type L modes, travelling outwards from the bulkhead in both directions. These again decay rapidly, producing the local maximum.

As one would have expected, in the presence of coupling the very low levels, especially those associated with Type L modes, are raised. In compensation, the rate of decay of the Type IS modes becomes progressively faster, as more energy leaks out of these modes into other, more highly damped, mode types. By the case shown in Fig. 5(d), all four mode types get rather rapidly locked together, and decay along parallel tracks. The particular proportions of energy in the four types when they are thus locked together are those of the eigenvector having the lowest decay rate. This is always the only eigenvector all of whose terms are positive, so that it is the only one which has physical significance in isolation. The proportions given by this eigenvector play somewhat the same role in this coupled system as does the condition of "equipartition of energy" in normal SEA: it is the state the system tends towards given sufficient length for the pattern to develop.

## 6. Conclusions

A statistical approach for modelling the transmission of vibration along a realistic submarine pressure hull has been developed. Fluid-loading effects are included in the modelling and are significant. Standard Statistical Energy Analysis is not adequate to deal with the rather special geometry of the submarine pressure hull, but the proposed new model captures details of behaviour which are in accordance with experimental findings. In particular, "leakage" of energy between angular orders as a result of irregularities in the hull structure can "short-circuit" a reflector such as a bulkhead.

## 7. Acknowledgements

The authors are grateful to Dr I Roebuck and Dr D J W Hardie of the DRA for providing invaluable support. ©British Crown Copyright 1997/DERA.

## STATISTICAL POWER FLOW

to the coupling, to the extent where they were comparable with that of type L.

To gain some physical insight into the effect of coupling, we present some plots of spatial energy distribution. The energy density is plotted at each mid-bay position. The bulkhead is at the end of bay 10, and an obvious drop of levels occurs there. Figures 5(a) and (b) show two representative results without coupling, for two different frequency bands. Figures 5(c) and (d) show the results for the same frequency band as Fig. 5(b), with coupling equal to  $\Delta_{struct}/1000$  (as in Fig. 4) and  $\Delta_{struct}/10$ , respectively.

The non-reverberant nature of some of the subsystems is immediately apparent in the cases without coupling. For the higher frequency shown here, in Fig. 5(b), the Type L modes particularly are showing a very rapid spatial decay. This can be attributed mainly to their high damping (predominantly by radiation). It is no wonder, with such extreme non-reverberant behaviour, that SEA does not predict the response at all accurately. Notice in Fig. 5(b) that because the Type L modes show rapid spatial decay and are also coupled to the Type IS modes, the resulting pattern has a local maximum near the bulkhead. What is happening is that energy initially fed into the Type L modes decays rapidly, so that little of it reaches the bulkhead. However, energy reaches the bulkhead quite efficiently via the Type IS modes, and some of it is then scattered into Type L modes, travelling outwards from the bulkhead in both directions. These again decay rapidly, producing the local maximum.

As one would have expected, in the presence of coupling the very low levels, especially those associated with Type L modes, are raised. In compensation, the rate of decay of the Type IS modes becomes progressively faster, as more energy leaks out of these modes into other, more highly damped, mode types. By the case shown in Fig. 5(d), all four mode types get rather rapidly locked together, and decay along parallel tracks. The particular proportions of energy in the four types when they are thus locked together are those of the eigenvector having the lowest decay rate. This is always the only eigenvector all of whose terms are positive, so that it is the only one which has physical significance in isolation. The proportions given by this eigenvector play somewhat the same role in this coupled system as does the condition of "equipartition of energy" in normal SEA: it is the state the system tends towards given sufficient length for the pattern to develop.

## 6. Conclusions

A statistical approach for modelling the transmission of vibration along a realistic submarine pressure hull has been developed. Fluid-loading effects are included in the modelling and are significant. Standard Statistical Energy Analysis is not adequate to deal with the rather special geometry of the submarine pressure hull, but the proposed new model captures details of behaviour which are in accordance with experimental findings. In particular, "leakage" of energy between angular orders as a result of irregularities in the hull structure can "short-circuit" a reflector such as a bulkhead.

## 7. Acknowledgements

The authors are grateful to Dr I Roebuck and Dr D J W Hardie of the DRA for providing invaluable support. ©British Crown Copyright 1997/DERA.

## 8. References

1. D.G. Crighton. The Interaction Between Sound and Vibration, *Proc. I.O.A.*, 10, 2, 1-35 (1988).
2. C.H. Hodges, J. Power and J. Woodhouse. The Low Frequency Vibration of a Ribbed Cylinder, Part 1: Theory. *J. Sound Vib.*, 101, 219-235 (1985).
3. C.H. Hodges and J. Woodhouse. Theories of Noise and Vibration in Complex Structures. *Rep. Prog. Phys.*, 49, 107-170 (1986).
4. R.H. Lyon and R.G. De Jong. *Theory and Application of Statistical Energy Analysis*, Butterworth-Heinemann (1995).
5. K. H. Heron, Advanced statistical energy analysis, *Phil. Trans. Roy. Soc. London A346*, 501-510 (1994).

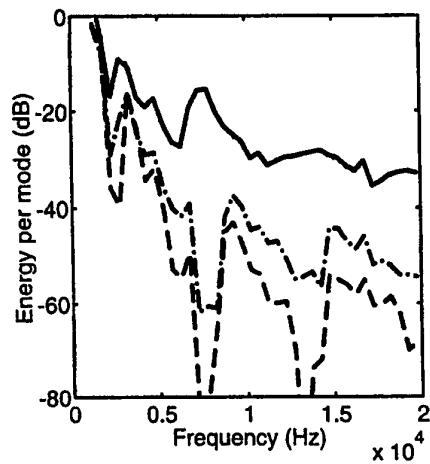


Figure 3(a). Comparison of power-flow modelling with SEA, in the absence of leakage coupling, for the Type L modes. Solid line: section A, SEA; dash-dot line: section B, SEA; dotted line: section A, power flow; dashed line: section B, power flow.

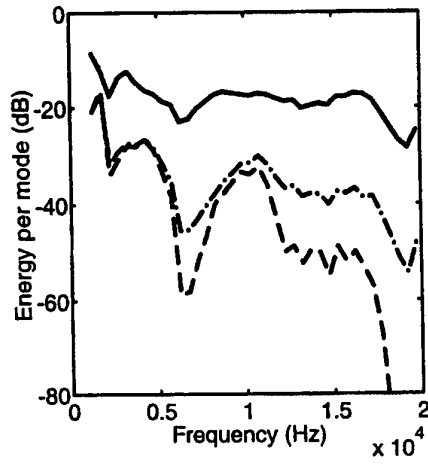


Figure 3(b). Comparison of power-flow modelling with SEA, in the absence of leakage coupling, for the Type C modes. Solid line: section A, SEA; dash-dot line: section B, SEA; dotted line: section A, power flow; dashed line: section B, power flow.

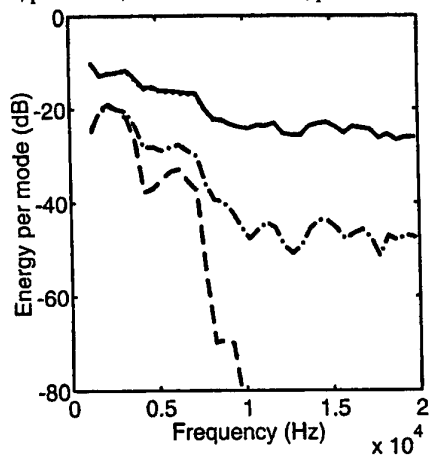


Figure 3(c). Comparison of power-flow modelling with SEA, in the absence of leakage coupling, for the Type R modes. Solid line: section A, SEA; dash-dot line: section B, SEA; dotted line: section A, power flow; dashed line: section B, power flow.

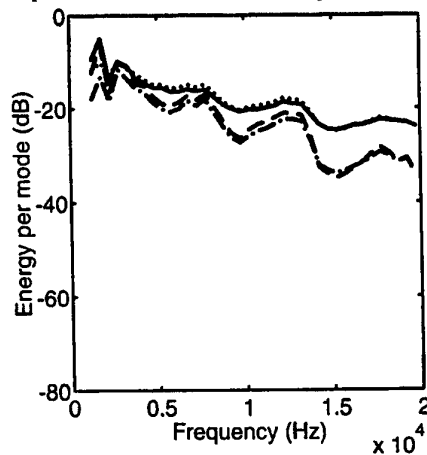


Figure 3(d). Comparison of power-flow modelling with SEA, in the absence of leakage coupling, for the Type IS modes. Solid line: section A, SEA; dash-dot line: section B, SEA; dotted line: section A, power flow; dashed line: section B, power flow.

# STATISTICAL POWER FLOW

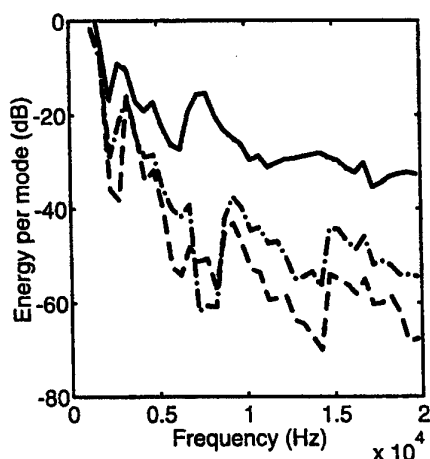


Figure 4(a). Comparison of power-flow modelling with SEA with constant leakage coupling of  $\alpha_{ij} = \Delta_{struct} / 1000$ , for the Type L modes. Solid line: section A, SEA; dash-dot line: section B, SEA; dotted line: section A, power flow; dashed line: section B, power flow.

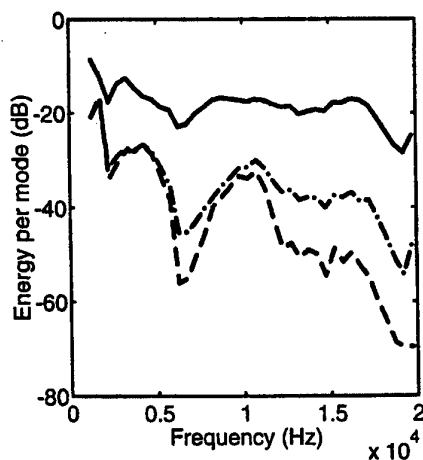


Figure 4(b). Comparison of power-flow modelling with SEA with constant leakage coupling of  $\alpha_{ij} = \Delta_{struct} / 1000$ , for the Type C modes. Solid line: section A, SEA; dash-dot line: section B, SEA; dotted line: section A, power flow; dashed line: section B, power flow.

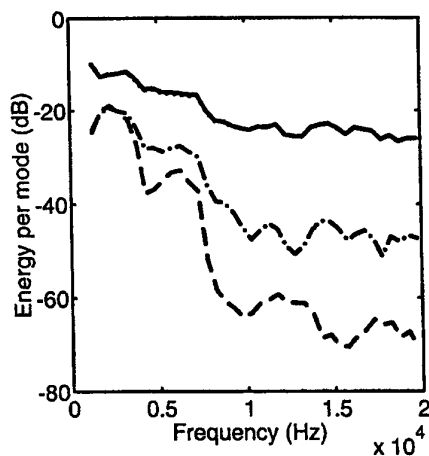


Figure 4(c). Comparison of power-flow modelling with SEA with constant leakage coupling of  $\alpha_{ij} = \Delta_{struct} / 1000$ , for the Type R modes. Solid line: section A, SEA; dash-dot line: section B, SEA; dotted line: section A, power flow; dashed line: section B, power flow.

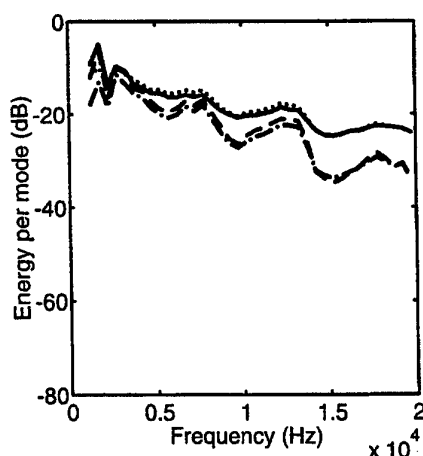


Figure 4(d). Comparison of power-flow modelling with SEA with constant leakage coupling of  $\alpha_{ij} = \Delta_{struct} / 1000$ , for the Type IS modes. Solid line: section A, SEA; dash-dot line: section B, SEA; dotted line: section A, power flow; dashed line: section B, power flow.

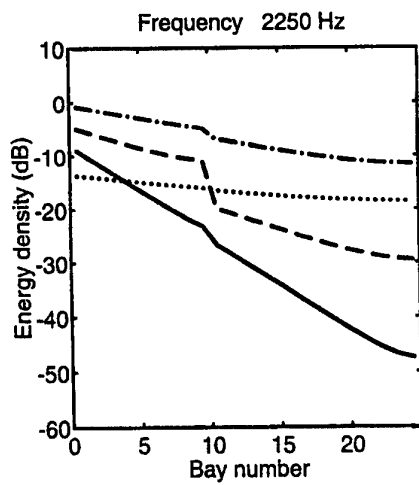


Figure 5(a). Spatial distribution of energy along the two-chunk model, without leakage coupling, in the frequency band centred on 2250 Hz. Solid line: Type L modes; dashed line: Type C modes; dash-dot line: Type R modes; dotted line: Type IS modes.

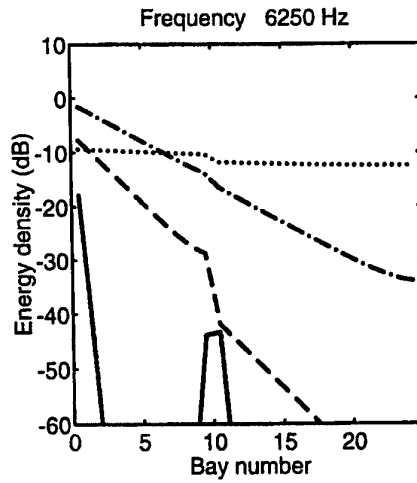


Figure 5(b). Spatial distribution of energy along the two-chunk model, without leakage coupling, in the frequency band centred on 6250 Hz. Solid line: Type L modes; dashed line: Type C modes; dash-dot line: Type R modes; dotted line: Type IS modes.

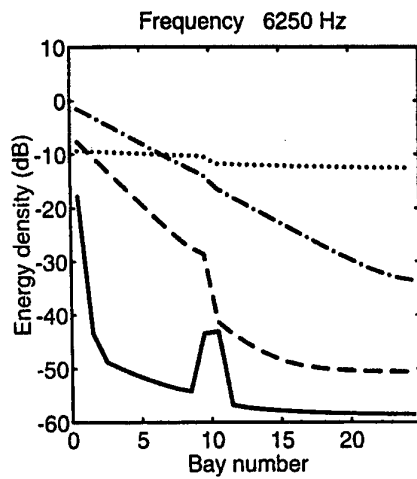


Figure 5(c). Spatial distribution of energy along the two-chunk model, with leakage coupling at level  $\alpha_{ij} = \Delta_{struct} / 1000$ , in the frequency band centred on 6250 Hz. Solid line: Type L modes; dashed line: Type C modes; dash-dot line: Type R modes; dotted line: Type IS modes.

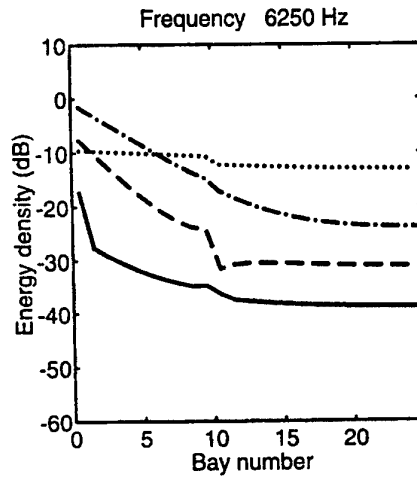


Figure 5(d). Spatial distribution of energy along the two-chunk model, with leakage coupling at level  $\alpha_{ij} = \Delta_{struct} / 10$ , in the frequency band centred on 6250 Hz. Solid line: Type L modes; dashed line: Type C modes; dash-dot line: Type R modes; dotted line: Type IS modes.

# **THE ESTIMATION OF DYNAMIC STRESS AND STRAIN IN BEAMS, PLATES AND SHELLS USING STRAIN-VELOCITY RELATIONSHIPS**

Denis G. Karczub and Michael P. Norton  
Department of Mechanical and Materials Engineering  
Centre for Acoustics, Dynamics and Vibration  
University of Western Australia  
Nedlands, WA, Australia, 6009

## **ABSTRACT**

This paper reviews recent research into the development of simple relationships between mean-square dynamic strain and vibrational velocity for the estimation of maximum dynamic strain levels in randomly vibrating structures. These relationships provide a consistent approach with a firm theoretical basis for the estimation of dynamic strain from vibrational velocity in all types of structures, independent of the type of structural element (beam, plate or cylindrical shell) and the frequencies of excitation (resonant, non-resonant, multi-modal and broad-band vibration in the low-, mid- and high-frequency ranges). The relationships developed are based on farfield relationships, factors for the effects of evanescent waves, and correlations between the spatial maxima of dynamic strain and velocity.

## **1. Introduction**

Analyses of dynamic stress and fatigue are necessary for structures and piping systems that are subject to random vibration caused by mechanical, acoustic or flow-induced forces. These analyses should be performed during design, after installation and commissioning, and on existing plants and structures to identify potential failures before they occur. Problems with dynamic fatigue occur regularly and often result from a failure to take dynamic stress and fatigue into account, either during design or after changes in plant and excitation levels. The situation is also hampered by a lack of suitable methods for predicting dynamic stress during design and after installation.

The objective of the present work is to develop simple relationships for determining dynamic stress and strain levels in randomly vibrating structures and piping systems from either calculated or measured vibrational velocity levels. Relationships have previously been developed for single mode resonant vibration of beams [1,2,3] and broad-band resonant



vibration of plates and cylindrical shells [4,5], but the problems of (i) non-resonant vibration and multi-modal resonant vibration of beams, plates and cylindrical shells and (ii) the single mode resonant vibration of plates and cylindrical shells have not been considered. The work presented here addresses these additional cases and provides a consistent approach which is the same for all cases irrespective of the type of excitation or the type of structure.

One of the key applications of the techniques considered here is the measurement of maximum dynamic strain in structures and piping systems using portable accelerometers in place of permanently mounted strain gauges. The use of relationships between dynamic strain and velocity to estimate dynamic strain provides a practical alternative to the use of strain gauges that is less susceptible to environmental conditions, is less sensitive to the location of maximum dynamic stress, and which can be undertaken at lower cost.

A more detailed literature review and treatment of the work contained here is given in Reference [6].

## 2. Overview of Method

Using travelling wave solutions as the basis of the theoretical framework to be developed, farfield relationships are derived between the propagating wave components of dynamic strain and velocity. These relationships are derived for beam, plate and cylindrical shell structural elements. Formal relationships for the correlation of dynamic strain and velocity spatial maxima are then defined. These latter relationships incorporate explicit factors for the effects of evanescent waves on farfield relationships between dynamic strain and velocity, and are based on analyses of dynamic strain and velocity spatial distributions (Karczub[6]). Factors for the effects of evanescent waves are subsequently incorporated in a single overall factor relating the spatial maxima of dynamic strain and velocity for practical applications. Theoretical spatial distributions and some experimental data demonstrating these relationships are then presented.

## 3. Farfield Relationships

### 3.1 FLEXURAL VIBRATION OF A BEAM

The dynamic bending strain for flexural vibration of a beam is related to the transverse velocity at the same location by a frequency-independent constant  $K_{\text{shape}}/c_L$  if the evanescent wave components are neglected. Dividing the farfield dynamic strain at position  $x$  and frequency  $f$ ,  $\xi_{FF}(x, f) = y_m k^2 (A_1 e^{-ikx} + A_2 e^{ikx})$ , by the farfield velocity at the same location and frequency,  $v_{FF}(x, f) = i2\pi f (A_1 e^{-ikx} + A_2 e^{ikx})$ , and expressing in terms of mean-square values, yields

$$\frac{\langle \xi_{FF}^2(x,f) \rangle}{\langle v_{FF}^2(x,f) \rangle} = \left( \frac{y_m k^2}{i2\pi f} \right)^2 = \left( \frac{K_{shape}}{c_L} \right)^2, \quad (1)$$

where  $K_{shape} = y_m \sqrt{A/I}$  is the non-dimensional geometric shape factor, the subscript FF denotes farfield conditions where evanescent waves can be neglected,  $y_m$  is the distance of the outermost fibre from the centroidal axis,  $k$  is the wavenumber,  $i$  is  $\sqrt{-1}$ , the  $A$ , are complex constants which vary with frequency,  $c_L = \sqrt{E/\rho}$  is the longitudinal wave speed,  $A$  is cross-sectional area, and  $I$  is the area moment of inertia. The frequency independent constant is a function of only cross-sectional geometry  $K_{shape}$  and the longitudinal wavespeed  $c_L$ . The value of  $K_{shape}$  is equal to  $\sqrt{3}$  for solid rectangular beams, and lies in the range of  $\sqrt{2}$  for a very thin walled hollow bar to 2 for a solid circular bar.

### 3.2 FLEXURAL VIBRATION OF A PLATE

Using the propagating wave components of the travelling wave solution for flexural vibration of plate, and dividing the farfield dynamic bending strain components  $\xi_{x,FF}$  and  $\xi_{y,FF}$  by the farfield velocity  $v_{FF}$  gives

$$\frac{\xi_{x,FF}(x,f)}{v_{FF}(x,f)} = \frac{y_m k_B^2 \cos^2 \theta}{i2\pi f} = \frac{-iK_{shape}}{c_L} \cos^2 \theta \quad (2)$$

and

$$\frac{\xi_{y,FF}(x,f)}{v_{FF}(x,f)} = \frac{y_m k_B^2 \sin^2 \theta}{i2\pi f} = \frac{-iK_{shape}}{c_L} \sin^2 \theta, \quad (3)$$

where  $K_{shape}$  is a non-dimensional geometric shape factor (which equals  $\sqrt{3}$  independent of plate thickness) and  $c_L$  is the longitudinal wavespeed for a plate given by  $c_L = \sqrt{E/\rho(1-\mu^2)}$ . These relationships are the same as for the flexural vibration of a beam except that for plate vibration there are two components of dynamic bending strain which are also a function of the direction of wave propagation. Since the dominant direction of wave propagation varies from one frequency to the next and is generally not known from vibration measurements, exact predictions of dynamic bending strain from velocity using the above relationships are not possible.

If the dynamic bending strain component sum  $\xi_{x,FF} + \xi_{y,FF}$  is related to velocity (in place of the individual components of dynamic bending strain), the frequency independent relationship

$$\frac{\langle (\xi_{x,FF}(x,f) + \xi_{y,FF}(x,f))^2 \rangle}{\langle v_{FF}^2(x,f) \rangle} = \left( \frac{y_m k_B^2}{i2\pi f} \right)^2 = \left( \frac{K_{shape}}{c_L} \right)^2 = \frac{3}{c_L^2}, \quad (4)$$

results, where  $K_{shape} = \sqrt{3}$ . This relationship is equivalent to the farfield relationship between dynamic bending strain and velocity for beam flexural vibration. It is independent of plate

thickness and the direction of wave propagation. Since the sum of dynamic bending strains provides an upper bound limit on dynamic bending strain ( $\xi_{\max,FF} < \xi_{x,FF} + \xi_{y,FF}$ ), estimates of dynamic strain from Equation 4 provide an upper bound for predictions of fatigue life. Equation 4 should, as a minimum, find use for first pass vibration screening of flat plate structures.

### 3.3 VIBRATION OF CYLINDRICAL SHELLS

For the case of cylindrical shell vibration it is necessary to consider in-plane motions in addition to out-of plane motions. To permit the relationships between dynamic strain and velocity to be expressed in terms of only the readily measured out-of-plane motions, the in-plane wave amplitude coefficients  $U_{ns}$  and  $V_{ns}$  are eliminated from the travelling wave equations for dynamic bending strain and velocity by substituting the characteristic wave amplitude ratios  $\alpha_{ns}=U_{ns}/W_{ns}$  and  $\beta_{ns}=V_{ns}/W_{ns}$ . Hence,

$$\xi_{x,n}(x,\theta,f) = \sum_{s=1}^8 W_{ns} e^{k_{ns}x} \cos(n\theta) \{k_{ns}\alpha_{ns} - zk_{ns}^2\}, \quad (5)$$

$$\xi_{\theta,n}(x,\theta,f) = \sum_{s=1}^8 W_{ns} e^{k_{ns}x} \cos(n\theta) \left( \frac{1}{R^2 + Rz} \right) \{R + n^2 z + nR\beta_{ns} + nz\beta_{ns}\} \quad (6)$$

and

$$v_n(x,\theta,f) = i2\pi f \sum_{s=1}^8 W_{ns} \cos(n\theta) e^{k_{ns}x}, \quad (7)$$

where  $\xi_x$  is the axial dynamic bending strain,  $\xi_\theta$  is the circumferential dynamic bending strain,  $v$  is the transverse velocity and the only unknowns are the out-of-plane wave amplitude coefficients  $W_{ns}$ . Only axial and circumferential dynamic strains are considered since the shear strain is zero at angular positions where the axial and circumferential dynamic strains are largest. Maximum dynamic strain occurs at  $z=\pm y_m$ .

Farfield relationships derived in this sub-section are expressed in the non-dimensionalised form

$$K_{FF}(f) = \frac{\xi_{FF} c_L}{v_{FF}} = \frac{y_m k_B^2}{2\pi f} c_L \equiv K_{shape}, \quad (8)$$

where  $K_{FF}$  is the non-dimensional farfield correlation ratio. Substituting Equations 5, 6 and 7 into Equation 8 for axial waves  $s=1,2$  with the lowest cut-on frequencies, the farfield relationships between dynamic bending strain and velocity for cylindrical shell vibration are given by

$$K_{FF,axial,ns}(f) = \frac{\xi_{x,ns} c_L}{v_{ns}} = \left| \frac{k_{ns}\alpha_{ns} - zk_{ns}^2}{i2\pi f} \right| c_L, \quad (9)$$

and

$$K_{FF, circ, ns}(f) = \frac{\xi_{\theta, ns} c_L}{v_{ns}} = \left( \frac{1}{R^2 + R_z} \right) \left| \frac{\{R^2 + n^2 z + nR\beta_{ns} + nz\beta_{ns}\}}{i2\pi f} \right| c_L. \quad (10)$$

These relationships for the components of dynamic bending strain are a function of the direction of wave propagation and it is necessary to relate the sum of dynamic bending strains to velocity in the same way as for flexural vibration of a plate (Equation 4). The resulting relationship between the sum of dynamic bending strains and velocity is plotted in Figure 1 for  $n=1..3$ . The ratio of farfield dynamic strain to velocity is bounded and essentially frequency independent for vibration of circumferential modes  $n \geq 3$ , and the vibration of circumferential modes  $n=1$  and  $n=2$  at frequencies above the ring frequency (refer Figure 1).

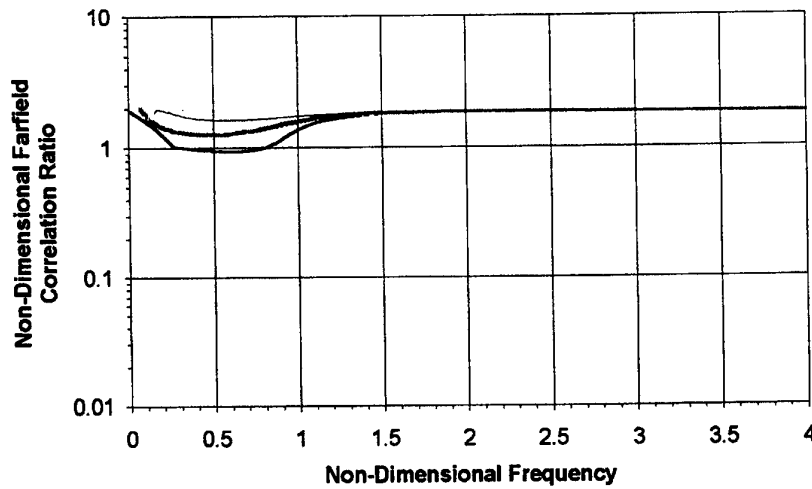


Figure 1. Non-Dimensional Farfield Correlation Ratio for Cylindrical Shell Vibration  
( —  $n=1$ ; - -  $n=2$ ; —  $n=3$ )

The relationship between the propagating wave components of dynamic strain and velocity plotted in Figure 1 does not consider the effects of additional propagating waves that cut-on at higher frequencies. To calculate these effects it is necessary to revert to the use of numerical calculations of the vibrational response for actual cylindrical shell systems. The results of investigations undertaken for a clamped cylindrical shell are that the pairs of axial waves which cut-on at the lowest frequencies for each circumferential mode  $n$  dominate the response at all resonant frequencies, with the result that the non-dimensional correlation ratio in Figure 1 also applies at higher frequencies where there are additional pairs of propagating waves. Only a small increase in the non-dimensional farfield correlation ratio of approximately five per cent is required to take these additional propagating waves into account.

### 3.4 GENERALISED FARFIELD RELATIONSHIP

The resulting generalised farfield relationship between the dynamic strain and velocity at the same position for flexural vibration of beams, plates and cylindrical shells is given by

$$\langle \xi_{FF}^2(x, f) \rangle = \left( \frac{K_{FF}}{c_L} \right)^2 \langle v_{FF}^2(x, f) \rangle, \quad (11)$$

where  $\xi_{FF} = \xi_{x,FF} + \xi_{y,FF}$  for plates,  $\xi_{FF} = \xi_{x,FF} + \xi_{\theta,FF}$  for cylindrical shells,  $K_{FF}/c_L$  is defined as the farfield correlation ratio, and the non-dimensional farfield correlation ratio  $K_{FF}$  is equal to  $K_{shape}$  for beams and plates. Since  $K_{FF}$  is frequency independent for beams and plates, and is approximately frequency independent and bounded for cylindrical shell vibration, the relationship in Equation 11 between farfield dynamic strain and farfield velocity is also frequency independent. Values of  $K_{FF}$  for beams, plates and cylindrical shells are summarised in Table 1.

TABLE 1. Non-Dimensional Correlation Ratios between Dynamic Strain and Velocity

	$K_{FF}$	$K$	$K_{vFF}$
Beams	$\sqrt{3}$	2.3	2.46
Solid rectangular bars			
Pipe, wall thickness up to Schedule 80			
Beams	2	2.65	2.84
Solid circular bars			
Pipe, wall thickness above Schedule 80			
Plates	$\sqrt{3}$	2.3	2.46
Cylindrical Shells	$\sqrt{3.5}$	2.0	2.0

### 4. Estimation of Maximum Dynamic Strain from Velocity

The objective of the present work is to develop relationships for estimating the spatial maximum dynamic strain in simple structures from the measured or calculated velocity response. The farfield relationship in Equation 11 provides exact estimates of dynamic strain from velocity at the same position in farfield regions, and can be used to determine the spatial maximum farfield dynamic strain  $\xi_{max,FF}$  in each frequency band. This involves measuring or calculating the spatial maximum farfield velocity  $v_{max,FF}$  in each frequency band and evaluating Equation 11 for  $\xi_{max,FF}$ . The farfield relationship in Equation 11 does not, however, apply in nearfield regions due to the different effects of evanescent waves on the propagating wave components of dynamic strain and velocity (Karczub[6]) preventing the direct application of farfield relationships to the estimation of maximum dynamic strain. In

this section, expressions for the estimation of maximum dynamic strain from velocity that take into account the complicating effects of evanescent waves are derived from the farfield relationship in Equation 11.

#### 4.1 EVANESCENT WAVE EFFECTS

The general effects of evanescent waves are to increase the spatial maxima of dynamic strain and velocity above their spatial maximum farfield levels at different locations and by different amounts. The different effects of evanescent waves on dynamic strain and velocity are due to the opposite phase of evanescent waves in the travelling wave solutions dynamic strain and velocity. Spatial distributions demonstrating these effects are plotted in Figure 2 for the resonant vibration of a transversely excited clamped beam, and in Figure 3 for the resonant vibration of a clamped cylindrical shell. The effects of evanescent waves are shown by overlaying spatial distributions of the propagating and evanescent wave components of the response. Velocity is plotted in these figures as predicted dynamic strain calculated from Equation 11 using velocity in place of the farfield velocity. It should be noted that in the case of cylindrical shell vibration there may be additional pairs of evanescent waves that have short wavelength and produce larger levels of dynamic strain concentration than in a beam. Dynamic strain concentration is defined as the increased dynamic strain at a boundary or discontinuity due to evanescent wave effects (Ungar[7]).

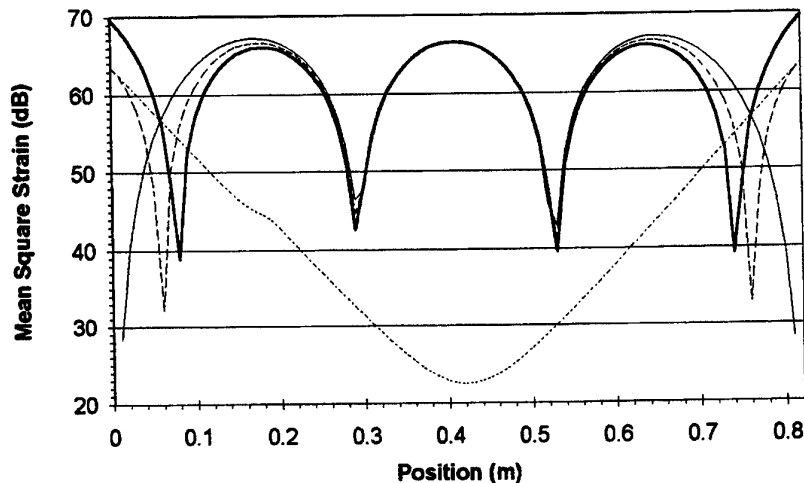


Figure 2. Spatial Distributions of the Dynamic Strain and Velocity Response in a Clamped Beam  
( — Strain; — — Predicted Strain; - - - Farfield Strain; . . . Nearfield Strain)

#### 4.2 CORRELATION OF SPATIAL MAXIMA

The generalised farfield relationship between dynamic strain and velocity in Equation 11 provides an exact relationship between the spatial maxima of dynamic strain and velocity in

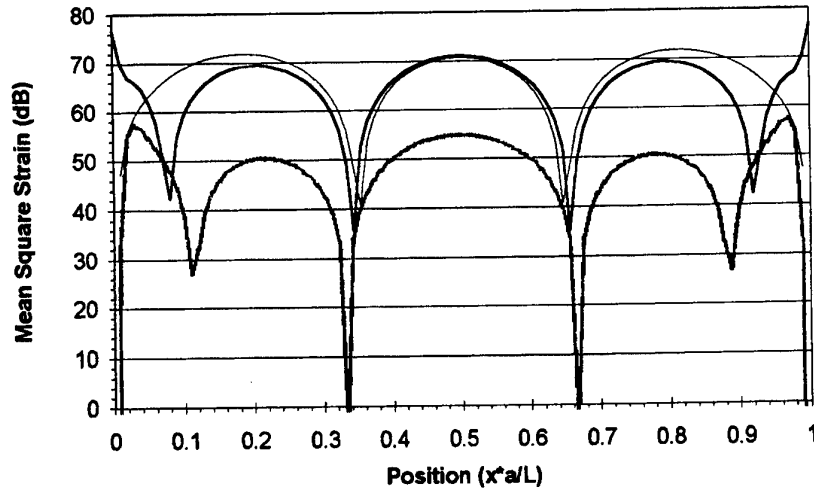


Figure 3a. Dynamic Strain and Velocity in a Clamped Cylindrical Shell  
( — Axial Strain; - - - Circumferential Strain; — Predicted Strain)

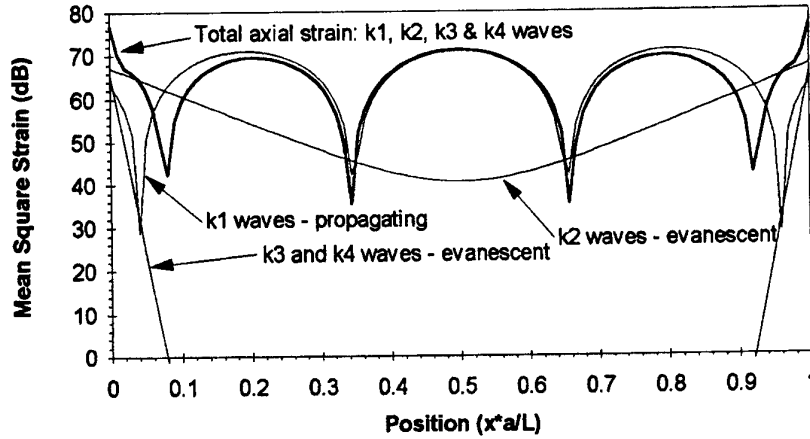


Figure 3b. Propagating and Evanescent Wave Components of Axial Dynamic Strain  
in a Clamped Cylindrical Shell

the absence of evanescent waves which is only slightly modified by evanescent wave effects when the complete response is considered. Evaluating Equation 11 at a position  $x_{\max,FF}$  where the propagating wave components of both dynamic strain and velocity attain their spatial maximum levels gives

$$\frac{\xi_{\max,FF}(f)}{v_{\max,FF}(f)} = \frac{\xi_{FF}(x_{\max,FF}, f)}{v_{FF}(x_{\max,FF}, f)} = \frac{K_{FF}}{c_L}, \quad (12)$$

where  $\xi_{\max,FF}$  is the predicted maximum farfield dynamic strain and  $K_{FF}/c_L$  is the farfield

correlation ratio as before. Evanescent wave effects are taken into account by incorporating factors for the increases in dynamic strain and velocity levels above maximum farfield levels. If  $\xi_{\max}(f)/\xi_{\max,FF}(f)$  is the increase in maximum dynamic strain above the maximum farfield dynamic strain and  $v_{\max}(f)/v_{\max,FF}(f)$  is the increase in maximum velocity above the maximum farfield velocity, then the ratio of maximum dynamic strain to maximum velocity is given by

$$\frac{\xi_{\max}(f)}{v_{\max}(f)} = \frac{\xi_{\max}(f)/\xi_{\max,FF}(f)}{v_{\max}(f)/v_{\max,FF}(f)} \frac{K_{FF}}{c_L} = \frac{K'(f) K_{FF}}{c_L}, \quad (13)$$

where

$$K'(f) = \frac{\xi_{\max}(f)/\xi_{\max,FF}(f)}{v_{\max}(f)/v_{\max,FF}(f)}. \quad (14)$$

The factor  $K'(f)$  represents the increase or decrease in the non-dimensional farfield correlation ratio  $K_{FF}$  due to the effects of evanescent waves on the dynamic response.

The relationship in Equation 14 states that the maximum dynamic strain in a structure is related to the maximum velocity by the farfield correlation ratio  $K_{FF}/c_L$  and a frequency dependent factor,  $K'(f)$ . Defining

$$K(f) = K'(f) K_{FF}, \quad (16)$$

the ratio of maximum dynamic strain to maximum velocity is re-expressed as

$$\frac{\xi_{\max}(f)}{v_{\max}(f)} = \frac{K(f)}{c_L}, \quad (17)$$

where  $K$  is defined as the non-dimensional correlation ratio between dynamic strain and velocity.

In cases involving high frequency vibration, it is more practical to rely on measurements of the spatial maximum farfield velocity rather than the spatial maximum velocity as it is more readily measured and provides conservative estimates if the spatial maximum velocity is detected instead of the maximum farfield velocity. Correlating the spatial maximum dynamic strain with the spatial maximum farfield velocity at frequency  $f$  gives

$$\frac{\xi_{\max}(f)}{v_{\max,FF}(f)} = \left( \frac{\xi_{\max}(f)}{\xi_{\max,FF}(f)} \right) \frac{K_{FF}}{c_L} = \frac{K'_{vFF}(f) K_{FF}}{c_L} = \frac{K_{vFF}(f)}{c_L}, \quad (17)$$

where  $K_{vFF}$  is the non-dimensional correlation ratio between dynamic strain and farfield velocity.

#### 4.3 NON-DIMENSIONAL CORRELATION RATIO

The non-dimensional correlation ratio defined above is a frequency dependent factor but is found to be frequency independent for the flexural vibration of simple beams, and approximately frequency independent and bounded for the resonant vibration of plates and



cylindrical shells (refer Table 2 for the case of thin plate flexural vibration). Calculated data for a beam (Karczub[6]), and the experimental data in Section 5 for plates and cylindrical shells, also supports the application of the same frequency independent non-dimensional correlation ratios to vibration at non-resonant frequencies. Frequency independence is an essential property as it permits estimates of maximum dynamic strain to be obtained without consideration for the frequency of vibration; in particular, this permits the estimation of maximum dynamic strain using strain-velocity relationships to be applied directly to the multi-modal and broad-band vibration of resonant structures.

TABLE 2. Non-Dimensional Correlation Ratios for Clamped Plate Vibration

$m$	$n$	$f_{m,n}$	$\theta$	$K$
1	1	51.5Hz	57.6°	1.95
2	1	83.8Hz	37.1°	1.91
1	2	125.3Hz	71.8°	2.21
3	1	138.1Hz	26.2°	2.11
2	2	154.8Hz	56.3°	1.97
3	2	205.6Hz	44.4°	1.74
4	1	212.4Hz	20.0°	2.20
1	3	236.6Hz	77.4°	2.28

Values of  $K$  and  $K_{vff}$  to be used with Equations 16 and 17 for the estimation of maximum dynamic strain in beam, plate and cylindrical shell structures are given in Table 1. These values can be used in practically all cases except for the low frequency vibration of structures containing concentrated masses and vibration of a system below the first natural frequency. The non-dimensional correlation ratio is significantly increased in these latter cases resulting in non-conservative predictions if the factors in Table 1 are erroneously used.

#### 4.4. OVERALL MEAN-SQUARE RESPONSE LEVELS

Conservative predictions of the maximum overall mean-square dynamic strain are obtained by constructing a spectrum of maximum predicted mean-square dynamic strain in each frequency band  $f_i$  from Equation 16 or Equation 17, and then summing the mean-square values in each frequency band:

$$\langle \xi_{\max}^2 \rangle \leq \sum_{i=1}^{\infty} \langle \xi_{\max}^2(f_i) \rangle. \quad (18)$$

Equation 18 is accurate in cases where the maximum dynamic strain in each frequency band occurs at the same location for all frequencies  $f_i$ . For systems that do not have maximum dynamic strain at the same location at all frequencies this approach provides a conservative upper-bound prediction of the maximum overall mean-square dynamic strain.

## 5. Experimental Results

Experimental results for the prediction of dynamic bending strain from velocity in narrow frequency bands are presented in Figure 4 and Figure 5. The results in Figure 4 are for the flexural vibration of a clamped plate and represent the predicted maximum dynamic strain and the maximum measured dynamic strain along a line normal to one of the clamped boundaries. The maximum overall predicted dynamic strain was 65dB and the measured overall dynamic strain was 65.1dB. The results in Figure 5 are for the vibration of a

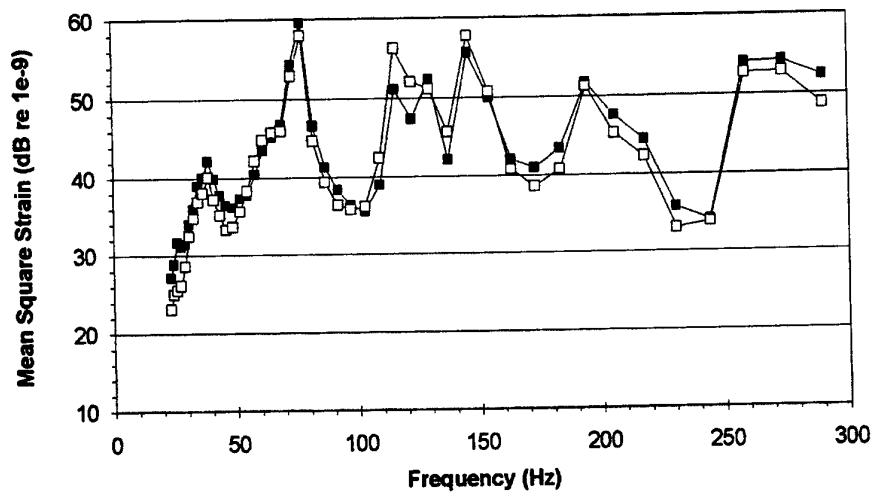


Figure 4. Measured and Predicted Dynamic Strain Autospectra at the Clamped Boundary of a Fully Clamped Rectangular Plate (—■— Measured; -□- Predicted)

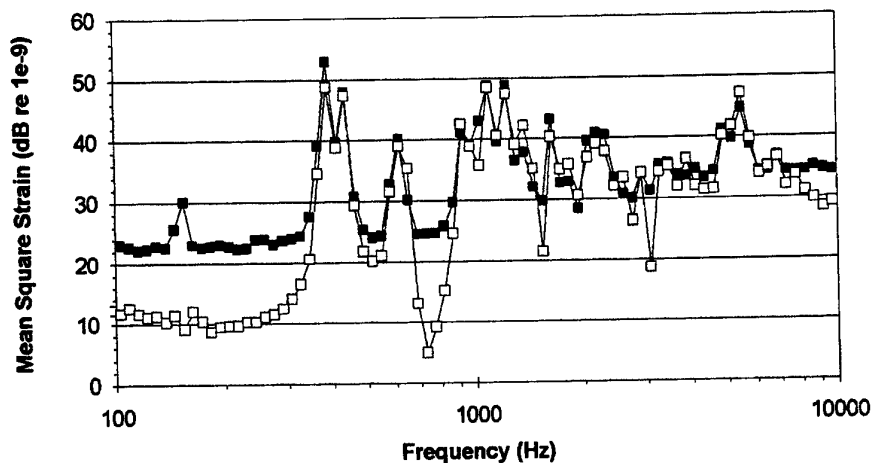


Figure 5. Measured and Predicted Dynamic Strain Autospectra in a Cylindrical Shell (—■— Measured Axial plus Circumferential Strain; -□- Predicted Strain)

cylindrical shell and represent the predicted dynamic strain and the measured dynamic strain at the same location. The measured dynamic strain was obtained by measuring the axial and circumferential strains and then adding the autospectra for these two measurements. The overall predicted dynamic strain was 57.2dB and the measured overall dynamic strain was 58.4dB. In both cases there is very good agreement between measured and predicted.

## 6. Conclusions

The main conclusion of this work is that there exists largely frequency independent relationships between dynamic strain and velocity which (i) have a firm theoretical and physical basis, (ii) are the same for beams, plates and cylindrical shells, and (iii) can be applied in a consistent manner to the narrow-band, multi-modal and broad-band vibration of simple structural elements in the low-, mid- and high-frequency ranges. These relationships can be used with measured, calculated or Statistical Energy Analysis determined vibrational velocity data to obtain narrow-band and overall estimates of maximum dynamic strain. The accuracy of the method is supported by theoretical and experimental data gathered to date.

## 7. References

1. HUNT, F.V. "Stress and Strain Limits on the Attainable Velocity in Mechanical Vibration", *The Journal of the Acoustical Society of America*, **32**(9), 1960, 1123-1128.
2. UNGAR, E.E. "Transmission of Plate Flexural Waves through Reinforcing Beams; Dynamic Stress Concentrations", *The Journal of the Acoustical Society of America*, **33**(5), 1961, 633-639.
3. WACHEL, J.C. et al, "Vibrations in Reciprocating Machinery and Piping Systems", *EDI Report 85-305, Engineering Dynamics Incorporated, San Antonio Texas*, 1985.
4. STEARN, S.M. "Stress Distributions in Randomly Excited Structures", *Ph.D. Thesis, Southampton University*, 1970.
5. NORTON, M.P. and FAHY, F.J. "Experiments on the Correlation of Dynamic Stress and Strain with Pipe Wall Vibrations for Statistical Energy Analysis Applications", *Noise Control Engineering Journal*, **30**(3), 1988, 107-117.
6. KARCZUB, D.G. "The Prediction of Dynamic Stress and Strain in Randomly Vibrating Structures Using Vibrational Velocity Measurements", *Ph.D. Thesis, The University of Western Australia*, 1996.
7. UNGAR, E.E. "Transmission of Plate Flexural Waves through Reinforcing Beams; Dynamic Stress Concentrations", *The Journal of the Acoustical Society of America*, **33**(5), 1961, 633-639.

# STATISTICAL ENERGY ANALYSIS OF THE PARAMETRIC RESONANCE IN STRUCTURAL MEMBERS

A.K. BELYAEV

*Institute of Technical Mechanics, Johannes Kepler University of Linz  
Altenbergerstr. 69, A-4040, Linz, Austria*

**Abstract.** The case where one structural member of a structure experiences a dynamic instability is studied. The principal regions of instability of a member is shown to depend very strongly on the axial vibration in the structure. Its boundary turns out to be very complicated if the frequency band of the instability zone contains many resonant modes which are very sensitive to fabrication and assemblage details. Two variants of the frequency averaging are proposed. Phase averaging across a small frequency band of each resonant mode of axial vibrations yields a smooth interior approximation to the instability zone. An energy-based averaging results in an external envelope. The latter may be viewed as a stability chart of a structural member in an engineering structure in which one has confidence.

## 1. Introduction

The case where one structural member of a structure experiences a dynamic instability is addressed. It is customary to analyse the stability of a mechanical component alone and to ignore its mechanical environment. The exceptions are aeroelasticity and fluid-structure interaction. However, even in these theories the interaction of a structural member with other structural members is ignored and only the interaction with fluids or gases is considered. Nevertheless it is intuitively clear that the influence of the whole structure on the stability of its particular component may be considerable.

In the present investigation we restrict ourselves to the mutual interaction of components in a complex structure. The main intent of the present study is to reveal the regions of dynamical stability of a structural component and to analyse the influence of the structure on the dynamic stability of the component.

The paper is organised as follows. The boundary value problem governing the interaction of the local dynamics of a potentially unstable structural member and the overall structure's dynamics is derived in Part 2. By using the Galerkin approach the partial differential equation governing the beam buckling reduces to an ordinary differential equation which is similar to the Mathieu equation. A simple closed form expression for the boundaries of the principle instability zones is derived. Results of

numerical computations are presented and discussed in Part 3. The influence of the large vibrating structure on the stability of a particular component is shown to be considerable and it changes drastically the stability chart of the component. It is shown that the boundaries of the instability zone are very complicated. Besides, they are fuzzy because of the structural parameters' uncertainty. For this reason, a phase average and an energy-based average over the fast variable are performed in Part 4. It is shown that the energy-based average which is similar to that of the Statistical Energy Analysis yields an external boundary of the instability zone in which one has confidence.

## 2. The governing equations of the problem

We model a potentially unstable component by a simply supported Bernoulli-Euler beam on which a periodic force  $P(t) = P_0 + P_1 \cos \omega t$  is imposed at the end  $x=l$ , cf. Fig.

1. At the end  $x=0$  the beam is attached to another structural member or an extended structure which is assumed to be dynamically stable, i.e. it does not exhibit any lateral instability.

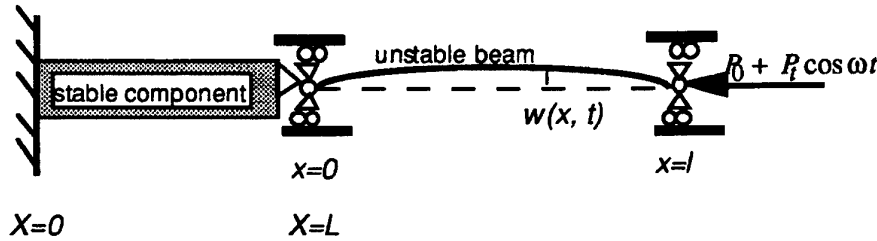


Figure 1. Schematic of the problem

Taking into account the terms describing the geometrical nonlinearity up to quadratic included results in the following nonlinear partial integro-differential equations for the beam vibrations (for details see Bolotin, 1964)

$$EF \frac{\partial^2 u}{\partial x^2} - \rho F \frac{\partial^2 u}{\partial t^2} = \rho F \int_0^x \left[ \frac{\partial w}{\partial \xi} \frac{\partial^3 w}{\partial \xi \partial t^2} + \left( \frac{\partial^2 w}{\partial \xi \partial t} \right)^2 \right] d\xi, \quad 0 < x < l \quad (1)$$

$$EI \frac{\partial^4 w}{\partial x^4} - \frac{\partial}{\partial x} \left[ EF \frac{\partial u}{\partial x} \frac{\partial w}{\partial x} \right] + \rho F \frac{\partial^2 w}{\partial t^2} = 0, \quad 0 < x < l \quad (2)$$

Here  $EI$  and  $EF$  are the flexural and axial rigidities, respectively,  $u$  and  $w$  are the axial and lateral deflections, respectively,  $\rho$  is the mass density and  $F$  is the cross-sectional area. Equation (1) describes the axial vibration of the beam while eqn (2) describes the bending vibration. The beam is assumed to be undamped.

As the boundaries of the instability zones are sought, one can neglect the non-linear

terms in the right-hand side of eqn (1), cf. Bolotin (1964), to obtain the following equation for the longitudinal vibration in the beam

$$\frac{\partial^2 u}{\partial x^2} - \frac{1}{a^2} \frac{\partial^2 u}{\partial t^2} = 0, \quad a = \sqrt{\frac{E}{\rho}} \quad (3)$$

where  $a$  is the velocity of sound. The longitudinal vibration in the structure is governed by the following differential equation

$$\left(1 + \beta \frac{\partial}{\partial t}\right) \frac{\partial^2 U}{\partial X^2} - \frac{1}{A^2} \frac{\partial^2 U}{\partial t^2} = 0, \quad 0 < X < L, \quad (4)$$

where  $U(X, t)$  is the axial displacement in the structure, and  $A$  is the velocity of sound in the structure. To account for material and structural damping in the structure, we assume the Kelvin-Voigt constitutive law, i.e. we introduce a viscosity by means of an viscous damping operator  $\beta \frac{\partial}{\partial t}$ . More sophisticated rheological model is not required since

harmonic vibration is considered. In what follows the capital letters are referred to the structure whereas the small letters to the beam. Boundary conditions and the conditions of the beam-structure interaction are given by

$$X = 0, \quad U = 0; \quad x = l, \quad -c \frac{\partial u}{\partial x} = P_o + P_t e^{i\omega t} \quad (5)$$

$$x = 0, \quad X = L, \quad u(0) = U(L), \quad C \left(1 + \beta \frac{\partial}{\partial t}\right) \frac{\partial U}{\partial X} = c \frac{\partial u}{\partial x} \quad (6)$$

where  $c = EF$  and  $C$  are the axial rigidities of the beam and the structure, respectively.

Solution of the boundary value problem, eqns (3)-(6), is given by

$$U(X, t) = H \frac{\sin \Lambda X}{\sin \Lambda L} e^{i\omega t} - \frac{P_o}{C} X; \quad \Lambda = \frac{\omega}{A\sqrt{1 + i\beta\omega}} \quad (7)$$

$$u(x, t) = (H \cos \lambda x + G \sin \lambda x) e^{i\omega t} - \frac{P_o}{c} x - \frac{P_o}{C} L; \quad \lambda = \frac{\omega}{a}$$

where  $\lambda$  and  $\Lambda$  are wave numbers of the beam and the structure, respectively. The expressions for  $H$  and  $G$  are as follows

$$H = \frac{\omega^{-1} P_t}{r \sin \lambda l - R\sqrt{1 + i\beta\omega} \cotan \Lambda L \cos \lambda l}, \quad G = \frac{\frac{R}{r} \sqrt{1 + i\beta\omega} \cotan \Lambda L \omega^{-1} P_t}{r \sin \lambda l - R\sqrt{1 + i\beta\omega} \cotan \Lambda L \cos \lambda l} \quad (8)$$

where  $r = ma$  and  $R = MA$  are the impedances of the beam and the absorber, respectively. Substituting eqn (7) into eqn (2) yields the following equation for the bending vibration in the beam

$$EI \frac{\partial^4 w}{\partial x^4} + P_o \frac{\partial^2 w}{\partial x^2} + EF \lambda \frac{\partial}{\partial x} \left( (H \sin \lambda x - G \cos \lambda x) \frac{\partial w}{\partial x} \right) e^{i\omega t} + \rho A \frac{\partial^2 w}{\partial t^2} = 0 \quad (9)$$

### 3. The principal instability zone of the beam attached to the structure

In order to define the principal zone of instability we assume  $w(x,t) = \varphi(x) q(t)$  where the fundamental function  $\varphi(x) = \sin \frac{\pi x}{l}$  is the first vibration mode and the static buckling form of the beam alone. We multiply eqn (9) by  $\varphi(x)$  and integrate along the length of the beam. The result is the following ordinary differential equation for the generalised coordinate  $q(t)$

$$\frac{d^2 q}{dt^2} + \Omega^2 [1 + 2\mu \Phi(\omega) e^{i\omega t}] q = 0 \quad (10)$$

Here the natural frequency of the bending vibration of the axially compressed beam  $\Omega$ , the first critical load  $P_c$  and dimensionless magnitude of the external force  $\mu$  are as follows

$$\Omega^2 = \left(\frac{\pi}{l}\right)^2 \frac{P_c - P_o}{\rho F}; \quad P_c = EI \frac{\pi^2}{l^2}; \quad \mu = \frac{P_t}{2(P_c - P_o)} \quad (11)$$

Function  $\Phi(\omega)$  is given by

$$\Phi(\omega) = \frac{2}{l} \frac{1}{r \sin \lambda l - R\sqrt{1 + i\beta\omega} \cotan \Lambda L \cos \lambda l} \int_0^l [r \sin \lambda x - R\sqrt{1 + i\beta\omega} \cotan \Lambda L \cos \lambda x] \cos^2 \frac{\pi x}{l} dx \quad (12)$$

which after the evaluation of the integral takes the following form

$$\Phi(\omega) = \frac{4 \sin \frac{\lambda l}{2} \lambda^2 l^2 - 2\pi^2}{\lambda l^2 - 4\pi^2} \frac{r \sin \frac{\lambda l}{2} - R\sqrt{1 + i\beta\omega} \cotan \Lambda L \cos \frac{\lambda l}{2}}{r \sin \lambda l - R\sqrt{1 + i\beta\omega} \cotan \Lambda L \cos \lambda l} \quad (13)$$

We intend to analyse the conditions under which the dynamic buckling of the beam occurs and obtain the boundaries of the principal zone of instability. To this end we rewrite eqn (10) in the form of the Mathieu equation

$$\frac{d^2 q}{dt^2} + \Omega^2 [1 + 2\mu |\Phi(\omega)| e^{i(\omega t + \arg \Phi(\omega))}] q = 0 \quad (14)$$

The first approximation to the boundaries is known to be determined by means of the following substitution, cf. Bolotin (1964) and Roseau (1987)

$$q(t) = q_1 \sin \frac{\omega t + \arg \Phi(\omega)}{2} + q_2 \cos \frac{\omega t + \arg \Phi(\omega)}{2} \quad (15)$$

which leads to the following equations for boundaries of the principal zone of instability, see Bolotin (1964) and Roseau (1987)

$$\omega = 2\Omega\sqrt{1 \pm |\Phi(\omega)|\mu} \quad (16)$$

The latter equation expresses a certain dependence between the frequency and the magnitude of the external axial force which is known to be the boundary of the principal zone of instability. The case  $|\Phi(\omega)| = 1$  corresponds to the boundary of the conventional principal instability zone of the Mathieu equation, cf. Bolotin (1964) and Roseau (1987). The function  $\Phi(\omega)$  reflects therefore the influence of the longitudinal vibration on the instability chart of the bending vibration. As  $|\Phi(\omega)|$  can vary arbitrarily (e.g. it can be very large or very small) the stability chart of the beam changes drastically. Hence, the influence of the vibrating structure on the stability chart of a component may be very considerable.

To begin with, the main instability zone of the beam alone without longitudinal vibration is shown in Fig. 2. The boundaries of this zone are obtained from eqn (16) under the assumption  $|\Phi(\omega)| = 1$ .

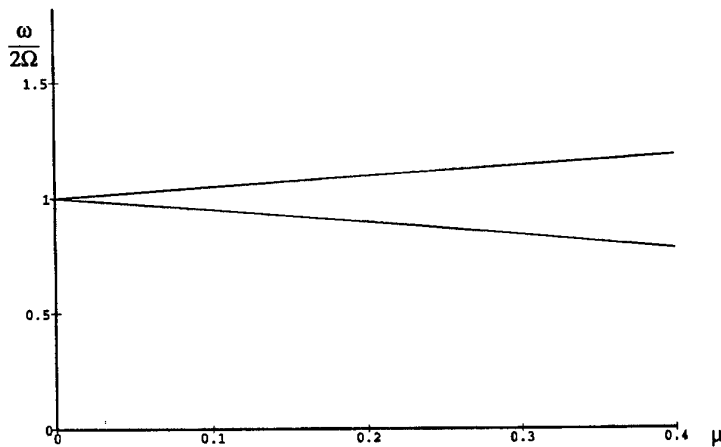


Fig.2. The principal instability zone of the beam alone

Another limiting case is obtained if one assumes that the structure is a rigid body, i.e.  $R = \infty$ . In this case only the longitudinal vibration of the beam alone affects the instability zone. Substituting  $R = \infty$  into eqn (13) delivers the following expression for  $\Phi(\omega)$

$$\Phi(\omega) = \frac{2 \tan \lambda l}{\lambda} \frac{\lambda^2 l^2 - 2\pi^2}{\lambda^2 l^2 - 4\pi^2} \quad (17)$$

which coincides with the known results of Bolotin (1964). The main instability zone is shown in Figure 3.



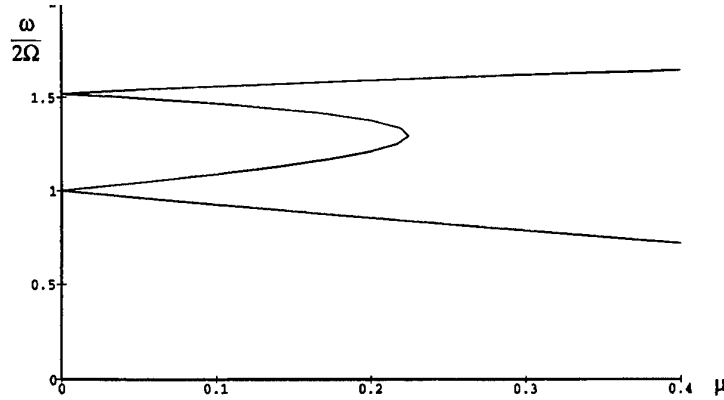


Fig.3. Influence of the axial vibration on principal instability zone of the beam

#### 4. Phase averaging and energy-based averaging

Function  $\Phi(\omega)$  takes into account effect of the interaction of axial vibration in the structural members. It is a rapidly changing function of frequency if the frequency band of the parametric resonance contains a number of resonant terms. Provided the structure is very large compared with the beam the modal density of the structure may be rather high in the frequency domain of the local parametric resonance of the structural member. Figure 4 shows  $|\Phi(\omega)|$  for following non-dimensional parameters of the model:

$\beta\Omega = 10^{-3}$ ,  $\frac{R}{r} = 1.94$ ,  $\frac{L}{l} \frac{a}{A} = 221$ ,  $\frac{al}{2\Omega} = 1$ . In this case the boundary of the instability

zone turns out to be very complicated as Fig. 5 displays.

When the structure has a high modal density then  $\Phi(\omega)$  contains two scales: slow variables  $\lambda l$  and  $\omega$  and a fast variable  $\lambda L$ . It seems reasonable to average the function with respect to the fast variable, i.e. across a small frequency band of each resonant mode of axial vibrations. To this aim, one can replace  $\Phi$  by a smooth function  $\hat{\Phi}$  which is obtained by means of the phase averaging with respect to the fast variable  $z = \omega L / A$

$$\hat{\Phi}(\omega) = \frac{4 \sin \frac{\lambda l}{2}}{\lambda l} \frac{\lambda^2 l^2 - 2\pi^2}{\lambda^2 l^2 - 4\pi^2} \frac{1}{2\pi} \int_0^{2\pi} \frac{r \sin \frac{\lambda l}{2} - R\sqrt{1+i\beta\omega} \cos \frac{\lambda l}{2} \cotan\left(\frac{z}{\sqrt{1+i\beta\omega}}\right)}{r \sin \lambda l - R\sqrt{1+i\beta\omega} \cos \lambda l \cotan\left(\frac{z}{\sqrt{1+i\beta\omega}}\right)} dz \quad (18)$$

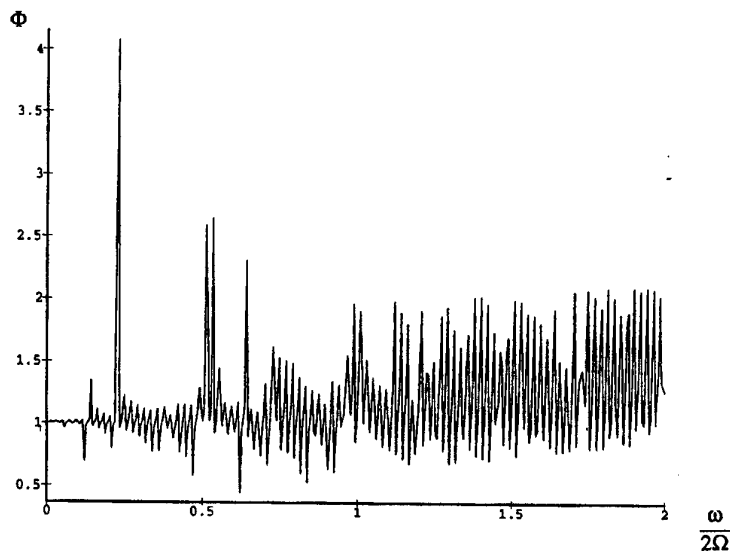


Fig.4. Absolute value of  $\Phi$  versus frequency

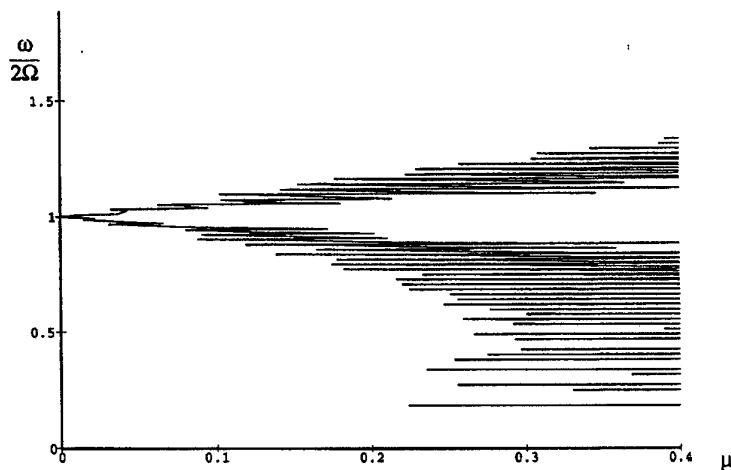


Fig. 5. The principal zone of instability of the beam attached to the structure.

The averaging sounds reasonable in view of the fact that the structural details, material and fabrication imperfections as well as the boundary conditions are uncertain, i.e. the eigenfrequencies and the places of the resonance peaks are uncertain as well, cf. Fahy (1994). Integral (18) allows analytic evaluation, cf. Gradsteyn and Ryzhik (1980), to give

$$\hat{\Phi}(\omega) = \frac{4 \sin \frac{\lambda l}{2} \lambda^2 l^2 - 2\pi^2}{2\pi \lambda l} \frac{1}{\lambda^2 l^2 - 4\pi^2 r^2 \sin^2 \lambda l + R^2(1 + i\beta\omega) \cos^2 \lambda l}$$

$$\left[ r R \sqrt{1 + i\beta\omega} \sin \frac{\lambda l}{2} \ln \frac{1 - \frac{R\sqrt{1 + i\beta\omega}}{r} \cotan \lambda l \tan \frac{2\pi}{\sqrt{1 + i\beta\omega}}}{\sqrt{1 + \tan^2 \frac{2\pi}{\sqrt{1 + i\beta\omega}}}} + \right.$$

$$\left. \frac{2\pi}{\sqrt{1 + i\beta\omega}} \left\{ r^2 \sin \lambda l \sin \frac{\lambda l}{2} + R^2(1 + i\beta\omega) \cos \lambda l \cos \frac{\lambda l}{2} \right\} \right] \quad (19)$$

The result of the computations is displayed in Fig. 6. One can see that the phase average with respect to the fast variable delivers a smooth internal boundary of the principal zone of instability.

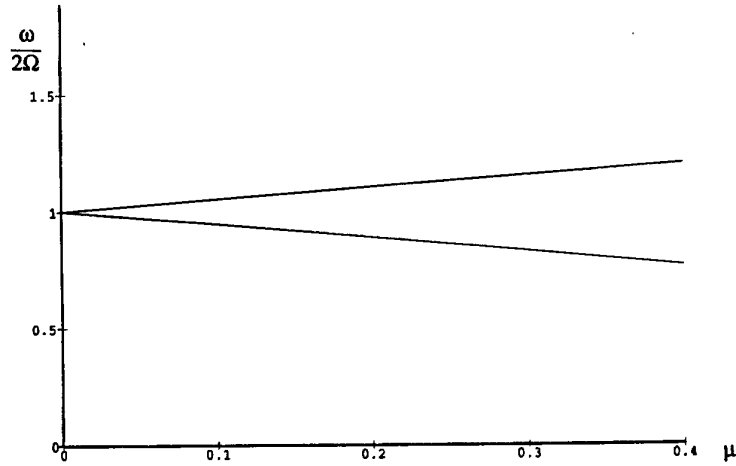


Fig. 6. Phase-averaged boundary of the principal instability zone.

As eqn (16) which determines the boundaries of the instability zone requires only the absolute value of  $\Phi$ , i.e.  $|\Phi(\omega)|$ , another possible average is an energy-based average with respect to the fast variable

$$|\tilde{\Phi}| = \frac{1}{2\pi} \int_0^{2\pi} \sqrt{|\Phi|^2} dz \quad (20)$$

where  $z = \omega l / A$  is the fast variable. An explicit expression for  $|\tilde{\Phi}|$  is as follows

$$|\tilde{\Phi}| = \frac{4 \left| \sin \frac{\lambda l}{2} \right|}{\lambda l} \frac{|\lambda^2 l^2 - 2\pi^2|}{|\lambda^2 l^2 - 4\pi^2|} \sqrt{\frac{1}{2\pi} \int_0^{2\pi} \left| \frac{r \sin \frac{\lambda l}{2} - R\sqrt{1+i\beta\omega} \cos \frac{\lambda l}{2} \cotan(z/\sqrt{1+i\beta\omega})}{r \sin \lambda l - R\sqrt{1+i\beta\omega} \cos \lambda l \cotan(z/\sqrt{1+i\beta\omega})} \right|^2 dz} \quad (21)$$

Estimation of the integral (21) yields

$$|\tilde{\Phi}| = \frac{4 \left| \sin \frac{\lambda l}{2} \right|}{\lambda l} \frac{|\lambda^2 l^2 - 2\pi^2|}{|\lambda^2 l^2 - 4\pi^2|} \sqrt{\frac{Bb + Kk}{b^2 + k^2} + \frac{1}{2\sqrt{y^2 - b^2 - k^2}} \left( Y - \frac{y(Bb + Kk)}{b^2 + k^2} \right)} \quad (22)$$

where the following denotations are made

$$b = -2 \frac{R}{r} \cotan \lambda l, \quad k = \frac{R^2}{r^2} (1 + i\beta\omega) \cotan^2 \lambda l - 1; \quad \Gamma = \text{Im} \frac{1}{\sqrt{1+i\beta\omega}} > 0 \quad (23)$$

$$y = \left( 1 + \frac{R^2}{r^2} (1 + i\beta\omega) \cotan^2 \lambda l \right) \cosh \frac{2\omega L \Gamma}{A} + 2 \frac{R}{r} \cotan \lambda l \sinh \frac{2\omega L}{A} \Gamma$$

The result of the numerical work is shown in Fig. 7. One can see that the latter estimation can be viewed as an external smooth border to the inherently complicated principal zone of instability in which one has confidence.

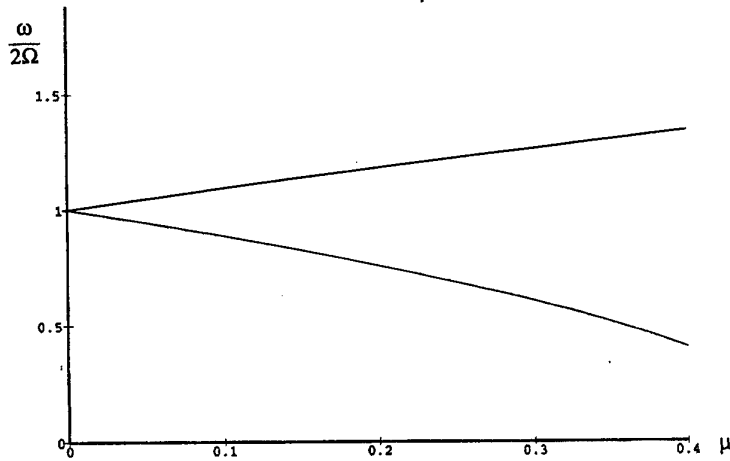


Fig.7. Energy averaged boundary of the principal instability zone

## 5. Conclusions

The original principal zone of instability and two smooth approximations are shown in Fig. 8.

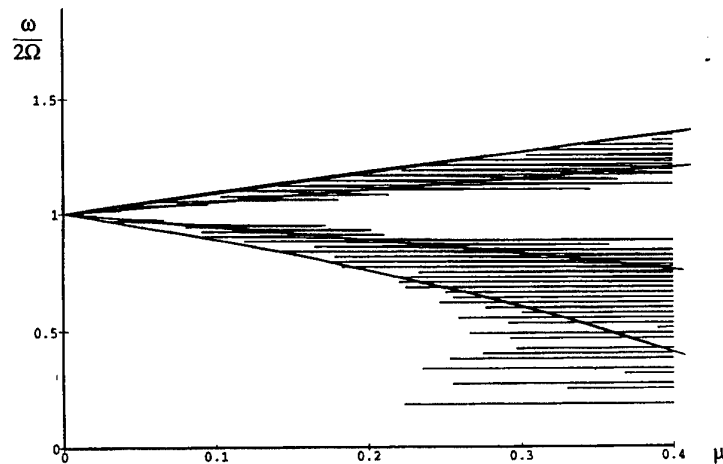


Fig.8. The principal instability zone together with its internal and external envelopes

The phase average may be viewed as an internal smooth envelope of the instability zone. This envelope is informative in that regard that the interior of this envelope contains unstable unbounded solutions. The energy based average is of crucial importance since it delivers a smooth external boundary of the inherently complicated principal zone of instability. This external boundary is not sensitive to uncertainties in engineering structures that is it should be viewed as the practical boundary of the principal instability zone in which one has confidence. The domain between the above smooth approximations is very specific. One can guarantee neither stability nor instability of the beam there. The study of this domain remains to tackle.

## References

- Bolotin, V.V. (1964) *The Dynamic Stability of Elastic Systems*. Holden-Day, San-Francisco.
- Fahy, F.J. (1994) Statistical Energy Analysis: a critical overview. *Phil. Trans. R. Soc. London A* 346, 431-447.
- Gradshteyn, I.S. and Ryzhik I.M. (1980) *Table of Integrals, Series and Products*, Academic Press, New York.
- Roseau, M. (1987) *Vibrations in Mechanical Systems*. Springer-Verlag, Berlin.

# ON THE EXTERNAL INPUT POWER INTO COUPLED STRUCTURES

G. MAIDANIK

DTMB

Bethesda, Maryland 20084-5000, USA

J. DICKEY

Center for Nondestructive Evaluation,

The Johns Hopkins University, Baltimore, MD 21218, USA

## 1. Abstract

In the application of the statistical energy analysis (SEA) it is commonly assumed that the external input power is independent of the coupling between an externally driven structure (a master structure) and an attached passive structure (an adjunct structure). It is argued that although this assumption may be reasonable for weak couplings and, with some reservation, for strongly coupled similar structures, it may be incorrect for strongly coupled dissimilar structures. The definitions of similar and dissimilar coupled structures, in this context, are explained. The implication to SEA of this dissimilarity in strongly coupled structures is discussed in the light of developing noise control criteria for complexes that are composed of these coupled structures.

## 2. Introduction

It has been customary, when using the statistical energy analysis (SEA) to derive the response (stored energy) of a complex composed of coupled structures, to assume that the couplings among the structures do not influence the external input powers. In this sense, the external input powers, injected into the structures in isolation, are assumed to be invariants when couplings are instituted. This assumption initially simplified the analysis and subsequently its validity was not challenged, presumably a matter of "letting sleeping dogs lie". Indeed, as long as the couplings could be considered "weak" the assumption felt comfortably valid. Questions regarding the validity of the assumption arise only when "moderate" and, especially, "strong" couplings are brought in as a possibility. Chandiramani and Smith attempted to account for changes in SEA as some of the couplings transit from weak to strong [1,2]. A major finding, in both efforts, is the convergence of the modal stored energies among those structures that are strongly coupled; as the couplings become stronger in these structures, there is a convergence toward equipartition of modal stored energies. In other words, as the coupling between two structures is increased, the coupled structures tend to merge and

the stronger the coupling the more complete is the merger. In both papers, however, the influence, that the changes in the couplings may induce on the external input powers, is neglected apriori [1,2]. This neglect is examined in this paper; not rigorously, but, rather, heuristically. It is argued that for couplings among "similar" structures the external input powers are not dependent on the strength of the couplings. However, for "dissimilar" structures the external input powers are dependent on the strength of the couplings and there may then be a significant difference between those external input powers pertaining to weak and those pertaining to strong couplings.

### 3. Rudimentary Statistical Energy Analysis (SEA)

The steady state equation of SEA for a complex composed of multiple coupled structures is

$$\underline{\underline{\omega}} \underline{\underline{\eta}}(\omega) \underline{\underline{E}}(\omega) = \underline{\underline{\Pi}}_e(\omega) \quad ; \quad \underline{\underline{E}}(\omega) = \{E_\alpha(\omega)\} \quad ; \quad \underline{\underline{\Pi}}_e(\omega) = \{\Pi_{e\alpha}(\omega)\} \quad ;$$

$$\underline{\underline{\omega}} = (\omega \delta_{\alpha\beta}) \quad ; \quad \underline{\underline{\eta}}(\omega) = \left( \left[ \sum_{\gamma} \eta_{\gamma\alpha}(\omega) \right] \delta_{\alpha\beta} - \eta_{\alpha\beta}(\omega) (1 - \delta_{\alpha\beta}) \right) \quad , \quad (1a)$$

where  $(\omega)$  is a center frequency of a frequency band of width  $(\Delta\omega)$ ,  $\eta_{\alpha\alpha}(\omega)$  is the loss factor associated with the  $(\alpha)$ th structure,  $\eta_{\gamma\alpha}(\omega)$  is the coupling loss factor associated with the attachment of the  $(\alpha)$ th structure to the  $(\gamma)$ th,  $E_\alpha(\omega)$  and  $\Pi_{e\alpha}(\omega)$  are the stored energy and the external input power; in and into, the  $(\alpha)$ th structure, respectively, and  $\delta_{\alpha\beta}$  is the Kronecker delta. Significantly, Eq. (1a) is proper in the sense that  $\underline{\underline{\eta}}(\omega)$  is a functional only of parameters that define the complex; it is independent of the elements of the stored energy vector  $\underline{\underline{E}}(\omega)$  and of the external input power vector  $\underline{\underline{\Pi}}_e(\omega)$ . [Propriety is an essential ingredient to any successful analysis; for this reason many of the quantities and parameters involved are often tested for propriety.] The modal SEA quantities and parameters that are implicitly stated in Eq. (1a) are

$$E_\alpha(\omega) = \Delta\omega n_\alpha(\omega) \epsilon_\alpha(\omega) \quad ; \quad \Pi_{e\alpha}(\omega) = \Delta\omega n_\alpha(\omega) \pi_{e\alpha}(\omega) \quad ;$$

$$[\eta_{\alpha\beta}(\omega)/\eta_{\beta\alpha}(\omega)] = \lambda_{\beta}^{\alpha}(\omega) = [n_\alpha(\omega)/n_\beta(\omega)] = [\lambda_{\alpha}^{\beta}(\omega)]^{-1} \quad , \quad (2)$$

where  $n_\alpha(\omega)$  is the modal density,  $\epsilon_\alpha(\omega)$  is the averaged modal stored energy and  $\pi_{e\alpha}(\omega)$  is the averaged modal external input power, all in reference to the  $(\alpha)$ th structure [3]. The averaging is either over the frequency within the bandwidth  $(\Delta\omega)$  or over an ensemble of complexes with differences that lie within that same bandwidth [3]. Since the "loss factor matrix"  $\underline{\underline{\eta}}(\omega)$  is, by definition, nonsingular, Eq. (1a) may be inverted

$$\underline{\underline{E}}(\omega) = \underline{\underline{\xi}}(\omega) (\underline{\underline{\omega}})^{-1} \underline{\underline{\Pi}}_e(\omega) \quad ; \quad \underline{\underline{\xi}}(\omega) = (\underline{\underline{\xi}}_{\alpha\beta}(\omega)) = [\underline{\underline{\eta}}(\omega)]^{-1} \quad . \quad (1b)$$

The inverted loss factor matrix  $\underline{\underline{\xi}}(\omega)$  may be dubbed the "gain factor matrix". Clearly, Eq. (1b), like Eq. (1a), is significantly proper. From Eq. (1a) one obtains

$$\sum_{\alpha} \omega \eta_{\alpha\alpha}(\omega) E_\alpha(\omega) = \Pi_e(\omega) \quad ; \quad \Pi_e(\omega) = \sum_{\alpha} \Pi_{e\alpha}(\omega) \quad , \quad (3a)$$

which simply expresses the equation of conservation of energy; it states that the dissipated power in the complex;  $[\omega \eta_{\alpha\alpha}(\omega) E_{\alpha}(\omega)]$  in the  $(\alpha)$ th structure, is equal to the external input power into the complex;  $[\Pi_{e\alpha}(\omega)]$  into the  $(\alpha)$ th structure. Similarly, from Eq. (1b) one obtains

$$E_{\alpha}(\omega) = \sum_{\gamma} E_{\alpha}^{\gamma}(\omega) \quad ; \quad E_{\alpha}^{\gamma}(\omega) = \xi_{\alpha\gamma}(\omega) [\Pi_{e\gamma}(\omega)/\omega] \quad , \quad (3b)$$

which simply accounts for the contributions, to the stored energy  $E_{\alpha}(\omega)$  of the  $(\alpha)$ th structure, by the external input powers into the various structures that compose the complex; e.g.,  $E_{\alpha}^{\gamma}(\omega)$  is contributed to  $E_{\alpha}(\omega)$  by the external input power  $[\Pi_{e\gamma}(\omega)]$  into the  $(\gamma)$ th structure.

An "effective loss factor"  $\eta_e(\omega)$  may be defined in the form

$$\omega \eta_e(\omega) E(\omega) = \sum_{\alpha} \omega \eta_{\alpha\alpha}(\omega) E_{\alpha}(\omega) \quad ; \quad E(\omega) = \sum_{\alpha} E_{\alpha}(\omega) \quad . \quad (4a)$$

In this form  $\eta_e(\omega)$  is a measure of the ability of the complex as a whole to dissipate the stored energy  $E(\omega)$  in it [3-5]. Casting Eq. (4a) in the algebraically manipulated form

$$\eta_e(\omega) = \left[ \sum_{\alpha} \eta_{\alpha\alpha}(\omega) E_{\alpha}(\omega) / \sum_{\beta} E_{\beta}(\omega) \right] \quad , \quad (4b)$$

interprets the effective loss factor  $\eta_e(\omega)$  to be the "average loss factor"; averaged over the stored energies of the structures comprising the complex. Similarly, an "effective gain factor"  $\xi_{e\alpha}(\omega)$  is defined in the form

$$\xi_{e\alpha}(\omega) [\Pi_e(\omega)/\omega] = \sum_{\gamma} \xi_{\alpha\gamma}(\omega) [\Pi_{e\gamma}(\omega)/\omega] \quad . \quad (5a)$$

In this form  $\xi_{e\alpha}(\omega)$  is a measure of the transfer of energy from the external input powers to the  $(\alpha)$ th structure. Casting Eq. (5a) in the form

$$\xi_{e\alpha}(\omega) = \Pi_{e\gamma}(\omega) \left[ \sum_{\gamma} \xi_{\alpha\gamma}(\omega) \Pi_{e\gamma}(\omega) / \sum_{\beta} \Pi_{e\beta}(\omega) \right] \quad , \quad (5b)$$

interprets the effective gain factor  $\xi_{e\alpha}(\omega)$  of the  $(\alpha)$ th structure to be the "average gain factor" of that structure; averaged over the external input powers of the structures comprising the complex. From Eqs. (3a) and (4) one obtains

$$\omega \eta_e(\omega) E(\omega) = \Pi_e(\omega) \quad ; \quad \eta_e(\omega) = [\Pi_e(\omega) / \omega E(\omega)] \quad , \quad (6a)$$

and from Eqs. (3b) and (5) one obtains

$$\xi_{e\alpha}(\omega) [\Pi_e(\omega)/\omega] = E_{\alpha}(\omega) \quad ; \quad \xi_{e\alpha}(\omega) = [\omega E_{\alpha}(\omega) / \Pi_e(\omega)] \quad . \quad (6b)$$

From Eqs. (6a) and (6b), the identity

$$\eta_e(\omega) = [\xi_e(\omega)]^{-1} \quad ; \quad \xi_e(\omega) = \sum_{\alpha} \xi_{e\alpha}(\omega) \quad , \quad (7)$$

emerges.

As usual, for good and bad reasons, a complex consisting of merely two structures



is chosen to demonstrate the notions and concepts that lie within SEA and to illustrate results obtained by rendering SEA to such a complex. A SEA model of a two-structures complex is depicted in Fig. 1; one structure is designated the (s)th structure (the master structure) and the other the (b)th structure (the fuzz in a structural fuzzy) [4-6]. A question is then posed: May an externally driven structure (the (s)th structure) be adjoined by another (the (b)th structure) in order to improve the noise control integrity of the union; e.g., by increasing the effective loss factor  $\eta_e(\omega)$  of the combined structures beyond that of the initial structure? For the two-structures complex Eq. (4b), after straightforward algebraic manipulations, yields

$$\eta_{es}(\omega) = [\eta_e(\omega)/\eta_{ss}(\omega)] = [1 + \eta_s^b(\omega) \zeta_s^b(\omega)] [1 + \zeta_s^b(\omega)]^{-1} ;$$

$$\eta_s^b(\omega) = [\eta_{bs}(\omega)/\eta_{ss}(\omega)] ; \quad \zeta_s^b(\omega) = [E_b(\omega)/E_s(\omega)] . \quad (4c)$$

Using Eq. (4c), Fig. 2 is presented. In this figure values of  $\eta_{es}(\omega)$  are depicted as a function of  $\eta_s^b(\omega)$  and  $\zeta_s^b(\omega)$ . It is revealed that for a practical range of  $\{\eta_s^b(\omega), \zeta_s^b(\omega)\}$  there exist a region in which  $\eta_{es}(\omega)$  exceeds unity, notwithstanding that in another region,  $\eta_{es}(\omega)$  is less than unity. The region in Fig. 2 for which  $\eta_{es}(\omega) \geq \sqrt{10}$ , establishes a set of criteria that needs to be satisfied by parameters that define the two-structures complex to affirmatively answer the question posed. However, as argued in Reference 4, that  $\eta_{es}(\omega)$  exceeds unity may be a necessary, but is not a sufficient condition for achieving an effective noise control. To achieve and effective noise control a more comprehensive analysis, than that involved in the determination of  $\eta_{es}(\omega)$ , is required

#### 4. Stored Energy Ratios in Noise Control Criteria

To examine more comprehensively the noise control criteria it is convenient to model the complex in terms of unattached structures. Whereas Eq. (1) is the insitu description of the complex, the equation of SEA for a complex in which the structures are artificially, but appropriately, isolated from each other is

$$\underline{\omega} \underline{\eta}^0(\omega) \underline{E}^0(\omega) = \underline{\Pi}_e^0(\omega) ; \quad \underline{E}^0(\omega) = \{E_\alpha^0(\omega)\} ; \quad \underline{\Pi}_e^0(\omega) = \{\Pi_{e\alpha}^0(\omega)\} ,$$

$$\underline{\omega} = (\omega \delta_{\alpha\beta}) ; \quad \underline{\eta}^0(\omega) = (\eta_{\alpha\alpha}^0(\omega) \delta_{\alpha\beta}) ; \quad (8a)$$

or invertedly

$$\underline{E}^0(\omega) = \underline{\xi}^0(\omega) \underline{\omega}^{-1} \underline{\Pi}_e^0(\omega) ; \quad \underline{\xi}^0(\omega) = (\xi_{\alpha\alpha}^0(\omega) \delta_{\alpha\beta}) ; \quad \underline{\xi}^0(\omega) = [\underline{\eta}^0(\omega)]^{-1} . \quad (8b)$$

A typical equation of motion for a structure may be selected from Eq. (8). It reads

$$\omega \eta_{\alpha\alpha}^0(\omega) E_\alpha^0(\omega) = \Pi_{e\alpha}^0(\omega) ; \quad E_\alpha^0(\omega) = \xi_{\alpha\alpha}^0(\omega) [\Pi_{e\alpha}^0(\omega)/\omega] . \quad (9)$$

This equation states that the stored energy  $E_\alpha^0(\omega)$  is attained by the isolated ( $\alpha$ )th

structure in response to an external input power  $\Pi_{e\alpha}^0(\omega)$  that is directly injected into it; this power is dissipated, in this structure in isolation, by the loss factor  $\eta_{\alpha\alpha}(\omega)$ . From Eqs. (1b) and (8) one may define three useful forms of stored energy ratios:  $\mathcal{E}_\alpha(\omega)$ ,  $\mathcal{E}_{0\alpha}^Y(\omega)$  and  $\mathcal{E}_\alpha^Y(\omega)$ . The first ratio is defined

$$\mathcal{E}_\alpha(\omega) = [E_\alpha(\omega)/E_\alpha^0(\omega)] = \xi_0^\alpha(\omega) P_0^\alpha(\omega) \quad ; \quad \xi_0^\alpha(\omega) = [\xi_{\alpha\alpha}(\omega) \eta_{\alpha\alpha}^0(\omega)] \quad ;$$

$$P_0^\alpha(\omega) = [\Pi_{e\alpha}(\omega)/\Pi_{e\alpha}^0(\omega)] \quad , \quad (10a)$$

and may be used, for example, to assess the influence, on the stored energy of the  $(\alpha)$ th structure, due to the incorporation of this structure to be an insitu member of the complex. Clearly  $\mathcal{E}_\alpha(\omega)$  is proportional to the ratio  $P_0^\alpha(\omega)$  of the insitu external input power into the  $(\alpha)$ th structure to that in isolation; i.e., before it is incorporated in the complex. The second stored energy ratio is defined

$$\mathcal{E}_{0\alpha}^Y(\omega) = [E_\alpha^Y(\omega)/E_\alpha^0(\omega)] = \xi_0^{\alpha Y}(\omega) P_{0\alpha}^Y(\omega) \quad ; \quad \xi_0^{\alpha Y}(\omega) = [\xi_{\alpha Y}(\omega) \eta_{\alpha\alpha}^0(\omega)] \quad ;$$

$$P_{0\alpha}^Y(\omega) = [\Pi_{eY}(\omega)/\Pi_{e\alpha}^0(\omega)] \quad , \quad (10b)$$

and may be used, for example, to assess the influence, on the stored energy of the  $(\alpha)$ th structure, due to the incorporation of this structure to be an insitu member of the complex when the external input power into that complex is applied to another structure; e.g., to the  $(Y)$ th structure. Clearly  $\mathcal{E}_{0\alpha}^Y(\omega)$  is proportional to the ratio  $P_{0\alpha}^Y(\omega)$  of the external input power into the  $(Y)$ th structure insitu and the external input power into the  $(\alpha)$ th structure in isolation. The third ratio is defined

$$\mathcal{E}_\alpha^Y(\omega) = [\mathcal{E}_{0\alpha}^Y(\omega)/\mathcal{E}_\alpha(\omega)] = [E_\alpha^Y(\omega)/E_\alpha(\omega)] = \xi_\alpha^{\alpha Y}(\omega) P_\alpha^Y(\omega) \quad ,$$

$$\xi_\alpha^{\alpha Y}(\omega) = [\xi_{\alpha Y}(\omega)/\xi_{\alpha\alpha}(\omega)] \quad ; \quad P_\alpha^Y(\omega) = [\Pi_{eY}(\omega)/\Pi_{e\alpha}(\omega)] \quad ; \quad (10c)$$

and may be used, for example, to assess the influence, on the stored energy of the  $(\alpha)$ th structure, of injecting the external input power into the  $(Y)$ th structure versus injecting it into the  $(\alpha)$ th structure itself. The ratio between these two external input powers is designated  $P_\alpha^Y(\omega)$  and the stored energy ratio  $\mathcal{E}_\alpha^Y(\omega)$  is proportional to this external input power ratio under the conditions just specified.

If noise control of the  $(\alpha)$ th structure is the criterion of import, then the desire is to minimize, in each case, the one relevant ratio of the three; either  $\mathcal{E}_\alpha(\omega)$ ,  $\mathcal{E}_{0\alpha}^Y(\omega)$  or  $\mathcal{E}_\alpha^Y(\omega)$ . Minimization of this kind renders the selected ratio small compared with unity; the smaller, the more commendable is the noise control achievement. The first factor in each of these three stored energy ratios; namely,  $\xi_0^\alpha(\omega)$ ,  $\xi_0^{\alpha Y}(\omega)$  and  $\xi_\alpha^{\alpha Y}(\omega)$ , respectively, are proper quantities. The propriety is in the sense that these quantities are functional only of the properties of the structures and the couplings among them; they are independent of the stored energies in, and the external input powers into the individual structures that comprise the complex. These properties, in SEA, are defined in terms of the elements of the loss factor matrix  $\eta(\omega)$  and/or of the gain factor matrix  $\xi(\omega)$ . For a prescribed model of the complex, these elements are assumed known and changes in these elements, to achieve a desired noise control condition, are also assumed known. A question arises with respect to the second factor

in each of the three stored energy ratios: Are these second factors; namely,  $P_0^\alpha(\omega)$ ,  $P_{0\alpha}^\gamma(\omega)$  and  $P_\alpha^\gamma(\omega)$ , respectively, which consist of various ratios of external input powers into specific structures, directly or indirectly dependent on the properties of the structures and especially of the couplings among them? If the external input powers are assumed to be independent of the couplings

$$P_0^\alpha(\omega) \Rightarrow P_0^{0\alpha}(\omega) = 1 \quad , \quad (11a)$$

$$P_{0\alpha}^\gamma(\omega) \Rightarrow P_{0\alpha}^{0\gamma}(\omega) = [\lambda_\alpha^\gamma(\omega) (M_\alpha/M_\gamma)] \quad , \quad (11b)$$

$$P_\alpha^\gamma(\omega) \Rightarrow P_\alpha^{0\gamma}(\omega) = P_{0\alpha}^{0\gamma}(\omega) \quad . \quad (11c)$$

On the other hand, if the external input powers are dependent on the couplings, changes in these couplings, which are designed to achieve desired noise control condition with respect to the first factors, may influence, adversely or beneficially, the corresponding second factors. The central theme of this paper is the investigation of the influence of the couplings on these second factors.

## 5. External Input Power at SEA

It is usual to specify the external drive, to which a structure may be subjected, by an external force-source or an external velocity-source; in the first the external force is specified, in the second the externally imposed velocity is specified. When the external force-source is employed the external input power into a structure is

$$\begin{aligned} \Pi_e(\omega) &= \langle |F_e(\omega)|^2 \rangle \langle G(\omega) \rangle \quad ; \quad S_e(\omega) \Delta \omega = 2\pi \langle |F_e(\omega)|^2 \rangle \quad ; \\ \langle G(\omega) \rangle &= [(\pi/2) n(\omega)/M] \quad , \end{aligned} \quad (12a)$$

and when the external velocity-source is employed the external input power into a structure is

$$\Pi_e(\omega) = \langle |V_e(\omega)|^2 \rangle \text{Re} \{ \langle [G(\omega) - iB(\omega)]^{-1} \rangle \} \quad ; \quad (12b)$$

where  $G(\omega)$  is the conductance and  $B(\omega)$  is the susceptance, with both these quantities being real,  $S_e(\omega)$  is the quadratic spectral distribution of the force-source,  $n(\omega)$  is the modal density and  $M$  is the mass of the structure [3]. In order to avoid difficulties, without loss in insight, Eq. (12a) is used in this paper and the use of Eq. (12b) is deferred to another. Figure 3a depicts the single structure on which attention is now focused. The SEA equation of motion for this structure is given by

$$\omega \eta(\omega) E(\omega) = \Pi_e(\omega) \quad , \quad (13)$$

where  $\eta(\omega)$  is the loss factor and  $E(\omega)$  is the stored energy that is generated by the external input power  $\Pi_e(\omega)$ . The external input power  $\Pi_e(\omega)$  into this structure is stated, as agreed, in Eq. (12a). It may be instructive to subdivide this structure into two substructures; one designated (1) and the other (2), as prescribed in Fig. 3b. The SEA

equation of motion for the two-structures complex is given by

$$\omega [\eta_{11}(\omega) + \eta_{21}(\omega)] E_1(\omega) - \omega \eta_{12}(\omega) E_2(\omega) = \Pi_{e1}(\omega) \quad , \quad (14a)$$

$$\omega [\eta_{22}(\omega) + \eta_{12}(\omega)] E_2(\omega) - \omega \eta_{21}(\omega) E_1(\omega) = 0 \quad , \quad (14b)$$

$$\begin{aligned} \eta_{e1}(\omega) &= [\eta_e(\omega)/\eta_{11}(\omega)] = [1 + \eta_1^2(\omega) \zeta_1^2(\omega)] [1 + \zeta_1^2(\omega)]^{-1} ; \\ \eta_1^2(\omega) &= [\eta_{22}(\omega)/\eta_{11}(\omega)] \quad ; \quad \zeta_1^2(\omega) = [E_2(\omega)/E_1(\omega)] \quad . \end{aligned} \quad (14c)$$

[cf. Eqs. (1a) and (4).] Invoking Eq. (2), Eq. (14c) may be cast in terms of averaged modal quantities and parameters

$$\begin{aligned} \eta_{e1}(\omega) &= [\eta_e(\omega)/\eta_{11}(\omega)] = \{1 + \eta_1^2(\omega) [\lambda_1^2(\omega) \sigma_1^2(\omega)]\} \{1 + [\lambda_1^2(\omega) \sigma_1^2(\omega)]\}^{-1} ; \\ \zeta_1^2(\omega) &= [\lambda_1^2(\omega) \sigma_1^2(\omega)] \quad ; \quad \sigma_1^2(\omega) = [\epsilon_2(\omega)/\epsilon_1(\omega)] = [v_{12}^2(\omega) + 1]^{-1} ; \\ \lambda_1^2(\omega) &= [n_2(\omega)/n_1(\omega)] = [\eta_{21}(\omega)/\eta_{12}(\omega)] \quad ; \quad v_{12}^2(\omega) = [\eta_{22}(\omega)/\eta_{12}(\omega)] \quad . \end{aligned} \quad (15)$$

Thus, the "coupling quotient"  $v_{12}^2(\omega)$ , the modal density ratio  $\lambda_1^2(\omega)$ , the modal stored energy ratio  $\sigma_1^2(\omega)$  and the effective loss factor ratio  $\eta_{e1}(\omega)$  are all proper parameters of the two-structures complex. Clearly, if  $v_{12}^2(\omega) \gg 1$ , the coupling between the (2)th and (1)th structures, in this complex, is weak and  $\sigma_1^2(\omega) \ll 1$ ; if  $10 \geq v_{12}^2(\omega) \geq 1$ , the coupling is moderate and  $10^{-1} \leq \sigma_1^2(\omega) \leq (1/2)$ ; and if  $v_{12}^2(\omega) \leq 1$ , the coupling is strong and  $\sigma_1^2(\omega) \rightarrow 1$ . The classification is in accord with previous treatises on this subject [1,2,7,8]. This is not, however, the whole story; the material discussed in Section II is called upon to contribute to the story too. In this vein the (1)th structure is appropriately isolated and its SEA equation of motion is then stated in the form

$$\omega \eta_{11}^0(\omega) E_1^0(\omega) = \Pi_{e1}^0(\omega) \quad , \quad (16a)$$

and if the external force-source remains unaltered by the isolation, the external input power injected into the (1)th structure in isolation is

$$\Pi_{e1}^0(\omega) = \langle |F_e(\omega)|^2 \rangle \langle G_1^0(\omega) \rangle \quad ; \quad \langle G_1^0(\omega) \rangle = (\pi/2) [n_1(\omega)/M_1] \quad . \quad (16b)$$

[cf. Eqs. (8) and (12a), and Fig. 3b.] From Eqs. (10a) and (14) through (16) one derives

$$\mathcal{E}_1(\omega) = [E_1(\omega)/E_1^0(\omega)] = \xi_0^1(\omega) P_0^1(\omega) \quad , \quad (17)$$

$$\xi_0^1(\omega) = [\xi_{11}(\omega) \eta_{11}^0(\omega)] \quad ; \quad \xi_{11}(\omega) = \{ \eta_e(\omega) (1 + [\lambda_1^2(\omega) \sigma_1^2(\omega)]) \}^{-1} \quad , \quad (18a)$$

$$P_0^1(\omega) = [\Pi_{e1}(\omega)/\Pi_{e1}^0(\omega)] \quad . \quad (18b)$$

To set the stage, it is contrived that the division of the structure into a two-structures complex is constructed at a "controlled boundary"; i.e., at a thought boundary that involves no change in the physical properties of the original structure. Under this construction SEA would demand that quantities and parameters in Eqs. (12) and (13) match those in Eqs. (17) and (18) in the form

$$\sigma_1^2(\omega) \rightarrow 1 \quad ; \quad \eta(\omega) \rightarrow \eta_e(\omega) \quad ; \quad \Pi_e(\omega) \rightarrow \Pi_{e1}(\omega) \quad . \quad (19)$$

The first of these matchings signifies that the couplings at the controlled boundary is strong, as a merged structure would; after all, the complex is, in fact, a single structure! From Eqs. (17) through (19) one finds

$$\mathcal{E}_1(\omega) = [\eta_{11}^0(\omega)/\eta(\omega)] [M_1/M] \quad ; \quad M = M_1 + M_2 \quad , \quad (20)$$

$$\xi_0^1(\omega) = [\eta_{11}^0(\omega)/\eta(\omega)] [n_1(\omega)/n(\omega)] \quad ; \quad n(\omega) = n_1(\omega) + n_2(\omega) \quad , \quad (21a)$$

$$P_0^1(\omega) = [n(\omega)/M] [M_1/n_1(\omega)] = [1 + \lambda_1^2(\omega)] [1 + (M_2/M_1)]^{-1} \quad . \quad (21b)$$

Two major points emerged: The first is the simplicity of Eq. (20) and the second is the particular form of  $P_0^1(\omega)$ , as stated in Eq. (21b). This particular form of  $P_0^1(\omega)$  may be summarized

$$P_0^1(\omega) \begin{cases} > 1 & , & \lambda_1^2(\omega) > (M_2/M_1) & , & (22a) \\ = 1 & , & \lambda_1^2(\omega) = (M_2/M_1) & , & (22b) \\ < 1 & , & \lambda_1^2(\omega) < (M_2/M_1) & , & (22c) \end{cases}$$

and one is reminded that  $\lambda_1^2(\omega) = [n_2(\omega)/n_1(\omega)]$ . Equation (22b) defines the two structures; (1)th structure and (2)th structure, to be similar and Eqs. (22a) and (22c) define them to be dissimilar; Eq. (22a) defines a "light" and Eq. (22c) defines a "heavy" adjoined (2)th structure. In Eq. (22) the notion that the external input power into a structure is independent of the coupling when another is adjoined to it, is challenged, notwithstanding that if the structures are similar, as just defined, the challenge is muted.

The contrived division of the structure, just discussed, brings out another topic of significance. The division clearly results in two structures, each of which has a resonance frequency distribution that occupies a higher region of the  $\omega$ -domain than the original. Indeed, in the lower frequency region, where "global-modes" lie, the division of the single structure cannot be strictly entertained. As suggested by the global-modes designation, in that lower frequency region in which these global-modes reside, the (1)th and (2)th structures must be assumed merged apriori. This merger, in turn, validates apriori the matching, stated in Eq. (19), for the global-modes.

Returning to the central topic of discussion, the boundary between the two structures is assumed physical rather than controlled, and, therefore, Eq. (19) could no longer be validated a priori. One expects that if the coupling of the (2)th structure to the (1)th structure, at this boundary, is weak, the external input power ratio  $P_0(\omega)$  converges onto unity. Heuristically, the bridge between weak and strong coupling, and vice versa, can be expressed, for the two-structures complex, in the form

$$P_0^1(\omega) = \{ 1 + \lambda_1^2(\omega) [\sigma_1^2(\omega)]^q \} \{ 1 + (M_2/M_1) [\sigma_1^2(\omega)]^q \}^{-1} ;$$

$$\sigma_1^2(\omega) = [1 + v_{12}^2(\omega)]^{-1} < 1 , \quad (23a)$$

where the index  $q$  is yet to be determined; a likely candidate, however, is  $q = 1$ . In Eq. (23a) a weak coupling is characterized by a small value, compared with unity, for  $\sigma_1^2(\omega)$  and, in accord with Eq. (19), a strong coupling is characterized by a value of  $\sigma_1^2(\omega)$  that converges on unity. In any case, for the two-structures complex, as Eq. (15) attests, the quantity  $\sigma_1^2(\omega)$  is a proper parameter. In this sense Eq. (23a) also defines a proper quantity;  $P_0^1(\omega)$  is proper. Using Eq. (23a), Fig. 4 is presented. In this figure values of  $P_0^1(\omega)$  are depicted as a function of  $(M_2/M_1)$  and  $\lambda_1^2(\omega)$  for two fixed values of  $\sigma_1^2(\omega)$ ; in Fig. 4a,  $\sigma_1^2(\omega) = 1$ , which is commensurate with strong coupling and in Fig. 4b,  $\sigma_1^2(\omega) = 0.2$ , which is commensurate with a fairly weak coupling. Analogously, the external input power ratio  $P_{01}(\omega)$ , as stated in Eqs. (10b) and (12a), can be expressed, for the two-structures complex, in the form

$$P_{01}^2(\omega) = P_{01}^{02}(\omega) \{ 1 + \lambda_2^1(\omega) [\sigma_2^1(\omega)]^q \} \{ 1 + (M_1/M_2) [\sigma_2^1(\omega)]^q \}^{-1} ;$$

$$P_{01}^{02}(\omega) = [\lambda_1^2(\omega) (M_1/M_2)] ; \quad \sigma_2^1(\omega) = [1 + v_{21}^1(\omega)]^{-1} < 1 ;$$

$$v_{21}^1(\omega) = [\eta_{11}(\omega)/\eta_{21}(\omega)] , \quad (23b)$$

and again,  $P_{01}^2(\omega)$ , in Eq. (23b), as Eq. (15) attests, is proper. [cf. Eq. (11b).] The criterion for weak or strong coupling in Eq. (23b) is characterized by whether  $\sigma_2^1(\omega)$  is small compared with unity or approaches unity, respectively. Finally, from Eqs. (23a) and (23b) and Eqs. (10c) and (12a) one obtains

$$P_1^2(\omega) = \{ [P_{01}^2(\omega)] (\sigma_2^1(\omega) < 1) / [P_0^1(\omega)] (\sigma_1^2(\omega) < 1) \} , \quad (23c)$$

and, clearly,  $P_1^2(\omega)$  is proper. [The product or the ratio of two proper quantities is proper!] From Eq. (23) it emerges, again, that if the two structures are similar

$$\lambda_1^2(\omega) = (M_2/M_1) , \quad (24)$$

the external input power ratios, just stated, are all substantially equal to unity, independently of the coupling [1,2,4]. It also emerges, again, that if the two structures are dissimilar and the coupling is strong in the sense that the coupling quotient  $v_{12}^2(\omega)$  is small compared with unity so that  $\sigma_1^2(\omega) \rightarrow 1$ , the external input power ratio  $P_0(\omega)$  differs from unity. Notwithstanding that for weak coupling in the sense that the

coupling quotient  $v_{12}^2(\omega)$  is large compared with unity so that  $\sigma_2^1(\omega) \ll 1$ ,  $P_0^1(\omega)$  approaches unity even if the structures are not similar; i.e., when Eq. (23) is violated. Analogous assessment can be conducted with respect to  $P_{01}^1(\omega)$ , stated in Eq. (23b), and  $P_1^1(\omega)$ , stated in Eq. (23c).

The generalization of Eq. (23) can be readily made. Following the definitions of  $P_0^\alpha(\omega)$ ,  $P_{0\alpha}^\gamma(\omega)$  and  $P_\alpha^\gamma(\omega)$ , stated in Eq. (10), utilizing Eq. (12a) and the procedure that led to Eq. (23), one may readily extrapolate and state

$$P_0^\alpha(\omega) = \left\{ \sum_{\beta} \lambda_{\alpha}^{\beta}(\omega) [\sigma_{\alpha}^{\beta}(\omega)]^q / \sum_{\beta} (M_{\beta}/M_{\alpha}) [\sigma_{\alpha}^{\beta}(\omega)]^q \right\} ,$$

$$\sigma_{\alpha}^{\beta}(\omega) = [\xi_{\beta\alpha}(\omega)/\lambda_{\alpha}^{\beta}(\omega) \xi_{\alpha\alpha}(\omega)] < 1 ; \quad (25a)$$

$$P_{0\alpha}^\gamma(\omega) = P_{0\alpha}^{0\gamma}(\omega) \left\{ \sum_{\beta} \lambda_{\gamma}^{\beta}(\omega) [\sigma_{\gamma}^{\beta}(\omega)]^q / \sum_{\beta} (M_{\beta}/M_{\gamma}) [\sigma_{\gamma}^{\beta}(\omega)]^q \right\} ,$$

$$P_{0\alpha}^{0\gamma}(\omega) = [\lambda_{\alpha}^{\gamma}(\omega) (M_{\alpha}/M_{\gamma})] ; \quad \sigma_{\gamma}^{\beta}(\omega) = [\xi_{\beta\gamma}(\omega)/\lambda_{\gamma}^{\beta}(\omega) \xi_{\gamma\gamma}(\omega)] < 1 ; \quad (25b)$$

$$P_{\alpha}^{\gamma}(\omega) = [P_{0\alpha}^{\gamma}(\omega)](\sigma_{\gamma}^{\beta}(\omega) < 1) / [P_0^{\alpha}(\omega)](\sigma_{\alpha}^{\beta}(\omega) < 1) , \quad (25c)$$

where use is made of Eqs. (1b) and (2) and  $P_{0\alpha}^{0\gamma}(\omega)$  is defined in Eq. (11b). Since the elements in the gain factor matrix  $\xi_{\alpha\beta}(\omega)$  are proper and so are the modal density ratios, the external input power ratios, stated in Eq. (25), are also proper. Thus, in this generalization to a multi (more than two)-structures complex the quantities  $P_0^\alpha(\omega)$ ,  $P_{0\alpha}^\gamma(\omega)$  and  $P_\alpha^\gamma(\omega)$  are proper, notwithstanding that once the first two are, the propriety of the third follows. Moreover, it remains invariant that if the structures are similar

$$\lambda_{\alpha}^{\beta}(\omega) = (M_{\beta}/M_{\alpha}) , \quad (26)$$

the external input power ratios, stated in Eq. (25), are all equal to unity. When the structures are dissimilar, deviations from unity of these ratios may occur; such deviations from unity need to be estimated when noise control criteria are being developed for multi-structures complexes [4,8]. Of particular import in these estimates is the influence of the couplings, among the various structures, on these ratios. The manner of estimating these deviations, as they relate to the couplings among the structures, is presented in this paper. Equation (25) in conjunction with Eq. (10) may be efficaciously employed to establish noise control criteria in situations in which dissimilar structures are coupled members in the same complex.

## 6. References

1. K. L. Chandiramani, "Some simple models describing the transition from weak to strong coupling in statistical energy analysis," J. Acoust. Soc. Am. 63, 1081-1083 (1978)
2. P.W. Smith, Jr., "Statistical models of coupled dynamical systems and the transition from weak to strong coupling," J. Acoust. Soc. Am. 62, 695-698 (1979).

3. R. H. Lyon, Statistical Energy Analysis of Dynamical Systems (MIT, Cambridge, 1975).
4. G. Maidanik and J. Dickey, "Design criteria for the damping effectiveness of structural fuzzies," J. Acoust. Soc. Am. **100**, 1-5 (1996).
5. R. H. Lyon, "Statistical energy analysis and structural fuzzy," J. Acoust. Soc. Am. **97**, 2878-2881 (1995).
6. G. Maidanik and J. Dickey, "On the fuzz in a structural fuzzy," Proceeding of Internoise 96, 1297-1302 (1996).
7. R. H. Lyon and G. Maidanik, "Power flow between linearly coupled oscillators," J. Acoust. Soc. Am., **34**, 623-639 (1962).
8. G. Maidanik and J. Dickey, "Loss factors of pipe-like structures containing beads," J. Acoust. Soc. Am. **99**, 1-9 (1996).

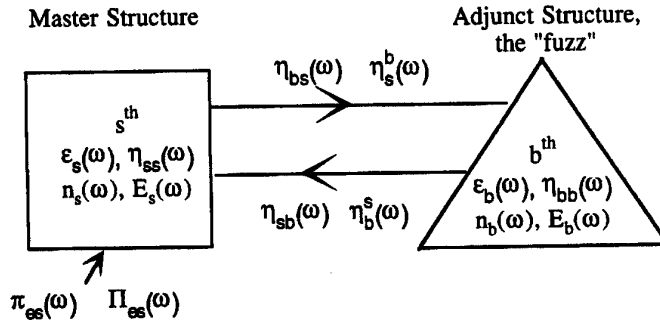


Figure 1, A SEA model of two coupled structures.

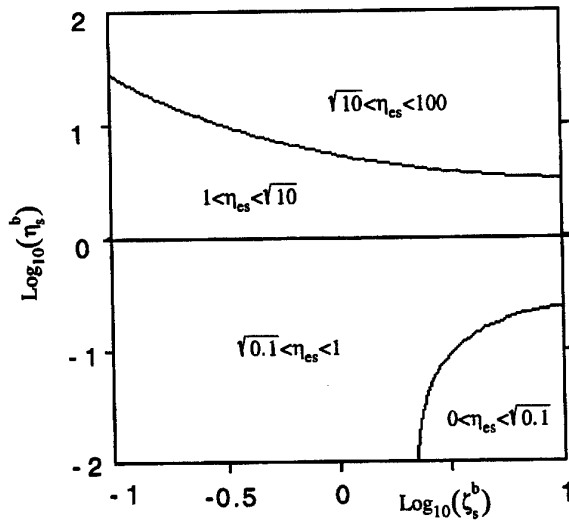
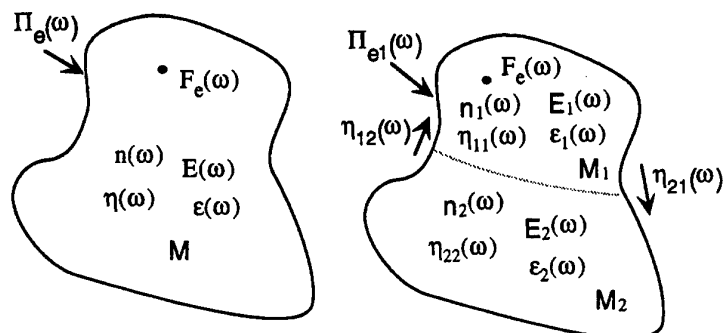


Fig. 2 The effective loss factor ratio  $\eta_{es}(\omega)$  as a function of the stored energy ratio  $\zeta_s^b(\omega)$  and the loss factor ratio  $\eta_s^b(\omega)$ .





a) An externally driven SEA model of a simple structure.

b) A two-structure complex obtained by appropriate division of the structure depicted in Fig. 3a.

Fig. 3

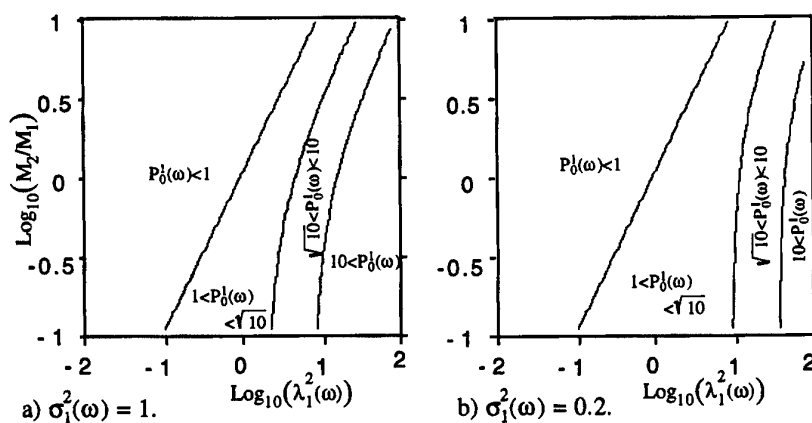


Fig. 4. The external input power ratio  $P_0^1(\omega)$  as a function of  $(M_2/M_1)$  and  $\lambda_1^2(\omega)$  for a fixed value of the modal energy ratio,  $\sigma_1^2(\omega)$ .

# Statistical Energy Analysis in View of Stochastic Modal Analysis

H. J. Pradlwarter and G. I. Schuëller

*Institute of Engineering Mechanics  
Leopold-Franzens University, Innsbruck, Austria*

## Abstract

Exact expressions for the SEA power flow relation between substructures are presented. The approach is based on stochastic modal analysis and is capable to treat non-conservative and strong coupling. Moreover, energy distributions within subsystems are obtained.

## Introduction

SEA is a well established procedure to evaluate the vibration in complex substructures controlled by the energy dissipation and coupling. The methodology is applied mainly in the high frequency domain for which mode shapes cannot be predicted deterministically. SEA is well documented and the recent book by Keane and Price (1996) summarises essential developments in that field. In the critical overview of this book by F. J. Fahy it is mentioned that the accuracy might not be satisfactory for strong non-conservative coupling. Moreover, it is not applicable for the low frequency range. The present approach tries to fill this gap.

## Method of Analysis

### Stationary Stochastic Modal Response

In typical application of SEA, the amplitudes of vibration are generally quite small, and all components react essentially linear. It is therefore justified to confine the following considerations to a linear structural system, of which the equation of motion may read,

$$M \cdot \ddot{x} + C \cdot \dot{x} + K \cdot x = f(t) \quad (1)$$

where  $M$ ,  $C$  and  $K$  denotes the mass, viscous damping and stiffness matrix, and  $x$  and  $f(t)$  represent the generalised displacement and force vector, respectively.

For the derivation of the stochastic response, it is advantageous to rewrite the equation of motion (1) in a first order form,

$$\dot{\mathbf{y}} = \mathbf{A} \cdot \mathbf{y} + \mathbf{g} \quad (2)$$

introducing the state vector  $\mathbf{y}$ ,  $\mathbf{g}$  and the matrix  $\mathbf{A}$  as specified in the following where  $\mathbf{U}$  denotes the identity matrix:

$$\mathbf{y}^T = \{\mathbf{x}^T, \dot{\mathbf{x}}^T\} \quad ; \quad \mathbf{g}^T = \{0^T, \mathbf{f}^T \mathbf{M}^{-1}\} \quad ; \quad \mathbf{A} = \begin{bmatrix} 0 & \mathbf{U} \\ -\mathbf{M}^{-1} \mathbf{K} & -\mathbf{M}^{-1} \mathbf{C} \end{bmatrix} \quad (3)$$

There are well established procedures to determine the stochastic response of linear systems (see e.g. Lin (1976)). The main features of the stochastic response can be characterised by its first two moments, i.e. the mean vector  $\mathbf{E}\{\mathbf{y}\}$  and the covariance matrix  $\mathbf{D} = \mathbf{E}\{\mathbf{y}\mathbf{y}^T\} - \mathbf{E}\{\mathbf{y}\} \cdot \mathbf{E}\{\mathbf{y}\}^T$ , where  $\mathbf{E}\{\cdot\}$  denotes the mathematical expectation or average.

The mean vector  $\mathbf{E}\{\mathbf{y}\}$  is obtained by taking the expectation of eq.(2) leading to eq.(4). Since the mean  $\mathbf{E}\{\mathbf{y}\}$  must for a stationary response not change w.r.t. time, it follows that the right hand side of eq.(4) is zero, and the mean vector is determined analogously as in the static case where the loading is replaced by its time invariant expectation.

$$\mathbf{E}\{\dot{\mathbf{y}}\} = \mathbf{A} \cdot \mathbf{E}\{\mathbf{y}\} + \mathbf{E}\{\mathbf{g}\} \quad (4)$$

$$\text{for } \mathbf{E}\{\dot{\mathbf{y}}\} = 0 \quad : \quad \mathbf{E}\{\mathbf{x}\} = \mathbf{K}^{-1} \cdot \mathbf{E}\{\mathbf{f}\} \quad (5)$$

As it is common practice in random vibration analysis it will be assumed in the following, that the response  $\mathbf{y}$  and the excitation  $\mathbf{f}$  or  $\mathbf{g}$  have zero mean, i. e.  $\mathbf{E}\{\mathbf{y}\} = \mathbf{E}\{\mathbf{g}\} = 0$ , bearing in mind that the static part needs to be added if the total response is required.

The covariance matrix  $\mathbf{D}$  can be determined in a straightforward manner. The differentiation of the symmetric matrix  $\mathbf{D}$  w.r.t. time, and introducing eq.(2) in the expression below,

$$\dot{\mathbf{D}} = \frac{d}{dt} \mathbf{E}\{\mathbf{y}\mathbf{y}^T\} = \mathbf{E}\{\dot{\mathbf{y}}\mathbf{y}^T + \mathbf{y}\dot{\mathbf{y}}^T\} = \mathbf{A} \cdot \mathbf{D} + \mathbf{D} \cdot \mathbf{A}^T + \mathbf{B} = 0 \quad (6)$$

lead to the so called Lyapunov equation for the stationary case ( $\dot{\mathbf{D}} = 0$ ), where the matrix  $\mathbf{B}$  denotes the symmetric matrix:

$$\mathbf{B} = \mathbf{E}\{\mathbf{g}\mathbf{y}^T\} + \mathbf{E}\{\mathbf{y}\mathbf{g}^T\} = \begin{bmatrix} 0 & \mathbf{E}\{\mathbf{x}\mathbf{f}^T\} \cdot \mathbf{M}^{-1} \\ \mathbf{M}^{-1} \mathbf{E}\{\mathbf{f}\mathbf{x}^T\} & \mathbf{M}^{-1} \mathbf{E}\{\mathbf{f}\dot{\mathbf{x}}^T\} + \mathbf{E}\{\dot{\mathbf{x}}\mathbf{f}^T\} \mathbf{M}^{-1} \end{bmatrix} \quad (7)$$

The above relation defines a linear equation system to determine uniquely all  $2N^2 + N$  components of the symmetric covariance matrix  $\mathbf{D}$ , provided the matrix  $\mathbf{B}$  and the matrices defining the structure are known.

Note that no restricting assumptions have been made in eq.(6) with eq.(7) regarding the stochastic characteristics of the excitation. Considerable effort is

needed to determine the sub-matrices  $E\{f x^T\}$  and  $E\{f \dot{x}^T\}$  for the general case, where the random loading  $f(t)$  and the stochastic response  $x(t)$  are correlated. Only for the special case of a purely random process, i.e. so called white noise, these two matrices can be formulated independently from the specific response  $x(t)$  and  $\dot{x}(t)$ . Let the random excitation be represented as

$$f(t) = G \cdot \xi(t) \quad (8)$$

where  $\xi(t)$  represents a vector of  $M$  uncorrelated white noise components  $\xi_k(t)$  and  $G$  a matrix of dimension  $N \times M$  with constant coefficients. Using such a representation spatially correlated white noise excitation can be described. The components  $\xi_k(t)$  are assumed to be uncorrelated since it is always possible to introduce a linear transformation leading to the above representation. In most cases, the distributions of the excitation are close to a normal one for which the components  $\xi_k(t)$  can be regarded as independent. Each white noise component  $\xi_k(t)$  is characterised by the Dirac delta correlated auto-covariance function  $R_{kk}(\tau)$

$$R_{kk}(\tau) = E\{\xi_k(t)\xi_k(t+\tau)\} = I_{kk} \cdot \delta(\tau) \quad (9)$$

or its Fourier transform resulting in a constant spectral density  $S_{kk} = I_{kk}/(2\pi)$ .

$$S_{kk}(\omega) = \frac{1}{2\pi} \int_{-\infty}^{+\infty} R_{kk}(\tau) e^{-i\omega\tau} d\tau = \text{const} = \frac{1}{2\pi} I_{kk} \quad (10)$$

White noise is a fairly accurate substitute in case of a broad band excitation as commonly met in problems of noise transmission. However, coloured noise can also be treated by utilising filtered white noise. Bearing in mind that a generalisation to coloured noise is possible, the excitation will be regarded in the following as white noise only. For white noise excitation, the force vector  $f(t)$  is statistically independent from the displacement vector  $x(t)$ , and also independent from the velocity  $\dot{x}(\tau < t)$  and  $E\{f \dot{x}^T\}$  is only function of the white noise intensity matrix  $I$  and mass matrix  $M$ ,

$$E\{f x^T\} = E\{f\} \cdot E\{x\}^T = 0 \quad ; \quad E\{f \dot{x}^T\} = \frac{1}{2} G \cdot I \cdot G^T \cdot M^{-1} \quad (11)$$

where the white noise intensity matrix  $I$  is a diagonal matrix and the matrix  $B$  defined in eq.(7) simplifies to:

$$B = \begin{bmatrix} 0 & 0 \\ 0 & M^{-1} \cdot G \cdot I \cdot G^T \cdot M^{-1} \end{bmatrix} \quad (12)$$

For further considerations, eq.(3) and the above relation for matrix  $B$  is introduced into the Lyapunov eq.(7), leading to three equivalent relations for the stationary stochastic response,

$$E\{x \dot{x}^T\} + E\{\dot{x} x^T\} = 0 \quad (13)$$

$$K \cdot E\{x x^T\} - C \cdot E\{x \dot{x}^T\} - M \cdot E\{\dot{x} \dot{x}^T\} = 0 \quad (14)$$

$$\begin{aligned}
& K \cdot E\{\dot{x}\dot{x}^T\} \cdot M - M \cdot E\{\dot{x}\dot{x}^T\} \cdot K + \\
& C \cdot E\{\dot{x}\dot{x}^T\} \cdot M + M \cdot E\{\dot{x}\dot{x}^T\} \cdot C = G \cdot I \cdot G^T \quad (15)
\end{aligned}$$

where eq.(13) has been introduced into the last two equations.

Utilising the last three equations, all  $K = 2N^2 + N$  components of the symmetric covariance matrix  $D$  can be determined uniquely by solving a linear equation system of dimension  $K$ . For large  $N$ , however, due to its size, the solution of the  $K$ -dimensional equation system becomes cumbersome. This difficulty can be circumvented using modal decomposition as shown subsequently.

Assuming modal damping, the equation of motion (1) decouples by using modal coordinates  $z(t)$ ,

$$x(t) = \Phi \cdot z(t) \quad (16)$$

$$\ddot{z}_j(t) + 2\zeta_j\omega_j\dot{z}_j(t) + \omega_j^2 z_j(t) = q_j(t) = \phi_j^T \cdot f \quad ; \quad 1 \leq j \leq N \quad (17)$$

where the matrix  $\Phi$  contains all eigenvectors of the characteristic equation,

$$K \cdot \Phi = M \cdot \Phi \cdot \Lambda \quad (18)$$

where  $\Lambda = [\text{diag}(\omega_j^2)]$  is a diagonal matrix comprising all eigenvalues. The eigenvectors are orthogonal with respect to the stiffness matrix  $K$  and mass matrix  $M$  and are normalised to satisfy the relations:

$$\Phi^T \cdot K \cdot \Phi = \Lambda \quad ; \quad \Phi^T \cdot M \cdot \Phi = U \quad (19)$$

Assuming further that the damping matrix  $C$  decouples using the transformation,

$$\Gamma = \Phi^T \cdot C \cdot \Phi = [\text{diag}(\gamma_j)] \quad ; \quad \gamma_j = 2\zeta_j\omega_j \quad (20)$$

and introducing the last two relations into eqn.(13)-(15), these equations assume for modal coordinates the following simple form:

$$E\{zz^T\} + E\{\dot{z}\dot{z}^T\} = 0 \quad (21)$$

$$\Lambda \cdot E\{zz^T\} - \Gamma \cdot E\{z\dot{z}^T\} - E\{\dot{z}z^T\} = 0 \quad (22)$$

$$\begin{aligned}
& \Lambda \cdot E\{z\dot{z}^T\} - E\{\dot{z}z^T\} \cdot \Lambda + \Gamma \cdot E\{\dot{z}\dot{z}^T\} + E\{\dot{z}\dot{z}^T\} \cdot \Gamma = \\
& \hat{I} = \Phi^T \cdot G \cdot I \cdot G^T \cdot \Phi \quad (23)
\end{aligned}$$

Utilising a modal representation, one is in the favourable position to give an explicit solution in closed form for all components of the covariance matrix  $D$  as shown in the following. Considering the  $j$ -th row and  $k$ -th column of eq.(22) and next the  $k$ -th row and  $j$ -th column leads to the following two equations,

$$\omega_j^2 E\{z_j z_k\} - \gamma_j E\{z_j \dot{z}_k\} - E\{\dot{z}_j z_k\} = 0 \quad (24)$$

$$\omega_k^2 E\{z_j z_k\} k + \gamma_k E\{z_j \dot{z}_k\} - E\{\dot{z}_j z_k\} = 0 \quad (25)$$

where  $E\{z_j \dot{z}_k\} = -E\{z_k \dot{z}_j\}$  (see eq.(21)) has been used in the last eq.(25). The terms  $E\{z_j z_k\}$  and  $E\{z_j \dot{z}_k\}$  can be eliminated from the above two equations, i. e. expressed as function of  $E\{\dot{z}_j \dot{z}_k\}$ :

$$\begin{Bmatrix} E\{z_j z_k\} \\ E\{\dot{z}_j \dot{z}_k\} \end{Bmatrix} = \frac{E\{\dot{z}_j \dot{z}_k\}}{\gamma_j \omega_k^2 + \gamma_k \omega_j^2} \begin{Bmatrix} \gamma_j + \gamma_k \\ \omega_j^2 - \omega_k^2 \end{Bmatrix} \quad (26)$$

Eq.(23) can also be represented by its components which read,

$$(\omega_j^2 - \omega_k^2)E\{z_j \dot{z}_k\} + (\gamma_j + \gamma_k)E\{\dot{z}_j \dot{z}_k\} = \hat{I}_{jk} \quad (27)$$

leading to the solution,

$$E\{\dot{z}_j \dot{z}_k\} = \frac{\hat{I}_{jk}}{\gamma_j + \gamma_k + \frac{(\omega_j^2 - \omega_k^2)^2}{\gamma_j \omega_k^2 + \gamma_k \omega_j^2}} \quad (28)$$

by utilising eq.(26). The last relation completes the solution in closed form for the second moments in modal coordinates and will be the basis for deriving the following SEA relations.

### Spatial Distribution of Kinetic Energy

Statistical Energy Analysis relates the power  $p$  introduced into the system by the external excitation to the vibrational energy  $E$  of the structural components. To simplify the derivation, it will be assumed that the mass matrix is diagonal, which corresponds to lumped mass points instead of a continuous mass distribution. This simplification, however, has a negligible effect on the deterministic and stochastic response of a structure respectively. To derive such a relation, the white noise intensity matrix  $I$  must be related to the power of the excitation introduced into the system. Recall from eq.(8) that the intensity matrix  $I$  is a diagonal matrix because the components  $\xi_k(t)$  of the vector  $\xi$  are uncorrelated. Each component  $\xi_k(t)$  introduces on the average a certain amount  $p_k$  of power into the system

$$p_k = \sum_{i=1}^N E\{f_i \dot{x}_i[\xi_k]\} = \frac{1}{2} I_{kk} \sum_{i=1}^N \frac{g_{ik}^2}{m_i} \quad (29)$$

where the first index  $i$  in  $g_{ik} \in G$  denotes the DOF and the second index  $k$  refers to the white noise component. Thus the white noise intensity  $I_{kk}$  of the component  $\xi_k(t)$  can be related with the average power  $p_k$  of the stationary white noise process  $\xi_k(t)$ . For the special case for which the excitation  $\xi_k(t)$  acts independently on a single mass point  $m_k$ , the power simplifies to  $p_k = I_{kk}/(2m_k)$ .

For continuous structures modelled by a FE-model, the above relations between white noise intensity and power is not convenient. First of all, the excitation  $\xi_k(t)$  can not be white, but is specified by a power spectrum  $S_{kk}$  which might have negligible power outside a certain frequency range. Moreover, there are actually no discrete mass points where the excitation acts upon. Therefore, an alternative

expression will be given. In case the excitation  $\xi_k(t)$  acts only on the  $k$ -th DOF, the following relation can be derived by modal analysis,

$$p_k = E\{f_k \dot{x}_k\} = \frac{1}{2} I_{kk} \sum_{i=1}^N \phi_{ki}^2 = \pi S_{kk} \sum_{i=1}^N \phi_{ki}^2 \quad (30)$$

where the first index in  $\phi_{ki}$  refers to the DOF and the second index to the mode. The above expression can be generalised for broad band excitation:

$$p_k = \pi \sum_i S_{kk}(\omega_i) \phi_{ki}^2 \quad (31)$$

For the general case where the possible correlated excitation is defined by eq.(8), the input power reads:

$$p_k = \sum_{i=1}^N E\{f_i \dot{x}_i[\xi_k]\} = \pi \sum_n S_{kk}(\omega_n) \left( \sum_{i=1}^N g_{ik} \phi_{in} \right)^2 \quad (32)$$

Next, the modal density  $\hat{I}_{jk}$  is related with the power  $p_k$  of the external white noise excitation.

$$\hat{I}_{jk} = \phi_j^T \cdot \mathbf{G} \cdot \mathbf{I} \cdot \mathbf{G}^T \cdot \phi_k = \sum_{i=1}^M I_{ii} \left( \sum_{l=1}^N \phi_{lj} g_{li} \right) \left( \sum_{l=1}^N \phi_{lk} g_{li} \right) \quad (33)$$

Relating the white noise intensity  $I_{ii}$  to the power  $p_i$

$$\hat{I}_{jk} = 2 \sum_{i=1}^M c_{i(j,k)} p_i \quad (34)$$

the coefficients  $c_{i(j,k)}$  are determined from eq.(32) leading to the dimensionless quantities

$$c_{i(j,k)} := \frac{\sqrt{S_{kk}(\omega_j) S_{kk}(\omega_k)} \left( \sum_{l=1}^N \phi_{lj} g_{li} \right) \left( \sum_{l=1}^N \phi_{lk} g_{li} \right)}{\sum_n S_{kk}(\omega_n) \left( \sum_{l=1}^N \phi_{ln} g_{ln} \right)^2} \quad (35)$$

where  $c_{i(j,k)}$  is a dimensionless quantity.

Denoting the averaged kinetic energy of each DOF  $j$  as  $e_j$  and recalling the modal representation in eq.(16) leads to

$$e_j = \frac{1}{2} m_j E\{\dot{x}_j^2\} = \frac{1}{2} m_j \sum_{n=1}^N \sum_{l=1}^N \phi_{jn} \phi_{jl} E\{\dot{z}_n \dot{z}_l\} \quad (36)$$

where the first index  $j$  in  $\phi_{jn}$  denotes the DOF of the  $n$ -th normalised eigenvector or mode. Nothing further than for small damping ratios  $\xi_n$ , which are usually in the range of a few percent and less, the main contribution to the kinetic energy

of the structure stems from the diagonal terms  $E\{\dot{z}_n^2\}$  and closely spaced modes with  $\omega_n^2 \approx \omega_l^2$ , and assuming further that the eigenpairs  $(\omega_n^2, \phi_n)$  are ordered,

$$\omega_1^2 \leq \omega_2^2 \leq \dots \leq \omega_N^2 \quad (37)$$

eq.(28) can be replaced by the following expression:

$$e_j = \sum_{n=1}^N \frac{m_j}{2} \phi_{jn}^2 E\{\dot{z}_n^2\} + 2 \sum_{n=1}^{N-1} \frac{m_j}{2} \phi_{jn} \phi_{j,n+1} E\{\dot{z}_n \dot{z}_{n+1}\} + \dots \quad (38)$$

Introducing the notation,

$$h_{j(n,l)} = m_j \phi_{jn} \phi_{jl} \quad ; \quad \gamma_{(n,l)} = \gamma_n + \gamma_l + \frac{(\omega_n^2 - \omega_l^2)^2}{\gamma_n \omega_l^2 + \gamma_l \omega_n^2} \quad (39)$$

the terms  $E\{\dot{z}_n \dot{z}_l\}$  read,

$$E\{\dot{z}_n \dot{z}_l\} = \frac{2}{\gamma_{(n,l)}} \sum_{i=1}^M c_{i(n,l)} p_i \quad (40)$$

and thus the kinetic energy of the  $j$ -th DOF specified in eq.(38) becomes:

$$e_j = \sum_{n=1}^N \frac{h_{j(n,n)}}{\gamma_{(n,n)}} \sum_{i=1}^M c_{i(n,n)} p_i + \sum_{n=1}^{N-1} \frac{h_{j(n,n+1)}}{\gamma_{(n,n+1)}} \sum_{i=1}^M c_{i(n,n+1)} p_i + \dots \quad (41)$$

Introducing the vectors,

$$\begin{aligned} \mathbf{e}^T &= \{e_1, e_2, \dots, e_N\} \quad ; \quad \mathbf{h}_{(n,l)}^T = \{h_{1(n,l)}, h_{2(n,l)}, \dots, h_{N(n,l)}\} \\ \mathbf{p}^T &= \{p_1, p_2, \dots, p_M\} \quad ; \quad \mathbf{c}_{(n,l)}^T = \{c_{1(n,l)}, c_{2(n,l)}, \dots, c_{M(n,l)}\} \end{aligned} \quad (42)$$

the above equation can be generalised to establish a relation for the spatial distribution of the energy  $e$  for all DOFs of the structure subjected to white noise excitation  $\mathbf{p}$ :

$$\mathbf{e} = \left[ \sum_{n=1}^N \frac{\mathbf{h}_{(n,n)} \cdot \mathbf{c}_{(n,n)}^T}{\gamma_{(n,n)}} + 2 \sum_{n=1}^{N-1} \frac{\mathbf{h}_{(n,n+1)} \cdot \mathbf{c}_{(n,n+1)}^T}{\gamma_{(n,n+1)}} + \dots \right] \cdot \mathbf{p} \quad (43)$$

The above relation is the main result of this paper and deserves a more detailed discussion.

Consider first the vector  $\mathbf{h}_{(n,l)}$  defined in eq.(39). Since the eigenvectors  $\phi_n$  or modes are normalised w.r.t. the mass matrix, the vector  $\mathbf{h}_{(n,l)}$  satisfies the property:

$$\sum_{j=1}^N h_{j(n,n)} = 1 \quad ; \quad 0 \leq h_{j(n,n)} \leq 1 \quad (44)$$

$$\sum_{j=1}^N h_{j(n,l)} = 0 \quad ; \quad -1 \leq h_{j(n,l)} \leq 1 \quad ; \quad \text{for } l \neq n \quad (45)$$



Looking at the total kinetic energy  $e_{tot}$  of the system,

$$e_{tot} = \sum_{j=1}^N e_j = \left[ \sum_{n=1}^N \frac{c_{(n,n)}^T}{\gamma_{(n,n)}} \right] \cdot \mathbf{p} \quad (46)$$

it becomes apparent, that only the first term in eq.(43) contributes to the total energy of the system, while the second and higher terms vanish due to eq.(45). Thus, the second term in eq.(43) accounts for a redistribution of the kinetic energy within the system letting the total amount of energy constant. The effect of the redistribution is in most cases negligible where the eigenfrequencies are well separated and become important only for pairs of closely spaced eigenfrequencies as it will be demonstrated in the numerical examples.

For the special case in which independent excitations act on single masses  $m_k$  introducing the external power  $E\{f_k \dot{x}_k\}$  into the structural system, it is readily verified ( $I_{kk} = 2m_k p_k$  (see eq.(29)) and  $\hat{I}_{n,l} = \phi_{kn} \phi_{kl} I_{kk}$ ) that

$$c_{k(n,l)} = m_k \phi_{kn} \phi_{kl} = h_{k(n,l)} \quad (47)$$

hold for which eq.(43) reads:

$$\mathbf{e} = \left[ \sum_{n=1}^N \frac{h_{(n,n)} \cdot h_{(n,n)}^T}{\gamma_{(n,n)}} + 2 \sum_{n=1}^{N-1} \frac{h_{(n,n+1)} \cdot h_{(n,n+1)}^T}{\gamma_{(n,n+1)}} + \dots \right] \cdot \hat{\mathbf{p}} \quad (48)$$

where the  $k$ -th component of the vector  $\hat{\mathbf{p}}$  denotes the input power  $\hat{p}_k = E\{f_k \dot{x}_k\}$ .

## SEA of Coupled Structural Components

The SEA method can be regarded as procedure to determine the vibration energy balance in complex coupled systems. The subsystems in the SEA model are either weakly coupled structural components or "blocks of similar modes". The external excitation introduces in each subsystem an input power  $\Pi_{in}$  which is dissipated by internal damping, but also transmitted to neighbouring subsystems by the coupling. The dissipation of the power  $\Pi_{i,in}$  of the  $i$ -th subsystem is expressed by the so called loss factor  $\eta_i$  multiplied by the kinetic energy  $E_i$  of the subsystem. The power flow  $\Pi_{ij}$  from the  $i$ -th to the  $j$ -th neighbouring subsystems is measured by the coupling loss factor  $\eta_{ij}$  multiplied by the difference  $(E_i - E_j)$  of energies. Hence, SEA states that power is transmitted only from subsystems of higher kinetic energy towards neighbouring systems with lower energy. In case the systems consist of  $J$  subsystems the following typical energy flow equation is established,

$$\omega_c \begin{bmatrix} \eta_1 + \sum_{j \neq 1} \eta_{1j} & -\eta_{12} & \dots & -\eta_{1J} \\ -\eta_{21} & \eta_2 + \sum_{j \neq 2} \eta_{2j} & \dots & -\eta_{2J} \\ \vdots & \vdots & \ddots & \vdots \\ -\eta_{J1} & -\eta_{J2} & \dots & \eta_J + \sum_{j \neq J} \eta_{Jj} \end{bmatrix} \cdot \begin{Bmatrix} E_1 \\ E_2 \\ \vdots \\ E_J \end{Bmatrix} = \begin{Bmatrix} \Pi_1 \\ \Pi_2 \\ \vdots \\ \Pi_J \end{Bmatrix} \quad (49)$$

for certain frequency bands  $[\omega_l, \omega_u]$  with  $\omega_c = (\omega_l + \omega_u)/2$  and where the coupling loss factors are symmetric, i.e.  $\eta_{ij} = \eta_{ji}$ . For substructures  $S_i$  and  $S_j$  which are not directly coupled, the coupling loss factors are assumed to vanish, i.e.  $\eta_{ij} = 0$ .

For a shorter notation, the above SEA power flow relation is expressed in matrix notation,

$$\hat{\Gamma} \cdot \{E\} = \{\Pi_{in}\} \quad (50)$$

with

$$\hat{\gamma}_{ij} \in \hat{\Gamma} \quad ; \quad \hat{\gamma}_{ii} = \omega_c(\eta_i + \sum_{j \neq i} \eta_{ij}) \quad ; \quad \hat{\gamma}_{ij} = -\omega_c \eta_{ij} \text{ for } j \neq i \quad (51)$$

where the "hat" in  $\hat{\gamma}$  is introduced to distinguish these coefficients clearly from modal damping  $\gamma_i$  defined in eq.(20).

The above SEA equation (49) is now compared with the exact solution stated in eq.(43) and eq.(48). The solution in eq.(43) is given in the form

$$e = \bar{\Gamma}^{-1} \cdot p \quad (52)$$

corresponding to an inverse formulation of (49). The eq.(43) can be easily specified for energies  $E_i$  in substructures  $S_i, i = 1, 2, \dots, L$ . Let  $\{J_i\}$  be the set DOF belonging to the substructure  $S_i$ . Since the kinetic energy  $E_i$  of substructure  $S_i$  is just the sum of all energies  $e_j$  of the DOF  $j$  belonging to  $S_i$ , eq.(43) reads for substructures,

$$E = \left[ \sum_{n=1}^N \frac{\bar{h}_{(n,n)} \cdot c_{(n,n)}^T}{\gamma_{(n,n)}} + 2 \sum_{n=1}^{N-1} \frac{\bar{h}_{(n,n+1)} \cdot c_{(n,n+1)}^T}{\gamma_{(n,n+1)}} + \dots \right] \cdot p \quad (53)$$

with:

$$E_i = \sum_{j \in \{J_i\}} e_j \quad (54)$$

$$\bar{h}_{i(n,l)} = \sum_{j \in \{J_i\}} h_{j(n,l)} \quad ; \quad \bar{h}_{(n,l)}^T = \{\bar{h}_{1(n,l)}, \bar{h}_{2(n,l)}, \dots, \bar{h}_{L(n,l)}\} \quad (55)$$

In a next step, the power input  $\Pi_i$  in a substructure  $S_i$  is defined as the sum of single sources  $p_j$

$$\Pi_i = \sum_{j \in \{J_i\}} p_j \quad (56)$$

where it is assumed that there is no correlation in the excitation across substructures, i.e. the coefficients  $g_{lj} \neq 0$  (see eq.(8)) belong for all  $l$  to the same substructure. Introducing the quantities

$$\bar{c}_{i(n,l)} = \frac{\sum_{j \in \{J_i\}} c_{j(n,l)} p_j}{\sum_{j \in \{J_i\}} p_j} \quad ; \quad \bar{c}_{(n,l)}^T = \{\bar{c}_{1(n,l)}, \bar{c}_{2(n,l)}, \dots, \bar{c}_{L(n,l)}\} \quad (57)$$

the kinetic energy in the substructures is determined by the linear relation,

$$E = \Upsilon \cdot \Pi \quad (58)$$

or equivalently in the standard SEA form

$$\bar{\Gamma} \cdot E = \Pi \quad \text{with} \quad \bar{\Gamma} = \Upsilon^{-1} \quad (59)$$

where the matrix  $\Upsilon$  reads:

$$\Upsilon = \left[ \sum_{n=1}^N \frac{\bar{h}_{(n,n)} \cdot \bar{c}_{(n,n)}^T}{\gamma_{(n,n)}} + 2 \sum_{n=1}^{N-1} \frac{\bar{h}_{(n,n+1)} \cdot \bar{c}_{(n,n+1)}^T}{\gamma_{(n,n+1)}} + \dots \right] \quad (60)$$

Please note, that the coefficients  $\bar{c}_{i(n,l)}$  are determined uniquely only in case it is additionally specified at which DOFs the power inputs  $p_j$  are introduced into the subsystem. In other words, the specification of the power  $\Pi_{i,in}$  introduced into the elastic subsystem  $S_i$  is in general not sufficient to specify uniquely the average kinetic energies or stationary stochastic response of the system. Only for the case that the whole substructure  $S_i$  vibrates uniformly over its domain and quasi independent from neighbouring substructures (weak coupling), the specification of the power input is sufficient to determine uniquely all energies in the substructures.

Another important aspect is the symmetry (see eq.(49) and eq.(59)) of the SEA power flow relation. For arbitrary strong coupling between substructures, the matrix  $\bar{\Gamma}$  is non-symmetric contrary to the matrix  $\bar{\Gamma}$  in eq.(50). Considering eq.(48) the matrix  $\bar{\Gamma}$  is symmetric under the assumption that substructures do behave like mass point with a single DOF each mass point. Thus, in case the substructures are very rigid in comparison to the coupling the matrix  $\bar{\Gamma}$  tends to be symmetric.

## Numerical Examples

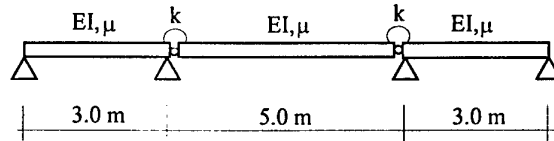


Figure 1: Structural System

The power flow relation in an elastic beam as shown below in Fig.1 is investigated in the following. Due to its symmetry closely spaced modes occur. The beam has a constant mass density  $\mu$  and two elastic torsional couplings  $k$ . Due to space limitations, only the case where  $k \rightarrow \infty$  is presented, representing strong coupling.

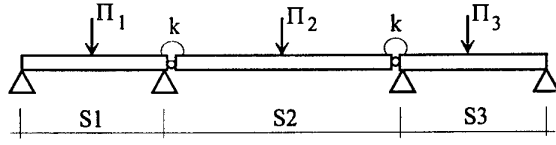


Figure 2: Partition of beam-structure into three sub-structures S1, S2 and S3

Modal analysis has been performed for the shown beam structure using 19 modes.

In a first case the structure is partitioned into three substructures as shown in Fig.3 where the supports represent natural boundaries of the substructure. The results depend according to eq.(60) mainly on the specific modal damping  $\gamma_{(n,n)} = 4\zeta_n\omega_n$ . The results obtained for constant  $\gamma_{(n,n)}$  are presented below.

For  $\zeta_j\omega_j = \text{const}$  ;  $k \rightarrow \infty$  ; modes  $\in [1, 19]$

$$\begin{Bmatrix} E_1 \\ E_2 \\ E_3 \end{Bmatrix} = \frac{1}{4 \langle \zeta\omega \rangle} \begin{bmatrix} 0.87825 & 0.01758 & 0.08737 \\ 0.03438 & 0.96485 & 0.03485 \\ 0.08737 & 0.01759 & 0.87825 \end{bmatrix} \cdot \begin{Bmatrix} \Pi_1 \\ \Pi_2 \\ \Pi_3 \end{Bmatrix}$$

$$4 \langle \zeta\omega \rangle \begin{bmatrix} +1.1507 & -0.01889 & -0.1137 \\ -0.0370 & +1.0378 & -0.0370 \\ -0.1137 & -0.0189 & +1.1507 \end{bmatrix} \cdot \begin{Bmatrix} E_1 \\ E_2 \\ E_3 \end{Bmatrix} = \begin{Bmatrix} \Pi_1 \\ \Pi_2 \\ \Pi_3 \end{Bmatrix}$$

The above shows the results according to eqn.(58) and (59) using all first 19 modes. Next the same quantities are shown using only the first four modes.

For  $\zeta_j\omega_j = \text{const}$  ;  $k \rightarrow \infty$  ; modes  $\in [1, 4]$

$$\begin{Bmatrix} E_1 \\ E_2 \\ E_3 \end{Bmatrix} = \frac{1}{4 \langle \zeta\omega \rangle} \begin{bmatrix} 0.60127 & 0.02818 & 0.34163 \\ 0.05710 & 0.94364 & 0.05710 \\ 0.34163 & 0.02818 & 0.60127 \end{bmatrix} \cdot \begin{Bmatrix} \Pi_1 \\ \Pi_2 \\ \Pi_3 \end{Bmatrix}$$

$$4 \langle \zeta\omega \rangle \begin{bmatrix} +2.4580 & -0.0318 & -1.3936 \\ -0.0644 & +1.0636 & -0.0644 \\ -1.3936 & -0.0318 & 2.4580 \end{bmatrix} \cdot \begin{Bmatrix} E_1 \\ E_2 \\ E_3 \end{Bmatrix} = \begin{Bmatrix} \Pi_1 \\ \Pi_2 \\ \Pi_3 \end{Bmatrix}$$

Finally strong coupling is investigated using a partition into substructures as shown in Fig.3. One can observe that the presentation according to eq.(58) is quite reasonable in contrast to the standard SEA representation (59), which is admittedly not designed for strong coupling.

For  $\zeta_j\omega_j = \text{const}$  ;  $k \rightarrow \infty$  ; modes  $\in [1, 19]$

$$\begin{Bmatrix} E_1 \\ E_2 \\ E_3 \\ E_4 \end{Bmatrix} = \frac{1}{4 \langle \zeta\omega \rangle} \begin{bmatrix} 0.38358 & 0.38788 & 0.00603 & 0.03053 \\ 0.53705 & 0.53954 & 0.01155 & 0.05684 \\ 0.01299 & 0.01086 & 0.96485 & 0.03438 \\ 0.06638 & 0.06172 & 0.01758 & 0.87825 \end{bmatrix} \cdot \begin{Bmatrix} \Pi_1 \\ \Pi_2 \\ \Pi_3 \\ \Pi_4 \end{Bmatrix}$$

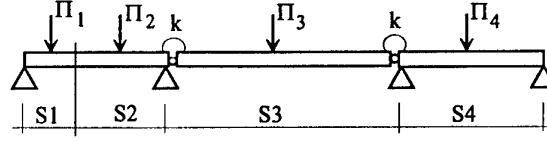


Figure 3: Partition of beam-structure into four sub-structures S1, S2, S3 and S4.

$$4 < \zeta\omega > \begin{bmatrix} -409.20 & +294.74 & -0.8859 & -4.8200 \\ +407.04 & -291.32 & +0.8611 & +4.6746 \\ +0.8438 & -0.6241 & +1.0392 & -0.0296 \\ +2.3069 & -1.7925 & -1.4350 & +1.1750 \end{bmatrix} \cdot \begin{Bmatrix} E_1 \\ E_2 \\ E_3 \\ E_4 \end{Bmatrix} = \begin{Bmatrix} \Pi_1 \\ \Pi_2 \\ \Pi_3 \\ \Pi_4 \end{Bmatrix}$$

## Conclusions and Outlook

The following conclusion are drawn from the presented results:

- (1) Exact expressions for the SEA power flow relations have been obtained. These expressions are exceptionally simple and allow to consider strong coupling (not just in the SEA sense) and energy dissipation in the couplings. It has been shown that a inverse representation is for arbitrary strong coupling better suited than the present standard form.
- (2) A SEA expression for the energy distribution has been derived based on deterministic modal analysis. The derived expressions might be used also for non deterministic modes, considering the mean and variance of the modes shapes. Spatially averaging leads to accurate estimates also for unknown modes shapes.
- (3) The presented approach is expecially suitable for the low frequency domain and for strong non-conservative coupling. It allows to account for specific modal damping ratios, which might be quite different especially in the low frequency domain.

## Acknowledgement

This research was partially supported by the Austrian Industrial Research Fund (FFF) under contract No. 6/752 which is gratefully acknowledged by the authors.

## References

- [1] Keane, A. J. and W. G. Price (1996). Statistical energy analysis, Cambridge University Press, England.
- [2] Lin, Y. K. (1976). Probabilistic Theory of Structural Dynamics, Robert E. Krieger Publishing Company, Huntington, New York.

## INPUT POWER MODULATION METHOD

KARL-OLA LUNDBERG  
Engineering Acoustics  
Lund Institute of Technology/Lund University  
P.O. Box 118 SE-221 00 Lund  
Sweden

### 1. Introduction

There is a need for *in situ* experimental estimation of loss factors and proper subsystem division when analysing assembled systems using statistical energy analysis (SEA). On the basis of a physical measure, the modulation transfer function computed from the squared impulse-response, a method has been developed for this purpose, see Fahy and Ruivo (1997), Lundberg (1997).

The SEA power balance equations in a narrow band  $(\omega_0, \Delta\omega)$  are for two coupled subsystems

$$\begin{bmatrix} \frac{dE_1(t)}{dt} \\ \frac{dE_2(t)}{dt} \end{bmatrix} = \begin{bmatrix} -\omega_0 \eta_1 & \omega_0 \eta_{12} \\ \omega_0 \eta_{21} & -\omega_0 \eta_2 \end{bmatrix} \begin{bmatrix} E_1(t) \\ E_2(t) \end{bmatrix} + \begin{bmatrix} \Pi_1(t) \\ \Pi_2(t) \end{bmatrix} \quad (1.)$$

where  $\eta_1 = \eta_{11} + \eta_{21}$  and  $\eta_2 = \eta_{22} + \eta_{12}$ .  $\eta_{ji}$  is the coupling loss factor describing the energy flow from the *i*:th to the *j*:th subsystem and  $\eta_{ii}$  the internal dissipation loss factor in subsystem *i*.  $E_i(t)$  is the resonant vibrational energy stored in subsystem *i* and  $\Pi_i(t)$  the external input power injected into subsystem *i*.

The equations can be Fourier transformed, rearranged, inverted and put on the form of power-energy transfer functions (Lindblad 1974), which are of low-pass character:

$$\begin{bmatrix} \hat{E}_1(\Omega) \\ \hat{E}_2(\Omega) \end{bmatrix} = \frac{1}{(j\Omega + \omega_0 \eta_1)(j\Omega + \omega_0 \eta_2) - \omega_0 \eta_{21} \omega_0 \eta_{12}} \begin{bmatrix} j\Omega + \omega_0 \eta_2 & \omega_0 \eta_{12} \\ \omega_0 \eta_{21} & j\Omega + \omega_0 \eta_1 \end{bmatrix} \begin{bmatrix} \hat{\Pi}_1(\Omega) \\ \hat{\Pi}_2(\Omega) \end{bmatrix} \quad (2.)$$

$\wedge$  indicates the transformed functions and  $\Omega$  is the transform variable equal to an ordinary angular frequency. The upper left element, e.g., in the square matrix of (2) is  $\left( \frac{\hat{E}_1}{\hat{\Pi}_1} \right)_{\hat{\Pi}_1}$ , where the index indicates that only  $\hat{\Pi}_1$  is active.

In principle the SEA parameters in a transfer function model in (2) could be identified from e.g. a least square fit to a corresponding measured function. However a transfer function in the diagonal of (2), though of second order, deviates very little from a first order if  $\eta_{21} \ll \eta_{11}$  and / or  $\eta_{12} \ll \eta_{22}$ . Then the results from such an identification will have no meaning and a necessary further step is to normalise on the source.

Take the quotient between transfer functions with the same source, i.e. between elements within the same column of (2), e.g.

$$\frac{\left( \frac{\hat{E}_2}{\hat{\Pi}_1} \right)_{\hat{\Pi}_1}}{\left( \frac{\hat{E}_1}{\hat{\Pi}_1} \right)_{\hat{\Pi}_1}} = \frac{\omega_0 \eta_{21}}{j\Omega + \omega_0 \eta_2} \quad (3.)$$

which is a robust lower order model. Notice that the input power can be reduced and thus does not have to be measured.

In earlier days when measuring response, one tried to use ideal sources like constant force or constant velocity sources, giving the boundary conditions  $F=0$  and  $v=0$ , respectively. Nowadays when transfer functions are measured, one must pay attention to the virtual boundary condition introduced. It can be achieved by putting the variable in the denominator of the transfer function equal to zero. Transferring this to (3) where  $\hat{E}_1$  is (secondary) generator, it means that the virtual boundary condition is given by  $\hat{E}_1=0$ , i.e. subsystem 1 is energy earthed. Let a plate be imaginary divided into two parts, 1 and 2. Then  $\eta_{12}$  is large which implies that  $\eta_2$  will be large and consequently the quotient (3) will be flat up to a (high) crossover frequency  $\omega_0 \eta_2$ . The more the boundary actually is reflecting, the smaller  $\eta_{12}$  and then  $\omega_0 \eta_2$  is lowered and in the limit it will be determined by the internal dissipation factor which gives  $\omega_0 \eta_{22}$ .

## 2. The relation between the physical system and the SEA formulation

A structure or an acoustic indoor channel may with high accuracy be modelled into a linear, time-invariant and causal system. This means that an impulse-response completely describes the system. Let a structure be excited in a position  $\mathbf{r}_0$  by a force  $F_0$ , which is a single-frequency modulated white noise signal:

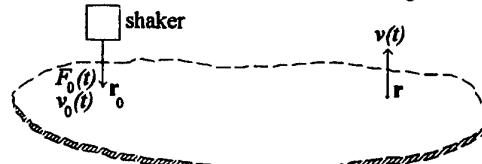


Figure 1. A structure excited by a point force

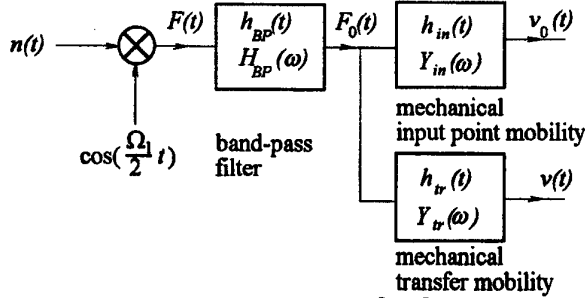


Figure 2. The linear system and in and outputs.  $\{n(t)\}$  is a stationary

stochastic process,  $\cos \frac{\Omega_1}{2} t$  a deterministic function and the force  $\{n(t)\} \cdot \cos \frac{\Omega_1}{2} t$  a nonstationary process.

The velocity response  $v(t)$  in an observation position  $\mathbf{r}$  is

$$v(t) = h * \left( n(t) \cos \frac{\Omega_1}{2} t \right) \quad (4.)$$

where the star denotes convolution and  $h$  is the band-pass filtered impulse-response i.e.

$$h = h_{tr}(t, \mathbf{r}, \mathbf{r}_0) * h_{BP} \quad (5.)$$

$h$  could include all linear distortions (e.g. of loudspeakers).

The ensemble average over many realisations of the squared velocity response process is

(Using the calculation trick  $\left( \int dx \right)^2 = \int dx_1 \int dx_2$ ):

$$\begin{aligned} E\{v^2(t)\} &= \\ &= \int_{-\infty}^{\infty} \int_{-\infty}^{\infty} E \underbrace{\{n(t-x)n(t-y)\}}_{=\delta(x-y)} \cdot \cos \frac{\Omega_1}{2} (t-x) \cos \frac{\Omega_1}{2} (t-y) h(x) h(y) dx dy = \\ &= h^2 * \cos^2 \frac{\Omega_1}{2} (t) \end{aligned} \quad (6.)$$

where it is used that the auto-correlation of white noise is a Dirac delta function.

The Fouriertransform of the squared impulse-response is essentially the complex modulation transfer function (CMTF), which is defined by Schröder (1981) and Polack and Schröder (1984) as

$$CMTF(\Omega) = \int_{-\infty}^{\infty} h^2(t) e^{-j\Omega t} dt \cdot H_{LP}(\Omega) \quad (7.)$$

where  $H_{LP}$  is an ideal low-pass filter. The CMTF can be computed by post-processing the impulse-response by squaring followed by Fouriertransforming.

If two plates of area  $S_1$  and  $S_2$  and of equal mass per unit area are coupled, then

$$\frac{\langle CMTF(\Omega, \mathbf{r}_0) \rangle_{21} \cdot S_2}{\langle CMTF(\Omega, \mathbf{r}_0) \rangle_{11} \cdot S_1} \quad (8.)$$



will be strongly related at low frequencies to the SEA expression in (3).  $\langle \rangle$  denotes spatial average, the right index in the double subscripts denotes the externally excited plate and the left the observed. Let the result of a fit of (8) to a system where the orders of the denominator and numerator polynomials are given and equal to 1 and 0, respectively, be the coefficients in the expression

$$\frac{b_0}{j\Omega + a_0} \quad (9.)$$

Identification yields that the following pairs are related:

$$\begin{cases} \omega_0 \eta_{21} \leftrightarrow b_0 \\ \omega_0 \eta_2 \leftrightarrow a_0 \end{cases} \quad (10.)$$

Incidentally one may derive an expression corresponding to (6) for the instantaneous input power  $\Pi(t) = F_0(t)v_0(t)$ , see appendix.

### 3. State of method development

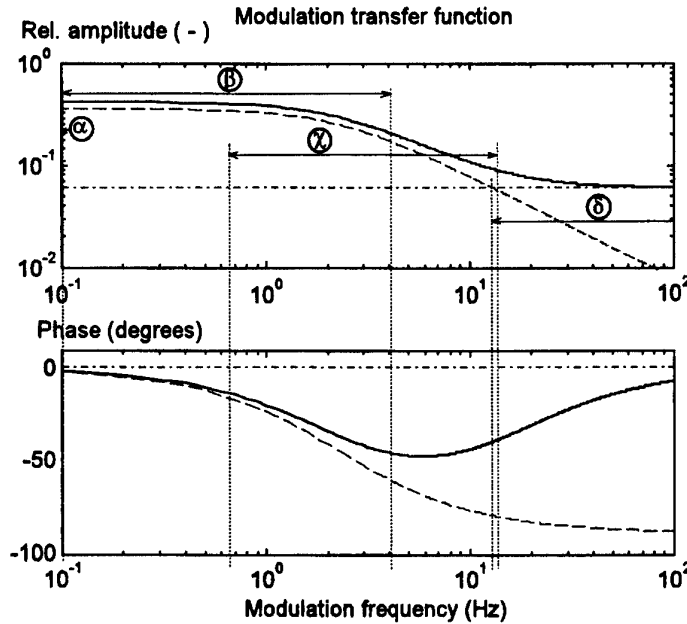


Figure 3. Idealised modulation transfer function representing the resonant (reverberant) field (—), the direct field (---) and the total field (— · —).  $\omega_0 \eta = 13.8$  (1/s) and  $t_f = 0.001$ s, see section 4.

Ranges of applicability:

- (a) SEA
- (b) Quasi steady-state SEA. The upper limit is approximate
- (c) [0.63, 12.5] Hz, range for calculation of Speech Transmission Index (STI). A different application of the CMTF is in room acoustics. There is a procedure to convert CMTF data into a

single figure called the "speech transmission index" (STI). It has been shown that the STI is very closely related to speech intelligibility

⑤ Direct field modulation is dominant. At the left end of the range, the magnitudes of the modulation of the direct and the reverberant field are equal, which could define a "modulation direct field radius", see section 4.

Up to now, the method has been used for estimation of SEA coupling and dissipation loss factors in built up structures and rooms, see Fahy and Ruivo (1997), Lundberg (1997). Till now, the method has been used rather heuristic in range ⑤ see figure 3, which upper limit arbitrary has been chosen to where the phase-function is approximately  $-\pi/4$ .

#### 4. The direct field and the modulation transfer function

Let the squared impulse response consists of two parts, the direct field and a purely exponential reverberant field (Houtgast T. et al (1980)):

$$h^2(t) \propto \frac{const.}{|r - r_0|^2} \cdot \delta(t) + e^{-\omega_0 \eta (t - t_i)} \theta(t - t_i) \quad (11.)$$

$t_i$  is the initial time delay gap,  $\theta(t)$  the Heaviside's unit step function,  $\delta(t)$  Dirac's delta function and  $\omega_0 \eta = 13.8 / T$ , where  $T$  is the reverberation time.

The direct field is attenuated with the distance from the source. A point source in a room will have a direct field that decreases at 6 dB per doubling of distance. The CMTF results from application of (7):

$$CMTF(\Omega) \propto \frac{const.}{|r - r_0|^2} + e^{-j\Omega t_i} \frac{1}{j\Omega + \omega_0 \eta} \quad (12.)$$

The part referring to the direct field is modulation frequency-independent and constitutes a "floor" for the amplitude of the CMTF. At higher modulation frequencies the contribution of the direct field becomes significant, as is shown in the example in figure 3, where the ratio between the energy in the direct field to the reverberant field is 0.17. The distance where the magnitudes of the modulation of the direct field and the reverberant field are equal, could be called "modulation direct field radius". Derived from (12) and normalised on the ordinary direct field radius, it is equal to

$$\left( \left( \frac{\Omega}{\omega_0 \eta} \right)^2 + 1 \right)^{1/4} \quad (12.)$$

When estimating SEA parameters, the contribution from the modulation of the direct field should not be dominating.

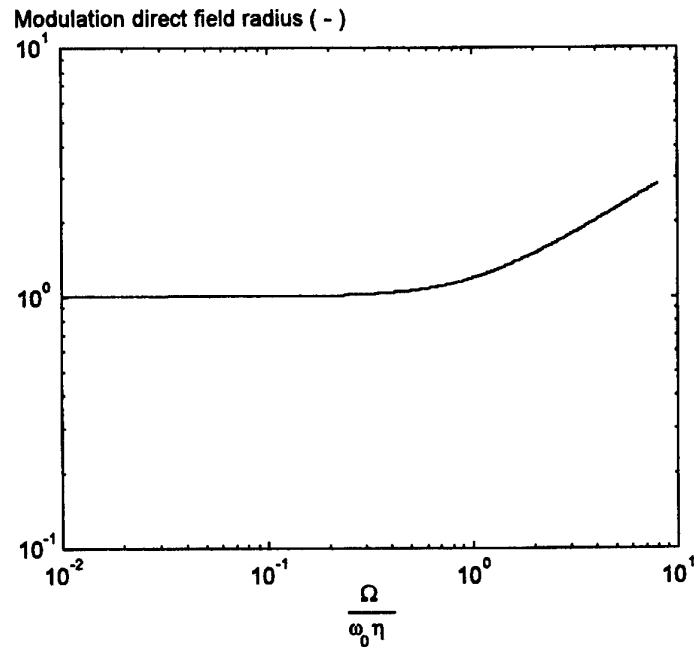


Figure 4. The modulation direct field radius (normalised). Incidentally this has applications at investigations of slit leakage.

### 5. Subsystem modulation homogeneity

In experiments on structures and rooms it has been observed that within the subsystems the relative variance of the amplitude and phase of the *CMTF* increases as the modulation frequency rises.

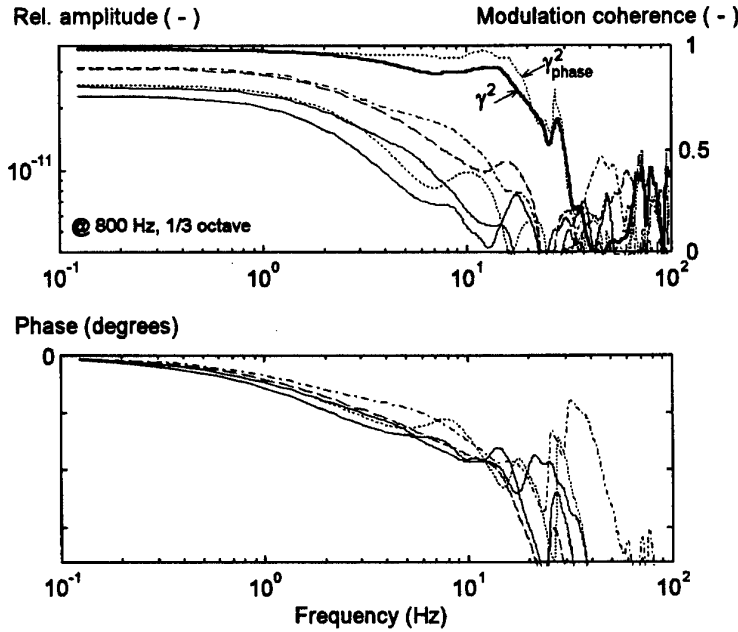


Figure 5. CMTF's for five observation positions, one source position. From experiments on a steel-plate of area 1.7 m<sup>2</sup> and thickness 2 mm. The right-hand ordinate represents the modulation coherence as specified by (13) and (14).

It is important that the model behaviour of the physical system holds above the crossover frequency, else there is no point in doing the parameter estimation. The spatial homogeneity could be quantified by a computed modulation coherence function

$$\gamma^2(\Omega, \mathbf{r}_0) = \frac{\left| \sum_{k=1}^n \text{CMTF}(\Omega, \mathbf{r}_k, \mathbf{r}_0) \right|^2}{n \sum_{k=1}^n |\text{CMTF}(\Omega, \mathbf{r}_k, \mathbf{r}_0)|^2} \quad (13.)$$

where the summation is over the observation positions. Fahy and Ruivo (1997) have pointed out that the modulation phase dispersion phenomenon appears to place considerable doubt on the validity of extension of the SEA equations to represent non-stationary vibrational energy flow between subsystems. Also a modulation "phase coherence" function could be computed from

$$\gamma^2_{\text{phase}}(\Omega, \mathbf{r}_0) = \frac{1}{n} \sum_{k=1}^n \frac{|\text{CMTF}(\Omega, \mathbf{r}_k, \mathbf{r}_0)|^2}{|\text{CMTF}(\Omega, \mathbf{r}_k, \mathbf{r}_0)|} \quad (14.)$$

The SEA-model designer must group modes that are "similar" together. It is possible that the modulation transfer function could be used as a "tool" for this:

- The quotient between modulation transfer functions (same source) at two observation positions supposed to be within the same subsystem, should be flat and not differ to much from unity, up to a frequency above the crossover frequency.
- The slopes of the amplitude and phase-function of the high frequency asymptote of a power-energy transfer function in the SEA model tell the number of subsystems "in between" the observed one and the directly driven.

## 6. Propagation delay between subsystems

In the SEA power balance equations for two coupled rooms, the energy incident to the coupling area is assumed to be immediately available for absorption and transmission by the other system. But physically this is not the case due to the finite energy velocity. Assume there is a delay  $\Delta t$  between the subsystems which is estimated by the travel time between the centroids of the systems (Lyle 1981). Then in the power balance of system 2,  $E_1(t)$  should be replaced by  $E_1(t - \Delta t)$  (and in the balance of system 1,  $E_2(t)$  by  $E_2(t - \Delta t)$ ). In the frequency domain this corresponds to a multiplication by  $e^{-j\Omega\Delta t}$  and then

$$\left( \frac{\hat{E}_2}{\hat{E}_1} \right)_{\Omega_1} = \frac{\omega_0 \eta_{21}}{j\Omega + \omega_0 \eta_2} \cdot e^{-j\Omega\Delta t} \quad (15.)$$

To make (15) a minimum-phase-shift function, a phase lead compensation,  $e^{j\Omega\Delta t}$ , could be introduced. This is done in an experiment with two coupled rooms, see next section.

## 7. Airborne sound insulation measurement

In the International Standard for measurements of airborne sound insulation between rooms, ISO 140-3, the equivalent absorption area in the receiver room is evaluated from a separate measurement of e.g. the reverberation time. Additionally, if the background level in the receiving room is larger than the sound pressure level due to the sound source, a precise value of the latter cannot be determined. However the estimation of the equivalent absorption area is time consuming and the desire to get received sound levels 10 dB above the background noise level makes demands upon the source.

The energy density in a wave is  $I/c$  and the total energy in the receiving room is  $I_2(t)V/c$ . Under the assumption of diffuse sound fields, the power balance equation for the receiving room in a specific frequency band is:

$$\frac{d}{dt} \left( \frac{I_2(t)}{c} V \right) = \frac{I_1(t)}{4} \cdot S \cdot \tau - \frac{I_2(t)}{4} \cdot A \quad (16.)$$

Taking the Fourier transform of (16) one obtains:

$$j\Omega \cdot \frac{\hat{I}_2(\Omega)}{c} V = \frac{\hat{I}_1(\Omega)}{4} S \cdot \tau - \frac{\hat{I}_2(\Omega)}{4} A \quad (17.)$$

Rearranging (17) yields:

$$\frac{\hat{I}_2(\Omega)}{\hat{I}_1(\Omega)} = \frac{S \cdot c \cdot \tau}{4V} \cdot \frac{1}{j\Omega + \frac{Ac}{4V}} \quad (18.)$$

Let

$$\frac{\langle CMTF(\Omega, \mathbf{r}_0) \rangle_{21}}{\langle CMTF(\Omega, \mathbf{r}_0) \rangle_{11}} \quad (19.)$$

be fitted to (9). Identification yields:

$$\tau \leftrightarrow \frac{b_0 4V}{S \cdot c} \quad (20.)$$

$$(\text{and } A \leftrightarrow \frac{a_0 4V}{c})$$

### 7.1. EXPERIMENTS IN TWO COUPLED ROOMS

Twelve observation positions in each room were used and one source position. The pressure impulse-responses in the standardised one-third octave bands with centre frequencies 100 to 3150 Hz were measured. The test signal was a maximum length sequence of length 65535. It is deterministic and periodic and its period length is matched to the record length of the analyser. The sampling frequency in the bands 100 - 800 Hz was 4000 Hz and the record length 16.384 s giving a frequency resolution of 0.061 Hz.

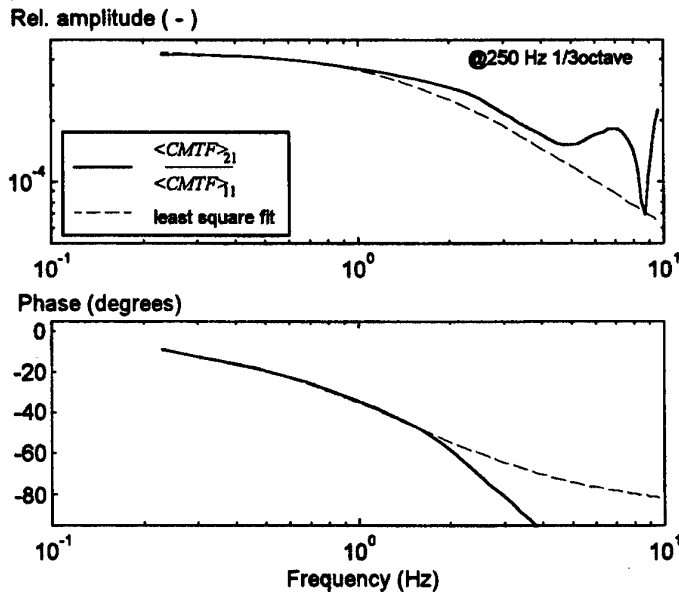


Figure 6. The quotient (19) in a specific band and a least-square fit.

The impulse-responses were post-processed in Matlab according to eq. (7) by  $CMTF = \text{fft}(h.^2)$ ; In figure 6, the solid line is the mean of the  $CMTF$ 's in the receiving room divided by the mean of the  $CMTF$ 's in the driving room. The model first order curve, denoted by the dash line, is fitted to the low frequency part of the solid line using the function `invfreqs` in Matlab Signal Processing Toolbox:

$[b,a] = \text{invfreqs}(\text{mean}(CMTF21(1:n))/\text{mean}(CMTF11(1:n)), w(1:n), 0, 1)$ ;  $b$  and  $a$  will contain the coefficients of the numerator and denominator polynomials, respectively,  $w$

is the frequency vector and "0" and "1" specify the desired orders of the numerator and denominator polynomials. The *CMTF*'s are truncated at  $n$ , corresponding to the frequency where the phase-function is approximately  $-\pi/4$ .

In another computation, a phase lead compensation,  $e^{j\Omega t_\Delta}$ , where the delay was put to  $t_\Delta = 7.8/340$ s, was multiplied with (19) before the fit procedure. In figure 7 and 8 the corresponding results are denoted "compensated".

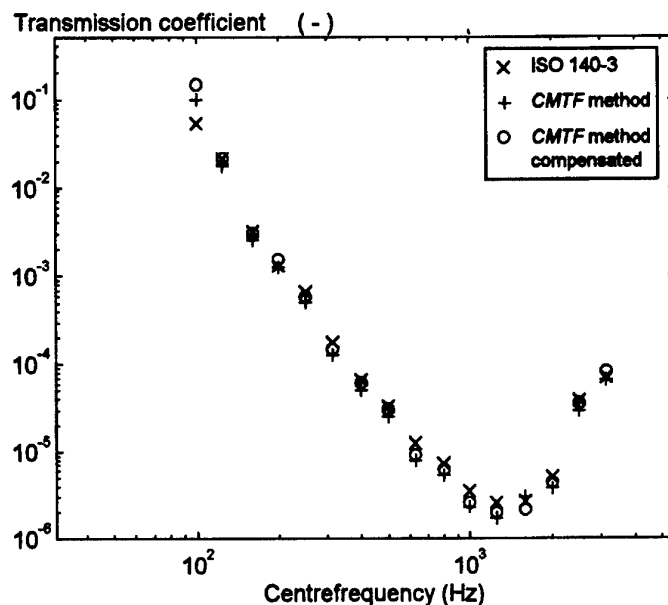


Figure 7. The transmission coefficient.

The results of the *CMTF* method are systematically smaller than those from ISO 140-3, with exception of the bands 100 Hz and 1600 Hz.

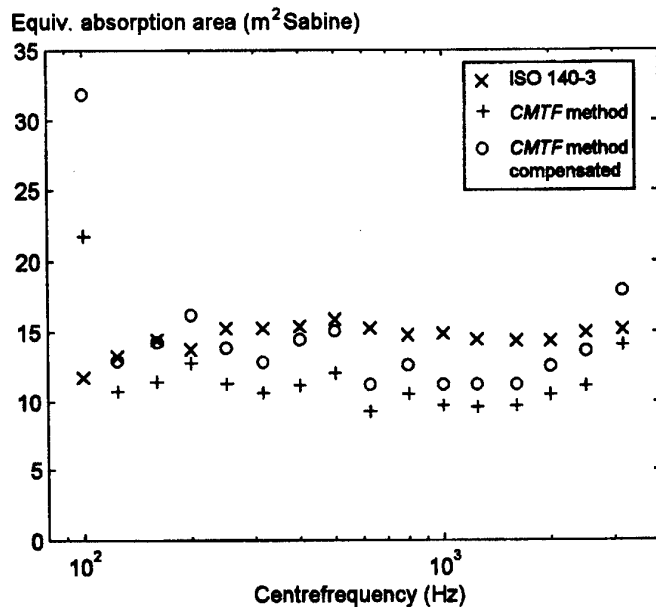


Figure 8. The equivalent absorption area.

The linear system description provides the opportunity for reducing the influence of the background noise and narrow-band analysis, see figure 9.

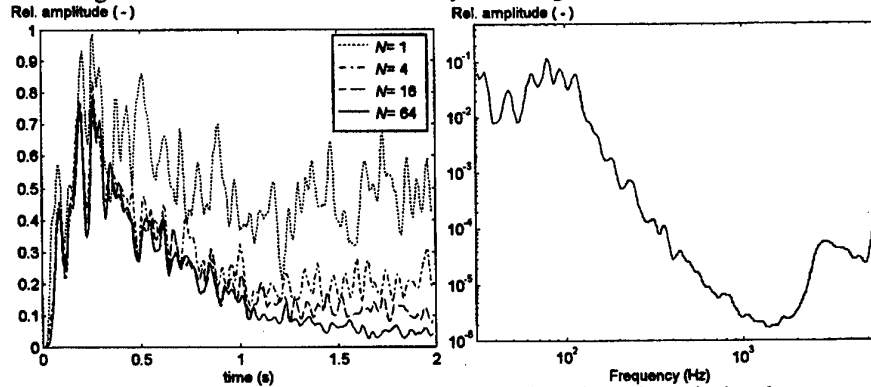


Figure 9. Left: Increasing the Signal-to-Noise Ratio by time averaging  $N$  times. The graphs show the impulse-response (envelopes smoothed) in a position in the receiving room, in a one-third octave band with centre frequency 1000 Hz. The SNR when  $N=1$  is equal to -8 dB.

Right:  $\frac{\langle |Z(\omega, r_0)|^2 \rangle_{21}}{\langle |Z(\omega, r_0)|^2 \rangle_{11}}$ , where  $Z$  are the acoustical transfer impedances. The expression is frequency smoothed with a sweeping Gauss-window of constant-percentage bandwidth (3 %).



## 9. References

- Fahy F.J. and Ruivo H.M. (1997) *Determination of Statistical Energy Analysis Loss Factors by Means of an Input Power Modulation Technique* to be published in Journal of Sound and Vibration
- Houtgast T. et al (1980) *Speech intelligibility in rooms. Part 1. Acustica* 46, 60-72
- Lindblad S. (1974) *Analytical models report 54*, dissertation Building Acoustics, Lund Institute of Technology, Lund, Sweden
- Lundberg K-O. (1997) *A method for estimating SEA loss factors Acustica united with acta acustica*, 83, 1-9
- Lundberg K-O. (1997) *A method for estimating SEA loss factors applied on a structure submitted to Acustica united with acta acustica*
- Lyle C.D. (1981) *An improved theory for transient sound behaviour in coupled diffuse spaces Acoustics Letters* 4, no 12
- Polack J-D. Schröder M.R. (1984) *The modulation transfer function of music signals and its applications to reverberation measurements, Acustica* vol. 54, 257-265
- Schröder M.R. (1981) *The modulation transfer function: Definition and measurements Acustica* 49, 179-182

## APPENDIX

Proceeding in a manner indicated by (6) it can be shown that the ensemble average is

$$E\{\Pi(t)\} = ((h_{in} * h_{BP})h_{BP}) * \cos^2 \frac{\Omega_1}{2}(t) \quad (A1)$$

Then in the frequency domain, the quotient between the kinetic energy density and the input power is equal to:

$$\frac{\mathcal{F}\left\{\frac{\rho}{2}(h_{tr} * h_{BP})^2\right\}}{\mathcal{F}\left\{((h_{in} * h_{BP})h_{BP})\right\}} \quad (A2)$$

where  $\mathcal{F}$  is the Fourieroperator and  $\rho$  the density.

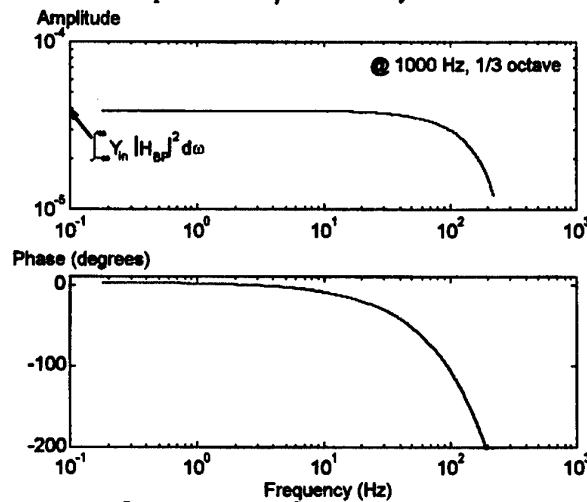


Figure A1.  $\mathcal{F}\left\{((h_{in} * h_{BP})h_{BP})\right\}$ . From experiments on a steel-plate of area 1.7 m<sup>2</sup> and thickness 2 mm.

## AN INDICATOR OF COUPLING STRENGTH BETWEEN SEA SUBSYSTEMS

F. J. FAHY

ISVR

University of Southampton

Southampton SO17 1BJ, UK

P. P. JAMES

Société Européenne de

Propulsion,

Vernon, France

### 1. Introduction

A judicious choice of subsystems for an SEA model is essential to the reliability of both theoretical and experimental applications of SEA. Although there exist no universally established criteria or guidelines on which to base this crucial fundamental decision, it is generally recommended that the chosen subsystems should be 'weakly coupled' to their immediate neighbours. Here too, there is no universally accepted definition or criterion of 'weak' coupling [1]. Among previously proposed weak-coupling conditions are the following: (i) coupling loss factors (CLFs) of a subsystem much smaller than its internal (dissipation) loss factor [2]; (ii) wave power transmission coefficient  $\tau_{ij}$  across a subsystem interface much less than unity; (iii)  $\tau_{ij}/2\pi^2 M_i M_j \ll 1$ , where  $M_i$  denotes modal overlap factor of subsystem  $i$  [3,4]; (iv) Green functions (or frequency response functions) of an uncoupled subsystem little affected by coupling to the rest of the system [5,6].

Although it is not clear which, if any, of these is most the appropriate, the *desiderata* associated with weak coupling may be expressed in qualitative terms as follows: (i) a substantial difference between the modal-average energy of a subsystem which directly receives input power from an external source and that of any other subsystem which is not directly excited; (ii) coupling loss factors between directly coupled subsystems much greater than those between subsystems separated by other interposed subsystems; (iii) frequency-average coupling loss factors which correspond closely with those based upon the wave power transmission coefficients between the corresponding infinitely extended (non-modal) subsystems; (iv) coupling loss factors insensitive to subsystem damping.

These conditions militate against the existence of 'global' modes which have significantly different natural frequencies from those of the uncoupled subsystems and in which modal energy is distributed over two or more subsystems. Under conditions of weak coupling, the system modes are 'localised' in the sense that they closely resemble in natural frequency and shape the modes of the uncoupled subsystems (given the appropriate boundary conditions), and that their energies reside principally within the corresponding subsystems. The modes of many practical structures, particularly those which are highly non-uniform (e.g. beam-stiffened), constitute a mix of global and local modes, a state which offers a serious difficulty for SEA modellers (this problem is currently being addressed by the development of hybrid global/local models).

## 2. Coupling strength and experimental SEA

Experimental SEA has two principal modes of application: (i) Determination of internal and coupling loss factors on the basis of controlled excitations; (ii) Inference of input powers on the basis of an SEA model derived in the laboratory together with estimates of subsystem response energies derived from vibration measurements made during system operation [7].

The first mode is implemented by means of the power injection technique, in which broad band forces are applied sequentially at a number of different points on each subsystem and, for each input point, the resulting responses are measured at a rather large number of points on each subsystem. The power inputs and response energies are estimated from signals generated by force and acceleration transducers. Alternatively, the equivalent powers and energies are derived from the Fourier transforms of applied impulsive forces and the resulting transient responses. Determination of the loss factors requires inversion of the matrix of estimated energies. Strong coupling between selected subsystems produces a matrix which is ill-conditioned for inversion because the associated subsystems tend to a state of equipartition of modal energy, and some of the off-diagonal elements can equal, or even exceed, the diagonal elements. The elements of the energy matrix are subject to uncertainty associated with spatial sampling error, spectral estimation error and with the assumption of equivalent mass which is employed to convert estimates of measured response velocities to kinetic energy. This uncertainty is propagated throughout the inverted matrix and often leads to serious errors in the estimates of loss factors: it is not uncommon for negative loss factors to emerge.

Strong coupling between any one or more pairs of subsystems is clearly undesirable. Unfortunately, the presence of strong coupling is usually detected only after a lengthy, time consuming measurement exercise has been completed. The following sections describe the results of an attempt to develop a rapid, preliminary test for subsystem coupling strength which is applied prior to implementation of the power injection method. The aim is to provide SEA experimenters with an indicator which 'sounds the alarm' when strong coupling is detected.

## 3. Energy impulse response

At the beginning of the research programme which led to the development of the indicator proposed herein it was decided that the most appropriate of the previously mentioned conditions associated with a state of weak coupling is that of Langley [5,6], since it relates to the existence, or otherwise, of global modes which involve highly correlated motions in two, or more, contiguous subsystems. This condition violates one of the principal assumptions of SEA, namely that all modal responses are uncorrelated. The employment of a number of 'randomly' located excitation points on each subsystem may provide an approximation to uncorrelated modal forces, as required by SEA theory, but it does nothing to mitigate the disruptive effect of the presence of global modes. [Note: it is not appropriate to attempt to overcome this difficulty by an appeal to notions of ensemble statistics in relation to tests on *single* physical samples].

However, it is not practicable to attempt to quantify the effect of subsystem coupling on Green functions in the frequency domain [8]. Uncoupled subsystems are not usually available and the question of appropriate boundary conditions is problematic. Consequently, attention has been directed to the response behaviour in the time domain. It seemed likely, on physical grounds, that the impulse response of a directly-excited subsystem would closely resemble that of another subsystem to which it is strongly coupled, but would differ significantly from that of another subsystem to which it is weakly coupled in terms of the wave power transmission coefficient. This 'hunch' was partly stimulated by the results of early work on the impulse response behaviour of coupled oscillators [9,10] and more recent work on transient SEA by Pinnington and Lednik [11]. A programme was initiated to investigate whether the postulated difference exists and, if so, how it could be quantified to form the basis of an 'indicator' of coupling strength.

SEA employs subsystem energy as the expression of vibrational state, and because it is common practice to measure structural response with accelerometers, from which kinetic energy density can be estimated, it was decided to investigate by means of theoretical analysis the temporal evolution of the kinetic energies of a number of simple subsystems consequent upon impulsive excitation. Vibrational kinetic energy is an oscillatory quantity, unlike total energy, so it was necessary to devise a procedure for suppressing these oscillations, while retaining the longer-time-scale evolution of the total energy. The impulse responses were Fourier Transformed, band-pass filtered and Inverse Fourier Transformed; the resulting filtered impulse responses were squared, scaled appropriately to give subsystem energies, and the time-histories of the kinetic energy were integrated over a time interval which was twenty times the inverse of the lower frequency limit of the band: the start of this time interval was moved along the time axis to produce a 'temporal moving average', or envelope, of the kinetic energy: examples are presented in Fig. 1. [Note: the integration interval was selected on an *ad hoc* basis.]

#### 4. Theoretical models

Systematic parametric studies have been made of a number of models of idealised subsystems of which the vibrational behaviour admits closed form analytic solutions [8]. The first model comprises a pair of uniform elastic rods of length, supporting quasi-longitudinal waves. Each rod is clamped at one end and coupled at the other end by an elastic spring of which the strength is systematically increased. One subsystem is subjected to an Dirac force impulse. When the spring is very strong, the energy impulse responses of both subsystems exhibit the simple exponential decay; with very weak coupling, the energy impulse response of the indirectly-excited rod exhibits a clear build up to a peak, followed by a decay, as shown in Fig. 1. The time delay to the peak is normalised on the characteristic time for wave energy to travel the length of the excited rod; it is denoted by  $\theta$ .

A study of the variation of  $\theta$  with non-dimensional spring strength  $\kappa$  for a rod length ratio of 3/7 shows that, over a large range of 'low' spring stiffness,  $\theta$  remains constant. As the spring stiffness is increased beyond a certain value,  $\theta$  falls rather rapidly and approaches zero, as shown in Fig. 2. Analysis of the natural frequencies and mode shapes of the coupled system shows that in the range of  $\kappa$  when  $\theta$  falls sharply,

the vibrational behaviour of the system changes from that of two clamped-free rods to a single clamped-clamped rod, suggesting that the fall in  $\theta$  indicates a transition from local to global modal behaviour. Fig. 2 also shows the variation of  $\theta$  with  $\kappa$  for a rod length ratio of 1/2. In this case,  $\theta$  remains close to zero over the whole range of spring strength. Subsequent studies revealed that the reason for this marked difference in behaviour lies in the fact that there is *coincidence* between the natural frequencies of at least one pair of the *uncoupled* (clamped-free) modes of the rods in the first case, but not in the second. The time-histories of the power transferred from the directly-driven rod to other rod in the two cases is presented in Fig. 3; there is a clear morphological and quantitative distinction between the two forms.

The variation of  $\theta$  with coupling spring stiffness was also studied for pairs of subsystems consisting of beams and also pairs of thin, flat, rectangular plates [8]. The characteristic fall, which was assumed to indicate the transition between weak (local mode) and strong (global mode) behaviour, is observed in all cases, *provided that coincidence exists between at least one pair of uncoupled modal natural frequencies*. Also studied was a system consisting of two end-connected rods of different cross-sectional area which support quasi-longitudinal waves. Conditional upon 'modal coincidence', the transitional fall in  $\theta$  is observed, the value approaching zero for an area ratio of unity (no discontinuity). The relevant uncoupled natural frequencies are those corresponding to a free boundary condition at the coupled end for the thicker rod and a fixed boundary condition for the thinner rod. This observation is important because it demonstrates that the definition of 'uncoupled' in the present context depends upon the form of constraint offered by one subsystem to the other when coupled.

The fact that no significant time delay to the peak of the energy impulse is observed if modal coincidence does not occur in a selected frequency band, *however weak the coupling*, would appear to present a serious obstacle to the feasibility of basing an indicator of coupling strength on this delay. Subsequent studies, however, indicate that the problem is more of academic interest than practical significance.

## 5. An indicator of coupling strength

Although the non-dimensional time delay to the peak of the kinetic energy impulse response is sensitive to coupling strength, subject to satisfaction of the condition of modal coincidence, it is also sensitive to subsystem damping. Since the purpose of the research was to seek a universal indicator of coupling strength which exclusively relates to the facility with which waves cross subsystem interfaces, it was necessary to suppress the effect of subsystem damping. This was achieved by defining a new non-dimensional quantity denoted by  $C_S$  as illustrated by Fig. 4. Evaluation of  $C_S$  for the idealised systems described above revealed a remarkable degree of uniformity of form and of values associated with very weak coupling, irrespective of system topology and wave type, as illustrated by Fig. 5, and a fair degree of immunity to large changes of damping (Fig. 6). On the basis of these analyses, we postulate a 'threshold' for  $C_S$  of 0.07, and suggest that values below this serve a warning that the choice of subsystems may not be appropriate.

## 6. The modal coincidence problem

As described above, a significant time delay to the peak of kinetic energy was observed only if the natural frequencies of at least one pair of uncoupled subsystem modes were equal (coincident), irrespective of the coupling strength. If this very restrictive condition were strictly necessary,  $C_S$  would be of little practical use, since one would not know whether a value below 0.07 is due to lack of modal coincidence or to a condition of strong coupling. Physical reasoning suggests that perfect coincidence is unlikely to be necessary, and that a sufficient degree of modal *proximity*, may be sufficient. Consequently, a series of theoretical studies of this phenomenon have been made in order to develop a proximity criterion.

As a prelude to the analysis of extended, multi-mode subsystems, the behaviour of  $C_S$  for a pair of coupled, viscously damped, spring-coupled oscillators has been analysed. The variation of  $C_S$  with the strength of the coupling spring has been evaluated for a range of damping ratios representative of those exhibited by practical structures. The ratio of uncoupled natural frequencies has been varied by varying the mass of the indirectly-excited oscillator. Examples of the results are shown in Fig. 7. The upper asymptote of  $C_S$  is very similar to that for rods, beams and plates. The frequency ratio below which  $C_S$  falls below 0.07, even with weak damping, decreases as damping is increased. The most significant feature is the confluence of all curves close to the proposed threshold of 0.07. For a given damping, the value of spring strength corresponding to the threshold value of  $C_S$  does not change with frequency ratio. This characteristic reinforces the argument for the selection of this threshold value and for  $C_S$  as a valid indicator of the transition from strong to weak coupling. However, Fig. 7 does suggest that the value of spring strength which corresponds to this threshold is sensitive to damping: the implication is that coupling strength (in the present sense) produced by a given spring can be weakened by increasing subsystem damping.

A similar analysis has been carried out for two rectangular flat plates of equal width plates coupled along the interface by a combination of linear and torsional line springs. Because of the multi-mode nature of this system it is not possible to vary the frequency ratio systematically as it is for discrete oscillators; consequently the variation of  $C_S$  for two different plate length ratios was investigated. It was found that the value of the indicator varied considerably with locations of the points of force input and response measurement: consequently, a set of values for twenty five different combinations of input and output locations was computed. The mean and 90% confidence limits of  $C_S$  are presented in Fig. 8; the former as functions of the strength of the torsional coupling spring exhibit the same confluence behaviour as the oscillators. The damping could not be varied for reasons of unacceptable demands in computer run time. The observed spatial variability suggests that it may be necessary to measure  $C_S$  at a number of points in experimental evaluations.

The principal conclusion from these analyses is that *if modal proximity is adequate to ensure that  $C_S$  is greater than 0.07 in the case of very weak coupling, it will ensure that it remains above this threshold if coupling is not strong.* The vital implication is that a modal proximity criterion can be validly derived on the basis of models incorporating very weak coupling which are amenable to analytic approximations.

## 7. Derivation of a modal proximity criterion

### 7.1. WEAKLY-COUPLED OSCILLATORS

A closed form analytic solution is available for the impulse response of two spring-coupled oscillators in the limit of vanishingly small coupling [12]. This expression has been used to evaluate  $C_s$  as a function of the four variables  $\omega_1$ ,  $\omega_2$ ,  $\zeta_1$  and  $\zeta_2$  which represent the uncoupled natural frequencies and damping ratios of the oscillators. Combinations of these variables are sought that produce a value of  $C_s$  which exceeds 0.07 with very weak coupling: the associated domain is defined as that of 'modal proximity'. Fig.9 reveals that, if the damping ratios are held constant, the boundaries of the domain correspond to constant frequency ratio  $\omega_1/\omega_2$ , independent of  $\omega_1$ : the domain expands as damping is increased. With  $C_s$  as a function of three variables, the boundary of the domain of modal proximity can be determined as a surface, as illustrated by Fig. 10. Modal proximity is clearly related to combined oscillator bandwidth.

### 7.2 WEAKLY-COUPLED MULTI-MODE SUBSYSTEMS

A deterministic form of analysis is not appropriate to multi-mode systems because it cannot be generalised. Hence a statistical approach was adopted with subsystem asymptotic modal densities and modal-average loss factors as independent variables. The probability of occurrence degree of modal proximity in a frequency band is determined by the probability distribution of the minimum difference between uncoupled mode natural frequencies. On the basis of the conventional SEA assumption of uniform probability of occurrence of a natural frequency within a given frequency band, a Monte Carlo simulation procedure was used to generate frequency separation statistics for two independent distributions. The generated distribution closely resembled a gamma distribution having both mean and standard deviation given by  $1/2N_1N_2$ , where  $N_i$  is the expected number of natural frequencies in band  $i$ ; this, of course, depends upon modal density and selected bandwidth. Hence the frequency separation  $\Delta\Omega_{90}$  corresponding to 90% cumulative probability may be defined; this also depends upon bandwidth. Finally, a Modal Proximity Indicator may be defined as

$$M_p = \omega_{min} \min(|1-x_1|, |1-x_2|) / \Delta\Omega_{90}$$

where  $x_1$  and  $x_2$  are the frequency ratios which bound the modal proximity domain for the given assumed or measured loss factors (as shown in Fig.10) and  $\omega_{min}$  is the lower limit of the selected frequency band. If  $M_p$  is greater than unity, a value of  $C_s$  of less than 0.07 indicates the existence of strong coupling at a confidence level of 90%. Note that  $M_p$  is sensitive to damping through  $x_1$  and  $x_2$ .

### 8. Some tests of $M_p$

As mentioned in Section 4, values of  $C_s$  have been determined for various models of coupled idealised subsystems. Calculations of  $M_p$  for weakly coupled rods and beams produced values much less than unity, thereby confirming the observed sensitivity to

small geometric variations associated with low modal density, which makes  $C_S$  unreliable. Calculations of  $M_P$  have been made for a theoretical model of two rectangular, steel, flat plates vibrating in flexure and coupled along one edge by a combination of a linear and torsion line springs. They both have a width of 2.31m, a length of 2.95m, a thickness of 3mm, a modal overlap factor of 0.07 and a modal density of 0.75 modes/Hz. In a frequency range where  $N_1 = N_2 = 8$ ,  $M_P = 3.3$ . This indicates that the modal proximity criterion is satisfied and the value of  $C_S$  with weak coupling springs would be greater than 0.07 and insensitive to small variations of the plate length ratio. However, estimates of  $C_S$  for one pair of input and response points suggested that it was, in fact, sensitive to such variations [8]. Subsequent estimates of the values of  $C_S$  at 25 pairs of input and response points on the plate yielded 90% confidence limits of 0.079 and 0.188, which clearly indicates adequate modal proximity.

Experiments on a pair of flat steel plates coupled by a variable number of short steel straps [13] showed  $C_S$  to be a stable and reliable indicator of coupling strength which was insensitive to a range of selected bandwidths of between 50 and 200Hz, and to the addition of 1% of plate mass in the form of a concentrated mass.  $M_P$  varied between 2 in a 200 Hz band centred on 200Hz and 278 in the same bandwidth centred on 6900 Hz, confirming a high degree of modal proximity.

## 9. Conclusion

A novel indicator of coupling strength between SEA subsystems, denoted by  $C_S$ , is proposed. It is rapidly determined from the band-filtered impulse response of a subsystems when indirectly excited by another subsystem which is directly excited. Theoretical and experimental evidence suggests that  $C_S$  for a particular subsystem should be determined at a number of points on any one subsystem to yield a good estimate of the temporal evolution of the subsystem energy.  $C_S$  exhibits a form of variation with coupling strength which appears to be universal and independent of subsystem form and wave type. The upper value associated with very weak coupling also seems to vary little from system to system, provided that a modal proximity criterion is satisfied as indicated by a modal proximity indicator denoted by  $M_P$  which can be evaluated from estimates of the modal densities and loss factors of the subsystems concerned. Provided that  $M_P$  is greater than unity, a value of  $C_S$  below a defined threshold value indicates the existence strong coupling between selected subsystems in the form of global modes. This condition is not conducive to accurate experimental determinations of SEA parameters or to accurate theoretical SEA response predictions. An SEA model which exhibits this behaviour should be modified to integrate strongly coupled subsystems into one subsystem.

## Acknowledgement

The authors gratefully acknowledge the Société Européenne de Propulsion and the Centre National d'Etudes Spatiales for financing this work within the R&T programme.



## 10. References

1. Fahy, F.J and James, P.P.: Weak coupling in statistical energy analysis, *ISVR Technical Report No. 228*, University of Southampton, 1994
2. Chandiramini, K.L.: Some simple models describing the transition from weak to strong coupling in statistical energy analysis, *J. Acoust. Soc. Am.* **63** (1978), 1081-1083.
3. Finnveden, S. F.: Ensemble averaged vibration energy flows in a three element structure, *J. Sound Vib.* **187** (1995), 495-529.
4. Mace, B. R.: The statistical energy analysis of two continuous one-dimensional subsystems, *J. Sound Vib.* **166** (1993), 429-461.
5. Langley, R. S.: A general derivation of the statistical energy analysis equations for coupled dynamic systems, *J. Sound Vib.* **135** (1989), 499-508.
6. Langley, R. S.: A derivation of the coupling loss factors used in statistical energy analysis, *J. Sound Vib.* **141** (1990), 207-219.
7. Fahy, F. J.: Statistical energy analysis: a critical overview review, *Phil. Trans. R. Soc. London A* **346** (1994), 431-447
8. Fahy, F. J.: A study of the kinetic energy impulse response as an indicator of the strength of coupling between SEA subsystems, *J. Sound Vib.* **190** (1996), 363-383.
9. Mercer, C.A., Rees, P.L. and Fahy, F.J.: Energy flow between two weakly coupled oscillators subject to transient excitation, *J. Sound Vib.* **15** (1971), 373-379.
10. Newland, D.: Calculation of power flow between coupled oscillators, *J. Soun Vib.* **3** (1966), 262-274.
11. Pinnington, R. J. and Lednik, D.: Transient statistical energy analysis of an impulsively excited two oscillator system, *J. Sound Vib.* **189** (1996), 265-287.
12. Fahy, F. J. and James, P. P.: Evolution of the energy impulse response in the case of two very weakly coupled systems: a mathematical model, *ISVR Technical Report No. 243*, University of Southampton, 1995.
13. James, P. P. and Fahy, F. J.: A technique for the evaluation of strength of coupling between SEA subsystems: experiments with two coupled plates and two coupled rooms, *ISVR Technical Report No. 242*, University of Southampton, 1995. Accepted for publication in *J. Sound Vib.*

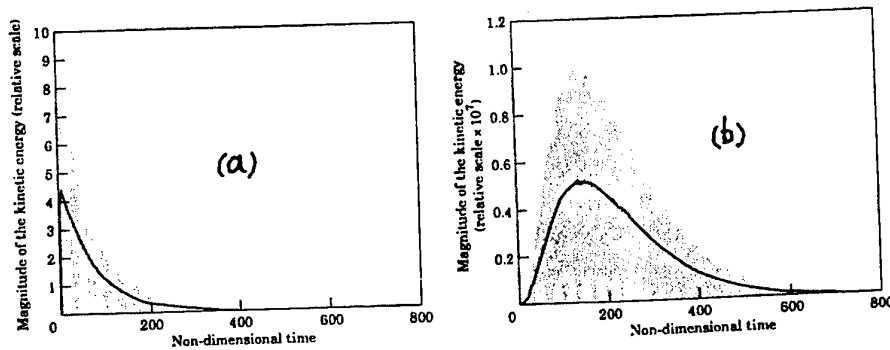


Fig.1 Kinetic energy impulse responses for weakly coupled subsystems: (a) directly-driven subsystem; (b) indirectly-driven subsystem.

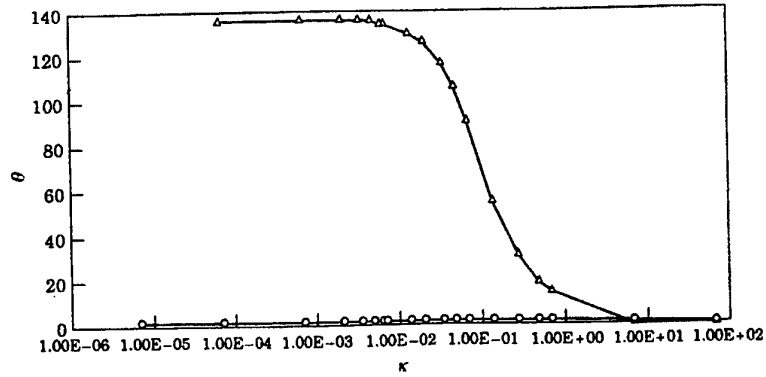


Fig.2 Variation of  $\theta$  with non-dimensional coupling spring strength  $\kappa$  for rods of length ratios 3/7 ( $\Delta$ ) and 1/2 (O).

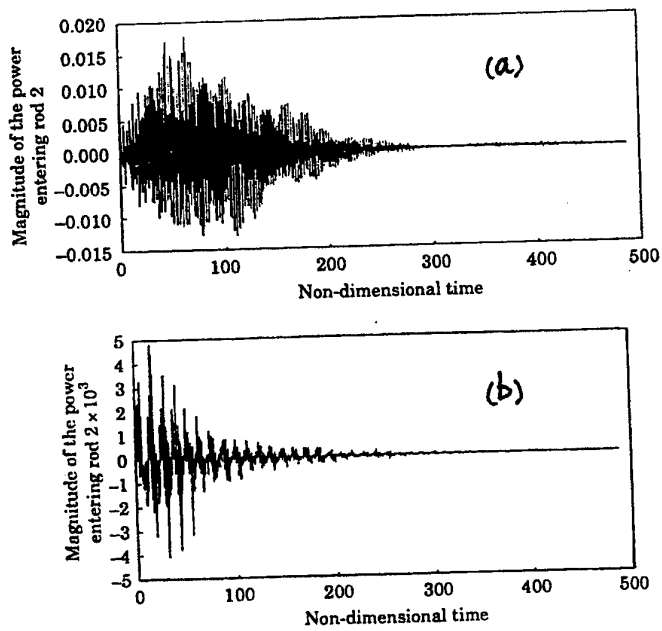


Fig.3 Temporal variation of transmitted power : (a) length ratio 3/7; (b) length ratio 1/2.

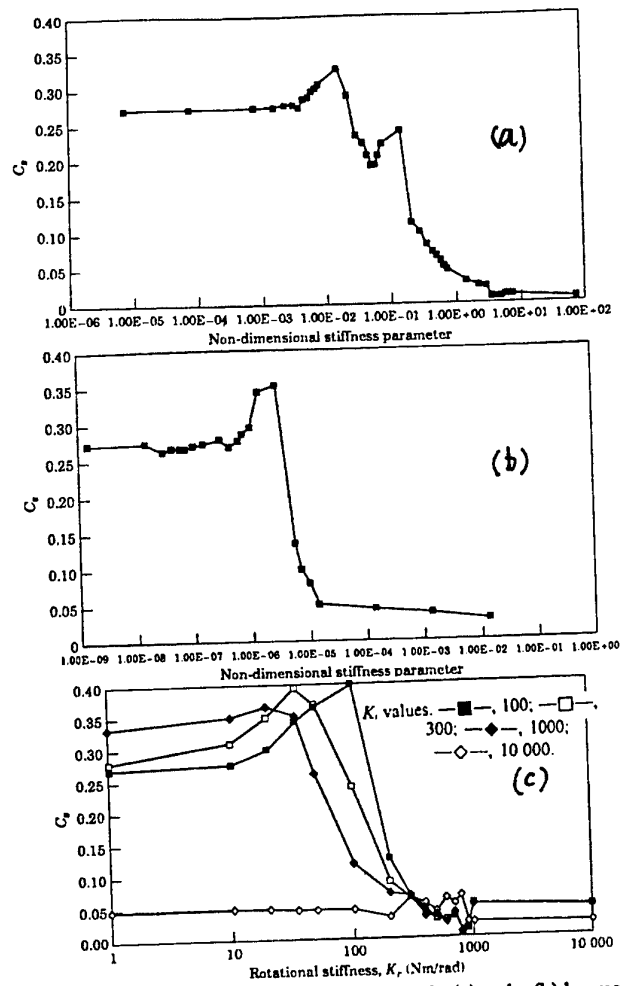


Fig.5 Variation of  $C_s$  with coupling spring strength: (a) rods; (b) beams; (c) plates

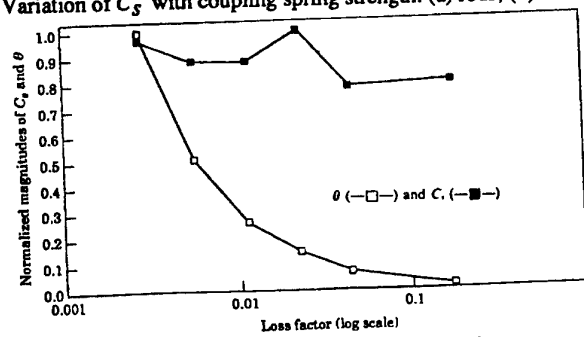
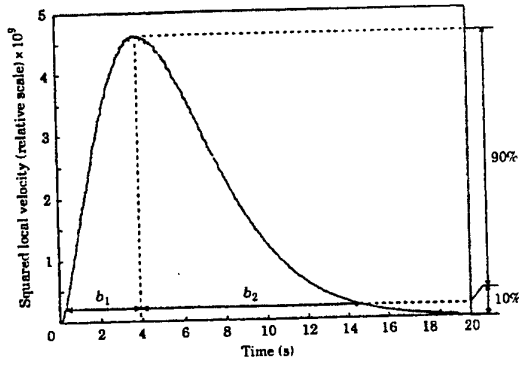
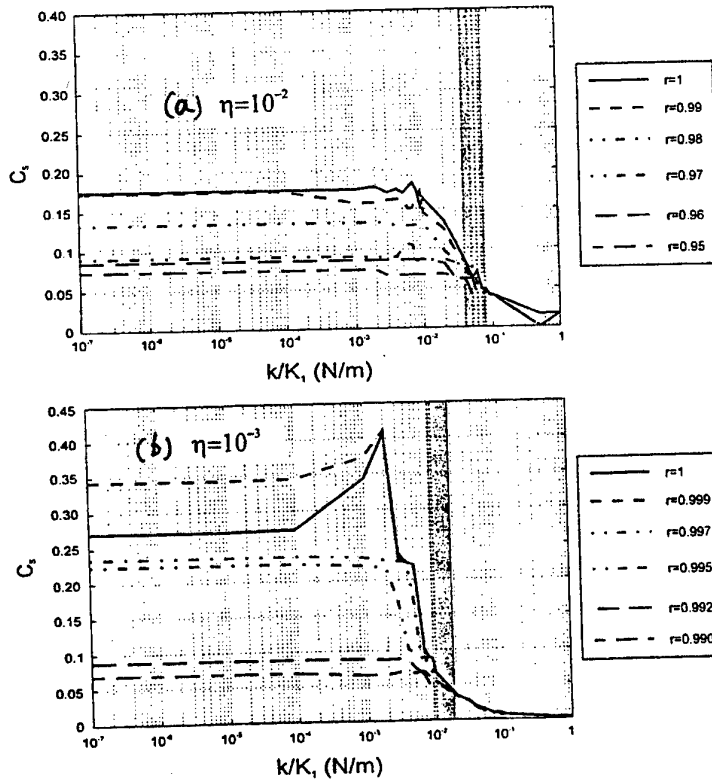


Fig.6 Variation of  $\theta$  and  $C_s$  with damping.

Fig.4 Definition of  $C_S$ Fig.7 Variation of  $C_S$  with non-dimensional coupling stiffness for a range of ratios of uncoupled oscillator natural frequencies: (a)  $\eta = 10^{-2}$ ; (b)  $\eta = 10^{-3}$ .

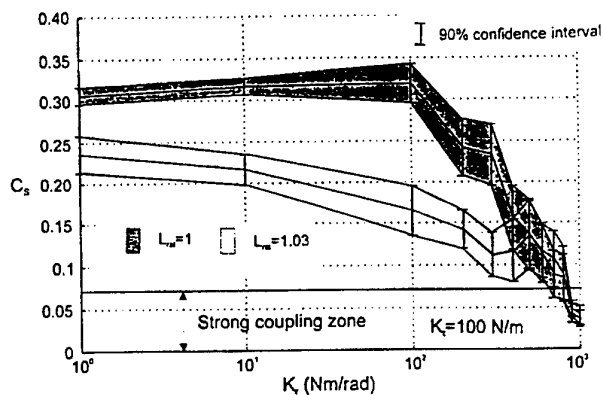


Fig.8 Variation of mean and 90% confidence interval of  $C_s$  for coupled plates with non-dimensional coupling spring strength for two plate length ratios.

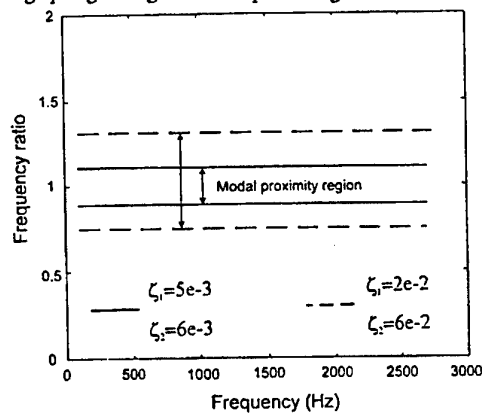


Fig.9 Frequency ratio bounds for modal proximity as a function of frequency for weakly coupled oscillators.

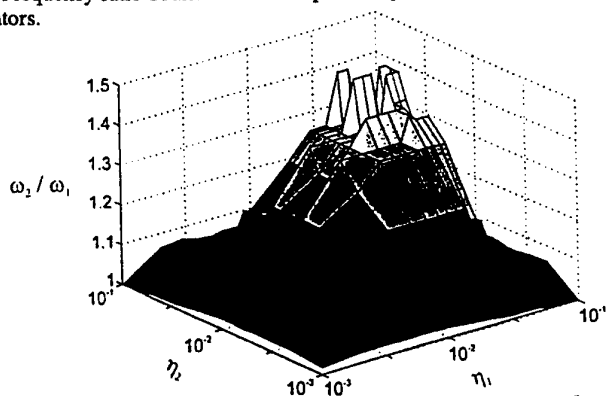


Fig.10 Bounding surface of modal proximity as a function of oscillator loss factors and uncoupled natural frequency ratio.

# ON THE CALCULATION OF CONFIDENCE LEVELS OF THE EXPERIMENTALLY DERIVED INTERNAL AND COUPLING LOSS FACTORS

L. HERMANS, K. DE LANGHE AND L. DEMEESTERE

*LMS International NV,  
Interleuvenlaan 68,  
3001 Leuven, Belgium*

## 1. Abstract

This paper deals with the statistical aspects of the Power Injection Method (PIM), a well-established technique to experimentally derive the SEA loss factor model. It is outlined how the variances of the energies measured in the power injection process can be obtained and how approximate analytical expressions describing the propagation of the energy variances through the loss factor calculation can be derived based on a first order Taylor expansion. The expressions giving the loss factor variances as functions of the energy variances offer the practical advantage that they can be quickly evaluated during the acquisition process. Subsequently, it is discussed how the confidence levels of the SEA predictions can be obtained. The practical usefulness and limitations of the derived analytical expressions are investigated based on a Monte-Carlo variability analysis. The statistical theory is then applied to a railway carriage of a high-speed train, illustrating how the effectiveness of loss factor modifications can be evaluated in terms of confidence levels.

## 2. Introduction

SEA is a high-frequency vibro-acoustic modeling technique which works with the averaged response taken in the time, frequency and spatial domain instead of local response variables. The successful application of SEA relies on a high modal density and high modal overlap to ensure that the average is a useful and reasonably accurate quantity [1]. SEA adopts the concept that the time averaged net power flow between two subsystems varies at a rate proportional to the difference in modal energy in a given frequency band and that the time averaged power internally dissipated in a subsystem is proportional to the total energy level of this subsystem. Both assumptions of proportionality give rise to the coupling and the internal loss factors which

constitute the basic SEA model. The global SEA equation is obtained by balancing the time averaged external power input to each subsystem with the power dissipated in the subsystem and the net power flows to the coupled subsystems. This results in the following equation :

$$\begin{bmatrix} \sum_{i=1}^N \eta_{1i} & -\eta_{21} & \cdots & -\eta_{N1} \\ -\eta_{12} & \sum_{i=1}^N \eta_{2i} & \cdots & -\eta_{N2} \\ \vdots & \vdots & \ddots & \vdots \\ -\eta_{1N} & -\eta_{2N} & \cdots & \sum_{i=1}^N \eta_{Ni} \end{bmatrix} \begin{bmatrix} E_1 \\ E_2 \\ \vdots \\ E_N \end{bmatrix} = \begin{bmatrix} \frac{P_1}{\omega} \\ \frac{P_2}{\omega} \\ \vdots \\ \frac{P_N}{\omega} \end{bmatrix} \quad \text{or} \quad [L]\{E\} = \frac{1}{\omega}\{P\} \quad (1)$$

where  $N$  is the total number of subsystems,  $E_i$  represents the time averaged total energy of the  $i$ -th subsystem,  $P_i$  is the time averaged power input to the  $i$ -th subsystem,  $\omega$  is the radian center band frequency,  $\eta_{ij}$  is the coupling loss factor between subsystems  $i$  and  $j$  and  $\eta_{ii}$  is the internal loss factor of subsystem  $i$ . The matrix  $[L]$  in equation (1), composed of the internal and coupling loss factors, is further referred to as the total loss factor matrix.

The Power Injection Method (PIM) is the most widely used technique to experimentally derive the SEA loss factor model without the need to disassemble the structure into components [2]. It basically comes down to exciting each subsystem in turn and measuring the response energies on all subsystems. The difficulty that arises in the experimental approach is the measurement of the total resonant energy of the  $i$ -th subsystem,  $E_{ij}$ , due to excitation in subsystem  $j$ . In order to cope with this, the vibrating or acoustical field is sampled at several discrete points. The measured point velocities or pressures are squared and spatially averaged to respectively yield the space averaged square velocity  $\langle \dot{X}_{ij}^2 \rangle$  or pressure  $\langle p_{ij}^2 \rangle$ . The brackets  $\langle \rangle$  denote the spatial averaging. For sake of simplicity, the variable  $\langle R_{ij} \rangle$  is introduced which represents  $\langle \dot{X}_{ij}^2 \rangle$  in case of a structural subsystem and  $\langle p_{ij}^2 \rangle$  in case of an acoustical subsystem. The energy of the  $i$ -th subsystem due to excitation in the  $j$ -th subsystem is then estimated by multiplying  $\langle R_{ij} \rangle$  with the total subsystem mass  $M_i$  or the subsystem volume  $V_i$  :

$$E_{ij} = M_i \langle R_{ij} \rangle \quad (\text{structural}) \quad \text{or} \quad E_{ij} = V_i \langle R_{ij} \rangle \frac{1}{\rho c^2} \quad (\text{acoustical}) \quad (2,3)$$

where  $\rho$  is the medium (mostly air) density and  $c$  the sound velocity in the medium. The total subsystem mass,  $M_i$ , in equation (2) can only be used in the calculation of the total energy for uniform structures of constant thickness (plate) or cross-section

(beam). In order to overcome this, it has been suggested to use the "equivalent" mass/volume in equations (2,3) instead of the real mass/volume [3].

The loss factors can be derived from the PIM-energies as follows [4] :

$$\begin{bmatrix} \sum_{i=1}^N \eta_{1i} & -\eta_{21} & \cdots & -\eta_{N1} \\ -\eta_{12} & \sum_{i=1}^N \eta_{2i} & \cdots & -\eta_{N2} \\ \vdots & \vdots & \ddots & \vdots \\ -\eta_{1N} & -\eta_{2N} & \cdots & \sum_{i=1}^N \eta_{Ni} \end{bmatrix} = \frac{1}{\omega} \begin{bmatrix} E_{11}^n & E_{12}^n & \cdots & E_{1N}^n \\ E_{21}^n & E_{22}^n & \cdots & E_{2N}^n \\ \vdots & \vdots & \ddots & \vdots \\ E_{N1}^n & E_{N2}^n & \cdots & E_{NN}^n \end{bmatrix}^{-1} \quad \text{or } [L] = \frac{1}{\omega} [E^n]^{-1} \quad (4)$$

where  $E_{ij}^n = \frac{E_{ij}}{P_j}$  denotes the normalized energy in subsystem i due to power input,  $P_j$ , in subsystem j.

Approximate formulas can also be derived on the basis that the energy in non-driven subsystems is significantly lower than in the directly driven subsystem (weak coupling assumption), guaranteeing positive loss factor values [5] :

$$\eta_{ij} \cong \frac{1}{\omega} \left( \frac{E_{ji}^n}{E_{ii}^n} \right) \left( \frac{1}{E_{jj}^n} \right) \quad \text{and} \quad \eta_{ii} \cong \frac{1}{\omega} \frac{1}{E_{ii}^n} \quad (5,6)$$

An important aspect of equation (5) is that it enables the coupling loss factors between two coupled subsystems to be calculated from measurements made only on those two subsystems, regardless of the other subsystems.

### 3. The Statistical Aspects of PIM

In the power injection process, each subsystem is excited at 3 or more points chosen at random in order to simulate statistical independence of the modes [2]. The responses at different locations are measured for each subsystem. Typically, about 5 to 10 response points per subsystem are measured. The square velocities/pressures are individually normalized by unity input power, subsequently linearly averaged and multiplied by the mass/volume, yielding the normalized energies  $E_{ij}^n$  appearing in equations (4) and (5,6).

The accuracy of the experimental SEA model will depend on the specific number of excitation and response points chosen on each subsystem. There will always be a certain spread associated with the normalized space averaged square velocity/pressure  $\langle R_{ij}^n \rangle$  due to the averaging of a finite number of values. Therefore, it is meaningful to calculate the associated confidence levels of  $\langle R_{ij}^n \rangle$  and to comprehend how these confidence levels can be translated into the confidence levels of the loss factors.



### 3.1. THE MEAN AND VARIANCE OF THE POPULATION OF THE NORMALIZED RESPONSES

The population of normalized square velocities/pressures which are dealt with in PIM are infinite because of an infinite number of potential excitation and response points. From the measurements, only a sample of normalized responses is obtained, each corresponding to a specific excitation and response point. If  $R_{ij,pq}^n$  denotes the normalized square velocity/pressure measured at response location  $p$  of the  $i$ -th subsystem due to excitation at location  $q$  of the  $j$ -th subsystem, the mean value and the variance of the population of the normalized square velocities/pressures of subsystem  $i$  for excitation in subsystem  $j$  can be estimated as follows [6] :

$$\mu_{R_{ij}^n} \equiv \bar{R}_{ij}^n = \frac{1}{N_{resp} N_{inp}} \sum_{q=1}^{N_{inp}} \sum_{p=1}^{N_{resp}} R_{ij,pq}^n \quad (7)$$

$$\sigma_{R_{ij}^n}^2 \equiv s_{R_{ij}^n}^2 = \frac{1}{N_{resp} N_{inp} - 1} \sum_{q=1}^{N_{inp}} \sum_{p=1}^{N_{resp}} (R_{ij,pq}^n - \bar{R}_{ij}^n)^2 \quad (8)$$

where  $N_{resp}$  is the number of response locations of response subsystem  $i$  and  $N_{inp}$  the number of excitation locations of the excited subsystem  $j$ . The overbar  $\bar{\phantom{x}}$  denotes the estimated mean value. It corresponds to the brackets  $\langle \phantom{x} \rangle$  denoting the spatial averaging, i.e.  $\langle R_{ij}^n \rangle = \bar{R}_{ij}^n$ . Note the difference in annotation between the (unknown) mean and variance representing the entire population, respectively denoted by the Greek letters  $\mu$  (population mean) and  $\sigma$  (population variance) and the mean and variance estimated from a sample of quantitative data ( $R_{ij,pq}^n$  for  $p = 1 \dots N_{resp}$ ,  $q = 1 \dots N_{inp}$ ) respectively designated by the overbar  $\bar{\phantom{x}}$  (sample mean) and the Roman letter  $s^2$  (sample variance). The sample standard deviation,  $s$ , is the non-negative square root of the sample variance. It is a measure of spread expressed in the units of the original data. The relative standard deviation which allows comparison of the spread of different data sets on a relative basis is defined as the ratio between the standard deviation and the mean.

### 3.2. THE VARIANCE OF THE NORMALIZED ENERGIES

For experimental SEA, the main result of interest is not the estimated mean and variance of the population of the normalized responses as such, but rather the mean and the variance of the space averaged square velocity/pressure  $\langle R_{ij}^n \rangle$  or the sample mean  $\bar{R}_{ij}^n$ . In other words, what is e.g. the 90% interval bracketing the unknown mean of the entire (infinite) population of the normalized responses.

The Central Limit Theorem says that, for a large number of samples  $N_{resp}N_{inp}$ , the sample mean  $\bar{R}_{ij}^n$  is approximately normally distributed with the mean  $\mu_{R_{ij}^n}$  and a variance given by

$$\sigma_{\bar{R}_{ij}^n}^2 \equiv s_{\bar{R}_{ij}^n}^2 = \frac{s_{R_{ij}^n}^2}{N_{resp} N_{inp}} = \frac{1}{N_{resp} N_{inp}} \left( \frac{1}{N_{resp} N_{inp} - 1} \sum_{q=1}^{N_{inp}} \sum_{p=1}^{N_{resp}} (R_{ij,pq}^n - \bar{R}_{ij}^n)^2 \right) \quad (9)$$

The interval  $[\bar{R}_{ij}^n - 1.645s_{\bar{R}_{ij}^n}, \bar{R}_{ij}^n + 1.645s_{\bar{R}_{ij}^n}]$  brackets the unknown mean with 90% interval.

Assuming then that there is no uncertainty on the subsystem mass/volume, the estimated variance of the normalized energies is given by

$$s_{E_{ij}}^2 = M_i^2 s_{\bar{R}_{ij}^n}^2 \text{ (structural) or } s_{E_{ij}}^2 = \frac{V_i^2}{\rho^2 c^4} s_{\bar{R}_{ij}^n}^2 \text{ (acoustical)} \quad (10,11)$$

It can be shown that, from an experimental point of view, the assumption of no uncertainty on the mass/volume is justified when computing the variances of the loss factors. Reason hereto is the fact that the mass/volume of the i-th subsystem is actually a scaling factor for the loss factors  $\eta_{ij}$  for  $j=1 \dots N$  [7,8].

#### 4. The Calculation of the Variances of the Loss Factors

The objective is now to study the transmission of the variances of the normalized energies through the loss factor calculation. Two methods can be distinguished to calculate the loss factor variances. On the one hand, the application of the statistical propagation of error formulas giving an approximate analytical expression for the loss factor variance as function of the variances of the normalized energies. These expressions can be quickly evaluated during the acquisition process. On the other hand, based on a Monte-Carlo variability analysis which requires much more computational effort and time, but offers the advantage to be more accurate if a sufficiently high number of experiments are evaluated. The statistical Monte-Carlo method also provides the possibility to evaluate the probability distribution of the loss factors.

##### 4.1. ANALYTICAL APPROACH

The variance calculation for the loss factors derived from either full matrix inversion (see equation (4)) or from approximate formulas (see equations (5,6)) is outlined.

##### 4.1.1. Full Matrix Inversion

The loss factors are estimated through the inverse of the normalized energy matrix. The statistical transmission of variance or propagation of error formula says that the mean of the loss factors can be approximated by evaluating equation (4) for the estimated mean of the normalized energies and that, based on performing a first order Taylor expansion, the variance of the total loss factor  $l_{ij}$  is approximately given by :

$$s_{l_{ij}}^2 \cong \sum_{k=1}^N \sum_{l=1}^N \left( \frac{\partial l_{ij}}{\partial E_{kl}^n} \right)^2 s_{E_{kl}^n}^2 \quad (12)$$

It can then be shown that the variance associated with the coupling loss factor between subsystems i and j is given by [9] :

$$s_{\eta_{ij}}^2 \equiv \frac{1}{\omega^2} \sum_{k=1}^N \sum_{l=1}^N (\bar{l}_{jk} \bar{l}_{li})^2 s_{E_{kl}}^2 \quad (13)$$

In case of weak coupling, the major contribution to the variance of the coupling loss factor  $\eta_{ij}$  will occur if  $k=j$  and if  $l=i$  as then the product of two total loss factors  $l_{ii}$  and  $l_{jj}$  occurs. This means that it is important that the variance of the normalized energy  $E_{ji}^n$  is low to get a high precision for the loss factor  $\eta_{ij}$ . Formula (13) also shows that in case of strong couplings, the variance will be higher in comparison with weak coupling.

Similar to the derivation of expression (13), it can be shown that the variance of the internal loss factor of subsystem  $i$  is given by [8]:

$$s_{\eta_{ii}}^2 \equiv \frac{1}{\omega^2} \sum_{k=1}^N \sum_{l=1}^N (\bar{l}_{li} \cdot \bar{\eta}_{kk})^2 s_{E_{kl}}^2 \quad (14)$$

#### 4.1.2. Approximate Formulas

The propagation of error formula can also be applied to equations (5,6), giving a good approximation for the loss factors in case of weakly coupled subsystems. By performing the first order Taylor expansion, the following expressions can be derived for respectively the coupling and the internal loss factor [7]:

$$s_{\eta_{ij}}^2 \equiv \frac{1}{\omega^2} \bar{\eta}_{ij}^2 \left( \frac{s_{E_{ji}}^2}{(\bar{E}_{ji}^n)^2} + \frac{s_{E_{ii}}^2}{(\bar{E}_{ii}^n)^2} + \frac{s_{E_{jj}}^2}{(\bar{E}_{jj}^n)^2} \right) \text{ and } s_{\eta_{ii}}^2 \equiv \frac{1}{\omega^2} \bar{\eta}_{ii}^4 s_{E_{ii}}^2 \quad (15,16)$$

One should realize that the formulas (15,16) describe how variability of error is propagated or transmitted through a mathematical function. In this case, the mathematical formula is an approximate method to compute the loss factors. The formulas will not take into account the bias error made due to using the approximate loss factor calculation instead of the full matrix inversion. This error is however of second order and typically, the approximation will result in a slight overestimation of the loss factors. The quality of the approximate loss factor calculation can be assessed by synthesizing the energies and comparing these with the measured energies obtained from the PIM tests [10].

#### 4.1.3. Usefulness of the analytical expressions

The approximate analytical expressions transforming the variances of the normalized energies into variances of the loss factors are extremely helpful to decide whether or not PIM measurements can be terminated. By analyzing the different contributions to the loss factor variance, it can be seen which critical subsystems require a higher discrete spatial sampling of the response field. The confidence levels also contribute to gaining more insight about the sub-division into subsystems, the key-stage in the whole SEA-process. As SEA deals with the reverberant response field, one would expect that the spread of the normalized point responses within the same subsystem is quite low.

The latter implies that the variance of the population of the normalized square velocities/pressures given by equation (8), is low. A fairly low number of excitation and response points is then sufficient to accurately estimate the true average. A high variance of the normalized energy for a reasonable number of excitation and response points might indicate that the subsystem division does not comply with the SEA basic assumptions. From equation (9), it can be seen that increasing the number of excitation and response points will narrow down the confidence interval, but precautions have to be taken with this. In case of large spread of the responses within the same subsystem, it might be more meaningful to re-partition the subsystem into smaller subsystems, having a response population with a lower variance.

#### 4.2. THE MONTE-CARLO APPROACH

The Monte-Carlo method computes the loss factor mean and the loss factor variance based on conducting experiments or simulations. In each experiment, the normalized energies are perturbed conform to a normal or Gaussian distribution having the sample mean  $\bar{E}_{ij}^n$  and sample variance  $s_{E_{ij}^n}^2$ . It is assumed that each term of the normalized

energy matrix can be independently perturbed. The loss factor calculation is then performed for a vast amount of possible combinations of disturbances of the normalized energies. In case  $M$  evaluations are carried out, for each loss factor,  $M$  values will be produced,  $\eta_{ij}^1, \eta_{ij}^2, \eta_{ij}^3, \dots, \eta_{ij}^M$ . The mean of the loss factor is then estimated by

$$\bar{\eta}_{ij\ MC} = \frac{1}{M} \sum_{k=1}^M \eta_{ij}^k \quad (17)$$

and the variance is given by

$$s_{\eta_{ij\ MC}}^2 = \frac{1}{M-1} \sum_{k=1}^M (\eta_{ij}^k - \bar{\eta}_{ij\ MC})^2 \quad (18)$$

Contrary to the analytical expressions which yield approximations for the loss factor mean and variance, if the number of simulations  $M$  is sufficiently high, an accurate result for the loss factor mean and variance is obtained. Additionally, the data set,  $\eta_{ij}^1, \eta_{ij}^2, \eta_{ij}^3, \dots, \eta_{ij}^M$ , allows to compute the probability histogram for each loss factor which can be visualized to check whether a normally distributed population is found. The disadvantage of the Monte-Carlo approach however lies within the significant amount of computation time in case the number of subsystems included in the SEA-model becomes large. In case of  $N$ -subsystems,  $N^2$  variables can be independently perturbed in each experiment and it can be easily understood that the number of experiments,  $M$ , should be much larger than  $N^2$  in order to get reliable estimates.

## 5. The Variance of the SEA Predictions

Assuming that the operational power inputs into different subsystems are given, the mean energy level of each subsystem can be estimated by applying the SEA power balance equation :

$$\{\bar{E}_{oper}\} = \frac{1}{\omega} [\bar{L}]^{-1} \{P_{oper}\} \quad (19)$$

where  $\{\bar{E}_{oper}\}$  represents the mean levels of the predicted response energies and  $\{P_{op}\}$  is the known operational input power vector. As the loss factors are experimentally identified by inverting the normalized energy matrix as expressed by equation (4), it is more convenient to rewrite equation (19) in terms of the normalized energies which were measured in the power injection process :

$$\{\bar{E}_{oper}\} = [\bar{E}^n] \{P_{oper}\} \quad or \quad \bar{E}_{i,oper} = \sum_{k=1}^N \bar{E}_k^n P_{k,oper} \quad (20)$$

Consequently, the variance of the predicted energy level of subsystem  $i$  is given by

$$s_{E_{oper,i}}^2 = \sum_{k=1}^N s_{E_k^n}^2 P_k^2 \quad (21)$$

As equation (20) is a linear equation, the probability distribution of the predicted operational energy will be normal if the normalized PIM-energies are normally distributed.

## 6. Test Results and Discussions

### 6.1. EVALUATION OF THE ACCURACY OF THE ANALYTICAL VARIANCE EXPRESSIONS BASED ON A MONTE-CARLO VARIABILITY ANALYSIS

In order to assess the practical usefulness and limitations of the analytical expressions which are approximate due to the involved first order Taler expansion in the derivation, the analytical formulas were applied to a numerical example and compared with the statistical Monte-Carlo approach. The normalized PIM energy matrix of a 6 fairly weakly coupled subsystem model, resembling a box structure with an opening, forms the basis for the numerical simulation. The coupling loss factors are about 6 to 10 times smaller than the internal loss factors and the weak coupling condition is better fulfilled for the higher frequencies. Three cases for the variances of the normalized PIM energies were investigated : relative standard deviation of all normalized energies equal to 10%, 20% and 30%. Figures 1, 2 and 3 compare the relative standard deviation of the internal loss factor  $\eta_{44}$  and the coupling loss factor  $\eta_{45}$  estimated by using equations (14) and (13) with the Monte-Carlo result. The number of experiments in the Monte-Carlo approach was chosen equal to 100000, guaranteeing a high confidence in the obtained results. It can be clearly observed from

figure 1 that excellent agreement is obtained in case the relative standard deviation of the PIM energies equals 10%. Figures 2 and 3 show that the analytical expressions are less good in case of higher relative standard deviations (20% and 30%). The estimates are better for the higher frequencies due to weaker coupling between the subsystems. In general, the analytical expressions tend to underestimate the Monte-Carlo variance, but the tendency and the relative importance are well predicted. So, from an engineering point of view, the analytical expressions yield a useful result and offer the practical advantage that they can be quickly evaluated. The histograms of the internal loss factor  $\eta_{44}$  and the coupling loss factor  $\eta_{45}$  have also been evaluated for the one-third octave band 1000Hz and are depicted in figures 4 and 5. It can be seen that the loss factor's distributions are not completely symmetric anymore, especially in case the relative standard deviation of the PIM-energies equals 20% and 30%. However, practically speaking, the assumption of a normal distribution with respect to the loss factor confidence calculation is adequate. Note also that for some experiments in the Monte-Carlo approach, negative loss factors were obtained.

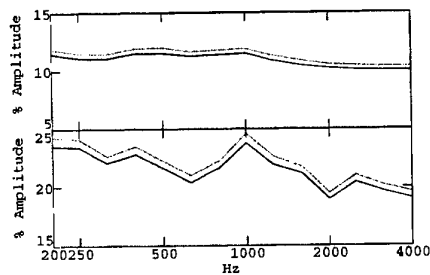


Figure 1: Relative standard deviation of internal loss factor  $\eta_{44}$  (upper) and coupling loss factor  $\eta_{45}$  (lower). Relative standard deviation of PIM-energies equal to 10%. Solid line : analytical expressions Dotted line : Monte-Carlo approach.

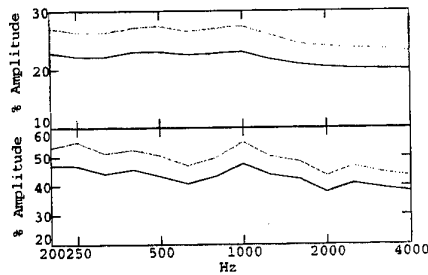


Figure 2: Relative standard deviation of internal loss factor  $\eta_{44}$  (upper) and coupling loss factor  $\eta_{45}$  (lower). Relative standard deviation of PIM-energies equal to 20%. Solid line : analytical expressions Dotted line : Monte-Carlo approach.

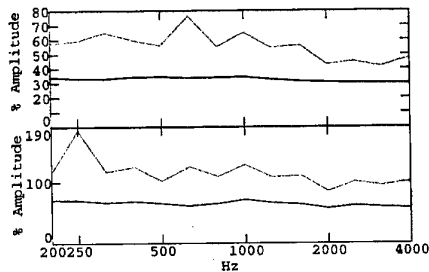


Figure 3: Relative standard deviation of internal loss factor  $\eta_{44}$  (upper) and coupling loss factor  $\eta_{45}$  (lower). Relative standard deviation of PIM-energies equal to 30%. Solid line : analytical expressions Dotted line : Monte-Carlo approach

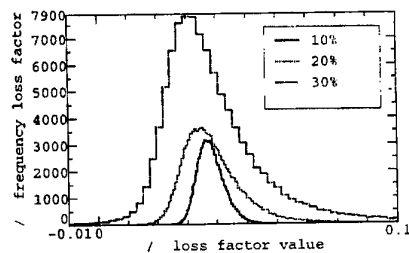


Figure 4: Histogram of the internal loss factor  $\eta_{44}$  for the one-third octave band 1000Hz. Relative standard deviation of PIM-energies equal to 10%, 20% and 30%.

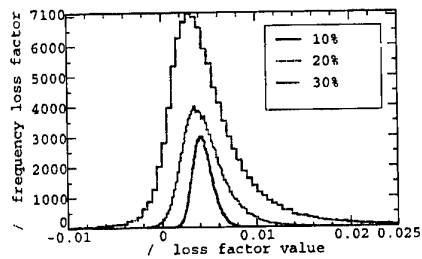


Figure 5: Histogram of the coupling loss factor  $\eta_{as}$  for the one-third octave band 1000Hz. Relative standard deviation of PIM-energies equal to 10%, 20% and 30%.

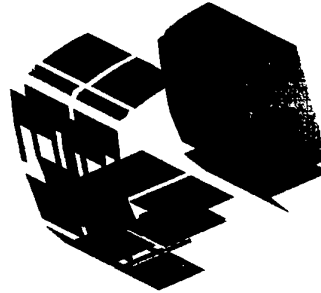


Figure 6: Geometry model of two vertical sections of railway carriage of the high-speed train.

## 6.2. APPLICATION OF THE STATISTICAL FORMULAS TO A RAILWAY CARRIAGE OF A HIGH-SPEED TRAIN

The experimental SEA model of a railway carriage of a high-speed train has been derived [11]. Justified by the repetitive nature of the structure, only two adjacent vertical sections of the railway carriage were studied. Taking two adjacent sections instead of one allowed to investigate the energy transfer in longitudinal direction. The two sections were divided in 18 structural components which were the roof, the roof edge, the upper part of the side wall, the lower part of the side wall, the wooden floor, the supporting steel floor, the supporting beam of the floor, the closing plate of the underfloor cavity, the exterior and interior windows and the inner mask around the windows. Including the passenger compartment and the underfloor cavity containing the auxiliary equipment as 2 acoustical subsystems yielded a SEA model consisting of 20 subsystems. A geometry model showing the subsystems of both sections is shown in figure 6.

In the power injection process, each subsystem was excited in 3 different input locations while the responses at 5 to 8 locations chosen differently from the input locations to exclude nearby field effects were measured for all subsystems. The relative standard deviations of the normalized energies (equations (9) and (10,11)) are typically in the range of 25 to 35%. Figure 7 depicts the normalized energy in respectively the upper part and the lower part of the side wall due to excitation in the upper part of the side wall. The 90% confidence levels are computed on the basis of a normal or Gaussian distribution. The internal and coupling loss factors were derived based on the approximate equations (5,6), assuming that the energy matrix normalized by unit input power is diagonal dominant. The obtained loss factors were validated by superposing and comparing the measured and the synthesized response energies, confirming that the approximate methods gave good results. The confidence levels of the loss factors were calculated according to equations (15) and (16). Figures 8 and 9 respectively show the internal loss factor for the interior cavity and the coupling loss factor between

the upper part and lower part of the side wall and their corresponding 90% confidence intervals.

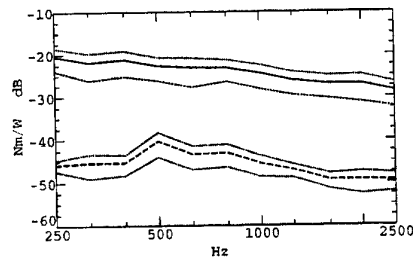


Figure 7: Normalized energy and associated 90% confidence intervals (dotted lines) for the response in the upper part (solid line) and lower part (dashed line) of the side wall due to excitation in the upper part of the side wall.

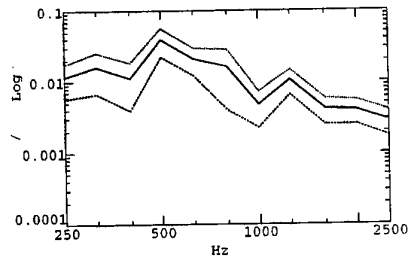


Figure 8: Internal loss factor of the interior cavity (solid line) and associated 90% confidence interval (dotted lines).

The derived loss factor model was then used to determine the way power flows through the structure for known power inputs. Figure 10 depicts the predicted energy level (equation (20)) and the associated 90% confidence levels (equation (21)) for the interior cavity when input power is applied at the supporting beams of the floor. Subsequently, two effective modifications in terms of adding damping treatment were determined from sensitivity studies. The internal loss factors of the supporting steel floor and the lower part of the side wall were doubled. Figure 10 shows that the predicted energy level for the modified structure is significantly lower than the original level.

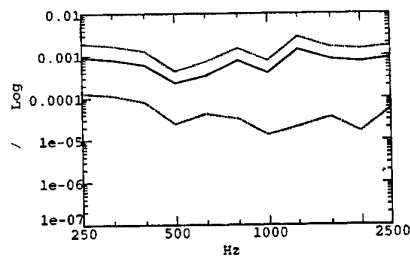


Figure 9: Coupling loss factor between upper part of side wall and lower part of side wall (solid line) and the associated 90% confidence interval (dotted lines).

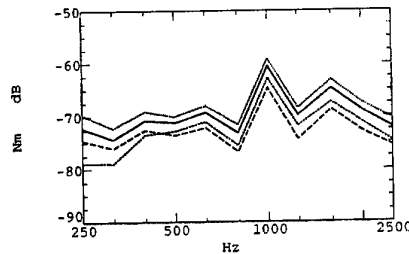


Figure 10: Predicted energy level (solid line) and associated 90% confidence interval (dotted lines) for the interior cavity due to operational input in the beam. The predicted energy level for modification in two internal loss factors is superposed (dashed line).

## 7. Summary and Conclusions

This paper has presented the statistical aspects concerning the Power Injection Method, a well-known technique to experimentally derive the loss factors. It has been shown



that analytical expressions can be deduced describing the loss factor variance in terms of the variances of the normalized energies. These formulas are approximate as they are based on a first order Taylor expansion. However, a Monte-Carlo variability analysis on a numerical example of 6 subsystems points out that they are of practical usefulness. The analytical expressions allow a quick assessment of the confidence levels of the variances during the PIM-tests, aiding the user to decide whether the desired accuracy has been achieved and whether or not the PIM-measurements can be terminated. The statistical theory has been applied to a railway carriage of a high-speed train, illustrating how the confidence levels of the loss factors and the SEA-predictions can be obtained and how the effectiveness of loss factor modifications can be evaluated in terms of confidence levels.

## 8. Acknowledgments

The presented work has been carried out within the framework of the IWT-project no AUT/940090, supported by the Flemish institute for the promotion of scientific and technological research in Industry.

## 9. References

- [1] R.H. Lyon, "Statistical Energy Analysis of Dynamical Systems: Theory and Practice", MIT Press, Cambridge, 1975.
- [2] D.A. Bies and S. Hamid, "In situ determination of loss and coupling loss factors by the power injection method, *Journal of Sound and Vibration*", 70(2), pp. 187-204, 1980.
- [3] N. Lalor, "The experimental determination of vibrational energy balance in complex structures", *Proc. SIRA Conference on Stress and Vibration - Recent Developments in Industrial Measurements and Analysis*, London, 1989.
- [4] L. Hermans, K. Wyckaert, K. De Langhe, "The Process to Experimentally Identify the Statistical Energy Analysis Parameters of Industrial Structures : Step by Step", *Proc. of ISMA21*, Leuven, 1996.
- [5] N. Lalor, "Practical considerations for the measurements of internal and coupling loss factors on complex structures", *ISVR Technical Report No. 182*, June 1990.
- [6] Stephen B. Vardeman, "Statistics for Engineering Problem Solving", IEEE Press - PWS Publishing Company, New York - Boston, 1994.
- [7] L. Hermans, K. De Langhe and L. Demeestere, "Methods to Estimate the Confidence Level of the Experimentally Derived Statistical Energy Analysis Model: Application to Vehicles", *Proc. SAE Noise and Vibration*, Traverse City, 1997.
- [8] L. Hermans, "On the Influence of the Subsystem Mass or Volume in Experimental Statistical Energy Analysis", to be published in *Proc. Inter-Noise 97*, Budapest, August, 1997.
- [9] K. Delanghe, "High Frequency Vibrations : Contributions to Experimental and Computational SEA Parameter Identification Techniques", Ph.D. dissertation, Department PMA, K.U.Leuven, 1996.
- [10] L. Hermans, K. Wyckaert, "Experimental Statistical Energy Analysis : Internal and Coupling Loss Factor Matrix Validation", *Proc. Inter-noise, Inter-Noise 96*, Liverpool, July-August 1996.
- [11] K. De Meester, L. Hermans, K. Wyckaert, N. Cuny, "Experimental SEA on a Highspeed Train Carriage", *Proc. of ISMA21*, Leuven, 1996.

## THE PRACTICAL IMPLEMENTATION OF SEA

N. Lalor  
*Institute of Sound and Vibration Research*  
*University of Southampton , SO17 1BJ*

### 1. Introduction

For the past three decades, structural dynamics prediction models have been almost exclusively based on the Finite Element Method (FEM) together with its Experimental Modal Analysis (EMA) counterpart. Although this tool has proved highly successful for stress and low frequency vibration modelling, it has been found to have severe limitations for noise. This is because the accuracy of many finite element structural models becomes unacceptably poor by about the 10th to 20th mode, particularly if there are bolted or spot-welded joints. The important acoustic frequency range, however, often extends beyond the 100th mode. It is for this reason that there has recently been a renewed interest in the Statistical Energy Analysis (SEA) technique for high frequency vibration and noise prediction. The successful application of SEA in its standard form relies on high modal density, high modal overlap and short wavelengths, ie the very factors which render FEM inaccurate. This is because SEA works with the average response of a structure and it needs these factors to ensure that the average is a realistic and thus a useful quantity. SEA and FEM are therefore complementary rather than competitive techniques - FEM for low frequency and SEA for high frequency.

In spite of the need to produce theoretical predictive models, experimentally based models are also extremely useful in practice. Apart from their use in predicting the effect of small modifications to a standard structure, they can also be used for sensitivity and diagnostic purposes. In the same way that EMA is the experimental counterpart of FEM, SEA also has an experimental counterpart, sometimes termed Energy Flow Analysis (EFA). It is the purpose of this paper to show how EFA can be used to diagnose and solve some of the noise and vibration problems that can occur with complex structures.

### 2. Theoretical Concepts

#### 2.1 APPLICATION OF SEA THEORY TO COUPLED SUBSTRUCTURES

The basic theory of SEA as formulated by Lyon[1] showed that the net steady-state frequency band averaged power flowing between two coupled oscillators is proportional to the difference in their vibrational energy levels, ie

$$P_{ij} = \beta (E_i - E_j) \quad (1)$$

where,

$P_{ij}$  = net power flowing from oscillator i to oscillator j  
 $E_i, E_j$  = energy of oscillators  
 $\beta$  = constant of proportionality =  $\omega_1 \eta_{12} = \omega_2 \eta_{21}$

$\omega_1, \omega_2$  = uncoupled natural frequencies of oscillators  
 $\eta_{ij}$  = coupling loss factor from oscillator i to oscillator j

It should be noted that E and  $\beta$  are also time and frequency band averaged.

Cremer and Heckl have shown [2] that for stiffness (spring) coupling  $\beta$  can be expressed as:

$$\beta = \frac{2(\delta_i + \delta_j) k_{ij}^2}{m_i m_j \{ (\omega_i^2 - \omega_j^2)^2 + 4(\delta_i + \delta_j)(\delta_i \omega_j^2 + \delta_j \omega_i^2) \}} \quad (2)$$

where,  
 $m_i, m_j$  = oscillator masses  
 $\delta_i, \delta_j$  = oscillator bandwidths  
 $k_{ij}$  = stiffness of coupling spring

Application of equation (1), together with the definition of the internal loss factor (see below) enables the power balance equations to be written for each oscillator viz:

$$\begin{aligned} P_1 &= \omega_1 \eta_1 E_1 + \omega_1 \eta_{12} (E_1 - E_2) \\ P_2 &= \omega_2 \eta_2 E_2 + \omega_2 \eta_{21} (E_2 - E_1) \end{aligned} \quad (3)$$

where,  
 $P_i$  = external input power to oscillator i  
 $\omega_i \eta_i E_i$  = power dissipated in oscillator i due to damping  
 $\eta_i$  = internal loss factor of oscillator i

These power balance equations for two coupled oscillators can be applied to the case of two weakly coupled structures (subsystems) provided certain assumptions are made. For example, it is assumed that, within the frequency band of interest, each mode absorbs the same amount of power, stores the same amount of energy and has the same internal loss factor. Thus, if the first subsystem has  $N_1$  modes within the band, the input power to each mode will be  $\frac{P_1}{N_1}$  and the energy stored by each mode will be  $\frac{E_1}{N_1}$  ( $P_1$  and  $E_1$  are band totals). Similar assumptions are made with regard to the second subsystem.

Examination of equation (2) shows that, because of the term  $(\omega_i^2 - \omega_j^2)^2$  in the denominator,  $\beta$  will be negligibly small unless  $\omega_i \approx \omega_j$ . Hence, each mode of the first subsystem will only couple significantly with the mode of the second subsystem that is nearest to it in frequency. The average value of  $\beta$  for these  $N_1$  couplings gives the average value of the coupling loss factor,  $\eta_{12}$ . A similar argument can be made regarding the coupling of each of the  $N_2$  modes of the second subsystem with those of the first, giving an average coupling loss factor in that direction of  $\eta_{21}$ .

Thus, the coupling between any pair of modes can be assumed to be equivalent to two coupled oscillators, so that equation (3) is applicable ie

$$\frac{P_1}{N_1} = \omega \eta_1 \frac{E_1}{N_1} + \omega \eta_{12} \left( \frac{E_1}{N_1} - \frac{E_2}{N_2} \right)$$

$$\therefore P_1 = \omega \eta_1 E_1 + \omega \eta_{12} \left( E_1 - \frac{N_1}{N_2} E_2 \right) \quad (4a)$$

$$\text{and} \quad \frac{P_2}{N_2} = \omega \eta_2 \frac{E_2}{N_2} + \omega \eta_{21} \left( \frac{E_2}{N_2} - \frac{E_1}{N_1} \right)$$

$$\therefore P_2 = \omega \eta_2 E_2 + \omega \eta_{21} \left( E_2 - \frac{N_2}{N_1} E_1 \right) \quad (4b)$$

Note that in the absence of any information regarding the natural frequencies of the modes, the band centre frequency has been assumed for both.

Summing equations (4a) and (4b) gives:

$$P_1 + P_2 = \omega (\eta_1 E_1 + \eta_2 E_2) + \omega \left\{ \eta_{12} \left( E_1 - \frac{N_1}{N_2} E_2 \right) + \eta_{21} \left( E_2 - \frac{N_2}{N_1} E_1 \right) \right\}$$

Now,  $(P_1 + P_2)$  is the total input power to the system and  $\omega(\eta_1 E_1 + \eta_2 E_2)$  the total losses of the system and, under steady-state conditions, these must be equal. Hence,

$$\eta_{12} \left( E_1 - \frac{N_1}{N_2} E_2 \right) + \eta_{21} \left( E_2 - \frac{N_2}{N_1} E_1 \right) = 0$$

$$\text{or} \quad \frac{\eta_{12}}{N_2} (N_2 E_1 - N_1 E_2) + \frac{\eta_{21}}{N_1} (N_1 E_2 - N_2 E_1) = 0$$

Thus, for

$$(N_2 E_1 - N_1 E_2) \neq 0$$

$$N_1 \eta_{12} = N_2 \eta_{21} \quad (5)$$

This is the well known reciprocity relationship, which shows that the total coupling strength (number of modes times the coupling strength of each mode) is the same in both directions - as it is with the two coupled oscillators, since  $\omega_1 \simeq \omega_2$ . If  $(N_2 E_1 - N_1 E_2) = 0$ , the condition of equipartition of modal energy exists and it can be seen from equations (4) that this would prevent any power flowing between the subsystems, regardless of the value of the coupling loss factors.

Equations (4) can be used for any practical structure provided that the modal densities of each subsystem are known. Since this is rarely the case, it is usual to eliminate the ratio  $\frac{N_1}{N_2}$  between equations (4) and (5) to give:

$$P_1 = \omega \eta_1 E_1 + \omega (\eta_{12} E_1 - \eta_{21} E_2) \quad (6a)$$

$$P_2 = \omega \eta_2 E_2 + \omega (\eta_{21} E_2 - \eta_{12} E_1) \quad (6b)$$

This analysis can be extended to any number,  $N$ , coupled subsystems to give:

$$\begin{bmatrix} P_1 \\ \vdots \\ P_N \end{bmatrix} = \omega \begin{bmatrix} \sum_{k=1}^N \eta_{1k} & \dots & -\eta_{N1} \\ \vdots & & \vdots \\ -\eta_{1N} & \dots & \sum_{k=1}^N \eta_{Nk} \end{bmatrix} \begin{bmatrix} E_1 \\ \vdots \\ E_N \end{bmatrix} \quad (7a)$$

or  $[P] = \omega [L] [E]$  (7b)

It should be noted that the  $\eta_{ij}$  element in a leading diagonal term of  $[L]$  represents the internal loss factor,  $\eta_j$ .

## 2.2 COUPLING LOSS FACTORS

It is important at this stage to understand the physical significance of the coupling loss factor,  $\eta_{ij}$ . As originally defined in relation to the coupled oscillators, it represents the coupling strength between their two modes. Extending this definition to the case of many coupled substructures,  $\eta_{ij}$  could in principle represent the average modal coupling between any two subsystems, whether they are physically connected or not. In practice, the necessary condition for weak coupling (to prevent equipartition of energy) generally reduces the coupling strength between unconnected subsystems to negligible proportions. It is therefore usual to consider these indirect coupling loss factors as equal to zero - indeed, it is usually more accurate to do this, particularly for an experimentally based model, as will be shown later.

There are, however, some notable exceptions to this rule. Figure 1 shows a structure comprised of 3 flat plates (each considered as a subsystem) joined at right angles. The in-plane modes of plate 2 will be at much higher frequencies than the flexural modes of plates 1 and 3. Therefore the low frequency flexural modes of plate 1 will couple with those of plate 3 via (non-resonant) in-plane motion of plate 2.

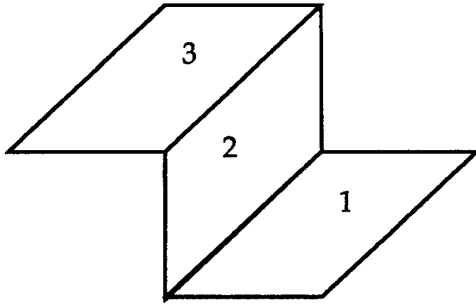


Figure 1

In this case plate 2 is merely acting as a connector. Another well known example of this "tunnelling" phenomenon, as it is known, is where two acoustic cavities are separated by a panel. Acoustic modes of each cavity can couple together via non-resonant (mass law) motion of the panel. In general tunnelling occurs when two similar subsystems are connected via a third dissimilar subsystem.

It is therefore very important when setting-up an SEA model to include tunnelling connections; however, it is also important not to include these connections where tunnelling does not exist.

### 2.2.1 Measurement of $\eta_{ij}$

Most of the problems associated with the measurement of the coupling loss factors on practical structures, such as car body shells, have now been solved and these techniques have been reported in detail elsewhere (eg [3], [4], [5]). Nevertheless, in view of the comments made earlier concerning the advisability of setting all coupling loss factors between unconnected subsystems to zero, it is worth reviewing the  $E_{\alpha\alpha}$  method [4].

By use of the power injection technique [6], elimination of the internal loss factors and conversion of measured  $\langle v^2 \rangle$  values to subsystem energies (via  $M_{eq}$ ), the coupling loss factors can be expressed uniquely in terms of the measured input powers and subsystem energies. Equation (8) gives this relationship for a 3 subsystem model. It should be noted here that  $E_{ij}$  = energy of subsystem  $i$  when subsystem  $j$  is excited by a shaker.

$$\omega \begin{bmatrix} \left( \frac{E_{11}}{E_{21}} - \frac{E_{12}}{E_{22}} \right) & 0 & 0 & 0 & 0 & \left( \frac{E_{31}}{E_{21}} - \frac{E_{32}}{E_{22}} \right) \\ 0 & \left( \frac{E_{22}}{E_{12}} - \frac{E_{21}}{E_{11}} \right) & 0 & \left( \frac{E_{32}}{E_{12}} - \frac{E_{31}}{E_{11}} \right) & 0 & 0 \\ 0 & 0 & \left( \frac{E_{11}}{E_{31}} - \frac{E_{13}}{E_{33}} \right) & 0 & \left( \frac{E_{21}}{E_{31}} - \frac{E_{23}}{E_{33}} \right) & 0 \\ 0 & \left( \frac{E_{23}}{E_{13}} - \frac{E_{21}}{E_{11}} \right) & 0 & \left( \frac{E_{33}}{E_{13}} - \frac{E_{31}}{E_{11}} \right) & 0 & 0 \\ 0 & 0 & \left( \frac{E_{12}}{E_{32}} - \frac{E_{13}}{E_{33}} \right) & 0 & \left( \frac{E_{22}}{E_{32}} - \frac{E_{23}}{E_{33}} \right) & 0 \\ \left( \frac{E_{13}}{E_{23}} - \frac{E_{12}}{E_{22}} \right) & 0 & 0 & 0 & 0 & \left( \frac{E_{33}}{E_{23}} - \frac{E_{32}}{E_{22}} \right) \end{bmatrix} \begin{bmatrix} \eta_{12} \\ \eta_{21} \\ \eta_{13} \\ \eta_{31} \\ \eta_{23} \\ \eta_{32} \end{bmatrix} = \begin{bmatrix} P_2/E_{22} \\ P_1/E_{11} \\ P_3/E_{33} \\ P_1/E_{11} \\ P_3/E_{33} \\ P_2/E_{22} \end{bmatrix} \quad (8)$$

Equation (8) is valid for the case where each subsystem is physically connected to the other two. If, however, subsystem 2 is disconnected from subsystem 3, in the absence of tunnelling,  $\eta_{23}$  and  $\eta_{32}$  will be equal to zero. Equation (8) can therefore be partitioned in the following manner.

$$\omega \begin{bmatrix} E_{\alpha\alpha} & E_{\alpha\beta} \\ E_{\beta\alpha} & E_{\beta\beta} \end{bmatrix} \begin{bmatrix} \eta_{\alpha} \\ 0 \end{bmatrix} = \begin{bmatrix} P_{\alpha} \\ P_{\beta} \end{bmatrix} \quad (9)$$

where  $[\eta_{\alpha}]$  represents the matrix of non-zero coupling loss factors. It can be seen from the first equation of (9) that

$$[\eta_{\alpha}] = \begin{bmatrix} \eta_{12} \\ \eta_{21} \\ \eta_{13} \\ \eta_{31} \end{bmatrix} = \frac{1}{\omega} [E_{\alpha\alpha}]^{-1} [P_{\alpha}] \quad (10)$$

The importance of this method is that, if subsystem 2 is not connected to subsystem 3, the energy matrix in equation (8) is badly conditioned - note the  $E_{23}$  and  $E_{32}$  terms, which will be very small and subject to noise contamination, on the denominators of the  $E_{\beta\alpha}$  part of the matrix. In addition, although  $E_{\beta\beta}$  is essentially well conditioned, the large leading diagonal terms will be suspect, again due to the presence of the  $E_{23}$  and  $E_{32}$  terms on the denominators.  $E_{\alpha\alpha}$  does not suffer from these problems and hence equation (10) will give much more accurate values of the non-zero coupling loss factors. In fact

$E_{\alpha\alpha}$  is so well conditioned that it can be approximated to a diagonal matrix, which uncouples the equations. The coupling loss factors can then be expressed simply as [4]:

$$\eta_{ij} \approx \frac{P_j E_{ji}}{\omega E_{ii} E_{jj}} \quad (11)$$

It has been found from experience that, provided weak coupling conditions are satisfied, equation (11) gives acceptable results even if subsystem 2 is connected to subsystem 3. Indeed, it can be used for much larger models but, again, weak coupling conditions should prevail.

Before leaving the subject of coupling loss factors, a further new development should be mentioned. Recent research at ISVR has shown [7] that the coupling loss factors can be expressed directly in terms of the measured input powers and  $\langle v^2 \rangle$  values. For example, for a 3 subsystem model:

$$\eta_{12} = \frac{\eta_1 (v_{21} v_{33} - v_{23} v_{31})}{(v_{22} v_{33} - v_{23} v_{32} + v_{23} v_{31} - v_{21} v_{33} + v_{21} v_{32} - v_{22} v_{31})} \quad (12a)$$

$$\eta_{21} = \frac{\eta_2 (v_{12} v_{33} - v_{13} v_{32})}{(v_{11} v_{33} - v_{13} v_{31} + v_{13} v_{32} - v_{12} v_{33} + v_{12} v_{31} - v_{11} v_{32})} \quad (12b)$$

where  $v_{ij} = \frac{\langle v_i^2 \rangle}{P_j}$

The 3 subsystem model is particularly important here, as it is in relation to equation (8), because the third subsystem can be considered to be "the rest of the structure", ie the influence of the rest of the structure is taken into account when evaluating the coupling loss factors between two subsystems within it. The result shown in equations (12) above has now been generalised for any number of subsystems [8]. It should also be noted that dividing equations (12) by the appropriate loss factor gives the Smith criterion [9] uniquely in terms of measured velocities and input powers.

Since equations (12) rely on a knowledge of the internal coupling factor, some consideration should be given here to its evaluation. Although the loss factors of individual modes within a frequency band may differ significantly, it is usually found that the band average values follow a smooth trend with frequency. Thus, it is now the usual practice at ISVR to measure the octave band decay ( $T_{60}$ ) values and interpolate the curve to obtain the  $1/3$  octave values. This is done because it is not uncommon for individual  $1/3$  octave bands to contain no modes, although this is quite rare for octave bands.

### 2.3 EQUIVALENT MASS

Although the frequency band total of the kinetic energy (KE) and the strain energy (SE) of a mode is constant, their relative amplitudes depend upon the frequency of vibration. Below its natural frequency SE will be the larger of the two and the position is reversed above this frequency. When the vibration is exactly at the natural frequency, then the two are equal. Thus, the band averages of KE and SE can be considered approximately equal, provided that the natural frequency is near the centre of the band. This is why the natural

frequency of the "average mode" of each subsystem is considered to be equal to the band centre frequency, and is the reason for the assumption made earlier for the oscillators that  $\omega_1 \approx \omega_2$ . Because KE and SE vary harmonically with time, it is convenient to express them in terms of their amplitudes, or maximum values. Thus, the time and frequency band averaged total energy can be expressed as:

$$(KE)_{\max} = (SE)_{\max} = \text{total energy}$$

This is a particularly useful relationship because it is much easier to measure KE than it is to measure SE. Unfortunately, even the measurement of KE presents significant problems, except with very simple structures. For one of the uniform flat plates shown in Figure 1, the maximum KE is given by

$$(KE)_{\max} = E_{\text{tot}} = M \langle v^2 \rangle \quad (13)$$

where,

$M$  = mass of plate

$\langle v^2 \rangle$  = mean square velocity averaged over the surface of plate.

However, equation (13) is not valid for a more complex structure such as the door of a car, regardless of how many sampling points are used to obtain the value of  $\langle v^2 \rangle$ .

It was research carried out at ISVR as part of the UK government's Quiet Heavy Vehicle project (QHV90) that first showed the way out of this difficulty [10]. Very carefully conducted experiments on diesel engine components, which were bolted to blocking masses, revealed a discrepancy between the directly measured input power from the shaker and that back-calculated from the relation,

$$P = \omega M \langle v^2 \rangle \eta_i$$

In this case the damping loss factor was obtained from vibration decay ( $T_{60}$ ) measurements, and the value of  $\langle v^2 \rangle$  from a large number of accelerometer measurements. At the time it was decided to introduce a correction factor  $K$ , which was found to be frequency dependent. This was later developed into the Equivalent Mass ( $M_{\text{eq}}$ ) concept [11].

There are three basic reasons why  $M_{\text{eq}}$  differs from the actual mass:

1. The number of velocity samples used to compute  $\langle v^2 \rangle$  is not sufficient.
2. The simple energy formulation of equation (13) is only applicable to uniform structures.
3. The frequency band totals of KE and SE are not equal.

For a simple uniform flat plate 10 samples are usually sufficient to provide a stable average, provided that some are not made redundant by placing them either side of an axis of symmetry. In the case of a more complex structure it is quite difficult to separate the first two aspects mentioned above, although the combined effect can be quite considerable. Figure 2 shows the results of two KE computations made on a finite element model of a 4 cylinder diesel engine block [12]. In the first instance, the total KE was computed from



$\frac{1}{2} \dot{X}^T M \dot{X}$ , where  $\dot{X}$  is the velocity vector and  $M$  is the mass matrix. The KE was then computed using equation (13), where  $M$  is the block mass and  $\langle v^2 \rangle$  was calculated from all the nodes forming the sides of the block ie the sites that could be sampled for an experimental test although, in practice, far fewer would normally be chosen. The figure shows how the ratio  $M \langle v^2 \rangle / \frac{1}{2} \dot{X}^T M \dot{X}$  varies with frequency.

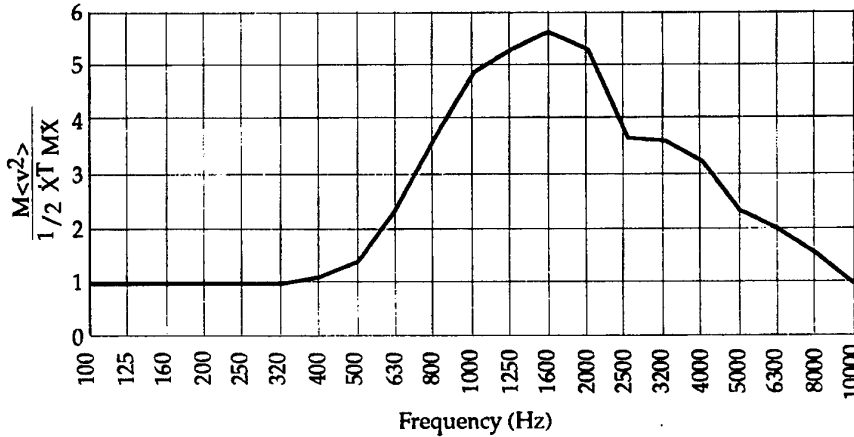


**Figure 2 Ratio of Apparent KE to Actual KE for Engine Block**

At low frequency (below the first mode of the block) the ratio is unity because the block vibrates as a rigid body. However, it can be seen that the ratio increases to a maximum of nearly 6 at around 1600 Hz. This represents an error of about 7.5 dB.

Although the third source of error has previously been discussed in Reference [13] it is worth repeating the main argument here. For a simple mass ( $m$ ) and spring ( $k$ ) system vibrating with amplitude  $x_0$  at frequency  $\omega$ , the total energy ( $E_{tot} = \overline{E}_{tot}$ ) is given by:

$$E_{tot} = \frac{1}{2} \{ m \omega^2 \cos^2(\omega t) + k \sin^2(\omega t) \} x_0^2 = (\overline{SE}) + (\overline{KE})$$

where the bars represent time averaged quantities and

$$(\overline{SE}) = \frac{1}{4} k x_0^2 : (\overline{KE}) = \frac{1}{4} m \omega^2 x_0^2$$

Hence

$$\frac{\overline{E}_{tot}}{\overline{E}_{KE}} = R = \frac{(\overline{SE}) + (\overline{KE})}{(\overline{KE})} = \frac{k + m \omega^2}{m \omega^2}$$

or

$$\overline{E}_{tot} = R \overline{E}_{KE} = \frac{1}{2} R m \langle v^2 \rangle$$

$\therefore$

$$M_{eq} = \frac{1}{2} R m$$

When  $\omega < \omega_n$ ,  $R$  and therefore  $M_{eq}$  approach infinity. At resonance,  $R = 2$  and therefore  $M_{eq} = m$ . At very high frequency  $M_{eq}$  approaches  $\frac{m}{2}$ .

However, when considering band totals rather than values at a particular frequency,  $M_{eq}$  can be very significantly different. For example, Figure 3 shows the variation of  $M_{eq}/\text{Actual mass}$  with frequency for the previously mentioned engine block, computed from the finite element model and confirmed by experiment [12]. It can be seen that the ratio rises to a maximum of at least 30. This represents an error of over 15 dB.

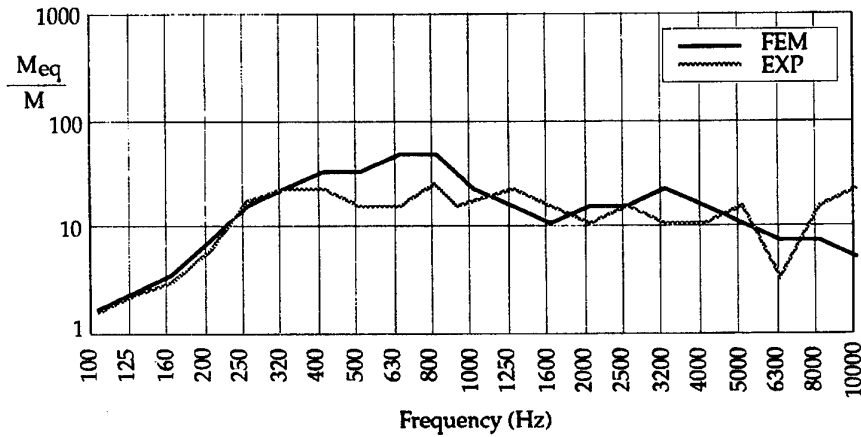


Figure 3 Ratio of Equivalent Mass to Actual Mass for Engine Block

### 2.3.1 Measurement of $M_{eq}$

Recent research at ISVR has shown [8] that the method used to calculate  $M_{eq}$  from measured results is, in fact, not quite correct. Previously, the method developed in Reference [11] has been used. ie for subsystem  $i$ :

$$(M_{eq})_i = \frac{P_i(T60)_i}{13.82 \langle \bar{v}_i^2 \rangle} = \frac{P_i}{\omega \eta_i \langle \bar{v}_i^2 \rangle}$$

However, certain discrepancies in predicted results have indicated that this relationship for 2 coupled subsystems should be:

$$(M_{eq})_i = \frac{(v_{jj} - v_{ji})}{\omega \eta_i (v_{ii} v_{jj} - v_{ij} v_{ji})} \quad (14)$$

where  $v_{ij}$  has the same meaning as with equation (12).

For more than 2 subsystems the relevant expression becomes increasingly complex, although a generalised solution has now been obtained [8].

### 3. Practical Applications of Experimental SEA Model

Once the internal loss factors, the coupling loss factors and the equivalent masses have been obtained, it is possible to directly relate input powers to subsystem velocities (or sound pressures, in the case of acoustic subsystems). This has a number of very important practical uses, which are outlined below.

#### 3.1 INPUT POWER DETERMINATION

If the surface average of the squared vibration velocity is measured on each subsystem, when the system is operating normally, the operational subsystem energies can be obtained by multiplying by the appropriate equivalent masses. The input powers are thus derived from the power balance equations (7) ie from the product  $\omega[L][E]$ .

Figure 4 shows the input powers calculated for a saloon car, using this technique [14].

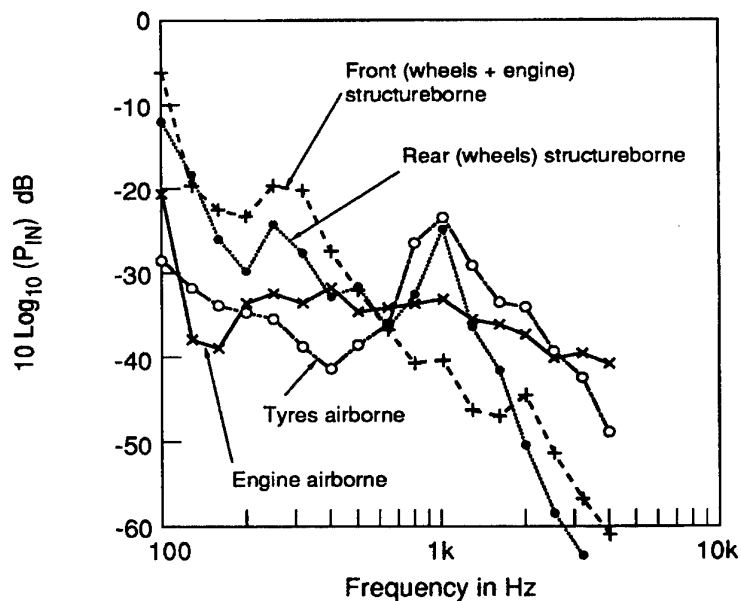


Figure 4 Input Powers to Car at 100 km/hr

#### 3.2 SOURCE CONTRIBUTIONS

Having determined the input powers, the subsystem energies (and hence their radiated noise) can be obtained from a recast version of the power balance equations ie

$$[E] = \frac{1}{\omega} [L]^{-1} [P]$$

By setting all the elements of [P] to zero, except the one under investigation, the noise due to it alone can be calculated. This process is then repeated for all the other elements of [P] in turn. Figure 5 shows the results of such an analysis carried out to determine the source contributions to the interior noise of the same car.

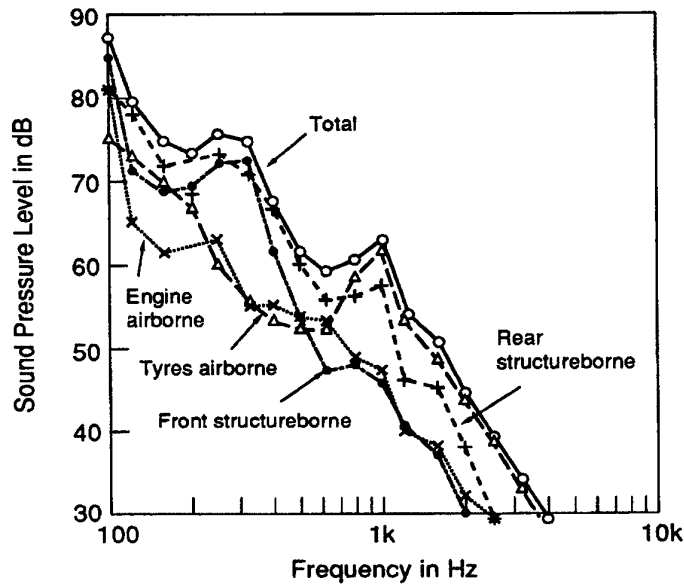


Figure 5 Source Contributions to Interior Noise

### 3.3 POWER FLOW DIAGRAMS

The derived input powers can also be used in combination with the SEA model to determine vibrational power flow round the structure. This is made possible because the power balance equations can be rearranged to give;

$$\text{Net power flow from } i \text{ to } j = \omega (E_i \eta_{ij} - E_j \eta_{ji})$$

Such diagrams are of considerable value to the noise control engineer, for they clearly show how each component that radiates noise gets its energy.

### 3.4 SENSITIVITY AND OPTIMISATION

It is possible to determine the sensitivity to each SEA parameter by perturbing it from its normal value and calculating the effect on the subsystem energies through the power balance equations. However, it is much more efficient to directly differentiate the power balance equations [15]. These sensitivities can then be used as the first stage of an automatic optimisation process, and a computer program has been written at ISVR to do this. Experience has shown that around 5 dB reduction can be achieved by simply moving

existing damping material around, and significantly more if coupling loss factors are also allowed to change - a result that would be almost impossible to achieve by trial and error.

#### 4. Acknowledgements

The author wishes to thank his colleagues, G. Stimpson and P. Faulstroh, for providing the results presented in the paper. Many thanks are also due to Mrs S. Greenwood for preparing the manuscript.

#### 5. References

- [1] Lyon, R.H. *Statistical Energy Analysis of Dynamic Systems: Theory and Application*. Cambridge Mass: MIT Press, 1975.
- [2] Cremer, L. Heckl, M. and Ungar, E.E. *Structure-Borne Sound*. Chap 8, 2nd edition published by Springer-Verlag.
- [3] Lalor, N. *The measurement of SEA Loss Factors on a Fully-Assembled Structure*. ISVR Technical Memorandum No. 150, University of Southampton, 1987.
- [4] Lalor, N. *Practical Considerations for the Measurement of Internal and Coupling Loss Factors of Complex Structures*. ISVR Technical Report No. 182, University of Southampton, June 1990.
- [5] Walsh, S.J. and Lalor, N. *Optimisation of Noise Control Measures in Complex Lightweight Sheetmetal Structures by Using Energy Flow Analysis*. Proc. BRITE EURAM 2nd Technological Days, 1989.
- [6] Bies, D.A. and Hamid, S. *In Situ Determination of Loss and Coupling Loss Factors by the Power Injection Method*. J.S.V. Vol 90(2), 187-204, 1980.
- [7] Lalor, N. *The Evaluation of SEA Coupling Loss Factors Directly From Vibration Measurements*. ISVR Technical Memorandum No. 789, University of Southampton, September 1996.
- [8] Gelat, P. and Lalor, N. *The Experimental Determination of Equivalent Mass for an SEA Subsystem*. Paper submitted to J.S.V 1997.
- [9] Smith, jnr P.W. *Statistical Models of Coupled Dynamical Systems and the Transition from Weak to Strong Coupling*. JASA, Vol 65(3), 695 - 698, 1979.
- [10] Carr, I. and Lalor, N. *The Prediction and Reduction of Noise from Engine Covers Using Energy Methods*. ISVR Contract Report No. 89/13, University of Southampton, 1989.
- [11] Lalor, N. *The experimental determination of vibrational energy balance in complex structures*. Proc. SIRA Conference on Stress and Vibration - Recent Developments in Industrial Measurement and Analysis, London, 1989.
- [12] Faulstroh, P. and Lalor, N. *Statistical Energy Analysis of I.C. Engines*. ISVR Contract Report No. 94/18, University of Southampton, 1994.
- [13] Lalor, N. *A Note on Equivalent Mass/Volume*. ISVR Technical Memorandum No. 740, University of Southampton, 1994.
- [14] Lalor, N. and Bharj, T. *The Application of SEA to the Reduction of Passenger Car Interior Noise*. Proc. 27th ISATA Conference on Mechatronics, Aachen, 1994. 343 - 349.
- [15] Lalor, N. and Stimpson, G. *FEM + SEA + Optimisation = Low Noise*. Proc. ATA Conference on Vehicle Comfort, Bologna, 1992.

## **Application of Statistical Energy Analysis (SEA) to the Development of a Light Truck Sound Package**

Xianli Huang, Mark J. Moeller, James J. Lee and Robert E. Powell  
Ford Motor Company  
P.O. Box 2053, Dearborn MI 48121-2053

### **Abstract**

This paper describes the application of Statistical Energy Analysis to the development of a light truck sound package. The development concerns addressed included airborne engine noise, tailpipe exhaust noise and rear road noise. SEA provided a framework to investigate different sound package configurations quickly and easily. SEA helped prioritize design alternatives to maximize benefit/cost ratio and to shorten development time. The project resulted in significant contributions to the development and optimization of the sound package and added value to the vehicle.

The first section describes the development and baseline validation of the SEA model. The model was checked and updated based on data gathered by "Engine Noise Simulator" (ENS) testing, and similar testing for tailpipe and underbody noise. Both microphone and acoustic intensity data were collected and compared to model performance. Once the model was baselined, it was used to develop sound package alternatives. For airborne engine noise, a model and physical Designed Experiment (DEX) was carried out to verify that the model accurately spanned the design space. The model results and hardware DEX gave similar trends. Design recommendations were made to the vehicle program and proved out in hardware. The model was also used to drive sound package design changes for airborne noise in the rear.

### **1. Introduction**

Shorter design cycle times are requiring manufacturers to rely increasingly on computer aided engineering (CAE) to verify performance of new designs. Interior noise has become an important performance attribute in modern passenger vehicles, as quiet and comfortable interiors are routinely expected by the customer. Accurate high frequency CAE models are required in order to design vehicles to meet targets for interior noise.

While no existing single technology offers sufficient accuracy to cover vehicle noise prediction over the full frequency range of human hearing, current CAE practice appears to divide the noise, vibration, and harshness (NVH) spectrum into two ranges: low and high

frequency. Low frequency models use a deterministic approach, usually based on finite element or boundary element representations of acoustic spaces. High frequency models use a statistical approach, usually based on some form of SEA. The statistical approach works with energy and power, predicting mean-square acoustic responses averaged over spatial volumes and frequency bands. The dividing line between the low and high frequency ranges is quite blurred – vehicle excitation and response appear to be mainly deterministic below 80 Hz, and mainly statistical above 250 Hz, with both aspects apparent in the intermediate or middle frequency range. For development of vehicle sound package, SEA is the most appropriate system modeling tool since the sound package performance is targeted at the higher frequency range, and in fact has limited effect at lower frequencies.

The SEA technique is rooted in the work of the early 1960's when working groups attempted to address serious structural acoustics problems in defense and aerospace applications. The concept of power flow in structures was developed. Considerable success was recognized in aerospace structures during this time period. In the late 1960's, increasing publication activities were seen on the development of a theoretical basis for working methods [1]. The applications spread into shipboard and building acoustics fields. In the 1970's, routine uses of SEA were seen in navy surface and submarine applications.

The first full motor vehicle SEA model presented in the literature was developed by DeJong in 1985 [2]. Interest in applying this technology to vehicle development has steadily increased since then. DeJong's was a relatively coarse model containing 36 subsystems for a 1/2 car model. The analysis range was from 63 Hz to 2 kHz for road, powertrain and wind noise sources. Analytical SEA models of passenger vehicles have been reported by Steel [3], Cimerman [4], Dong [5], Moeller [6], and Lee [7]. Because of concern over the complexity in automotive systems, a test based procedure for building SEA-like coupling matrices has also evolved. These procedures have been reported by Shaw [8], Lalor [9], Walsh [10], and Bharj [11]. Chen [12] compared a test based model to an analytical model for a light truck. Bharj [13] combined a test based and analytical model into a hybrid coupling loss factor matrix.

The analytical SEA modeling technique was applied in the program described here. The approach selected was to develop a single general purpose SEA model of a light truck. The SEA truck model has been applied in the simulation of airborne noise transmission phenomena. Presented here are three cases to evaluate the body design in terms of powertrain and road noise:

1. Airborne Engine Noise – The engine noise simulation was to investigate the noise insulation performance of the front end of the body system. The engine noise source was replaced by a simulator which was a cluster of loud speakers distributed on the envelope of the engine and transmission blocks.

2. Airborne Tailpipe/Exhaust Noise – For the evaluation of noise performance due to the exhaust tailpipe noise source, a tailpipe noise simulator was used in the vehicle design stage. The tailpipe simulator was basically an electric horn to excite acoustically at the exhaust location.

3. Airborne Tire Noise – To evaluate tire noise, the airborne sound radiated from the interaction of tire and road was required. The reverberant sound pressure in the wheelwell measured in chassis dynamometer testing was imposed as the model excitation. In this study, only the rear wheels were used.

## **2. Model Development and Validation**

### **2.1 GENERAL APPROACH TO MODELING**

The modeling philosophy adopted in this investigation was to build one general purpose SEA model to describe the light truck interior acoustic response to a variety of external loads. In SEA modeling, it is imperative to capture the detail necessary to describe the dynamics of the critical, or dominant, path. The model will be less sensitive to any modeling details on non-dominant paths. Realistic sound package optimization for simulation of “key life” events requires having multiple sources active over fairly wide frequency ranges. The sources can include road noise, both structureborne through the tire and airborne radiated from the tire; airborne and structureborne powertrain noise; wind noise; aspiration noise; component noises; and tailpipe/exhaust noise. There are a multitude of paths active from each of these sources with strengths varying widely with frequency. Any sound package optimization for one source acting independently would be less than optimum for the vehicle as a whole. Also, different events will have very different excitations, or load cases. Some “key life” events of interest include rough road at 35 mph, smooth road at 85 mph, steady acceleration, as well as impact and transient events.

The sound quality of the result must be considered as well as the overall level. To meet these challenges, a very detailed SEA model was developed that has sufficient detail to capture a variety of sources and their associated paths. An analytical model was chosen so that the predictions could be applied early in the program before representative hardware was available. Acoustic refinement in hardware requires nearly production level vehicles to produce meaningful results. The SEA model allowed estimates to be made earlier in the program. One advantage of an analytical coupling matrix is the ability to compute design sensitivities, either directly from the matrix or by differencing results of two different model runs. There is no direct way to tie sensitivities to design variables in the test based technique.

Two different techniques for sound package modeling have evolved as well. The technique adopted here is to explicitly model the sound package as elements in an SEA model. This



technique is described in Powell [14]. It is an asymptotic technique that captures the high frequency behavior of the lay up of materials. Another technique is described by Cimerman [4] and involves using apriori information about the lay up behavior in terms of transmission loss and insertion loss. The apriori information can come from test or external analysis. The advantage of the former method is that parameter sensitivity is directly available from the code and does not need to be externally generated.

The SEA approach adopted here is a general purpose analytical model with self contained full parameter design sensitivity. This allowed the model to be used for multiple sources with extensive sensitivity calculation and optimization.

## 2.2 STRUCTURAL MODELING

For the vehicle structure, the sheet metal components were modeled with elementary structural members for which wave propagation theories have been developed. The systems used in this model were beams, plates, and cylindrical shells. However, the wave modes on the structure were the principal entities. The bending and inplane waves on the structural members were treated separately. The inplane waves combine both the longitudinal and shear waves since the wave properties are similar and the two are strongly coupled to each other.

Plate subsystems were used to model most of the sheet metal panels. In the high frequency range, where wave lengths are much shorter than the radii of curvature, the effects of curvature can often be ignored. This simplification generated acceptable results. Many of the structural members were modeled as beams or shells with thin circular cross section, that included both one-dimensional and two-dimensional deformations. Inplane subsystems were included for all of the structure, in parallel with the flexural subsystems.

A junction is a connection between structural/acoustical subsystems defined by a common motion. In this model only the local geometry at the junction was used to define the interaction between component modes. The major junctions were the interfaces among the plates, shells and acoustic spaces.

## 2.3 SOUND PACKAGE MODELING

The trim and sound package design play two roles in isolating the car passenger interior from unwanted noise. Its design is to insulate the interior from airborne noise by increasing the transmission loss of the structure. Transmission loss is the ratio of sound power incident on the body structure to the sound power transmitted to the interior, expressed in decibels. The second role is to reduce the level of structureborne noise radiated to the interior at high frequency. This reduction is also expressed in decibels as the insertion loss. The trim and sound package design decouples the steel panels from the interior at higher frequencies.

The sound package design can also affect the absorption of sound in the interior. It is important to characterize all of these effects in the SEA model.

In the special case of trim added on top of a structural member or carpet over a panel, the increased transmission loss and insertion loss were modeled using five subsystems and two junctions. The subsystems were: outside air, plate bending, trim enclosed air, trim mass/bending layer, and inside air. The trim enclosed air represents the acoustic space between the structural member and the trim. If the trim air space is fiber filled, as under a carpet layer, the damping should be high to represent the sound attenuation in a porous material.

The coupling through sound package decoupler was specified by two junctions. The outside air was connected to the trim air with the plate bending as a barrier. Then the trim was connected to the inside air with the trim layer as the barrier. For holes in the trim, an additional area junction was used to connect the trim air to the inside air. The mass of the air column in the opening was explicitly modeled to capture the Helmholtz effect.

## 2.4 BASELINE VALIDATION OF THE MODEL

The baseline validation of the light truck SEA model with Engine Noise Simulator (ENS) test results was important for several reasons: verification of the configuration assumptions adopted in building the model, guidance for improvement in the model building process, and for the product's NVH improvement. The ENS equipment was simply a set of speakers mounted on an engine-shaped wooden box, as described in Griffiths [15]. There were low and high frequency loudspeakers installed on six faces of the box. The loudspeakers on each face were excited while loudspeakers on the other faces were inactive. The most important feature for the ENS facility was its good repeatability of test results (within 1 dB) with a white noise excitation. During the test, the vehicle's power train and drive-line were removed. The test was conducted in a semi-anechoic room.

The ENS airborne noise test for the light truck SEA model validation included 77 microphone and 11 acceleration measurements that were grouped into 4 clusters: source (engine compartment), environment (exterior), structure radiation (vibration) and target (interior) as shown in Figure 1. Twelve microphones were placed in the engine compartment to characterize the noise source. The exterior sound pressures were surveyed at locations underneath the floor panels, over the hood, windshield and roof, and beside the outer panels and glass. Eleven vibration measurements were concentrated on the frontal areas such as dashboard, floor panel, roof, windshield glass, door panel and side glass. Twenty microphones were located in the interior at driver's and passenger's ears, knees and toe board areas, inside the hinge-pillar and behind the instrument panel to survey the major noise transmission path characteristics from the engine compartment to the passenger cabin.

The SEA model validation process involved checking, verifying and modifying the model to capture the dynamics of the hardware, as shown in the test data. The first step was to use the SEA model predicted "thermal graph" described by Moeller [6,16], which represents the modal energy response, to check the model connectivity. The criterion was that the modal energy should diffuse smoothly from the source to the far-field sink. The phenomena were easily visualized through a finite element display model. The second step was to correlate the model response predictions to the test data. The discrepancy information between the predicted and measured responses, combined with model predicted power flow information, was used to locate and correct model building errors, as well as to verify and validate the model assumptions and strategies. The correlation process follows the noise transmission paths from source to the target. In this case the target was driver's and passenger's ear locations. The model predictions and test measurements are shown in Figure 2. The results show good agreement to the ENS test measurements, suggesting that the model captured the major dynamics of the hardware.

The light truck SEA model, validated by the ENS tests for engine presence, was then applied to evaluate and develop the sound package in the cargo area for the tailpipe noise excitation. Since the SEA model was refined to include more details in the vehicle cargo area, additional validation was conducted for the rear part. The Tailpipe Noise Simulator (TNS) was used to excite the vehicle in the same facility used for the ENS test. The noise source for the SEA model was described by a series of sound pressure measurements around the TNS and the measured sound pressures were imposed as the excitation to drive the model. Transfer function comparisons around the second seat passenger's head position are shown in Figure 3. It can be seen that the transfer functions at this position have some discrepancy over 2,500 Hz, which was assumed to be caused by the directionality of the acoustic power radiated from the tailpipe simulator.

## 2.5 INTENSITY VALIDATION OF THE MODEL

A sound intensity test for the vehicle in the semi-anechoic room was conducted to further verify the SEA model predictions. The above model validations for engine and tailpipe noise sources were carried out to correlate the predicted model responses with the measurements in terms of sound pressure levels (SPL). The point SPL and/or spatially-averaged SPLs in a subsystem are a scalar index which contains all contributions from adjacent subsystems and no information on power flow directionality. It requires a large amount of measurements along the noise path to capture the major dynamics of the system. Sound intensity scanning over the surfaces of subsystems captures both the magnitude and the directionality of energy flow. The sound intensity predictions on subsystem surfaces in SEA models were compared to the measured sound intensities over the hardware surfaces to further validate the SEA model.

Instruments used in the test included a B&K 2144 Real Time Intensity Analyzer with B&K 4181 and 4183 Sound Intensity Probes. The sound intensity scanning was performed under

the Tailpipe Noise Simulator excitation. The scanning areas included the surfaces of the cargo floor panel, quarter panel trim, quarter panel glass, and the liftgate panels inside the rear cabin.

Figures 4 and 5 show the power flow comparison over the cargo floor panel carpet and headliner surfaces. The gray areas in the figures denote the power flows into the vehicle interior from the surface over which the sound intensity was scanned and the white areas indicate the power flows into the surface. The SEA model power flow predictions show a good similarity to the power flows recorded on the hardware surfaces. Especially in the cargo floor carpet case, not only does it show the similar pattern but also accurately predicts the transition frequency at which power flows change direction. In addition, the information on the power flow patterns over the sound package surface provided a framework for thinking about development of sound package designs.

### 3. Exercising SEA for Design

The light truck SEA model was intensively validated under different loads and by different criteria. The results show that the model was robust in terms of predicting the trends and patterns of the hardware dynamics. The validation process itself provided good insight on where and how the sound package should be developed. The SEA model was then used to explore the design space, to improve the acoustic performance of the vehicle, and to evaluate and assess the sound package design alternatives.

The model was first used to address engine presence NVH issues and to guide the evaluation and development of sound package designs for airborne noise. Eight sound package changes were proposed for evaluation. The dash doubler was a composite of two sheet metal layers with mastic in between. The engine side dash insulator was a sheet of fiber glass material placed in the central part of the dash on the engine compartment side. The hood absorber was a sheet of fiber glass attached beneath the hood. Hush panels were plastic panels with a layer of foam attached to close out the bottom of the instrument panel openings.

The design variables were converted to the appropriate SEA model parameters and implemented in the SEA model to conduct a DEX to predict effectiveness of the proposed sound package. The hardware was tested on the light truck for the same DEX. Comparing the effects plots in Figures 6 and 7 show that the light truck model captured the major dynamics of the hardware and was capable of identifying the response change patterns and trends when the hardware was modified.

The model was also used to develop sound package in the rear part of the vehicle to reduce the noise due to the tailpipe and road noise excitations. The target was to reduce the sound pressure levels at the second row passenger's ear locations. To achieve this goal optimally,

the model was used to identify the major sound transmission paths from the noise source subsystem to the target subsystem where the second row passenger's heads are located. This process was performed beginning at the target. First, power flows into the target from its adjacent subsystems were checked. Then the subsystem which had the maximum contribution was selected. That subsystem's maximum contributor was followed and so forth until the source subsystem was reached. The sequentially selected subsystems constitute the major noise transmission path. The maximum contributors to 2nd row passenger's ear subsystem were the cargo upper acoustic space below 1,000 Hz, and the rear door window above 1,000 Hz. Then we traced the major contributor to the cargo upper subsystem, which showed that below 1,000 Hz the major contributor is the cargo lower subsystem. The major contributor to the cargo lower subsystem was identified as the lift-jack compartment, Figure 8, which is directly connected to the rear wheel well, i.e., the noise source. Based on these analyses, a decoupler consisting of a barrier with foam was recommended to cover the rear wheel well to block and absorb the sound transmission from the rear wheel well. Figure 9 shows that noise reduction difference between the baseline and the baseline plus rear decoupler averaged about 1.3 dB across the frequency spectrum.

#### 4. Conclusions

A multipurpose SEA model of a light truck was built to evaluate its airborne noise insulation performance.

1. The model was validated against three different criteria: steady state field response, acoustic intensity/power flow comparisons and software/hardware DEX.
2. The validated model was used to guide development of the vehicle sound package resulting in shortened vehicle development time.

#### Acknowledgments

The authors would like to thank Taner Onsay and William Hanke who both contributed to this effort.

#### References

1. Lyon, R.H. and DeJong, R.G., (1995) *Theory and Application of Statistical Energy Analysis*, 2nd Edition, Butterworth-Heinemann, Boston.
2. DeJong, R.G. (1985) A Study of Vehicle Interior Noise Using Statistical Energy Analysis, SAE Paper 850960.
3. Steel, J.A., (1996) The Prediction of Structural Vibration Transmission Through a Motor Vehicle Using Statistical Energy Analysis, *Journal of Sound and Vibration*, Vol 193(3), pp691-703.
4. Cimerman, B. et al. (1995) Incorporating Layered Acoustic Trim Materials in Body Structural-Acoustic Models, SAE Paper 951307.
5. Dong B. et al. (1995) Road Noise Modeling Using Statistical Energy Analysis Method, SAE Paper 951327.

6. Moeller, M.J. et al. (1995) A Novel Approach to Statistical Energy Analysis Model Validation, SAE Paper 951328.
7. Lee, J.J., et al. (1996) High Frequency Modeling of Vehicle Noise Performance of Aluminum Body Structure, presented at Acoustical Society of America Meeting, May 1996, Indianapolis
8. Shaw, S. (1987) Analysis and Prediction of the Acoustical Characteristics of Automobile Bodies Using Statistical Energy Analysis, Unikeller Conference, Switzerland.
9. Lalor, N. and Bharj, T. (1994) The Application of SEA to the Reduction of Passenger Car Interior Noise, 27<sup>th</sup> ISATA, Belgium
10. Walsh, S.J., Stimpson, G., and Lalor, N. (1990) A Computer System to Predict Internal Noise in Motor Cars Using Statistical Energy Analysis, *InterNoise 90*.
11. Bharj, T. and Pham, H. (1996) Application of Energy Flow Analysis (EFA) to Reduce Structure-Borne Noise Inside a Passenger Vehicle, *Internoise 96 Proceedings*, Liverpool, UK
12. Chen, H.Y., et al. (1995) A Comparison of Test-Based and Analytic SEA Models for Vibro-Acoustics of a Light Truck, SAE Paper 951329.
13. Bharj, T. and Cimmerman, B. (1996) Application of Statistical Energy Analysis (SEA) to a Passenger Vehicle, Combining Analytical and Test Based Prediction in a Hybrid Model, *InterNoise 96*, Liverpool, UK.
14. Powell, R.E., Zhu, J., Manning, J.E. (1997) SEA Modeling and Testing for Airborne Transmission Through Vehicle Sound Package, SAE Paper 971973.
15. Griffiths, D., Farahanchi, F., Mayer, T. (1995) Experimental Analysis of Interior Noise Due to Powerplant Radiated Noise, SAE 951266.
16. Moeller, M.J. (1994) Visualization of Statistical Energy Analysis Results, Acoustical Society of America Meeting, Cambridge Massachusetts, June 1994.

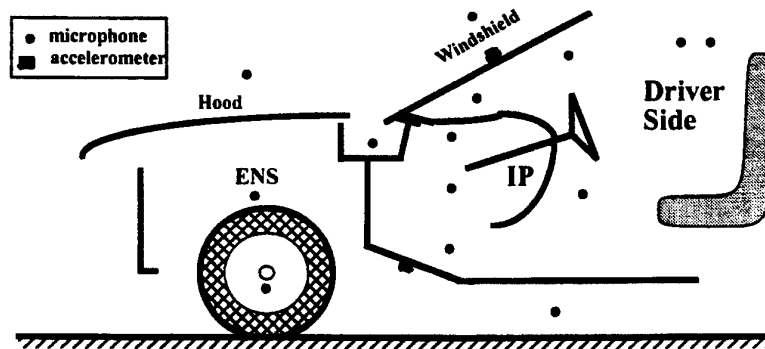


Figure 1. Sensor locations for engine noise simulator test.

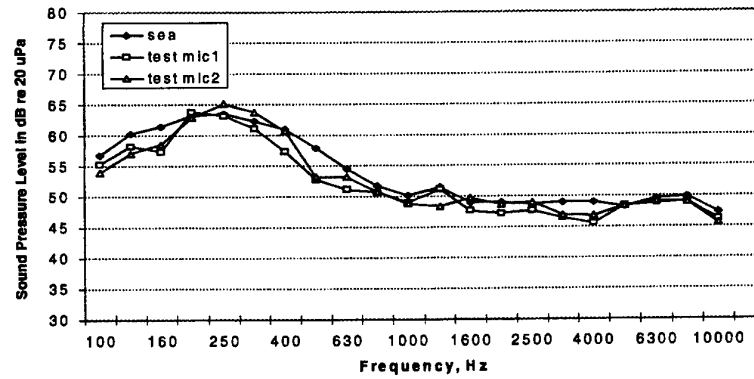


Figure 2. SEA model prediction and ENS test measurement, driver head space.

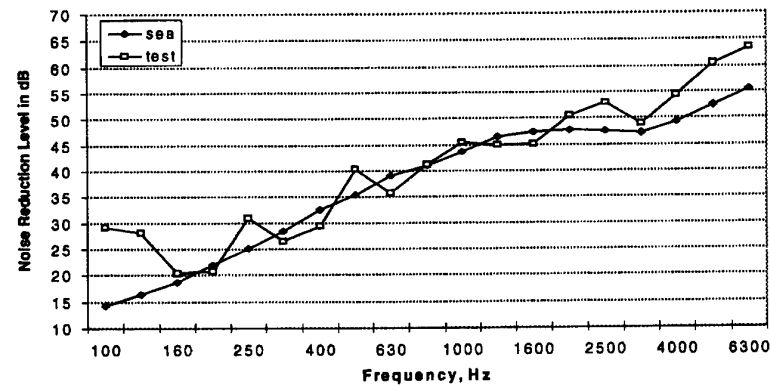


Figure 3. SEA model prediction and tailpipe simulator test measurement, second seat passenger head.

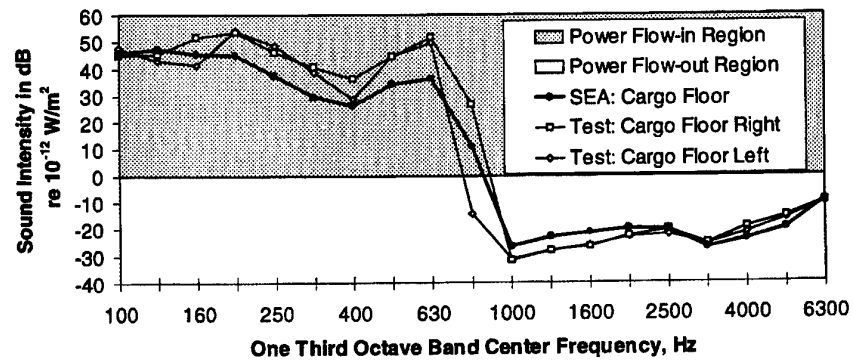


Figure 4. Tailpipe noise simulator, sound intensity, cargo area floor.

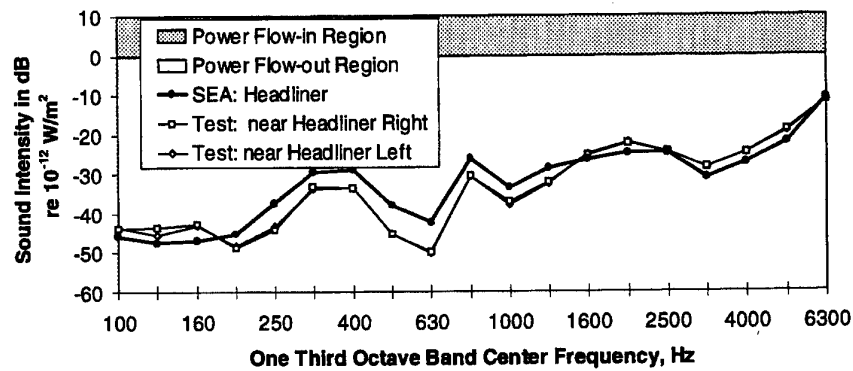


Figure 5. Tailpipe noise simulator, sound intensity scan, headliner area.

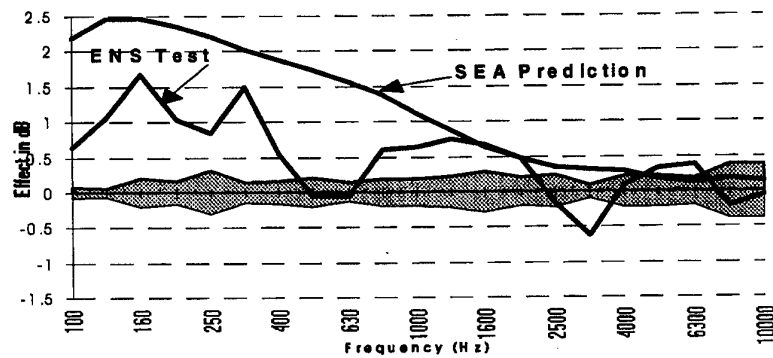


Figure 6. Engine noise simulator designed experiment, dash doubler effect at driver head.

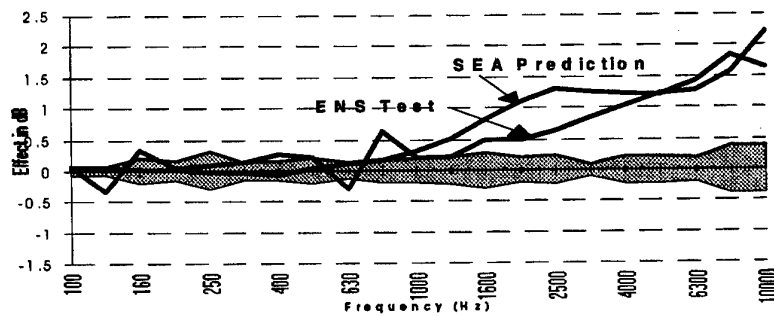


Figure 7. Engine noise simulator designed experiment, cowl side insulator effect at driver head.



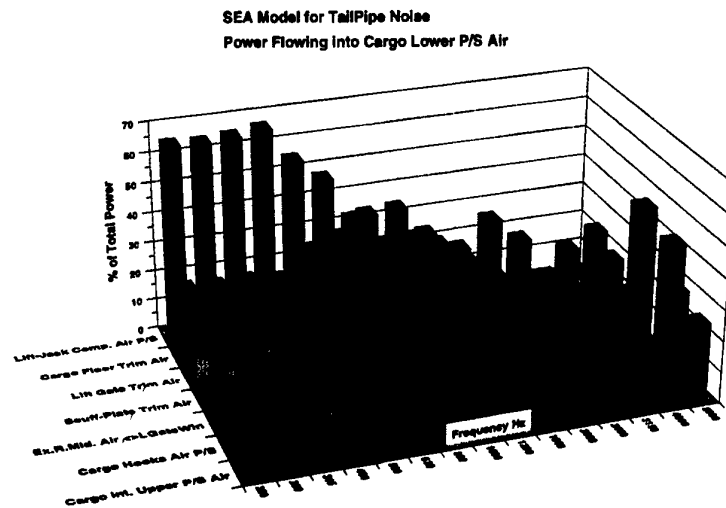


Figure 8. Power flowing into passenger side cargo lower acoustic space

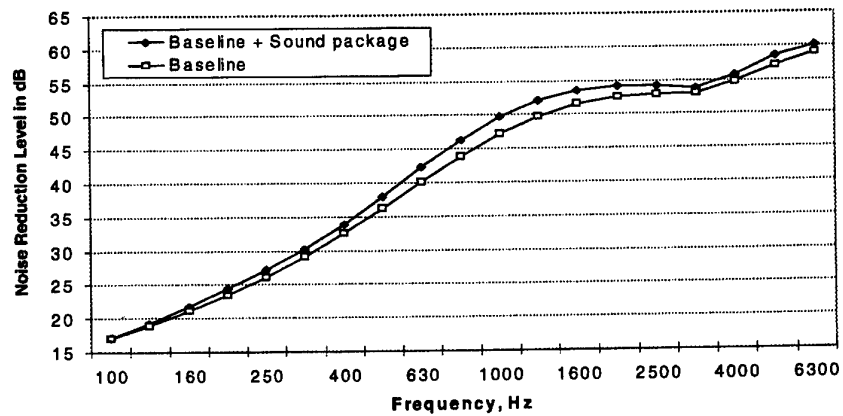


Figure 9. Second row passenger's ear noise reduction prediction comparison between the baseline SEA model and baseline plus sound package under rear wheel well excitation.

## **PREDICTING NOISE TRANSMISSION IN A TRUCK CABIN USING THE STATISTICAL ENERGY ANALYSIS APPROACH**

**Dr. GERARD BORELLO**

*InterAC*

*10, impasse Borde-Basse ZA La Violette 31240 L'Union France*

A Statistical Energy Analysis (S.E.A.) based model of a truck cabin has been developed in collaboration with the Research Center of RVI (Renault Véhicules Industriels) in Lyon, France. The aim of the associated study was the determination of virtual (as for numerical but realistic) potential solutions for improving the sound quality within the driver's cabin. It was why this model was initially planned to predict the internal noise due to an external acoustic loading and due to mechanical forces applied to the chassis expected to be the main sources for this type of vehicle. An hybrid approach, mixing experimental SEA and analytical SEA modeling, was chosen from the beginning to reach the virtual noise reduction objectives.

### **1. Testing the actual cabin**

Prior to investigate noise control solutions, the robustness of the model needed to be proven.

A five days test campaign on a truck vehicle was undertaken for creating the S.E.A. experimental database.

The main following tests were performed on the RVI vehicle :

- Identification of coupling and damping loss factors by the power injection method using a 18 subsystem experimental SEA model. This task implies measuring the power injected in the different subsystems with a calibrated excitation as well as measuring the corresponding energy transfers by recording all cross transfer inertances between coupled subsystems. An impact hammer was used as the excitation process.
- Measurement of sound pressure levels (SPL), acceleration in some locations and power injected under steady state excitation using a shaker attached to the chassis.
- Measurement of reverberation time in the cabin.
- Simulation of an external acoustic loading using a loudspeaker located underneath the cabin and collect of subsystem accelerations and SPL's.
- Internal excitation of the cabin using a loudspeaker and collect of some accelerations and SPL's.

The experimental S.E.A analysis has allowed the identification of experimental damping loss factors (DLF) and coupling loss factors (CLF) of the different panels constitutive of the cabin. The other test results were used to compare with corresponding simulations using the analytical SEA model of the cabin developed with the AutoSEA software.

## 2. The SEA experimental model

Only direct coupling loss factors corresponding to direct links between subsystem (as sketched in Figure 1) were computed using the AutoSEA-X [3] software developed by InterAC company.

In this software the DLF's are calculated separately from the CLF's using the following matrix equations where  $C_{ij}$  corresponds to the normalized transfer energy between subsystems  $i$  and  $j$  and  $P_i$  to the normalized power injected ('normalized' meaning dividing each quantity by the excitation force autospectrum). These equations are assuming no damping losses within joints.

$$\begin{bmatrix} \eta_1 \\ \eta_i \\ \eta_N \end{bmatrix} = \begin{bmatrix} C_{11} & C_{1i} & C_{1N} \\ C_{i1} & C_{ii} & C_{Ni} \\ C_{iN} & C_{iN} & C_{NN} \end{bmatrix}^{-1} \begin{bmatrix} \frac{P_1}{\omega_o |F_1|^2} \\ \frac{P_i}{\omega_o |F_i|^2} \\ \frac{P_N}{\omega_o |F_N|^2} \end{bmatrix}$$

*Equations for DLF identification*

The calculation of CLF's is based on the herebelow equations and associated theory can be found in [1,2].

$$\begin{bmatrix} \dots \\ \eta_{ki} \\ \dots \end{bmatrix}_{k=\alpha, N \text{ et } k \neq i} = \begin{bmatrix} \frac{C_{\alpha\alpha}}{C_{i\alpha}} - \frac{C_{\alpha\alpha}}{C_{ii}} & \dots & \frac{C_{N\alpha}}{C_{i\alpha}} - \frac{C_{N\alpha}}{C_{ii}} \\ \vdots & \frac{C_{kk}}{C_{ik}} - \frac{C_{ki}}{C_{ii}} & \vdots \\ \frac{C_{\alpha N_i}}{C_{iN_i}} - \frac{C_{\alpha i}}{C_{ii}} & \dots & \frac{C_{N_i N_i}}{C_{iN_i}} - \frac{C_{N_i i}}{C_{ii}} \end{bmatrix}^{-1} \begin{bmatrix} \frac{P_i}{\omega_o C_{ii} |F_i|^2} \\ \frac{P_i}{\omega_o C_{ii} |F_i|^2} \\ \frac{P_i}{\omega_o C_{ii} |F_i|^2} \end{bmatrix}$$

*Equations for CLF identification*

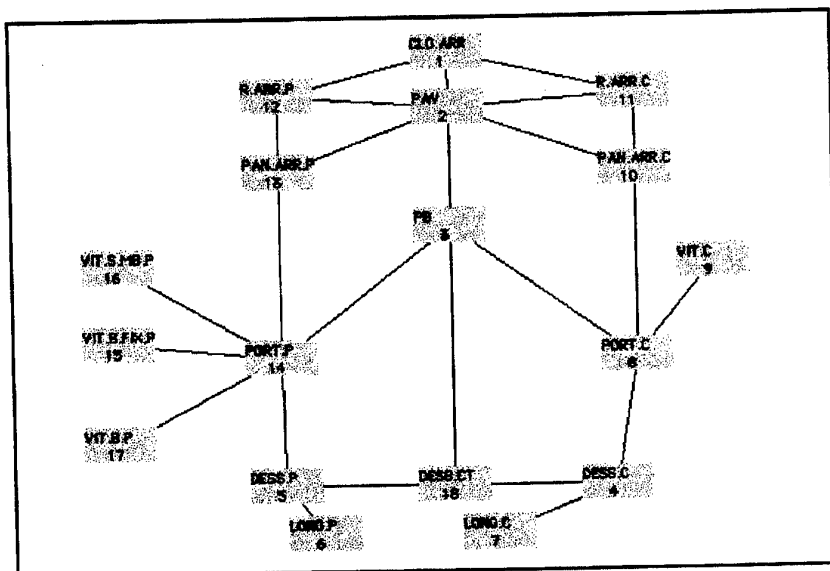


Figure 1. Connectivity of the 18 subsystem experimental SEA model

Rather large standard deviation were found in space frequency averaged velocity squared estimates used for the computation of normalized transfer energies (see Figure 2) due to some complexity on corresponding structures and the limited duration of the experimental SEA testing (limited number of transfer inertances for each subsystem).

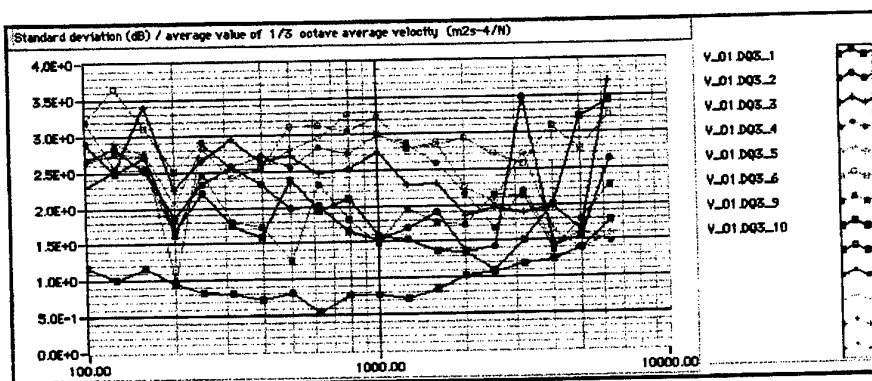


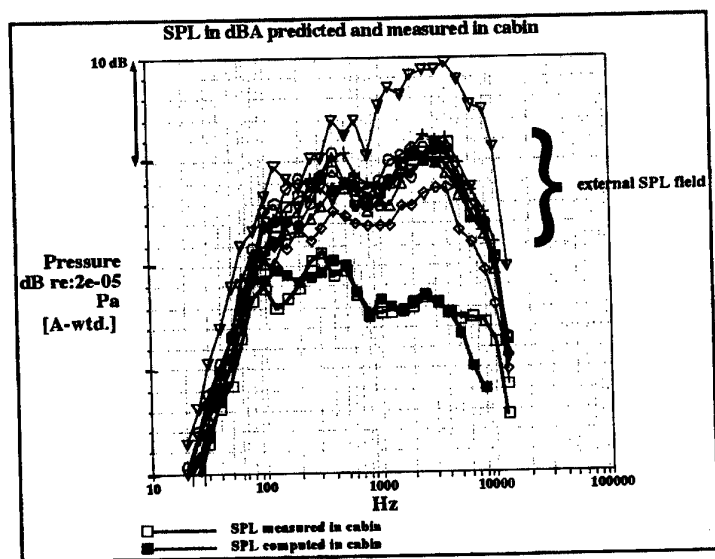
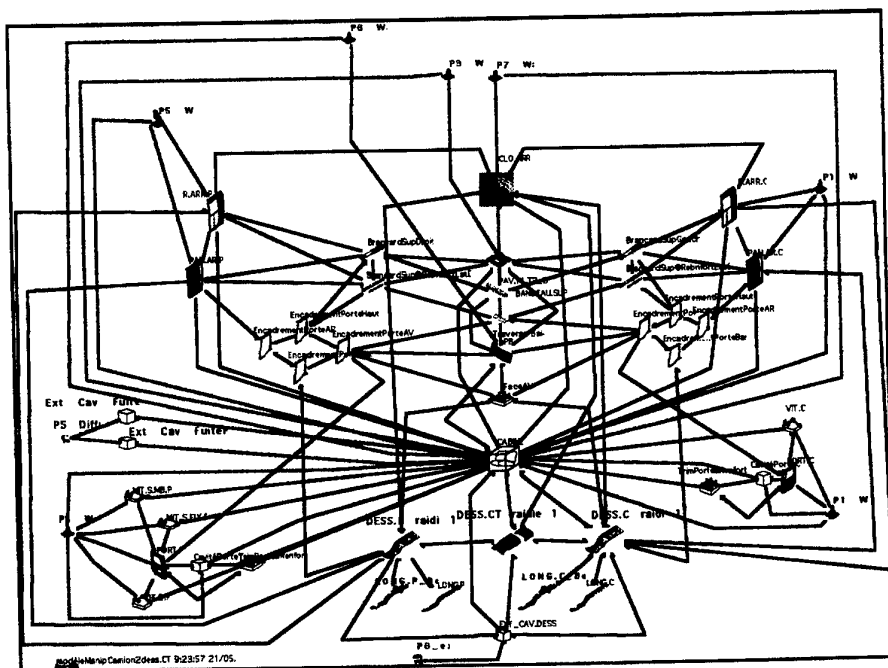
Figure 2. Standard deviation in dB in subsystem velocity squared estimates

### 3. The analytical SEA model

The model was graphically constructed within AutoSEA [4] from RVI sketches and drawing as shown in Figure 3. This model was built using the standard AutoSEA of flexural plate and cylinder SEA elements. Then the measured DLF's were imported within the model through the neutral file format of AutoSEA. Some measured injected power were used to validate asymptotic SEA input mobilities calculations on subsystems where simple theory needed to be tuned. Simulating an external acoustic loading with the analytical model leads to the comparison given in Figure 4. We can see the prediction of the cabin SPL is pretty good in a frequency bandwidth that starts from around 100 Hz up to 5 to 6 kHz. This result has only been obtained after import of experimental DLF's within the analytical model. Prior to this import, using preliminary constant value of DLF vs frequency was leading to SPL discrepancy of about 6 to 10 dB between test and prediction in many frequency bands making the correlation with the test a nearly impossible task. After DLF import, the discrepancy was reduced to a few dB, allowing then for a better interpretation of differences between test and prediction and some improvement of the modeling was achieved by playing on the structural characteristics of some subsystems.

When loading the chassis using a randomly excited shaker, the analytical model shows satisfactory trends in term of noise transmission in the frequency bands where the comparison is possible (when above the background noise of the test work room). Good correlation with acceleration measurements in some reference points was also observed, leading to the conclusion the model was also suitable for analyzing structural transmission coming from the engine attachment points (most of the CLF's were analytical in this case).

Accurate prediction of the behavior of some particular subsystems was not achievable but these singularities were identified and recommendations given to RVI as using alternative SEA libraries or local finite element results but it was still possible to frame the trends.



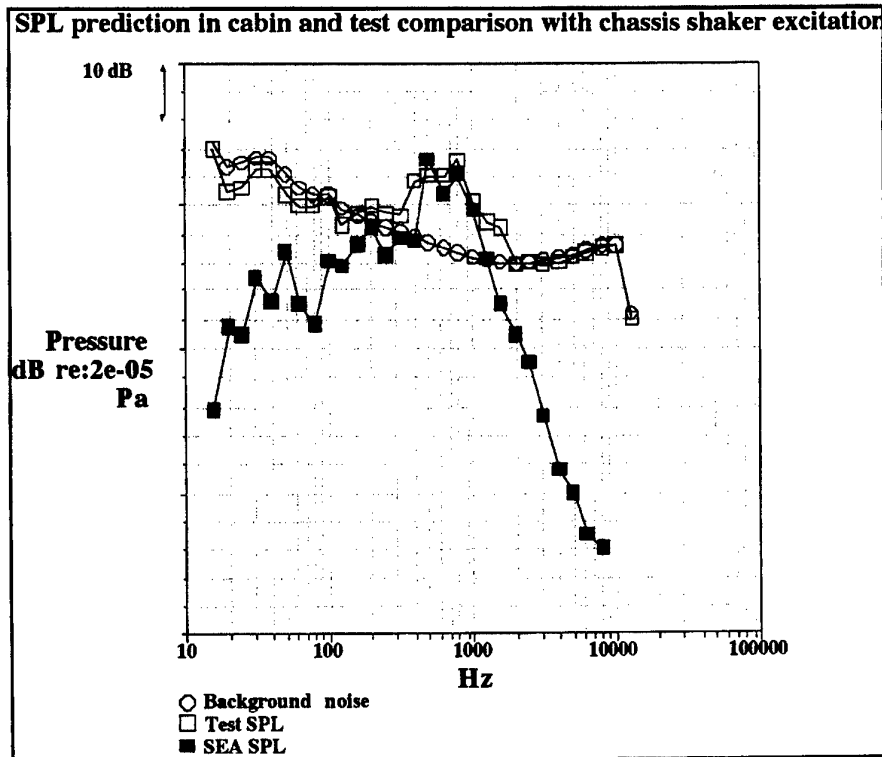


Figure 5. Predicting SPL inside cabin and comparing with corresponding measurement in exciting the chassis with a shaker. The cabin experimental SPL only emerges from the background noise between 300 and 1000 Hz

#### 4. The optimization of sound transmission in cabin

The base of the optimization of sound pressure levels in the cabin is to minimize (in the analytical model) input powers from all connected sources radiating within the cabin after appropriate ranking. These contributions are shown in Figure 6.

From this analysis, floor and side panels are mainly contributing on a frequency broad band scale but with different paths (resonant or non resonant depending of the frequency band).

The model also shown that noise reduction solutions based on increase of internal damping were rather inefficient. Performance of solutions based on improved trim panels or mass adjunction were evaluated that showed improvement of around 10 dB mainly above 500 Hz.

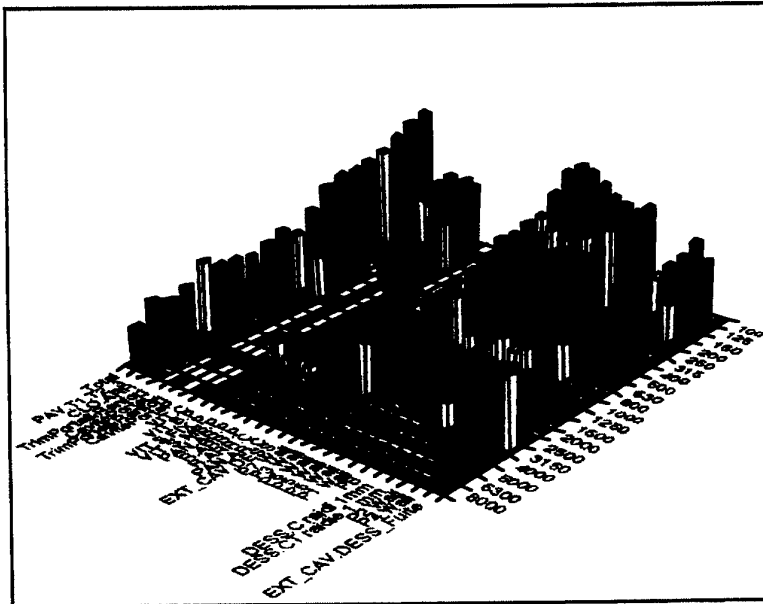


Figure 6. Distribution of power inputs within the cabin acoustic space vs subsystems and frequency

## 5. Conclusions

A theoretical model of a truck cabin was developed for understanding the respective contributions of the different structural components to the internal sound pressure level. This model shows that using an analytical SEA model enhanced by the import of experimental damping loss factors, it is possible to predict the global vibroacoustic behavior of the cabin to various external loading : external acoustic sound field to simulate engine noise radiation and force punctual excitation to simulate input of structural vibration by the engine mounting blocks. This model is then used to find solutions for noise reduction and to quantify their performance.

## 6. References

1. N.Lalor : The measurement of SEA loss factors on a fully assembled structures, *ISVR Technical Memorandum n° 150*, August 1987.
2. R.S.Ming, G.Stimpson, N.Lalor, On the measurement of individual coupling loss factor in a complex structure, *INTERNOISE 90 Conference*, Gotheburg 1990, 961-964.
3. AutoSEA-X, software for data acquisition and experimental SEA : *user guide of version 1.1*.
4. AutoSEA software for analytical SEA modeling *user guide of version 1.5*.



## STATISTICAL ENERGY ANALYSIS OF FLUID-FILLED PIPES

S. FINNVEDEN<sup>†</sup>  
*I.S.V.R., University of Southampton*  
*Southampton, SO17 1BJ, England*

### 1. Introduction

It is possible to make predictions of pipework vibrations at low frequencies using beam models. However, once the shell modes in the pipe walls are cut-on, the number of degrees of freedom required for classical methods increases dramatically. Today, the general trend to save costs and weight results in that higher quality steels are introduced to allow for a reduction of wall thickness. This reduces the cut-on frequencies for higher order radial-axial modes considerably and, as a consequence, 'high frequency' methods are needed also at 'lower' frequencies.

In an ongoing project in Southampton the feasibility of using statistical energy analysis (SEA) for screening pipeworks to find potential risks for fatigue is investigated. In this project, first a direct dynamic FEM was developed for analysing vibrations of fluid-filled pipes [1]. The objective was to have an accurate tool for performing numerical experiments and for verifying approximate theory. Second, based upon the experience gained, a simplified theory for the radial-axial vibrations was developed and was used for deriving closed form expressions for wave numbers, modal density and input power from point sources [2, 3]. Third, a 3-d.o.f. SEA element was formulated. This element is useful when, because of damping, the energy density varies within an element [4]. Fourth, methods and software were developed for calculating SEA coupling loss factors. So far these routines have been applied to flange connections [5].

Here, the results in [2, 3, 5] are compiled and are used to formulate a SEA model for a small pipe structure. The results are compared to those from calculations using the spectral FEM [1] showing good agreement. It is believed, SEA has the potential to become a standard method for predicting noise and vibration in pipeworks at somewhat higher frequencies, thus complementing beam models.

### 2. Waves in fluid-filled pipes

The waves in fluid-filled pipes were originally investigated by Fuller and Fahy using a semi-analytical method [6]. To increase efficiency, Finnveden [1] developed a FE method in which the radial dependence of the sound pressure was approximated with polynomial trial functions.

The first step in an analysis of pipes is to decompose the motions circumferential dependence in a Fourier series. In this series, the first,  $n = 0$ , term has no circumferential dependence; the  $n = 1$  term has one wavelength around the circumferential; the  $n = 2$  term has two wavelengths; and so on. At lower non-dimensional frequencies, there are four

<sup>†</sup> Also at the Dept. Vehicle Engineering, KTH, SE-100 44 Stockholm, Sweden

types of waves that can propagate in fluid-filled pipes: 1) Torsional,  $n = 0$ , waves in the pipe wall which are not coupled to the fluid motion; 2) Beam-type,  $n = 1$ , bending waves with the fluid mass added to that of the pipe; 3) Coupled axi-symmetric,  $n = 0$ , dilatational waves which are predominately as: a) Longitudinal waves in the pipe wall with some radial motion because of 'Poison coupling'; b) Plane acoustic waves forcing some radial motion of the pipe wall.

At somewhat higher frequencies, higher order radial-axial ( $n = 2$ , 'ovaling',  $n = 3$ , 'teddy bear', ...) waves can propagate. The cut-on frequencies for these waves are [2]

$$f_{c,n} = \frac{c_L}{2\pi R} \sqrt{\frac{\beta(n^2 - 1)^2}{1 + 1/n^2 + \mu/n}}; \quad (1)$$

$$c_L = \sqrt{E'/\rho}; \quad E' = E/(1 - \nu^2); \quad \mu = R\rho_f/(2T_c\rho); \quad \beta = T_c^2/12R^2.$$

$E$  is Young's modulus,  $\rho$  is the pipe wall density,  $\nu$  is Poison's number,  $R$  is the cylinder radius,  $T_c$  is the pipe wall thickness and  $\rho_f$  is the fluid density.

Besides these waves, at even higher frequencies, there is the axi-symmetric flexural wave, cut-on at the ring-frequency, and non-planar predominantly acoustic waves as well as non-planar longitudinal and torsional waves. For commonly used engineering materials, the first of these waves that can propagate is the first higher order acoustic wave, the  $n = 1$  mode, which is cut-on approximately at a frequency

$$f_{c,a} = 1.8 c_f / 2\pi R. \quad (2)$$

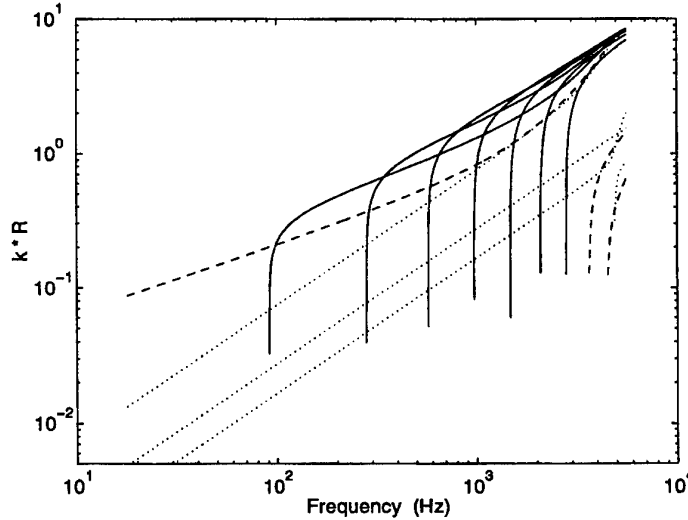


Figure 1. Wavenumbers in fluid-filled pipe. '...',  $n = 0$ , with increasing wavenumbers: longitudinal, torsional and fluid wave, plus flexural mode at 6 kHz; '—',  $n = 1$ , beam bending mode plus acoustic and torsional modes at high frequencies; '—',  $n = 2, 3, \dots, 8$ , radial-axial waves with increasing cut-on frequencies.

TABLE 1 Geometrical and material parameters

Material	Poissons ratio $\nu$	Density $\rho$ ( $\text{kg/m}^3$ )	Free wave speed $\sqrt{E/\rho}$ , $c_f$ (m/s)	Loss factors $\eta_e, \eta_v, \eta_f$
Steel	0.3	7800	4961	0.01, 0.01
Water	-	1000	1500	0.01

	Outer diameter (mm)	Wall thickness (mm)
Pipe	273	4.19
Flange	406	2*38

In the present work a thin-walled water-filled steel pipe is considered, the data are found in Table 1. It has a ring frequency,  $f_r = 5.9$  kHz and a cut-on frequency for the first higher order fluid mode,  $f_{c,a} = 3.2$  kHz. In Figure 1 wave numbers are shown for the propagating modes. In what follows, calculations are made for frequencies up to, and including, the 2 kHz octave band. The excitation will be a point force in the radial direction and the torsional wave is not excited. Consequently, included in the analysis are the  $n = 0$  longitudinal and acoustic waves and the radial axial waves of order  $n = 1$  until order  $n = 8$ .

### 3. Simplified equations of motion

Simplified equations of motion for the  $n \geq 1$  modes in fluid-filled pipes have been derived [2]. These derivations are based on the Lagrange formulation of the Arnold and Warburton equations for cylinder motion [7, equation (2.12a)] extended with terms modelling the fluid motion and the coupling between fluid and cylinder [1]. The same approach is here used to find equations for the  $n = 0$  modes. These simplified equations are useful for deriving the SEA parameters.

#### 3.1 AXI-SYMMETRIC MOTION

For  $n = 0$  modes the tangential (torsional) motion is uncoupled from the radial-axial cylinder motion and from the fluid. For frequencies well below the ring frequency, the axial flexural stiffness of the cylinder is negligible. Thus, as a first step, terms describing the tangential motion and the axial flexural stiffness are neglected in the Lagrangian for the cylinder motion. Second, at lower frequencies the fluid motion is to a good approximation plane, that is, without radial dependence. So, the fluid sound pressure is assumed to be

$$p(x, r) = \psi(x) / \rho \omega, \quad (3)$$

where  $p$  is the sound pressure and  $\psi$  is an analogy to the fluid velocity potential. This expression for the sound pressure is inserted into the Lagrangian, the corresponding Euler-Lagrange equations are derived and after some simplifications the equations of motion are found to be

$$\frac{\partial^2 u}{\partial x^2} + k_L^2 u + \frac{2\nu \rho \mu \omega}{E(1 - \Omega^2 - \nu^2)} \frac{\partial \psi}{\partial x} = 0; \quad (4a)$$

$$\frac{\partial^2 \psi}{\partial x^2} + k_f^2 \psi - \frac{2\nu\omega}{1-\Omega^2} \frac{\partial u}{\partial x} = 0; \quad w(1-\Omega^2) = \frac{\rho_f R^2 \omega}{E T_c} \psi - \nu R \frac{\partial u}{\partial x}, \quad (4b,c)$$

where  $u$  is the axial displacement and  $w$  is the radial displacement and where

$$k_L^2 = \frac{\omega^2}{c_L^2} \frac{1-\Omega^2}{1-\Omega^2-\nu^2}; \quad k_f^2 = \frac{\omega^2}{c_f^2} (1+\gamma); \quad (5)$$

$$\Omega = \omega R/c_L; \quad \gamma = 2\rho_f c_f^2 R / (E T_c (1-\Omega^2)).$$

These equations are similar to those derived by Pinnington and Briscoe [8].

*Wavenumbers and modeshapes.* Solutions of the form  $e^{ikx}$  are applied to equations (4) giving an eigenvalue problem for the wavenumbers. The four solutions,  $\pm\alpha$  and  $\pm\beta$ , are

$$\alpha^2 = k_p^2 + \sqrt{k_p^4 - k_f^2 k_L^2}, \quad \beta^2 = k_p^2 - \sqrt{k_p^4 - k_f^2 k_L^2};$$

$$k_p^2 = (1+q)(k_f^2 + k_L^2)/2; \quad (6)$$

$$q = \nu^2 \gamma / ((1-\Omega^2 - \nu^2)(1+\gamma) + (c_f^2/c_L^2)(1-\Omega^2)).$$

The corresponding eigenvectors are found when these values for  $\alpha$  and  $\beta$  are substituted into equations (4). It is seen that if the non dimensional number  $q$  is small, the wave numbers are close to  $k_L$  and  $k_f$ . Since the coupled solutions are pushed apart they are identifiable, so that if  $k_f > k_L$  then  $\alpha$  corresponds to the wave that is predominantly of fluid character and  $\beta$  corresponds to the predominantly structural wave.

### 3.2 RADIAL-AXIAL WAVES

For frequencies below the ring frequency, cylinder cross sectional breathing is greatly restrained. This is verified by inspection in [7, Table 2.11] where it is seen that the cross sectional mode shapes for propagating radial-axial modes are almost in-extensional. That is, to a good approximation, the circumferential strain,  $\varepsilon_\phi$  and the tangential displacement,  $v$ , are

$$\varepsilon_\phi = (n\nu + w)/R = 0; \quad v = -w/n. \quad (7)$$

This is the fundamental assumption for the derivation of the simplified theory for radial-axial motion of fluid-filled pipes [2]. Additionally, the axial flexural stiffness of the pipe wall is neglected and analysis is restricted to lower frequencies for which the pipe motion is subsonic and the fluid compressibility and fluid axial inertia are negligible. Finally, a trial function for the fluid sound pressure is found by retaining only the first term in a series expansion of the exact solution [6]:

$$p(x, r, \phi) = \psi(x) r^n \cos(n\phi), \quad n = 1, 2, \dots \quad (8)$$

Upon this basis, the expressions for the tangential displacement (7) and sound pressure (8) are inserted into the Lagrangian, the corresponding Euler-Lagrange equations are derived and after eliminating  $\psi$  the equations of motion are found

$$\begin{aligned} EI_n \frac{\partial^2 \theta}{\partial x^2} &= GA_c K_n \left( \theta + \frac{\partial w}{\partial x} \right) - \rho \omega^2 I_n \theta; \\ GA_c K_n \left[ \frac{\partial}{\partial x} \left( \theta + \frac{\partial w}{\partial x} \right) + C_n \frac{\partial^2 w}{\partial x^2} \right] &= (K_w - \omega^2 M_e) w, \end{aligned} \quad (9)$$

where  $G$  is shear modulus and where

$$\theta = n^2 u / R. \quad (10)$$

Above, the cross sectional area  $A_c$ , equivalent area moment of inertia  $I_n$ , equivalent shear factor  $K_n$ , equivalent mass per unit length  $M_e$ , stiffness  $K_w$  and factor  $C_n$  are

$$\begin{aligned} A_c &= 2\pi T_c R; \quad K_n = 1/(2n^2); \quad I_n = I_y / n^4; \quad I_y = \pi T_c R^3; \\ M_e &= \rho A / 2 (1 + 1/n^2 + 2\mu/n); \quad K_w = \beta E' A / 2 (n^2 - 1)^2 / R^2; \\ C_n &= 2\beta(n-1/n)^2 / K_n; \quad \mu = \rho_f \pi R^2 / \rho 2\pi R T_c. \end{aligned} \quad (11)$$

In equation (9), the term proportional to  $C_n$  describes the restraint against twist of the pipe wall. For thin-walled pipes, low order  $n$  and, or, low frequencies, this term may be neglected. Equations (9) are then equal to those for a Timoshenko beam on a Winkler foundation having stiffness per unit length,  $K_w$ . This "foundation stiffness" describes the circumferential flexural stiffness of the pipe-wall.

**Wavenumbers.** Using the equivalent Timoshenko beam theory (9), the propagating wave number for the mode with circumferential non-dimensional wavenumber  $n$  is given by the non-parenthesised signs in

$$\begin{aligned} k_n R &= \left[ H^2 + M(Q - \Omega_1^2) \right]^{1/2}, \\ H &= (M + \Omega_1^2 - Q C_n / (1 + C_n)) / 2; \quad \Omega_1 = \omega R / \sqrt{E / \rho} = \Omega / \sqrt{1 - \nu^2} \\ M &= (\omega^2 M_e - K_w) R^2 / (GA K_n (1 + C_n)); \quad Q = n^2 G / E. \end{aligned} \quad (12)$$

In [2] numerical experiments are made in which results from equation (12) are compared to those found using accurate thin-walled cylinder theory and Helmholtz equation for the fluid. Criteria for the application of the simplified beam theory are given.

#### 4. SEA formulation

Traditionally, using the wave approach to SEA, different wave components are assumed incoherent and of equal magnitude. For cylinders with contained fluid, SEA models are made regarding the cylinder and fluid as separate sub systems [9, 10]. The modal densities are calculated assuming the mode count a continuous function of both the axial and circumferential wave numbers, e.g., originally by Heckl [11] or most recently by Langley [12]. The normalised mode count for cylinders is defined  $N_n = T_c / L N_c$ , where  $N_c$  is the mode count. It is a function of only  $\beta$  and the non-dimensional frequency  $\Omega$  [3]. In Figure 2 are shown the normalised mode counts found using Arnold and Warburton cylinder theory and the ones found from references [11, 12]. These results are independent of  $\beta$  and are, as stated by the authors, not correct for frequencies where only the beam mode can propagate. Also, these theories do not account for the increase in the mode count at the cut-on frequencies.

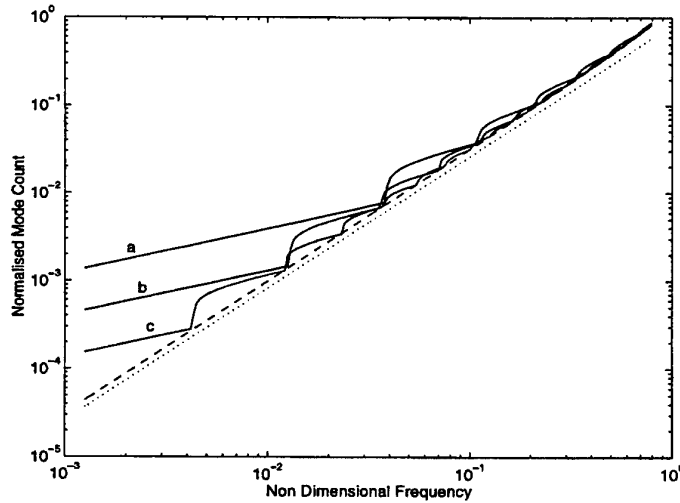


Figure 2. Normalised mode count in cylinders (From [2]). '.....', [11]; '---', [12]; '—', Arnold and Warburton theory; a,  $T_c = R/20$ ; b,  $T_c = R/60$ ; c,  $T_c = R/180$ .

##### 4.1 THE WAVE GUIDE APPROACH TO SEA

Many structures, e.g., cylinders, are geometrically orthotropic, resulting in that the speed of energy propagation is dependent on the direction. As can be deduced from Figure 2, the modal density, the derivative of the mode count, is also dependent on the direction of propagation. Additionally, for many connections the energy transmission between sub structures depends strongly on the angle of incidence. Examples of such connections are: coupling between cylinder and contained fluid [9], plate/beam junctions [13] and flange connected pipes [5]. This strong dependence on angle of incidence makes the SEA diffuse field assumption dubious.

To overcome this, Langley proposed the 'wave intensity method' [14]. Using this method the SEA assumptions are relaxed. The wave components are still assumed in-

coherent but their amplitudes are calculated explicitly. The total wave energies are then found by integrating over all possible directions of propagation.

Here, the alternative the 'wave guide approach to SEA' is proposed. Using this approach, first the waves that can transmit in the wave guide are calculated from the dispersion relations. Then, each of these wave types is considered as a one-dimensional SEA element. The advantages of this approach are that: 1) It is focused on the waves, or standing waves (modes), that carries energy; 2) It does not rely on a sometimes false assumption of in-coherence but on the ortogonality of modes; 3) Much of what has been learnt over the years on the application of SEA to one-dimensional systems applies. Of course, the wave guide approach is in principle equal to the standard wave approach [15].

#### 4.2 SEA PARAMETERS

To formulate SEA models for the energy balance in a pipe structure the input power to each element is needed as are the modal overlaps, describing the damping within the elements, and the coupling factors, describing the energy flow between them. Additionally, the modal densities are required for calculating the total vibration energies from the calculated modal energies.

##### 4.2.1 Modal density

In one-axial, prismatic, wave guide systems the resonances occur approximately when

$$kL = N\pi, \quad (13)$$

where  $k$  is a wavenumber in the direction of the wave guide,  $L$  is the length and  $N$  is any positive integer. The non-dimensional Helmholtz number,  $kL$ , is a measure of the size of the wave guide. For thin-walled cylinders, equation (13) is exact if the boundary conditions are "simply supported", that is, if they are  $\partial u/\partial x = v = w = \partial^2 w/\partial x^2 = 0$ . Also for a fluid-filled cylinder, equation (13) is exact, if the cylinder is simply supported and if the fluid obeys pressure release conditions,  $p = 0$ , at the pipe ends.

The mode count,  $N_c = N_c(\omega)$ , is the number of modes having resonance below the frequency  $\omega$ . If the mode count is considered as a continues variable of the Helmholtz number, it is, for each wave type in the wave guide, given by equation (13). It must, however, also be accounted for that for  $n \geq 1$  there are two waves with equal wave numbers but with different polarisation's.

In SEA, the modal density is central. It is defined for a frequency band between frequencies  $\omega_l$  and  $\omega_u$ :

$$n_{dens} = \frac{N_c(\omega_u) - N_c(\omega_l)}{\omega_u - \omega_l}. \quad (14)$$

Often the limit  $\omega_u \rightarrow \omega_l$  is taken, thus resulting in an expression valid for a particular frequency. However, this limiting expression is singular at cut-on if the mode count is based on (13). Here, calculations are made in third octave bands and equation (14) is used

to calculate the modal density, where the mode counts are given by equation (13) (and for  $n \geq 1$  multiplied by 2) and the wavenumbers are given by equation (6) or (12).

#### 4.2.2 Modal overlap

The dissipated power in an element is by definition,

$$P_d = \eta \omega E = M Em; \quad M = \eta \omega n_{dens}; \quad Em = E / n_{dens}, \quad (15)$$

where  $\eta$  is the loss factor and  $E$  is the total vibration energy in the element,  $n_{dens}$  is the modal density,  $Em$  is the modal energy and  $M$  is the modal overlap. In SEA, equations for energy conservation are formulated with the modal energy as independent variable. Then, the modal overlap based on the 3 dB bandwidth is the parameter describing the dissipation of energy.

#### 4.2.3 Coupling factor

In SEA, the energy flow between two directly coupled elements is

$$P_{i,j} = C(Em_i - Em_j), \quad (16)$$

where the coupling factor, or 'modal energy conductivity', is defined by this equation. Using the wave approach, the conductivity is calculated assuming that only element  $i$  is directly excited and that element  $j$  has a large modal overlap. For this case,  $C$  is related to  $\tau_{\infty}$ , the transmission factor for two semi infinite elements [16]

$$C = \tau_{\infty} / \pi (2 - \tau_{\infty}). \quad (17)$$

In [5] transmission factors for flange-coupled fluid-filled pipes are calculated and the routines presented are here used to calculate the conductivity,  $C$ . It should be noted, for geometrical reasons, waves of different trigonometric orders,  $n$ , are not coupled.

#### 4.2.4 Input power

The investigated structure is excited by a radial point force with time-rms amplitude  $f_0$ . For the radial-axial modes, the elegant expression in [17, Section v.4.c] is used to calculate the frequency band averaged input power [3]

$$P_{in} = \frac{\pi (\text{modal force})^2}{2 \text{ total mass}} \text{ modal density} = \frac{\pi / 2 f_0^2}{\rho A_c \left( 1 + 1/n^2 + 2\mu/n + (k_n R / n^2)^2 \right)} \frac{k_n(\omega_u) - k_n(\omega_l)}{\omega_u - \omega_l}, \quad (18)$$

where  $\mu$  and  $A_c$  are defined in equation (11). The wavenumbers are given by equation (12), using the convention that the wave number is zero below the cut-off frequency. This expression for the input power is investigated in [3] where criteria for its application are found.



The input power in the axi-symmetric modes is calculated from the equations of motion (4) applied to an infinite pipe that is excited by a radial point force at  $x = 0$ . The solutions are

$$u(x) = \begin{cases} A_+ U_1 e^{i\alpha x} + B_+ U_2 e^{i\beta x}, & x > 0 \\ A_- U_3 e^{-i\alpha x} + B_- U_4 e^{-i\beta x}, & x < 0 \end{cases}; \quad \psi(x) = \begin{cases} A_+ e^{i\alpha x} + B_+ e^{i\beta x}, & x > 0 \\ A_- e^{-i\alpha x} + B_- e^{-i\beta x}, & x < 0 \end{cases} \quad (19)$$

where  $A_+$ ,  $A_-$ ,  $B_+$  and  $B_-$  are constants. The eigenvectors have been scaled so that their  $\psi$ -component is unity while their  $u$ -components are  $U_i$  respectively. From the equations of motion it is deduced that  $\psi$  and  $\partial u / \partial x$  are continuous at  $x = 0$  whereas

$$\lim_{\varepsilon \rightarrow 0} [u(+\varepsilon) - u(-\varepsilon)] = \frac{\nu R f_0}{E A_c}; \quad \lim_{\varepsilon \rightarrow 0} \left[ \frac{\partial \psi(+\varepsilon)}{\partial x} - \frac{\partial \psi(-\varepsilon)}{\partial x} \right] = \frac{2 \omega R f_0}{E A_c}. \quad (20)$$

These four continuity conditions are used to find the constants  $A_+$ ,  $A_-$ ,  $B_+$  and  $B_-$  and the radial displacement is calculated using equation (4c). The input power is

$$P_{in} = \text{Re}(-i \omega w f_0). \quad (21)$$

The results using the simplified formulations are in Figure 3 compared to those found with the spectral FEM in [1] showing good agreements.

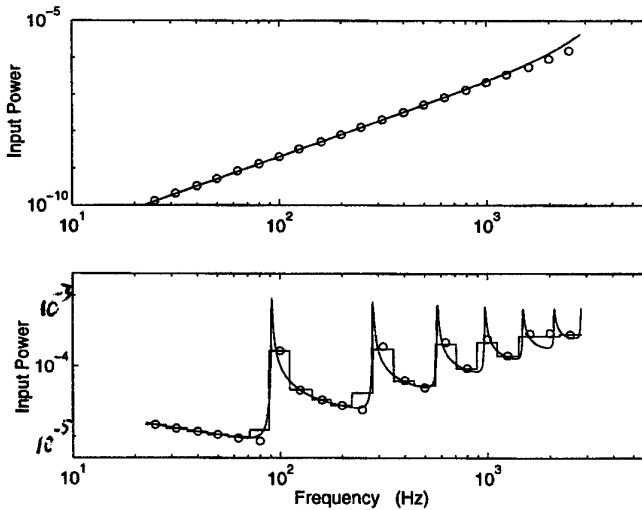


Figure 3. Input power to infinite fluid-filled pipe. Upper, axi-symmetric modes; lower, radial-axial mode; '—', SFEM, narrow band and third octave band averages; 'O', SEA

### 5. Numerical example

A simple un-supported pipe structure with three sections in a row, joined with flanges, is considered. The pipe and flange dimensions are defined according to standards [18, 19]. The material data are found in Table 1 and the three section lengths are respectively 9.5m, 5.27m and 7.57m. The excitation is a radial point force 3.49m from the end of section 1. Dissipative losses are described using a complex Young's modulus and complex densities,  $E = E_o(1 - i\eta_e)$ ,  $\rho = \rho_o(1 + i\eta_v)$  and  $\rho_f = \rho_{fo}(1 + i\eta_f)$ .

The third octave band average of the energies and energy flows in the structure are calculated with SEA. The SEA model is, for each trigonometric order, formulated with the SEA parameters presented above. The results are compared to those found with the spectral FEM (SFEM) presented in [1]. Calculations are made for frequencies from the 31.5 Hz octave band until the 2 kHz octave band. The deterministic calculation is made with 1500 logarithmic spaced frequency points, ensuring approximately 2.5 points within resonances 3 dB bandwidth. It should be pointed out, to use standard FE calculations for benchmark testing the SEA model would require extensive calculations. Using the rule of thumb of six nodes per wave length results in a FE model with almost 100.000 d.o.f. for the cylinders and perhaps as many for the fluid.

In Figure 3 are shown the calculated energy flow in the second flange connection and in Figure 4 are the total energies in the first and third pipe sections. At lower frequencies, the modal density and the modal overlap are small and the results are not in good agreement. However, once the  $n = 2$  mode is cut-on, at 90 Hz, the frequency averaged results agrees very well. At higher frequencies, above 1 kHz, there is a tendency for the SEA model to over predict energy transmission. Probably, since SEA does not account for that, because of damping, the energy density can decay within an element. Finally, in Figure 5 are shown the energy level difference between the end sections. It is not effected by errors in the SEA prediction of input power. Hence, the agreements are better at lower frequencies while the high frequency deviations are equal to those in Figure 4.

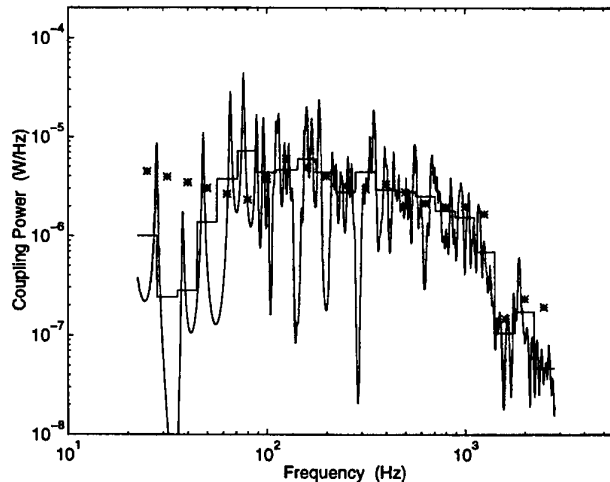


Figure 3. Energy flow in second connection; '—', SFEM, narrow band and third octave band averages; '\* \*', SEA

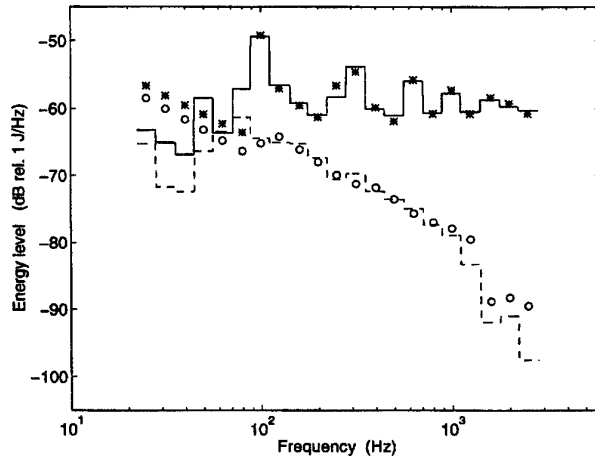


Figure 4. Third octave band averaged total vibration energies. '—', Section 1, SFEM; '\* ', Section 1, SEA; '- -', Section 3, SFEM; 'O ', Section 3, SEA.

## 6 Conclusions

Statistical energy analysis is applied to predict the vibrational energies in a small fluid-filled pipe structure consisting of three sections joined with flanges. The SEA model is based on a wave guide approach. Using this approach, first the waves that can propagate in the wave guide are calculated from the dispersion relations. Then, each of the wave types is considered as a one-dimensional SEA element. The advantages of this approach are that: 1) It is focused on the waves, or standing waves (modes), that carries energy; 2) It does not rely on a sometimes false assumption of in-coherence but on the orthogonality of modes; 3) Much of what has been learnt over the years on the application of SEA to one-dimensional systems applies.

The propagating waves for the  $n \geq 1$  modes are described with a previously reported equivalent beam theory [2, 3] whereas those for the  $n = 0$  modes are described with a similar theory presented here. The coupling factors are found with a FE-technique [5].

The SEA predictions are compared to those from a spectral FE calculation [1] showing good agreements. However, at lower frequencies, when only the  $n = 0$ , longitudinal and fluid modes and the  $n = 1$  beam mode can propagate, the results are not so good. This confirms that beams are not suitable for SEA, unless they are very long. At higher frequencies, above 1 kHz, standard SEA over predicts energy transfer because, when the modal overlap is high, the SEA assumption of constant energy density within the elements is violated. This error can be corrected with a 3-d.o.f. SEA element formulation [4].

In summary, the feasibility of using SEA to predict vibrations in pipeworks has been demonstrated. It is believed that the method has the potential to become a standard method for predictions at frequencies where the shell modes in the pipe wall are cut-on, thus complementing beam models. However, the major contribution of this work is considered to be the introduction of the wave guide approach to SEA. This approach, combined with the FE-technique discussed in [1, 5, 20] may become a very powerful tool for generating data to SEA models.

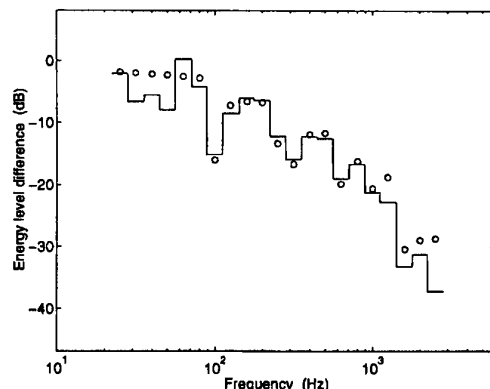


Figure 5. Energy level difference between Section 1 and Section 3. '—', SFEM; 'O', SEA.

### Acknowledgement

The financial supports from TFR, Sweden, and EPSRC, UK, are gratefully acknowledged. The discussions with Dr. Roger Pinnington have been of great help.

### References

1. S. Finnveden 1997 *J. Sound and Vibration* **199**, 125-154. Spectral finite element analysis of vibration of straight fluid-filled pipes with flanges.
2. S. Finnveden *J. Sound and Vibration* (Accepted for publication). Simplified equations of motion for the radial-axial vibrations of fluid-filled pipes.
3. S. Finnveden *J. Sound and Vibration* (Accepted for publication). Formulas for modal density and for input power from mechanical and fluid point sources in fluid-filled pipes.
4. S. Finnveden 1996 *Proc. Inter-Noise* 2951-2956. A 3-d.o.f. SEA element for modelling one-dimensional structures with high modal overlaps.
5. S. Finnveden 1997 *Proc. Sixth International Conference on Recent Advances in Structural Dynamics* (In press). Vibration energy transmission in fluid-filled pipes connected with flanges.
6. C. R. Fuller and F. J. Fahy 1982 *J. Sound and Vibration* **81**, 501-518. Characteristics of wave propagation in cylindrical elastic shells filled with fluid.
7. A. W. Leissa 1973 *Vibrations of shells* (NASA SP-288). Washington DC: U.S. Gov. Printing Office.
8. R. J. Pinnington, A. R. Briscoe 1994 *J. Sound and Vibration* **173**, 503-516. Externally applied sensor for axisymmetric waves in a fluid filled pipe.
9. F. J. Fahy *J. Sound and Vibration* **13**, 171-194. Response of a cylinder to random sound in the contained fluid.
10. M. P. Norton and A. Pruiti 1991 *Applied Acoustics* **33**, 313-336. Universal prediction schemes for estimating flow-induced industrial pipeline noise and vibration.
11. M. Heckl 1962 *J. the Acoustical Soc. of America* **34**, 1553-1557. Vibrations of point-driven cylindrical shells.
12. R. S. Langley 1994 *J. Sound and Vibration* **169**, 43-53. The modal density and mode count of thin cylinders and curved panels.
13. R.S. Langley and K.H. Heron 1990 *J. Sound and Vibration* **143**, 241-253. Elastic wave transmission through beam plate junctions.
14. R. S. Langley and A.N. Bercin *Phil. Trans. of the Royal Society series A* **346**, 489-499. Wave intensity analysis of high frequency vibrations
15. K.H. Heron 1990 *Proc. Inter-Noise* 973-976. *The development of a wave approach to SEA.*
16. S. Finnveden 1995 *J. Sound and Vibration* **187**(3) 495-529. Ensemble averaged vibration energy flows in a three element structure.
17. Cremer L., Heckl M. and Ungar E. E. 1988 *Structure-borne sound*. Springer-Verlag, 2 edition.
18. British Standard *BS 1600:91*. Dimensions for steel pipes for the petroleum industry.
19. British Standard *BS 1560:89*. Circular flanges for pipes (Class designated).
20. U. Örenius and S. Finnveden 1996 *J. Sound and Vibration* **198**, 203-224. Calculation of wave propagation in rib-stiffened plate structures

## SEA FOR PREDICTING THE EFFICIENCY OF NOISE REDUCTION SOLUTIONS

### SEA FOR PREDICTING THE EFFICIENCY OF NOISE REDUCTION SOLUTIONS APPLIED TO AN AIR CONDITIONER UNIT

A. ADOBES\*, L. RICOL\*, Y. ROUSSEL\*\*

\*EDF-DER-AMV

1, Avenue du Général-de-Gaulle, 92141 Clamart, France

\*\*CETIAT

27-29, Bd du 11 novembre BP 2042 Villeurbanne Cedex, France

#### 1. Introduction

Nowadays aspiration for a better quality of life includes a growing demand for lower noise air conditioners. There consequently seems to be a need for tools that would help manufacturers to understand both the generation of noise in a device and its propagation to the surrounding medium. In the present paper, we propose a modelling tool for making a global diagnosis of the propagation of mechanical and acoustical waves inside and from an existing air conditioner. We also use that tool to try to foresee the efficiency of a noise reduction solution.

Air conditioners are complex systems to be modelled : their radiation spectrum is rather broadband, their geometry is intricate, they are composed of a number of heterogeneous elements and include structure and air-borne propagation paths. A thorough modelling, e.g. based on the finite element method, seems therefore to be out of reach.

Although all the hypothesis for application of SEA are not quite fulfilled in the case of an air conditioner, we decided to simplify its modelling by considering that theory as a starting point of the approach. Our added value consisted then in trying to make the SEA model as accurate as possible by paying special attention both to the measurement of the data and the phase consisting in the updating of the model. A specific method for data fitting and model parameter estimation was actually used during the updating phase.

We now present our methodology and the results obtained by applying it to foresee the efficiency of a noise reduction solution applied to a real life air conditioner.

## 2. Elaboration of the initial vibroacoustic model

The first step of our methodology is devoted to the elaboration of the initial SEA vibroacoustic model. This step is based on a thorough observation of the unit and includes several tasks.

The first task is the choice of the subsystems. For each subsystem, one has to collect the relevant data. In the case of cavities, those data are the density of the fluid, the speed of sound in the fluid and the dimensions of the cavity. In the case of structures, the relevant data are the mass of the structure and its dimensions.

Another task consists in characterising the connections between all the subsystems. There exist three kinds of such connections : structure-structure, cavity-cavity and cavity-structure.

Special attention must furthermore be paid to classifying each subsystem into one of the two following categories : the category of subsystems that directly radiate sound into the room and the category of those that do not.

The device under study is the external unit of an individual split air conditioner (see figure 1). It includes two sound sources : an axial fan and a compressor. In figure 1, one of the panels which compose the envelop of the device has been taken out to display the compressor in its cavity.

The observation of the unit leads us to consider eleven subsystems : nine structures and two cavities (see figure 2). The nine structures are the top, the heat exchanger, the partition which separates the compressor cavity from the fan cavity, the fan support, the side panel, the front panel, the rear angle panel, the front panel and the base. The two cavities are the one which contains the compressor and the one which contains the fan. The latter cavity is composed of two sub-cavities : one can be seen on the heat exchanger side and one on the front panel side.

The full list of SEA modelling parameters includes : the vibroacoustic power injected into each subsystem by external forces, the damping loss factor of each subsystem and the coupling loss factors associated to any pair of subsystems. Note that the list of coupling loss factors includes the unidirectionnal coupling loss factors from the radiating subsystems to the surrounding medium. We use version 1.2 of standard SEA software AutoSEA® to provide us with the required coupling loss factors [1]. We furthermore collect in literature the required values for representing damping loss factors [2]. The analysis is performed by third-octave band in the frequency range [200 Hz - 2500 Hz].

# SEA FOR PREDICTING THE EFFICIENCY OF NOISE REDUCTION SOLUTIONS

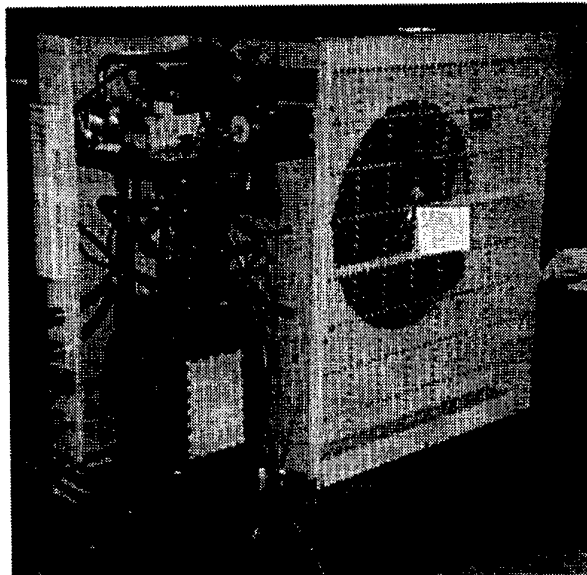


Figure 1 : photograph of the air conditioner unit under study.  
One of the panels has been taken out to display the compressor in its cavity.

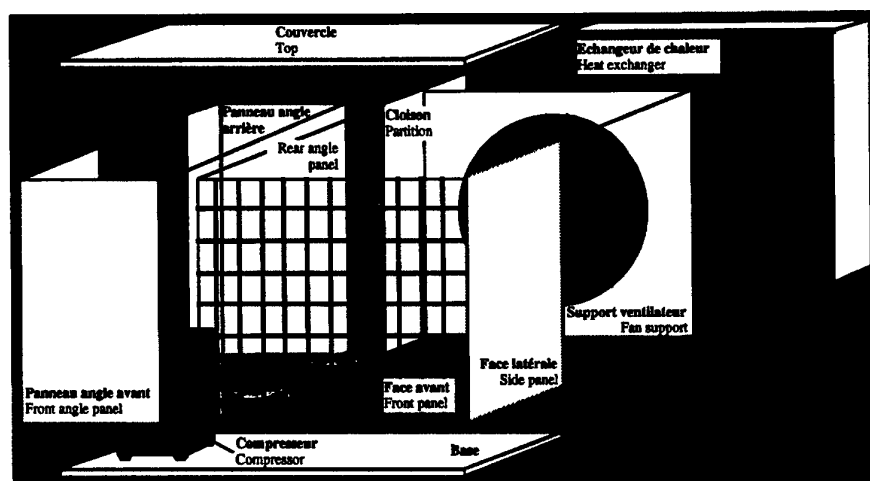


Figure 2 : exploded view of the unit and definition of the eleven subsystems which compose the SEA vibroacoustic model of the unit.

### 3. Data collection

Two operating conditions of the device are considered. The compressor is switched off in the first one. Both the fan and the compressor are switched on and in the second one. For each operating conditions, the total energy of the eleven subsystems and the sound power level radiated by the device are measured. The energy of each subsystem is determined by frequency averaging in third octave band the measured digital spectra, and spatially averaging over the subsystem domain the frequency averaged spectra. The formulas for deriving the energies are detailed hereafter both for the structure and the cavity subsystems.

Let  $M$  denote the number of measurement points taken on a subsystem.

In the case of structures, the energy  $E_i^{rk}$  of subsystem «  $i$  » for operating condition «  $r$  » and third-octave band «  $k$  » is derived by using :

$$E_i^{rk} = \frac{m_i}{M} \sum_{j=1}^M (v_{ij}^{rk})^2 \quad (1)$$

Where  $m_i$  is the mass of subsystem «  $i$  » and  $v_{ij}^{rk}$  is the third-octave band average of the velocity spectrum measured at point «  $j$  ». The measured data being non stationary and all the spectra being not simultaneously measured, velocities (as well as pressures in the case of the cavities) are referenced to the magnitude of the signal delivered by a fixed accelerometer.

In the case of cavity subsystems,  $E_i^{rk}$  is given by :

$$E_i^{rk} = \frac{V_i}{\rho c^2 M} \sum_{j=1}^M (p_{ij}^{rk})^2 \quad (2)$$

Where  $V_i$ ,  $\rho$  and  $c$  respectively denote the cavity volume, the fluid density and the speed of sound in the fluid.  $p_{ij}^{rk}$  denotes the third-octave band average of the acoustic pressure measured at point «  $j$  ».

Sound power levels are determined by integrating the sound intensity vector measured at the nodes of a parallelepipedical mesh enclosing the device. Figure 3 displays the sound power level in third-octave band for the two operating conditions.



## SEA FOR PREDICTING THE EFFICIENCY OF NOISE REDUCTION SOLUTIONS

### 4. A specific method for data fitting and SEA model parameter estimation

#### 4.1. SUMMARY OF MAIN SEA EQUATIONS

According to SEA theory, the state of the unit can be described by :

$$\omega_0^k \sum_{j=1}^N \bar{\eta}_j^{ik} E_j^{ik} = P_i^{ik} \quad (3)$$

Where superscript  $k$  indicates the pulsation band,  $\omega_0^k$  is the central pulsation of the band,  $N$  denotes the number of subsystems,  $E_j^{ik}$  is the energy of the  $j$ -th part for the  $r$ -th operating condition and  $P_i^{ik}$  denotes power injected by external forces into the  $i$ -th part for the  $r$ -th operating condition.

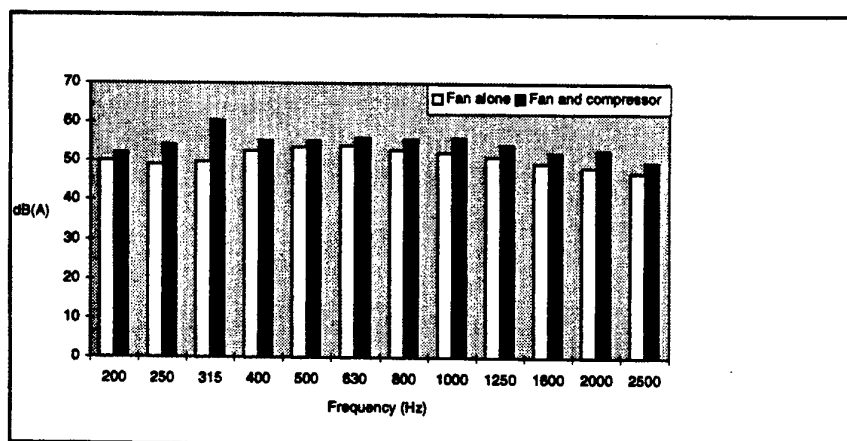


Figure 3 : sound power level in third octave band for the two operating conditions in the frequency range [200 Hz-2500 Hz]

The meaning of  $\bar{\eta}_j^{ik}$  is detailed in equations (4) and (5). Since equation (3) is considered for  $N$  subsystems,  $B$  pulsation bands and  $R$  operating conditions, it provides a set of  $N \times B \times R$  equations. Let  $\eta_i^{ik}$  denote the structural damping loss factor of the  $i$ -th subsystem and  $\alpha_i^{ik}$  an additional loss factor that accounts for the loss in energy by radiation of the  $i$ -th subsystem into the surrounding medium. Let furthermore  $\eta_j^{ik}$  denote the coupling loss factor from the  $i$ -th part to the  $j$ -th part.  $\bar{\eta}_j^{ik}$  is computed by using the following equations :

$$\text{Case } i=j, \quad \bar{\eta}_i^{ik} = \eta_i^{ik} + \alpha_i^{ik} + \sum_{\substack{j=1 \\ j \neq i}}^N \eta_j^{ik} \quad (4)$$

$$\text{Case } i \neq j, \quad \bar{\eta}_j^{ik} = -\eta_i^{ik} \quad (5)$$

Among the  $R$  conditions considered in equation (3), one can define  $N$  special operating conditions after switching the device (fan and compressor) off : during the  $p$ -th of those conditions, the operator injects and measures a power denoted by  $\delta_i^p P_p^{ik}$  into the  $i$ -th subsystem. By definition of Kronecker's symbol

$\delta_i^p$ , the  $p$ -th subsystem is the only one to be excited during the  $p$ -th special condition. The definition of those  $N$  special further conditions is of particular interest. It allows one to calibrate the response of the device by measuring the energies of all the subsystems that are generated by the input of a known power into a single one of them [3], [4]. Equation (3) is completed by equation (6) that allows one to calculate the sound power level  $\mathcal{P}_r^k$  radiated into the surrounding medium during the  $r$ -th operating condition :

$$\omega_0^k \sum_{j=1}^N \alpha_j^k E_r^{jk} = \mathcal{P}_r^k \quad (6)$$

#### 4.2. MODEL PARAMETERS AND DATA

Let us now consider the application of general inverse problem theory to try to improve our SEA model. That theory draws up a distinction between the parameters of the considered model and the data the model is provided with. The former are not measurable so that one can only obtain them by using some identification mean. The latter are on the contrary directly measurable. In the frame of inverse problem theory, equations (3) and (6) are therefore to be seen as relations between some model parameters (which are  $\eta_j^{ik}$ ,  $\alpha_j^k$  and  $P_r^{ik}$  in the frame of SEA), and some data (which are  $E_r^{jk}$ ,  $\mathcal{P}_r^k$  and  $P_r^{ik}$  in the frame of SEA). Note that the  $P_r^{ik}$  belong either to the family of parameters or to the one of data, depending on whether they are the unknown powers injected into the device by the fan and the compressor, or the ones applied (e.g. with a shaker) and measured by the operator during the calibration phase.

## 4.3. THE BAYESIAN APPROACH IN INVERSE PROBLEM THEORY

Among the available inverse methods, the bayesian approach appears to be well suited to update SEA models because it is, like SEA, based on a statistical approach. Let us now present that approach from a general point of view [5]. Let  $X$  be a vectorial space and  $x$  a vector of that space whose components are the model parameters and the data of the problem. One can arrange equations (3) and (6) in the form «  $f(x)=0$  », where  $0$  denotes the null vector, and  $f$  is a function that maps  $X$  into a space of residuals. Let  $\Theta(x)$  be a law of probability density describing the a priori state of information on the physical correlations assumed in-between the components of vector  $x$ . Note that those correlations are simply equations (3) and (6) in the frame of SEA. Let  $\rho(x)$  be a law of probability density representing the a priori state of information on the components of vector  $x$ . From now on, is superscript «  $k$  » omitted to simplify equations. In the bayesian approach, states of information  $\Theta(x)$  and  $\rho(x)$  combine one with each other to provide a more informative state called a posteriori state of information, represented by law of probability density  $\sigma(x)$  :

$$\sigma(x) = \rho(x)\Theta(x) \quad (7)$$

SEA being not an exact theory, we assume some kind of uncertainty on its fundamental equations (3) and (6), by assuming  $\Theta(x)$  is gaussian :

$$\Theta(x) = \frac{(2\pi)^{-\frac{NF}{2}}}{\sqrt{\det(C_{\text{prior}}^f)}} \exp\left(-\frac{1}{2} f(x)^t (C_{\text{prior}}^f)^{-1} f(x)\right) \quad (8)$$

Where  $NF$  is the dimension of the space of residuals,  $C_{\text{prior}}^f$  is an a priori covariance matrix on the physical correlations and  $\det(C_{\text{prior}}^f)$  denotes the determinant of  $C_{\text{prior}}^f$ . Since all the data and the parameters considered in SEA are positive, one has to search for them as such. One of the way for doing that is to make a change in variables so that data and parameters are sought for as powers of ten. We therefore introduce vector  $x^*$  and function  $\varphi$  defined as :

$$x_i = 10^{x_i^*} \Rightarrow x_i^* = \log_{10}(x_i) = x_i^* = \varphi(x_i) \quad (9)$$

Where  $x_i$  (resp.  $x_i^*$ ) denotes the general term of vector  $x$  (resp.  $x^*$ ). A gaussian law of probability density is assumed for vector  $x^*$  :

$$\rho(x) = \frac{(2\pi)^{\frac{NX}{2}}}{\sqrt{\det(C_{prior}^{x*})}} \exp\left(-\frac{1}{2}(\varphi(x) - \varphi(x_{prior}))^t (C_{prior}^{x*})^{-1} (\varphi(x) - \varphi(x_{prior}))\right) \quad (10)$$

Where  $NX$  is the dimension of space  $X$ ,  $C_{prior}^{x*}$  is an a priori covariance matrix associated to  $x^*$  and  $x_{prior}$  is an assumed a priori value of  $x$ . After replacing in equation (7)  $\rho(x)$  and  $\Theta(x)$  by their expressions (see eq. (8) and (10)), we get a new expression for  $\sigma(x)$  :

$$\sigma(x) = \text{constant} \cdot \exp\left\{-\frac{1}{2} \left[ \begin{aligned} &(\varphi(x) - \varphi(x_{prior}))^t (C_{prior}^{x*})^{-1} (\varphi(x) - \varphi(x_{prior})) \\ &+ \\ &f(x)^t (C_{prior}^f)^{-1} f(x) \end{aligned} \right] \right\} \quad (11)$$

Where « constant » denotes a positive real constant. Although  $\sigma(x)$  is not gaussian, it appears to be a bell shaped law of probability density, so that the information contained in it can be summarised by a central estimator and an estimator of dispersion. The simplest central estimator is the vector of Maximum Likelihood denoted  $x_{ML}$ , such that  $\sigma(x)$  is maximum for  $x = x_{ML}$ . Note that vector  $x_{ML}$  that maximises  $\sigma(x)$  also minimises the argument  $S(x)$  of the exponential in (11).  $S(x)$  is defined as :

$$S(x) = (\varphi(x) - \varphi(x_{prior}))^t (C_{prior}^{x*})^{-1} (\varphi(x) - \varphi(x_{prior})) + f(x)^t (C_{prior}^f)^{-1} f(x) \quad (12)$$

Since  $S(x)$  is non quadratic,  $x_{ML}$  is found by applying an iterative minimisation procedure [5]. One will find the matricial expressions to be used for computing the a posteriori estimators of dispersion  $C_{post}^{x*}$  and  $C_{post}^f$  in [5].

## 5. Application of the bayesian inversion method to the case of the unit

The bayesian inversion method described in section 4 has been programmed as a function inside LADY<sup>®</sup>, a general software devoted to signal processing and data management, developped in the frame of a partnership between EDF and INTESPACE. The model parameters elaborated in section 2, as well as the results of measurements described in section 3 were provided to that function in the form of twelve a priori vectors (one for each third octave band)

respectively associated to twelve covariance matrices. To simplify the problem, covariance matrices were assumed to be diagonal. Since the function  $S(x)$  to be minimised depends on a covariance matrix  $C_{\text{prior}}^*$  that contains the variances both on parameters and data, the ranking of the a priori uncertainties on parameters and data determines the result of the identification and should therefore be carefully established. The identification provides us with twelve a posteriori vectors and a posteriori covariance operators. The vectors components are data and parameters that satisfy equations (3) and (6) better than did the a priori vectors. Note that the lower the uncertainty associated to a data or to a parameter in the a priori covariance matrix, the closer its a posteriori value lies from the a priori one. In the limiting case where the user provides a null a priori uncertainty on some data or parameter (that means that the user is sure of the value of it), the identification outputs a solution that equals the a priori value of the data or parameter. As a piece of example, figure 4 displays the a priori and a posteriori spectra of the radiation loss factor  $\alpha$  of the side panel (see figure 2).

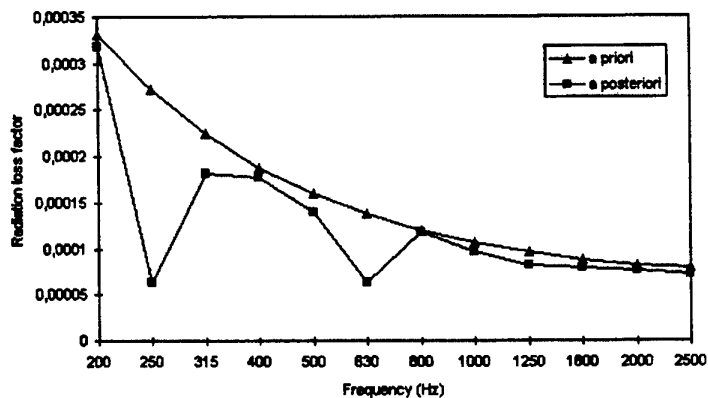


Figure 4 : radiation loss factor a priori and a posteriori spectra of the side panel by third octave band in the frequency band [200-2500 Hz]

The a priori values of  $\alpha$  are determined in the frame of classical SEA by using AutoSEA<sup>®</sup>. In the higher frequency range (from 800 to 2500 Hz) those values are representative of reality so that they are only slightly corrected by the updating method : the derived spectrum is smooth and the a posteriori values nearly equal the a priori ones. In the lower frequency range however, the a posteriori loss radiation factor output by the updating method exhibits large variations because of the strong modal behavior of the unit. The a posteriori values are moreover quite different from the a priori ones.

## 6. Application of noise reduction methods to the unit

Several noise reduction solutions were applied to the air conditioner. The most effective of them was the one that consisted in covering the internal faces of the compressor cavity with a viscoelastic fibrous layer. After application of that solution, the unit was submitted to the operating condition where both the fan and the compressor are switched on. The energies of all the subsystems and the sound power level of the unit were measured again. Figure 5 allows one to appreciate the noise reduction by comparing the sound power level radiated by the unit, before and after the pasting of the viscoelastic fibrous layer.

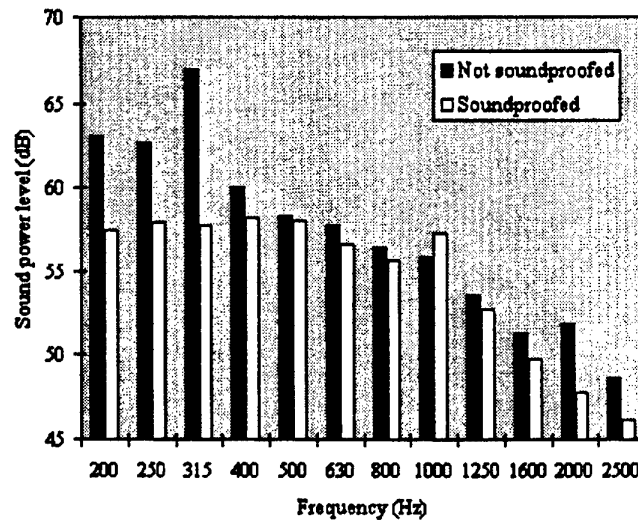


Figure 5 : sound power level by third octave band in the band [200-2500 Hz] after covering the internal faces of the cavity with a viscoelastic fibrous layer

It appears that noise reduction achieved depends on the frequency band. It is the higher (approximately 10 dB) in the 315 Hz third octave. Sound power level unexpectedly increases by 2 dB in the 1000 Hz third octave. After assessing experimentally the reduction in sound power level, we try in next section to estimate it by using the updated SEA model obtained in previous section.

## 7. Modification of the values of the updated model parameters

We now use the updated SEA model to try to foresee the reduction in sound power level. We first have to simulate the noise reduction solution itself by

## SEA FOR PREDICTING THE EFFICIENCY OF NOISE REDUCTION SOLUTIONS

correspondingly modifying the values of the model parameters. The SEA model is used afterwards to recompute a new sound power, which in turn is to be compared to the one measured in section 3.

Since we lacked of experience in that domain, we performed the modification of the model parameters values rather arbitrarily. We could neither find any reference about the values of SEA parameters to be chosen in the case of our assembly made of a viscoelastic fibrous layer pasted to a plate, nor assess the modifications of the coupling loss factors of the panel induced by the pasting of the layer on it.

The covering of the internal faces of the compressor cavity with the fibrous viscoelastic layer was eventually simulated by :

- increasing the updated damping loss factor of the subsystems corresponding to the plates pasted with the layer to take into account the viscoelastic effect,
- increasing the updated damping loss factor of the subsystem associated to the compressor cavity to take into account the damping effect due to the fibres,
- leaving unchanged all the coupling loss factors, the radiation loss factors and the powers injected by external forces into the unit.

The damping factors were increased in the same proportion in the whole frequency range.

After modification of its parameters, the SEA model was run again in two steps. The energy of all the subsystems was first computed after injecting the parameters new values into equation (3). The sound power level was then computed by injecting the previously determined energies, as well as the radiation loss factors, into equation (6). Figure 6 displays the comparison between the measured sound power levels spectrum (black bars), and the predicted one (white bars). It also reminds the sound power level spectrum before application of the noise reduction solution (solid line).

It appears that the difference between predicted and measured levels ranges from 0 to 4 dB, depending on the third-octave : prediction overestimates reality in the first three third octaves bands and underestimates it beyond the fourth band. Note that although the damping loss factors were increased in the same proportion in the whole frequency range, the proportion of the computed noise reduction does vary with frequency. The trends in noise reduction is globally well simulated by the model. The results would have probably been improved by using some model parameter variations more representative of the pasting of the layer on the panels.

## 8. Conclusion

We have presented a methodology devoted to foresee the efficiency of a noise reduction solution applied to a real life air conditioner. That methodology is

based on SEA and on a bayesian approach for data fitting and model parameter estimation. It appears that theoretical SEA parameters are, as expected, not suitable for the vibroacoustic modelling of air conditioners. One can however consider them as the a priori information to be input to a bayesian process of parameter identification. Provided the number of measurements taken into account by that process is large enough, one eventually gets more representative parameters. The vibroacoustic model elaborated by using that method allows one to foresee the trends in sound power level reduction. In the absence of any alternative method, that methodology appears to be able to provide an approximate vibroacoustic model of an air conditioner and can therefore be considered as an acceptable engineering design tool.

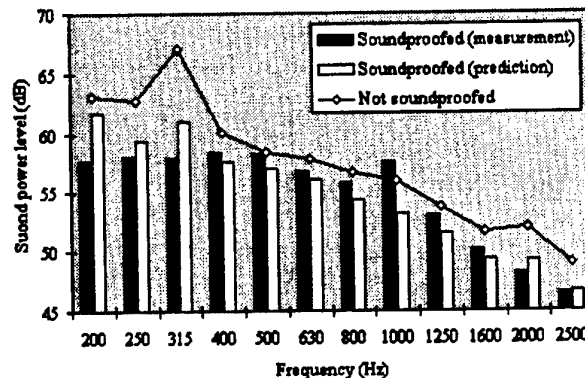


Figure 6 : sound power level after applying the noise reduction solution : predicted and measured effect of soundproofing, not soundproofed.

## 9. References

- [1] Vibroacoustic Sciences Limited 1992. *User guide AutoSEA 1.0*. Sydney : VSL.
- [2] Lyon, R.H. 1975. *Statistical analysis of dynamical systems : theory and applications*. Cambridge MA : The M.I.T. Press
- [3] Lalor N. 1990. *Practical considerations for the measurement of internal and coupling loss factors on complex structures*. Technical Report n°182 Southampton : ISVR.
- [4] Borello G. 1991. Identification of SEA coupling loss factors on liquid rocket engine. *Proc. Internoise 91* : pp. 1193-1196.
- [5] Tarantola, A. 1987. *Inverse problem theory : methods for data fitting and model parameter estimation* Elsevier science publishing BV.



# **STATISTICAL ENERGY ANALYSIS OF NONCONSERVATIVELY COUPLED SYSTEMS AND ITS APPLICATIONS TO ENGINEERING**

**YAO DE-YUAN**

*Department of Flight Vehicle Engineering,  
Beijing Institute of Technology, Beijing 100081,  
the People's Republic of China*

## **1. Introduction**

The development of statistical energy analysis (SEA) arose from a need by aeronautical and aerospace designers in the earlier time of 1960s to predict the dynamic response of flight vehicles and payloads to rocket jet noise and aerodynamic noise, which are broad-band excitations. So far there has been no effective method for prediction of the dynamic response except SEA. The aeronautical and aerospace structures, characterized by higher structural factor ( i.e. the ratio of structural surface area to mass itself ), produce a vast number of condensed vibration modes under such excitations as jet noise, aerodynamic noise, impulsive thrust, aerodynamic loads in the transonic and reentry flight phases etc.. Although computational methods for predicting vibration modes of structures were available, the size of the models which could be handled ( i.e. the number of degrees of freedom ), and the speed of computation, were such as to allow designers to predict only a few of the lowest order modes of rather idealized models. This posed a serious difficulty because the frequency range of significant response encompassed the natural frequencies of a multitude of higher order modes, the structures could support a number of different wave types, the payload structures were indirectly excited via structural wave transmission, and the transmission paths were circuitous and involved many different forms of structure and contained fluids.

Historically, most of the catastrophic accidents of satellite launch

vehicles or other large-size flight vehicles were caused by an unsuccessful prediction of dynamic environments ( mainly imply shock, vibration and noise environments ). During the development of a late-model flight vehicle, if the determined dynamic loads and dynamic environments were over-low, under-test and under-design could occur, reliability of the developed flight vehicle could not be fully tested and some problems or imperfections in design, technology, material, elements, etc. could not be fully revealed, consequently the failure of flight must be caused under the real adverse dynamic environment when the flight vehicle with hidden troubles was launched. On the contrary, if the provided dynamic loads and dynamic environments were over-high, the developed flight vehicle could not passed the environmental tests which conditions are artificially formulated, re-design and re-correction must be performed, in the end, either the developing period of time for the flight vehicle was enlarged, the structural weight and cost increased, or the flight vehicle under development could not come true at all. This forces the designers to improve the precision to predict the dynamic environment using SEA. One of the most important approaches for the solution of the problem is to make coupling property close to real coupling case as far as possible. The assumption of weak coupling, conservative coupling in conventional SEA, which is one of the most main causes for poor predicting precision using SEA, should be re-considered. i.e. great attention should be paid to the development of SEA of nonconservatively coupled system.[1]

## **2. SEA of Nonconservatively Coupled Systems**

Traditional statistical energy analysis is based on such assumptions as conservatively coupled, weakly coupled systems, proportional power flow, reciprocal principle etc.. The rigorous assumptions have placed serious restrictions on the improvement of estimate accuracy of dynamic responses using SEA and the extension of the applications of SEA in engineering. There exists connecting damping in almost all the real structural systems. Moreover the connecting damping, e.g. in common screwing, riveting structures, is non-negligible compared with the structural damping itself. The connecting damping is one of the main sources in damping of the composite structural systems, which include the damping caused by gas pumping, friction between the connections etc.. The solution to the problem in SEA of nonconservatively coupled systems is founded on the

basis of the power flow analysis of the coupled systems.

## 2.1. POWER FLOW ANALYSIS OF NONCONSERVATIVELY COUPLED OSCILLATORS

The power flow between nonconservatively coupled oscillators has been analytically studied by researchers. Inductively, two approaches were used in the analysis of the power flow. One is so-called equivalent approach ( or approximate approach ), in which the nonconservatively coupling problem is equalized to a conservative problem by introducing the effect of coupling damping on the power flow.[2][3] The other is the exact solution approach in which the expressions of the power flow with coupling damping are directly derived from the dynamic equations of oscillating system on the basis of the theory of random vibration and mechanical impedance.[4][5][6] The latter is beneficial to revealing the effecting law of coupling damping on the power flow and extending the analytical results into the analysis of the power flow of a multi-mode system, however the process is tedious. Although the former is relatively simple due to the use of the concerned results from conservatively coupling system, the extension of the results into multi-mode systems is rather difficult due to the introduction of varied correction coefficients.

It is found in the study on the power flow between nonconservatively coupled oscillators that the power flow is not proportional to the energy difference between oscillators while:[4]

$$P_{ij} = \alpha(E_i - E_j) + \beta E_i + \gamma E_j \quad (1)$$

Where  $\alpha$ ,  $\beta$ ,  $\gamma$  are the coefficients depending upon oscillators' parameters and coupling parameters. And the direction of power flow is not reversible, i.e.  $P_{ij} \neq -P_{ji}$ . The description of power flow in the frequency domain is given in reference [5]

$$\begin{aligned} P_{12} &= \text{Re}\{F_{12}V_2^*\} \\ P_{21} &= \text{Re}\{F_{21}V_1^*\} \end{aligned} \quad (2)$$

Where  $F_{ij}$  ( $i \neq j, i, j = 1, 2$ ) are Fourier transformations of the forces on oscillator  $j$  applied by the motion of oscillator  $i$ ,  $V_1^*, V_2^*$  are the conjugates of Fourier transformations of the oscillator's velocities. There exists an obvious imperfection in the description of the reaction between oscillators as it ignores the coupling action between oscillators. The power flow obtained from the results of conservatively coupled oscillators[6] could not

be directly extended to multi-mode systems.

## 2.2. NONCONSERVATIVELY COUPLING ANALYSIS OF MULTI-MODE SYSTEMS

### 2.2.1. Equivalent Method

Reference [7] gives the generalized energy balance equation of nonconservatively coupled system with correlative excitations:

$$[\eta^*]\{E\} = \frac{1}{\omega}\{P^*\} \quad (3)$$

where  $[\eta^*]$  is the loss factor matrix of nonconservatively coupled system under the correlative excitation. The equivalent input power matrix  $\{P^*\}$  of nonconservatively coupled system can be written:

$$\{P^*\} = \{P\} - [CR]\{S_R\} - [CI]\{S_I\} \quad (4)$$

Where  $[CR]$  is the inphase power coefficient matrix,  $[CI]$  is the orthogonal power coefficient matrix,  $\{S_R\}$  inphase spectral density matrix,  $\{S_I\}$  is the orthogonal spectral density matrix. Eq. (3) states clearly that the power flow equation of the nonconservatively coupled system with correlative excitation is the same as that of the conservatively coupled system with non correlative excitation as long as the real input power  $\{P_{in}\}$  is replaced with the equivalent input power and the conventional conservative loss factor matrix is replaced with the nonconservative loss factor matrix. Eq. (3) also states the following points: (1) the equation is the power flow expression of conservatively coupled system with correlative excitation if the system is conservative; (2) the equation is the power flow expression of conservatively coupled system with real correlative excitation if the system is conservative and the imaginary parts of cross spectral density between excitations are all zero; (3) the equation is the power flow balance expression of non-conservatively coupled system with real correlative excitation if the imaginary parts of cross spectral density between excitations are all zero; (4) the equation is the power flow balance expression of non-conservatively coupled system if the excitations are independent each other.

### 2.2.2. Unknown Parameter Reduction Method

Considering a nonconservatively coupled system consisting of two

subsystems with multi-modes, which can be either structural or acoustic. The following assumptions are used in the analysis: (1) each mode has similar energy in either subsystem; (2) the mode distributions follow an equal-probability law within the analyzed frequency bands; (3) the coupling properties of each pair of modes are similar in either subsystem.

Let the modal densities of two subsystems be  $n_1, n_2$ , respectively. The coupling output powers of two subsystems are  $P_{12}, P_{21}$ , respectively. The coupling loss factors of subsystems 1, 2 on mode-average are  $\eta_{12}^{(1)}, \eta_{21}^{(1)}, \eta_{12}^{(2)}, \eta_{21}^{(2)}$ , respectively. The internal loss factors of subsystems 1, 2 are  $\eta_1, \eta_2$ , respectively. The coupling output power flows of subsystems 1, 2 are respectively:

$$\begin{aligned}\langle P_{12} \rangle &= \omega (\eta_{12}^{(1)} \langle E_1 \rangle - \eta_{21}^{(1)} \langle E_2 \rangle) \\ \langle P_{21} \rangle &= \omega (\eta_{21}^{(2)} \langle E_2 \rangle - \eta_{12}^{(2)} \langle E_1 \rangle)\end{aligned}\quad (5)$$

Where  $\langle \rangle$  denotes that the parameters in brackets are on time-average. The internal loss factors of subsystems 1, 2 are respectively:

$$\begin{aligned}\langle P_{d1} \rangle &= \frac{c_1}{m_1} \langle E_1 \rangle = \eta_1 \omega \langle E_1 \rangle \\ \langle P_{d2} \rangle &= \frac{c_2}{m_2} \langle E_2 \rangle = \eta_2 \omega \langle E_2 \rangle\end{aligned}\quad (6)$$

The energy balance equations of two subsystems are:

$$\omega \begin{bmatrix} \eta_1 + \eta_{12}^{(1)} & \eta_{21}^{(1)} \\ -\eta_{12}^{(2)} & \eta_2 + \eta_{21}^{(2)} \end{bmatrix} \begin{Bmatrix} \langle E_1 \rangle \\ \langle E_2 \rangle \end{Bmatrix} = \begin{Bmatrix} P_{in,1} \\ P_{in,2} \end{Bmatrix}\quad (7)$$

It should be noted that the coupling output power flows between two subsystems are expressed in  $P_{12}, P_{21}$  in Eq. (5) instead of  $P_{in,1}, P_{in,2}$  in order to be beneficial to the extension of the analytical results into multi-subsystems.  $P_{12}$  is the coupling output power flow of subsystem 1 which is caused by the coupling action between the two subsystems, while  $P_{21}$  is the coupling output power flow of subsystem 2 which is caused by the coupling action between the two subsystems. The value of  $P_{12}, P_{21}$  can be either positive or negative, for each subsystem, "positive" denotes that the power flow is output from the subsystem itself, "negative" denotes that the power flow is input into the subsystem. Therefore the power loss in

coupling element can be written as:

$$P_d^{12} = P_{12} + P_{21} \quad (8)$$

The parameter  $P_d^{12}$  describes the coupling property between two subsystems, the coupling is conservative if  $P_d^{12} = 0$ ; the coupling is non-conservative if  $P_d^{12} \neq 0$ .

The analytical results for two-subsystem can be conveniently extended into the analysis for multi-subsystem. Let the number of multi-subsystem be  $N$  ( $N > 2$ ). Considering two coupling subsystems  $i, j$  ( $i \neq j$ ), we can write the coupling output power flow of subsystem  $i$  caused by coupling action as follows that:

$$P_{ij} = \omega(\eta_{ij}^{(i)} E_i - \eta_{ji}^{(i)} E_j) \quad (9)$$

As a result, the coupling output power flow of subsystem  $i$  in multi-subsystem should be:

$$P_{i0} = \sum_{\substack{j=1 \\ j \neq i}}^N P_{ij} = \omega \sum_{\substack{j=1 \\ j \neq i}}^N (\eta_{ij}^{(i)} E_i - \eta_{ji}^{(i)} E_j) \quad (10)$$

The energy balance equation of subsystem  $i$  is:

$$P_{di} + P_{i0} = P_{in,i} \quad (11)$$

The energy balance equations of  $N$  coupling subsystems are:

$$\omega \begin{bmatrix} \eta_1 + \sum_{j=2}^N \eta_{1j}^{(1)} & -\eta_{21}^{(1)} & \cdots & -\eta_{N1}^{(1)} \\ -\eta_{12}^{(2)} & \eta_2 + \sum_{\substack{j=1 \\ j \neq 2}}^N \eta_{2j}^{(2)} & \cdots & -\eta_{N2}^{(2)} \\ \cdots & \cdots & \cdots & \cdots \\ -\eta_{1N}^{(N)} & -\eta_{2N}^{(N)} & \cdots & \eta_N + \sum_{j=1}^{N-1} \eta_{Nj}^{(N)} \end{bmatrix} \begin{Bmatrix} E_1 \\ E_2 \\ \vdots \\ E_N \end{Bmatrix} = \begin{Bmatrix} P_{in,1} \\ P_{in,2} \\ \vdots \\ P_{in,N} \end{Bmatrix} \quad (12)$$

Or:

$$\omega[\eta]\{E\} = \{P\}$$

It is clearly found from Eq. (12) that (1) for nonconservatively coupled system,  $\eta_{ij}^{(i)} \neq \eta_{ij}^{(j)}$ ,  $\eta_{ji}^{(i)} \neq \eta_{ji}^{(j)}$ , and there exist reciprocal relations between  $\eta_{ij}^{(i)}$  and  $\eta_{ji}^{(i)}$  and between  $\eta_{ij}^{(j)}$  and  $\eta_{ji}^{(j)}$ , but no reciprocal

relations between  $\eta_{ij}^{(i)}$  and  $\eta_{ji}^{(i)}$  and between  $\eta_{ij}^{(j)}$  and  $\eta_{ji}^{(j)}$ ; (2) for conservatively coupled system,  $\eta_{ij}^{(i)} = \eta_{ij}^{(j)}$ ,  $\eta_{ji}^{(i)} = \eta_{ji}^{(j)}$ , and there exists a reciprocal relation between  $\eta_{ij}^{(i)}$  and  $\eta_{ji}^{(j)}$ ; (3) the number of unknown parameters increases greatly in the energy balance equations of non-conservatively coupled system, the unknown number in the coefficient  $\eta$  matrix is  $2N^2 - N$ , while the unknown number is  $N^2$  for conservatively coupled system. It can be found through the practical analysis of structural or acoustic systems that the number of unknown parameters can be reduced by the reduction of number of coupling relation i.e. by using varied methods in the division of subsystems. For nonconservatively coupled system, only the case of two coupling subsystems is solvable even if the internal damping of all the subsystems is known. Because coupling with two subsystems can produce four unknown parameters if internal loss factors are both known, missing one coupling relation can eliminate four unknown parameters. As a result, in order to make a nonconservative system solvable, the reduced coupling relation number  $N_{r,c}$  should satisfy:

$$N_{r,c} \geq \frac{N^2 - 2N}{4} \quad (13)$$

For a nonconservatively coupled system with  $N$  subsystems, the fact that coupling number  $N_c$  between subsystems is less than maximum solvable coupling number  $N_{s,max,c}$  ( $N_c < N_{s,max,c}$ ) is a necessary condition under which the on-line identification technique for coupling loss factor in traditional SEA is suitable for SEA of non-conservatively coupling system. The maximum coupling number  $N_{max,c}$ , the minimum coupling number  $N_{min,c}$  and the solvable maximum coupling number  $N_{r,max,c}$  can be respectively calculated according to the following formulas:

$$N_{max,c} = \sum_{i=1}^{N-1} i, \quad N_{min,c} = N - 1, \quad N_{s,max,c} = N_{max,c} - N_{r,c} \quad (14)$$

### 3. Applications to Engineering

To examine the effectiveness of SEA of nonconservatively coupled system and to provide theoretical preparation for the optimized control of vibroacoustic environment, the prediction of vibroacoustic environment for an instrument cabin (an enclosed cylindrical shell) of a flight vehicle

was performed as an applied example. The enclosed cylindrical shell with 2.0 m high, 0.8 m in diameter and 0.0022 m in thickness is in reverberation sound field. The inside construction is shown in Fig. 1. The original data of the cylindrical shell for the predict of vibroacoustic environment are shown in Table 1. The vibroacoustic environmental predict for three serious models of SEA is performed.

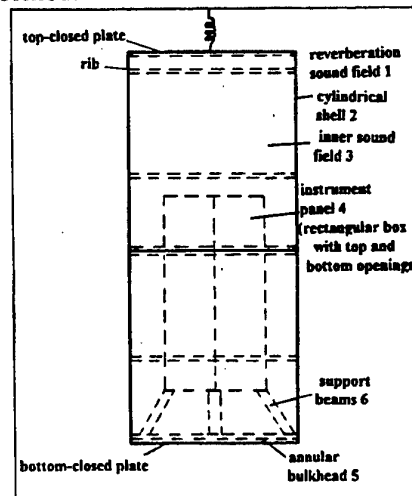


Fig.1 Sketch map of cylindrical shell with inside instrumental construction

Table 1.Original Data for Vibroacoustic Environment Predict

Subsystem	Parameter Name	Symbol	Value
reverberation field 1	volume	$\nabla_1$	$82.12 \text{ m}^3$
	mass density	$\rho_a$	$1.2 \text{ kgm}^{-3}$
	sound speed	$C_a$	$344 \text{ ms}^{-1}$
cylindrical shell 2	surface area	$A_2$	$4.757 \text{ m}^2$
	area density	$\rho_a$	$3.784 \text{ kgm}^{-2}$
	longitudinal sound speed	$C_{12}$	$3597 \text{ ms}^{-1}$
	thickness	$t_2$	$2.2 \text{ mm}$
	rotatory radius	$R_2$	$0.635 \text{ mm}$
	diameter	$D_2$	$0.813 \text{ m}$
	elastic modulus	$\gamma_2$	$2.23 \times 10^{10} \text{ Nm}^{-2}$
	volume density	$\rho_2$	$1714 \text{ kgm}^{-3}$



internal sound field 3	volume	$V_3$	0.966 $m^3$
instrument panel 4	surface area	$A_4$	1.36 $m^2$
	area density	$\rho_{14}$	1.86 $kgm^{-2}$
	bending inertial moment	$I_4$	9.0 $mm^3$
	bending rotatory radius $R_4$ , longitudinal sound speed $C_{14}$	$R_4, C_{14}$	18.3 $m^2 s^{-1}$
bulkhead 5	length	$l_5$	2.39 $m$
	line density	$\rho_{15}$	1.3 $kgm^{-1}$
	vertical plane rotatory radius	$R_{\rho 5}$	11.0 $mm$
	horizontal plane bending rotatory radius	$R_{\rho 5}$	12.7 $mm$
	twist rotatory radius	$R_{t5}$	16.8 $mm$
	polar inertial moment	$J_{15}$	13.7 $cm^4$
	twist stiffness constant	$K_{t5}$	1.12 $cm^4$
	longitudinal sound speed	$C_{15}$	5182 $ms^{-1}$
	shear sound speed	$C_{s5}$	3048 $ms^{-1}$
supporter 6	4 supporter's length	$l_6$	1.02 $m$
	line density	$\rho_6$	0.488 $kgm^{-1}$
	vertical plane bending rotatory radius	$R_{PV6}$	12.7 $mm$
	horizontal plane bending rotatory radius	$R_{PH6}$	16.8 $mm$
	twist rotatory radius	$R_{t6}$	21.1 $mm$
	polar inertial moment	$J_{16}$	8.03 $cm^4$
	twist stiffness constant	$K_{t6}$	0.015 $cm^4$
	longitudinal sound speed	$C_{16}$	5182 $ms^{-1}$
	shear sound speed	$C_{s6}$	3048 $ms^{-1}$
	static force stiffness	$K_6$	1.38 $Nm$
	angle made with cylindrical shell axis	$\theta$	20°

### 3.1. JOINT ENERGY TRANSFER TEST ALONG BOTH SOUND AND MECHANICAL ROUTES AND SEA PREDICT

Acoustic experiment of the cylindrical shell with instrument construction is performed when the shell is hanged through a spring in reverberation room ( sound field 1 ). Cylindrical shell 2 is reinforced by four annular bulkheads fixed on the inner wall. There are four supporters 6 on the bottom annular bulkhead 5, on which rectangular box 4 with openings at both the top end and the bottom end is supported. Vibration energy is transferred into the instrumental panel of rectangular box 4 through inner sound field 3 and support beams 6 to develop the acceleration response level of rectangular box 4. Predict results for various SEA models are shown in Fig.2. The symbol's meanings in the Figures are:

$$AL4_{re1g} = 10\log_{10} \frac{\langle a_4^2 \rangle}{g^2}, \quad SPL1_{re20\mu Pa} = 10\log_{10} \frac{\langle p_1^2 \rangle}{p_r^2}, \quad p_r = 20\mu Pa$$

Where  $\langle a_4^2 \rangle$  is acceleration average square value of 4th subsystem,  $\langle p_1^2 \rangle$  is pressure average square value of 1st subsystem,  $p_r$  is reference pressure,  $g$  is gravity acceleration.

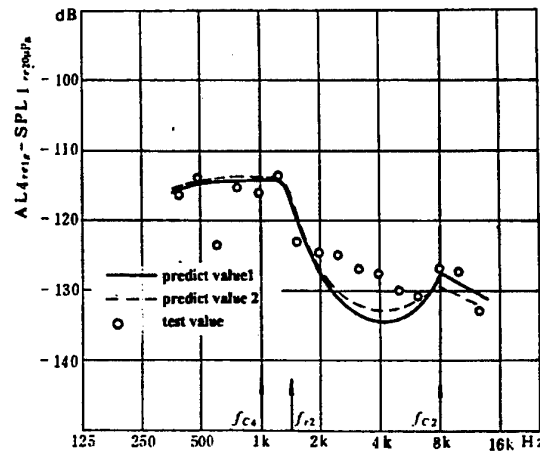


Fig. 2 Predict and test results for energy transfer through both sound and mechanical routes

### 3.2. ENERGY TRANSFER TEST ALONG SOUND ROUTE AND SEA PREDICT

Supporters 6 are removed and rectangular box 4 is hanged by soft spring

instead onto the top end of the cylindrical shell. The cylindrical shell is still hanged in reverberation room and excited by reverberation sound field 1. Energy is transferred only along the route: sound field 1 → cylindrical shell 2 → inner sound field 3 → instrumental panel of rectangular box 4, and to develop the dynamic response of box 4. The predict and test results are shown in Fig.3 where  $f_{c,i}$  is critical frequency of subsystem  $i$ ,  $f_{r,2}$  is ring frequency of subsystem 2.

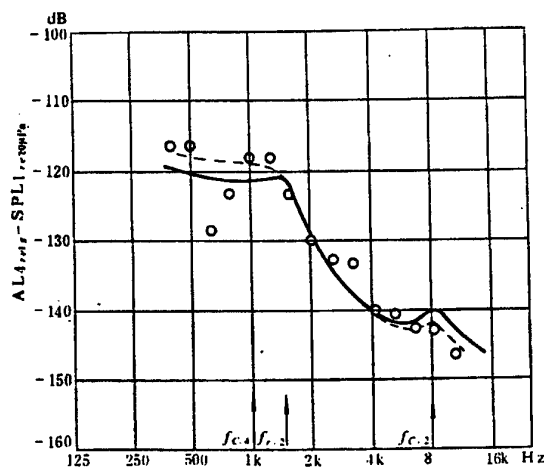


Fig.3 Predict and test results for energy transfer through sound route

### 3.3. ENERGY TRANSFER TEST ALONG MECHANICAL ROUTE AND SEA PREDICT

The instrumental panel of rectangular box 4 is insulated by sound-reduction shroud so that box 4 is not excited by inner sound field 3. Then vibration of box 4 is excited only by the energy transferred from support beams 6 to develop its vibration response. The cylindrical shell is still hanged by spring in reverberation room and excited by inner reverberation field. The transfer of vibration energy is only along the mechanical route: reverberation sound field 1 → cylindrical shell 2 → annular bulkhead 5 → supporters 6 → instrumental panel of rectangular box 4, to develop the dynamic response of the instrumental panel of rectangular box 4. The predict and test results are shown in Fig.4.

It is found in the comparison of the results shown in the three figures that both the predict results and the test results are in a satisfactory agreement. Particularly the results from through sound transfer route are

better than ones from through mechanical transfer route.

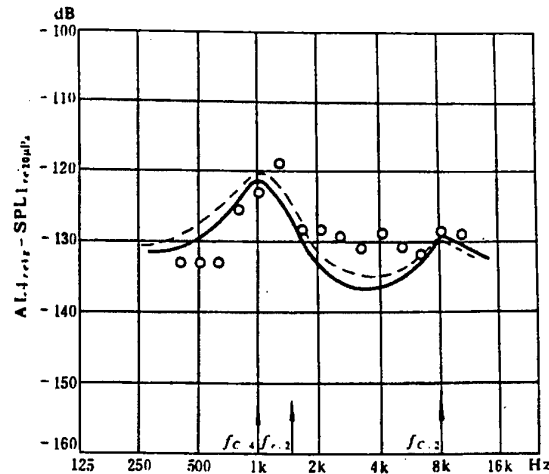


Fig 4. Predict and test results for energy transfer through mechanical route

#### References

- [1] Yao D.Y. and Wang Q.Z. (1995) *Statistical Energy Analysis Principle And Its Applications*, Beijing Institute of Technology Press, Beijing.
- [2] Ming R.S. and Sun J.C. ( 1989 ) Coupling element loss energy distribution of nonconservative coupled system, *Vibration and Shock*, No.4.
- [3] Luo S.H. (1988) *Application of SEA in vibration isolation of torpedo dynamic system*, Ph.D Thesis, Shanghai Jiaotong University.
- [4] Fahy, F. J. and Yao D.Y. (1987) Power flow between non-conservatively coupled oscillators, *Journal of Sound and Vibration*, Vol. 114 (1).
- [5] Sun J.C., Lalor L. and Richards E.J. ( 1987 ) Power flow and energy balance in nonconservatively coupled structures, Part I: Theory, *Journal of Sound and Vibration* 112.
- [6] Chen G.D. and Song T.T. (1991) Power flow and energy balance between nonconservatively coupled oscillators, *Transactions of ASME*, Vol.113 pp.331-343.
- [7] Yao D.Y., Liu S.W., Ning Y. & Pang H.S. ( 1991 ) Theoretical and experimental studies for x x flight vehicle structural vibration, China

## **SOUND TRANSMISSION THROUGH BUILDINGS USING SEA**

Robert J M Craik  
Department of Building Engineering and Surveying  
Heriot-Watt University  
Riccarton  
Edinburgh  
EH14 4AS

### **Introduction**

When Statistical Energy Analysis was first introduced in the early 1960s it brought together two existing bodies of knowledge. One of these was work on coupled oscillators and the second was on statistical room acoustics. This work on room acoustics was part of a well established philosophy in Building Acoustics which treated both the acoustic pressure in rooms and vibration of the structure in a statistical manner. This meant that when SEA was formally established in all its depth and complexity it was rapidly adopted by Building Acoustics groups around the world.

Since then SEA has been widely used in Building Acoustics and has been one of the most successful areas of the application of SEA. For sound transmission in buildings there is no serious competition to SEA as an approach to solving problems and although some specific problems require specialist techniques for their analysis and study, SEA is generally the preferred method. Although SEA notation is not always used, the fundamental concepts of averaging over space and frequency are widely accepted. It is this long acceptance of the SEA principles which has led to its wide scale adoption.

The application of SEA has developed to a point where the basic framework is accepted. There is still work to be done in developing and refining SEA but SEA has matured to a point where it is being used as a tool to solve real problems rather than as a research tool that has to be justified by comparison with other techniques.

Current problems in Building Acoustics being addressed using SEA can be broadly classified into three distinct groups. On the smallest scale there are problems of sound transmission and particularly sound transmission through multi-layer walls and floors. On a larger scale SEA is increasingly being used to study flanking transmission between adjacent rooms and finally, SEA is being used for the study of full sized buildings to help with general design and layout problems.

Similar developments are being undertaken in other areas of acoustics and the signs that the pattern of development is similar to that in Building Acoustics. Thus the current trends in Building Acoustics may give an insight into the future of other acoustics disciplines.

In this paper each of these three areas are reviewed briefly and some current work that is ongoing is described.

### Sound transmission through double walls

One of the earliest applications of SEA was to sound transmission through walls. In 1970 Price and Crocker [1] used SEA to study sound transmission through a wall consisting of two thin aluminium sheets. Although this form of construction is quite different from real building structures, nevertheless the application to other types of structure was immediately obvious and since then a range of types of construction have been examined.

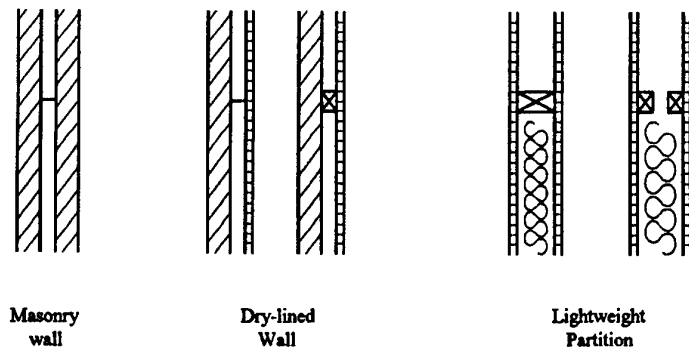


Figure 1. Section through typical double walls

There have been many studies of sound transmission through double walls some of which pre-date the introduction of SEA and today both classical and SEA approaches are used. Whilst classical approaches have been successful for the simpler form of construction they have tended to be unable to cope with more complex structures where there may be structural as well as airborne connections between two leaves of the wall.

Double walls can be classified into three broad types as shown in Figure 1. There are masonry cavity walls, dry-lined masonry walls and lightweight partitions. In masonry double walls two layers of masonry, typically brick or concrete block, are structurally connected by metal ties which are inserted for stability reasons [2]. In dry-lined walls, a masonry core wall provides the structural support and a secondary leaf is attached either by discreet points, such as nails, screws or plaster dabs, or by connection along lines through timber battens or metal channels [3]. Absorption may be added to the cavity.

The most acoustically complex form of construction is the lightweight double leaf partition which typically consists of two layers of plasterboard attached to some form of frame. There may or may not be absorption in the cavity and in cases where sound transmission is important two separate frames may be used. In most cases a common frame is used and plasterboard is attached to the frame either by nails or by screws.

Most of the difficulties with modelling this form of lightweight construction using SEA is with the frame. One approach is to model the frame as a connecting element between the two plates and to use standard theories for transmission between plates along a line connection. In this case the frame is not included in the model as a subsystem but is merely the connecting element between the two plates. The SEA model of a complete wall would be as shown in Figure 2. The properties of the frame may be included either by modelling it as a beam [4] or as a finite length plate [5]. The frame subdivides each leaf into

a number of sub-panels each of which would be modelled as a subsystem though for clarity only one is shown in Figure 2. This can lead to problems as there will be a low mode count in each sub-panel and there may be a non-diffuse sound field.

An alternative method of modelling the coupling is to assume that the connection between the plasterboard and the frame occurs only at a few discrete points. The coupling can then be computed from the mobility of the elements. In this case the frame has to be modelled as a subsystem and usually the coupling between the plasterboard on one side and the frame can be treated independently from the coupling between the frame and the plasterboard on the other side. This then gives the SEA model that is shown in Figure 3. This is similar to the model of Figure 2 but has the frame as a subsystem. The plasterboard on each side behaves as 1 subsystem so there are no special problems of low modal density. However, if the wall is made from several sheets of plasterboard then experimental data suggests that each sheet should be modelled as a separate subsystem. In practise, for airborne sound transmission, each leaf can be modelled as one subsystem and the effective perimeter length and area increased.

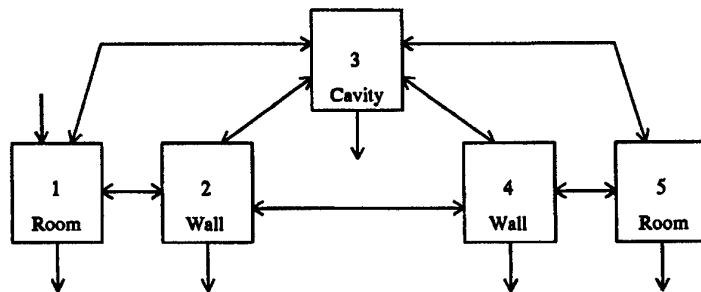


Figure 2. SEA model of a double leaf lightweight partition where the structural connection is a LINE connection

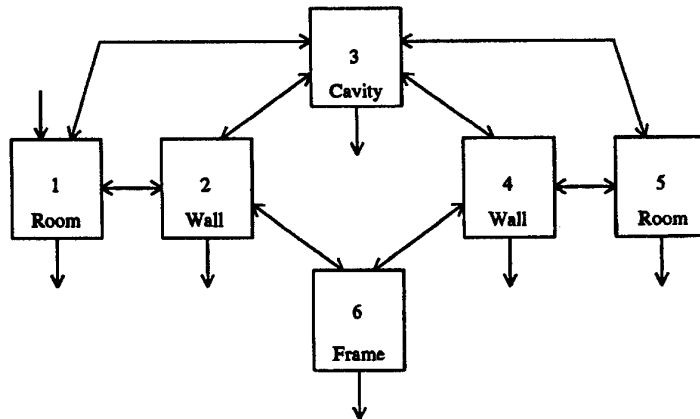


Figure 3. SEA model of a double leaf lightweight partition where the structural connection is a series of INDEPENDENT POINTS.

The decision as to when to use one model and when to use the other must clearly be addressed and a good strategy that works well in practice is to assume that the connection between the frame and the plasterboard is behaving as a series of independent points when the nails or screws are more than half a bending wavelength apart. Thus at low frequencies the joint between plates will be modelled as a line connection and at high frequencies the joint will be as a series of independent points. This clearly involves a certain amount of approximation but seems to work well in practice.

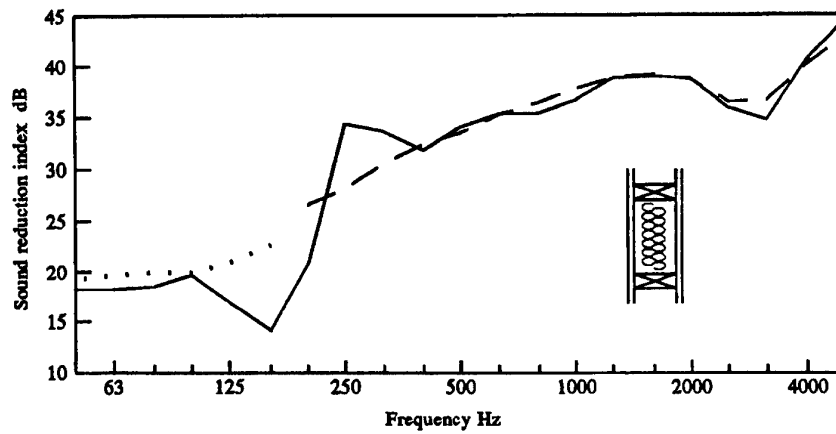


Figure 4. Measured and predicted transmission through a lightweight partition where the structural connection can be modelled as a LINE. —, measured; ----, predicted; ·····, predicted at low frequencies where the wall is a single subsystem.

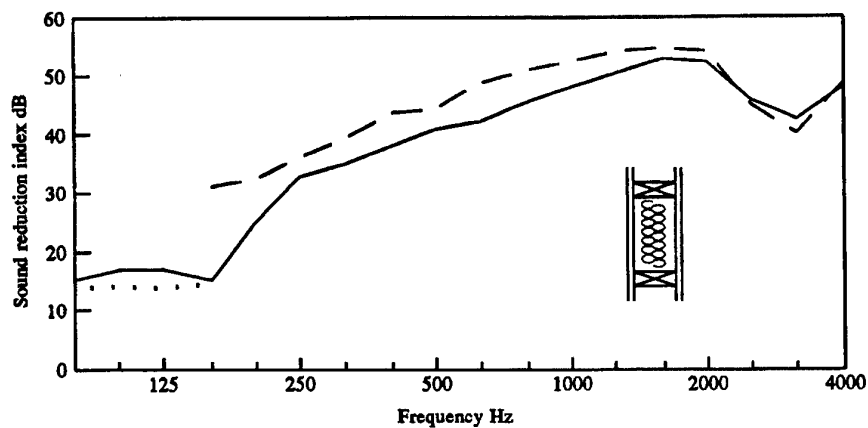


Figure 5. Measured and predicted transmission through a lightweight partition where the structural connection can be modelled as a SERIES OF POINTS. —, measured; ----, predicted; ·····, predicted at low frequencies where the wall is a single subsystem.



An example of measured predicted sound transmission through a lightweight plasterboard wall where the point connections are sufficiently close that they can be modelled as a line can be seen in Figure 4. It can be seen that there is good agreement between the measured and predicted results over the entire frequency range. At low frequencies, below 160 Hz, the wall should be modelled as a single subsystem and an appropriate prediction is included.

An example of measured and predicted transmission through a lightweight partition where the nails are far apart and are modelled as a series of independent points can be seen in Figure 5. Again there is good agreement though not as good as Figure 4. Further studies have shown that the model correctly models the structural coupling but that transmission through the cavity is not predicted accurately.

In most practical cases the connection points between the frame and the plasterboard are sufficiently far apart that for most of the frequency range the connection can be modelled by a series of points. Since the coupling is directly proportional to the number of points, it follows that sound transmission through the wall will be directly proportional to the number of nails in the wall. This clearly assumes that transmission through the wall is being dominated by the structural path and this will generally be the case if there is absorption in the cavity to reduce paths through the cavity. If there is no absorption in the cavity then the cavity path will generally dominate and the number of nails in the wall will not have any effect. Where transmission is through the structure, doubling the number of nails on either side will give a 3 dB difference in the sound reduction index and so doubling the nails on both sides will give up to 6 dB. Experimental data confirms this theoretical prediction.

The ability to use SEA models to model such complex structures is very important and is likely to have an increasing effect on design of walls and floors. There is an increasing demand for lighter constructions and in order to meet specified acoustic performance criteria it is necessary that these constructions should become more complex with more components. The days when walls were simply made thicker or heavier to achieve good sound insulation have long gone and increasingly lightweight constructions are the norm. Unfortunately the increased complexity of these constructions means that it is no longer practical to test all possible combinations of components to establish which are the best. Numerical modelling offers an alternative approach to establish, if not the best construction, at least those which merit further study. It can already be used as a filtering technique to rule out unsuitable forms of construction and will increasingly be used in product development.

### **Short flanking transmission paths**

It has long been recognised that measurements made in the field differ considerably from laboratory measurements and apart from difficulties of workmanship this can often be attributed to flanking transmission. SEA provides simple procedures for predicting flanking transmission and therefore helps with the understanding of sound transmission between rooms. This is an area where SEA is having a significant impact on the organisations responsible for building codes in a number of different countries.

A typical situation consists of two adjacent rooms which share flanking walls or floors. Increasingly building codes, which try to maintain levels of acoustic insulation, need

to specify not only the properties of the common wall or floor but increasingly the properties of the flanking walls and floors. In Britain the Regulations [6] specify not only a range of wall and floor constructions that will give adequate insulation against direct sound transmission but also specify details of other components that could affect flanking transmission including detailed advice about construction materials and matters such as the position of windows.

When the Regulations were first being developed testing was carried out in large experimental facilities where different combinations of materials were studied. However, as the range of materials and construction forms increases, so this is becoming increasingly difficult and numerical models are being used in its place.

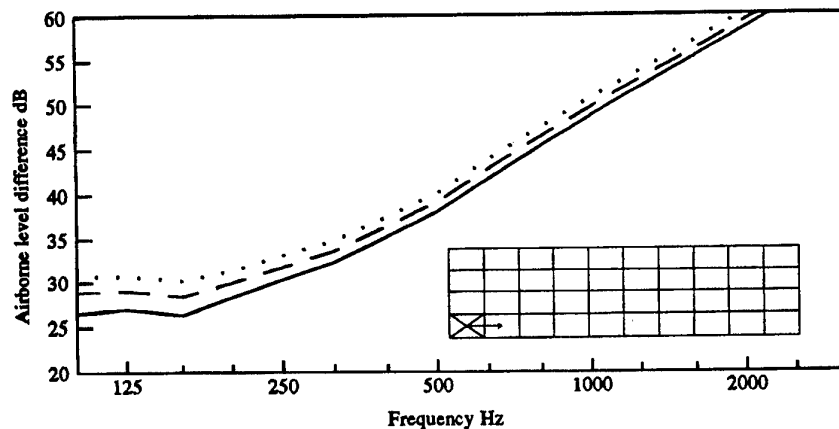


Figure 6. Sound transmission through a wall. ...., direct paths; ----, direct + 1st flanking paths; —, all paths. Insert shows a section through the idealised building.

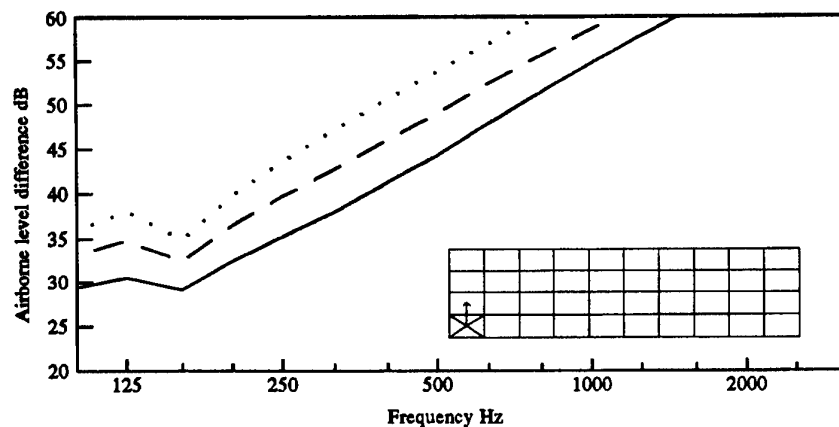


Figure 7. Sound transmission through a floor. ...., direct paths; ----, direct + 1st flanking paths; —, all paths. Insert shows a section through the idealised building.

A recently developed CEN standard [7] seeks to harmonise many of the calculation procedures across Europe and although not yet finalised it is helping to bring to attention many of the key features of flanking transmission. This document does not use SEA notation and instead describes sound transmission in terms of parameters such as transmission coefficient and radiation efficiency, which are familiar to SEA users, as well as others such as "characteristic junction transmission" which are new. The standard is designed mainly for use with measured data and this is reflected in the structure and notation used. However, it can also be used as a predictive tool. The theories then described are identical to those found in an SEA model and in some laboratories the SEA notation is being used in preference to the notation given in the standard. The mere existence of a standard of this type demonstrates the extent to which SEA type methods are embedded in thinking at all levels. The only difficulty with the standard is that it specifies exactly how to model each situation (often by ascribing each real system to its nearest idealised system). This approach may stifle new ideas and new approaches particularly for non-standard constructions where a good design may be discarded because its nearest idealised equivalent does not work well.

Although studying individual transmission paths can be very successful there are some difficulties which can be seen by considering sound transmission through a wall as shown in Figure 6 and transmission through a floor as shown in Figure 7. These figures show the predicted transmission for an idealised building with a 150 mm concrete floor and 100 mm concrete block walls. The shortest path is direct transmission through the wall or floor. For the wall most of the sound is transmitted through the wall and the difference between the direct path and all paths is less than 3 dB. Including the flanking paths that cross one structural joint increases the accuracy of the prediction to within 1.5 dB.

TABLE 1.  $D_{sT,w}$  of the wall and floor as the number of flanking paths is increased.

Subsystems in path	Wall	Floor
3 (Direct path)	42.8	54.6
4 (Direct + 1 st flanking)	41.6	50.7
5	41.2	49.3
6	41.0	48.5
7	40.9	48.0
8	40.8	47.6
9	40.8	47.4
10	40.7	47.2
Sum of all paths	40.5	46.4

However, for the floor it can be seen that the level difference due to transmission through the direct path is over 10 dB higher than the level difference due to all paths.

Adding all the first order flanking paths reduces the level difference by 5 dB but is still 5 dB above the overall transmission. Adding additional paths increases the accuracy of the prediction as can be seen in Table 1 which shows the single figure index  $D_{\text{tr},w}$  for both the wall and floor as additional paths are included. However, a path by path analysis is only useful if a few dominant paths control the overall transmission. In this example, a path analysis is useful for the wall but not the floor since too many paths need to be considered for reasonable levels of accuracy. Unfortunately, without carrying out the calculations it is not clear when a path analysis is going to be useful and when not.

The main advantage of a path analysis is its simplicity. The airborne level difference due to transmission along a path 1-2-3-4 can be given by [8]

$$D_{1-2-3-4} = 10 \log \frac{\eta_2 \eta_3 \eta_4 V_4}{\eta_{12} \eta_{23} \eta_{34} V_1} \quad (1)$$

where  $\eta_i$  is the total loss factor,  $\eta_{ij}$  is the coupling loss factor and  $V$  is the room volume. The equation for each of the loss factors is usually a simple algebraic expression or a list of measured data. It is therefore a simple matter to carry out the calculation by hand (or with a spreadsheet if it is to be repeated often) without the need for expensive "black box" software. This simplicity has always been one of the attractions of SEA.

### SEA as a design tool

The final area where SEA is being developed is for use as a design tool to examine the global properties of a building or structure. Increasing the size of the system being considered greatly increases the complexity of the model. When transmission is only over a short distance then it is generally sufficient to consider only bending wave transmission. However, when larger physical models are considered then in-plane waves must also be included. This increases the difficulty in calculating the structural transmission coefficients and simple algebraic expressions are rarely sufficient.

The best method of modelling the in-plane waves is sometimes a topic of discussion. In a large building (or other structure) there are large continuous floors and it is sometimes suggested that the entire floor should be modelled as a single subsystem for in-plane waves even if it is subdivided for bending waves. The alternative is to divide each separate floor into three separate subsystems (bending, longitudinal and transverse waves). This is a more elegant solution as there is then physical coincidence between the three subsystems and the mechanisms of wave conversion are then obvious. On the other hand the modal density and modal overlap of the longitudinal and transverse subsystems will be low.

If the floor is a single subsystem then the in-plane vibration will be constant for all floor slabs whereas if the floors are independent subsystems then the vibration level of each will be different. This provides an experimental method of determining the best approach.

An experiment was carried out to resolve this problem and also to establish whether or not the existing theoretical models [9] which are normally verified by comparison with bending wave energy also predict the in-plane vibration correctly.

The in-plane energy was measured by simply placing an accelerometer on its side. This limits the range of frequencies where reliable measurements can be made as bending waves are associated with rotation of the plate elements causing in-plane motion at the surface. In theory this unwanted vibration can be reduced by using two accelerometers on opposite sides of the floor but in practise this does not result in any significant improvement. The test was carried out of a series of floors marked 2 - 7 in the insert of Figures 8 and 9. The source was a transient excitation of a wall shown by an arrow in the figure. This generated in-plane vibration in the floors due to wave conversion at the boundary.

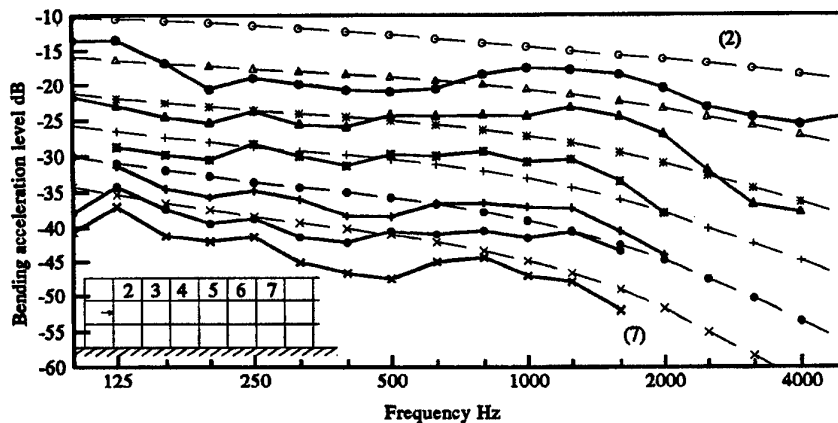


Figure 8. Measured and predicted BENDING vibration in a building as the distance from the source increases. —, measured; - - - - - , predicted

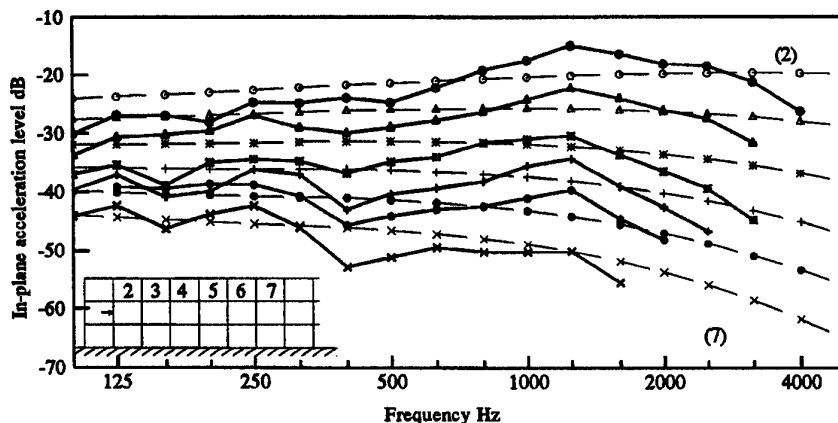


Figure 9. Measured and predicted IN-PLANE vibration in a building as the distance from the source increases. —, measured; - - - - - , predicted

A comparison of the measured and predicted bending vibration can be seen in Figure 8. This confirms what other measurements have already shown [10] that the bending energy can be predicted for this building.

A comparison between the measured and predicted in-plane energy can be seen in Figure 9. Although there is good agreement between the measured and predicted results the results must be interpreted with care. The bending rotation induced in-plane vibration on the surface is greater than the predicted in-plane vibration at frequencies above 500 Hz and so at these frequencies the accelerometer is not measuring in-plane energy. The same problem occurs at low frequencies close to the source particularly for floor 2. The remaining data shows that the vibration level is different at each floor and so each floor section should be modelled as a separate subsystem. In addition there is good agreement between the measured and predicted results showing that existing theoretical models can be used with confidence.

One of the applications of these models is to calculate the effect of changes in room layout or material properties on sound transmission through large structures.

An example of this type of application can be seen in the results of Figure 10 which show a section through an idealised building. The building was taken to have 150 mm concrete floors and 100 mm concrete block walls (as in Figure 6 and 7) and a noise source was modelled as being located in the lower left hand room. Sound transmission through the entire building was then calculated and the values of  $D_{sT,w}$  (weighted standardised level difference) for transmission from the source room to the other rooms in the building was computed. The properties of the materials used in the internal walls were then increased by a factor of 2 (except in the case of the damping where all the walls and floors had their internal loss factor increased) and the change in the  $D_{sT,w}$  values was computed. The figure shows the section of the building and in each room is shown the change in  $D_{sT,w}$  in dB. A positive number indicates that the level difference has gone up (sound transmission has been reduced).

It can be seen that the change in Young's Modulus has a relatively small effect on transmission which decreases with distance from the source. The level difference has gone up by 1 dB for transmission to the room next door but goes down for the room above resulting from a redistribution of energy in the building. The increased stiffness of the walls has increased transmission vertically and reduced transmission horizontally. There is therefore a decrease for all of the top floor rooms. Despite the large change in the values of Young's modulus (a factor of 2) the change in level difference is relatively small.

Much larger changes occur when the thickness of the internal walls is increased. There is a significant improvement in transmission to the room next door and almost no change to the room above. The improvement is achieved for all ground floor rooms and again there is a redistribution of energy in a vertical direction.

Increasing the density of the internal walls improves the sound insulation for all rooms and the benefit generally increases with distance. Similarly increasing the internal loss factor (of all walls and floors) increases the sound insulation particularly for rooms that are far from the source.

Young's Modulus $\times 2$	-0.7	-0.7	-0.6	-0.5	-0.4	-0.3	-0.2	-0.2	-0.2	-0.1
	-0.5	-0.5	-0.4	-0.3	-0.2	-0.1	-0.1	-0.0	-0.0	0.1
	-0.5	-0.3	-0.1	0.1	0.1	0.1	0.1	0.2	0.2	0.3
	X	1.0	0.4	0.5	0.5	0.5	0.4	0.4	0.4	0.5
Density $\times 2$	1.1	1.5	1.8	2.2	2.5	2.9	3.2	3.6	4.0	3.9
	1.1	1.6	1.9	2.3	2.7	3.1	3.5	3.8	4.2	4.1
	1.0	2.0	2.2	2.5	2.9	3.2	3.6	4.0	4.4	4.3
	X	3.4	2.5	2.7	3.0	3.3	3.7	4.1	4.5	4.3
Thickness $\times 2$	-0.8	-0.5	-0.1	0.3	0.7	1.1	1.5	1.9	2.3	2.5
	-0.4	0.1	0.6	1.1	1.5	1.9	2.2	2.5	2.9	3.1
	0.1	1.3	1.9	2.2	2.4	2.7	3.0	3.3	3.6	3.8
	X	5.6	3.2	3.1	3.2	3.4	3.6	3.9	4.2	4.4
Internal loss factor $\times 2$	6.2	6.8	7.4	8.1	8.8	9.4	10.0	10.6	11.2	11.8
	5.4	6.0	6.7	7.4	8.1	8.9	9.6	10.2	10.8	11.3
	3.1	4.3	5.7	6.8	7.6	8.3	9.0	9.7	10.2	10.8
	X	2.2	5.0	6.3	7.3	8.0	8.5	9.1	9.7	10.2

Figure 10. Change in  $D_{nt,w}$  as the material properties of the internal walls (or all elements for the damping) are increased by a factor of 2.

### Conclusions

During the last 30 years there has been an increasing development of SEA and an increasing use of its application to Building Acoustics. The basic philosophy of SEA is firmly embedded in Building Acoustics and this has been one of the great strengths in its application. SEA is likely to continue to be the main conceptual model used in Building Acoustics and as more studies are carried out so there will be greater confidence in its application.

One of the fundamental remaining problems in SEA in general is in the analysis of the uncertainties of the theoretical model. Surprisingly this is not one of great importance to users of SEA in the field of Building Acoustics. In Building Acoustics there are relatively few tests that are routinely carried out (such as sound transmission) and all are based on robust procedures involving spacial, temporal and frequency averaging. Most users therefore have a "feel" for the measured data and particularly problems associated with spacial variation and low frequency.

In the future SEA will continue to develop. Fundamental work will result in more closely defined limits of applicability and uncertainty providing a firm theoretical basis. Other developments will take place extending the range of applications comparing SEA models with other theoretical models and with detailed laboratory results. This work is in progress in many disciplines of acoustics.

The biggest change will be in when industry takes these SEA models and uses them for design purposes. This will lead to further development of SEA and is a phase that is just beginning.

### References

- [1] Price, A. J. and Crocker, M. J. (1970) Sound transmission through double panels using statistical energy analysis. *Journal of the Acoustical Society of America*, 47, 683-693.
- [2] Craik, R.J.M. and Wilson, R. (1995) Sound transmission through masonry cavity walls. *Journal of Sound and Vibration*, 179, 79-96.
- [3] Wilson, R. and Craik, R.J.M. (1996) Sound transmission through dry lined walls. *Journal of Sound and Vibration*, 192, 563-579.
- [4] Langley, R. S. and Heron, K. H. (1990) Elastic wave transmission through plate/beam junctions. *Journal of Sound and Vibration*, 143, 241-253.
- [5] Bhattacharya, M. C., Mulholland, K. A. and Crocker, M. J. (1971) Propagation of sound energy by vibration transmission via structural junctions. *Journal of Sound and Vibration*, 18, 221-234.
- [6] Building Standards (Scotland) Amendment Regulations (1987), HMSO, London.
- [7] CEN/TC126/WG2 N96, (1994) Building Acoustics - Estimation of acoustic performance of buildings from the performance of products. Part 1: Airborne sound insulation between rooms. Sixth working draft.
- [8] Craik, R.J.M. (1996) Sound transmission through buildings using statistical energy analysis. Gower, UK, pp. 261.
- [9] Craven, P. G. and Gibbs, B. M. (1981) Sound transmission and mode coupling at junctions of thin plates, Part I: Representation of the problem. *Journal of Sound and Vibration*, 77, 417-427.
- [10] Craik, R.J.M. and Thancanarnootoo, A. (1992) The importance of in-plane waves in sound transmission through buildings. *Applied Acoustics*, 37, 85-109.

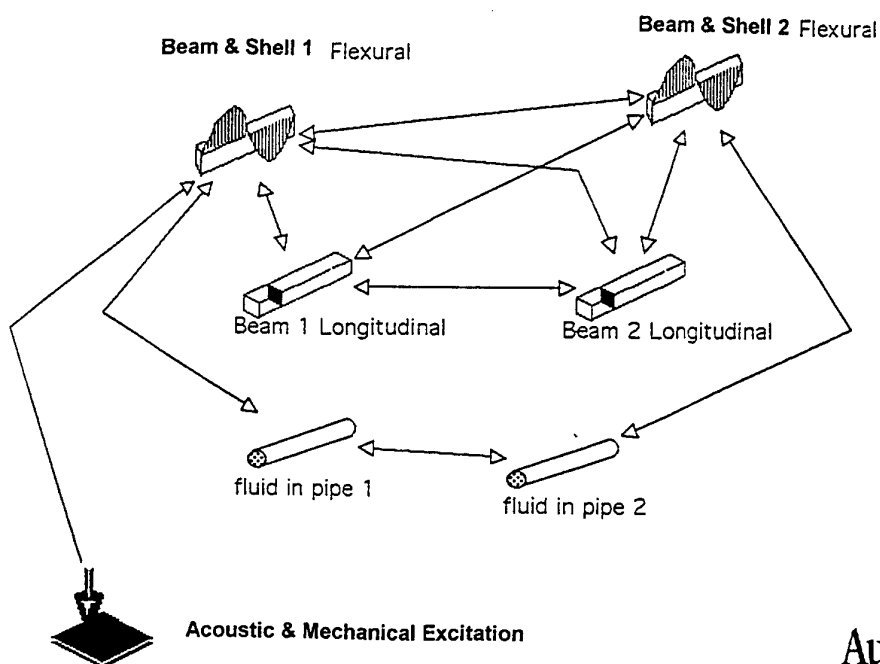


# Executive Summary

## Prediction of Noise from Pipework in Ships and Onshore & Offshore Installations

Industrial Design Study in Conjunction with CMPT

- ✓ Assess Compliance with Noise Limits
- ✓ Evaluate New and Modified Designs Quickly
- ✓ Identify Dominant Noise Radiators
- ✓ Confidence in Application of Noise Control Measures



## **A better design technique for controlling pipework noise.....**

- Noise is an important design issue for marine-structure and onshore plant designers and operators. Meeting regulations and clients' specifications for noise is of growing concern.
- A survey has revealed that most builders, contractors and operators see the need for more capable and reliable prediction and optimisation methods, to enable noise to be controlled to specific limits at the design stage and hence to comply with customers' specifications. Better design techniques can also assist competitiveness by aiding economical low noise design.
- A Managed Programme of the Centre for Marine and Petroleum Technology, which is being coordinated by Marinetechnic South Ltd, is combining the resources of a £0.5M research programme (now in mid-term) with multi-sponsor industrial design projects in order to develop applications of Statistical Energy Analysis (SEA) techniques to marine craft and offshore and related installations.
- Statistical Energy Analysis (SEA) is a noise and vibration modelling technique introduced 30 years ago, in particular to design spacecraft to resist damage from acoustically-induced vibration during the launch phase. SEA has since been developed for broader application, particularly for the prediction of sound levels in road vehicles, aircraft and buildings. Its benefits, including simplicity for the guided user, can now be applied to prediction of noise from pipework.
- Commercial SEA applications packages are available and it is the intention of this study to develop and verify the particular aspects required to allow application to pipework noise. The method could then be applied via a developed user interface.
- Currently, proposed noise models have been inadequate to give acceptable confidence in predicted levels because they omit important structural response factors and include internal attenuation uncertainties, which are to be addressed in this study.
- The application study is targeted primarily at gas-filled systems but can be extended to liquid-filled systems.
- The intended project is costed at £65k over a period of 15 months.
- Sponsors will have the opportunity of influencing the direction and emphasis of the study, at the project definition stage and throughout, and will receive early information on technical progress in this important area of design.
- Proposed deliverables include algorithms and guidelines for SEA modelling of noise from pipework.

If you are interested in knowing more about this programme, please contact:

Neil Pinder, Programme Coordinator  
Marinetechnic South Ltd  
Tizard Building (ISVR)  
University of Southampton  
Highfield  
Southampton SO17 1BJ, UK

Tel: +44 (0)1703 593756  
Fax: +44 (0)1703 592728  
E-mail: [jnp@isvr.soton.ac.uk](mailto:jnp@isvr.soton.ac.uk)